CHALMERS
UNIVERSITY OF TECHNOLOGY

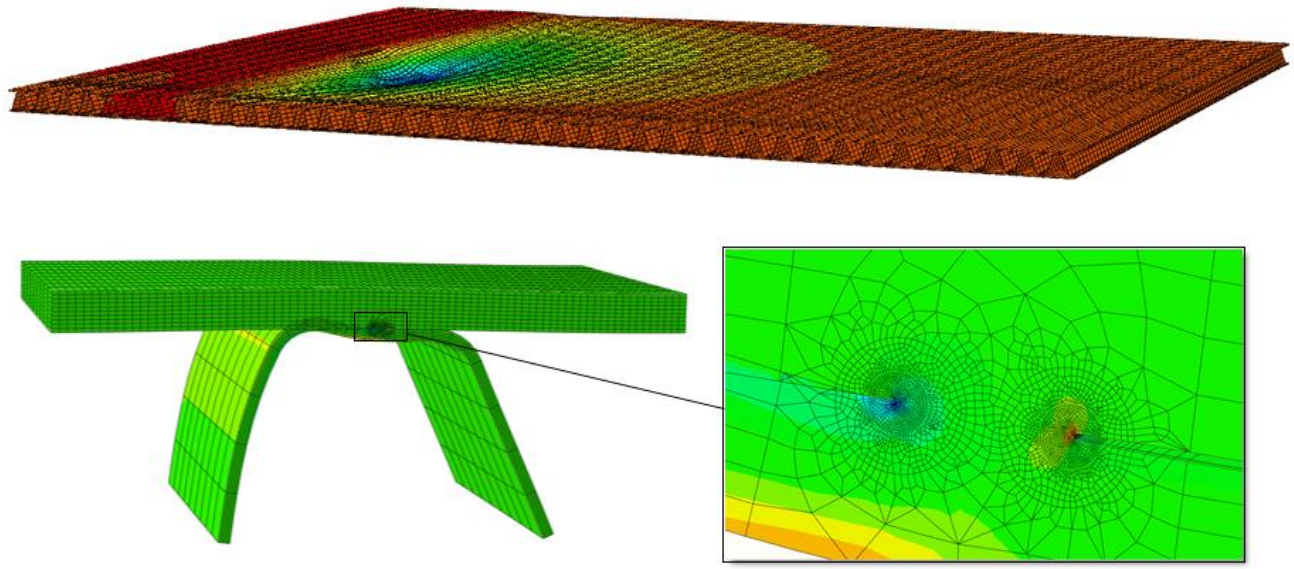

Fatigue Analysis of Hybrid Laser Welds in Steel Sandwich Bridge Decks

Master's Thesis in the Master's Programme Structural Engineering and Building Technology

AMANDA PALMKVIST
LINDA SANDBERG

Department of Civil and Environmental Engineering
Division of Structural Engineering
Steel and Timber Structures
CHALMERS UNIVERSITY OF TECHNOLOGY
Gothenburg, Sweden 2015
Master's Thesis 2015:11

MASTER'S THESIS 2015:11

Fatigue Analysis of Hybrid Laser Welds in Steel Sandwich Bridge Decks

Master's Thesis in the Master's Programme Structural Engineering and Building Technology

AMANDA PALMKVIST

LINDA SANDBERG

Department of Civil and Environmental Engineering
Division of Structural Engineering
Steel and Timber Structures
CHALMERS UNIVERSITY OF TECHNOLOGY
Göteborg, Sweden 2015

Fatigue Analysis of Hybrid Laser Welds in Steel Sandwich Bridge Decks
Master's Thesis in the Master's Programme Structural Engineering and Building Technology

AMANDA PALMKVIST
LINDA SANDBERG

Examensarbete 2015:11/ Institutionen för bygg- och miljöteknik,
Chalmers tekniska högskola 2015

Department of Civil and Environmental Engineering
Division of Structural Engineering
Steel and Timber Structures
Chalmers University of Technology
SE-412 96 Göteborg
Sweden
Telephone: + 46 (0)31-772 1000

Cover:
Photograph of a finite element model of the fatigue tested steel sandwich deck, together with submodel 1 and a close up of the weld region.

Department of Civil and Environmental Engineering
Göteborg, Sweden, 2015

Fatigue Analysis of Hybrid Laser Welds in Steel Sandwich Bridge Decks

Master's thesis in the Master's Programme Structural Engineering and Building Technology

AMANDA PALMKVIST
LINDA SANDBERG
Department of Civil and Environmental Engineering
Division of Structural Engineering
Steel and Timber Structures
Chalmers University of Technology

ABSTRACT

Steel sandwich panels are a concept that historically has been used in the shipbuilding industry. The panels are made with a core, which can be produced with different configurations, connected with welds to an upper and lower face plate. The panels have shown great advantages with not only good stiffness in both longitudinal and transverse direction but also a high stiffness- to weight ratio making the concept interesting for bridge design.

However, the concept has not yet been used in bridge design because of limitations in the welding techniques. By implementing the newly developed welding technique, hybrid laser arc welding, larger penetration depths are possible enabling the use of geometries relevant in bridge application. Despite great advantages with steel sandwich panels limited research exists, especially in the field of fatigue. Often the fatigue failure governs the design of steel bridges; therefore, it is of large importance to investigate the fatigue behaviour of these types of welds.

The aim of the master's thesis was thus to investigate the fatigue behaviour of hybrid laser welds in steel sandwich decks. The first objective was to create a SN-curve to represent the design strength for hybrid laser welds. The SN-curve was produced by modelling previously performed fatigue test specimens in FE-software Abaqus and analyse them using the effective notch stress method. The investigation indicated that a higher slope for the SN-curve than what is recommended by International institute of welding is possible. The fatigue strength was shown to be close to the recommended FAT225-curve. However, a large scatter of the results existed indicating on uncertainties in the results. Therefore, more fatigue tests need to be conducted to determine a reliable design strength.

The second objective for the thesis project was to identify critical weld details in a steel sandwich bridge deck under a moving static load and identify the governing load effects. In this study the effective notch stress method was used in conjunction with finite element analysis. The study was conducted by investigating the fatigue behaviour in welded details close to the support and in the mid span of the deck, both at the upper and lower face panels. By subjecting the deck to a moving load in transverse direction the detail subjected to maximum stress was detected. It was shown that the most critical detail was the one at the upper panel close to the support. The stress was of much greater magnitude and can be explained by the high impact of the large shear force at the position combined with a compressive local effect.

Key words: Steel Sandwich Panel, Hybrid laser arc weld, Fatigue design, Effective notch stress method, Bridge deck

Analys av utmattningsbrott i hybridlasersvetsar i stålsandwich-däck

Examensarbete inom mastersprogrammet Structural Engineering and Building Technology

AMANDA PALMKVIST
LINDA SANDBERG
Institutionen för bygg- och miljöteknik
Avdelningen för Konstruktionsteknik
Stål- och träkonstruktioner
Chalmers tekniska högskola

SAMMANFATTNING

Stålsandwichpaneler är ett koncept som historiskt har använts inom varvsindustrin. Panelerna är utformade med en kärna, som kan produceras med olika konfigurationer, som är ansluten med svetsar till övre och undre flänsar. Panelerna har inte bara visat bra egenskaper vad gäller styvhet i både längd- och tvärriktning utan även hög styvhet i förhållande till låg vikt vilket gör konceptet intressant för brokonstruktion.

Inom brokonstruktion har konceptet dock inte används på grund av begränsningar i svetstekniken. Genom att implementera den nyutvecklande svetstekniken, laserhybridsvetsning, har förmågan att skapa svetsar med tillräckligt penetrationsdjup gjort det möjligt att producera däck för brokonstruktioner. Trots stora fördelar med stålsandwichpaneler har begränsad mängd forskning gjorts på området, speciellt inom utmattning. Det är dock ofta utmattningsbrott som bestämmer livslängden för stålbroar och det är därför av stor vikt att undersöka utmattningsbeteendet hos dessa typer av svetsar.

Syftet med examensarbetet var att undersöka utmattningsbeteendet hos hybridlasersvetsar i stålsandwichdäck. Målet var att skapa en SN-kurva för att presentera en dimensionerande hållfasthet för hybridlasersvetsar. SN-kurvan framställdes genom modellering av gamla utmattningsprovkroppar i FE-programmet Abaqus som analyserades med ”effective notch stress” metoden. Undersökningen visade på en högre lutning för SN-kurvan än vad som rekommenderats av International institute of welding och resulterade i en utmattningshållfasthet nära den rekommenderade FAT225-kurvan. Dock visade analysresultatet på en stor spridning vilket indikerade på osäkerheter i resultaten. Därför bör fler utmattningstester utföras för att erhålla en pålitlig hållfasthet för hybrid laser svetsar.

Det andra målet för examensarbetet var att identifiera de styrande lasteffekterna samt de kritiska svetsdetaljerna i stålsandwich brodäcket under en rörlig last. Även i denna studie användes ”effective notch stress” metoden i samband med en finita element analys. Studien genomfördes genom att undersöka utmattningsbeteendet i svetsade detaljer nära stöd och i fältmitt, både i övre och nedre flänsen. Genom att utsätta däcket för en rörlig last i tvärriktningen kunde den detalj utsatt för maximal spänning bestämmas. Det visade sig att den mest kritiska detaljen var svetsen i den övre flänsen placerad nära stöd. Spänningen var av mycket större magnitud vilket kan förklaras av den stora skjuvkraften vid stödet kombinerat med ett stort lokalt tryck.

Nyckelord: Stålsandwichelement, Hybridlasersvets, Utmattningsdimensionering, Effective notch stress-metoden, Brodäck

Contents

Preface

This Master's thesis deals with fatigue design of hybrid laser welds in steel sandwich decks. The analysis has been carried out by using finite element analysis in conjunction with the effective notch stress method. The research has been carried out at the Department of Structural Engineering, Steel and Timber Structures, at Chalmers University of Technology, during January to June 2015. The thesis was a part of a research project founded by the Norwegian Public Roads Administration.

We would like to give a special thanks to our examinator and supervisor Prof. Mohammad Al-Emrani, who have offered us invaluable advice, consultation and guidance through this project.

Many thanks go to Farshid Zamiri Akhlaghi and Peter Nilsson, at the Division of Structural Engineering, for all the help they have given us. Finally, we would like to thank our opponents Evgenios Papadopoulos and Emmanouil Arvanitis for taking the time reading this thesis and giving their critical comments about it.

Göteborg June 2015

Amanda Palmkvist & Linda Sandberg

Notations

Roman upper case letters

A	Area
C	Fatigue strength constant
N	Normal force
N_0	Fatigue strength constant
N_i	Crack initiation time
N_p	Crack propagation time
N_t	Fatigue life
M	Moment
W	Bending stiffness

Roman lower case letters

m	Slope of the SN-curve (material constant)
$m_{natural}$	Natural slope of the SN-curve
s	Factor for stress multiaxiality and strength criterion

Greek letters

σ_r	*S*tress range
σ_{nom}	Nominal stress
ρ	Actual notch radius
ρ^*	Substitute micro structural length

Abbreviations

FAT	Fatigue class
FE	Finite Element
FEM	Finite Element Method
FLM	Fatigue Load Model
GMAW	Gas Metal Arc Welding
HAZ	Heat Affected Zone
HLAW	Hybrid Laser Arc Welding
IIW	International Institute of Welding
MAG	Metal Active Gas
MIG	Metal Inert Gas
SPS	Sandwich Plate System
SSD	Steel Sandwich Deck
SSP	Steel Sandwich Panel

1 Introduction

For long time the orthotropic bridge deck, consisting of a steel plate and longitudinal stiffeners, has been the most suitable concept in steel bridge design. The combination of a light-weight structure and satisfactory resistance against bending and torsion has made the deck an often used element. Over the years orthotropic steel decks have experienced extensive problems with fatigue cracks. The cracks have in some cases already been discovered after 20 years in service. Furthermore, due to high maintenance and lack of fully automated fabrication the cost is high for the orthotropic bridge deck (Bright & Smith 2004).

To overcome the disadvantages with the orthotropic steel deck, a steel sandwich deck (SSD) is in a theoretical aspect a more suitable option. The fact that the SSD is produced with an upper and lower face plate separated by the core, lower the neutral axis towards the centre of the cross-section. This result in a high strength- and stiffness to weight ratio. Furthermore, the level of anisotropy is significantly reduced, inducing load distribution in two directions.

The element has successfully been used in the ship industry for several years. The decks used in the ship industry are made of thin face plates and ordinary laser welding technique can be used to attach the panels to the core (Kujala & Klanac 2005). The concept to use SSD in bridge design is a relatively new design idea, because the welding techniques have been inadequate to weld through thicker plates that are needed in bridge design. Today a welding technique has developed by combining the laser welding process with arc welding (MAG/MIG). The technique is called hybrid laser arc welding (HLAW) and produce welds, through plates with larger thickness, with adequate quality (Abbott et al. 2007).

Despite the great advantages with SSD, the concept has not been applied yet in bridge design. One of the reasons is that the concept is not fully developed. Thus more research needs to be done to confirm critical details in the design concept. One of the critical aspects is the fatigue strength, often governing the design of steel bridges. No design methodology regarding hybrid laser welds exists and little research on the fatigue behaviour of steel sandwich bridge decks have been presented. Therefore, to be able to implement SSPs in steel bridge design one day it is crucial to get better understanding of the fatigue behaviour.

The Master thesis was a part of research project founded by the Norwegian Public Roads Administration. The research project aims to create a time effective transportation route along the western corridor (E39), from Trondheim to Kristianstad, eliminating all ferries. To create these long-span bridges, for the crossings, several structural concepts were investigated and one of these was the light-weighted steel sandwich panels.

1.1 Project Aim

The aim of this master thesis project was to study the fatigue strength of hybrid laser welds and the fatigue behaviour of welded details in steel sandwich bridge decks. The specific objectives were:

- Building of a SN-curve representing the fatigue life of hybrid laser arc welds
- Identify critical weld details in a SSD under a moving static load and the governing load effects

1.2 Method

To create a basic knowledge of the fatigue behaviour of hybrid laser arc welds and steel sandwich decks a literature study was initially performed. In addition a thorough study of previous preformed fatigue test on hybrid laser arc welds was conducted as a base for building a SN-curve representing the fatigue life. The purpose of producing the SN-curve was to compare it with the detail class recommended by the international institute of welding, IIW, and evaluating the fatigue strength of hybrid laser welds. Each test was modelled using the FE-software ABAQUS to localize the fatigue strength in terms of effective notch stress to be used in the SN-curve. The advantages of using the effective notch stress method are that the effect of the local weld geometry is included directly into the stress. Tests with different geometrical configurations can therefore be compared. The effective notch stress for each test was plotted in relation to the number of cycles to failure received from the tests.

To evaluate the fatigue behaviour of welded details a FE-analysis of the SSD was performed. A 3D solid model of the deck was set up in ABAQUS together with four attached submodels to identify critical weld details and the governing load effects. By applying submodels a refined region of the welds could be constructed at the critical positions of the deck. Further, the deck was subjected to a moving load and the notch stress at the weld regions were investigated for the different load steps. In this way the global and local load effects could be determined. Additionally, the most critical weld detail could be identified.

1.3 Limitations

- Several versions of hybrid welding techniques exists. However, this project will only cover hybrid welding combining laser with MAG/MIG welding.
- The welded connections between the steel sandwich elements in a bridge will not be considered in the report.
- When connecting the corrugated web to the flanges the welded connection can be produced with one or more strings. Only steel sandwich elements joint by one weld string was investigated in this project.
- The SSP can be produced with several different core configurations. Nevertheless, the project will only cover element with corrugated core.
- The SSP can be placed in either transverse or longitudinal direction of the bridge. Though, the study was limited to only study the fatigue behavior when the deck was placed with the webs of the corrugated core parallel to the main girder.
- In the FE-analysis of the SSD all loads where transferred between the face plates and the core by the weld. No face contact forces where considered.

1.4 Outline

Initially, a literature study is presented with the aim of creating a basic understanding of the subject for the reader. In the literature study a review of the completed fatigue tests are presented, to be used as base material when building the SN-curve representing the fatigue strength of hybrid laser welds.

The rest of the report is divided in two parts, Part A and Part B. A division of the report is done to increase the readability and the understanding for the reader.

Part A is focusing on defining a fatigue strength of hybrid laser welds. Consequently, this section contains the method used analysing the old fatigue test, the resulting SN-curves and a discussion concerning the obtained result.

Part B is focusing on the fatigue behaviour of steel sandwich bridge decks. The section covers the fatigue analysis of the SSD using FE-software Abaqus. Initially, a description of the modelling procedure of the 3D model and attached submodels are presented followed by respective verification. Additionally, the identified critical weld details and governing load effects are presented in a combined result and discussion chapter. Finally, the fatigue life of the SSD could be calculated by using the SN-curve produced in Part A.

The Master thesis's is summed up with conclusions regarding the project, but also suggestions of future studies.

2 Literature study

In this chapter, a literature study is presented regarding the keywords for the Master's thesis. Initially, information about steel sandwich decks is presented followed by welding techniques, especially regarding hybrid laser welding. The section about fatigue describes the basic information about the subject with the aim of creating understanding about the complex and critical failure mode which fatigue represents. The effective notch stress method was used during the fatigue analysis of the SSD, the literature study presents the method and how to use it. Finally, the fatigue behaviour of hybrid laser welds is presented and old fatigue tests that have investigated the behaviour of HLAW and produced SN-curves.

2.1 Steel sandwich decks

For many years the orthotropic steel deck has been a commonly used concept in several industries. The deck consists of an upper face plate connected to stiffeners by welds, see Figure 2.1. During service, critical aspects have been detected that threaten the capacity of the conventional stiffened plates. Fatigue cracks and the need of more frequent repairs of the surfacing than concrete decks are two examples (Bright & Smith 2004). It has also been shown that the deck has a lower stiffness in transverse direction compared to longitudinal direction. To improve the stiffness of the element a lower face panel can be added (Bright & Smith 2007) and thus is a closed sandwich element constructed, see Figure 2.2.

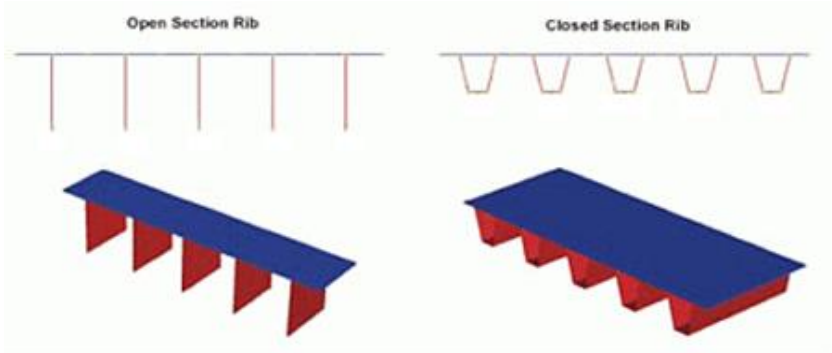

Figure 2.1 Orthotropic steel deck with open and closed stiffeners (Enginsoft 2014).

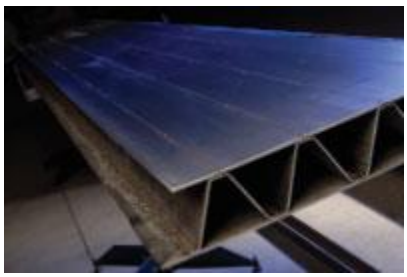

Figure 2.2 Steel sandwich panel (Welding design & fabrication 2008).

The sandwich panel concept has been under development during many years. Already in the 1950s the concept was tested in different industrial branches. However, the welding technique during that time had weaknesses and the idea was put on ice.

In the 1980s the US Navy continued to develop the sandwich panels. By that time, the welding technique had been improved and the laser welding technique made it possible to produce sandwich elements with required quality. The new welding technique required a low heat input and had the ability to create welds with sufficient depth (Kujala & Klanac 2005).

Furthermore, the development of the concept continued in Europe and especially in Great Britain, Germany and Finland (Kujala & Klanac 2005). The project SANDWICH was a European project involving eight countries. In the project there were twelve partners that had different expertise in special fields. The aim of the project was to develop the sandwich element and try to develop sufficient ways of improve the behaviour by filling them with different core material (Sandwich.balport n.d.).

2.1.1 Core configurations

There are many types of sandwich decks, two of them are the composite sandwich panels and metallic sandwich panels. The composite sandwich panel can be used either as a non-load carrying or a load carrying element. When producing this kind of element a part of the element consists of a non-metallic component, for example FRP or PU foam. Metallic sandwich panels can be classified by SPS or SSP. The SPS element is composed of two steel face pates and a bonded core. While the SSP is made of two steel face plates welded to a metal core. The core of the SSP can have different configuration depending on application (Kujala & Klanac 2005). Different configurations of the core can be seen in Figure 2.3.

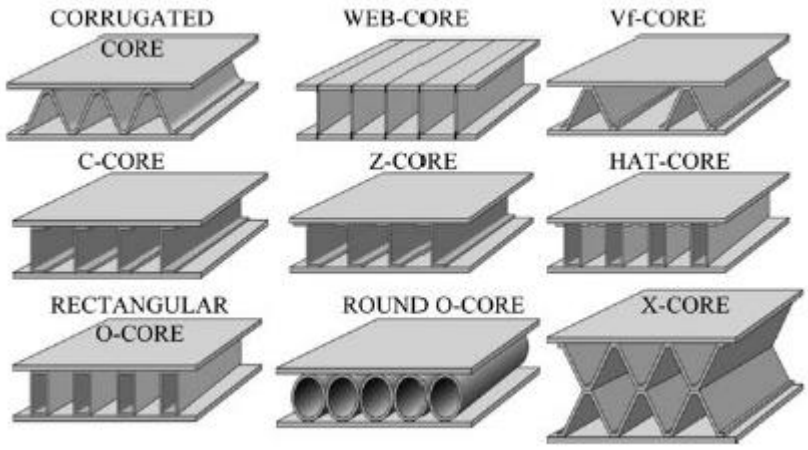

Figure 2.3 Different core configurations (Romanoff & Varsta 2007).

A SSP can have different benefits, depending on the core configuration, additional to the main advantages as a light structure and high transverse stiffness. For example the z- and hat-core are easier to produce, while the corrugated and I-core are more light-weighted. Further, for all configurations there is a possibility to improve the behaviour

of the structure by filling the sandwich panel with polymer or mineral wool etc. (Kujala & Klanac 2005).

2.1.2 Mode of action

The SSP is different to a conventional stiffened deck regarding the ability to distribute the load in two directions. This is due to the improved stiffness in transverse direction. The compression and tensile stresses are acting on the upper and lower face plate, while the core is carrying the shear force acting on the structure.

As already mentioned SSP's consists of both an upper and lower face plate. When the lower plate is added the efficiency of the cross-section improves, by influencing the neutral axis to be forced further down to the mid-depth of the cross-section. The effect of the lowered axis results in face panels that are highly stressed and are preferable for the structure. Furthermore, the added panel creates an element that has shown to be less orthotropic, which entails an improved and more efficient load distribution (Bright & Smith 2004).

For the different core configuration additional load effects can appear in the cross-section. For example, for the corrugated core an additional local moment will appear at the location of the connection of core and face panels, see Figure 2.4.

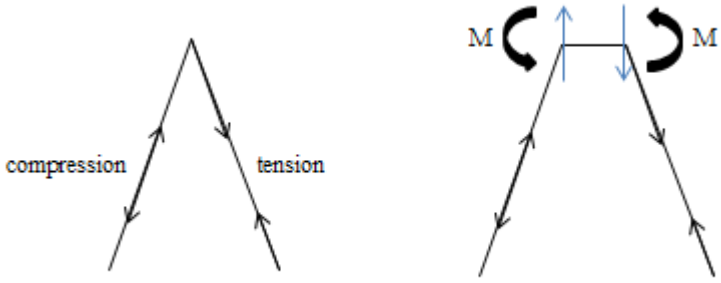

Figure 2.4 The force distribution for a V- and corrugated core (Alwan & Järve 2012).

2.1.3 Advantages of steel sandwich elements

Using the sandwich panel deck several advantages are obtained. Examples of the advantages for sandwich panels compared with traditional stiffened plates are presented below (Kujala & Klanac 2005), (Sandwich.balport n.d.):

- Sandwich panels are light, and have a weight saving potential of almost 50%
- High/good stiffness to weight ratio
- Fire safety
- Noise damping
- 50% space saving
- High pre-fabrication accuracy
- Significantly improves crashworthiness

2.1.4 Application of the steel sandwich panel

The SSP is today used in different industrial areas as the marine and aviator industry. The advantages of the SSP deck have made it attractive for bridge construction. There is no bridge that is built with the SSP deck today because of the need of more research. A limit for the development has for a long time been the welding process. The already mentioned laser welding is not enough to produce SSP decks for bridge constructions. Even if the laser welding produces welds with a large penetration depth it is not enough for bridge construction. The need of thicker face panels due to larger loads limits the application of SSP decks in bridge construction.

Today, a new welding technique has been developed, HLAW, see Section 2.2.3. This technique creates welds with adequate penetration depth and creates the possibility of using the sandwich element in bridges. The newly developed technique offers also an efficient production method with an automated method. In the method, first the core is laser welded to one of the face panels from the inside of the element. The other panel is then placed on top of the corrugated core and welded from the outside, see Figure 2.5.

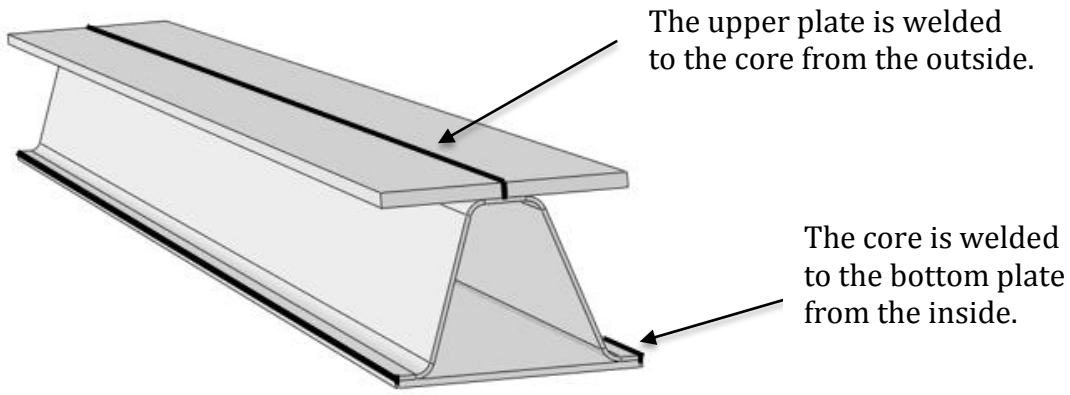

Figure 2.5 Illustration of the production method of the steel sandwich element.

However, there are not many companies that have the right equipment for this laser technique. This is due to high investment cost, and the request for hybrid laser welded structures is today low. Further, the fabrication cost is competitive with conventional steel structures.

2.2 Welding Techniques

There are several welding techniques used in industries today. Hybrid laser welding is a newly developed technique, and it is a combination of the more traditional welding techniques MIG/MAG and laser. In this section the different techniques are described with advantages and disadvantages, and also how the hybrid laser welding technique is created from the traditional techniques.

2.2.1 Gas Metal Arc Welding

The gas metal arc welding (GMAW), also known as MIG or MAG welding, is the most commonly used welding technique today. Gas metal arc welding is a welding process in which an electric arc forms in a "shield" gas between a consumable electrode and the work-piece. The arc itself is an ionized gas column, hot enough with to melt and join the continuously fed metal electrode and the work-piece metal(s), see Figure 2.6. The shielding gas is fed from the welding gun and is used to stabilize the arc and to shield the weld pool from oxidation (Frostevarg 2014).

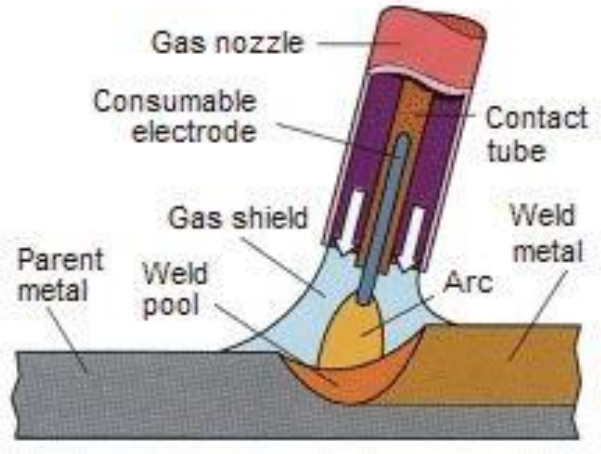

Figure 2.6 Gas metal arc welding (Frostevarg 2014).

The GMAW has several beneficial properties compared to laser welding. The affordable equipment and the easy-to-learn welding technique is possibly the main reasons why the GMAW is the most commonly used welding process. In contrast to laser welding, the GMAW has the ability to bridge joint gaps by adding material, allowing for expanded gap tolerances. Another benefit is that the metallurgical properties can be controlled by adding the desirable filler material.

However, the process has also some limitations, one of them the inability of deep penetration. This is particularly a problem for welding together steel sandwich panels since stake welds are necessary when connecting the core to the outer plats.

It should also be mentioned that the GMAW process is rather sensitive to the amount of heat going into the welding process. If welding with too low heat input it has a potential to result in lack of fusion, nevertheless, too high heat input can easily lead to plate distortion.

2.2.2 Laser beam welding

Laser beam welding is a relatively new welding technology which got its breakthrough as higher power laser sources became available with improved beam quality. The technique opened up for the possibility to construct closed steel sandwich panels, making it feasible to connect the face sheets to the core from the outside.

Laser beam welding can be divided into keyhole and conductive welding. The former being the one used in welding of steel sandwich panels. Keyhole welding is generating a deep narrow weld by using high energy laser to cause evaporation and thus forming

a capillary known as a "keyhole" that extend into the work-piece. The resulting capillary vapor pressure, hydrostatic pressure and the surface tension of the molten metal is maintaining the keyhole open. The process can be seen in Figure 2.7 (Frostevarg 2014).

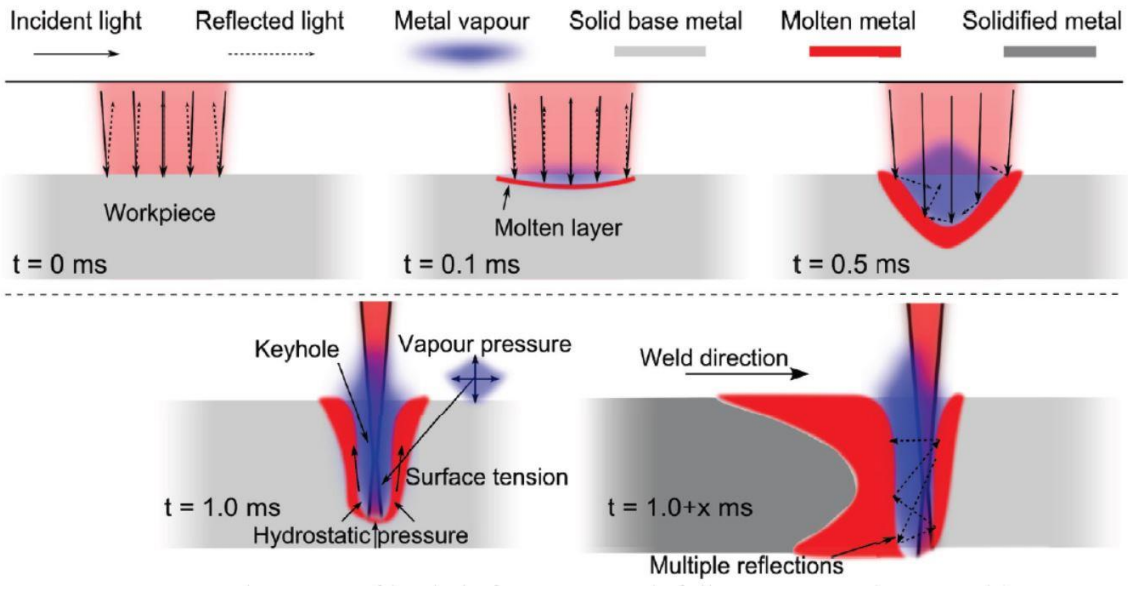

Figure 2.7 The process of keyhole formation (Frostevarg 2014).

The key advantages of laser beam welding compared to traditional welding techniques is connected to its speed and capability of making deep welds. It enables welding of diverse materials and thicknesses and allows flexibility in terms of geometry and use of complex connections (Alam 2012). The high welding speed save both manufacturing time and consequently money, but it also results in less heat input leading to less thermal distortion, and therefore, less residual stresses and a reduced heat affected zone (HAZ). A decrease of the HAZ is desired since it is softer than the base material and decreasing the strength of the welded structure (Frostevarg 2014).

However, occasional metallurgical problems have been noticed due to the fast welding process. The rapid cooling of the fusion zone could in some cases lead to solidification cracks and brittle hardening and therefore the steel chemistry need to be carefully controlled (Alam 2012).

Laser welding does also have some other disadvantages. The investment- and maintenance costs are higher than traditional arc welding and an accurate fit up of the joined parts is more important due to the absence of filler. The lack of filler could cause stress concentrations due to the weld geometry.

In the case of laser welded steel sandwich elements it has been proven that the weld is more sensitive to transverse bending moment than traditional joints, this is due to the cross section of the laser weld being smaller than the thickness of the stiffener (Kozak 2005).

2.2.3 Hybrid laser arc welding

Hybrid laser arc welding (HLAW) combines the conventional gas metal arc welding (GMAW) with laser beam welding into one hybrid process, see Figure 2.8.

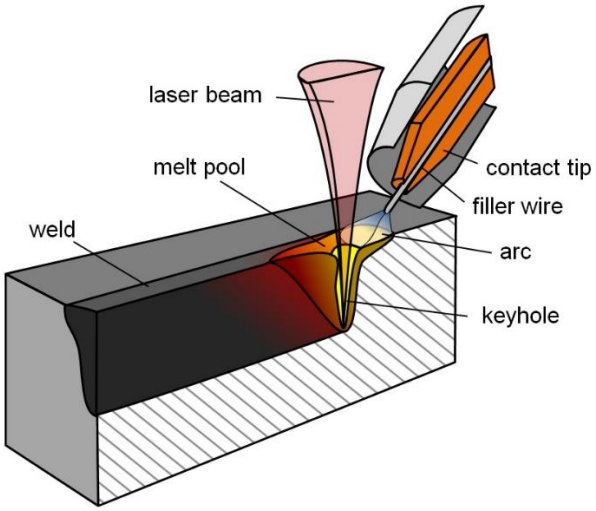

Figure 2.8 Hybrid laser arc welding (Ionix 2015).

These two processes with quite different heat sources can be unified into one, since both work in a gaseous shielding atmosphere, at ambient pressure, is making it possible (Frostevarg 2014).

The HLAW has the potential to combine the best attributes from both laser beam welding and GMAW improving both the productivity and quality. Laser welding offers, at a high speed and precision, deep penetration welds which enable a decreased number of weld passes. The low heat input results in low thermal stresses and distortions and a smaller HAZ zone compared with GMAW. The GMAW help to enhance the weld geometric profile for the HLAW by the use of filler wire to bridge joint gaps, improving the surface conditions and impurities, and improving the control of the weld metallurgy. Together they have the ability to achieving a wide and deep bead, see Figure 2.9. The HLAW is a promising welding technic, which with its advantages has the ability to make the steel sandwich panel applicable in bridge design.

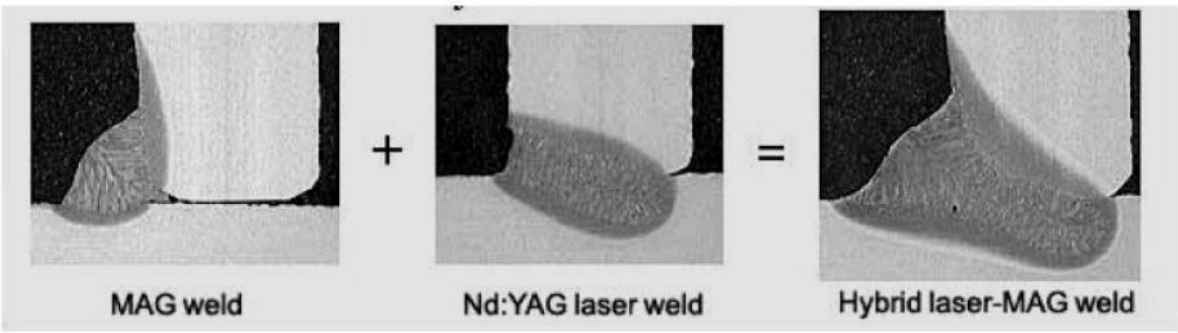

Figure 2.9 Hybrid laser arc weld profile (Alam 2012).

However, the process can be arranged in several ways, with the same or separate operation point, either with the GMAW tailing or at the lead, and the laser beam as the primary or secondary heat source. All these parameters influence the weld quality, for example, the energy ratio of the two heat sources decides if the characteristics of the weld will be more arc-like or laser-like, i.e., the penetration will increase with increased laser energy while the weld width will increase with more arc energy So all parameters are important and need to be carefully balanced and modified to get the optimal result for each case (Ionix 2015).

2.3 Fatigue

The ultimate state for structures can be of different character, and depends on material, load effect and type of structure etc. The elementary failure mode is reached when the load increases and reaches a magnitude over the yield strength of the material, at that time a collapse is to be expected. For steel structures fatigue failure is another example of failure. The load can be well below the yield strength but when a steel structure is exposed of a variable and varying load fatigue failure can occur (Al-Emrani & Åkesson 2013).

As mentioned, the load is often below the yield strength for a fatigue failure. The magnitude of the load is considered to be relatively low and results in failure after several load cycles, usually the amount of load cycles become as large as several millions before the structure fails. Because of the low magnitude of the applied load no distinct deformations will appear and the structure can without any obvious signs fail because of fatigue. Therefore, fatigue failure is considered to be a brittle failure.

Fatigue can be defined as a progressive process that will be localized in special details that are subjected to stresses with large magnitude. The detail has usually also some kind of defect that contributes to larger amount of stress in that area. The meaning of a progressive process is that the process takes time, both to initiate and develop. The damage created by fatigue is permanent and irreversible, and leads to formation of micro cracks. To describe fatigue failure, a bending test of a teaspoon is instructive. By repeatedly bend the teaspoon it will after a while become fragile and therefore easy to break. That type of failure mode is referred to as fatigue failure.

Fatigue failure and cracks can appear in different kind of structures, see Figure 2.10a and 2.10b. So, fatigue is a problem in several different engineering applications, such as construction of bridges, airplanes and ships etc. Fatigue failure might not be as common as other structural failure modes but if it developed it can have devastating structural and economic damage but also fatalities.

Figure 2.10 a) Fatigue crack in a bridge construction (Haghani et al. 2012) b) Fatigue failure in a ship (TWI 2015).

2.3.1 The process of fatigue

In a global aspect steel is an isotropic material with the same properties in all directions. Thus, steel is an alloy and on a micro level the material has a crystalline structure with the possibility of some inhomogeneity created during manufacturing.

To create the strongest bond in the material the melted metal needs to be densely packed. During the process iron and coal are molten, and hardening crystals are formed, also called grains. The grains increases in size until their outer shells are attached to another grain. The interface of different crystal is called grain boundary. The solid material, that is the final product, is formed of several small crystals. Sometimes a dislocation in the crystal is created; these dislocations are very small line defects and create the already mentioned inhomogeneity in the material. The dislocations have their explanation by incomplete creation of the lattice structure, affecting that some ions are missing, see Figure 2.11. These types of defects in the material have a big impact on the structural behaviour and the mechanical properties of the material (MAST n.d.).

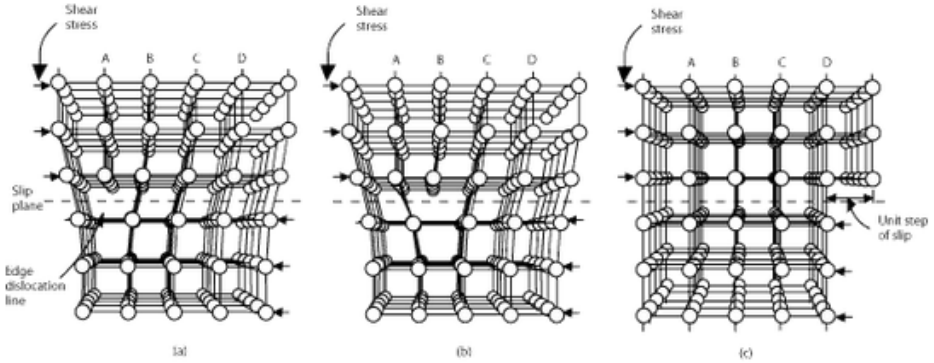

Figure 2.11 Dislocation movement (NDT Resource Center n.d.).

When a steel structure is exposed of loading the existing dislocation moves and creates so called slip bands, see Figure 2.12. The formation of the slip band is a shear stress driven process and will therefore exist in planes of 45° in the direction of the tensile stress. In addition, the slip band is created in planes where the dislocations easily can move. The slip band results in plastic deformation and the deformation are especially obvious at the surface of the material. During repeated loading and unloading new slip

band will be developed and result in extrusions and intrusions at the surface, see Figure 2.12.

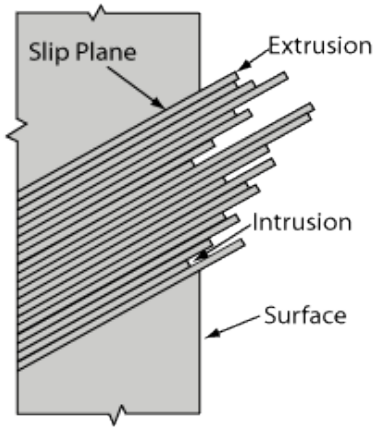

Figure 2.12 Slip band formations with extrusions and intrusions (Classle 2009).

As mentioned the slip band results in local irreversible plastic deformations which are the start of fatigue damage. The slip band will progressively result in formation of small micro cracks. This first phase is called the initiation phase of the fatigue life of a structure. The initiation phase depends on the characteristics of the surface of the structural detail as well as the metallurgical characteristics of the steel. Moreover, the mechanical properties of the structural detail also contribute to the initiation phase. Eventually, a dominant crack will develop when several micro cracks are coalescing to one crack. The crack propagation then changes from 45° in the direction of the tensile stress to become perpendicular to the direction of the maximum principal stress. This is called the crack propagation phase and depends on the material's crystal planes. Furthermore, the crack will propagate in a zigzag path.

The crack initiation and crack propagation represents the fatigue life of a structure. The fatigue life is represented by a number of load cycles that a structure can resist until failure. The fatigue life is expressed according to the equation below:

$$N_t = N_i + N_p \tag{2.1}$$

Where: N_t: fatigue life
N_i: crack initiation time
N_p: crack propagation time

The crack initiation time indicated how many load cycles that are needed to develop one crack, i.e. formation of slip band that depends on the movement of dislocations. Finally, extrusion and intrusions are formed and eventually one dominate crack. The crack propagation time is equal to fatigue failure of the structure. Crack propagation time is the number of load cycles that forces crack growth to its critical length that result in failure. The ratio of initiation and propagation time in the total fatigue life is different for different structures. For example, for a plain machined specimen the initiation phase can be 90% of the total fatigue life while the initiation phase can be 10% in a specimen with a notch.

The fatigue life is affected by several aspects. Three main areas can be identified; load-related factors, factors related to the structure and effects form the environment. The first category involves type of loading, load levels and number of load repetitions etc. while type of detail and properties of both material and geometry belong to the second category. The factor with largest impact on the fatigue life is the load level, i.e. the stress range. In a detail with high stress concentration fatigue cracks can be expected. The geometry of the detail can create a stress concentration and has therefore also a great impact on the development of fatigue cracks. If a detail has a change in the geometry a geometrical stress concentration is created. The change, for example a hole disturbs the stress flow and results therefore in a concentration of stress which can have a magnitude several times larger than the mean stress. Furthermore, welded details are also creating areas with concentration of stresses. Except from the geometric stress concentration that the weld develops, it also contains residual stresses and local stress raisers. The local stresses are made of different weld defects such as start-stop of the weld and porosity etc. Residual stresses are created during cooling of the welding process. When the weld reaches the surrounding temperature it wants to shrink. Thus, the parent material prevents the movement in the weld and both compressive and tensile stresses arise in the section.

2.3.2 SN-curves: representation of the fatigue life data

SN-curves represent the fatigue life of a specific specimen and are a common way to present this type of test results. The largest impact on the fatigue life is, as already mentioned, the stress range. Therefore, it is important to investigate what stress range and how many load cycles a specimen can resist until failure. The SN-curve also called Wöhler diagram presents fatigue test results in terms of stress range in relation to number of load cycles and are based upon constant amplitude fatigue tests, see Figure 2.13.

To create a Wöhler diagram several tests at different stress ranges, on the same type of specimen, need to be done. Several tests are also required for each stress range to ensure that the results become as accurate as possible. The results are plotted in a log-log graph, with the stress range on the vertical axis and number of cycle on the horizontal axis. The plotted values have a scatter but by doing a statistical analysis a mean value of the plotted values can be decided. The result becomes a line in the diagram which presents the mean fatigue strength of the specimen. Furthermore, to be able to use the curve for design a safety margin needs to be considered, this is accomplished by considering the standard deviation and results in a SN-curve representing the design fatigue strength of the tested detail. Each SN-curve are identified by a FAT value which is the characteristic strength at 2 million cycles.

In the graph, it exists stress ranges that never leads to fatigue failure, the number of load cycles can be infinite large. The magnitude of the stress range is so low that the structure is capable to resist infinite repetitions of loading at that range. This stress range is called fatigue limit. Compare the fatigue limit with the low cycle fatigue, the stress range has a large magnitude and fatigue failure will occur after a relatively low number of load cycles. The part of the graph that is between the fatigue limit and low cycle fatigue can be expressed with the linear relation presented below.

$$\log\left(\frac{N}{N_0}\right) = \log(C) - m * \log(\sigma_r) \quad \rightarrow \quad N_t = N_0 * \left(\frac{C}{\sigma_r}\right)^m \tag{2.2}$$

Where: N_t: the fatigue life
σ_r: the stress range
C, N_0: fatigue strength constants
m: Slope of the SN-curve (material constant)

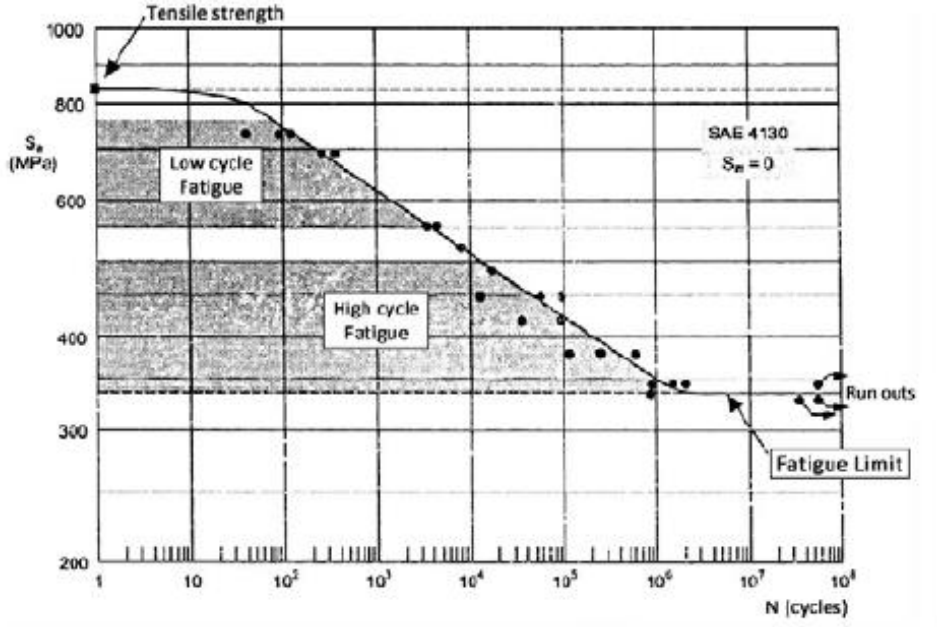

Figure 2.13 *SN-curve* (Al-Emrani & Åkesson 2013).

A slope constant of m=3 is conventionally used for welded details since it have proven to best fit a large numbers of structural details. From the fatigue test data a mean linear regression analysis can alternatively be carried out, calculating an m value assuming a straight line of the SN-curve. This is the natural slope and is calculated according to the equation below.

$$m_{natural} = \frac{n.\sum(logN.log\sigma_r) - \sum logN.\sum log\sigma_r}{(\sum log\sigma_r)^2 - n.\sum(log\sigma_r)^2} \quad (2.3)$$

The history of the stress range for a structure can be of constant or variable amplitude. The constant amplitude cyclic stress is the simplest load case where the load is assumed not to vary during the load history. The variable amplitude stress range is a loading pattern that is more realistic and a better way of describing the load history of many structures, for example bridges and offshore platforms. Further, the variable amplitude loading requires simplification and is transformed to a stress histogram. Stress histogram is created using many separate blocks. Each block represents an approximation of the stress range and the number of cycles of a specific part from the variable amplitude loading diagram.

2.4 Fatigue Assessment

Fatigue failure in superstructures is highly dependent on the structural connections and the geometry details of the weld. Several methods for fatigue life assessments are used in connections with welded structures. However, the two primarily used approaches are the fracture mechanics approach and the SN-curve approach. The fracture mechanics

approach is commonly used in fatigue assessment of a structure with an existing crack and it predicts the fatigue life up to a defined crack length. The crack initiation is negligible in this method and the stress-intensity factor only is used in the calculation of fatigue life. The SN-curve approach evaluating the fatigue life by the use of SN-curves. The curves are, as mentioned, based upon constant amplitude fatigue tests and the result is presented in a diagram as the stress range versus the numbers of cycles to failure, see Section 2.3.2. Three different methods are often used in the SN-curve approach, the nominal stress, the notch stress and the hot spot stress (Caccese et al. 2006).

Additionally, the methods of fatigue assessment are normally divided into global- or local approaches depending on the stress parameters involved. The global approach is based on the external loads or uniformly distributed stresses at the critical cross section. The nominal stress method and structural methods, such as the Hot spot method, are two examples of the global approach. On the other hand, the local approach is based on the stress or strain in the vicinity of the crack initiation location, commonly at the weld toe or -root. The notch stress method and fracture mechanics are both established on characteristics of the weld geometry and are thus local approaches (Heshmati 2012).

When choosing between the different approaches it is necessary to recognize that the accuracy of the method is dependent on the effort and time put in but also the complexity of the construction. Below in Figure 2.14 you can see a comparison of the mentioned approaches with regard to accuracy and work effort.

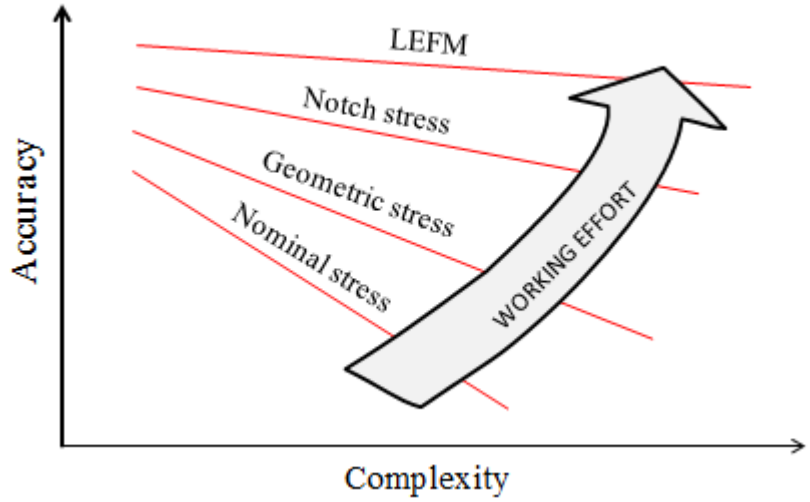

Figure 2.14 Comparison of accuracy and work effort for common used fatigue assessment approaches.

2.4.1 Nominal stress method

The nominal stress method is by far the most common fatigue approach and is included in most of the codes and standards such as IIW recommendations and Eurocode. The nominal stress approach is based on the nominal stress which is defined as the total bending and membrane stress in the structural detail calculated at the expected point of crack initiation, see Figure 2.15. The nominal stress excludes any stress raiser effects and can in simple cases be calculated using elementary theories of structural mechanics

based on linear elastic behavior. However in more complex cases finite element modeling can be used to determine the nominal stress (Al-Emrani & Åkesson 2013).

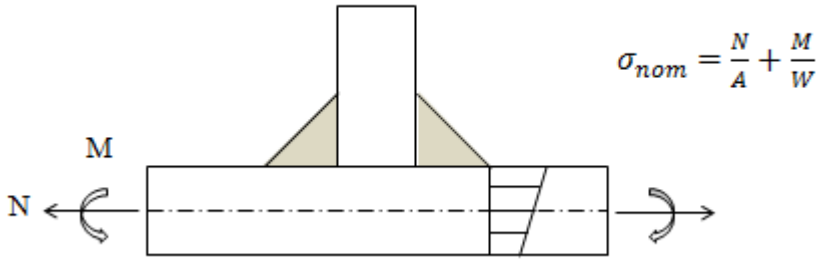

Figure 2.15 Definition of the nominal stress.

The calculated nominal stress is to be compared with the SN-curve of the appropriate detail category to determine the fatigue strength. As the nominal stress SN-curves are derived from laboratory tests thus the effect of geometry, shape and local stress raisers, which is excluded in the calculated nominal stress, are accounted for in the detail classes to a certain degree.

2.4.2 Effective notch stress method

The fatigue strength of weldments is significantly influenced by local stress raisers from geometrical discontinuities such as holes and sharp local changes. The total local stress at such critical points is often referred to as the "notch stress" and is based on the theory of elasticity. The fatigue assessment based on the notch stress is known as the effective notch stress method. Since the effective notch stress method includes the effect of the local weld geometry directly into the stress it is possible to compare different geometrical configurations with each other and accomplish optimizations (Al-Emrani & Aygül 2014).

The effective notch stress method was first introduced by Radaj, who took advantage of stress averaging in the micro-support theory developed by Neuber. The idea was to achieve a stress reduction in a notch as a result of averaging the stress over a defined depth by introducing a fictitious enlargement of the notch radius, see Figure 2.16 (Fricke 2012).

And the following formula for the fictitious radius, was proposed:

$$\rho_f = \rho + s\rho^* \qquad (2.4)$$

Where: ρ: actual notch radius
s: factor for stress multiaxiality and strength criterion
ρ*: substitute micro structural length

In the proposed approach by Radaj for welded joints the actual notch radius is chosen to zero assuming the worst case conditions. The constraint factor, s, is taken as 2.5 for steel members and micro structural length is assumed to 0.4, together increasing the actual radius with 1 mm.

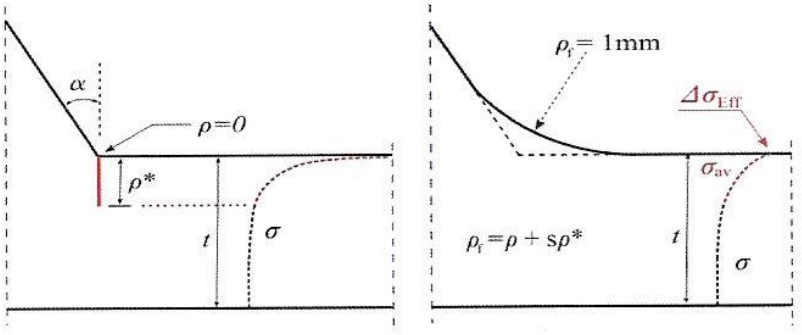

Figure 2.16 *Neuber's micro-support theory in welded joints (Al-Emrani et al. 2014).*

2.4.2.1 Principles of the method

When applying the effective notch stress method in fatigue assessment of welded joints the effective notch stress is generally determined through finite element analysis. In order for the FEM to calculate the accurate total stress at the weld toe or root it is important that a sufficient density of the finite elements is maintained. The effective stress notch method has since 1996 been included in the international institute of welding (IIW) recommendations and the recommended type and size of FE-elements in the notch regions can be seen in Table 2.1 below. The mesh can be obtained both by using 3D solid elements or 2D plane elements as long as the recommended element size is attained (Al-Emrani & Aygül 2014).

Table 2.1 *IIW Recommended element size for FE models using the effective notch stress method* (Al-Emrani & Aygül 2014).

Element type		***Element size***		
		Relative size	***r = 1 mm (t ≥ 5 mm)***	***r = 0.05 mm (t < 5 mm)***
Hexahedral	Quadratic	≤ r/4	0.25 mm	0.012 mm
	Linear	≤ r/6	0.15 mm	0.008 mm
Tetrahedral	Quadratic	≤ r/6	0.15 mm	0.008 mm

The region of the anticipated crack initiations, the weld toe and root, are modeled with the fictitious radius to avoid stress singularities and receiving a functional convergent stress value, see Figure 2.17. The IIW recommending a fictitious radius of 1 mm for plate thickness of 5 mm and above, while plates with thickness less than 5 mm is recommended a fictitious radius of 0.05mm.

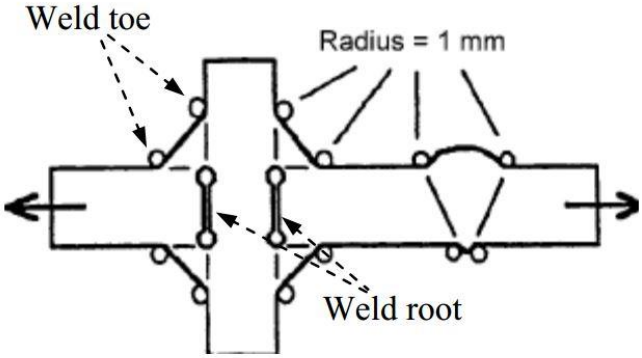

Figure 2.17 Factious rounding of weld toes and roots (Barsoum 2008).

The weld root can according to IIWs recommendations be modeled in two different ways; using U-shape or keyhole, see Figure 2.18. The method used depends if the weld is load carrying or not. IIW recommends U-shape should be used for non-load carrying welds and for load carrying weld both methods can be used.

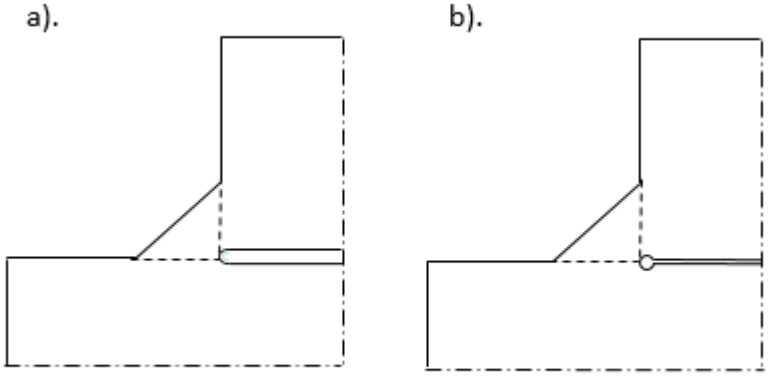

Figure 2.18 Rounding of weld root according to IIW:s recommendation a).U-shape b). Keyhole.

Since the effective notch stress method take into account both the global stress and the effect of the local geometry it is possible for one single SN-curve to represent all structural details irrespective of the loading type and geometry. The IIW recommend that the FAT225 fatigue SN-curve is to be used in design for plates thicker than 5 mm when based on principle stresses, see Figure 2.19. This will result in fatigue failure at the effective notch stress range of 225 MPa after $2*10^6$ number of load cycles. For plates smaller than 5 mm, IIW recommends the FAT630 SN-curve should be used.

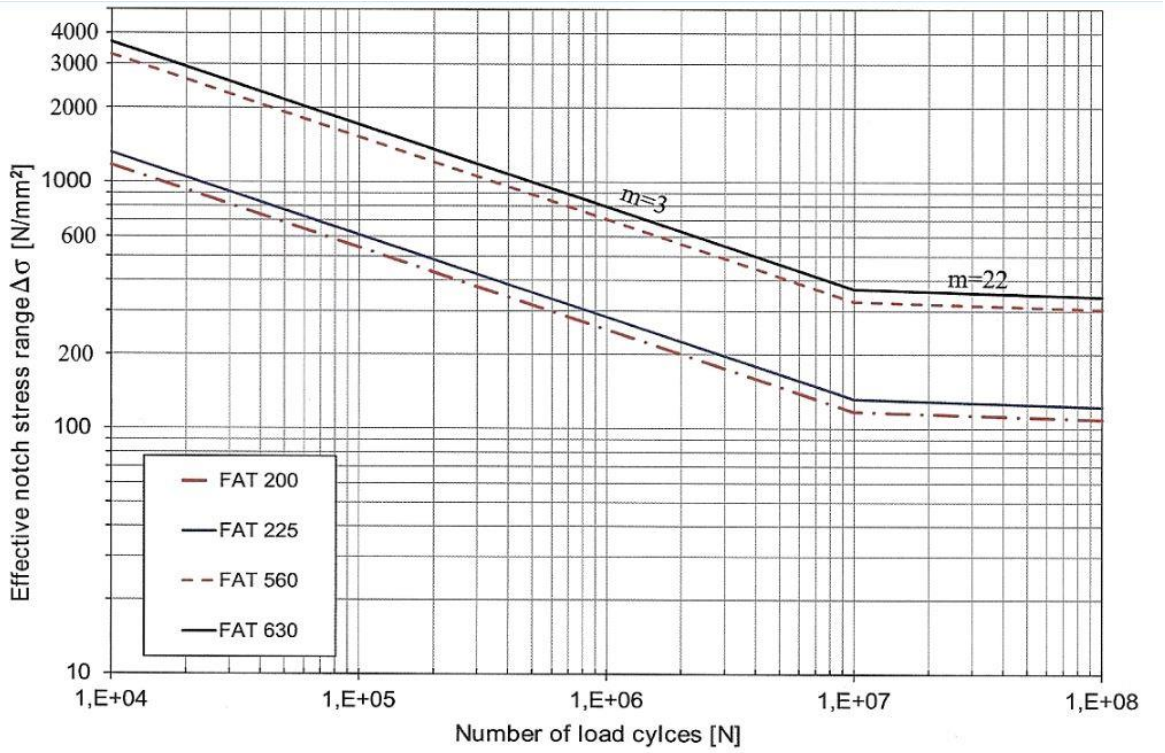

Figure 2.19 Effective notch stress SN-curves recommended by IIW (Al-Emrani & Aygül 2014).

2.5 Parameters affecting fatigue life

In this chapter parameters that have proven to affect the fatigue life will be presented. Among them are the local geometry, weld defects and residual stresses which all impact the fatigue strength and life of the material. Therefore, these parameters will during cyclic loading give rise to a large scatter in the fatigue life.

2.5.1 Residual stresses

Residual stresses in the welded detail can have a great impact on the fatigue life. It can both be beneficial or unfavourable depending on whether it is compressive or tensile stress. Often the tensile residual stresses will be negative since it keeps the crack open, thus, increase the crack growth rate. On the other hand compressive residual stresses will decrease the crack growth rate.

A study was conducted by (Barsoum 2008) examining the weld quality of HLAW and MAG welded non-load-carrying cruciform joints. The HLAW process resulted in lower tensile residual stresses close to the toe region compared to the MAG welding processes.

Residual stresses can not only give rise to earlier fatigue failure but it can also influence the position of the crack initiation point. In a study to investigate the change of fatigue crack initiation points in weld toe and root, (Kainuma & Mori 2008) preformed fatigue tests of ordinary welds in load-carrying cruciform joints. The study showed that low stress ranges resulted in root crack while high stress ranges caused toe failure. (Kainuma & Mori 2008) confirmed that the reason was the compressive residual

stresses found in the weld root while tensile residual stresses were observed in the weld toe.

2.5.2 Weld geometry

The weld geometry is of great interest when working with fatigue design. The geometry has a large impact on the fatigue life of a detail and the idea of finding the optimal weld geometry is of interest. It has also been shown that the weld geometry is strongly influenced by the used welding technique. For example, a laser-welded joint shows smaller dimensions of the weld bead due to the localized heat input and thus resulting in a narrow weld. The fatigue life becomes affected of the smaller bead dimension.

Furthermore, for welded joints a large statistical variation of the weld geometry is to be expected. (Remes & Varsta 2010) conducted a statistical analysis including both statistical variation of the weld geometry for different welding techniques but also comparison between the different techniques. The results can be seen in Figure 2.20 and 2.21, where the dimensions are presented at the probability levels 5%, 50% and 95%. A description of the notations in the figure can be seen in Figure 2.22 and the welding method in the figures are according the following explanation:

- Hybrid LF: CO_2-laser combined MAG welding, laser travels first
- Hybrid MF: CO_2-laser combined MAG welding, MAG travels first
- Laser: CO_2-laser welding without filler material
- SAW: submerged arc welding using two wires

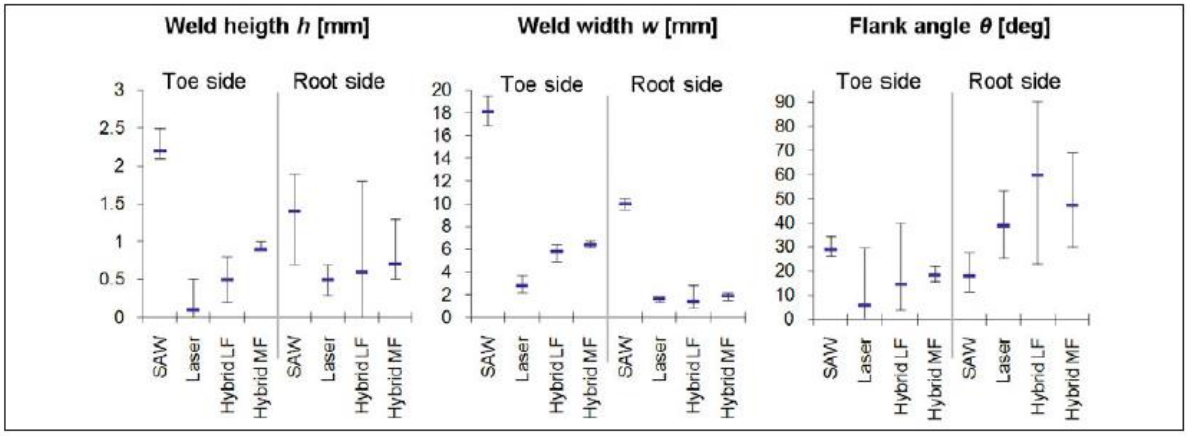

Figure 2.20 Weld bead dimensions at the 5%, 50% and 95% probability levels (Remes & Varsta 2010).

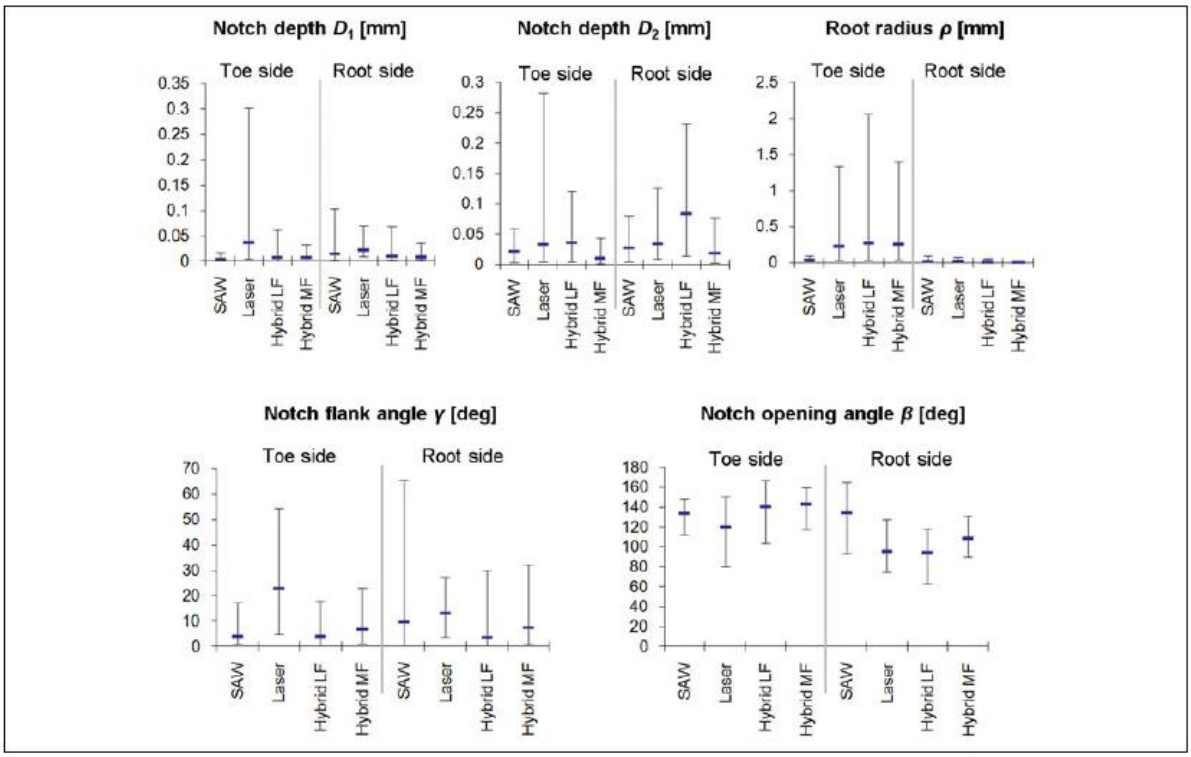

Figure 2.21 *Weld notch dimensions at the 5%, 50% and 95% probability levels* (Remes & Varsta 2010).

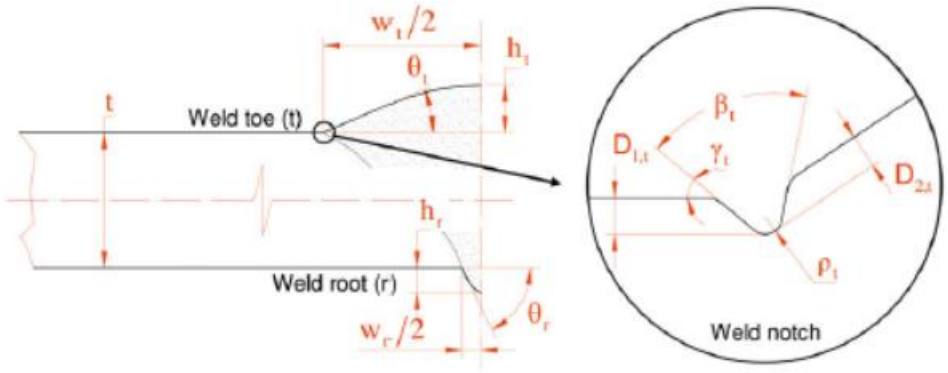

Figure 2.22 *Description of notations in figure 2.20-21.*

It is clear from the summary of the analysis that there are remarkable variations of the bead geometry of the welds. Especially, the root side shows larger variation than the toe side. Comparing laser-based joints with SAW the maximum value of the flank angle on the root side is considerably larger. Overall, the weld bead is smaller for laser-based welds than for arc joints. Furthermore, an investigation of the weld notch dimensions indicated that laser-based welds obtained larger specific values of the root radius on the toe side compared with the root side. The analysis also indicated on smaller values on the notch depth for laser-based welds.

In addition, (Remes & Varsta 2010) conducted a study with the aim of explaining how the notch stress is influenced by the weld geometry. A comparison of hybrid laser welds with arc- and laser-welded joints was presented. Finally, critical geometric parameters

for fatigue life were determined for each welding technique by analysing the stress concentration due to different geometries. Depending on used welding technique different geometrical parameters of the weld were showed to be critical. According to the study the weld height, weld width and notch depth showed the largest impact on the stress concentration for laser-base welded joints and are thus the critical geometrical parameters for these types of welds. While the flank angle showed less impact on the fatigue strength for laser-based joints

Finally, (Remes & Varsta 2010) concluded that the weld geometry has large impact on the fatigue life. Moreover, the stress concentration factor based on the critical and mean geometry showed a large variation, 11%-35%. Therefore, to improve the accuracy of fatigue assessment of laser hybrid welds (Remes & Varsta 2010) recommend that the critical geometry should be applied in the fatigue analysis instead.

Similarly, (Barsoum 2008) studied the effect of the geometry on the stress concentration. Comparing non-loadbearing cruciform welds with hybrid laser welds, MAG flux corde and solid wire. To investigate the stress concentration at the toe radius linear elastic FE models were carried out. By using the surface measuring technique plastic replicas the toe radius of each weld was measured and applied in the FE model. FE analysis was carried out and the stress concentrations for the different specimens were calculated. In Table 2.2, a summary of the stress concentration factor, mean stress respectively the stress deviation, for the different batches are presented.

Table 2.2 Mean value and standard deviation for measured toe radius in (mm) and by FE calculated stress concentration factors K_t (Barsoum 2008).

Batch: mean V./St. dev	**L**	**C**	**E**	**F**
Welding method	Hybrid Nd: Yag-laser/MAG	Tandem arc MAG solid wire	MAG flux cored wire	Tandem wire MAG flux cored
Toe radius (mm)	1,3/0,5	1,8/1,0	1,1/0,2	3,4/0,5
K_t	2,7/0,5	2,7/0,3	2,6/0,6	1,8/0,1

The study indicated that the weld reinforcement, i.e. general profile and size, is less significant than the geometry of the weld toe; especially the radius and toe angle, when analysing the stress concentration. A larger toe angle and a smaller radius tend to increase the stress concentration, see Figure 2.23.

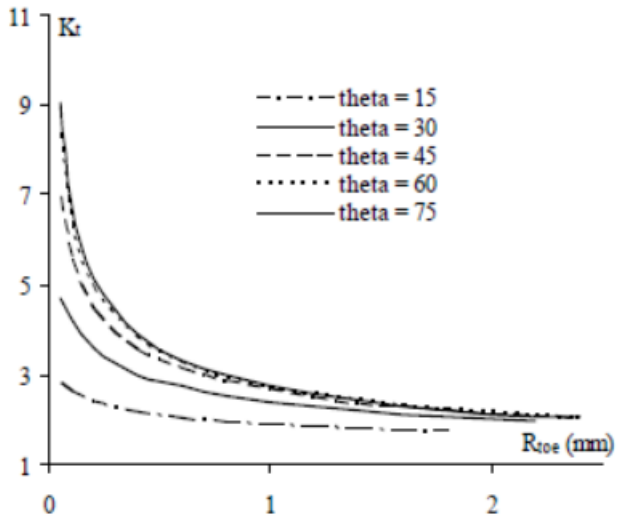

Figure 2.23 *Influence of toe radius, R_{toe}, and angle, theta, on the stress concentration factor, K_t* (Barsoum 2008)

Further, the study showed a plate thickness effect on the stress concentration, i.e. an increased plate thickness increased the stress concentration and thus decreased the fatigue strength of the specimen. In addition, due to distortion of plates after welding can angular misalignment appear and create problem, especially for thinner plates. Under fatigue loading the angular misalignment results in secondary bending stresses and negatively affects the fatigue strength.

Moreover, the geometry does not only have an impact on the fatigue life but can also have influence on the location of the crack initiation point. (Kainuma & Mori 2008) studied the relationship between the weld size and crack initiation point for ordinary welds in cruciform joints. The analysis was conducted on both non-load-carrying and load-carrying joints with a plate thickness of 20 mm and weld size between 9 and 30 mm. The study verified that the weld size influence the position of the fatigue failure. For the load-carrying joint the fatigue failure origin shifted from root to toe at a weld size of 24 mm, see Figure 2.24. Thus, the critical weld size ratio was 1.2. However, the ratio was slightly decreased when the influence of the penetration depth was considered. The non-load-carrying joint showed less dependency on the weld size, only cracking in the toe.

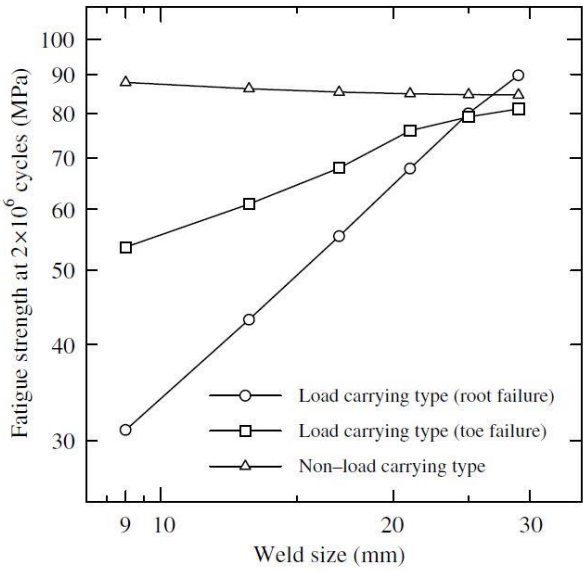

Figure 2.24 Effect of weld size on fatigue strength (Kainuma & Mori 2008).

2.5.3 Weld defects

Geometrical stress concentrations and residual stresses are not the only factors affecting the fatigue life. The weld process also produces several types of weld defects that act as local stress raisers creating possible locations for crack initiation. Common weld defects for hybrid laser arc welds are porosity, concavity, root humpling (root bead instability), incomplete fusion and incomplete penetration (Victor 2011).

The parameter with largest impact on the fatigue life differs. The parameter affecting the fatigue life most depends on type of structure and thus type of weld. Weld defects can have a significant impact on the fatigue strength. The defects can often be considered as crack-like flaws in the weld, and therefore can the initiation phase in the fatigue life be eliminated. So, when studying the fatigue life of such structure can focus be on the crack development in the structure.

2.6 Fatigue tests

As were stated in previous section, the fatigue performance is strongly dependent on the weld geometric profile. The hybrid laser welding process has shown to improve the weld geometry by producing a full penetration weld with reduced irregularities. Therefore, the fatigue life is affected by the welding process making it difficult to compare conventional welds or laser welds with HLAW without fatigue life experiments. Hybrid laser welding being a new technique not much fatigue tests have been performed on such details. However, in the following section completed fatigue tests are presented including discussion and conclusion of the results and methods. Parameters and aspects affecting the results are also discussed. The notations used in the chapter are according figure 2.25.

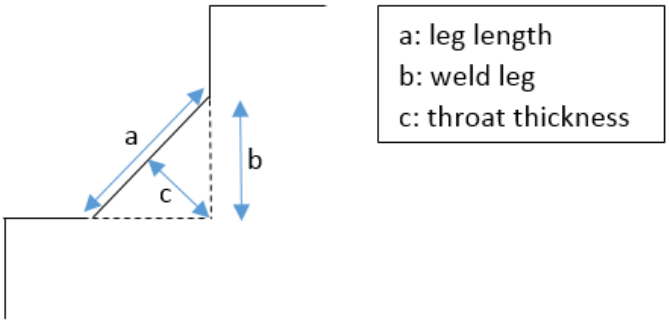

Figure 2.25 Notations for the weld geometry.

2.6.1 Test 1 - Fatigue test performed by (Caccese et al. 2006) on cruciform fillet welds

In a study done by (Caccese et al. 2006) tests were performed to measure the fatigue life of laser- and hybrid laser fabricated welds with different weld geometric profiles. The study was part of an ongoing research to measure the fatigue life of laser welded structures for application in naval vessels.

To investigate the effect of the local geometry the specimens weld profile were varied, measured and categorized. The fatigue testing were performed at the University of Maine using a 50 metric ton MTS 810 universal testing machine with a TestStar digital controller, see Figure 2.26 a). The test specimens used in the study were made of cruciform-shaped HSLA-65 steel plating, all with the same measurements, 355.6 mm long, 95.35 mm wide and with a thickness of 12.7mm, see Figure 2.26 b). The specimens were loaded axially, under completely reversed sinusoidal loading, at constant stress amplitude of 103.3 MPa, 206.8 and 310.3 MPa. The controller ended the test when a doubling of the measured extension recorded in the beginning of the test was achieved.

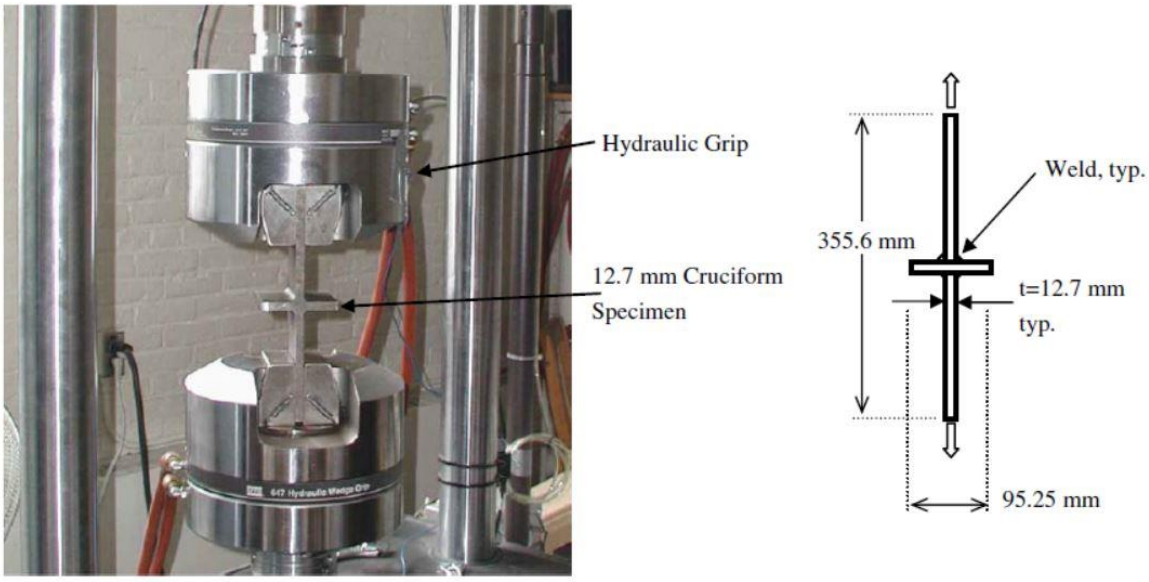

Figure 2.26 Fatigue test a) Specimen set-up in test machine b) Measurements of test specimens (Caccese et al. 2006).

The investigation was divided into four test series; series-A, fabricated using a laser cold-wire (LBW-CW) process at the research laboratory of Penn state University. The geometry was characterized by a small region that was flat in the center and a smooth radius toward the end. Series-B,-C and –D were all fabricated at Applied thermal science in Sanford and both series –B and –C was produced with the LBW-CW process. However, series-C was welded with a reduced process rate resulting in a larger fillet than in series-B. Series-D was produced using a hybrid CO_2 laser/GMAW process which resulted in a near to circular weld, see Figure 2.27.

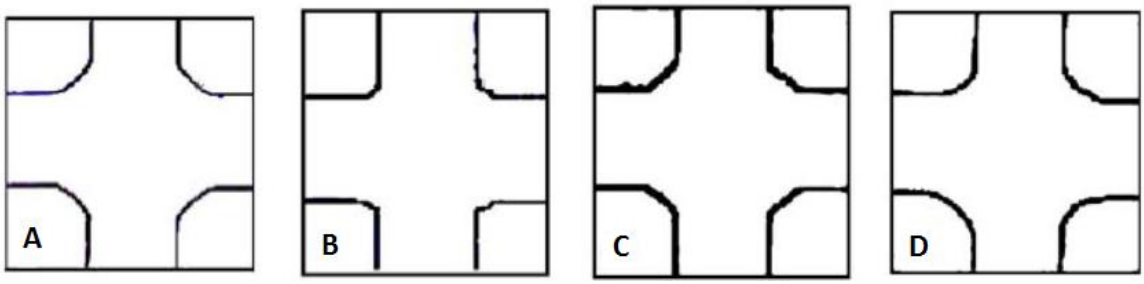

Figure 2.27 Traced weld profile of series A-D (Caccese et al. 2006).

The test results were compared with historical data reported by (Munse et al. 1983) on cruciform joints and tests done by (Kihl 2002) on conventionally welded HSLA-65 steel cruciform and can be seen in Figure 2.28.

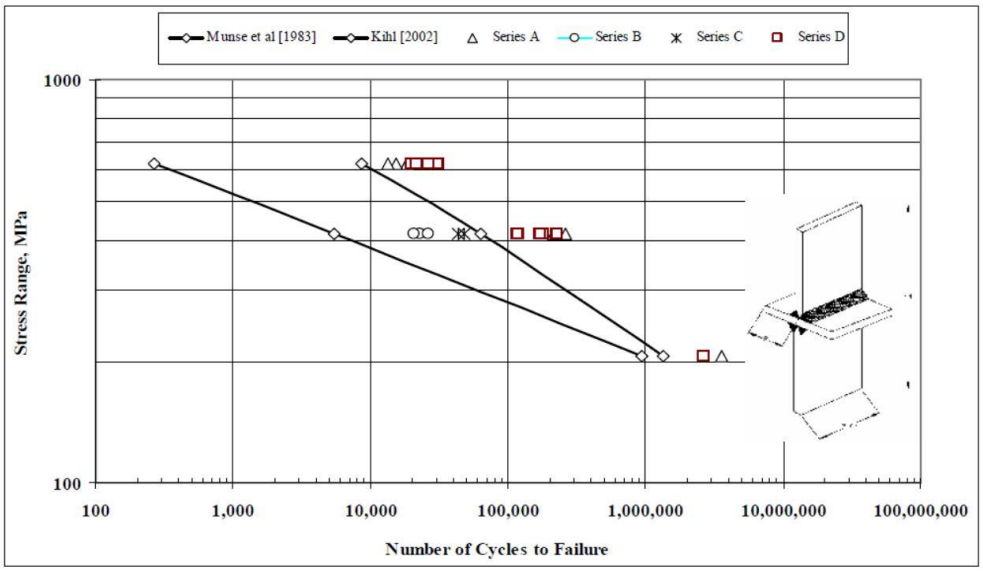

Figure 2.28 SN-curve obtained from the fatigue test study performed on cruciform welded profiles (Caccese et al. 2006).

The result showed that laser welded sections have as good, if not greater, fatigue life as conventional welded sections. If supplemented with the GMAW process, the nearly circular profile reduces the stress concentration to further improve the fatigue life. The exact fatigue test results of the laser-hybrid welded specimens, series-D, can be seen in Table 2.3 below.

Table 2.3 Result from the constant amplitude fatigue test on series-D (Caccese et al. 2006)

Constant-amplitude fatigue tests on laser-hybrid welded specimens, series D- 12.7 mm thick, laser hybrid weld process (L/GMAW)

Specimen ID	Specimen Thickness mm (in)	Stress Amplitude Mpa (ksi)	Specimen Condition[a]	Cycles to Failure	Geometric Mean
CR208-3	12.7 ($\frac{1}{2}$)	103.4 (15)	AF	20,000,000 +	
CR117-2	12.7 ($\frac{1}{2}$)	103.4 (15)	AF	2,658,000	> 12,075,6760
CR201-2	12.7 ($\frac{1}{2}$)	103.4 (15)	AF	20,000,000 +	
CR206-2	12.7 ($\frac{1}{2}$)	103.4 (15)	AF	20,000,000 +	
CR187A	12.7 ($\frac{1}{2}$)	206.8 (30)	AF	179,948	
CR187B	12.7 ($\frac{1}{2}$)	206.8 (30)	AF	228,982	169,853
CR211-2	12.7 ($\frac{1}{2}$)	206.8 (30)	AF	170,600	
CR209-4	12.7 ($\frac{1}{2}$)	206.8 (30)	AF	118,400	
CR210-4	12.7 ($\frac{1}{2}$)	310.03 (45)	AF	30,500	
CR202-2	12.7 ($\frac{1}{2}$)	310.03 (45)	AF	19,700	24,018
CR207-4	12.7 ($\frac{1}{2}$)	310.03 (45)	AF	21,300	
CR212-2	12.7 ($\frac{1}{2}$)	310.03 (45)	AF	26,000	

[a]AF, specimen tested as fabricated.

2.6.2 Test 2 - Fatigue test performed by (Barsoum 2008) of non-load-carrying cruciform fillet welds

In this study conducted by (Barsoum 2008), fatigue life test were performed to compare the fatigue strength of cruciform specimens welded with different welding techniques. The specimen used has a cruciform shape with a non-load carrying weld. Each specimen consisted of two panels with a width and thickness of 12mm. Before welding, the panels were shot blasted to minimize/avoid the risk of crack initiation from cold laps. The welded detail was made with a throat thickness of 6-7 mm and a leg length of 9 mm. Four different welding techniques were used to create the specimens:

- Batch L: Hybrid Nd: Yag-laser/MAG
- Batch C: Tandem arc MAG solid wire
- Batch E: MAG flux cored wire
- Batch F: Tandem wire MAG flux cored

In addition, the hybrid laser-welded specimens were only welded from one side, while the other specimens are welded from both side, i.e. top and bottom, see Figure 2.29.

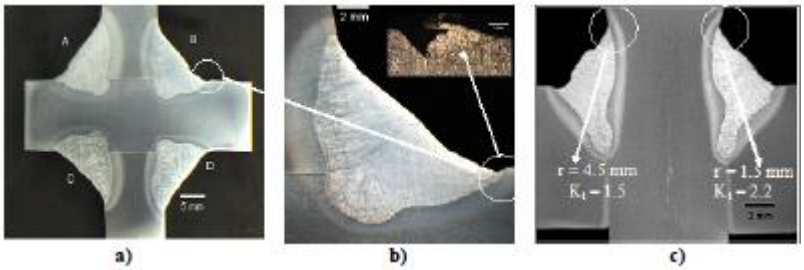

Figure 2.29 *Weld penetration of cruciform joints: a) batch C, E and F b) initial weld flaw – under cut – from specimen in batch E; c) batch L (Barsoum 2008).*

During the fatigue test the specimens were loaded with pulsating tension (R=0), with a constant stress amplitude of ±50 kN. According to the study all failure mode propagated form the toe side. When the propagation of the crack had reached half the thickness of the specimen the test was stopped. The fatigue test results together with the mean SN-curve and the characteristic FAT curves for the specimens produced with hybrid laser welding are presented in Figure 2.30. The fatigue test results were compared with IIW's recommendation of FAT80 as the detail class for a non-load carrying cruciform specimen. Table 2.4 summarizes the test results for batch L.

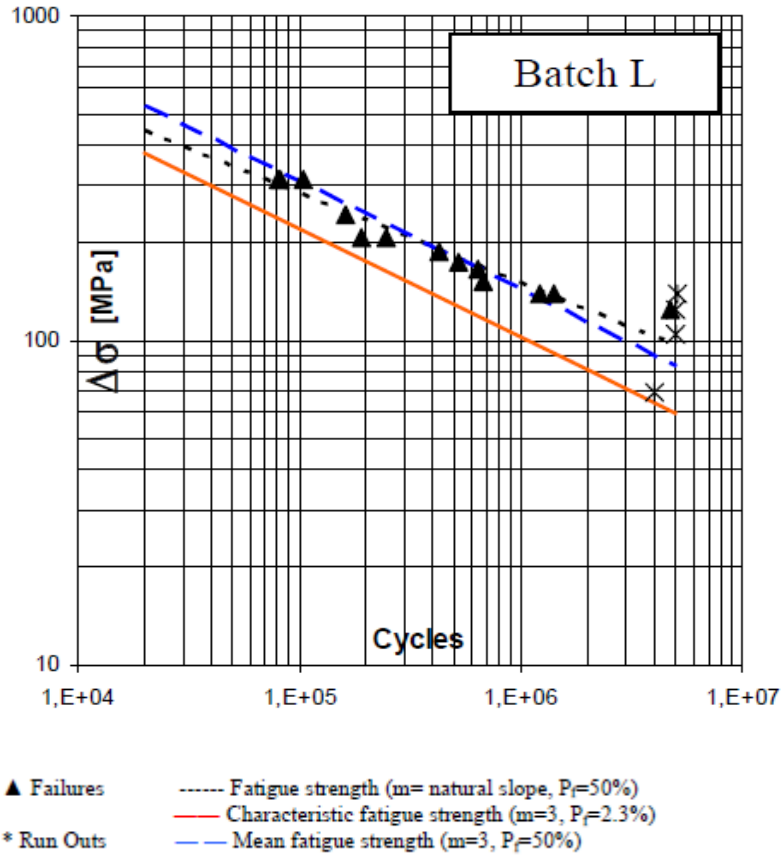

Figure 2.30 *Fatigue test result compiled in SN-curve, together with mean curve (50% failure probability) evaluated with m=, natural mean curve with m evaluated with linear regression and the FAT (2,3% failure probability) curve according to IIW (Barsoum 2008).*

Table 2.4 Summarizing results for batch L.

BATCH	**L: HYBRID ND: YAG-LASER/MAG**
m=natural slope	3.6
Mean value (P=50%, m=3)	113
Characteristic value (P=95%, m=3)	87
FAT according to IIW	80

(Barsoum 2008) concluded that welds made with laser hybrid and MAG flux cored wire technique had a better quality. Additionally, the test results indicated that the specimens made with these welding techniques had a SN-curve with higher slope and increased mean fatigue strength, which indicates better weld quality. The fatigue strength achieved through the fatigue test resulted in a higher value for all specimens when comparing with the recommended value according to IIW.

2.6.3 Test 3 - Fatigue test performed by (Alam et al. 2009) on eccentric fillet welds

The fatigue life tests were performed on 13 specimens with the same geometry and welded under the same conditions. Each specimen consisted of two plates placed with an eccentricity of 5 mm to each other. The base plates used had a dimension of 100x50x10 mm, i.e. a width of 50 mm, thickness of 10 mm and a length of 100mm. The specimens were produced using structural stainless steel SS142333 as base metal for all specimens. The two base plates were welded together with a fillet using hybrid laser welding. The weld was produced with throat thickness 6-7 mm and leg length 4 mm. To reduce the impact of welding defects, such as start and stop defects all specimens were milled on both sides in the longitudinal direction of the weld and thus achieving the final dimensions of 100x25x10 mm, see Figure 2.31. In addition, a small plate was welded to the eccentric base plate to make the specimen to be able to be placed stable in a horizontal position. This was done to create a stable specimen for the experimental fatigue test.

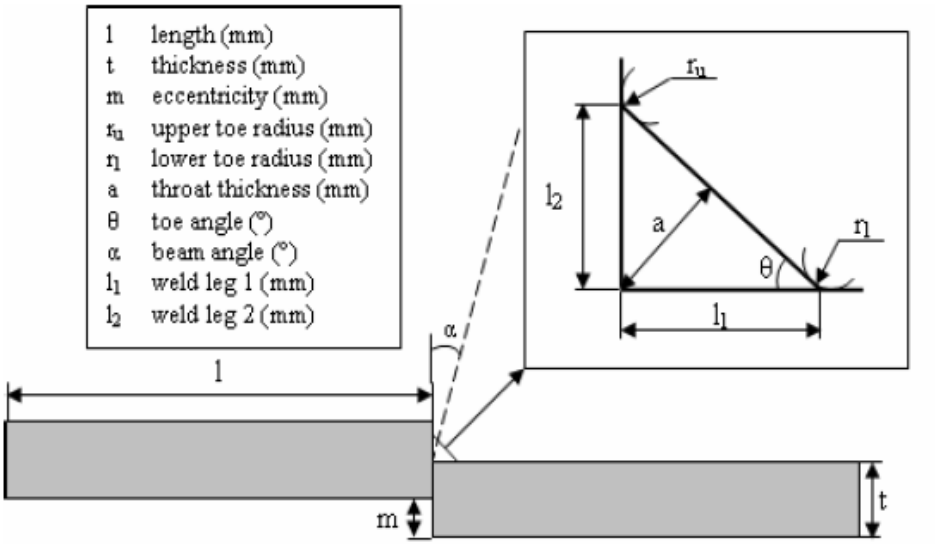

Figure 2.31 *Eccentric fillet joint* (Alam et al. 2009).

The fatigue test was carried out as a four point bending test, see Figure 2.32 a), with a constant amplitude loading in tension (R=0). According to the fatigue test the cracks started in the upper and lower toe. However, the test also indicated on crack development in the weld bead, see Figure 2.32 b).

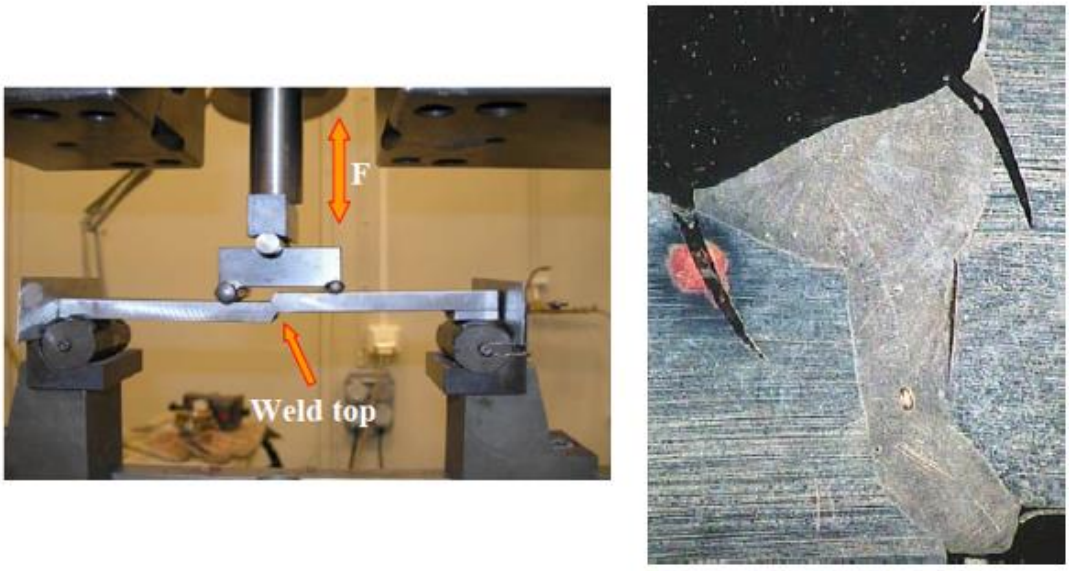

Figure 2.32 *Fatigue test a) Fatigue test arrangement b) Crack pattern in specimen* (Alam et al. 2009).

The fatigue analysis was based on the nominal stress method. The nominal stress was taken at the top surface, 24mm away from the joint edge. The results from the fatigue life test together with the mean SN-curve and characteristic FAT curve are shown in Figure 2.33. The SN-curve represents the fatigue life of hybrid laser welded eccentric fillet joints. Table 2.5 summarizing the results from the fatigue test.

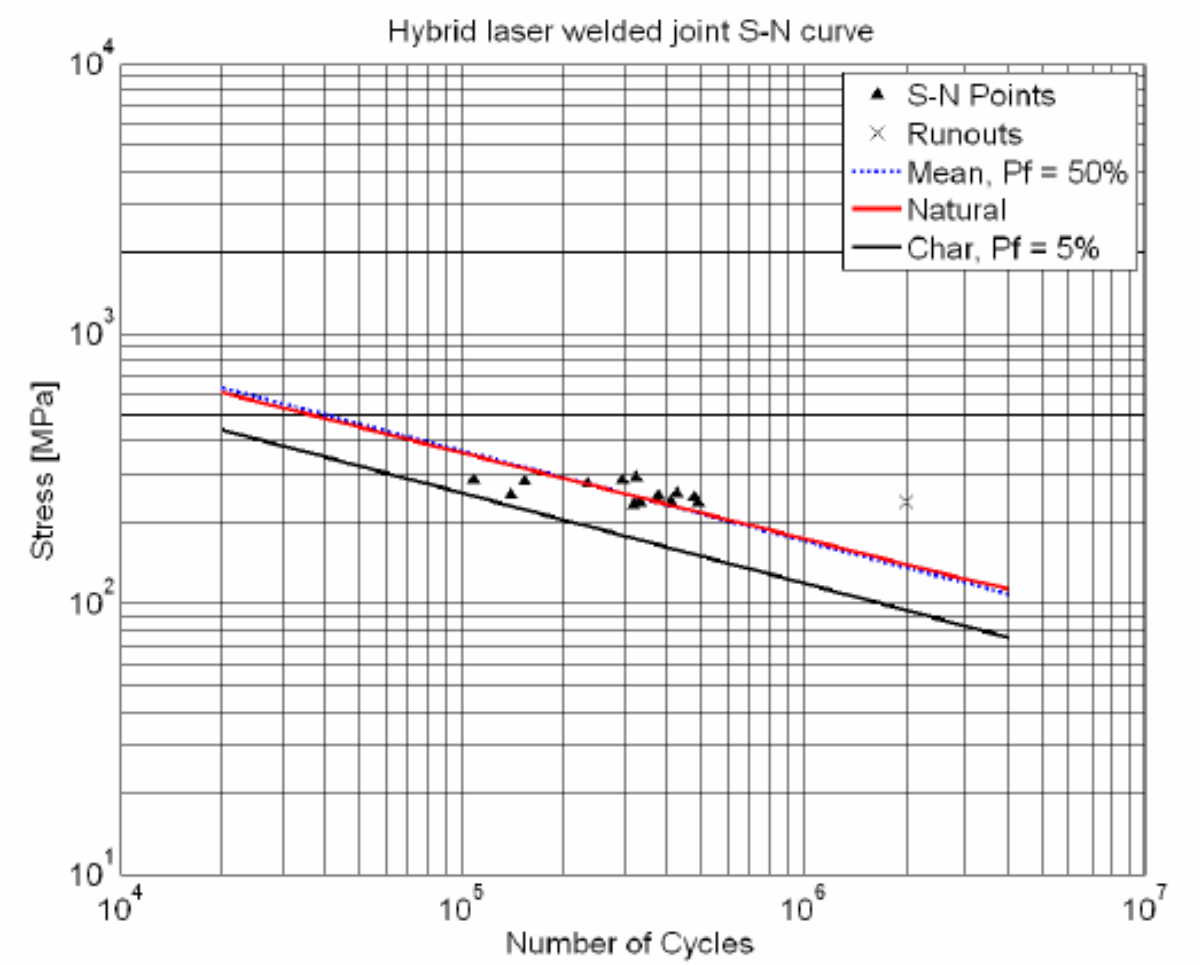

Figure 2.33 *Fatigue test result complied in SN-curves, together with mean curve (50% failure probability) evaluated with m=3, natural mean curve with m evaluated with linear regression and the FAT (5% failure probability) curve according to IIW* (Alam et al. 2009).

Table 2.5 *Summarizing results from the fatigue life test.*

WELDING METHOD	**HYBRID ND: LASER/MIG**
m=natural slope	3.16
Mean value (m=natural slope)	141
Mean value (P=50%, m=3)	137
Characteristic value (P=95%, m=3)	95

2.6.4 Test 4 - Fatigue test performed by (Narimani 2008) on butt welds

(Narimani 2008)investigated in his master thesis the efficiency of using hybrid laser welding. By comparing fatigue test results from specimens made with hybrid laser welding with conventional MAG-welding (Narimani 2008) was able to decide the efficiency of using the hybrid laser process, in addition different fatigue behaviour of the different weld techniques were investigated.

The fatigue test was made on specimens produced with steel sheets DOMEX 700 MC, which is a high strength steel. When using MAG-welding, specimens made with both one and two beads were produced. Two beads creates less deformation and better mechanical properties according to (Narimani 2008) and therefore great advantages are obtained using two beads compared to one. The test specimens were produced with the shape according to Figure 2.34.

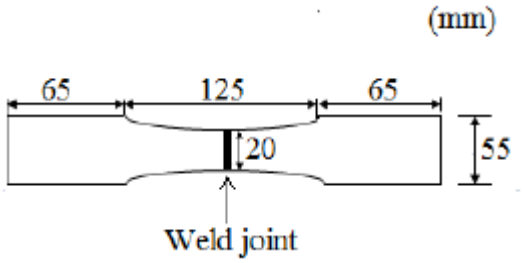

Figure 2.34 Test specimen for transverse fatigue testing (Narimani 2008).

The fatigue tests were performed as pure tensile load tests and 14 specimens for each welding technique were used. The tests were performed on different stress magnitudes to create a SN-curve.

Specimens with both transverse and longitudinal hybrid laser welds were produced for the fatigue study. The tests indicated a lower stress concentration for the longitudinal loaded welds because the applied stress direction are parallel to the weld joint. Therefore, the transverse hybrid laser welds are more critical and the detail of interest. For applied forces and results for the transverse hybrid laser welds see Table 2.6. (Narimani 2008) also presented the fatigue test results as a Wöhler curve, which can be seen in Figure 2.35.

Table 2.6 Results for hybrid laser welds (Narimani 2008).

Specimen	Area	σ_{min}	σ_{max}	σ_r	F_{min}	F_{max}	Cycles	Misalignment angle
Nr	[mm²]	[MPa]	[MPa]	[MPa]	[kN]	[kN]	[Nx10^6]	[°]
1	100,0	0	400	400	0,00	39,79	0,227	0,31
2	99,5	0	200	200	0,00	19,90	13,882	0,22
3	101,7	0	451	451	0,00	23,00	0,141	0,42
4	99,7	0	451	451	0,00	45,00	0,220	0,48
5	99,7	0	451	451	0,00	44,95	0,124	0,26
6	100,3	0	300	300	0,00	30,09	1,087	0,2
7	100,7	0	300	300	0,00	30,21	2,303	0,41
8	99,6	0	350	350	0,00	17,44	0,516	0,38
9	99,6	0	350	350	0,00	17,42	0,308	0,34
10	99,6	0	300	300	0,00	29,88	13,000	0,47
11	99,4	0	350	350	0,00	34,80	0,257	0,23
12	99,6	0	350	350	0,00	34,86	0,230	0,31
13	99,3	0	550	550	0,00	54,60	0,043	0,4
14	99,6	0	550	550	0,00	54,78	0,041	0,22

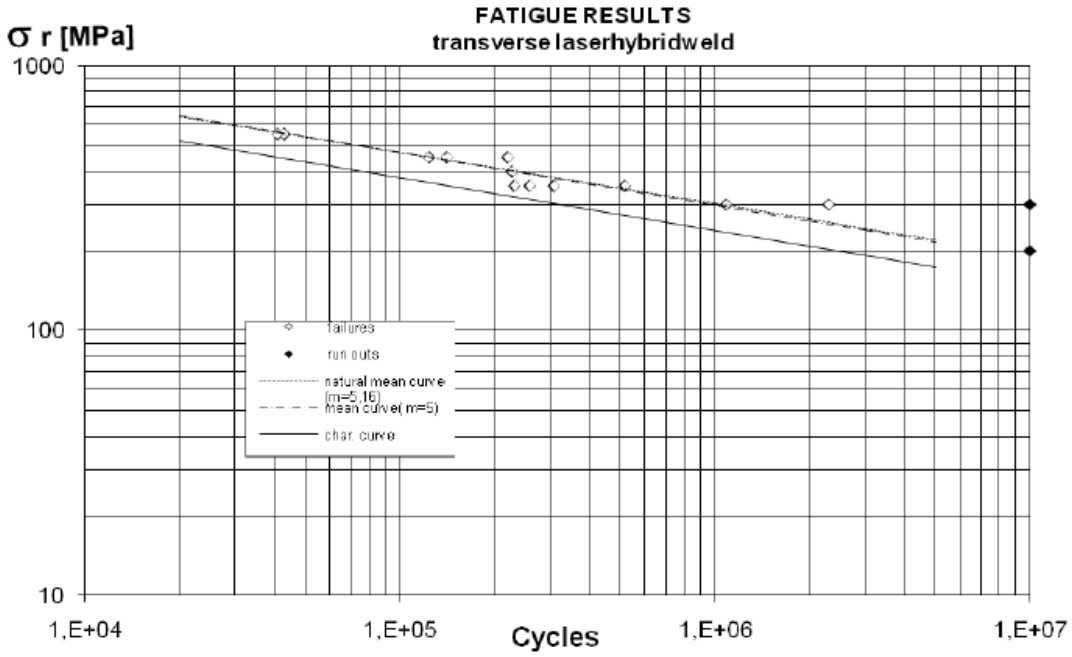

Figure 2.35 SN-curve for transverse hybrid laser weld (Narimani 2008).

The resulting SN-curve for the hybrid laser weld indicated good quality of the welds. The slope of the curve of the mean strength for the tested specimens was equivalent with an unwelded material. Further, using hybrid laser welding for joints using in structures made of high strength steel is beneficial (Narimani 2008). (Narimani 2008) also argues that the crack initiation will occur in the weld root due to higher stress concentration factor combined with tensile stress at the penetration bead. The assumption was confirmed by the fatigue test results which showed crack initiation in the weld root.

PART A

Building of SN-curve

3 Building of SN-curve

One of the main objectives in this master thesis project was to produce a SN-curve representing the fatigue life of hybrid laser welds. In Section 2.6 a thorough study of four fatigue tests on hybrid laser welds was completed. These tests were used as a base for creating the SN-curve. To be able to build one single SN-curve representing hybrid laser welds the effective notch stress method was applied. Each test was modelled using the FE-software Abaqus/CAE to find the effective notch.

The IIWs recommendations for using the effective notch stress method in FE-modelling were applied, see Section 2.4.2. The welds in the tests were thus idealizations, according to IIW recommendations, of the real weld geometries. In Section 2.4.2.1 it was mentioned that finite element analysis is the most appropriate method for fatigue life assessment when determining effective notch stresses. In the following sections the approach in Abaqus for each fatigue test is presented and discussed where general settings made in Abaqus are explained.

However, there are several settings and decision regarding geometry, mesh etc. made in Abaqus that need further explanation and discussion. Regarding the weld root, the recommendations of IIW include two different ways to model the root, either by keyhole or U-shape root. If it is a non-load carrying weld the effective stress will be different depending on method used. Therefore, IIW recommends that the U-shape should be used because the effective notch stress will attain a lower value and therefore result in underestimated fatigue strength.

However, if the joint is load-carrying both methods could be used because the method should result in similar values with a marginal difference (Al-Emrani & Aygül 2014). Therefore, investigation of the impact of the different methods was done for the load carrying specimen. The study indicated a marginal difference of 0.1 % of the resulting effective notch stress for the methods, and therefore it is possible to use both of the methods.

In the mesh settings it is possible to choose either linear or quadratic elements. Quadratic elements are higher order elements created with eight nodes, see Figure 3.1 b). In contrast a linear element, seen in Figure 3.1 a), is created with nodes only in each corner. Since the quadratic elements have several nodes at each side it is possible to receive a non-linear result over each element line. The impact of the two element types were studied and indicated on a small difference in the resulting effective notch stress of only 0.1%. Hence, both the element settings are possible to use.

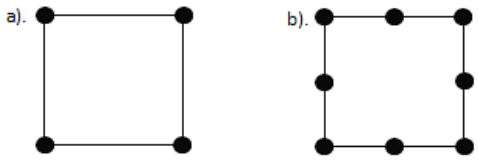

Figure 3.1 Mesh elements a) Linear element b) Quadratic element.

Finally, it was shown that the setting with largest impact on the resulting effective notch stress was the choice of reduced or full integration elements in the mesh module. The full integration integrates over all nodes in the element and will thus result in a more accurate result of the analysis. Whereas, the analysis over a reduced integration element

is carried out over a reduced number of node and can consequently create a difference between the resulting stresses received from the methods. This setting indicated the largest difference with a magnitude of almost 20 %.

3.1 Test 1 - Fatigue test performed by (Caccese et al. 2006) on cruciform fillet welds

In the following chapter the FE-analysis regarding the fatigue test performed by (Caccese et al. 2006) on cruciform specimens are presented. Furthermore, the choices made regarding the setup of the model and the settings in Abaqus are described and explained.

3.1.1 Geometry

The geometry of the cruciform specimen were modelled according to the measurements reported by (Caccese et al. 2006), see Figure 3.2. However, in the study the exact weld leg of the weld were not recorded and the dimensions were therefore determined by measuring the distances. (Caccese et al. 2006) presented a picture of the welded detail and the distances were measured from that figure. Thus, the technique entails uncertainties, which was indicated by the variation of the measured values 5.37-5.86 mm. The mean value 5.6 mm was used as the dimension of the weld leg in the model. The cruciform specimen was symmetrical around the X-axis, for simplicity only half the cruciform was therefore modelled.

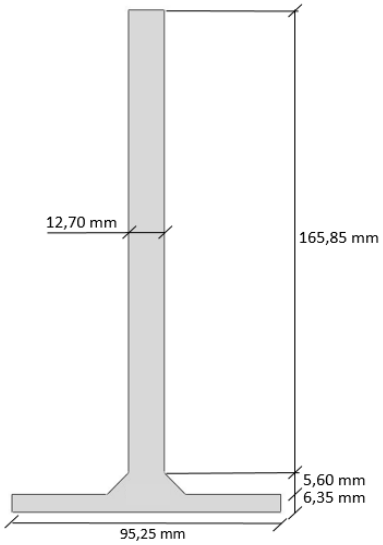

Figure 3.2 The geometry of the specimen.

As mentioned in Section 2.4.2, the finite element model used together with the effective notch stress method should be created with either 3D solid elements or 2D planar elements. In this case, the cruciform test specimen barley experience any stress variations through the depth during loading making it more suitable to use a 2D plane strain element model. This simplification not only reduced the work effort but also minimizing the computational effort for the FE-software.

Since the part was modeled using the type planar, the part was sketched in a two-dimensional sketch plane. The basic feature for the model had to be defined by two properties; shape and type. The shape indicating the basic topology of the feature, and the type the method which is used to generate the base features. In the model the shell

shape was used which is a simplification of the solid shape and has a small thickness in comparison with the width and depth. The part type was specified to deformable to be allowed to deform under load.

An idealized weld profile was created, as recommended by IIW, with a flank angle of 45^{o} for the fillet weld. As stated earlier a fictitious notch radius of 1mm had to be applied for plate thicknesses above 5 mm. Since the HSLA-65 steel plates had a thickness of 12.7mm the fictitious radius of 1 mm were used in the model, see Figure 3.3. The weld root was modelled by a U-shape, see Figure 3.3. However, according to (Al-Emrani & Aygül 2014) both root shapes, U-shape and Keyhole, generates the same effective notch stress for load-bearing welds.

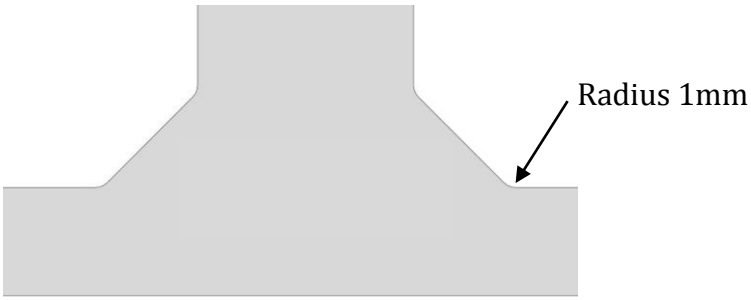

Figure 3.3 Fictitious radius 1mm and U-shape at weld root.

3.1.2 Material properties

Since elastic material behavior can be assumed for fatigue analysis using the effective notch stress, only elastic material properties were needed to define the model. A typical steel material with elastic modulus of E=200GPa and Poisson's ratio of v=0.3 was defined and assigned to the whole cross-section. The base metal and weld had thus the same material properties which was an idealization of the real situation. The idealization was possible because of the small difference in the result that the two different material properties would have generated. A section was defined, containing information about the material properties of the region. In this case a solid homogeneous section was chosen and the section was assigned to the created part.

The presented material properties are applied for all test specimens modeled in Abaqus, thus will the material properties not be further explained for the following specimens.

3.1.3 Load and boundary conditions

To reduce the work effort a pressure load equal to 1Pa was applied on the top edge of the model, see Figure 3.4. As a result, the effective notch stresses for the specimen at each loading level could be obtained by multiplying the analysis result by the actual applied load. This made it possible to only create one model for all loading levels.

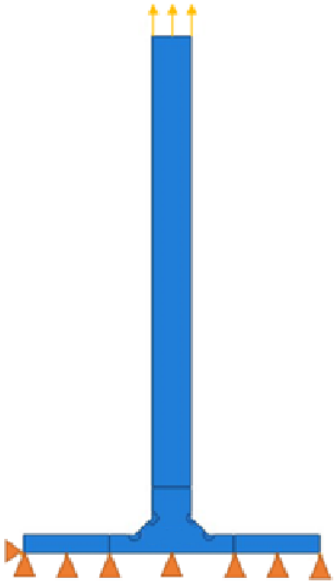

Figure 3.4 Load condition and boundary condition of the specimen.

When choosing the boundary conditions it was important to simulate the real applied boundaries during testing. Since only half the cruciform specimen was modeled the symmetry boarder was the main concern. The boundary conditions were chosen to avoid constrains and therefore a minimum of translation restrains in the x-direction were provided, i.e. the whole symmetry edge were restrained in the y-direction while only one node were restrained in the x-direction, see Figure 3.4.

3.1.4 Partitioning and meshing

The fatigue crack in the cruciform specimen could initiate from either the weld toe or the weld root. As stated earlier, it is important that a sufficient density of FE elements is maintained at these critical regions. However, the mesh size far from the notch does not need to be as fine as at the notch, thus, a courser mesh could be constructed in these areas. Nevertheless, it was essential to keep a smooth transition from the course mesh to the fine mesh.

To attain the required mesh density partitions were constructed and local seeding was used to obtain the element size recommended by IIW and to achieve a gradual transition, see Figure 3.5. Quadratic shaped elements were used for the mesh. Additional, quadratic geometric order was chosen which indicates how the integration scheme is within the elements. According to IIW's recommendation the element size 0.25 mm was selected for the region closest to the notch. The mesh density was increased further in the second partition to 0.75 mm and remaining part of the specimen was applied a mesh with a density of 4 mm. Furthermore, the analysis was not done with reduced integration which means that the integration was done over all nodes in the model.

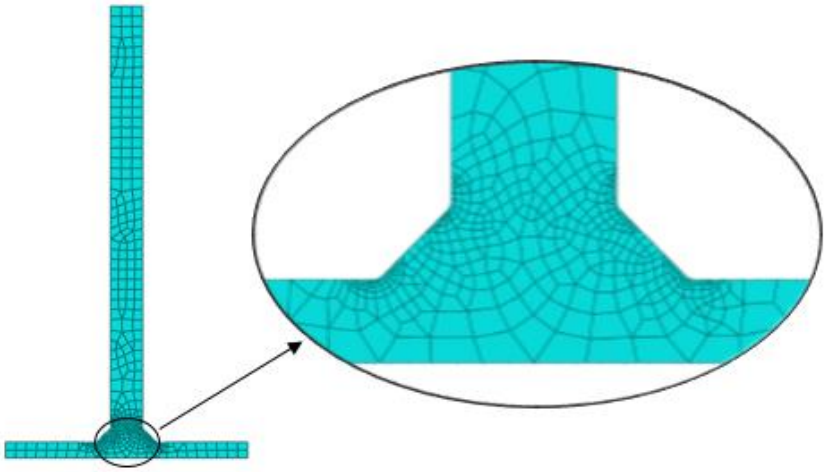

Figure 3.5 Meshed specimen and close up mesh at weld root and toe

3.2 Test 2 - Fatigue test performed by (Barsoum 2008) of non-load-carrying cruciform fillet welds

The second test investigated by FEM-analysis was the non-load bearing cruciform test done by (Barsoum 2008). Similarly, in this chapter the choices regarding the setup of the model and the settings in Abaqus are described and explained.

3.2.1 Geometry

The geometry was modeled according to the dimensions presented in the report (Barsoum 2008), see Figure 3.6. However, the height and the width of the specimen were not reported and had to be assumed. The length of the plate parts was however of less importance since it has no influence on the stress concentration at the notch.

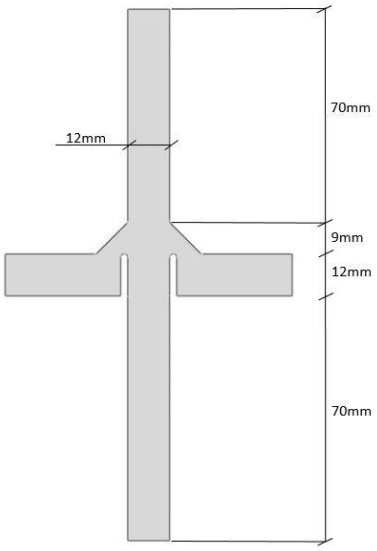

Figure 3.6 Geometry of the specimen.

The weld leg was put to 9mm as stated in the report by (Barsoum 2008) and an idealization of the weld profile according to IIW was created, with a flank angle of 45°

and a fictitious radius of 1mm. When modeling the U-shape it was important not to disturb the stress flow, by not allowing the U-shape to cross the border to the mid plate. To investigate the influence of the root position on the result two versions of the U-shape were modeled, one with an idealized position and one with the root deeper into the plate which representing the actual laser hybrid weld more accurately, see Figure 3.7.

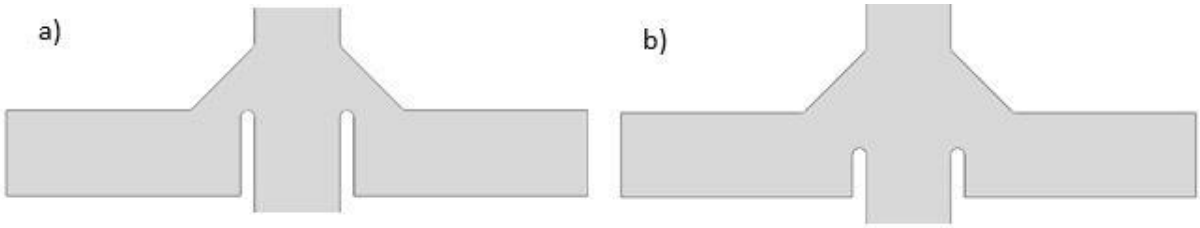

Figure 3.7 Versions of U-shape a) idealized b) representing actual weld.

The idealized U-shape resulted in an approximately 10% lower value of the stress concentration factor at both the toe and root. This was expected given that the longer U-shape gives cause to less stress flow through the region and thus lower stress concentration.

As for the former model the geometry was created with 2D plain strain elements to represent the test situation in a simple and accurate way. The other settings were done in the same way as in Section 3.1.1.

3.2.2 Load and boundary conditions& Partitioning and meshing

To simulate the loading situation a pressure load of 1Pa was applied on the top and bottom edge of the model, see Figure 3.8a. As in previous case, this made it possible to obtain the effective notch stress for each loading level with only one model.

The fatigue crack initiation point in the non-loadbearing cruciform could either start from the weld toe or the weld root, thus, partitioning of these regions were performed. Two partition faces around each toe and root were created. A density of 0.25 mm was put to the region closes to the weld notch as recommended by IIW and was subsequently increased to 0.75 mm and 4 mm for the regions further out, see Figure 3.8b.

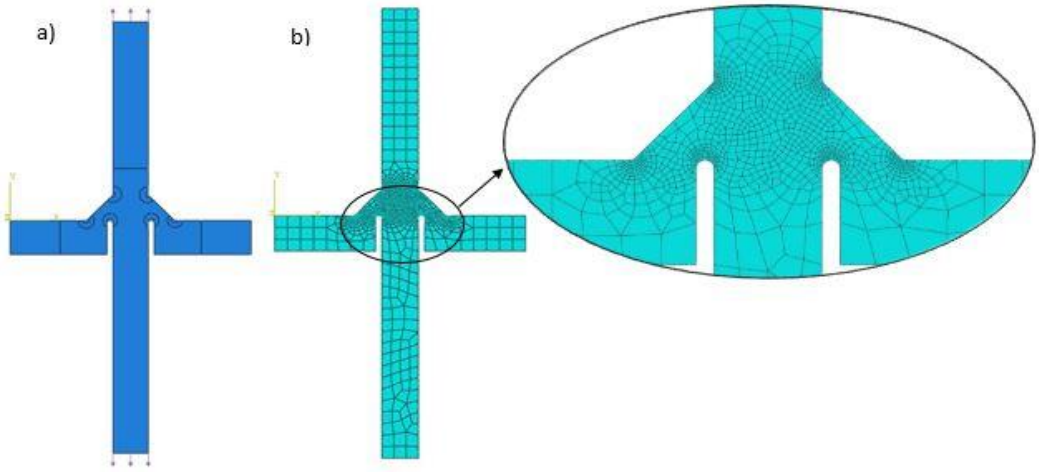

Figure 3.8 a) Applied load b) Meshed specimen.

3.3 Test 3 - Fatigue test performed by (Alam et al. 2009) on eccentric fillet welds

In the following section the FE-analysis of the fatigue test on eccentric fillet welds performed by (Alam et al. 2009) are presented. As in previous sections the choices made concerning the setup of the model and the settings in Abaqus are described and explained.

3.3.1 Geometry

In Abaqus the specimen was modelled with dimensions according to the fatigue test specimen presented by (Alam et al. 2009). The shape of the specimen is presented in Figure 3.9. The dimension of the weld was modelled with a leg length of 4mm. The idealizations of the weld recommended by IIW were applied as before, with a flank angle of 45^{o} for the fillet weld and a notch radius of 1 mm at the root. Because of the loading situation the weld root was not considered as a critical crack initiation detail and the geometry of the weld root was therefore not considered in the modelling of the specimen

Regarding the modelling of the geometry in Abaqus, the geometry and settings for the part was done in similar way presented in Section 3.1.1.

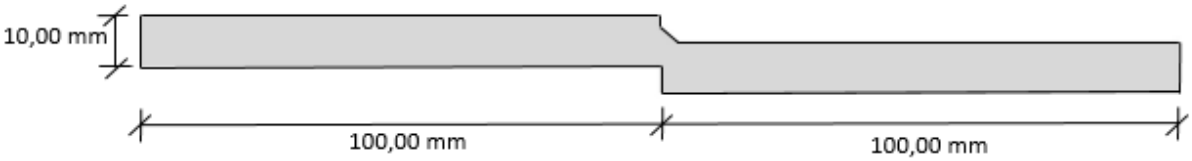

Figure 3.9 The geometry of the specimen used in Abaqus.

3.3.2 Load and boundary conditions

The test was a four point bending test with concentrated compressive forces, see Figure 3.10. The forces were applied 24 mm from the weld connection of the two plates as a concentrated force. The magnitude of the force was set to 0.5 N for each location. The boundary conditions were applied at the edges of the specimen, at the supports. The restraints are applied in single nodes, and the specimen was restrained at both edges in the vertical direction. In addition, the horizontal direction was only restrained at one edge. The restraints enabled translation in the x-direction and deflection due to bending.

Figure 3.10 Applied load and boundary conditions.

3.3.3 Partitioning and meshing

As mentioned in the geometry chapter the weld root were not considered as a critical crack initiation detail. Therefore, a mesh with a fine density was not needed in that region. Thus, the expected crack initiation points of the specimen were the weld toes and the region around them required a finer mesh. The area around the critical weld toe was portioned in two sections with a density of 0.25 mm closest to the weld radius. The mesh density was increased to 0.75 mm and 4 mm for the second section at the weld radius and for the rest of the specimen respectively. See Figure 3.11 for the applied mesh for the whole specimen and Figure 3.12 for the mesh density used in the region closest to the critical weld toe.

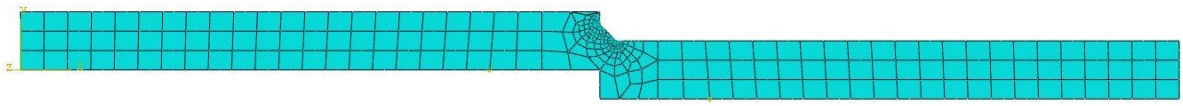

Figure 3.11 The meshed specimen.

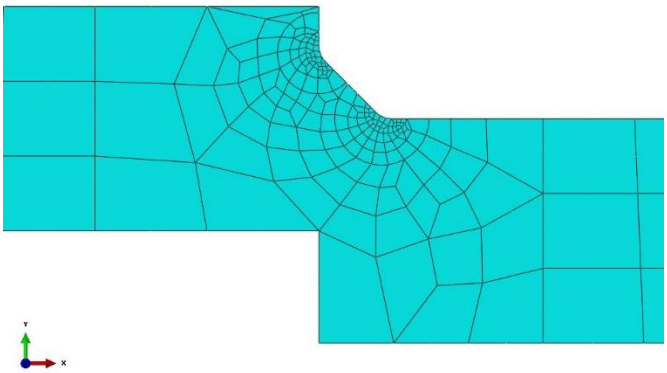

Figure 3.12 Mesh density at welded detail.

3.4 Test 4 - Fatigue test performed by (Narimani 2008) on butt welds

The last test studied by FE-analysis was a fatigue test on butt welds done by (Narimani 2008). In this chapter, as in previous sections, the choices made regarding the setup of the model and the settings in Abaqus are described and explained.

3.4.1 Geometry

The geometries of the specimen were taken from the report by (Narimani 2008) see Figure 2.30 in Chapter 2.6.4. However, the dimensions of the weld were not specified and had to be approximated decided by studying a photo of the produced butt weld, see Figure 3.13. The weld width of the toe side and root side are measured to 25-35mm respectively 9mm.

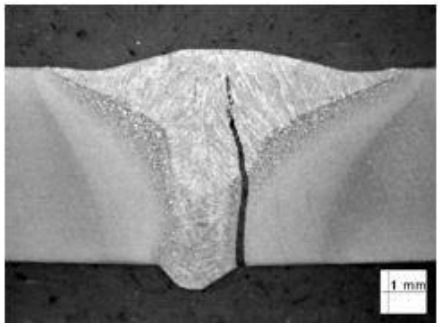

Figure 3.13 Geometry of the fatigue tested laser hybrid weld (Narimani 2008).

To achieve an idealized weld profile, the recommendations from IIW was used for rounding of the weld toe and root with a flank angel of 30 degrees and a notch radius of 1mm.

Further, due to poor documentation of the geometry, primarily in case of the weld size and the unspecified gradual change of the height of the cross section, the impact of these parameters were studied. To investigate the influence of the transition of the geometry near the weld two different shapes were created, see Figure 3.14.

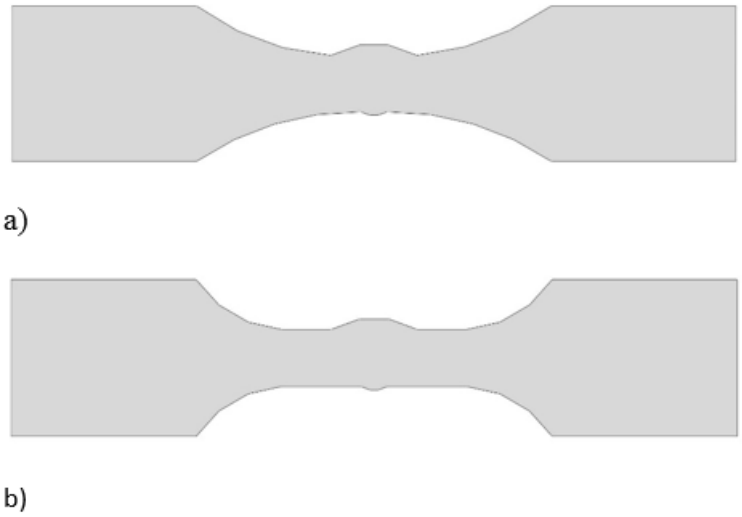

Figure 3.14 Two versions of transition of geometry a) Sharp transition b) Smooth transition.

The case with the sharper transition, seen in Figure 3.14 a), resulted in approximately 9.5% higher values of the notch stress than in the case of the smoother transition, seen in Figure 3.14 b) . The shape of the transition of the geometry also effected the position of the crack initiation, from toe to root. (Narimani 2008) reported that the crack initiated and propagated from the root for all performed tests, thus, the geometry with the smoother transition was more probable to reflect the test specimens of (Narimani 2008) experiments.

The effect of the weld size was studied as well by investigating the change in the notch stress when increasing the width of the bead from 25mm to 35mm. The study showed

a difference of 6.7% between the two weld sizes. Therefore a mean of 30mm width was used for further studies.

Regarding the modelling of the geometry in Abaqus all the settings were done in similar way as presented in Section 3.1.1.

3.4.2 Load, Partitioning & meshing

The loading situation was simulated by applying a pressure load of 1 Pa at the right and left edge of the model, as for the previous fatigue tests. For a butt weld the fatigue crack could either start from the weld root or the weld toe. Therefore, to attain a finer mesh density in those critical regions partition were constructed and local seeding were used to obtain the element size recommended by IIW and to achieve a gradual transition. The loading position and partitioning of the model can be seen in Figure 3.15 a) and the mesh in Figure 3.15 b).

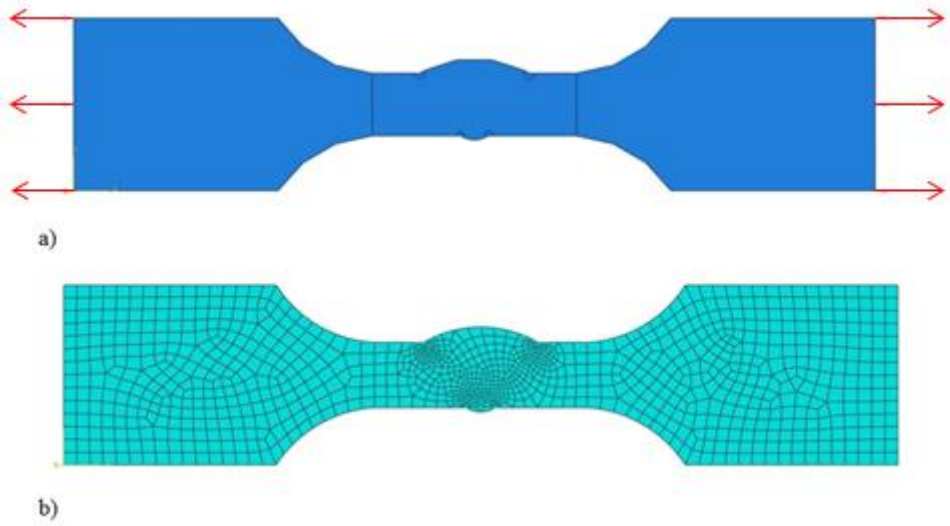

Figure 3.15 a) Load position and partitioning b) Mesh for the specimen.

4 Result PART A

The result for each specimen is presented separately with contour plots and a SN-curve for each specimen. Finally, a merged SN-curve with all results is presented and from this curve is the effective notch stress fatigue strength of hybrid laser welds decided.

4.1 Test 1 – Fatigue test performed by (Caccese et al. 2006) on cruciform fillet weld

The analysis resulted in a stress concentration at the weld root. (Caccese et al. 2006) did not report the failure location for the specimen and the analysis result could thus not be verified. The maximum principal stress were obtained at the left U-shape with a magnitude of 7.072 Pa, see Figure 4.1. (Caccese et al. 2006) reported applied stress range, where the relation between the applied stress range and the effective notch stress is the stress concentration factor. The received stress from Abaqus was considered as the stress concentration factor and was used to obtain the effective notch stress for the applied stress ranges, see Table 4.1. The table also presents the number of cycles to failure for respective notch stress.

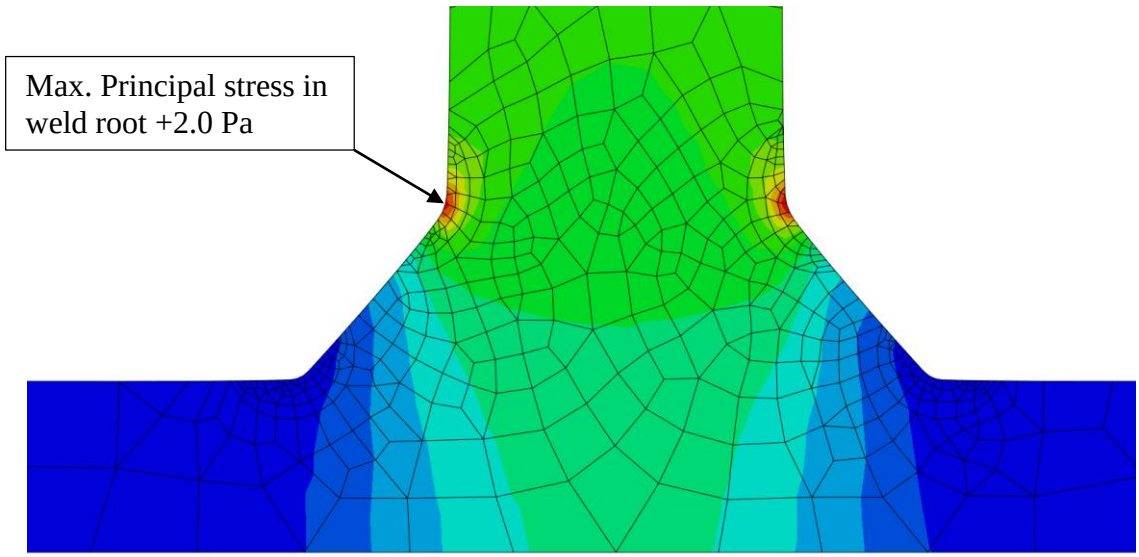

Figure 4.1 The stress variation form FEM analysis.

Table 4.1 Applied stress range, stress concentration factor, effective notch stress and number of cycles.

Applied stress range [MPa]	**Stress concentration factor, K**	**Effective notch stress** [MPa]	**Number of cycles** [N] (geometric mean)
620.6	2.0	1241.2	30 500
620.6	2.0	1241.2	19 700
620.6	2.0	1241.2	21 300
620.6	2.0	1241.2	26 000
413.6	2.0	827.2	179 948
413.6	2.0	827.2	228 982

413.6	2.0	827.2	170 600
413.6	2.0	827.2	118 400
206.8	2.0	413.6	20 000 000 +
206.8	2.0	413.6	2 658 000
206.8	2.0	413.6	20 000 000 +
206.8	2.0	413.6	20 000 000 +

Furthermore, the obtained results were used to build a SN-curve for the tested detail in accordance with the method described in Chapter 2.3.2. The same method was similarly used when building a SN-curve for the three other details. A modified excel sheet created by PhD student Mohsen Heshmati, at the Division of Structural Engineering at Chalmers, was used, see Appendix A. All SN-curves were calculated with a slope m=3 and m=5 excluding the run outs. From the analysis results a mean linear regression analysis was additionally carried out, assuming a straight line of the SN-curve resulting in a natural m value. For exact calculations see Appendix A.

A presentation of the analysis results together with the achieved mean values and the characteristic FAT curves can be seen in Graph 4.1. The FAT curves are calculated on a survival probability level of P=95%. As mentioned in Chapter 2.4.2.1, IWW have recommended that the FAT225 fatigue SN-curve should be used in design for plates thicker than 5mm when the effective notch stress is based on principle stresses. Thus, a comparison between the FAT225 curve and the FAT curves for the cruciform detail is presented in the graph.

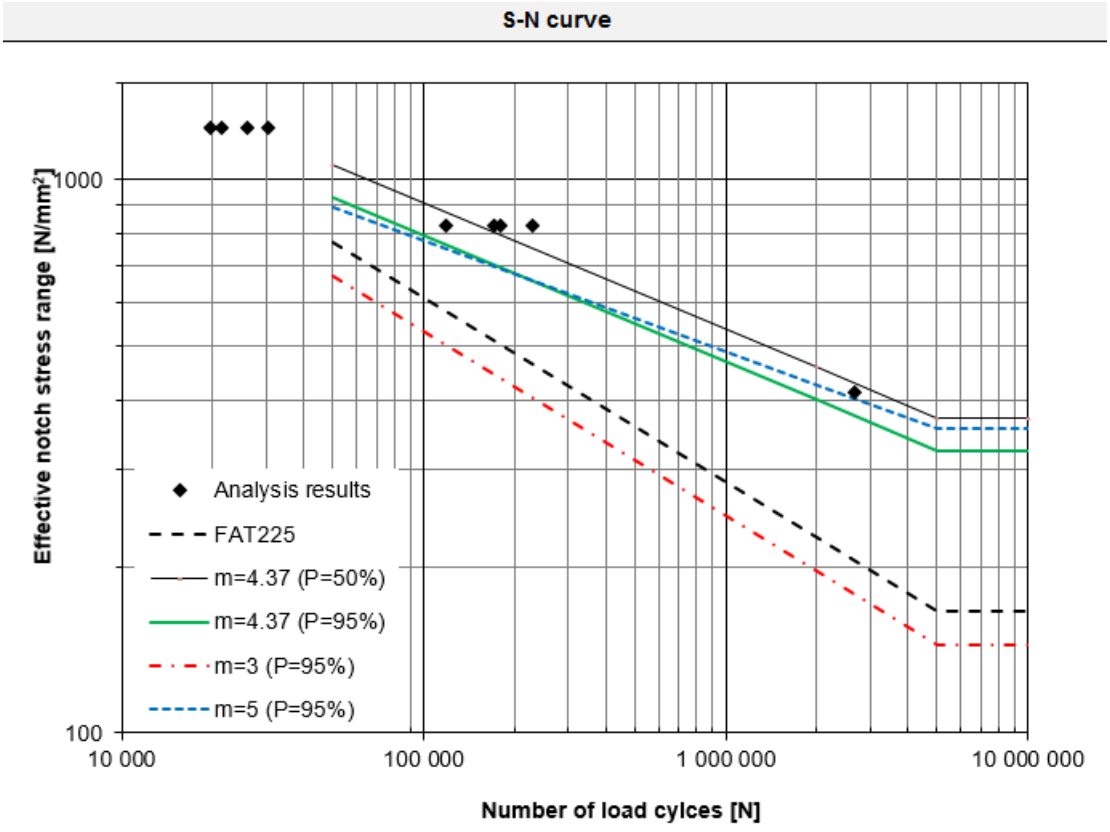

Graph 4.1 SN-curve for the cruciform detail and a comparison with FAT225

With the conventional slope of m=3 the SN-curve for the cruciform detail showed an effective notch stress range of 196 MPa after $2*10^6$ cycles, resulting in a lower detail class than has been recommended by IIW for other weld types.

The linear regression analysis for the analysis results of the cruciform detail resulted in a higher slope m of the SN-curve of 4.37 and a characteristic fatigue strength 400 MPa. A summarized table of the mean and characteristic SN-curves can be seen in Table 4.2.

Table 4.2 Summary of mean and characteristic SN-curve values at $2*10^6$ cycles.

Statistical evaluation of analysis data according to EN 1993-1-9:2005		
SLOPE	**Mean SN-curve (P=50%)**	**Characteristic SN-curve (P=95%)**
m=natural=4.37	458.5	400.2
m=3	334.1	195.9
m=5	500.4	426.4

4.2 Test 2 – Fatigue test performed by (Barsoum 2008) of non-load-carrying cruciform fillet welds

The analysis result for the non-load-carrying cruciform joint indicated fatigue failure in the weld root, with a maximum principle stress of 2.196 Pa. However, the test result reported by (Barsoum 2008) indicates crack initiation in the weld toe at the top. Residual stresses in the weld could be the reason for this, since the root usually experience compressive residual stresses which would counteract the tensile stresses developed from the load, see Section 2.5.1. Thus, the maximum principle stress in the toe region was used when creating the SN-curve, see Figure 4.2. Table 4.3 presents the summarized results from the analysis with included effective notch stress and number of cycles used for the SN-curve.

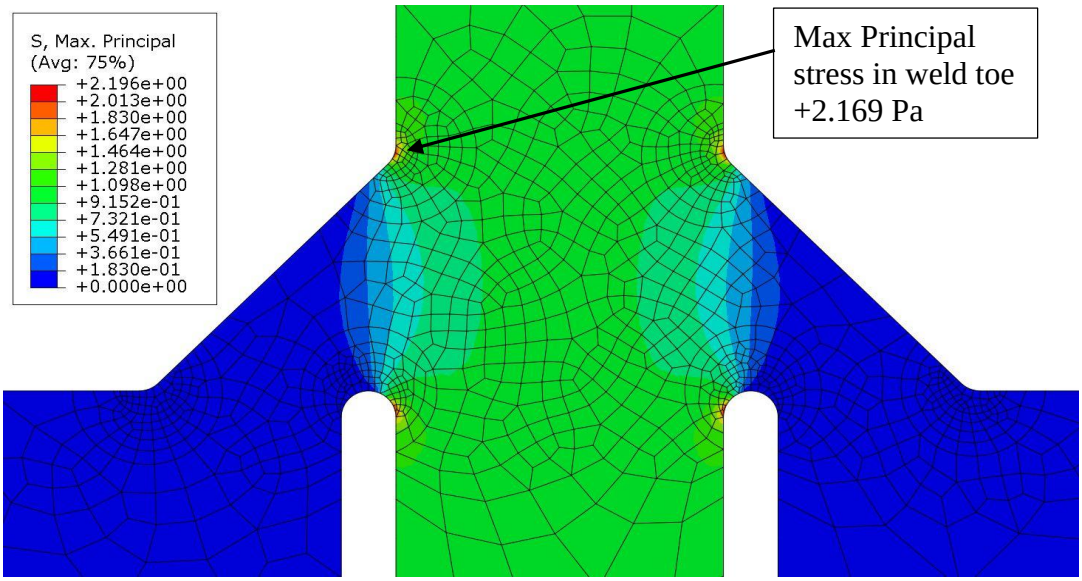

Figure 4.2 The stress variation from FEM-analysis.

Table 4.3 Nominal stress, stress concentration factor, effective notch stress and number of cycles for the analysis.

Nominal stress experiment [MPa]	**Stress concentration factor, K**	**Effective notch stress** [MPa]	**Number of cycles** [N]
302	2.169	655.038	8.1e4
302	2.169	655.038	1.01e5
230	2.169	498.870	1.5e5
201	2.169	435.969	1.9e5
201	2.169	435.969	2.35e5
180	2.169	390.42	4.2e5
160	2.169	347.04	5.2e5
150	2.169	325.35	6.3e5
141	2.169	305.829	6.7e5
128	2.169	277.632	1.2e6
128	2.169	277.632	1.3e6
110	2.169	238.59	4.55e6

Furthermore, the calculated effective notch stresses and number of cycles were used to build a SN-curve for the non-load-carrying cruciform detail that can be seen in Graph 4.2 below. Showed in the graph are both the analysis results, the mean, and the characteristic SN-curves together with the recommended FAT225 curve.

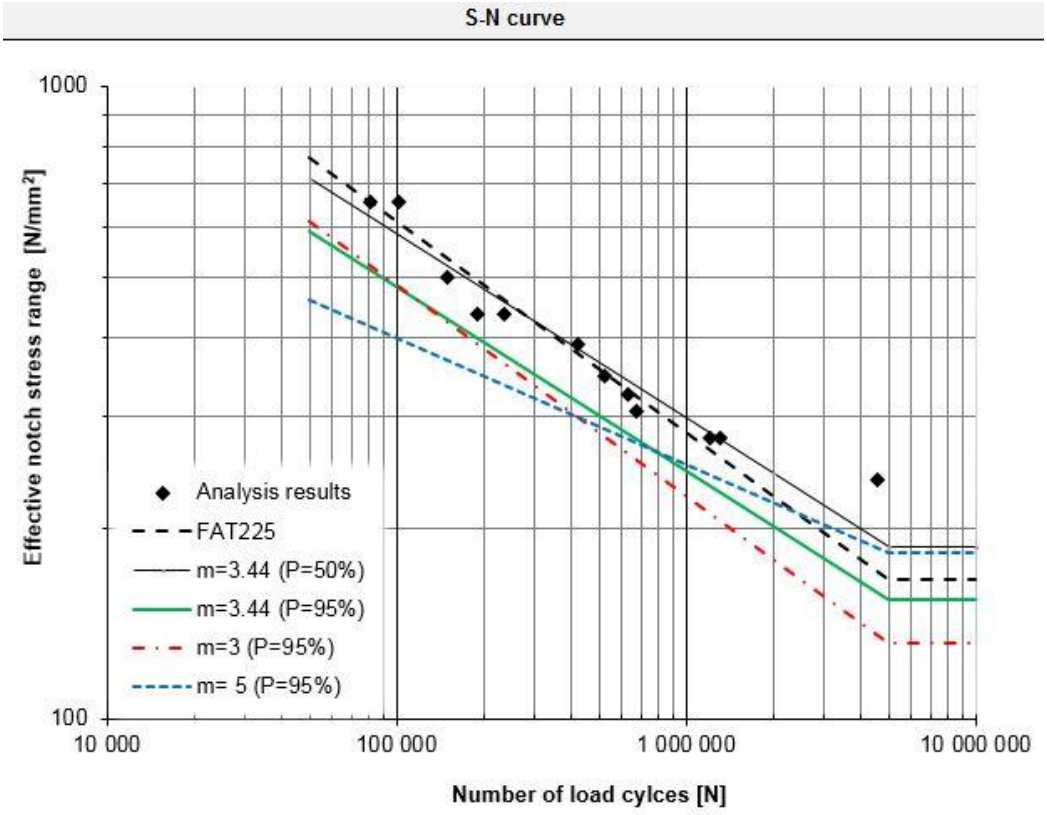

Graph 4.2 Characteristic SN-curve for the non-load-carrying cruciform detail and a comparison with FAT225.

The produced SN-curves indicating on a lower detail class than the one recommended by IIW. Applying the standard slope m=3 the detail class resulted in 178 MPa. However, the natural slope was calculated to a higher value of 3.44. Thus, the characteristic SN-curve increased to 202 MPa, see Table 4.4.

Table 4.4 Summary of mean and characteristic SN-curve values at $2*10^6$ cycles.

Statistical evaluation of analysis data according to EN 1993-1-9:2005		
SLOPE	**Mean SN-curve (P=50%)**	**Characteristic SN-curve (P=95%)**
m=natural=3.44	244,6	201,5
m=3	229	178
m=5	281,4	219,8

4.3 Test 3 – Fatigue test performed by (Alam et al. 2009) on eccentric fillet welds

The FE analysis indicated on failure in the lower weld toe and the result was consistent with reported results by (Alam et al. 2009). The result indicated that the lower weld toe was the most critical location for the specimen. The maximum principal stress received from Abaqus was $1{,}075*10^4$ Pa, see Figure 4.3. (Alam et al. 2009) presented the fatigue analysis based on the nominal stresses approach. The nominal stress were analysed at the top surface 24 mm from the welded joint, at the position of load application. In Abaqus the nominal stress was read at the same location but for a load application of 1 N. The resulting nominal stress from Abaqus was 2289 Pa and was further verified with hand calculations of the nominal stress of the cross section. The stress was calculated to 2280 Pa which indicated on an acceptable tolerance and that the obtained value was correct, see Appendix B.

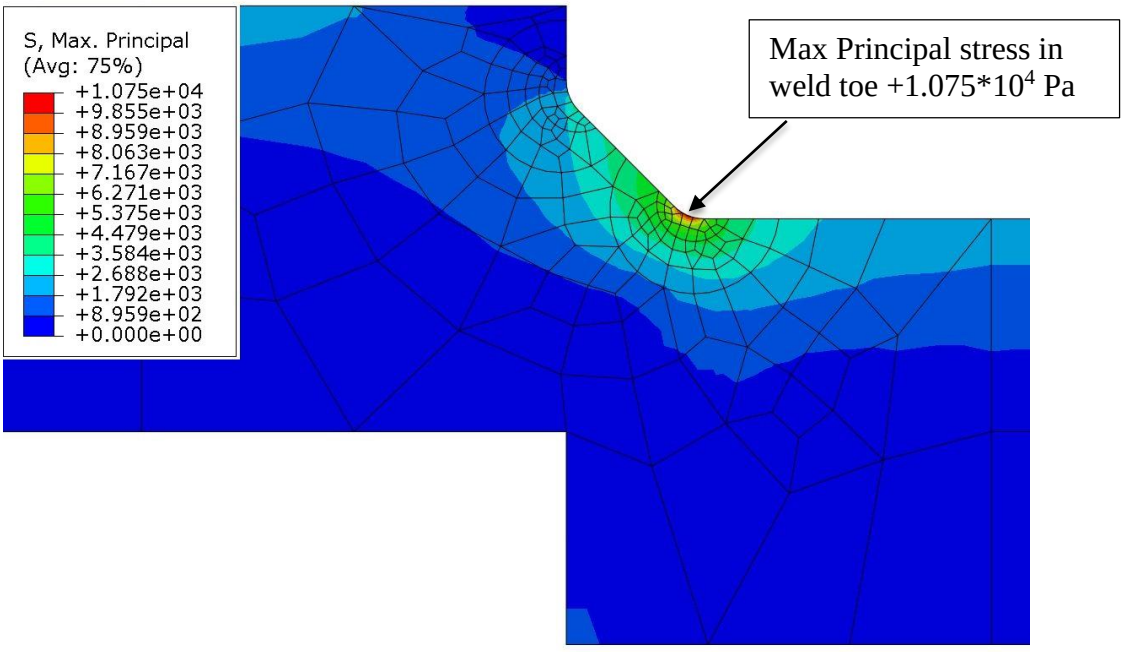

Figure 4.3 The stress variation from FEM analysis.

To transform the nominal stress into notch stress, nominal stresses from the fatigue test and Abaqus were weighted to each other resulting in a correlation factor. By dividing the nominal stress from the fatigue test with the nominal stress from Abaqus the correlation of these values was obtained. The maximum principal stress was then multiplied with the calculated factor to obtain the accurate effective notch stress. The results from the analysis are presented in Table 4.5, where the effective notch stress and number of cycles are the values used when building the SN-curve.

Table 4.5 Nominal stresses, relation factor, maximum principal stress, effective notch stress and number of cycles for the fatigue analysis.

Nominal stress from fatigue test [MPa]	**Nominal stress from Abaqus** [Pa]	**Correlation factor** [MPa]	**Principal stress Abaqus** [Pa]	**Effective notch stress** [MPa]	**Number of cycles** [N]
274	2289	$11.97*10^4$	10740	1286	112000
234	2289	$10.22*10^4$	10740	1098	130000
270	2289	$11.80*10^4$	10740	1267	140000
264	2289	$11.53*10^4$	10740	1239	222000
274	2289	$11.97*10^4$	10740	1286	290000
283	2289	$12.36*10^4$	10740	1328	318000
220	2289	$9.61*10^4$	10740	1032	314000
227	2289	$9.92*10^4$	10740	1065	321000
232	2289	$10.14*10^4$	10740	1089	361000
224	2289	$9.76*10^4$	10740	1051	412000
240	2289	$10.48*10^4$	10740	1126	417000
224	2289	$9.79*10^4$	10740	1051	480000
230	2289	$10.05*10^4$	10740	1079	454000

The analysis results together with the mean and characteristic SN-curves for the eccentric fillet weld is presented in Graph 4.3. A comparison with the FAT225 curve is also presented.

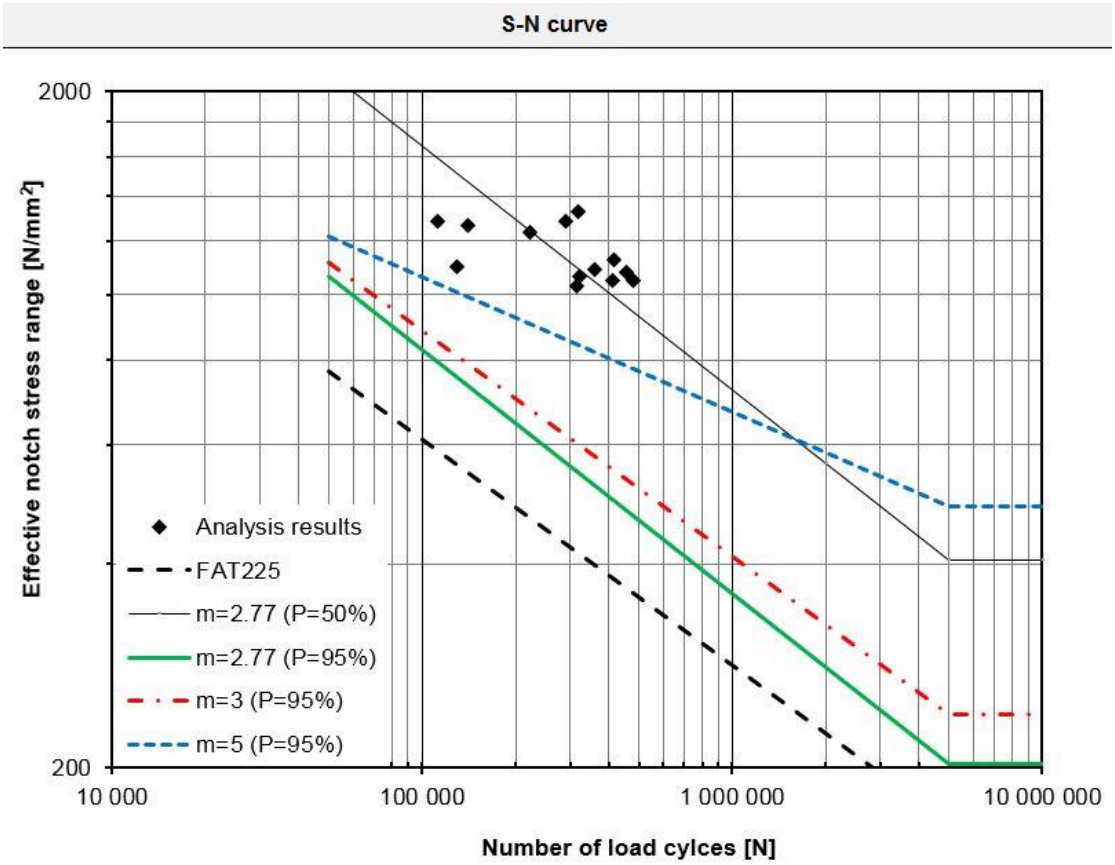

Graph 4.3 SN-curve for the eccentric fillet weld and a comparison with FAT225.

The produced SN-curves, all indicating on a higher detail class than FAT225. The characteristic SN-curve applying a slope of m=3 showed an effective notch stress of 326 MPa at $2*10^6$ cycles. The calculated natural slope of 2.77 was slightly lower than the conventional thus reducing the detail class to 282MPa. Table 4.6 presents the summarized results for the mean and characteristic SN-curves.

Table 4.6 Summarization of mean and characteristic SN-curve values at $2*10^6$ cycles.

Statistical evaluation of analysis data according to EN 1993-1-9:2005		
SLOPE	**Mean SN-curve (P=50%)**	**Characteristic SN-curve (P=95%)**
m=natural=2.77	563.2	281.8
m=3	594.5	326
m=5	773.8	583.9

4.4 Test 4 – Fatigue test performed by (Narimani 2008) on butt welds

The FE-analysis indicated on fatigue failure in the left root of the specimen which was consistent with the result reported by (Narimani 2008). However, as mentioned in Chapter 3.1.4.1 the crack initiation point was largely influenced by the transition of the geometry near the weld, which was assumed. The maximum principle stress extracted from Abaqus at this location was +6.248 Pa, see Figure 4.4.

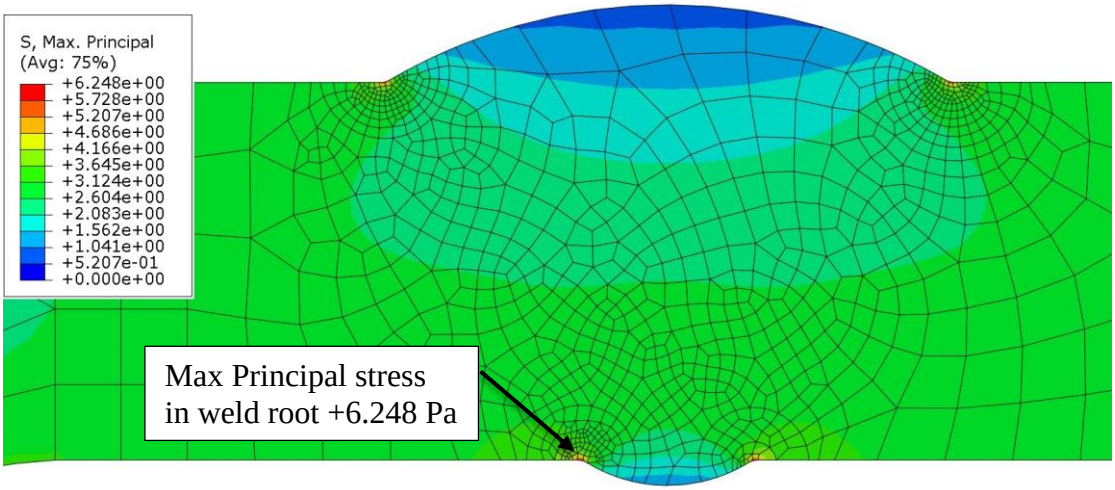

Figure 4.4 The stress variation from FEM analysis.

The fatigue analysis presented by (Narimani 2008) was based on the nominal stress. However, the particular location of the analyzed nominal stress was not evident in the reported documentation. The area for the calculated nominal stress was reported to 100mm^2, indicting an analysis position close to the weld. Therefore, the nominal stress from Abaqus was read at distance of 10.5 mm from the weld, giving the same area but still at enough distance to not be influenced by the concentrated stress close to the weld.

To obtain the effective notch stresses first the nominal stress from the fatigue test and Abaqus were weighted to each other resulting in a correlation factor. The maximum principle stress from Abaqus was then multiplied with the correlation factor resulting in the accurate effective notch stresses. The analysis result is summarized in Table 4.7.

Table 4.7 Nominal stresses, relation factor, maximum principal stress, effective notch stress and number of cycles for the fatigue analysis.

Nominal stress experiment [MPa]	**Mean Nominal stress from Abaqus [Pa]**	**Correlation factor [-]**	**Max principal stress Abaqus [Pa]**	**Effective notch stress [MPa]**	**Number of cycles [N]**
400	2.744	$145.77*10^6$	6.248	911	227 000
200	2.744	$72.89*10^6$	6.248	455	13 882 000
451	2.744	$164.36*10^6$	6.248	1027	141 000
451	2.744	$164.36*10^6$	6.248	1027	220 000
451	2.744	$164.36*10^6$	6.248	1027	124 000

300	2.744	$109.33*10^6$	6.248	683	1 087 000
300	2.744	$109.33*10^6$	6.248	683	2 303 000
350	2.744	$127.55*10^6$	6.248	797	516 000
350	2.744	$127.55*10^6$	6.248	797	308 000
300	2.744	$109.33*10^6$	6.248	683	13 000 000
350	2.744	$127.55*10^6$	6.248	797	257 000
350	2.744	$127.55*10^6$	6.248	797	230 000
550	2.744	$200.44*10^6$	6.248	1252	43 000
550	2.744	$200.44*10^6$	6.248	1252	41 000

Moreover, the obtained analysis result was then used to build a SN-curve for the butt weld. In Graph 4.4 the analysis result are presented together with the mean and characteristic SN-curves. Additionally, a comparison with the recommended FAT225 curve is showed the graph.

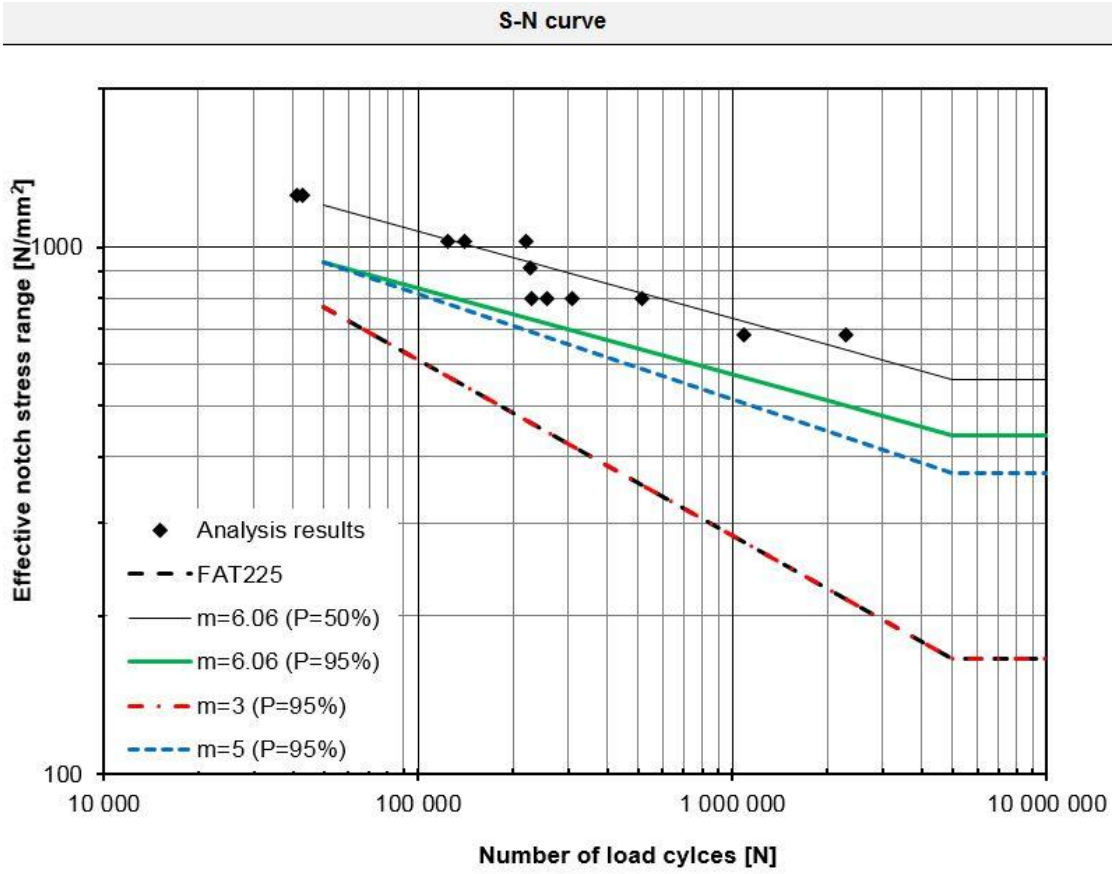

Graph 4.4 Characteristic SN-curve for the butt weld detail and a comparison with FAT225.

The SN-curves for the butt weld demonstrate a higher or equal detail class than FAT225. The SN-curve applying the slope of m=3 end up at a detail class of 225 while the SN-curve applying the natural slope of 6.06 attain a much higher value of 510MPa, see Table 4.8.

*Table 4.8 Summarization of mean and characteristic SN-curve values at 2*10^6 cycles.*

Statistical evaluation of analysis data according to EN 1993-1-9:2005		
Slope	**Mean SN-curve (P=50%)**	**Characteristic SN-curve (P=95%)**
m=natural=6.06	652.6	510.2
m=3	503.1	224.9
m=5	618.3	447.4

4.5 SN-curve representing hybrid laser welds

Since one of the main objectives in the project was to produce a SN-curve representing the fatigue life of hybrid laser arc welds, all received analysis results were finally put together to construct one single SN-curve. For exact calculation see Appendix A. The final characteristic SN-curve for laser hybrid welds together with the mean SN-curve and IIWs recommended FAT225 curve can be seen in Graph 4.5.

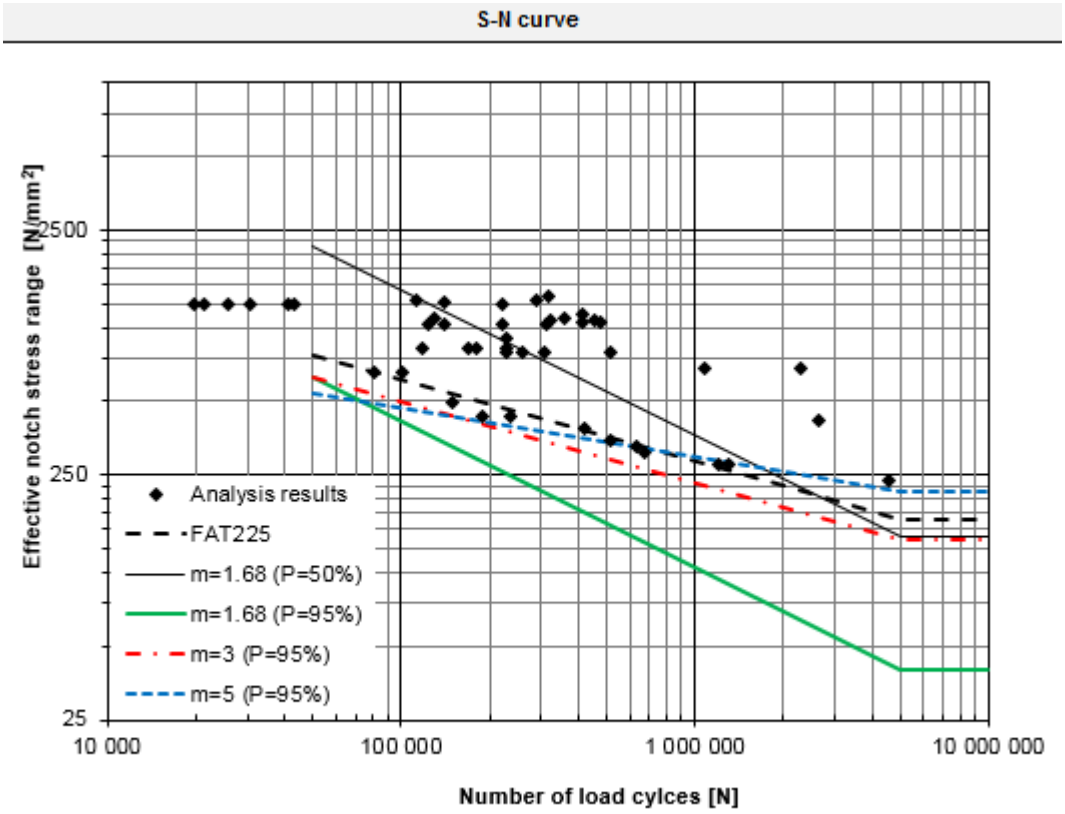

Graph 4.5 Final SN-curve representing the fatigue life of laser hybrid welds.

The graph showed a large scatter in the analysis result of the four analysed details. Moreover, the SN-curves representing hybrid laser welds indicated on a lower detail class than the detail class recommended by IIW. Applying the slope of m=3 a detail class of 185 was reached while using the natural slope of m=1.68 a drastically reduced

value of 69 MPa was attained. The values for the mean and characteristic SN-curves are presented in Table 4.9.

Table 4.9 Summarization of mean and characteristic SN-curve values at $2*10^6$ cycles.

Statistical evaluation of analysis data according to EN 1993-1-9:2005		
SLOPE	**Mean SN-curve (P=50%)**	**Characteristic SN-curve (P=95%)**
m=natural=1.68	240.7	69.1
m=3	400.4	184.6
m=5	518.7	258.6

5 Discussion PART A

In this part FE-analysis has been carried out on previously performed fatigue tests in order to study the fatigue strength of hybrid laser arc welds. In conjunction with the effective notch stress method one single SN-curve representing the hybrid laser welds was produced.

Initially a literature study was carried out which pointed at a higher fatigue strength for the HLAW than for ordinary MIG/MAG welds. The fatigue life test performed by (Caccese et al. 2006) on cruciform fillet welds indicated on an improved fatigue life compared to both historical test data on conventional weld but also in comparison with the laser cold-wire welds test series. Additionally, (Narimani 2008) results were consistent with (Caccese et al. 2006), again showing on an enhanced fatigue strength compared to conventional MAG welding. The only uncertainty of the improved fatigue strength were brought forward in (Barsoum 2008) study on non-load-carrying cruciform which did not show any increase in fatigue strength compared to the other tested welding technics. Although, it indicated on a higher fatigue strength than recommended by IIW.

Even though the literature study pointed at an enhanced fatigue strength, the FE-analysis showed inconsistency in the results. When studying the analysis result from the four fatigue tests separately, two of the tests showed a detail class equal to or above the recommended detail class by IIW. While two resulted in a slightly reduced detail class. However, depending on the slope applied the detail class varying substantially.

Therefore, it should be mentioned that when the results for the four analysis were compared three of the tests indicated on a higher natural slope than the one recommended by IIW of m=3. The exception was the fatigue test on the eccentric fillet weld. Though, the fatigue tested specimens were in this case subjected to stress ranges concentrated to a narrow interval making the natural slope non-representative of the analysis results. Consequently, a higher slope, m, might be more representative when analysing the fatigue strength of hybrid laser welds, and would thus result in a higher detail class than when applying a slope of m=3.

When evaluating the final characteristic SN-curve representing the hybrid laser welds a large scatter in the analysis results were displayed and therefore making the natural slope inapplicable. If instead applying a slope m=5, which was closer to the mean slope value for the four tests, a detail class of 257 MPa was achieved. Consequently, the conducted study did indicate on an slightly improved fatigue strength for hybrid laser welds compared to ordinary welding techniques.

Nonetheless, it was a lot of uncertainties in the results. In test 1 the weld size had to be measured due to poor documentation. The weld size being one of the most influential parameter for the notch stress it might have affected the result substantially. Additionally, since the crack initiation point was not reported for the fillet weld a verification of the result could not be done. The same problem were encountered for test 4, both the transition geometry and the weld size were not specified. As mentioned in Chapter 3.4.1 a difference of 9.5% in the notch stress were found when changing the geometry from a smooth to a sharper transition radius. Additionally, the change of the

weld size has proven to influence the resulting notch stress adding to the uncertainty of the result.

When using the effective notch stress method idealizations of the weld geometries are used, some of which is far from the reality for laser hybrid welds. For example, when idealizing butt welds a flank angel of 30 degrees is to be used for both the root and toe side. However, the statistical analysis done by (Remes & Varsta 2010) on variation of the weld geometry pointed at a larger flank angle of the root, with a variation from 30 to as high as 90 degrees. The enlarged flank angle of the root were also confirmed in the photo of the fatigue tested butt welds in test 4, see Figure 3.13. Large geometric variations such as this could of course be one of the reasons for the scatter in the results.

Another idealization which showed influence on the effective notch stress was the modelled root position in test 2. Because of the large penetration of the hybrid laser welds the root is positioned further down in the plate. As mentioned in Chapter 3.2.1, the idealized weld gave about 10% lower notch stress thus resulting in a lower detail class.

PART B

Fatigue analysis of welded details in a SSD under moving load

6 Fatigue analysis of welded details in SSD under moving load

The second objective in the master thesis project was to identify critical weld details in a steel sandwich bridge deck under a moving static load and the governing load effects. By investigating how welded details at critical locations in the deck were affected by the moving load the critical hot spot in the deck for fatigue could be detected.

The study involved modelling of a global 3D model where four sub-models were attached. The models were created using the FE-software ABAQUS version 6.13-3. The submodels represented critical weld details in the structure where fatigue failure was expected. The fatigue analysis of the steel sandwich deck was evaluated using the effective notch stress method.

6.1 Global model

In this section the methodology used to create the 3D-model for fatigue analysis of the SSD is explained. The used settings in Abaqus and other choices regarding geometry and material are presented and discussed.

6.1.1 Choice of Geometry

The 3D model represents a steel sandwich deck with a surface area of 4x4 m. The cross-section was constructed with a corrugated core attached to an upper and lower face panel. The created SSD represented a part of a road bridge construction. The corrugations are placed in the longitudinal direction of the deck.

The repeated corrugation of the core enabled the simplified and less time consumption method of only creating one parent part consisting of one corrugation, see Figure 6.1. The parent part was copied to the required length, and the copied elements were dependent on the parent part and adopted therefore the same geometry, material properties and mesh. As mentioned earlier, weld details should be modelled with U-shape or keyhole when using effective notch stress method. However, due to lack of interest of the local stress concentrations at the weld detail in the global model the U-shape or keyhole of the weld were excluded. The weld was modelled with a height of 0.1 mm which is the diameter used when applying the U-shape later. The parent part was modelled with no interactions included between different plates i.e. the web and upper and lower face panel.

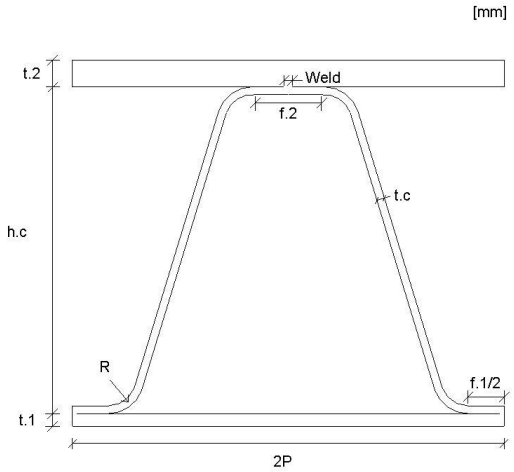

Figure 6.1 Geometry and dimensions of the parent part.

The applied dimensions of the geometry of the cross-section were determined with regard to two restrictions, deformations and local buckling. The global deformation was not allowed to exceed L/400 while the local deformations were not permitted to exceed 2P/400, according to Eurocode Load model 1 (LM1). Additionally, the cross-section class of the deck was limited to class 3 or lower. The dimensions are listed in Table 6.1 below.

Table 6.1 Notations and dimensions of the cross-section geometry of the SSD

Notations	***Dimensions [mm]***
2P	149.6
h_c	104.1
t_c	2.7
t_1	4.4
t_2	9.3
f_1	25
f_2	25
R	10.8 degrees
Weld	3

The parent part was modelled using 20 node solid elements without reduced integration. By extruding the part 4 m the required length was obtained. The desired width of 4 m required that the parent part was copied 26.7 times. For simplicity the part was only copied 26 times resulted in a total width of 3.9 m. Before the total area of the deck was

created the mesh was applied to the parent part. A convergence study of the applied mesh is presented in Section 6.2.3.

To prevent motion between two copied parts in the deck two different methods were investigated. Initially, the parts were merged into one part by using the setting "merge mesh", but this method showed unsatisfying results. The motion was not prevented between the parts, instead the parts separated during analysis and the deck demonstrated an incorrect deformed shape. The concept of using the merge setting was therefore excluded. In addition to the method of merging the parts into one element, the parts were connected to the adjacent parts using the setting "tie constraint". All parts were constrained to the adjacent part in all degrees of freedom. By modelling the deck as mentioned, the deck showed reliable and approved behaviour and the method was used to create the deck that was going to be used in the analysis.

6.1.2 Material properties

Before the parent part was multiplied the material properties were applied to the part. For fatigue analysis using the effective notch stress elastic material behaviour can be assumed. A typical steel material with Young's module E=200GPa and Poisson's ratio of 0.3 was assigned to the whole cross-section.

6.2 Verification

The verification involved two verifications, where initially the reaction forces for the deck were compared with the applied load to confirm that they resulted in an equal value. Secondly, a convergence study was conducted with the purpose of finding the most appropriate mesh for the model. Nine models were compared.

6.2.1 Load and boundary conditions for verification

As mentioned, the model represents a deck of a road bridge structure. Fatigue load model 3, FLM 3, according to SS-EN 1991-2 was applied, but with some simplifications, see Figure 6.2. Only half an axle, with a magnitude of 60 kN, was applied at the centre of the SSP deck. The area exposed for pressure was 400x400 mm, resulting in the total applied load 375 kPa.

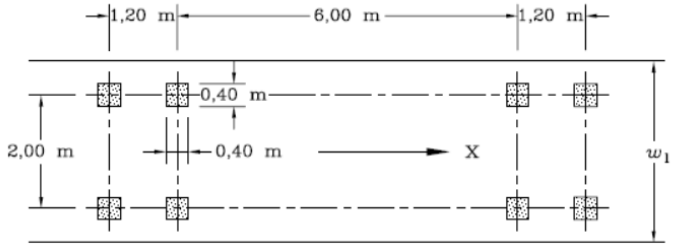

Figure 6.2 Fatigue load model 3.

To be able to apply the load an additional part was created. The created part had the same area as the applied axle load. The quadratic part was created as a shell element and with a tie constrain attached to the deck, thus preventing motion between the deck and the quadratic part. The shell element was assigned a thickness of 1 mm. The same Poisson's ration as for the deck was used but the Young's module was decreased to 100

Pa. If the stiffness of the plate was not decreased compared with the stiffness of the deck the deformation was influenced resulting in a smaller deformation at the applied load due to higher stiffness at that location. The load was applied as a pressure load on the shell element, see Figure 6.3. The mesh of the quadratic part was created as similar as the deck, so no conflicts between the meshes should occur.

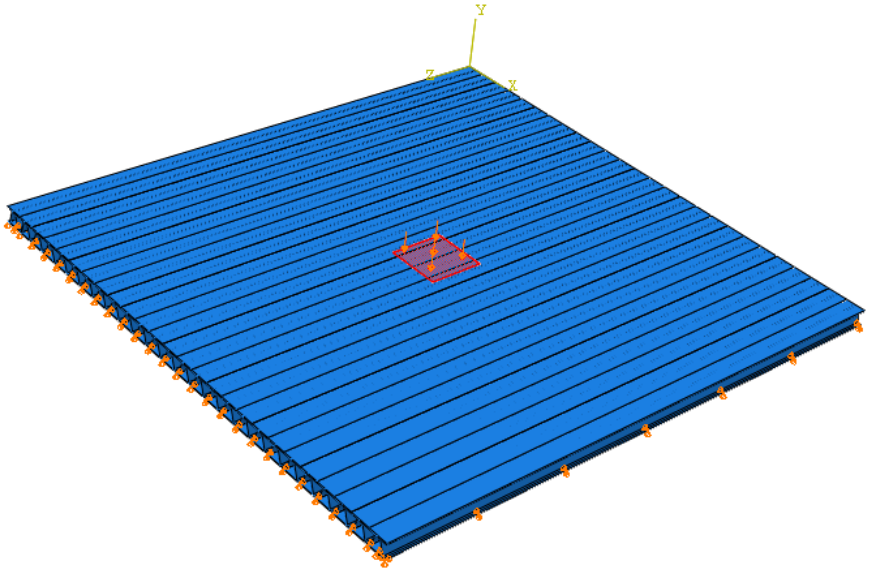

Figure 6.3 Applied load at the SSD.

The deck was restrained in the vertical direction at all four edges. To prevent the deck to rotate the deck was restraint in x- and z direction as well. Therefore, two perpendicular edges of the deck were restrained counteracting the motion in these directions.

6.2.2 Reaction force

The global model was verified by comparing the summation of reaction forces extracted from Abaqus with the total applied load. The applied load was a half axle load with a magnitude of 60kN. The reaction forces extracted from Abaqus resulted in a summation of 60 kN. Comparing the values showed thus a very good equality with 0 % difference.

6.2.3 Convergence study

The second step in the verification of the model involved a convergence study with the purpose of investigate the mesh and decide the most appropriate mesh density of the global model. The mesh was decided so the global model demonstrated a reasonable and correct response and behaviour. The study involved both local and global deformation at the upper and lower face panel. Additionally, a stress convergence were done both at the upper and lower face panel and at the boundaries to the submodels. All extracted values from the models were done at the depth 2 m of the deck. See Appendix C for the completed convergence study and the exact location for the extracted values.

Nine models were created with different mesh densities. The number of elements ranged from 5440 to 414096, see Figure 6.4 for the nine meshes.

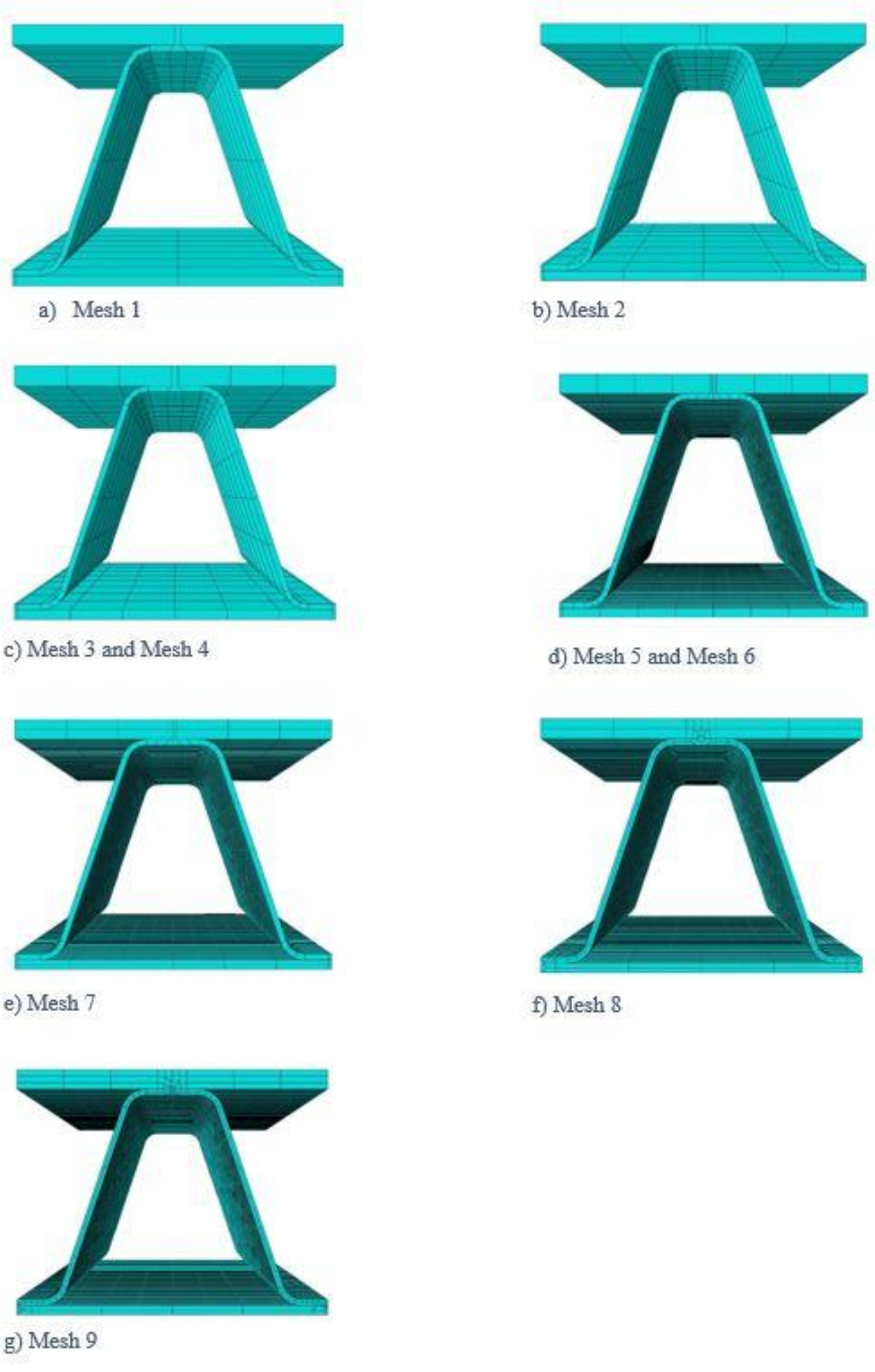

Figure 6.4 The cross-section of the nine meshes.

Initially, the deformation both global and local was investigated. With increased numbers of elements both global and local deformation increased gradually in the SSP deck, see Graph 6.1and 6.2. The global deflection indicated problems for the meshes with an element size of 500 mm in the depth. The plots of the deformation showed an unsmooth shape with distinct edges and thus an insufficient behaviour of the global behaviour, see Figure 6.1 b). As a result, Mesh 1, 2 and 3 were excluded in further analysis. Another reason to avoid element size 500 mm in the depth of the model was the ambition to keep the element ratio low in the model.

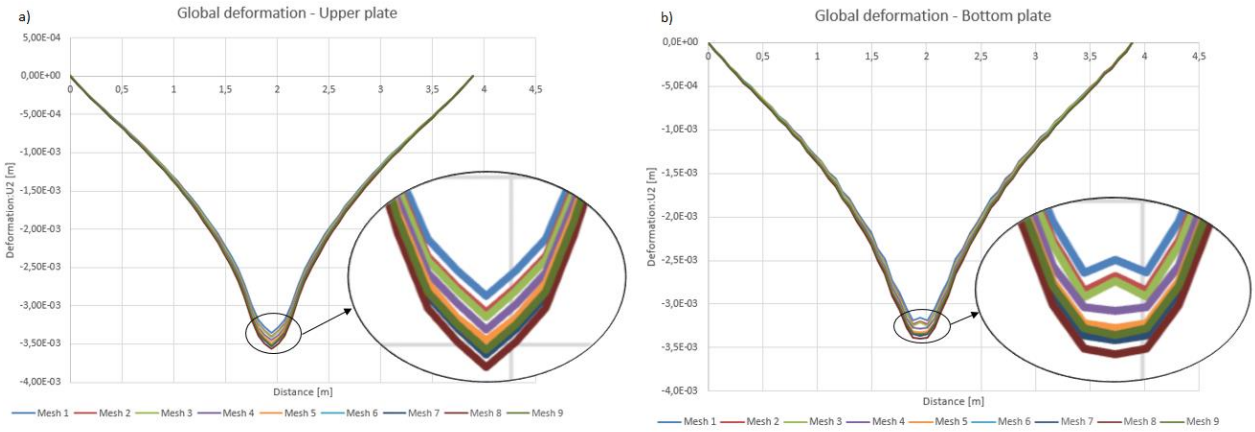

Graph 6.1 Global deformation a) Upper plate b) Bottom plate.

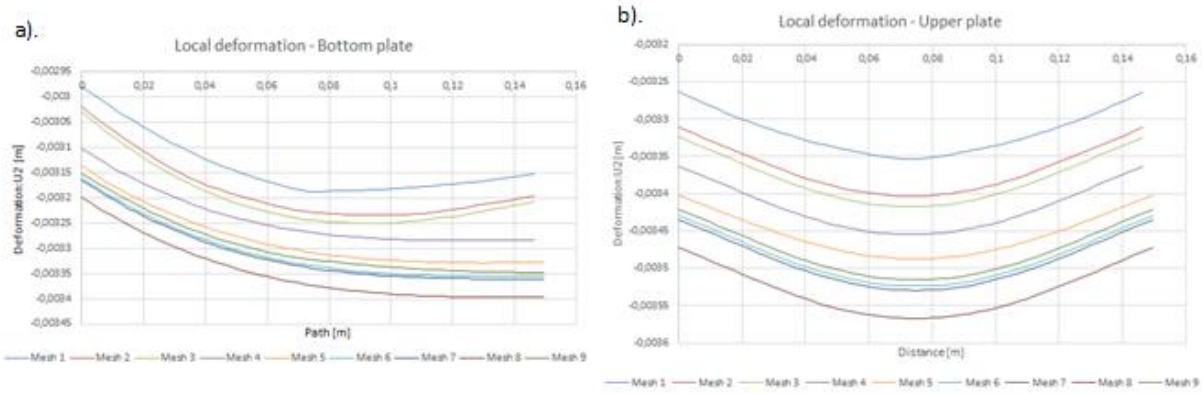

Graph 6.2 Local deformation a) Bottom Plate b) Upper plate.

The mesh density at the area of the weld was another interesting aspect that was investigated. Models with both one and several elements at the weld area were studied. The global deflection showed a minor difference in the magnitude when comparing the models with finer mesh densities with the more course ones. However, when the number of elements was increased at the area of the weld the time consumption to run the analysis was significantly increased. As a result, a model with few elements at the weld was to prefer due to less time consumption.

Secondly, a stress convergence were done to evaluate the meshes. The values were extracted at the upper and lower face panel, at the centre of the deck under the load. For the convergence to not be influenced by the local stress concentration at the weld region, causing misleading results, a point subjected to only nominal stress had to be obtained. The geometry of the structure enabled an analysis of the stresses according to beam theory. The face panels were seen as supported beams where the corrugations acted as supports. From the analysis normal stress in the x-direction was extracted. Complete linearity was found at a distance of 74.8 mm from the weld, i.e. in between two welds, see Appendix C. The stress convergence of Mesh 4-9 at the upper plate can be seen in Graph 6.3 a) and at the bottom plate in Figure 6.3 b). The comparison indicated good convergence between Mesh 4 and Mesh 6-9. However, Mesh 5 showed a discrepancy of 19% indicating on problems with element size 100mm in the depth.

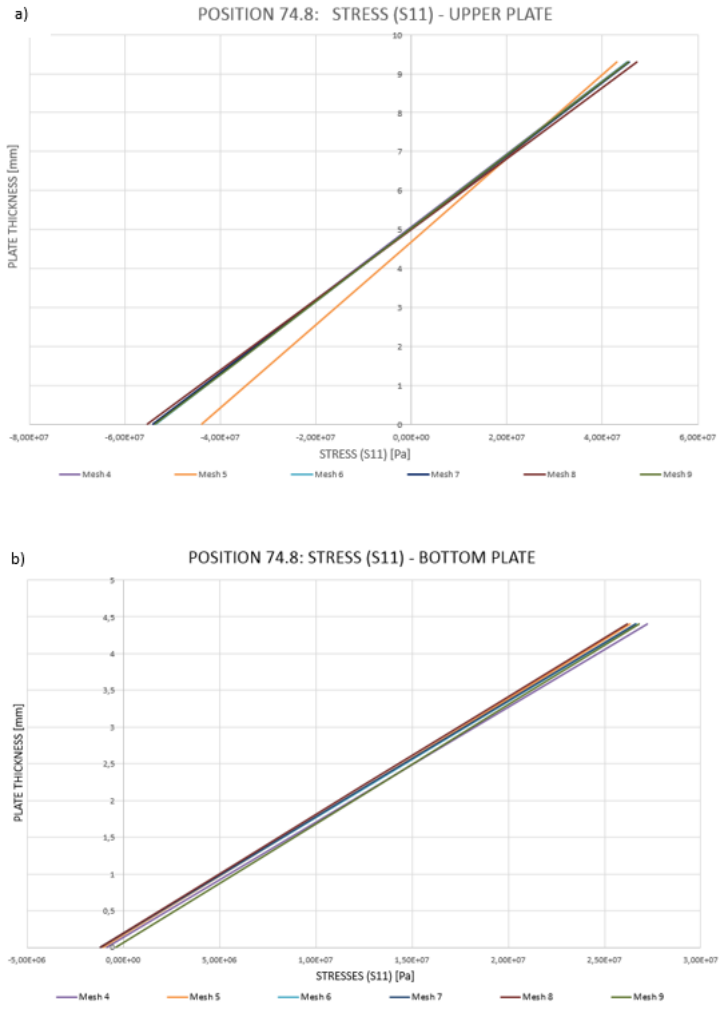

Graph 6.3 Stresses a) Upper plate b) Bottom plate.

In the fatigue analysis of the deck submodels were used, see Section 6.3-4. The submodels were created with an area of 149.6x149.6 mm, seen from the above. To verify a correct response at the boundaries of the supposed submodel a stress convergence were done at the boundaries ±74.8 mm from centre of the deck, see Figure 6.5. The stress component in the z-direction (S33) was extracted from the model, see Appendix C.

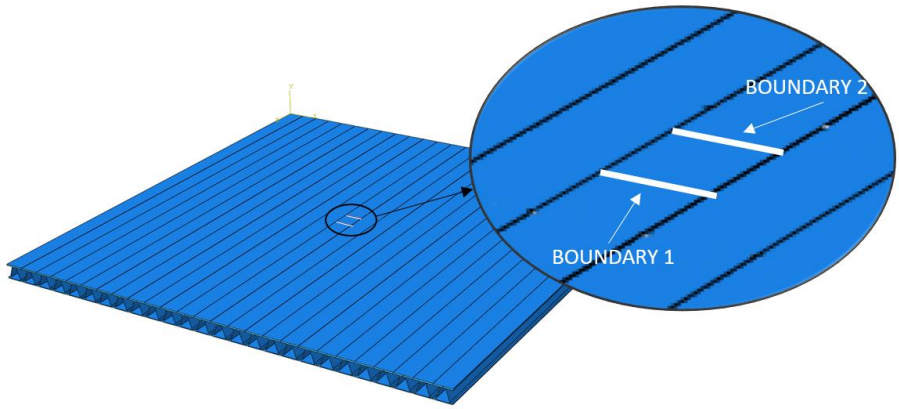

Figure 6.5 Stress convergence at boundaries of submodels.

The results from the stress convergence at the two boundaries can be seen in Graph 6.4 a) and b). The stress convergence showed good coherence between mesh 6, 7, 8 and 9. However, Mesh 4 and 5 indicated on inconsistencies. As for the previous stress convergence of the stress component in x-direction in the upper and lower face panel, Mesh 5 indicated now again on large variation compare to the other meshes. Consequently, an element size of 100mm in depth will not result in reliable result. Therefore, Mesh 5 was not used for further analysis. Additionally, Mesh 4 showed a 12% discrepancy indicating that the mesh had too few elements in the cross-section to give correct response. Mesh 4 were also excluded for further analysis.

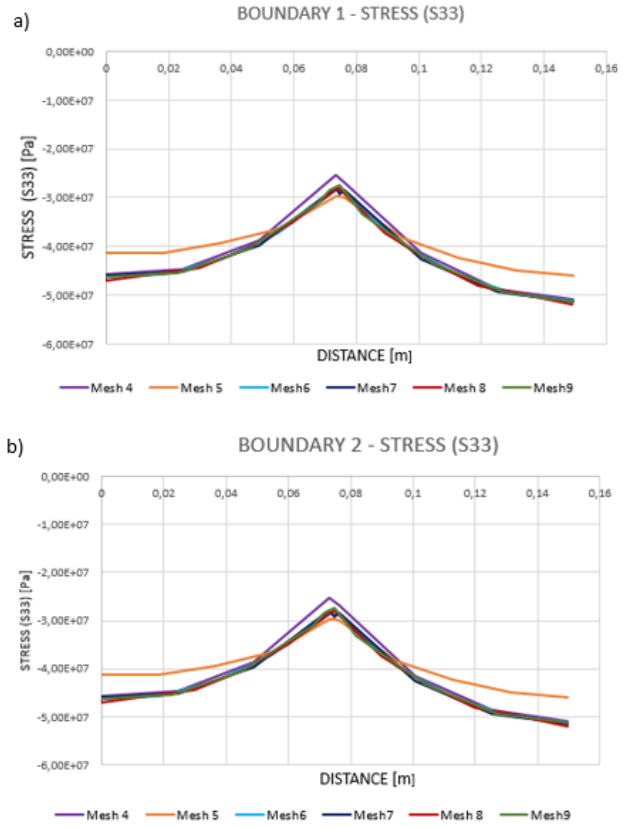

Graph 6.4 Stress verification at ±74.8 mm from centre a) boundary 1 b) boundary 2.

Mesh 6-9 showed similar results with low percentage differences after comparing deformation and stresses. However, the benefit of using a model with low analyse time was the main aspect for the choice of using Mesh 7 for further work. Mesh 7 fulfilled already mentioned aspects with a lower element size than 100 mm in the depth and showed thus reliable results during analysis.

6.3 Submodels

Submodels are used to investigate a specific area of a model that is of special interest. The area can represent a critical detail of the structure and it is therefore important to analyse this area in detail. Using submodels, it is possible to apply a finer mesh of the area of interest than for the remaining model and thus obtain a more accurate result and reduce the run time. A submodel is linked to the output database of the global model, which makes the submodel dependent of the results of the global model.

The submodel was created by first copying the global model and then removing regions of the geometry that were not of interest. To achieve shorter runt time, it was of great importance to create a submodel with as small geometry as possible. Three models were created, with different geometries that were going to be verified so that the most appropriate geometry of the submodel was selected for the fatigue analysis. Two of the models were formed with reduced geometry, "Submodel Large" and "Submodel Small", while the third submodel adopted the same geometry as the parent part, "Submodel Cell", see Figure 6.6. Even if a model with reduced geometry was preferable, stresses and deformations needed to be correct and not become affected of the reduced geometry. The submodels with reduced geometry were therefore verified by comparing deformation and stresses with "Submodel Cell". The verification in Chapter 6.3.1 indicated which submodel that was preferable to use for the fatigue analysis of the weld regions in the deck.

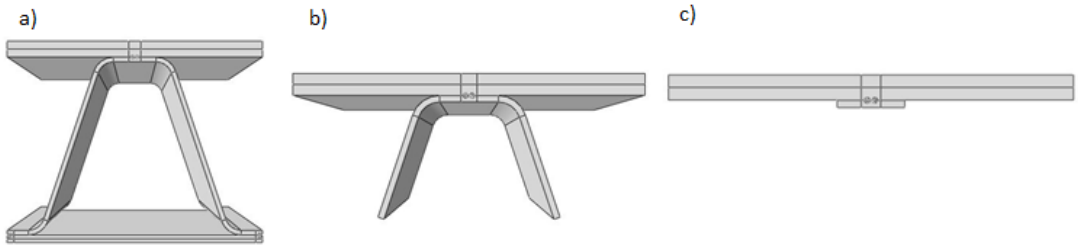

Figure 6.6 Geometry of the submodels a) Submodel Cell b) Submodel Large c). Submodel Small

The analysis of the stress concentration at the weld region was done according to the effective notch stress method. Therefore, the submodels were created with a U-shape at the region of the weld, see Figure 6.7. Following the recommendations of the IIW a radius of 1 mm were to be applied for plates above 5mm while a radius of 0.05 mm should be chosen for plates less than 5mm. However, since the top plate had a thickness of 9.3mm while the corrugated web plate had a thickness of 2.7 mm it made the choice of radius a bit unclear. However, a radius of 0.05 mm for the U-shape was chosen since a smaller gap between the face panels and the web give rise to less impact on the bending stiffness of the deck.

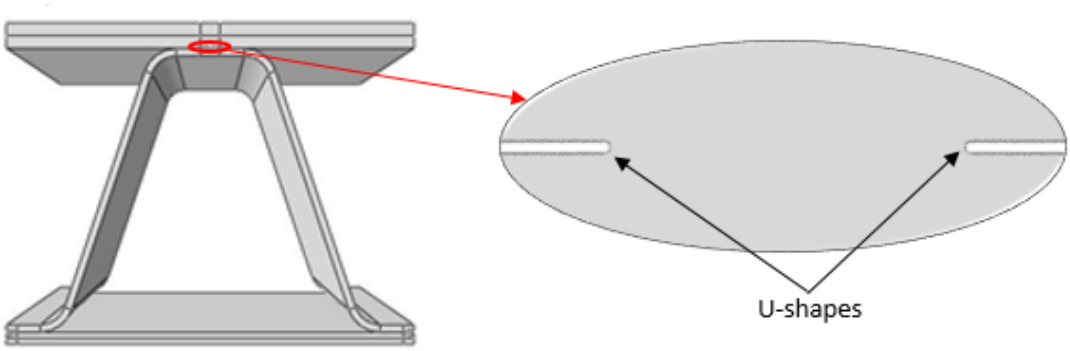

Figure 6.7 U-shapes created at the weld region at the submodels.

Moreover, the depth of the submodels was chosen so it became large enough for the centre not to be influenced by the boundary conditions applied at the edges. The depth of the models was thus taken to 149.6 mm creating a quadratic model.

The fatigue behaviour of the deck was to be investigated at weld details at a path in the middle of the deck i.e. half the depth. The verification of the submodels was done at the same location but at the middle of the deck i.e. half the transverse length. By using the coordinates of the position in the global model the submodels were translated to the correct location where the models were positioned.

The mesh of the submodels were created according to IIW:s recommendations presented in (Al-Emrani & Aygül 2014). According to the recommendations, element size 0.012 mm at the U-shape should be adopted when a radius of 0.05 mm is used. The element size was increased gradually in two steps; 0.036mm and 0.108mm. Remaining area was meshed using the seed by number of elements, where the number was chosen so the element ratio was approved. See Figure 6.8 for the meshed specimens of the different submodels and Figure 6.9 for a zoomed visualization of the mesh at the area of the U-shape. Element size of 8 mm was used for the mesh in the depth of the models.

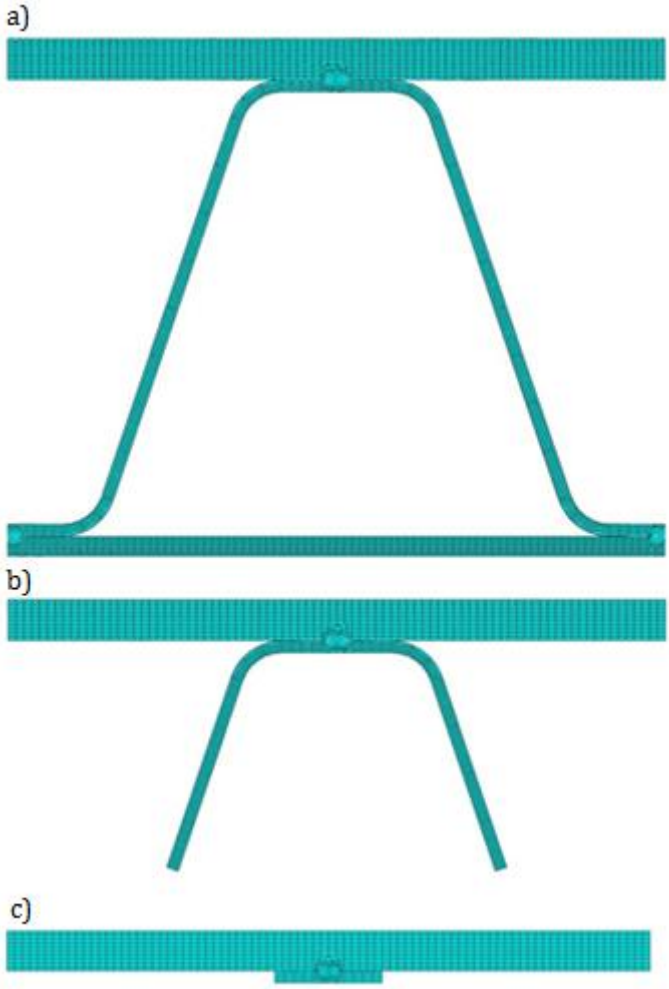

Figure 6.8 The meshed submodels a) Submodel Cell b) Submodel Large c) Submodel Small.

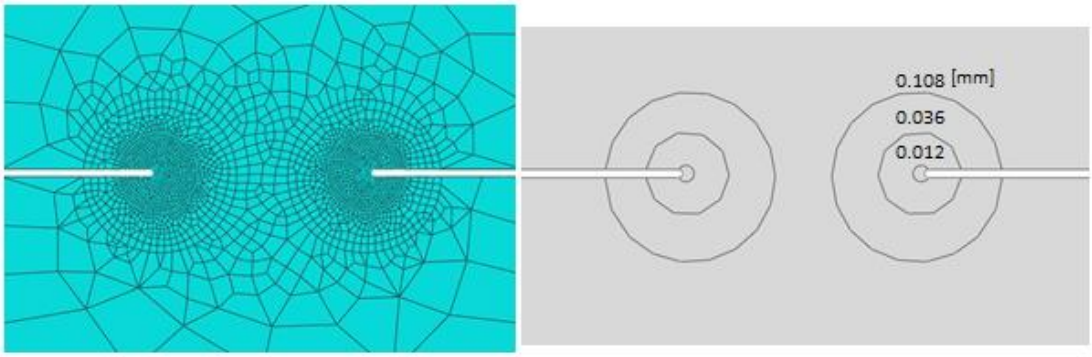

Figure 6.9 The mesh used at the U-shape for all submodels.

The submodels were coupled to the global model using node-based submodeling. This modelling technique makes it possible to interpolate the results from the global model to the submodel by using nodal result fields. By using this technique the boundary conditions for the submodel are defined. The boundary conditions were applied at the faces that were created when removing regions of the geometry when creating the submodels geometry.

6.3.1 Verification of submodels

Three submodels were created, by verification it was decided which of the models that was going to be used in the fatigue analysis. As mentioned, it was of interest to use a submodel with reduced geometry to decrease the run time. However, the models with decreased geometry had to show correct result and not jeopardize the accuracy of the result. For more detailed information regarding the verification see Appendix D.

The same load as presented in Chapter 6.2.1 was used again in the verification of the submodels. The verification involved comparison of deformation and Principal stress. The extracted values from Abaqus were taken from the centre line in the depth of the submodels. The results were not extracted from the edges of the submodels due to the large impact of the boundary conditions at the edges.

The comparison of the deformation showed good coherence of the models. The values of the deformations were extracted at a path placed at the upper plate including the total width of the submodels, see Figure 6.10. The values were extracted and plotted in Graph 6.5, which showed that the deformations for the different submodels almost were equal. Especially, the deformation for the "Submodel Cell" and "Submodel Large" showed almost identical results of the deformation. The deformation of the "Submodel Small" indicated a minor difference, smaller than 1%.

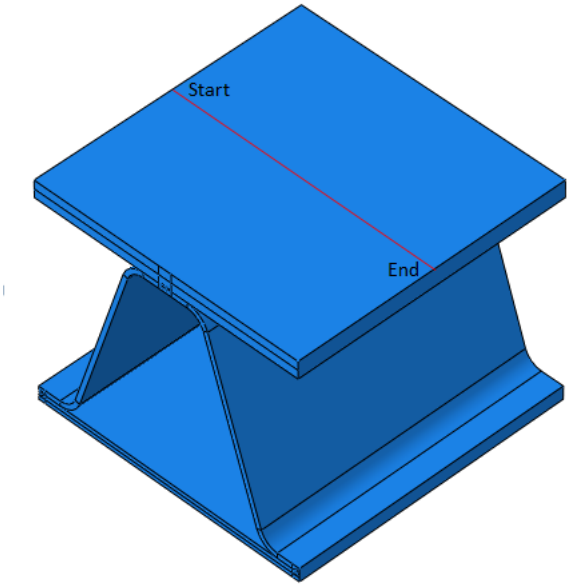

Figure 6.10 Path where the deformations values were extracted.

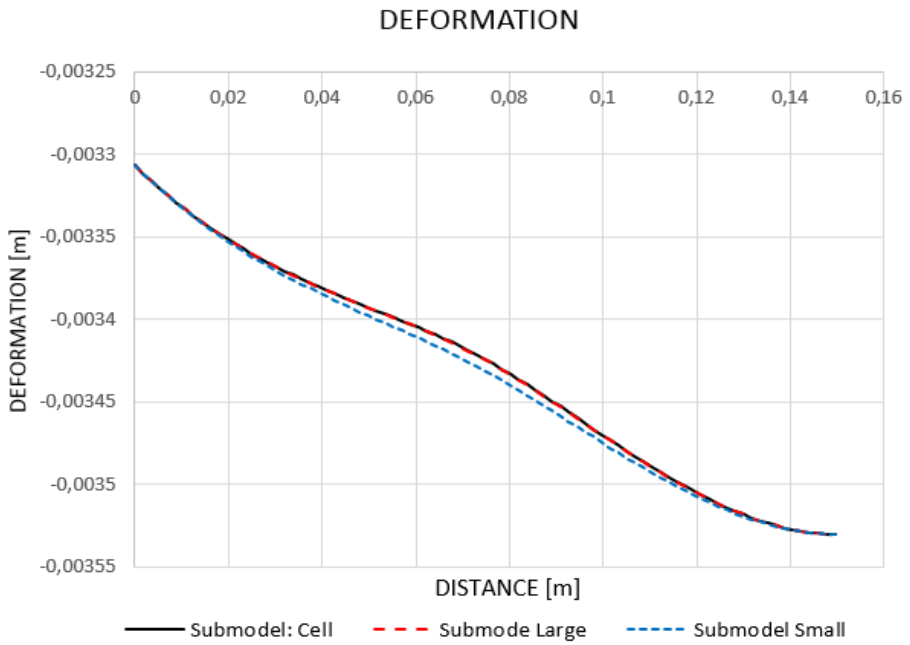

Graph 6.5 Deformation plots for the submodels.

However, the comparison of the stresses indicated on differences of the models, see Graph 6.6-7. The stresses were compared at the U-shapes, both at the left and right side. The small submodel showed large difference compared with the other models. The difference varied depending on where on the plots the values were compared. Therefore were the mean differences calculated and the comparison of the mean difference between submodel "Small" and "Cell" indicated on large discrepancy with 33% and 9.4% for the left and right U-shape respectively. However, comparing the mean difference of submodel "Large" and "Cell" showed good coherence with small differences of 1.2% for the left U-shape and 1.7% for the right. The remaining plots showed that the stresses for the "Submodel Small" had a difference in smaller magnitudes but still not approved. The difference in the stresses gave the conclusion that weld details could not be modelled according the geometry of "Submodel Small". The submodel was therefore excluded and it was decided that the model could not be used for further analysis of the fatigue behaviour of weld details in the SSD. The significantly reduced geometry of the submodel had too large impact of the behaviour.

In similar way, comparing the deformations, showed the stress plots of submodel "Cell" and "Large" good coherence. The values of the stresses for the models were almost equal. The high coherence of the stresses for the two models enabled to use "Submodel Large" for further analysis regarding the fatigue behaviour.

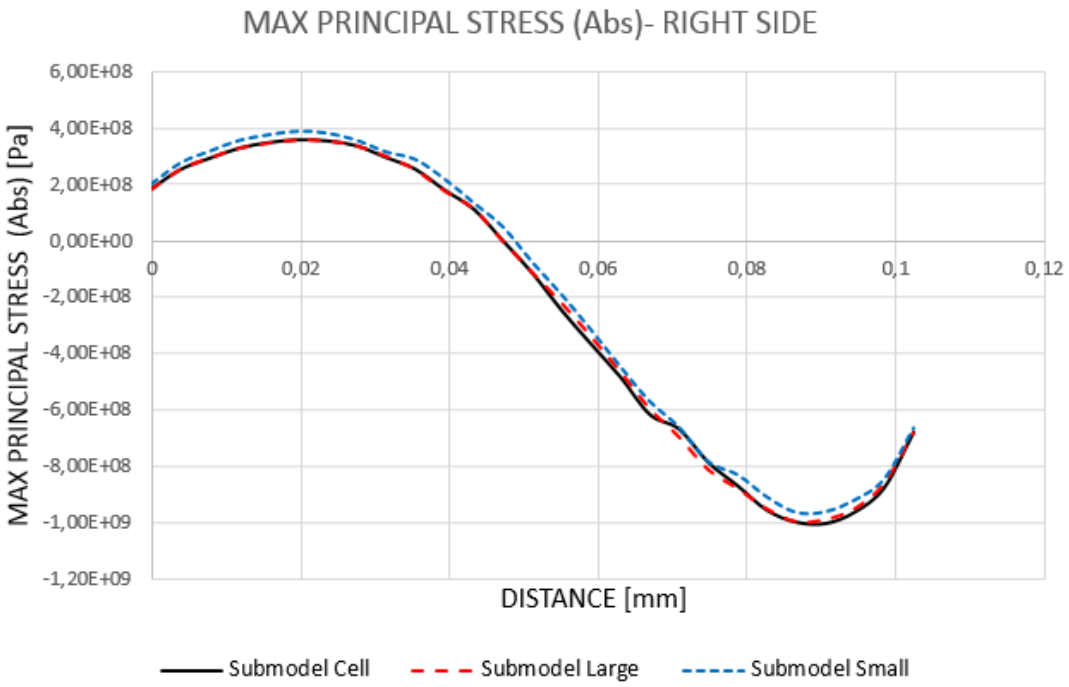

Graph 6.6 Principal stresses (Abs) at the right path.

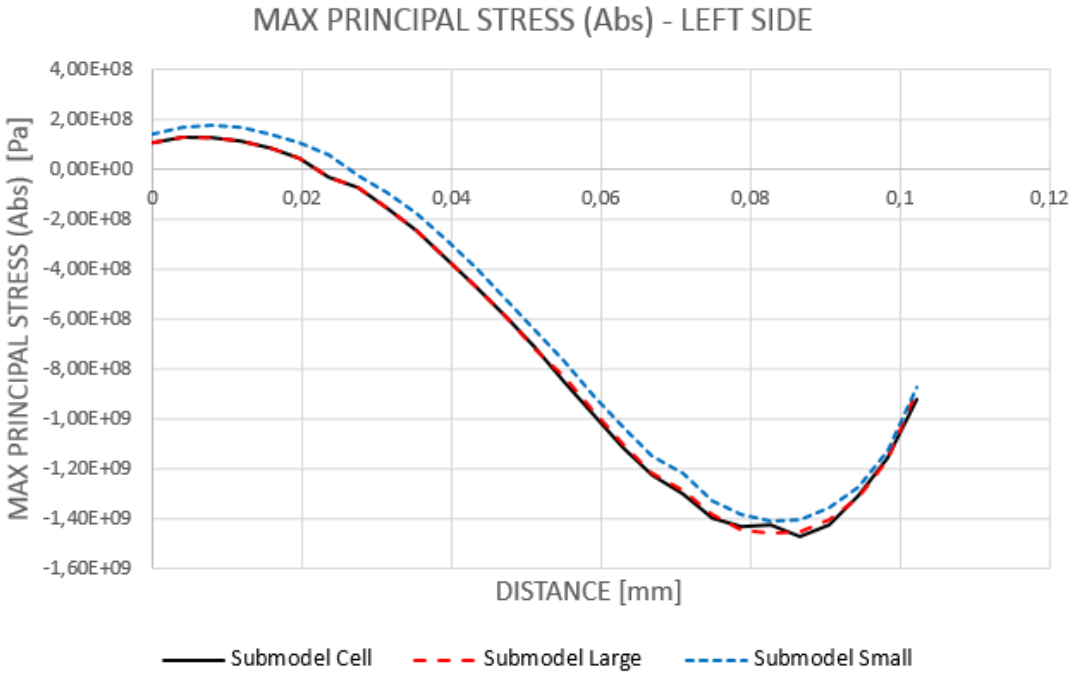

Graph 6.7 Principal stresses (Abs) at the left path.

The plotted values of the stresses of "Submodel Cell" showed a bump in the shape of the plots at the left U-shape. The sharp change in the shape of the plots can be explained by two elements in the mesh, placed at the position of the bump. The elements created a node that was affected by four other nodes. Compared with remaining nodes that was

only affected by three nodes, see Figure 6.11. The resulting stress at that node was therefore higher.

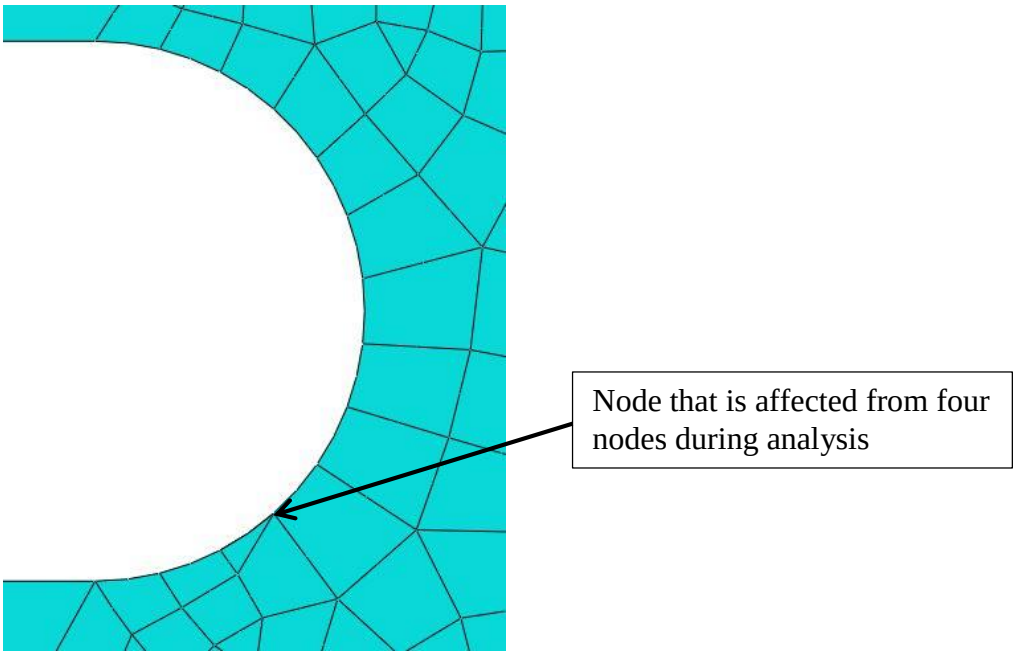

Figure 6.11 Critical node creating bump at the extracted stresses.

6.4 Fatigue analysis of Steel Sandwich Bridge deck

In previous chapters the verifications of the global model and the submodels were presented. The verification resulted in the most suitable models to be used for the fatigue analysis of the SSD.

The fatigue behaviour of the SSD was investigated by attaching four submodels at critical locations in the deck. The critical areas were expected to experience high stress concentration at the weld regions and might therefore govern the fatigue life of the structure. The positions of the submodels were at the middle of the deck and close to one boundary, both at the upper and bottom plate, see Figure 6.12. The locations were assumed to be affected by different stress components which might affect the fatigue behaviour in different ways and the positions were therefore interesting to investigate. It was assumed that the submodels close to the boundary would be exposed to large shear forces while at the middle of the deck bending moment has larger impact. Additionally, Submodel 1 and 3 were expected to be exposed to both global and local affects.

Furthermore, the fatigue analysis of the Submodel 1 and 2, close to the boundary, was expected to be influenced by the edge of the deck. Consequently, the width of the deck was increased by adding seven parent parts at each side of the boundary conditions, see Figure 6.12. The added parts resulted in a total increased width of 2094.4 mm of the deck. The boundary conditions were kept at the same positions and with the same constraints, i.e. all edges were restrained in the vertical direction while two perpendicular edges were counteracting movement in x- and z-direction.

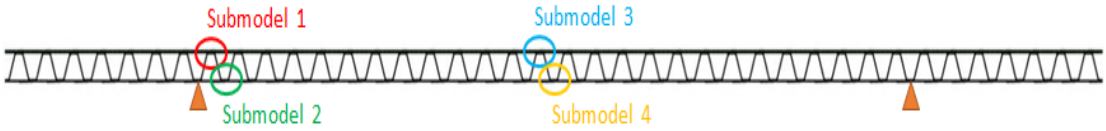

Figure 6.12 The developed model with positions of the submodels.

In the fatigue analysis the deck was subjected to a moving load in the transverse direction of the deck, going in a positive x-direction. The moving load represent half an axel of 60 kN, applied at an area of 400x400 mm. To be able to create the moving load, the load was applied through 42 steps with different locations. The load was moved in steps of 50 mm and 100 mm. The step intervals were decreased to 50 mm when the load was close to a submodel, otherwise load steps of 100 mm were used, see Figure 6.13. Start and stop of the load in the figure was calculated from the centre of the 400mm wide load area, when the deck was placed according the coordinate system in the figure. In the remaining report when a load step is denoted for example, "load step 1.2 m" this means that the centre of the load was applied at 1.2 m form the left edge when the deck is placed according the coordinate system in Figure 6.13. Due to symmetry of the deck, the load was only moved to the centre of the deck and would have otherwise resulted in the same results for the other half of the deck.

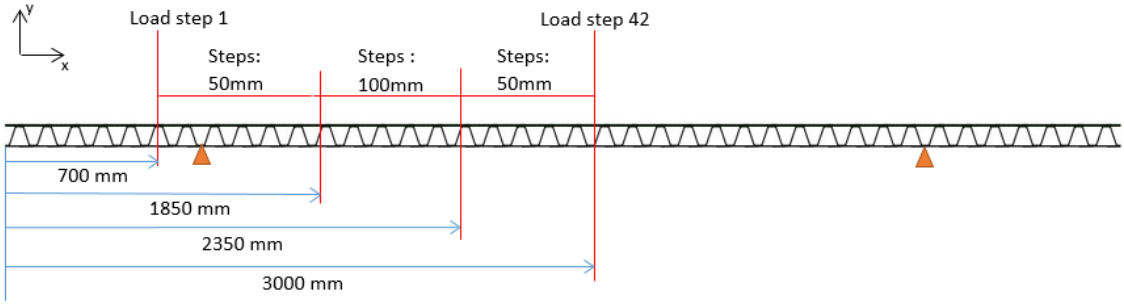

Figure 6.13 Load positions for the moving load.

The fatigue analysis of the deck was done by investigate the stress concentration at the U-shapes, i.e. the weld regions. To decide which weld that was the most critical one, influence lines for each U-shape at the submodels were created and compared. The influence lines represented the stress variation at the weld due to the moving load in transverse direction. As mentioned, each submodel consisted of two U-shapes, were the left one for each model was labelled A and the right B, see Figure 6.14. The stresses were extracted at paths at each U-shape, marked as red arcs in Figure 6.14. The path at the U-shapes consisted of 27 nodes. For each node at the paths influence lines were created, and it was possible to show not only at which U-shape the stress was highest but also where a crack would occur at the U-shape. In total, eight diagrams was created showing 27 influence lines representing the stress variation under the moving load at the 27 nodes at each path, see Appendix E.

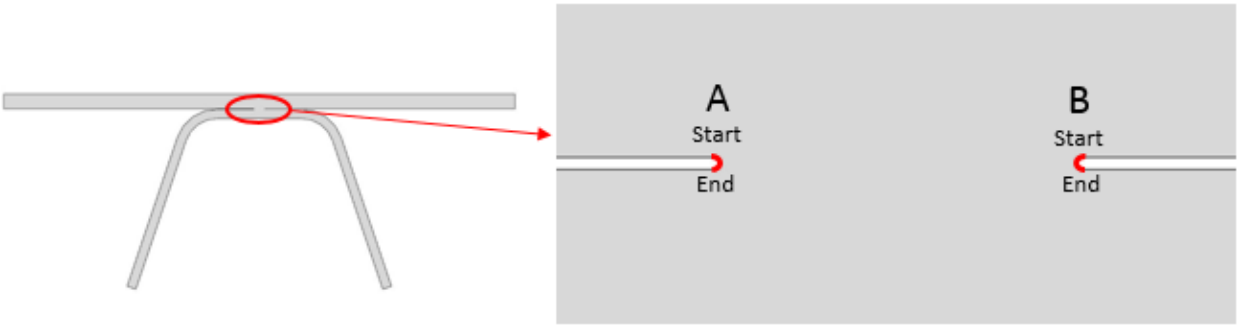

Figure 6.14 Labelling of the U-shapes of each submodel.

The influence lines for the submodels were compared, and critical details in the structure could be decided. The variation of the stresses was analysed, trying to understand the behaviour and what stress components that were affecting the models at which time. By comparing the resulted plots with influence lines representing the global shear and moment at the positions of the submodels the different stress components could be identified and also how and when they affected the weld details. The local moment was another aspect involved for the analysis with the purpose of understanding the stress variation at the welds. Simplified sketches of the influence lines representing shear and global moment and also local moment diagram were made, see Figure 6.15-17, and was then used for the analysis.

The influence lines of the submodels were analyzed so the most critical weld detail was determined. The most critical detail was decided by investigate maximum stress concentration, compression and tension, for each submodel. The stresses were compared and the maximum stress was obtained. The detail with the largest stress concentration was seen as the most critical weld region in the deck and it was also possible to indicate where in the weld the crack would occur.

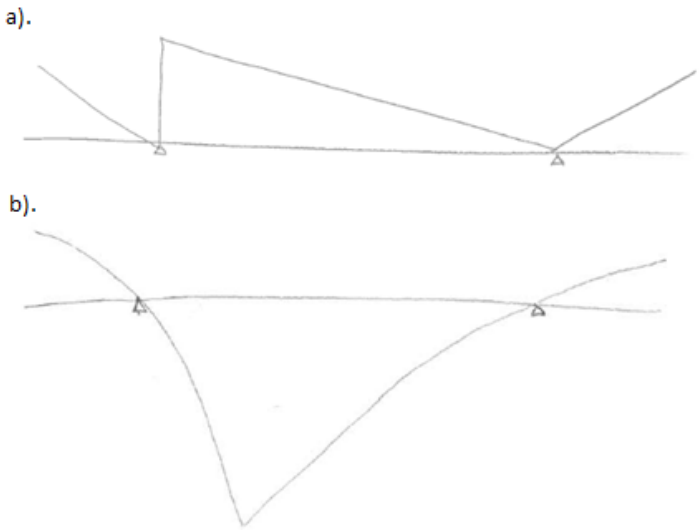

Figure 6.15 a). Influence line of shear force at Submodel 1 and 2 b). Influence line of global moment at Submodel 1 and 2.

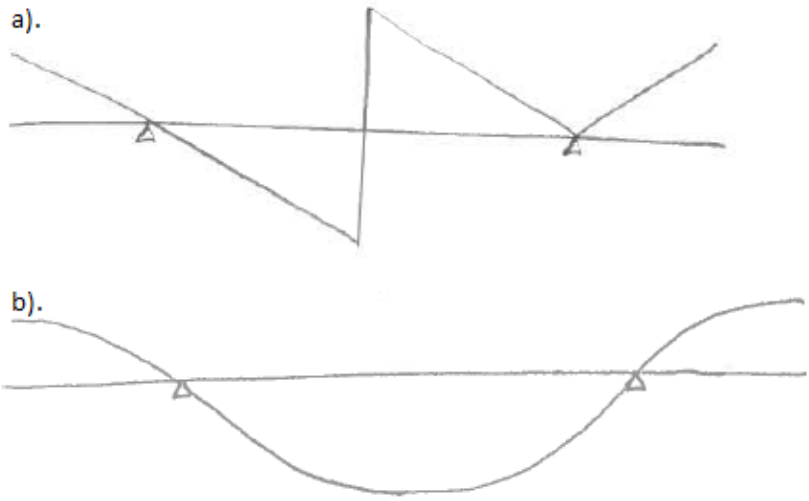

Figure 6.16 a). Influence line of shear force at Submodel 3and 4 b). Influence line of global moment at Submodel 3and 4.

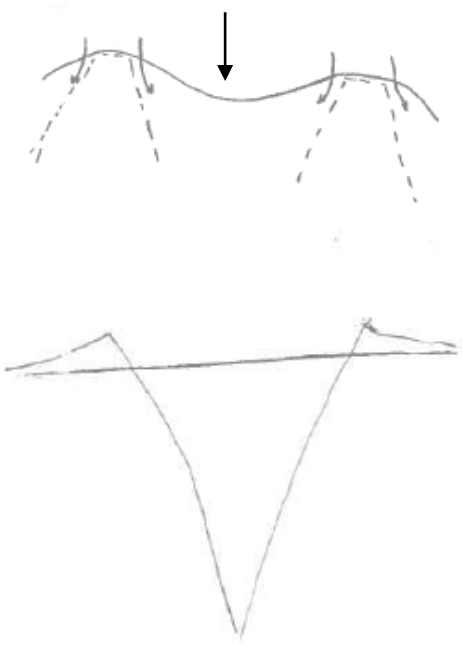

Figure 6.17 Local moment diagram.

7 Result and discussion PART B

The result of the fatigue analysis of the SSD is presented in the following chapter. The result is presented for one submodel at the time and ends with a summary and a conclusion of which weld detail is the most critical for fatigue in the deck. Contour plots are presented for each submodel with the expected crack initiation point in the weld. The chapter ends with a thorough discussion regarding the results and with the attempt of presenting which stress components that contribute to critical stress points in the submodels.

7.1 Submodel 1

7.1.1 Submodel 1A

Submodel 1A showed compressive stresses for all nodes at every step, see Graph 7.1. Node 1-10 showed highest stress at load step 1.45 m while node 11-27 hade largest stress in load step 1.2. The stress concentration was gradually increased for the load steps in the beginning, until the maximum stress concentration was obtained. After the nodes had reached the maximum stress the stresses were successively decreased in relation to the increased distance between the load and submodel. The maximum stress concentration was obtained in step 1.2 m, calculated from the edge of the deck. The magnitude of the maximum stress concentration was obtained in node 21 with a magnitude of 2366 MPa

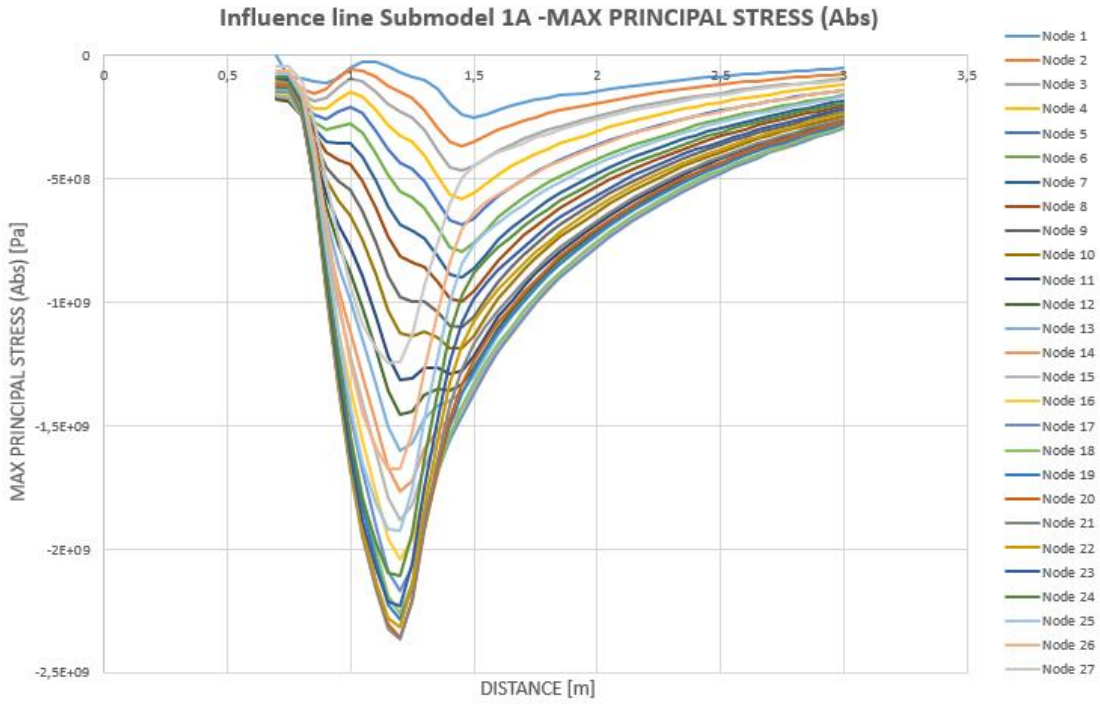

Graph 7.1 Influence lines of Submodel 1A – Max principal stress (Abs).

7.1.2 Submodel 1B

Analyzing the influence lines of Submodel 1B, see Graph 7.2, it was shown that the nodes were affected of both tension and compression stress depending on the load position. In a similar way as Submodel 1A, the maximum compression was gained when the load was applied over the submodel i.e. step 1.2. Moving the load further away from the submodel, the compression stress successively was decreased and reaches instead the maximum tension stress when the load was applied at step 1.45 m. The maximum stress concentration was shown in step 1.45m as tension with a magnitude of 1429 MPa at node 17.

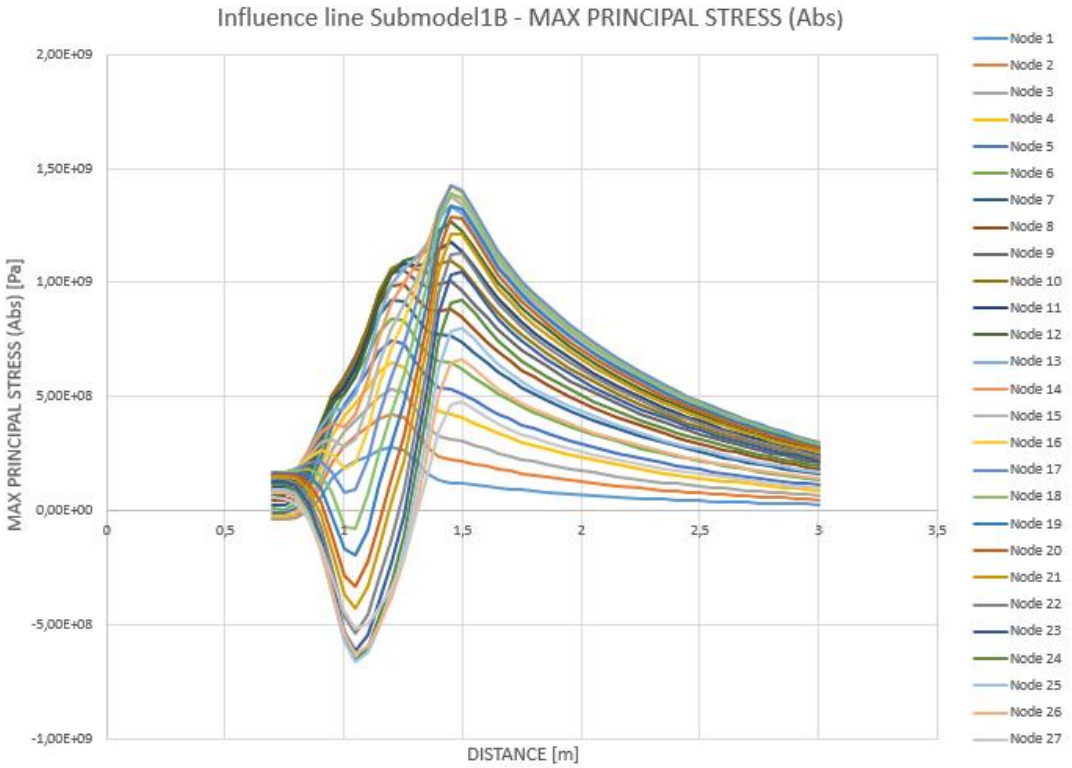

Graph 7.2 Influence line Submodel 1B – Max principal stress (Abs).

7.1.3 Crack initiation point of Submodel 1

Both Submodel 1A and 1B showed largest stress concentration at the lower nodes, at node 21 and 22 for Submodel 1A respectively Submodel 1B. The contour plots indicate the crack initiation points for Submodel 1, see Figure 7.1. The most critical position for initiation of a crack was though in Submodel 1A due to higher stress concentration.

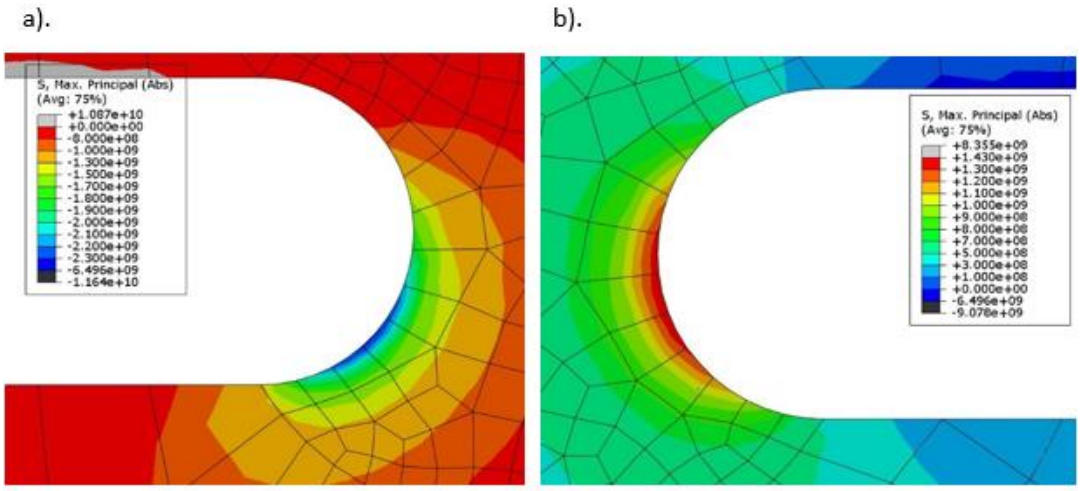

Figure 7.1 Crack initiation points for Submodel 1 a). Submodel 1A at step 1.2 m b) Submodel 1B at step 1.45 m.

7.2 Submodel 2

7.2.1 Submodel 2A

When the load was applied to the left of the support, the submodel experienced compression with the maximum compression at step 0.95, see Graph 7.3. However, the submodel was affected of the highest stress concentration when the load was moving away from the submodel towards the middle of the deck. The highest stress was obtained as tension at load step 1.4 m with a magnitude of 1227.19 MPa at node 12. The stresses were after the maximum stress position decreased gradually when the load was moving away. When the application point of the load was at the position of the submodel the stresses turned zero.

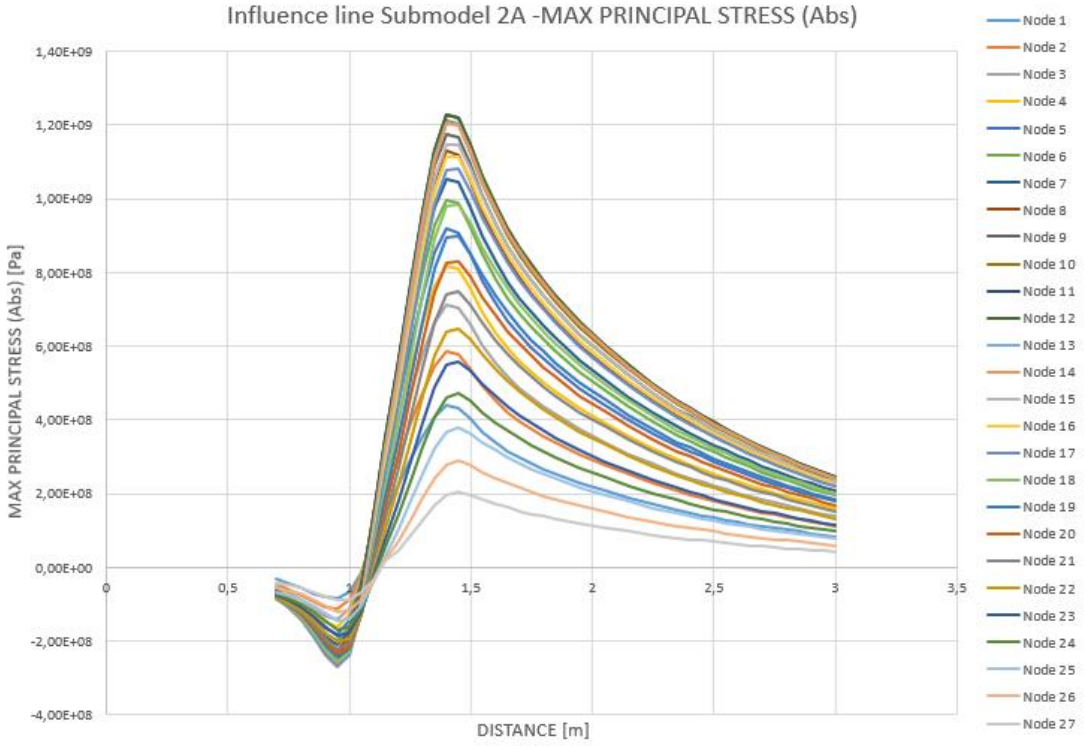

Graph 7.3 Influence line Submodel 2A – Max principal stress (Abs).

7.2.2 Submodel 2B

The influence lines representing the behaviour of the stress variation of Submodel 2B is presented in Graph 7.4. It is possible to see the mirroring behaviour and plots compared with the influence lines of Submodel 2A. The maximum stress affecting the submodel was localized in load step 1.45 m. Submodel 2A and 2B showed thus similarities with the highest stress components almost in the same load step. The stress was localized in node 12, the same as in Submodel 2A, as a compression stress of 1233 MPa. When the load was applied to the left of the support, the submodel was affected of tension but not in the same magnitude as the critical compression stress.

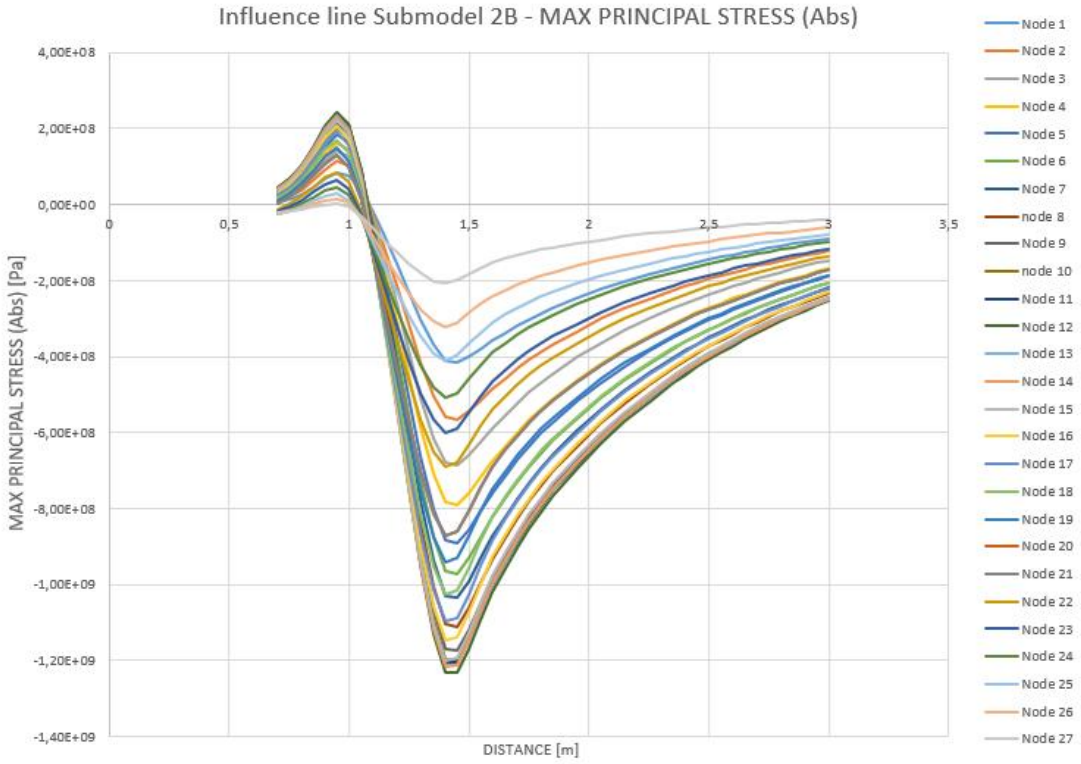

Graph 7.4 Influence line Submodel 2B – Max principal stress (Abs).

7.2.3 Crack initiation point of Submodel 2

The highest stress concentration was observed at node 12 for both Submodel 2A and 2B. The magnitude of the maximum stresses was almost the same, thus in tension for Submodel 2A and compression for Submodel 2B. The estimated crack initiation points at the weld detail are presented in Figure 7.2.

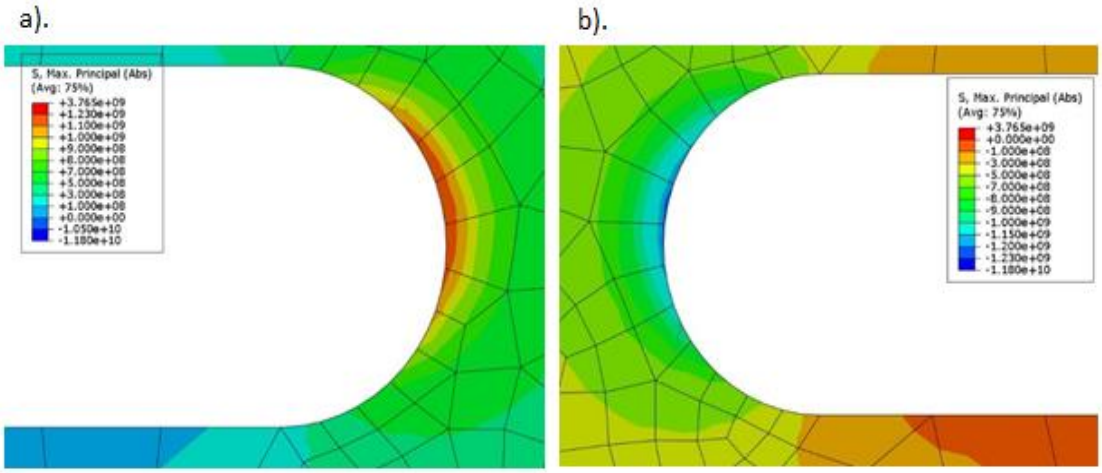

Figure 7.2 Crack initiation points for Submodel 2 a). Submodel 2A at step 1.4 m b) Submodel 2B at step 1.45 m.

7.3 Submodel 3

7.3.1 Submodel 3A

The model was exposed to both tension and compression. The maximum stress was observed at load step 3 m i.e. the middle of the deck. The compression was of a magnitude of 1461 MPa and was obtained at node 22, i.e. in the lower edge of the U-shape. Zero stress was observed at two locations; when the load was applied at the support all nodes are exposed to zero stress. Node 7-27 was affected by no stress again at step 2.7-3, depending on which node that was observed. The maximum tension was observed at load step 2.55 m, but with a lower magnitude than the compression, see Graph 7.5.

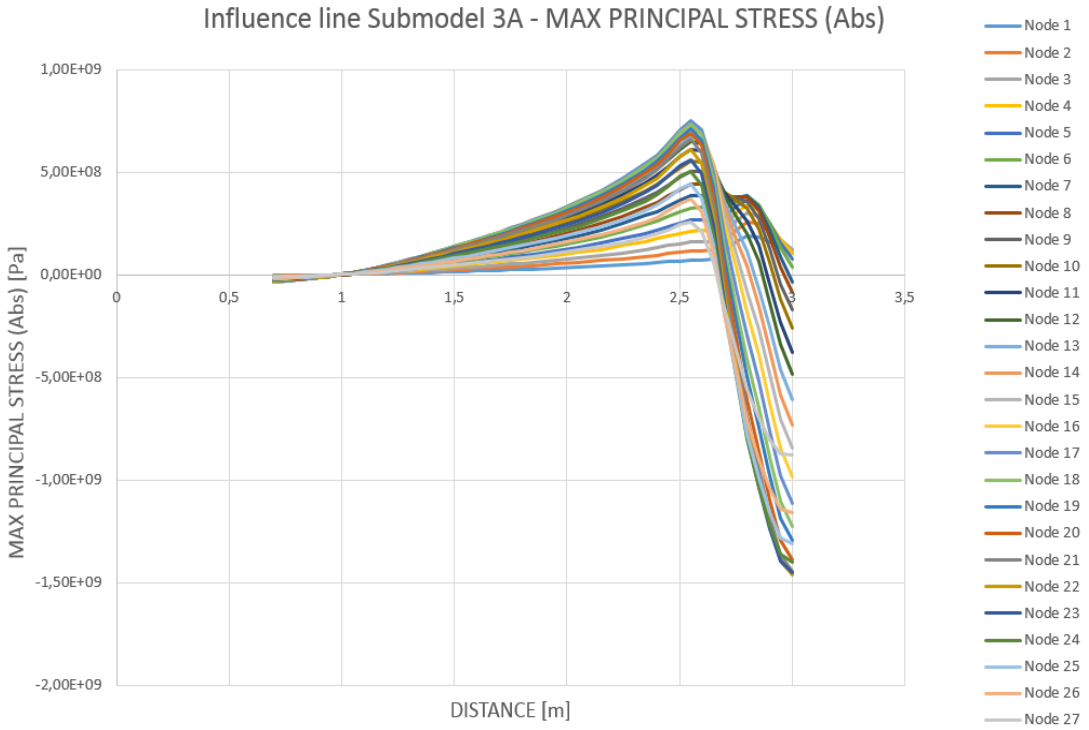

Graph 7.5 Influence line Submodel 3A – Max principal stress (Abs).

7.3.2 Submodel 3B

As for Submodel 3A, the highest stress was compressive, see Graph 7.6. The maximum compression was obtained at node 23 at load step 2.85 with a magnitude of 1456 MPa. The behaviour of the nodes at the upper edge of the U-shape differs from the node in the lower edge when the load was moving towards the middle of the deck. Node 14-27 was only exposed to compression and showed maximum compression in load step 2.85. However, node 1-13 had the largest compression in load step 2.6 and for increased load steps the compression was decreased and turned to tension.

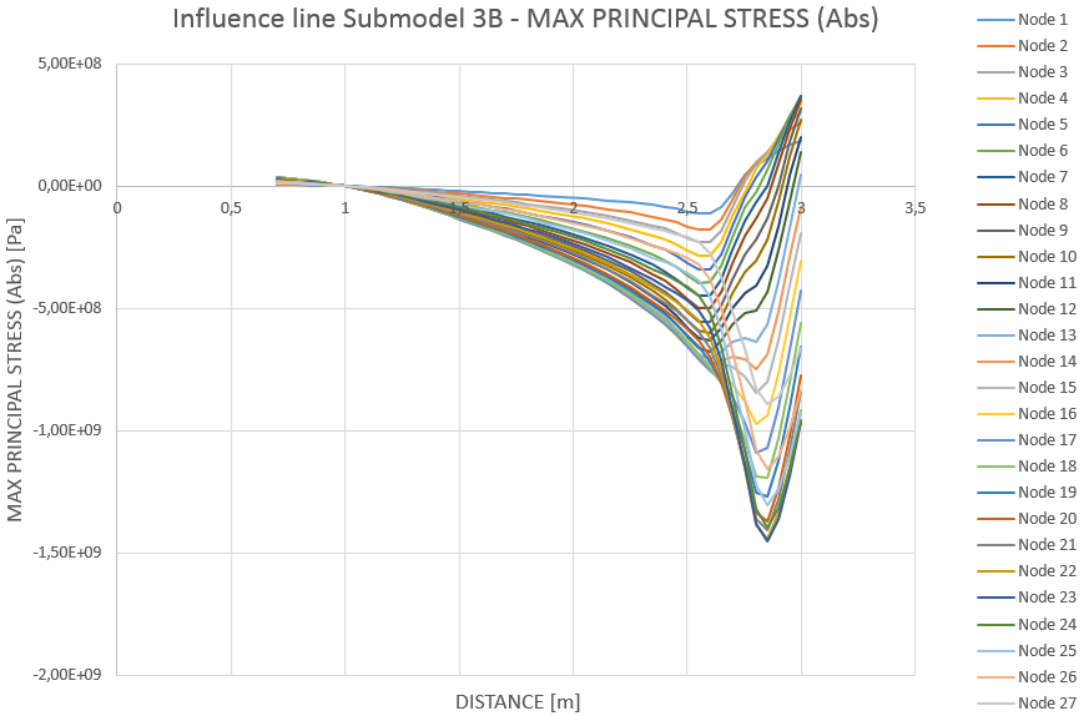

Graph 7.6 Influence line Submodel 3B – Max principal stress (Abs).

7.3.3 Crack initiation point for Submodel 3

The crack initiation point was expected in two adjacent nodes, node 22 and node 23 for Submodel 3A and 3B respectively. The difference in magnitude of maximum stresses for Submodel 3A and 3B, was less than one percent and it was therefore hard to identify the more critical crack initiation point in Submodel 3.

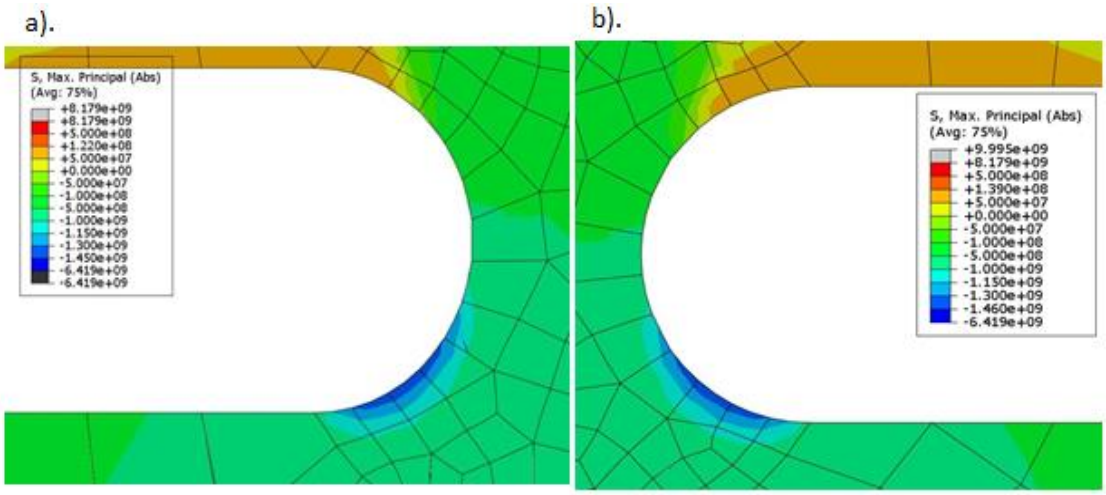

Figure 7.3 Crack initiation points for Submodel 3 a). Submodel 3A at step 3 m b) Submodel 3B at step 2.85 m.

7.4 Submodel 4

7.4.1 Submodel 4A

The critical stress component for Submodel 4A was compressive, which was the main stress component for the nodes. However, small tensile stresses between load step 0.7-1 and load step 3 was detected. All nodes showed similar behaviour and had largest compression at load step 2.75. When the load moved further towards the middle the plots showed a sharp upward behaviour with rapid decreasing compression. The maximum stress was 803 MPa and was obtained in node 12.

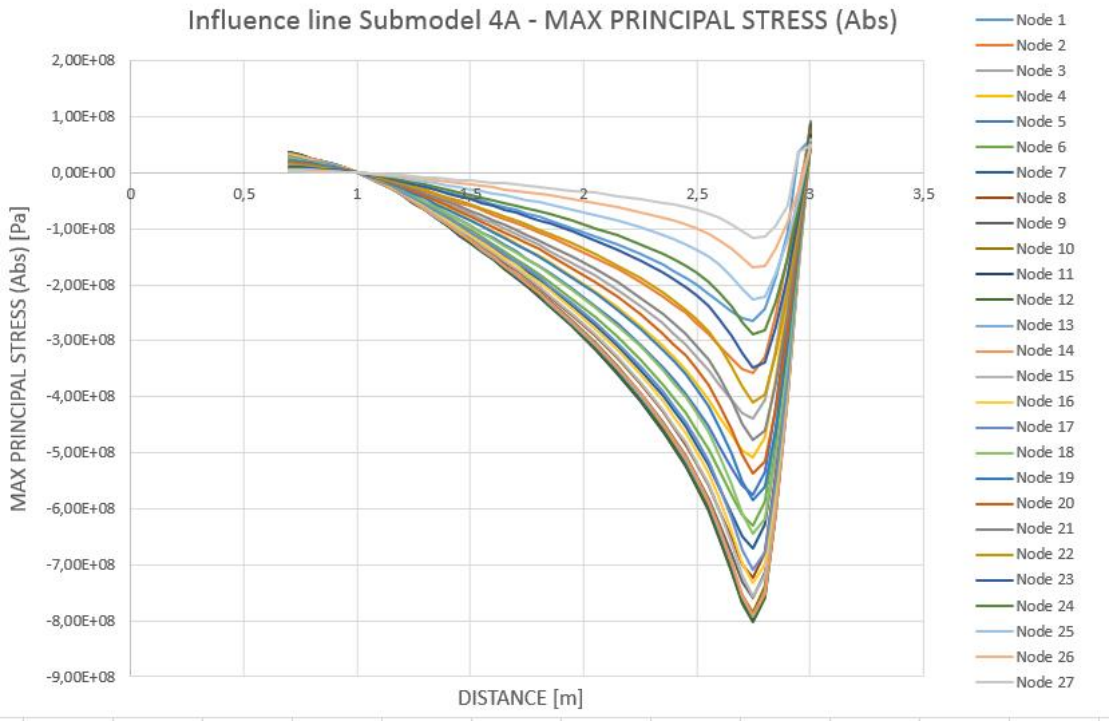

Graph 7.7 Influence line Submodel 4A – Max principal stress (Abs).

7.4.2 Submodel 4B

The influence lines of Submodel 4B was a mirroring of the influence lines representing Submodel 4A, see Graph 7.8. The critical stress component was tensile, and the maximum stress has a magnitude of 813 MPa and was detected in node 12 at load step 2.75.

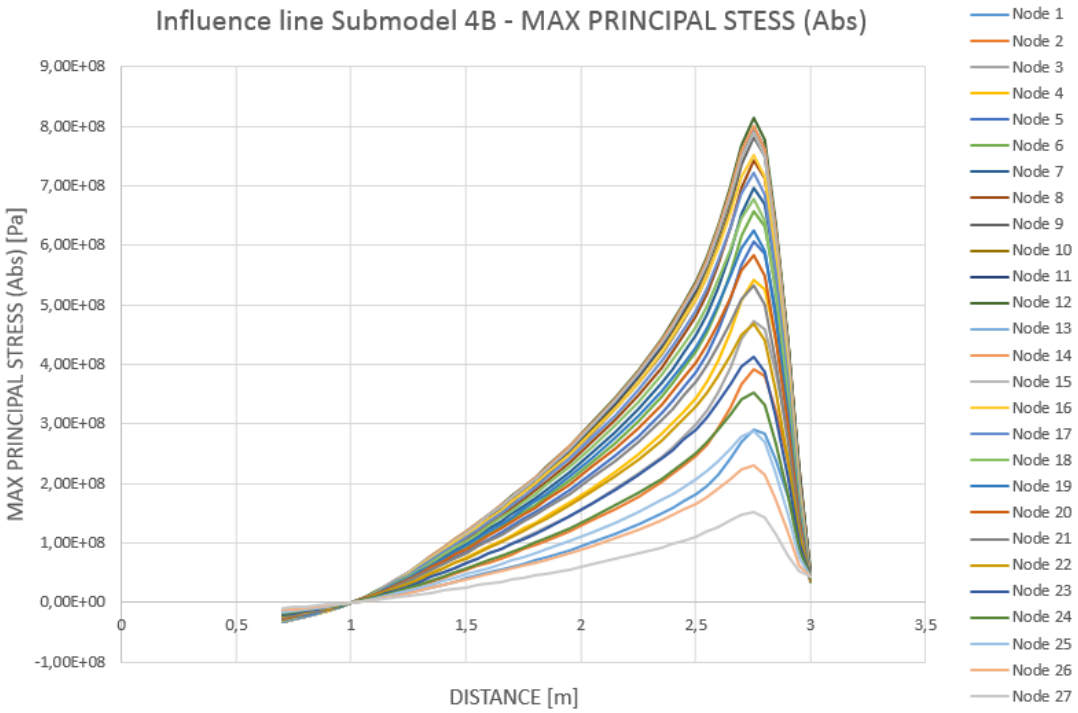

Graph 7.8 Influence line Submodel 4B – Max principal stress (Abs).

7.4.3 Crack initiation point

The maximum stress was observed in node 12 for both Submodel 4A and 4B, thus 4A was subjected to compression and 4B for tension at the critical stress point. Node 12 is almost in the centre of the U-shapes and the expected crack location is presented in Figure 7.4. The magnitude of the maximum stresses did not differ much for the U-shapes. The load step was the same for both maximum values.

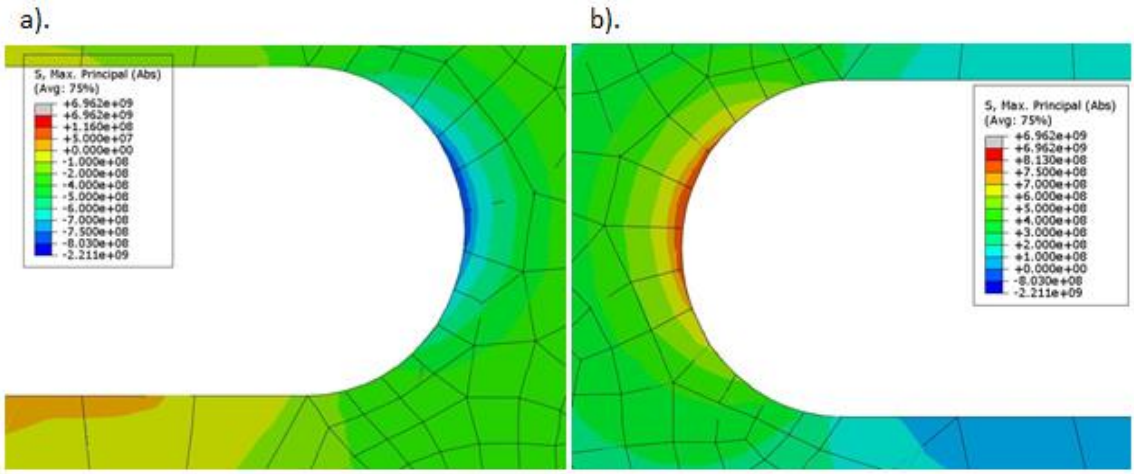

Figure 7.4 Submodel 4 a). Maximum stress for Submodel 4A at step 2.75 b) Maximum stress for Submodel 4B at step 2.75.

7.5 Governing load effects for fatigue failure

When starting the fatigue analysis of the deck the maximum stress was assumed to be obtained in the submodels placed at the upper plate, Submodel 1 or 3. The submodels were affected both by global and local load effects while the Submodel 2 and 4 were only affected by global effects. The local load effects were assumed to increase the stress concentration at Submodel 1 and 3 and thus create the largest stress concentrations. However, which model that would show the highest stress of Submodel 1 and 3 was difficult to predict before the analysis. The submodels were assumed to be affected by both shear force and bending, though, which load effect that would give greatest impact on the stress concentration was hard to foresee. Additionally, the submodels placed close to the support would show large impact due to the support reactions.

7.5.1 Global effects

The analysis of the result indicated that the global bending did not have any significant effect on the stresses at the weld region. No bending moment driven stresses was see in the influence lines for the different submodels. However, the global shear had a large effect on the stress concentration in the weld.

As explained in Section 2.1.3, the corrugated core was exposed to compression and tension as a result from the global shear. The weld details are therefore affected by these two counteracted shear forces that create a local moment in the weld region. The analysis of the influence lines showed this behaviour for the submodels. Figure 7.5 presents an idealization of the behaviour of the Submodel 1 and 3. It was found, as explained in the picture, that both tension and compression were acting in the web when the load was positioned between the submodels. The weld region for the submodels adopted overall the same stress as in the adjacent web part. So, Submodel 1A and 3B were subjected to compression while Submodel 1B and 3A were subjected to tension. For submodel 2 and 4 the behaviour was in similar way, with Submodel 2B and 4A exposed to compression whereas Submodel 2A and 4B were subjected to tension.

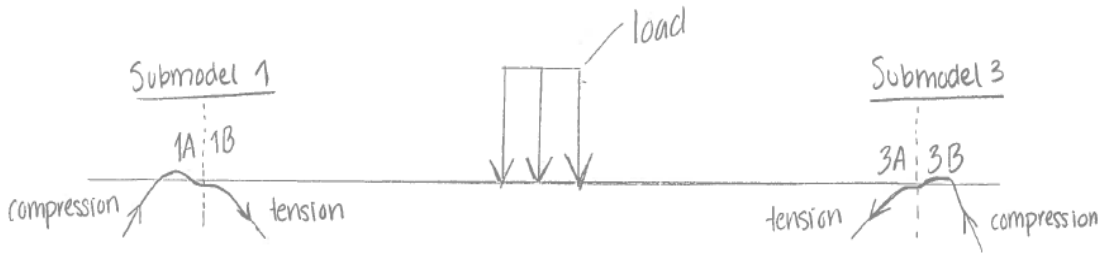

Figure 7.5 The behavior and the similarities of the different submodels.

In submodel 2 and 4, mainly this global effect contributed to the notch stress in the weld. When comparing the influence lines for the submodels with the influence lines representing the shear force, for the positions of the submodels, a clear similarity was presented. In Figure 7.6-7 a comparison of the influence lines of Submodel 2A, 4A and the shear force influence lines are presented, and the similarity is obvious. Remember that the influence lines of the submodels only represent the load steps until the middle of the deck. In other words, the stress component that has the greatest effect on the welds connecting the bottom plate with the core is the global shear.

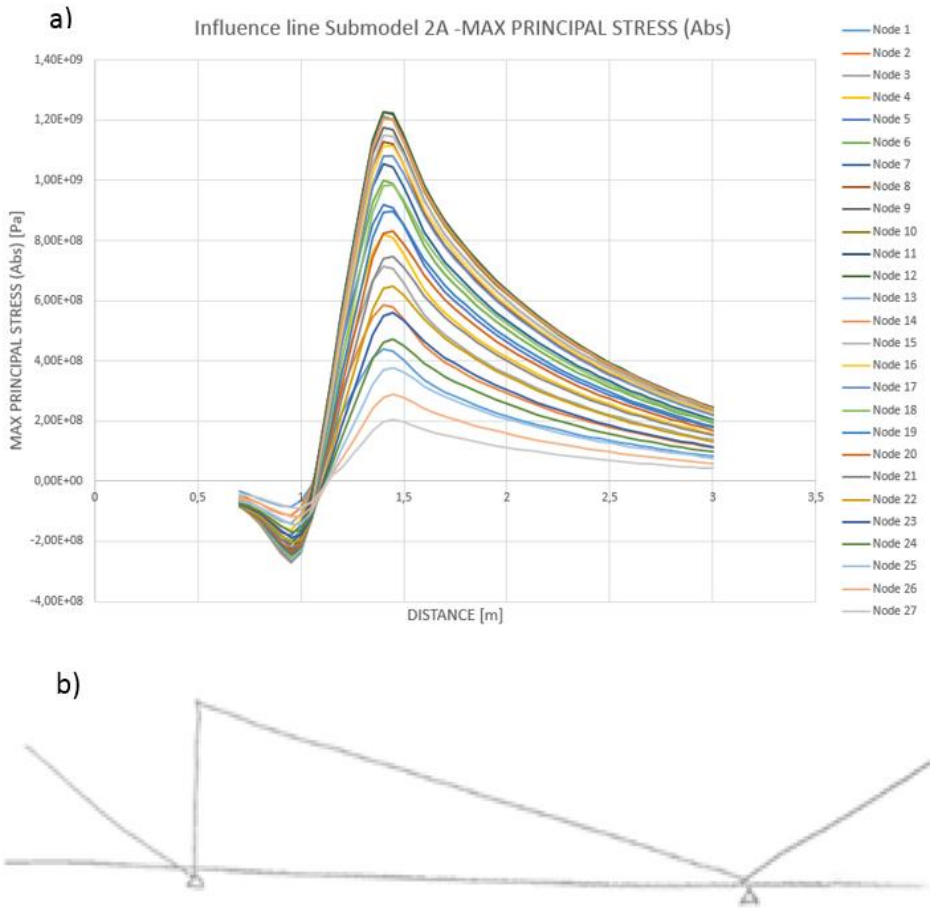

Figure 7.6 Comparing Submodel 2 with influence line representing shear force a) Submodel 2A b) Influence line representing shear force.

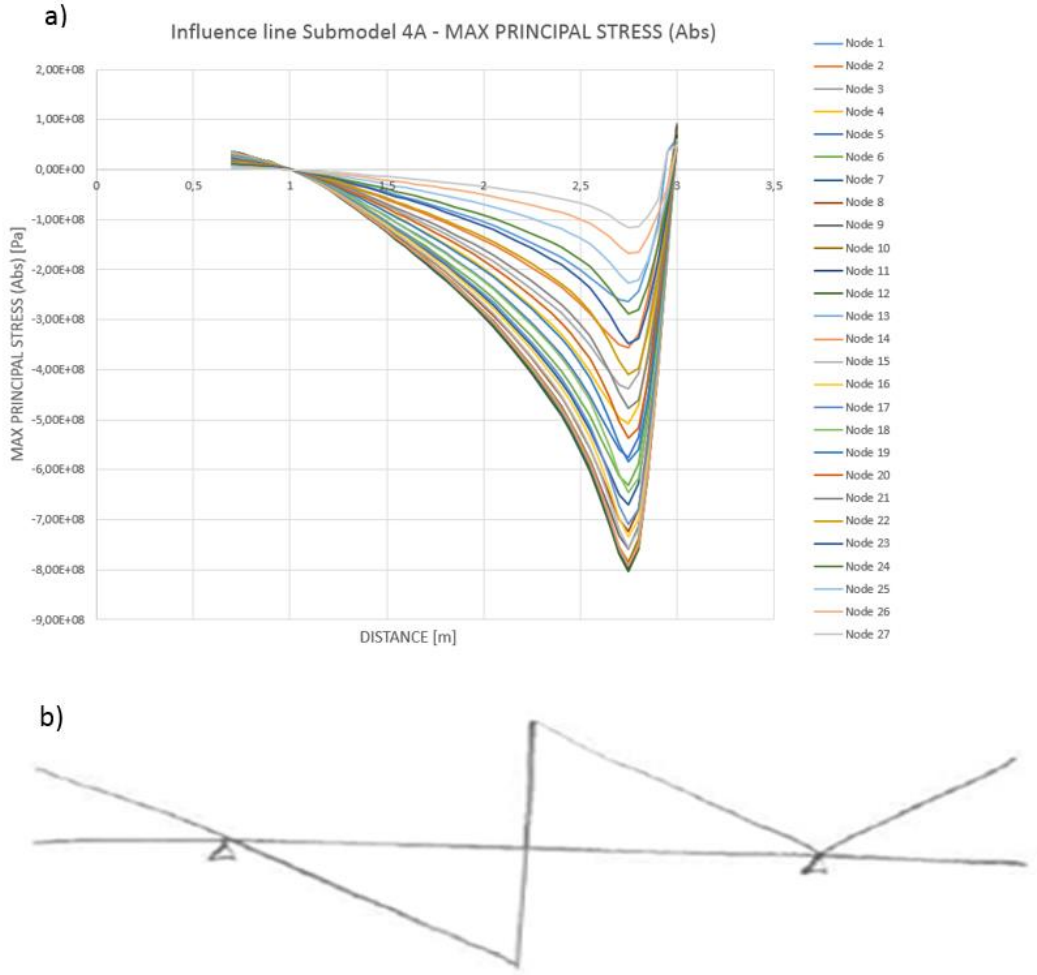

Figure 7.7 Comparing Submodel 4 with influence line representing shear force a) Submodel 4A b) Influence line representing shear force.

Additionally, the influence lines of the submodel 2 and 4 showed that the maximum stresses were obtained when the load was applied between 200-250 mm from the submodels. Meaning that the load had one edge on the position of the submodel i.e. the load applied on half the submodel, see Figure 7.8. These load application points give rise to the highest shear stress that these submodels can be exposed to.

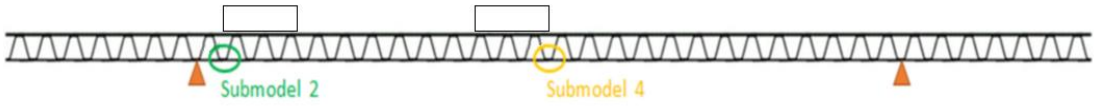

Figure 7.8 Load position contributing to the maximum stress in submodel 2 and 4.

Furthermore, the maximum stress for both the Submodel 2 and 4 was observed in node 12, i.e. in the middle of the U-shapes. This node will always be effected by highest shear stress if the weld is only effected by global load effects. Figure 7.9, show an illustration of the stress behaviour in the weld region and how the shear stress is changing and reaches the maximum magnitude in the position of node 12.

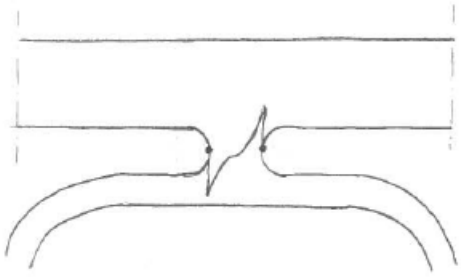

Figure 7.9 The shear stress behaviour at the weld region in Submodel 2 and 4.

Analysing Submodel 1 and 3 it was detected that the maximum stresses in these models were of higher magnitude than the maximum stresses in Submodel 2 and 4, which thus confirmed the assumption that the submodels placed at the upper face panel were more critical due to additional local load effects.

Submodel 1 and 3 showed similar behaviour as observed for Submodel 2 and 4, shear being the governing global parameter. Again, the stress variation showed large similarities with the influence lines representing shear force, see Figure 7.10. However, there were some exceptions where local effect showed large impact on the influence lines of Submodel 1 and 3, see Section 7.5.2. It was also observed that the U-shapes in Submodel 1 were connected in the way of how the values in the nodes were changing. In other words, the nodes at the upper edge in Submodel 1A reached their maximum stress concentration in the same load step as the nodes at the lower edge in Submodel 1B, and vice versa.

Moreover, for the last load steps for Submodel 3 a decreased stress concentration was seen. The decreased shear force at this location can be one explanation, see Figure 7.10 for the comparison with the shear force diagram.

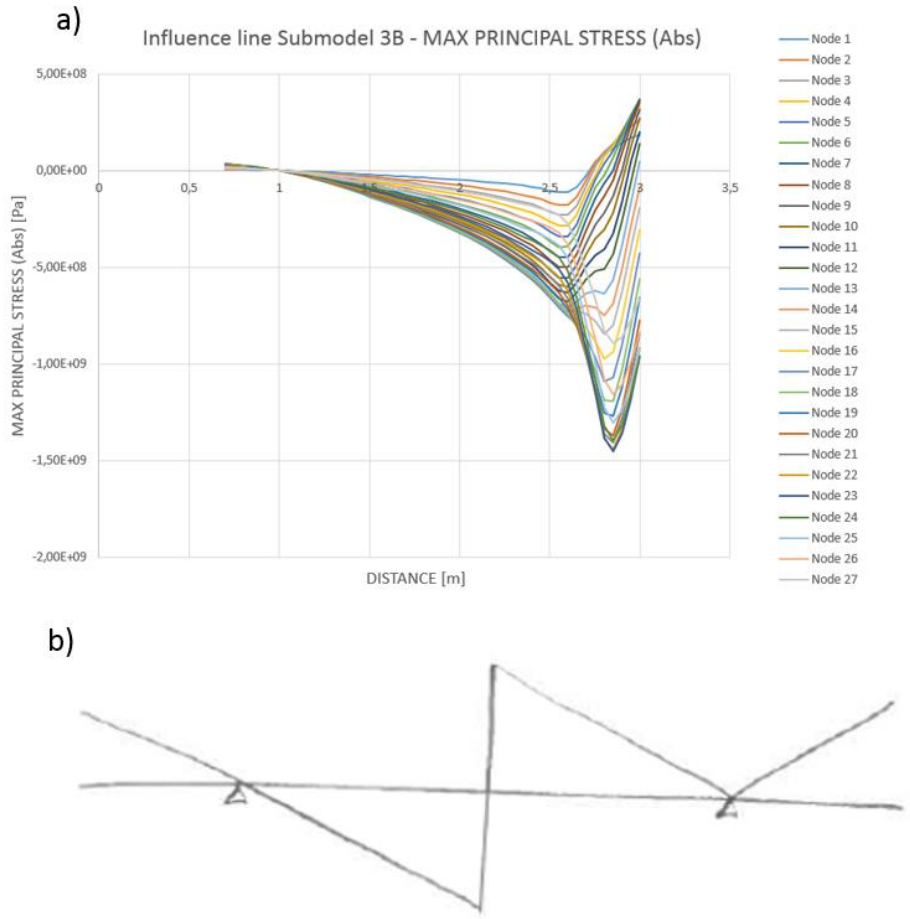

Figure 7.10 Comparison of Submodel 3B and shear force a) Influence lines Submodel 3B b) Influence lines of shear force.

Common for all comparisons between the influence lines of the submodels with the influence lines representing global moment and shear force, were that the positions for maximum and zero stresses was placed with some offset from the expected positions. The influence lines representing global moment and shear force, that were used for the analysis, was based on a moving point load while the real analysis involved a load with an application area of 400x400 mm. Due to the increased application area specific characteristic points i.e. maximum load, was positioned with some offset.

7.5.2 Local effects

As mentioned, the local load effects showed a large impact on the stress concentration in the upper welds, i.e. in Submodel 1 and 3. Overall the influence lines showed similar behaviour as the shear force but when the load was moving towards the submodels the impact of local load effects was clear. To investigate this a comparison of the stress concentration around the welds for Submodel 1A and 2B were done. And as can be seen in Figure 7.11 , when the load is far from the submodels, both welds experience the same stress as a result from the global shear, while when the load are close to the submodels the lower part of the U-shape for Submodel 1 experience a high compressive force. Therefore, lowering the position of the crack initiation point. And the same behaviour can be seen comparing submodel 3 and 4 as well.

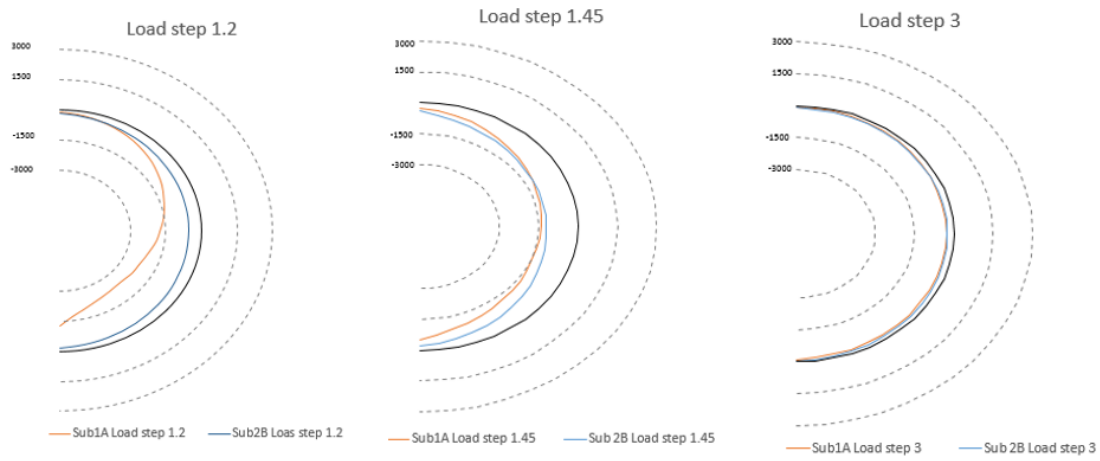

Figure 7.11 *Comparison of stress concentration around the weld for submodel 1A and 2B*

As illustrated in Figure 7.12, maximum local load effects were observed when the centre of the load surface was in the middle of two corrugations closest to the submodel. In the figure the effect on Submodel 1 is described. Analysing the local effect the upper plate can be seen as a beam supported on several supports i.e. the welds. The weld regions are therefore affected by maximum local compression forces which are affecting the lower nodes in the U-shape where compression was substantially increased. At the described load step maximum local load effects were observed for Submodel 1A, while Submodel 1B was affected by largest local effects when the load was applied between two corrugations but on the left side of the submodel. Submodel 3 showed the same behaviour but mirrored. However, if the load would have been a patch load the local load effects would have been increased significantly.

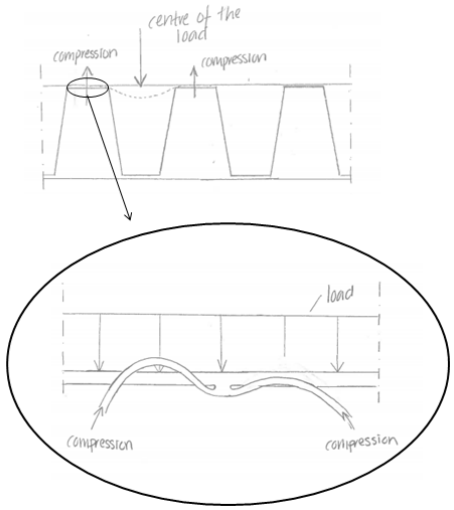

Figure 7.12 *Illustration of the behaviour of the submodels when affected by the highest local load effect. The deformation in the illustration is not reality based, it is greatly magnified to improve the understanding of the behavior.*

Submodel 1A and 3B were mainly affected by compression. Global shear force and maximum local load effects where both creating compression at the weld region and

contributed therefore to the maximum stress concentrations for Submodel 1A and 3B at the location with maximum local load effect.

In contrast, Submodel 1B and 3A was mainly affected by tension and the local load effect contributed with compression and was thus counteracting the tension in the lower nodes in the U-shapes, see Figure 7.13. The local effects in Submodel 1B are the main reason of the visible differences compared with the influence line of shear force. As mentioned in the previous section, the change of the stress variation in Submodel 3 at the last load step are the decrease in global shear. However, after analysing the local load effect it was detected that the local compression was adding to the stress magnitude.

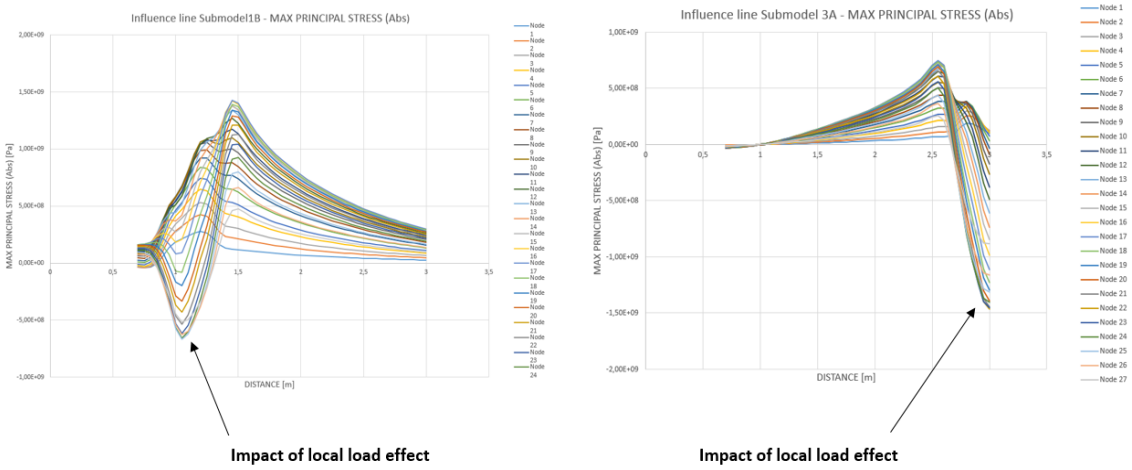

Figure 7.13 Impact of local load effects a) Submodel 1B b) Submodel 3A.

7.6 The most critical weld detail

The most critical detail was decided by investigating and comparing maximum stress concentrations of each submodel. A summary of the most critical stresses for the different submodels is presented in Table 7.1. The highest stress was obtained in Submodel 1A as compression with a magnitude of 2366 MPa.

Table 7.1 Maximum stresses for each submodel.

Submodel		**Maximum stress** [MPa]	**Step – max stress** [m]	**Node**
1	A	2366 (compression)	1.2	21
	B	1429 (tension)	1.45	17
2	A	1227 (tension)	1.4	12
	B	1233 (compression)	1.45	12
3	A	1462 (compression)	3	22
	B	1456 (compression)	2.85	23
4	A	803 (compression)	2.75	12
	B	813 (tension)	2.75	12

Submodel 1 showed the maximum stress concentration at the left U-shape, however the right U-shape also showed the highest tension. The submodel was placed close to the support causing high global shear stress which was one explanation of the high stress concentration in Submodel 1. It was also clear that the local load effects had impact on the model and contributed to the largely increased values of the stresses when the load was moving towards the submodel. Due to the large stress concentration observed at the position of the support, it might be advantageously to create a local design solution. For example, stiffeners can be added or increased thickness of the upper and lower face panel is another suggestion. These design proposals will contribute to higher stiffness in the area of the support and thus reduce the stress concentrations at the weld details.

7.7 The fatigue life of the SSD

With the most critical stress concentration identified it was of great interest to investigate the fatigue life of the SSD. By implementing IIW:s recommended fatigue strength FAT 630, for weld details with plate thickness smaller than 5 mm, and a slope of m=3, the fatigue life of the SSD was determined according to the equation:

$$N_t = N_0 * \left(\frac{C}{\sigma_r}\right)^m$$

The calculation showed that fatigue cracks would be developed after 37745 load cycles. The obtained stresses during the fatigue analysis were overall of large magnitude. Consequently, the analysis indicated that fatigue will be the critical aspect for SSD and govern the design of the structure. Especially, when studies regarding local and global deflection and buckling has been conducted in earlier studies, with the same dimensions of the deck, and resulted in sufficient strength and resistance. Consequently, the dimensions need to be increased so that the deck can withstand the large magnitude of the stresses and be applicable in bridge structures. It might also be advantageously to increase the amount of weld strings at each weld region. The deck that was analyzed in this thesis was modelled with one weld string at each weld detail. By increasing the amount the local moment in the weld region will be deceased due to decreased local shear forces.

7.8 General comments regarding PART 2

The models used in the analysis were not created with contact interaction between the plates i.e. between the web and the upper and lower panel. If interaction would have been included, the web would have created an extra support for the upper panel during deformation. That modelling method might contribute to decreased deformation and stresses. However, the analysis produced in the Master´s thesis did not investigate the differences in result and how much that would affect the results.

In this analysis the fatigue behaviour has been investigated by comparing maximum stress concentrations obtained at influence lines representing critical weld regions in the deck. The most critical position was determined by deciding which node at the U-shapes was that affected by the highest stress concentration. However, the fatigue analysis could also have been done by investigating which influence line that was affected by the highest load over longest distance i.e. the integral of the plotted values. The influence line with the highest value of the integral would then be the most critical

detail for fatigue, see a simplified illustration of the different methods and a comparison of the two different techniques in Figure 7.14.

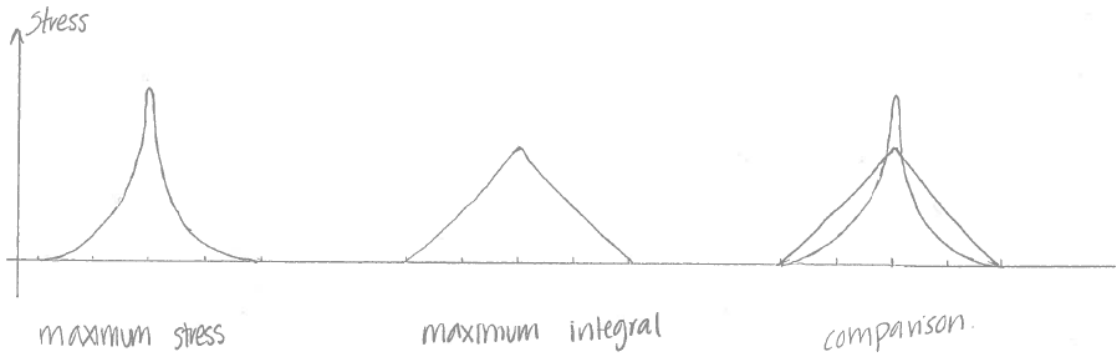

Figure 7.14 Different fatigue analysis methods and a comparison of these.

8 Conclusions

- The majority of the exanimated fatigue tests pointed to an increased slope m in the SN-curve. Thus, a higher slope might be more representative when analyzing the fatigue strength of hybrid laser arc welds.

- A slightly higher fatigue strength for hybrid laser welds was detected in the study of the fatigue strength, compared with the conventional welding techniques.

- Due to idealizations and poor test documentations the analysis results displayed a large scatter and pointed out uncertainties in the results. Therefore, more fatigue tests and further studies regarding the design strength of hybrid laser welds need to be conducted to determine a reliable design strength.

- Fatigue is a very important design parameter for SSD. The deck had in earlier studies showed sufficient resistance against bending and buckling but during the fatigue analysis high stress concentrations at the weld regions were observed and would thus be the dimensioning factor of SSD.

- The most critical weld detail, i.e. the position of the highest stress concentration, was detected in the upper plate in the weld region closest to the support, in the lower part of the left U-shape.

- The load effects that govern the critical stress concentration in the most critical weld detail were the compressive component coming from the global shear force together with a local compressive force.

- The most critical load position was attained when the loadcentre was applied with a distance of 2p/2 to the right of the weld region. This load position contributed to compression forces of both the local and global load effect.

- The welds in the lower plate showed constantly lower stress concentrations than the welds in the upper plate.

8.1 Suggestions for future work

- It is of large interest to investigate how different geometrical configurations of the cross-section would affect the fatigue behaviour of the deck. Therefore, a parametric study would be of interest.

- To be able to determine a reliable fatigue strength of hybrid laser welds more fatigue tests need to be done.

- Large stress concentrations were attained close to the support, therefore, it would be of interest to investigate local solutions for that area.

- In this research only steel sandwich decks with one weld string at each weld region were investigated. Since the welds experience very large stress concentrations it would be of interest to study steel sandwich decks with two parallel strings.

9 References

Abbott, S.P., Systems, P.L. & Caccese, V., 2007. Automated Laser Welded High Performance Steel Sandwich Bridge Deck Development. , pp.1–17.

Alam, M.M. et al., 2009. Fatigue Behaviour Study of Laser Hybrid Welded Eccentric Fillet Joints – Part I. *12th NOLAMP proceeding 2009 : Nordic Laser Materials Processing Conference*, pp.1–29.

Alam, M.M., 2012. *Laser welding and cladding : The effects of defects on fatigue behaviour*. Luleå University of Technology.

Al-Emrani, M. & Aygül, M., 2014. *Fatigue design of steel and composite bridges*, Göteborg.

Al-Emrani, M. & Åkesson, B., 2013. *Steel Structures*, Göteborg: Chalmers university of technology.

Alwan, U. & Järve, D., 2012. *New Concept for Industrial Bridge Construction*. Chalmers University of Technology.

Barsoum, Z., 2008. *Residual stress analysis and fatigue assessment of welded steel structures*. Kunglig Tekniska Högskolan. Available at: http://www.diva-portal.org/smash/record.jsf?pid=diva2:13428.

Bright, S.R. & Smith, J.W., 2007. A new design for steel bridge decks using laser fabrication. *The Structural Engineer*, 85(21), pp.49–57.

Bright, S.R. & Smith, J.W., 2004. Fatigue performance of laser-welded steel bridge decks. *The Structural Engineer*, 82(21), pp.31–39.

Caccese, V. et al., 2006. Effect of weld geometric profile on fatigue life of cruciform welds made by laser/GMAW processes. *Marine Structures*, 19, pp.1–22.

Classle, 2009. Crystal defects. Available at: https://www.classle.net/book/crystal-defects [Accessed February 5, 2015].

Enginsoft, 2014. Expert system for optimization of bridge orthotropic deck plates. Available at: http://www.enginsoft.it/applications/civil_engineering/bridge.html [Accessed January 29, 2015].

Fricke, W., 2012. *IIW Recommendations for the Fatigue Assessment of Welded Structures By Notch Stress Analysis : IIW-2006-09*, Cambridge: Woodhead Publishing Limited.

Frostevarg, J., 2014. *The Morphology of Laser Arc Hybrid Welds*. Luleå University of Technology.

Haghani, R., Al-Emrani, M. & Heshmati, M., 2012. Fatigue-Prone Details in Steel Bridges. *Buildings*, 2, pp.456–476. Available at: http://www.mdpi.com/2075-5309/2/4/456/.

Heshmati, M., 2012. *Fatigue Life Assessment of Bridge Details Using Finite Element Method*. Chalmers University of Technology.

Ionix, 2015. Hybrid laser welding. Available at: http://ionix.fi/en/technologies/laser-processing/hybrid-laser-welding/ [Accessed February 21, 2015].

Kainuma, S. & Mori, T., 2008. A study on fatigue crack initiation point of load-carrying fillet welded cruciform joints. *International Journal of Fatigue*, 30, pp.1669–1677.

Kihl, DP, 2002. *Fatigue strength of HSLA-65 weldments*, Naval Surface Warfare Center-Carderock Division.

Kozak, J., 2005. *Strength tests of steel sandwich panel*. Gdansk University of Technology.

Kujala, P. & Klanac, A., 2005. Steel sandwich panels in marine applications. *Brodogradnja*, 56, pp.305–314.

MAST, Scientific Principles. Available at: http://matse1.matse.illinois.edu/metals/prin.html [Accessed February 5, 2015].

Munse, W. et al., 1983. *Fatigue characterization of fabricated ship details for design*, Springfield.

Narimani, H., 2008. *Fatigue Strength of Laserhybridwelded High Strength Steel*. Luleå University of Technology.

NDT Resource Center, Linear Defects - Dislocations. Available at: https://www.nde-ed.org/EducationResources/CommunityCollege/Materials/Structure/linear_defects.htm [Accessed February 5, 2015].

Remes, H. & Varsta, P., 2010. Statistics of Weld Geometry for Laser-Hybrid Welded Joints and its Application within Notch Stress Approach. *Welding in the World*, 54, pp.R189–R207. Available at: http://link.springer.com/10.1007/BF03263505.

Romanoff, J. & Varsta, P., 2007. Bending response of web-core sandwich plates. *Composite Structures*, 81, pp.292–302.

Sandwich.balport, Sandwich.balport:home. Available at: http://sandwich.balport.com/index1.html [Accessed February 4, 2015].

TWI, 2015. Schenectady T2 tanker. Available at: http://www.google.com/imgres?imgurl=http://www.twi-global.com/EasysiteWeb/getresource.axd%253FAssetID%253D11017%2526type%253Dfull%2526servicetype%253DInline&imgrefurl=http://www.twi-

global.com/news-events/case-studies/schenectady-t2-tanker-165/&h=290&w=38 [Accessed February 4, 2015].

Welding design & fabrication, 2008. Design Implications of Sandwich Panels. Available at: http://weldingdesign.com/news/design-implications-sandwich-panels [Accessed January 29, 2015].

Victor, B.M., 2011. Hybrid Laser Arc Welding. *ASM Handbook*, 6A(Welding Fundamnetals and Processes), pp.321 – 328.

Appendix

Appendix A – Building of SN-curve

Appendix B – Calculation of nominal stress

Appendix C – Convergence study of the 3D model

Appendix D – Verification of submodels

Appendix E – Fatigue analysis of SSD

Appendix A - Building of SN-curve

With the ambition of investigate and decide the fatigue strength of hybrid laser welds a SN-curve was created. SN-curves present the fatigue life of details and are in this study based on results in terms of effective notch stresses in relation to number of cycles until failure.

A SN-curve represents the fatigue life of a detail or specimen. Normally, SN-curves are based on fatigue tests result in terms of stress range in relation to number of cycles to failure. The results are plotted in a log-log graph, with the stress range on the vertical axis and number of cycle on the horizontal axis. The plotted values shows mostly high scatter but by doing a statistical analysis a mean value of the plotted values can be decided. The result becomes a line which presents the mean fatigue strength of the specimen. Furthermore, to be able to use the curve for design a safety margin needs to be considered, this is accomplished by considering standard deviation. The fatigue strength of the detail is determined of the stress range received at 2 million cycles.

It is possible to read the number of cycles a structure can withstand for different stress ranges. However, it is also possible to calculate the number of cycles as well, see equation 1.

$$\log\left(\frac{N}{N_0}\right) = \log(C) - m * \log(\sigma_r) \quad \rightarrow \quad N_t = N_0 * \left(\frac{C}{\sigma_r}\right)^m \qquad (1)$$

A slope constant of m=3 is conventionally used for welded details since it have proven to best fit a large numbers of structural details. From the fatigue test data a mean linear regression analysis can alternatively be carried out, calculating a m-value assuming a straight line of the SN-curve. This is the natural slope and is calculated according to the equation below.

$$m_{natural} = \frac{n.\sum(logN.log\sigma_r) - \sum logN.\sum log\sigma_r}{(\sum log\sigma_r)^2 - n.\sum(log\sigma_r)^2} \qquad (2)$$

Normally, SN-curves represents only one specific detail. However, in this study was the effective notch stress method used which enabled to create one curve even if different specimens were used. The SN-curve was built by using test results from old fatigue tests. Four old fatigue tests were found and the specimens from the tests were modelled in ABAQUS. The specimens were created with dimensions according to the documentation but the weld regions were created as idealizations according to the effective notch stress method. The region of the anticipated crack initiations, the weld toe and root, was modeled with a fictitious radius to avoid stress singularities and receiving a functional convergent stress value.

The documentation regarding the old fatigue tests involved test trials at different stress ranges. For each stress range presented in the documentation a related effective notch stress was decided. The notch stress was observed either at the weld toe or root. The value of number of cycles was kept for the related notch stress. The SN-curve was built by plotting the effective notch stress in relation to number of cycles. In total four specimens were investigated, for each specimen one separate SN-curve was created. Finally, one SN-curve involving all tests was conducted and from that curve was the fatigue strength of hybrid laser welds decided.

Construction detail	**Load-carrying cruciform joint**	
Literatur	Effect of weld geometric profile on fatigue life of cruciform welds made by laser/GMAW processes. V.Caccese, P.A. Blomquist, K.A. Berube, S.R. Webber, N.J. Orozco	
Material	Denomination	HSLA-65 steel
	Delivery code	
	Plate thickness	12.7 mm
Mech. properties	$R_{p0,2}$	Mpa
	R_m	MPa
Fabrication	Welding process	Hybrid laser arc welding
	Welding material	---
	Post weld treatment	
Fatigue loading	Stress ration	0 [-]
	Type of loading	sine-wave
	Type of collective	constant amplidute

Sketch and dimension of test specimen and loading

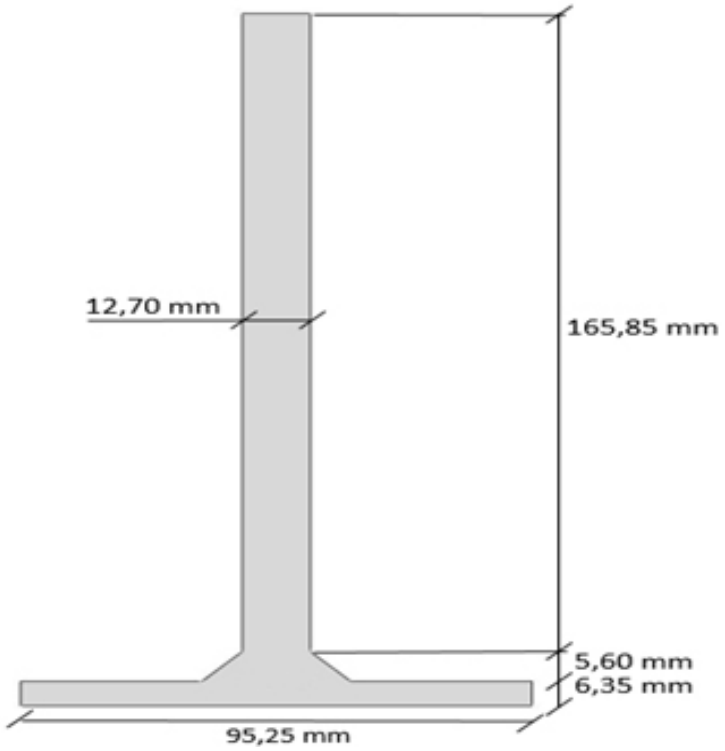

Versuchsergebnisse

n	stress range $\Delta\sigma$	load cycles N	Com. *
1	1241	30 500	1
2	1241	19 700	1
3	1241	21 300	1
4	1241	26 000	1
5	827	179 948	1
6	827	228 982	1
7	827	170 600	1
8	827	118 400	1
9	414	20 000 000	0
10	414	20 000 000	0
11	414	20 000 000	0
12	414	2 658 000	1
13			
14			
15			
16			
17			
18			
19			
20			
21			
22			
23			
24			
25			
26			
27			
28			
29			
30			

Origin and type of fatigue failure

Comments

* use "0" for a run-out that should not be taken into account for the statistical evaluation, "1" elsewhere

S-N curve

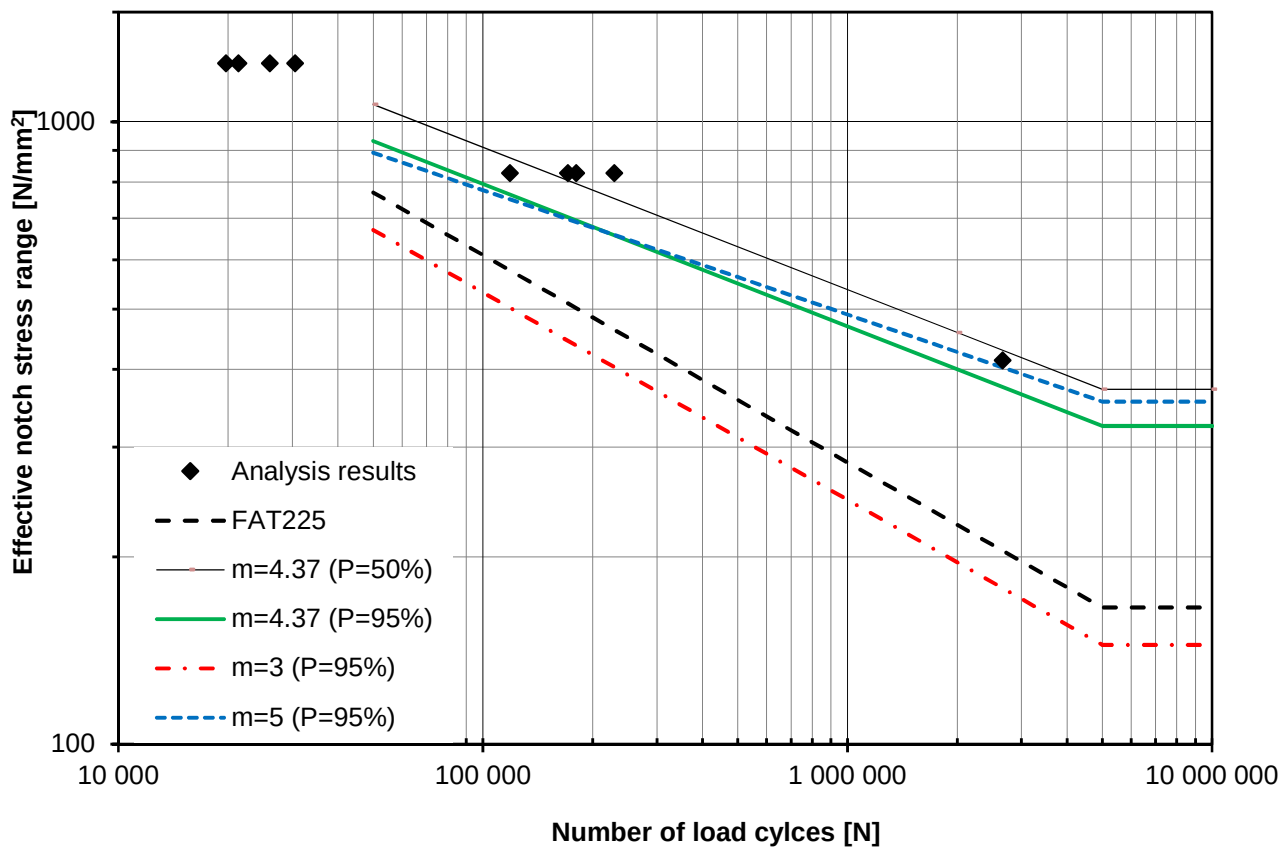

Statistical evaluation of test data according to EN 1993-1-9:2005

slope	mean S-N curve ($P_Ü$ = 50%) $\Delta\sigma_{50\%}$	characteristic S-N curve ($P_Ü$ = 95%) $\Delta\sigma_C$
m = variable = 4,37	**458,5**	**400,2**
m = fix = 3	334,1	195,9
m = fix = 5	500,4	426,4

Statistical evaluation of fatigue test data according to EN 1933-1-9:2005

		m = 4,37	m = 3	m = 5
Coeff. Regression line y = a + m · x :	a	17,929	13,873	19,798
	m	-4,37	-3,00	-5,00
Standard deviation:	s	0,109	0,254	0,152
	xm	2,661	2,524	2,699
	Sxx	0,197		
	Syy	3,838		
	Sxy	-0,860		
f - value:	f	1,572	2,089	1,463
k - value:	t(87.5;n-1)	1,240		
	χ(87.5;n-1)	3,797		
	Gauss(0.95)	1,645		
95%-fractile value of Student-distribution:	t(95)	1,895		
	k	2,801		

n	Δσ	N	y = log(N)	x = log(Δσ)	y^2	x^2	x·y	m = 3 $(y-a-m\cdot x)^2$	m = 5 $(y-a-m\cdot x)^2$
1	1241,2	30 500	4,48	3,09	20,11	9,57	13,87	0,011	0,024
2	1241,2	19 700	4,29	3,09	18,44	9,57	13,29	0,088	0,001
3	1241,2	21 300	4,33	3,09	18,73	9,57	13,39	0,069	0,000
4	1241,2	26 000	4,41	3,09	19,49	9,57	13,66	0,031	0,007
5	827,2	179 948	5,26	2,92	27,62	8,51	15,33	0,018	0,002
6	827,2	228 982	5,36	2,92	28,73	8,51	15,64	0,058	0,023
7	827,2	170 600	5,23	2,92	27,37	8,51	15,26	0,013	0,001
8	827,2	118 400	5,07	2,92	25,74	8,51	14,80	0,002	0,019
9	0	0	0,00	0,00	0,00	0,00	0,00	0,000	0,000
10	0	0	0,00	0,00	0,00	0,00	0,00	0,000	0,000
11	0	0	0,00	0,00	0,00	0,00	0,00	0,000	0,000
12	413,6	2 658 000	6,42	2,62	41,27	6,85	16,81	0,161	0,084
0	0	0	0,00	0,00	0,00	0,00	0,00	0,000	0,000
0	0	0	0,00	0,00	0,00	0,00	0,00	0,000	0,000
0	0	0	0,00	0,00	0,00	0,00	0,00	0,000	0,000
0	0	0	0,00	0,00	0,00	0,00	0,00	0,000	0,000
0	0	0	0,00	0,00	0,00	0,00	0,00	0,000	0,000
0	0	0	0,00	0,00	0,00	0,00	0,00	0,000	0,000
0	0	0	0,00	0,00	0,00	0,00	0,00	0,000	0,000
0	0	0	0,00	0,00	0,00	0,00	0,00	0,000	0,000
0	0	0	0,00	0,00	0,00	0,00	0,00	0,000	0,000
0	0	0	0,00	0,00	0,00	0,00	0,00	0,000	0,000
0	0	0	0,00	0,00	0,00	0,00	0,00	0,000	0,000
0	0	0	0,00	0,00	0,00	0,00	0,00	0,000	0,000
0	0	0	0,00	0,00	0,00	0,00	0,00	0,000	0,000
0	0	0	0,00	0,00	0,00	0,00	0,00	0,000	0,000
0	0	0	0,00	0,00	0,00	0,00	0,00	0,000	0,000
0	0	0	0,00	0,00	0,00	0,00	0,00	0,000	0,000
0	0	0	0,00	0,00	0,00	0,00	0,00	0,000	0,000
0	0	0	0,00	0,00	0,00	0,00	0,00	0,000	0,000
0	0	0	0,00	0,00	0,00	0,00	0,00	0,000	0,000
9		Summe	44,87	26,66	227,51	79,18	132,06	0,45	0,16
		Mittelwert	4,99	2,96	25,28	8,80	14,67	0,05	0,02

Statistical evaluation of fatigue test data according to EN 1933-1-9:2005

		m = 4,37	m = 3	m = 5
50%-fractile	N	$\Delta\sigma_{50\%}$	$\Delta\sigma_{50\%}$	$\Delta\sigma_{50\%}$
(mean S-N curve)	2,0E+06	458,5	334,1	500,4
95%-fractile	N	$\Delta\sigma_C$	$\Delta\sigma_C$	$\Delta\sigma_C$
(Chrakteristic S-N curve)	2,0E+06	400,2	195,9	426,4
	N*	1 104 067	403 299	898 760
	y*	6,043	5,606	5,954
	a	17,671	13,177	19,450
5%-Fraktile	N	$\Delta\sigma_{5\%}$	$\Delta\sigma_{5\%}$	$\Delta\sigma_{5\%}$
(upper 5%-fractile S-N curve)	2,0E+06	525,3	569,7	587,2
	N*	3 622 969	9 918 194	4 450 577
	y*	6,559	6,996	6,648
	a	18,187	14,568	20,145

					225
Wertepaare S-N Kurven	N	Mean value	95%-fractile	5%-fractile	Detail class 225
Variable slope, m = 4,37	5,E+04	1066,6	931,0	1222,0	769,5
	2,E+06	458,5	400,2	525,3	225
	5,E+06	371,8	324,5	425,9	165,8
	1,E+07	371,8	324,5	425,9	165,8
slope m = 3	5,E+04	1142,6	670,0	1948,5	
	2,E+06	334,1	195,9	569,7	
	5,E+06	246,2	144,4	419,8	
	1,E+07	246,2	144,4	419,8	
slope m = 5	5,E+04	1046,5	891,8	1228,0	
	2,E+06	500,4	426,4	587,2	
	5,E+06	416,6	355,0	488,9	
	1,E+07	416,6	355,0	488,9	

Construction detail	**Non-load carrying cruciform joint**		
Literatur	Fatigue assessment of cruciform joints welded with different methods. Zuheir Barsoum, J. Samuelsson		
Material	Denomination		
	Delivery code		
	Plate thickness	12	mm
Mech. properties	$R_{p0,2}$	360	Mpa
	R_m	515	MPa
Fabrication	Welding process	Hybrid Nd:Yag-laser/MAG	
	Welding material	---	
	Post weld treatment	Shot blasted	
Fatigue loading	Stress ration	0	[-]
	Type of loading	sine-wave	
	Type of collective	constant amplidute	

Sketch and dimension of test specimen and loading

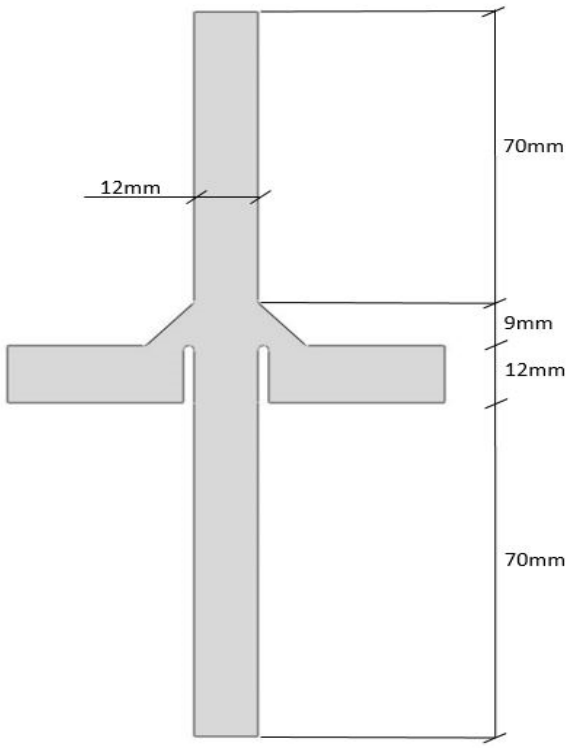

Versuchsergebnisse

n	stress range $\Delta\sigma$	load cycles N	Com. *
1	655	81 000	1
2	655	101 000	1
3	499	150 000	1
4	436	190 000	1
5	436	235 000	1
6	390	420 000	1
7	347	520 000	1
8	325	630 000	1
9	306	670 000	1
10	278	1 200 000	1
11	278	1 300 000	1
12	239	4 550 000	1
13			
14			
15			
16			
17			
18			
19			
20			
21			
22			
23			
24			
25			
26			
27			
28			
29			
30			

Origin and type of fatigue failure

Comments

* use "0" for a run-out that should not be taken into account for the statistical evaluation, "1" elsewhere

S-N curve

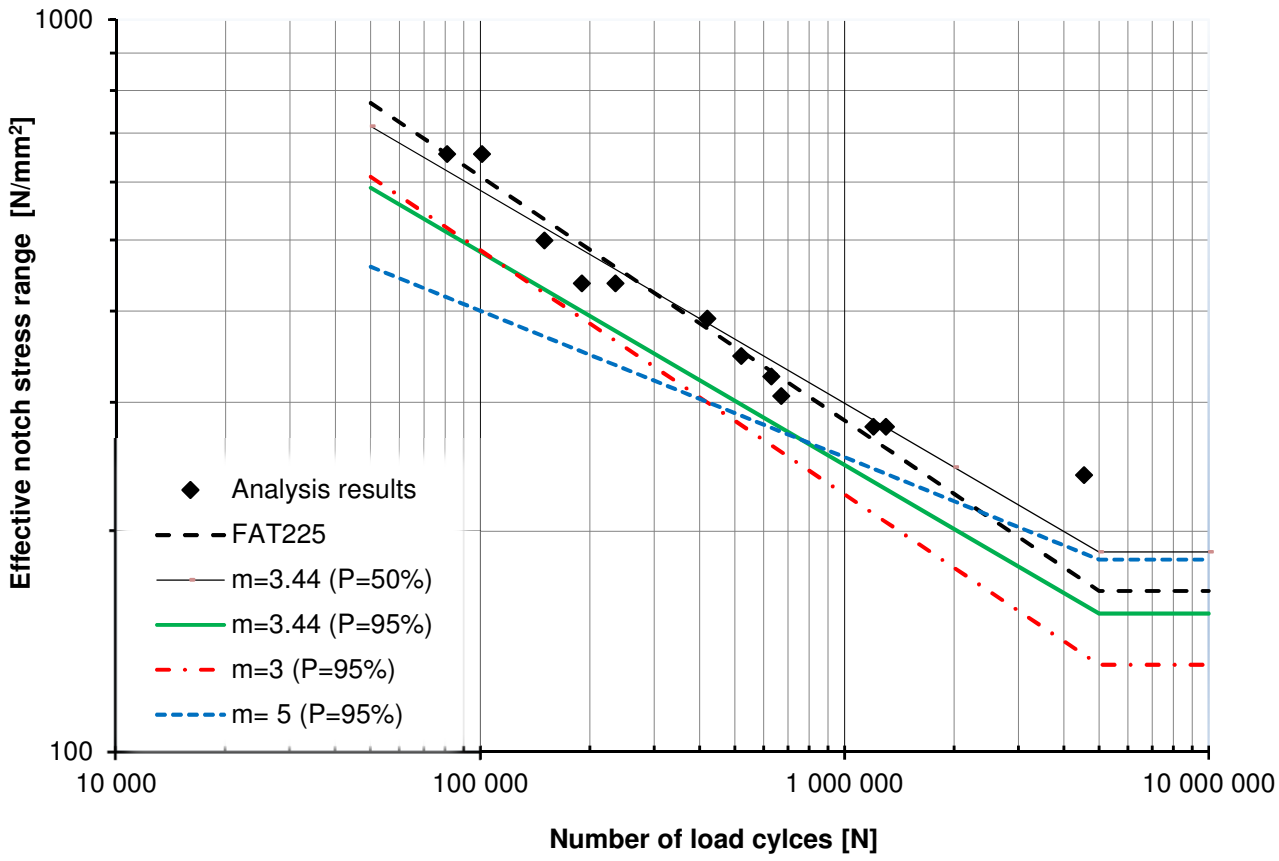

Statistical evaluation of test data according to EN 1993-1-9:2005

slope	mean S-N curve ($P_Ü$ = 50%) $\Delta\sigma_{50\%}$	characteristic S-N curve ($P_Ü$ = 95%) $\Delta\sigma_C$
m = natural = 3,44	**244,6**	**201,5**
m = fix = 3	229,0	178,4
m = fix = 5	281,4	219,8

Statistical evaluation of fatigue test data according to EN 1933-1-9:2005

		m = 3,44	m = 3	m = 5
Coeff. Regression line y = a + m · x :	a	14,516	13,380	18,548
	m	-3,44	-3,00	-5,00
Standard deviation:	s	0,143	0,157	0,275
	xm	2,388	2,360	2,449
	Sxx	0,226		
	Syy	2,876		
	Sxy	-0,777		
f - value:	f	1,252	1,305	1,163
k - value:	t(87.5;n-1)	1,214		
	χ(87.5;n-1)	5,975		
	Gauss(0.95)	1,645		
95%-fractile value of Student-distribution:	t(95)	1,812		
	k	2,583		

n	Δσ	N	y = log(N)	x = log(Δσ)	y^2	x^2	x·y	m = 3 $(y-a-m\cdot x)^2$	m = 5 $(y-a-m\cdot x)^2$
1	655,04	81 000	4,91	2,82	24,09	7,93	13,82	0,001	0,195
2	655,04	101 000	5,00	2,82	25,04	7,93	14,09	0,005	0,289
3	498,87	150 000	5,18	2,70	26,79	7,28	13,97	0,012	0,014
4	435,97	190 000	5,28	2,64	27,87	6,97	13,93	0,034	0,005
5	435,97	235 000	5,37	2,64	28,85	6,97	14,18	0,008	0,000
6	390,42	420 000	5,62	2,59	31,62	6,72	14,57	0,000	0,001
7	347,04	520 000	5,72	2,54	32,67	6,45	14,52	0,002	0,017
8	325,35	630 000	5,80	2,51	33,63	6,31	14,57	0,002	0,035
9	305,83	670 000	5,83	2,49	33,94	6,18	14,48	0,010	0,087
10	277,63	1 200 000	6,08	2,44	36,96	5,97	14,85	0,001	0,063
11	277,63	1 300 000	6,11	2,44	37,38	5,97	14,94	0,004	0,047
12	238,59	4 550 000	6,66	2,38	44,33	5,65	15,83	0,168	0,000
0	0	0	0,00	0,00	0,00	0,00	0,00	0,000	0,000
0	0	0	0,00	0,00	0,00	0,00	0,00	0,000	0,000
0	0	0	0,00	0,00	0,00	0,00	0,00	0,000	0,000
0	0	0	0,00	0,00	0,00	0,00	0,00	0,000	0,000
0	0	0	0,00	0,00	0,00	0,00	0,00	0,000	0,000
0	0	0	0,00	0,00	0,00	0,00	0,00	0,000	0,000
0	0	0	0,00	0,00	0,00	0,00	0,00	0,000	0,000
0	0	0	0,00	0,00	0,00	0,00	0,00	0,000	0,000
0	0	0	0,00	0,00	0,00	0,00	0,00	0,000	0,000
0	0	0	0,00	0,00	0,00	0,00	0,00	0,000	0,000
0	0	0	0,00	0,00	0,00	0,00	0,00	0,000	0,000
0	0	0	0,00	0,00	0,00	0,00	0,00	0,000	0,000
0	0	0	0,00	0,00	0,00	0,00	0,00	0,000	0,000
0	0	0	0,00	0,00	0,00	0,00	0,00	0,000	0,000
0	0	0	0,00	0,00	0,00	0,00	0,00	0,000	0,000
0	0	0	0,00	0,00	0,00	0,00	0,00	0,000	0,000
0	0	0	0,00	0,00	0,00	0,00	0,00	0,000	0,000
0	0	0	0,00	0,00	0,00	0,00	0,00	0,000	0,000
12		Summe	67,55	31,00	383,18	80,33	173,76	0,25	0,75
		Mittelwert	5,63	2,58	31,93	6,69	14,48	0,02	0,06

Statistical evaluation of fatigue test data according to EN 1933-1-9:2005

		m = 3,44	m = 3	m = 5
50%-fractile	N	$\Delta\sigma_{50\%}$	$\Delta\sigma_{50\%}$	$\Delta\sigma_{50\%}$
(mean S-N curve)	2,0E+06	244,6	229,0	281,4
95%-fractile	N	$\Delta\sigma_C$	$\Delta\sigma_C$	$\Delta\sigma_C$
(Chrakteristic S-N curve)	2,0E+06	201,5	178,4	219,8
	N*	1 027 426	945 300	581 280
	y*	6,012	5,976	5,764
	a	14,226	13,055	18,011
5%-Fraktile	N	$\Delta\sigma_{5\%}$	$\Delta\sigma_{5\%}$	$\Delta\sigma_{5\%}$
(upper 5%-fractile S-N curve)	2,0E+06	296,8	294,0	360,3
	N*	3 893 224	4 231 459	6 881 371
	y*	6,590	6,626	6,838
	a	14,805	13,706	19,084

					225
Wertepaare S-N Kurven	N	Mean value	95%-fractile	5%-fractile	Detail class 225
Variable slope, m = 3,44	5,E+04	714,8	589,0	867,6	769,5
	2,E+06	244,6	201,5	296,8	225
	5,E+06	187,4	154,4	227,4	165,8
	1,E+07	187,4	154,4	227,4	165,8
slope m = 3	5,E+04	783,1	610,0	1005,4	
	2,E+06	229,0	178,4	294,0	
	5,E+06	168,7	131,4	216,6	
	1,E+07	168,7	131,4	216,6	
slope m = 5	5,E+04	588,5	459,7	753,5	
	2,E+06	281,4	219,8	360,3	
	5,E+06	234,3	183,0	300,0	
	1,E+07	234,3	183,0	300,0	

Construction detail	**Eccentric fillet joint**		
Literatur	Fatigue behaviour study of laser hybrid welded eccentric fillet joints. M.M. Alam, Z. Barsoum, P. Jonsén, H.A. Häggblad, A.F.H. Kaplan		
Material	Denomination	Stainless steel SS142333	
	Delivery code		
	Plate thickness	10	mm
Mech. properties	$R_{p0,2}$	210	Mpa
	R_m	0-690	MPa
Fabrication	Welding process	Hybrid laser arc welding	
	Welding material	---	
	Post weld treatment	Milled	
Fatigue loading	Stress ration	0	[-]
	Type of loading	sine-wave	
	Type of collective	constant amplidute	

Sketch and dimension of test specimen and loading

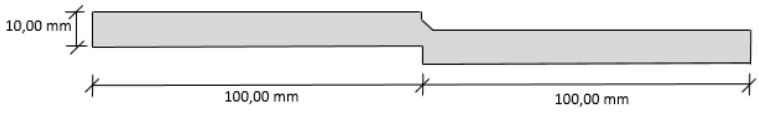

Versuchsergebnisse

n	stress range $\Delta\sigma$	load cycles N	Com. *
1	1286	112 000	1
2	1098	130 000	1
3	1267	140 000	1
4	1239	222 000	1
5	1286	290 000	1
6	1328	318 000	1
7	1032	314 000	1
8	1065	321 000	1
9	1089	361 000	1
10	1051	412 000	1
11	1126	417 000	1
12	1051	480 000	1
13	1079	454 000	1
14			
15			
16			
17			
18			
19			
20			
21			
22			
23			
24			
25			
26			
27			
28			
29			
30			

Origin and type of fatigue failure

Comments

* use "0" for a run-out that should not be taken into account for the statistical evaluation, "1" elsewhere

S-N curve

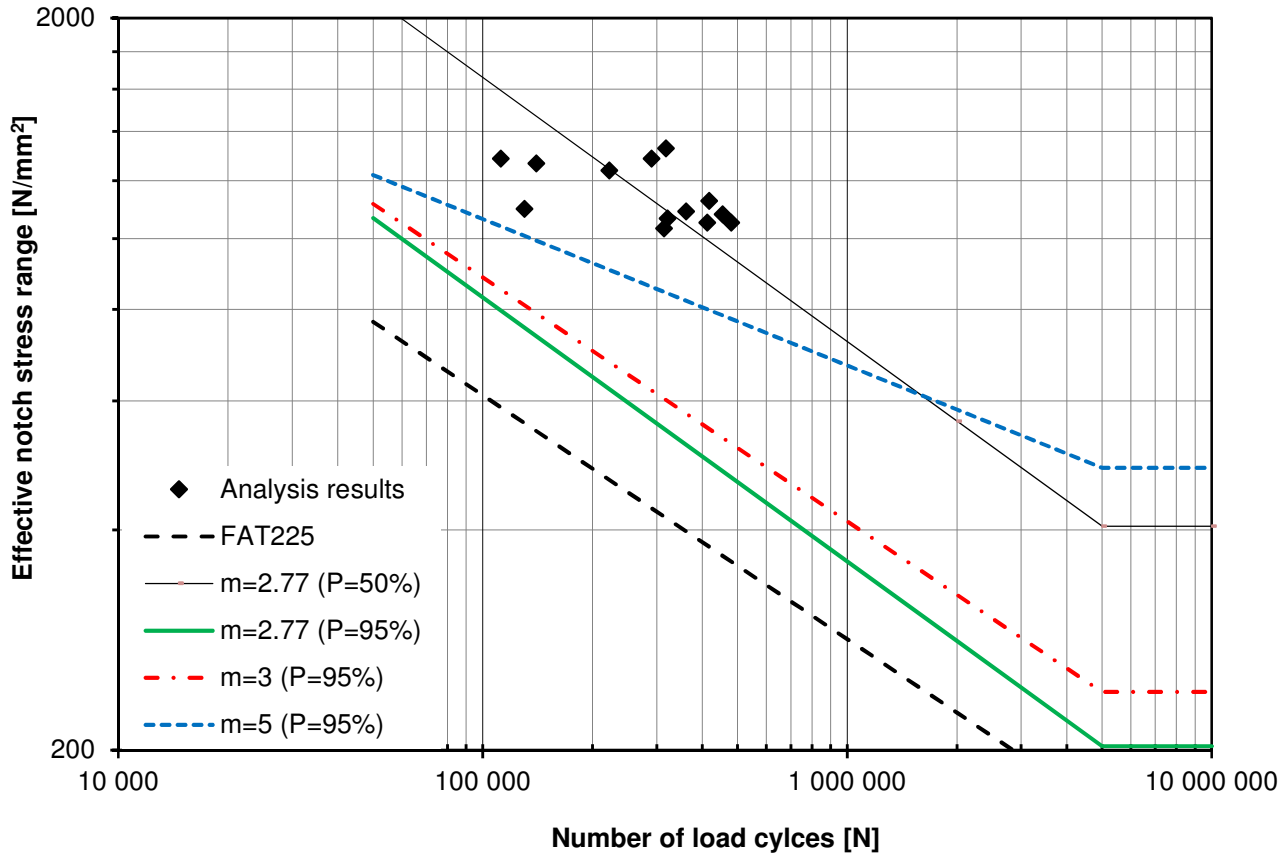

Statistical evaluation of test data according to EN 1993-1-9:2005

slope	mean S-N curve ($P_Ü$ = 50%) $\Delta\sigma_{50\%}$	characteristic S-N curve ($P_Ü$ = 95%) $\Delta\sigma_C$
m = variable = 2,77	**563,2**	**281,8**
m = fix = 3	594,5	326,0
m = fix = 5	773,8	583,9

Statistical evaluation of fatigue test data according to EN 1933-1-9:2005

		m = 2,77	m = 3	m = 5
Coeff. Regression line y = a + m · x :	a	13,926	14,624	20,744
	m	-2,77	-3,00	-5,00
Standard deviation:	s	0,190	0,190	0,212
	xm	2,751	2,774	2,889
	Sxx	0,020		
	Syy	0,548		
	Sxy	-0,054		
f - value:	f	5,961	5,247	2,578
k - value:	t(87.5;n-1)	1,209		
	χ(87.5;n-1)	6,729		
	Gauss(0.95)	1,645		
95%-fractile value of Student-distribution:	t(95)	1,796		
	k	2,532		

n	Δσ	N	y = log(N)	x = log(Δσ)	y^2	x^2	x·y	m = 3 $(y\text{-}a\text{-}m\cdot x)^2$	m = 5 $(y\text{-}a\text{-}m\cdot x)^2$
1	1286	112 000	5,05	3,11	25,49	9,67	15,70	0,061	0,022
2	1098	130 000	5,11	3,04	26,15	9,25	15,55	0,150	0,183
3	1267	140 000	5,15	3,10	26,48	9,63	15,97	0,029	0,007
4	1239	222 000	5,35	3,09	28,58	9,57	16,54	0,000	0,005
5	1286	290 000	5,46	3,11	29,84	9,67	16,98	0,028	0,070
6	1328	318 000	5,50	3,12	30,28	9,75	17,19	0,062	0,140
7	1032	314 000	5,50	3,01	30,22	9,08	16,57	0,007	0,032
8	1065	321 000	5,51	3,03	30,32	9,16	16,67	0,001	0,010
9	1089	361 000	5,56	3,04	30,89	9,22	16,88	0,002	0,000
10	1051	412 000	5,61	3,02	31,53	9,13	16,97	0,003	0,000
11	1126	417 000	5,62	3,05	31,59	9,31	17,15	0,023	0,018
12	1051	480 000	5,68	3,02	32,28	9,13	17,17	0,015	0,002
13	1079	454 000	5,66	3,03	32,00	9,20	17,16	0,018	0,006
0	0	0	0,00	0,00	0,00	0,00	0,00	0,000	0,000
0	0	0	0,00	0,00	0,00	0,00	0,00	0,000	0,000
0	0	0	0,00	0,00	0,00	0,00	0,00	0,000	0,000
0	0	0	0,00	0,00	0,00	0,00	0,00	0,000	0,000
0	0	0	0,00	0,00	0,00	0,00	0,00	0,000	0,000
0	0	0	0,00	0,00	0,00	0,00	0,00	0,000	0,000
0	0	0	0,00	0,00	0,00	0,00	0,00	0,000	0,000
0	0	0	0,00	0,00	0,00	0,00	0,00	0,000	0,000
0	0	0	0,00	0,00	0,00	0,00	0,00	0,000	0,000
0	0	0	0,00	0,00	0,00	0,00	0,00	0,000	0,000
0	0	0	0,00	0,00	0,00	0,00	0,00	0,000	0,000
0	0	0	0,00	0,00	0,00	0,00	0,00	0,000	0,000
0	0	0	0,00	0,00	0,00	0,00	0,00	0,000	0,000
0	0	0	0,00	0,00	0,00	0,00	0,00	0,000	0,000
0	0	0	0,00	0,00	0,00	0,00	0,00	0,000	0,000
0	0	0	0,00	0,00	0,00	0,00	0,00	0,000	0,000
0	0	0	0,00	0,00	0,00	0,00	0,00	0,000	0,000
13		Summe	70,75	39,78	385,64	121,77	216,48	0,40	0,49
		Mittelwert	5,44	3,06	29,66	9,37	16,65	0,03	0,04

Statistical evaluation of fatigue test data according to EN 1933-1-9:2005

		m = 2,77	m = 3	m = 5
50%-fractile	N	$\Delta\sigma_{50\%}$	$\Delta\sigma_{50\%}$	$\Delta\sigma_{50\%}$
(mean S-N curve)	2,0E+06	563,2	594,5	773,8
95%-fractile	N	$\Delta\sigma_C$	$\Delta\sigma_C$	$\Delta\sigma_C$
(Chrakteristic S-N curve)	2,0E+06	281,8	326,0	583,9
	N*	293 467	329 654	489 093
	y*	5,468	5,518	5,689
	a	13,093	13,841	20,133
5%-Fraktile	N	$\Delta\sigma_{5\%}$	$\Delta\sigma_{5\%}$	$\Delta\sigma_{5\%}$
(upper 5%-fractile S-N curve)	2,0E+06	1125,5	1084,4	1025,6
	N*	13 630 146	12 133 928	8 178 401
	y*	7,135	7,084	6,913
	a	14,760	15,407	21,356

					225
Wertepaare S-N Kurven	N	Mean value	95%-fractile	5%-fractile	Detail class 225
Variable slope, m = 2,77	5,E+04	2131,0	1066,4	4258,5	769,5
	2,E+06	563,2	281,8	1125,5	225
	5,E+06	404,7	202,5	808,7	165,8
	1,E+07	404,7	202,5	808,7	165,8
slope m = 3	5,E+04	2033,3	1114,8	3708,5	
	2,E+06	594,5	326,0	1084,4	
	5,E+06	438,1	240,2	799,0	
	1,E+07	438,1	240,2	799,0	
slope m = 5	5,E+04	1618,2	1221,0	2144,7	
	2,E+06	773,8	583,9	1025,6	
	5,E+06	644,2	486,1	853,8	
	1,E+07	644,2	486,1	853,8	

Construction detail	**Butt weld**	
Literatur	Fatigue strength of laser hybrid welded high strength steel. Hamid Narimani	
Material	Denomination	High strength steel DOMEX 700 MC
	Delivery code	
	Plate thickness	10 mm
Mech. properties	$R_{p0,2}$	714 Mpa
	R_m	MPa
Fabrication	Welding process	Hybrid laser arc welding
	Welding material	---
	Post weld treatment	Milled
Fatigue loading	Stress ration	0 [-]
	Type of loading	sine-wave
	Type of collective	constant amplidute

Sketch and dimension of test specimen and loading

Versuchsergebnisse

n	stress range $\Delta\sigma$	load cycles N	Com. *
1	911	227 000	1
2	455	13 882 000	1
3	1027	141 000	1
4	1027	220 000	1
5	1027	124 000	1
6	683	1 087 000	1
7	683	2 303 000	1
8	797	516 000	1
9	797	308 000	1
10	683	13 000 000	1
11	797	257 000	1
12	797	230 000	1
13	1252	43 000	1
14	1252	41 000	1
15			
16			
17			
18			
19			
20			
21			
22			
23			
24			
25			
26			
27			
28			
29			
30			

Origin and type of fatigue failure

Comments

* use "0" for a run-out that should not be taken into account for the statistical evaluation, "1" elsewhere

S-N curve

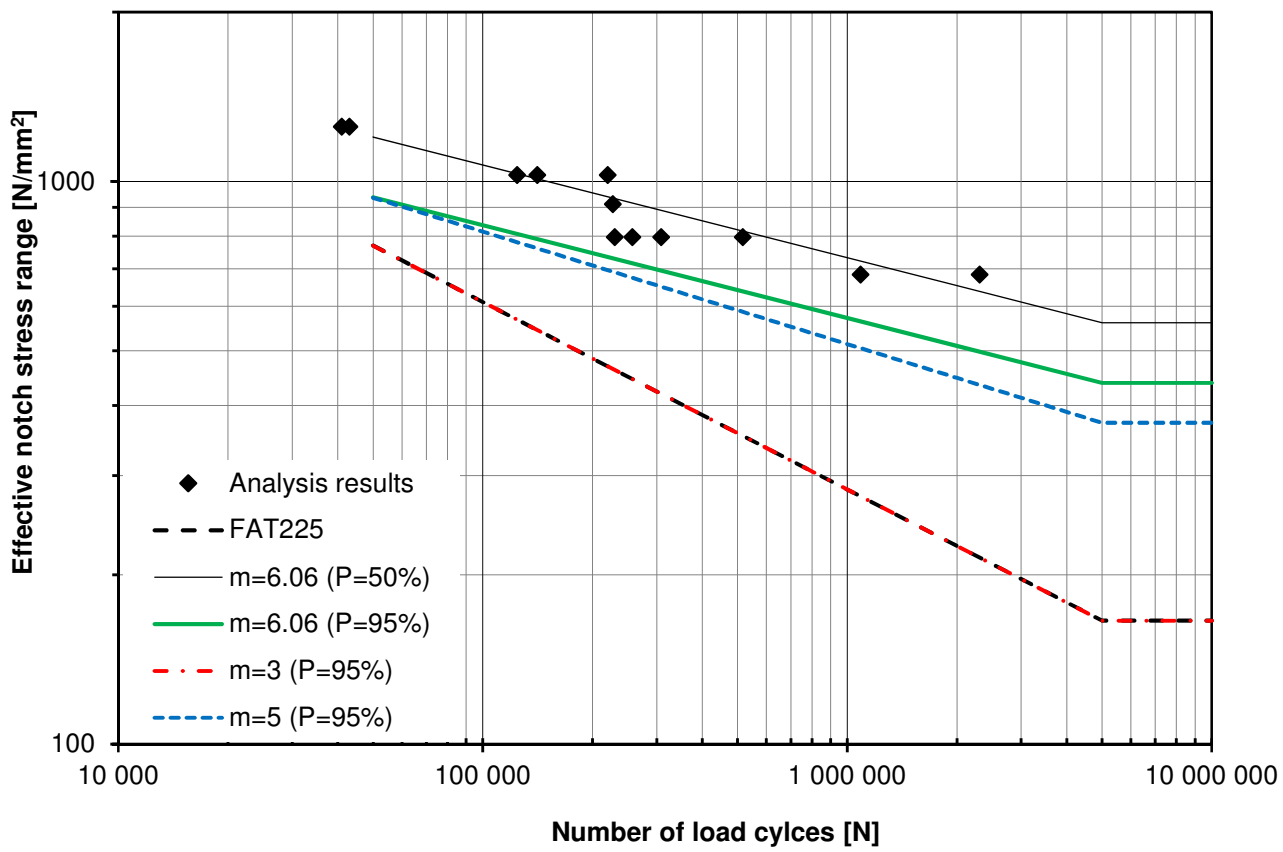

Statistical evaluation of test data according to EN 1993-1-9:2005

slope	mean S-N curve ($P_Ü$ = 50%) $\Delta\sigma_{50\%}$	characteristic S-N curve ($P_Ü$ = 95%) $\Delta\sigma_C$
m = variable = 6,06	**652,6**	**510,2**
m = fix = 3	503,1	224,9
m = fix = 5	618,3	447,4

Statistical evaluation of fatigue test data according to EN 1933-1-9:2005

		m = 6,06	m = 3	m = 5
Coeff. Regression line y = a + m · x :	a	23,348	14,406	20,257
	m	-6,06	-3,00	-5,00
Standard deviation:	s	0,340	0,507	0,364
	xm	2,815	2,702	2,791
	Sxx	0,181		
	Syy	8,043		
	Sxy	-1,098		
f - value:	f	1,139	1,348	1,171
k - value:	t(87.5;n-1)	1,204		
	χ(87.5;n-1)	7,493		
	Gauss(0.95)	1,645		
95%-fractile value of Student-distribution:	t(95)	1,782		
	k	2,489		

n	Δσ	N	y = log(N)	x = log(Δσ)	y^2	x^2	x·y	m = 3 $(y-a-m\cdot x)^2$	m = 5 $(y-a-m\cdot x)^2$
1	911	227 000	5,36	2,96	28,69	8,76	15,85	0,029	0,011
2	455	13 882 000	7,14	2,66	51,01	7,07	18,98	0,505	0,031
3	1027	141 000	5,15	3,01	26,51	9,07	15,51	0,049	0,002
4	1027	220 000	5,34	3,01	28,54	9,07	16,09	0,001	0,021
5	1027	124 000	5,09	3,01	25,94	9,07	15,34	0,077	0,011
6	683	1 087 000	6,04	2,83	36,44	8,03	17,11	0,018	0,002
7	683	2 303 000	6,36	2,83	40,48	8,03	18,03	0,211	0,077
8	797	516 000	5,71	2,90	32,63	8,42	16,58	0,000	0,001
9	797	308 000	5,49	2,90	30,12	8,42	15,92	0,045	0,068
10	683	13 000 000	7,11	2,83	50,61	8,03	20,16	1,467	1,059
11	797	257 000	5,41	2,90	29,27	8,42	15,70	0,085	0,115
12	797	230 000	5,36	2,90	28,75	8,42	15,56	0,116	0,151
13	1252	43 000	4,63	3,10	21,47	9,60	14,35	0,230	0,018
14	1252	41 000	4,61	3,10	21,28	9,60	14,29	0,250	0,024
0	0	0	0,00	0,00	0,00	0,00	0,00	0,000	0,000
0	0	0	0,00	0,00	0,00	0,00	0,00	0,000	0,000
0	0	0	0,00	0,00	0,00	0,00	0,00	0,000	0,000
0	0	0	0,00	0,00	0,00	0,00	0,00	0,000	0,000
0	0	0	0,00	0,00	0,00	0,00	0,00	0,000	0,000
0	0	0	0,00	0,00	0,00	0,00	0,00	0,000	0,000
0	0	0	0,00	0,00	0,00	0,00	0,00	0,000	0,000
0	0	0	0,00	0,00	0,00	0,00	0,00	0,000	0,000
0	0	0	0,00	0,00	0,00	0,00	0,00	0,000	0,000
0	0	0	0,00	0,00	0,00	0,00	0,00	0,000	0,000
0	0	0	0,00	0,00	0,00	0,00	0,00	0,000	0,000
0	0	0	0,00	0,00	0,00	0,00	0,00	0,000	0,000
0	0	0	0,00	0,00	0,00	0,00	0,00	0,000	0,000
0	0	0	0,00	0,00	0,00	0,00	0,00	0,000	0,000
0	0	0	0,00	0,00	0,00	0,00	0,00	0,000	0,000
0	0	0	0,00	0,00	0,00	0,00	0,00	0,000	0,000
14		Summe	78,82	40,96	451,74	120,00	229,47	3,08	1,59
		Mittelwert	5,63	2,93	32,27	8,57	16,39	0,22	0,11

Statistical evaluation of fatigue test data according to EN 1933-1-9:2005

		m = 6,06	m = 3	m = 5
50%-fractile	N	$\Delta\sigma_{50\%}$	$\Delta\sigma_{50\%}$	$\Delta\sigma_{50\%}$
(mean S-N curve)	2,0E+06	652,6	503,1	618,3
95%-fractile	N	$\Delta\sigma_C$	$\Delta\sigma_C$	$\Delta\sigma_C$
(Chrakteristic S-N curve)	2,0E+06	510,2	224,9	447,4
	N*	450 453	178 700	396 768
	y*	5,654	5,252	5,599
	a	22,700	13,357	19,554
5%-Fraktile	N	$\Delta\sigma_{5\%}$	$\Delta\sigma_{5\%}$	$\Delta\sigma_{5\%}$
(upper 5%-fractile S-N curve)	2,0E+06	834,7	1125,4	854,5
	N*	8 879 946	22 383 839	10 081 462
	y*	6,948	7,350	7,004
	a	23,995	15,455	20,959

					225
Wertepaare S-N Kurven	N	Mean value	95%-fractile	5%-fractile	Detail class 225
Variable slope, m = 6,06	5,E+04	1199,9	938,1	1534,7	769,5
	2,E+06	652,6	510,2	834,7	225
	5,E+06	560,9	438,6	717,5	165,8
	1,E+07	560,9	438,6	717,5	165,8
slope m = 3	5,E+04	1720,7	769,2	3848,8	
	2,E+06	503,1	224,9	1125,4	
	5,E+06	370,7	165,7	829,2	
	1,E+07	370,7	165,7	829,2	
slope m = 5	5,E+04	1293,0	935,6	1786,9	
	2,E+06	618,3	447,4	854,5	
	5,E+06	514,8	372,5	711,4	
	1,E+07	514,8	372,5	711,4	

Construction detail	**Final SN-curve based on previous specimens**	
Literatur		
Material	Denomination	Steel
	Delivery code	
	Plate thickness	>5 mm
Mech. properties	$R_{p0,2}$	Mpa
	R_m	MPa
Fabrication	Welding process	Hybrid laser arc welding
	Welding material	---
	Post weld treatment	
Fatigue loading	Stress ration	0 [-]
	Type of loading	sine-wave
	Type of collective	constant amplidute

Sketch and dimension of test specimen and loading

Versuchsergebnisse

n	stress range $\Delta\sigma$	load cycles N	Com. *
1	655	81 000	1
2	655	101 000	1
3	499	150 000	1
4	436	190 000	1
5	436	235 000	1
6	390	420 000	1
7	347	520 000	1
8	325	630 000	1
9	306	670 000	1
10	278	1 200 000	1
11	278	1 300 000	1
12	239	4 550 000	1
13	1241	30 500	1
14	1241	19 700	1
15	1241	21 300	1
16	1241	26 000	1
17	827	179 948	1
18	827	228 982	1
19	827	170 600	1
20	827	118 400	1
21	414	20 000 000	0
22	414	20 000 000	0
23	414	20 000 000	0
24	414	2 658 000	1
25	1286	112 000	1
26	1098	130 000	1
27	1267	140 000	1
28	1239	222 000	1
29	1286	290 000	1
30	1328	318 000	1
31	1032	314 000	1
32	1065	321 000	1
33	1089	361 000	1
34	1051	412 000	1
35	1126	417 000	1
36	1051	480 000	1
37	1079	454 000	1
38	911	227 000	1
39	455	13 882 000	1

40	1027	141 000	1
41	1027	220 000	1
42	1027	124 000	1
43	683	1 087 000	1
44	683	2 303 000	1
45	797	516 000	1
46	797	308 000	1
47	683	13 000 000	1
48	797	257 000	1
49	797	230 000	1
50	1252	43 000	1
51	1252	41 000	1
52			
53			

* use "0" for a run-out that should not be taken into account for the statistical evaluation, "1" elsewhere

S-N curve

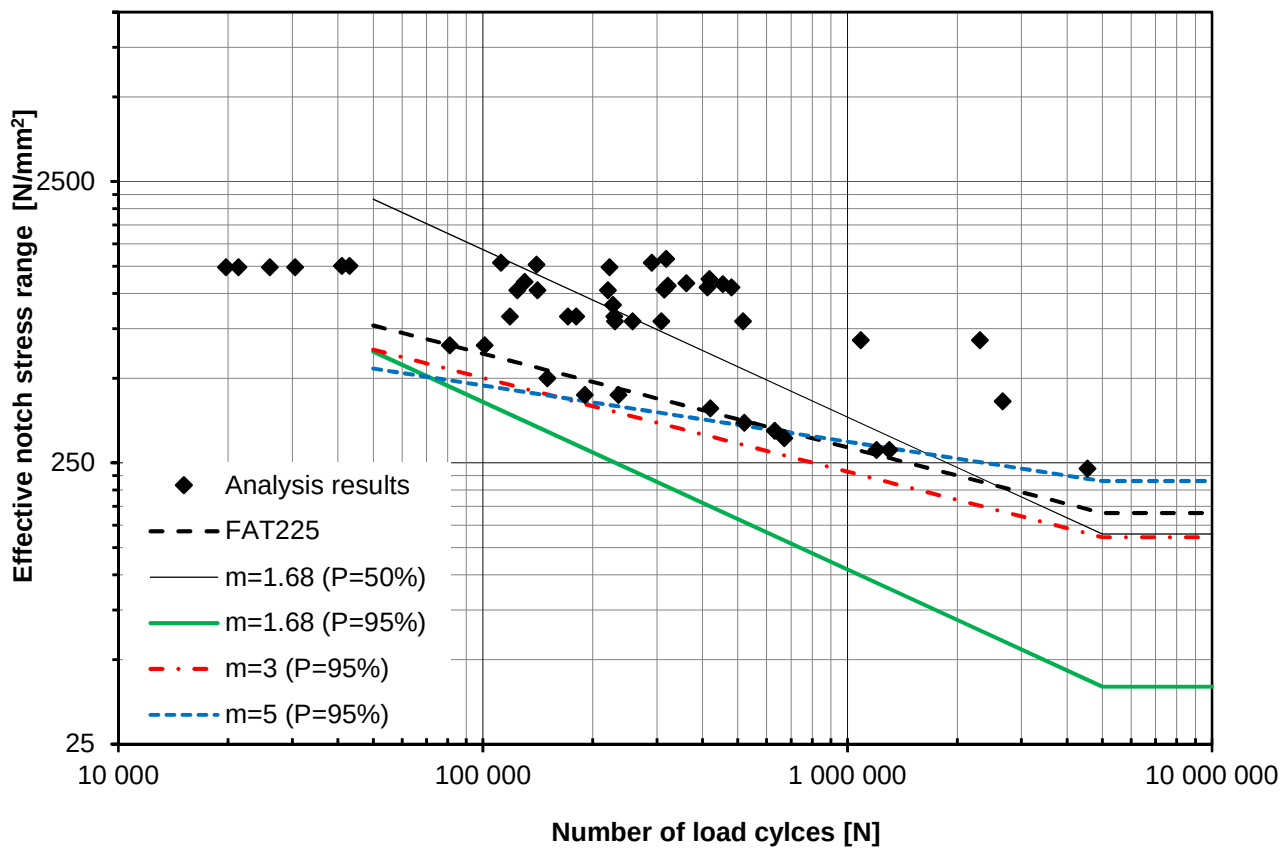

Statistical evaluation of test data according to EN 1993-1-9:2005

slope	mean S-N curve ($P_Ü$ = 50%) $\Delta\sigma_{50\%}$	characteristic S-N curve ($P_Ü$ = 95%) $\Delta\sigma_C$
m = variable = 1,68	**240,7**	**69,1**
m = fix = 3	400,4	184,6
m = fix = 5	518,7	258,6

Statistical evaluation of fatigue test data according to EN 1933-1-9:2005

		m = 1,68	m = 3	m = 5
Coeff. Regression line y = a + m · x :	a	10,300	14,109	19,876
	m	-1,68	-3,00	-5,00
Standard deviation:	s	0,509	0,585	0,885
	xm	2,382	2,603	2,715
	Sxx	2,190		
	Syy	18,085		
	Sxy	-3,677		
f - value:	f	1,136	1,057	1,034
k - value:	t(87.5;n-1)	1,165		
	χ(87.5;n-1)	36,138		
	Gauss(0.95)	1,645		
95%-fractile value of Student-distribution:	t(95)	1,679		
	k	2,044		

n	$\Delta\sigma$	N	y = log(N)	x = log($\Delta\sigma$)	y^2	x^2	x·y	m = 3 $(y-a-m\cdot x)^2$	m = 5 $(y-a-m\cdot x)^2$
1	655,04	81 000	4,91	2,82	24,09	7,93	13,82	0,564	0,784
2	655,04	101 000	5,00	2,82	25,04	7,93	14,09	0,430	0,624
3	498,87	150 000	5,18	2,70	26,79	7,28	13,97	0,703	1,463
4	435,97	190 000	5,28	2,64	27,87	6,97	13,93	0,831	1,959
5	435,97	235 000	5,37	2,64	28,85	6,97	14,18	0,671	1,709
6	390,42	420 000	5,62	2,59	31,62	6,72	14,57	0,505	1,676
7	347,04	520 000	5,72	2,54	32,67	6,45	14,52	0,595	2,125
8	325,35	630 000	5,80	2,51	33,63	6,31	14,57	0,596	2,293
9	305,83	670 000	5,83	2,49	33,94	6,18	14,48	0,682	2,631
10	277,63	1 200 000	6,08	2,44	36,96	5,97	14,85	0,489	2,493
11	277,63	1 300 000	6,11	2,44	37,38	5,97	14,94	0,441	2,385
12	238,59	4 550 000	6,66	2,38	44,33	5,65	15,83	0,101	1,767
13	1241,2	30 500	4,48	3,09	20,11	9,57	13,87	0,117	0,006
14	1241,2	19 700	4,29	3,09	18,44	9,57	13,29	0,284	0,013
15	1241,2	21 300	4,33	3,09	18,73	9,57	13,39	0,249	0,006
16	1241,2	26 000	4,41	3,09	19,49	9,57	13,66	0,170	0,000
17	827,2	179 948	5,26	2,92	27,62	8,51	15,33	0,010	0,001
18	827,2	228 982	5,36	2,92	28,73	8,51	15,64	0,000	0,005
19	827,2	170 600	5,23	2,92	27,37	8,51	15,26	0,015	0,003
20	827,2	118 400	5,07	2,92	25,74	8,51	14,80	0,080	0,046
21	0	0	0,00	0,00	0,00	0,00	0,00	0,000	0,000
22	0	0	0,00	0,00	0,00	0,00	0,00	0,000	0,000
23	0	0	0,00	0,00	0,00	0,00	0,00	0,000	0,000
24	413,6	2 658 000	6,42	2,62	41,27	6,85	16,81	0,027	0,135
25	1286	112 000	5,05	3,11	25,49	9,67	15,70	0,072	0,518
26	1098	130 000	5,11	3,04	26,15	9,25	15,55	0,016	0,195
27	1267	140 000	5,15	3,10	26,48	9,63	15,97	0,120	0,615
28	1239	222 000	5,35	3,09	28,58	9,57	16,54	0,267	0,876
29	1286	290 000	5,46	3,11	29,84	9,67	16,98	0,465	1,284
30	1328	318 000	5,50	3,12	30,28	9,75	17,19	0,583	1,545
31	1032	314 000	5,50	3,01	30,22	9,08	16,57	0,184	0,476
32	1065	321 000	5,51	3,03	30,32	9,16	16,67	0,230	0,589
33	1089	361 000	5,56	3,04	30,89	9,22	16,88	0,314	0,752
34	1051	412 000	5,61	3,02	31,53	9,13	16,97	0,326	0,718
35	1126	417 000	5,62	3,05	31,59	9,31	17,15	0,444	1,005
36	1051	480 000	5,68	3,02	32,28	9,13	17,17	0,406	0,835
37	1079	454 000	5,66	3,03	32,00	9,20	17,16	0,419	0,896

38	911	227 000	5,36	2,96	28,69	8,76	15,85	0,016	0,077
39	455	13 882 000	7,14	2,66	51,01	7,07	18,98	1,016	0,310
40	1027	141 000	5,15	3,01	26,51	9,07	15,51	0,006	0,110
41	1027	220 000	5,34	3,01	28,54	9,07	16,09	0,072	0,275
42	1027	124 000	5,09	3,01	25,94	9,07	15,34	0,000	0,076
43	683	1 087 000	6,04	2,83	36,44	8,03	17,11	0,186	0,111
44	683	2 303 000	6,36	2,83	40,48	8,03	18,03	0,573	0,434
45	797	516 000	5,71	2,90	32,63	8,42	16,58	0,095	0,119
46	797	308 000	5,49	2,90	30,12	8,42	15,92	0,007	0,014
47	683	13 000 000	7,11	2,83	50,61	8,03	20,16	2,276	1,990
48	797	257 000	5,41	2,90	29,27	8,42	15,70	0,000	0,002
49	797	230 000	5,36	2,90	28,75	8,42	15,56	0,002	0,000
50	1252	43 000	4,63	3,10	21,47	9,60	14,35	0,033	0,061
51	1252	41 000	4,61	3,10	21,28	9,60	14,29	0,041	0,051
48		Summe	261,99	138,41	1448,07	401,28	751,77	15,73	36,06
		Mittelwert	5,46	2,88	30,17	8,36	15,66	0,33	0,75

Statistical evaluation of fatigue test data according to EN 1933-1-9:2005

		m = 1,68	m = 3	m = 5
50%-fractile	N	$\Delta\sigma_{50\%}$	$\Delta\sigma_{50\%}$	$\Delta\sigma_{50\%}$
(mean S-N curve)	2,0E+06	240,7	400,4	518,7
95%-fractile	N	$\Delta\sigma_C$	$\Delta\sigma_C$	$\Delta\sigma_C$
(Chrakteristic S-N curve)	2,0E+06	69,1	184,6	258,6
	N*	245 844	195 819	61 644
	y*	5,391	5,292	4,790
	a	9,390	13,099	18,364
5%-Fraktile	N	$\Delta\sigma_{5\%}$	$\Delta\sigma_{5\%}$	$\Delta\sigma_{5\%}$
(upper 5%-fractile S-N curve)	2,0E+06	838,8	868,8	1040,2
	N*	16 270 485	20 427 046	64 889 015
	y*	7,211	7,310	7,812
	a	11,211	15,118	21,387

					225
Wertepaare S-N Kurven	N	Mean value	95%-fractile	5%-fractile	Detail class 225
Variable slope, m = 1,68	5,E+04	2165,6	621,5	7545,7	769,5
	2,E+06	240,7	69,1	838,8	225
	5,E+06	139,5	40,0	486,1	165,8
	1,E+07	139,5	40,0	486,1	165,8
slope m = 3	5,E+04	1369,4	631,2	2971,2	
	2,E+06	400,4	184,6	868,8	
	5,E+06	295,0	136,0	640,1	
	1,E+07	295,0	136,0	640,1	
slope m = 5	5,E+04	1084,7	540,9	2175,4	
	2,E+06	518,7	258,6	1040,2	
	5,E+06	431,8	215,3	866,0	
	1,E+07	431,8	215,3	866,0	

Appendix B – Calculation of nominal stress

Presentation of calculations of nominal stress to fatigue analysis of an eccentric filet weld.

Calculations for Eccentric fillet weld test

Calculations of the nominal stress at the top surface 24 mm away from the joint edge.
The calculated value was used for verification of the model in Abaqus.

- Nominal stress at top surface 24 mm away from the joint edge

$h_{EFW} := 0.01 \cdot m$ Hight specimen

$b_{EFW} := 1 \cdot m$ Width of the specimen

$P_{EFW} := 0.5 \cdot N$ Applied force

$L_{EFW} := 76 \cdot mm$ Length from support to 24mm away from joint

$M_{EFW} := P_{EFW} \cdot L_{EFW} = 0.038 \cdot N \cdot m$ Moment

$W_{EFW} := \frac{b_{EFW} \cdot h_{EFW}^{2}}{6} = 1.667 \times 10^{-5} \cdot m^{3}$ Bending stiffnes of the specimen

$\sigma_{nom.calculated} := \frac{M_{EFW}}{W_{EFW}} = 2.28 \cdot kPa$ Nominal stress 24 mm away from the joint

Appendix C - Convergence study of the 3D model

The convergence study was conducted with the aim of decide the most appropriate mesh density for the global model. The verification involved both local and global deformation at the upper and lower face panel. Additionally, stresses at the upper and lower face panel were investigated and then the stress behaviour at the boundaries of the submodels.

During the verification the deck was exposed to a pressure load representing half an axle load with a magnitude of 375 kPa. The load was applied at the center of the deck, and had a total application area of 400x400 mm.

In total nine models were verified, the different meshes are explained with the table C.1 and figure C.1.

Table C.1 How the different meshes was created.

	Number of elements used in the SSP								
	Mesh 1	Mesh 2	Mesh 3	Mesh 4	Mesh 5	Mesh6	Mesh 7	Mesh 8	Mesh 9
Upper weld	1	1	1	1	2	2	2	D2	D6
Lower weld	2	2	2	2	2	2	2	D2	D6
Upper plate	2	4	6	6	8	8	6	4	6
Lower plate	2	4	6	6	8	8	6	4	4
Radius	1	2	3	3	4	4	3	3	4
f2 (upper)	3	3	3	3	6	6	6	6	6-8
f1/2 (lower)	2	2	2	2	2	3	3	6	6-8
d1+d2	2	3	4	4	6	6	4	4	6
Depth	500 mm	500mm	500mm	50mm	100mm	50mm	50mm	50mm	50mm
Thickness	1	1	1	1	1	1	2	2	2-3
No elements	5440	7312	9392	93728	64568	133296	137408	216496	414096
Time									4h 45m

[mm]

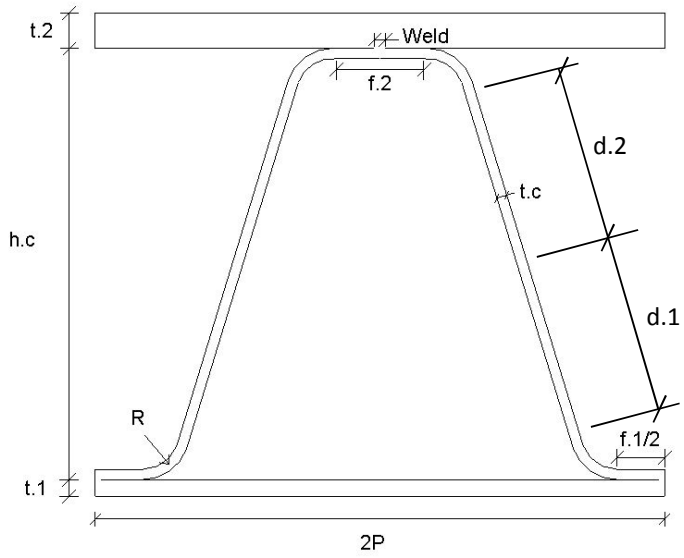

Figure C.1 Figure with notations of table C.1

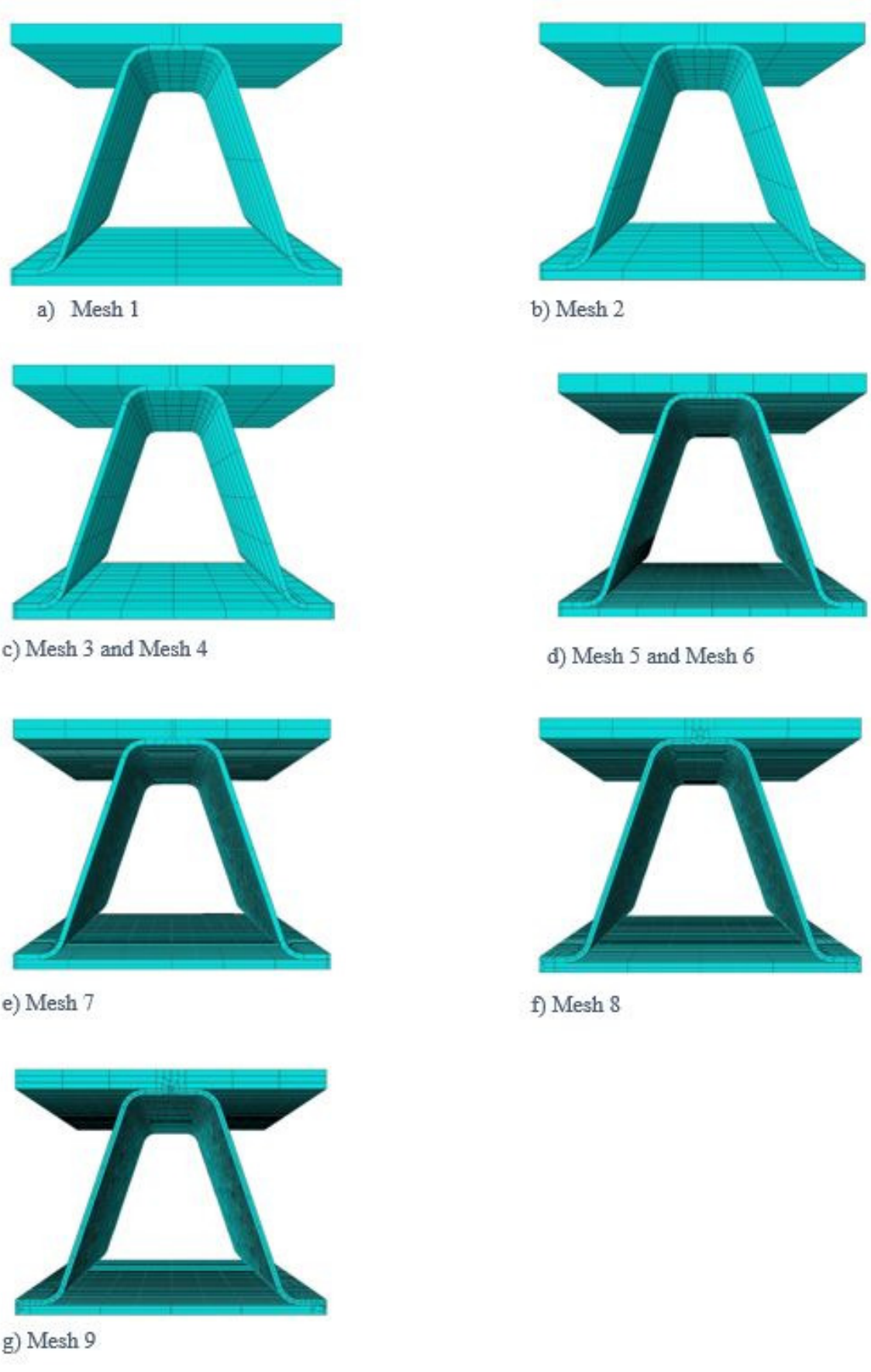

Figure C.2 The different meshes.

Global Deflection - Upper plate

To investigate the convergence of the mesh a study of the global deflection of the upper plate was done. The global deflection for the upper plate was taken at the center line of the model and at the top edge, see figure below,

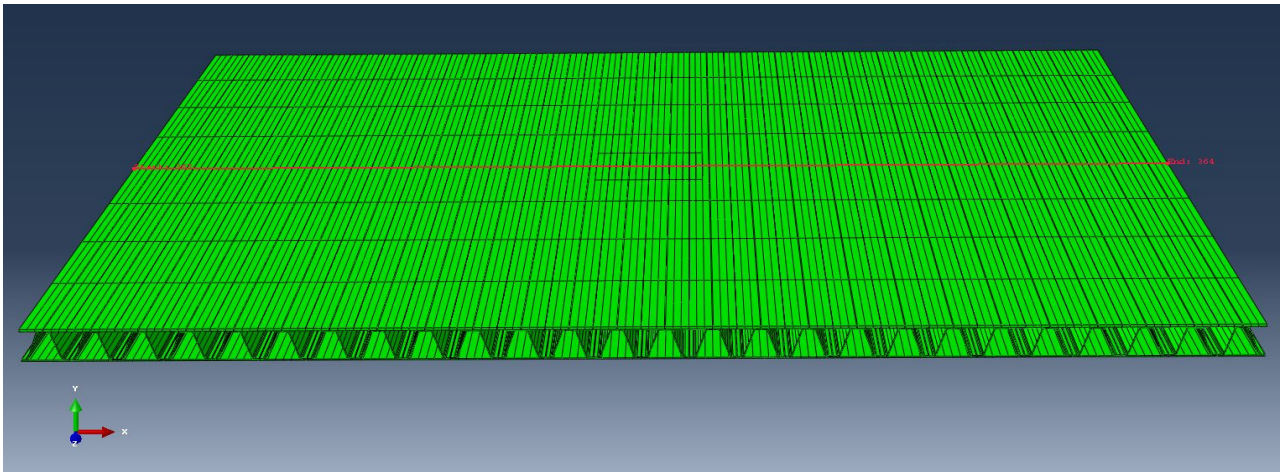

Mesh 1

Distance [m]	U2 [m]
0	6,84E-06
0,0648267	-9,54E-05
0,129653	-0,0001905
0,19448	-0,0002741
0,259307	-0,0003576
0,324133	-0,0004356
0,38896	-0,0005163
0,453787	-0,0005948
0,518613	-0,0006748
0,58344	-0,0007565
0,648267	-0,0008371
0,713093	-0,0009229
0,77792	-0,0010064
0,842747	-0,0010965
0,907573	-0,0011856
0,9724	-0,0012802
1,03723	-0,0013778
1,10205	-0,0014773
1,16688	-0,0015853
1,23171	-0,0016927
1,29653	-0,001812
1,36136	-0,0019315
1,42619	-0,0020634
1,49101	-0,0022007
1,55584	-0,0023492
1,62067	-0,0025196

Mesh 2

Distance [m]	U2 [m]
0	7,14E-06
0,0648267	-9,57E-05
0,129653	-0,000191
0,19448	-0,000275
0,259307	-0,00036
0,324133	-0,000439
0,38896	-0,00052
0,453787	-0,000599
0,518613	-0,00068
0,58344	-0,000762
0,648267	-0,000844
0,713093	-0,00093
0,77792	-0,001015
0,842747	-0,001106
0,907573	-0,001196
0,9724	-0,001292
1,03723	-0,00139
1,10205	-0,001491
1,16688	-0,001601
1,23171	-0,00171
1,29653	-0,001831
1,36136	-0,001953
1,42619	-0,002087
1,49101	-0,002227
1,55584	-0,002378
1,62067	-0,002551

Mesh 3

Distance [m]	U2 [m]
0	7,14E-06
0,0648267	-9,59E-05
0,129653	-0,00019
0,19448	-0,00028
0,259307	-0,00036
0,324133	-0,00044
0,38896	-0,00052
0,453787	-0,0006
0,518613	-0,00068
0,58344	-0,00076
0,648267	-0,00085
0,713093	-0,00093
0,77792	-0,00102
0,842747	-0,00111
0,907573	-0,0012
0,9724	-0,0013
1,03723	-0,00139
1,10205	-0,0015
1,16688	-0,00161
1,23171	-0,00172
1,29653	-0,00184
1,36136	-0,00196
1,42619	-0,00209
1,49101	-0,00223
1,55584	-0,00239
1,62067	-0,00256

1,68549	-0,0027151
1,75032	-0,0029812
1,81515	-0,0031838
1,87997	-0,0032797
1,9448	-0,0033541
2,00963	-0,00328
2,07445	-0,0031844
2,13928	-0,002982
2,20411	-0,0027163
2,26893	-0,0025212
2,33376	-0,0023512
2,39859	-0,002203
2,46341	-0,002066
2,52824	-0,0019344
2,59307	-0,0018152
2,65789	-0,0016961
2,72272	-0,001589
2,78755	-0,0014813
2,85237	-0,001382
2,9172	-0,0012846
2,98203	-0,0011902
3,04685	-0,0011013
3,11168	-0,0010113
3,17651	-0,0009279
3,24133	-0,0008422
3,30616	-0,0007616
3,37099	-0,00068
3,43581	-0,0005999
3,50064	-0,0005213
3,56547	-0,0004404
3,63029	-0,0003621
3,69512	-0,0002781
3,75995	-0,0001939
3,82477	-9,80E-05
3,8896	5,17E-06

1,68549	-0,002751
1,75032	-0,003023
1,81515	-0,003234
1,87997	-0,003326
1,9448	-0,003404
2,00963	-0,003327
2,07445	-0,003235
2,13928	-0,003024
2,20411	-0,002752
2,26893	-0,002553
2,33376	-0,00238
2,39859	-0,002229
2,46341	-0,002089
2,52824	-0,001956
2,59307	-0,001835
2,65789	-0,001713
2,72272	-0,001604
2,78755	-0,001495
2,85237	-0,001395
2,9172	-0,001296
2,98203	-0,001201
3,04685	-0,001111
3,11168	-0,00102
3,17651	-0,000935
3,24133	-0,000849
3,30616	-0,000767
3,37099	-0,000685
3,43581	-0,000604
3,50064	-0,000525
3,56547	-0,000444
3,63029	-0,000364
3,69512	-0,00028
3,75995	-0,000195
3,82477	-9,86E-05
3,8896	5,05E-06

1,68549	-0,00276
1,75032	-0,00304
1,81515	-0,00325
1,87997	-0,00334
1,9448	-0,00342
2,00963	-0,00334
2,07445	-0,00325
2,13928	-0,00304
2,20411	-0,00276
2,26893	-0,00256
2,33376	-0,00239
2,39859	-0,00224
2,46341	-0,0021
2,52824	-0,00196
2,59307	-0,00184
2,65789	-0,00172
2,72272	-0,00161
2,78755	-0,0015
2,85237	-0,0014
2,9172	-0,0013
2,98203	-0,0012
3,04685	-0,00111
3,11168	-0,00102
3,17651	-0,00094
3,24133	-0,00085
3,30616	-0,00077
3,37099	-0,00069
3,43581	-0,00061
3,50064	-0,00053
3,56547	-0,00044
3,63029	-0,00037
3,69512	-0,00028
3,75995	-0,0002
3,82477	-9,89E-05
3,8896	4,97E-06

Mesh 4

Distance [m]	U2 [m]
0	7,14E-06
0,0648267	-9,74E-05
0,129653	-0,0001947
0,19448	-0,0002805
0,259307	-0,0003667
0,324133	-0,000447
0,38896	-0,0005303
0,453787	-0,000611
0,518613	-0,0006932
0,58344	-0,0007773
0,648267	-0,0008602

Mesh 5

Distance [m]	U2 [m]
0	4,48E-06
0,0648267	-9,79E-05
0,129653	-0,000194
0,19448	-0,00028
0,259307	-0,000366
0,324133	-0,000448
0,38896	-0,000531
0,453787	-0,000613
0,518613	-0,000695
0,58344	-0,00078
0,648267	-0,000864

Mesh 6

Distance [m	U2 [m]
0	4,34E-06
0,0648267	-9,85E-05
0,129653	-0,0002
0,19448	-0,00028
0,259307	-0,00037
0,324133	-0,00045
0,38896	-0,00053
0,453787	-0,00062
0,518613	-0,0007
0,58344	-0,00078
0,648267	-0,00087

0,713093	-0,0009488		0,713093	-0,000953		0,713093	-0,00096
0,77792	-0,0010347		0,77792	-0,00104		0,77792	-0,00105
0,842747	-0,0011277		0,842747	-0,001133		0,842747	-0,00114
0,907573	-0,0012193		0,907573	-0,001226		0,907573	-0,00123
0,9724	-0,0013165		0,9724	-0,001325		0,9724	-0,00133
1,03723	-0,0014169		1,03723	-0,001426		1,03723	-0,00143
1,10205	-0,0015193		1,10205	-0,001531		1,10205	-0,00154
1,16688	-0,0016309		1,16688	-0,001644		1,16688	-0,00165
1,23171	-0,0017416		1,23171	-0,001757		1,23171	-0,00177
1,29653	-0,001865		1,29653	-0,001883		1,29653	-0,00189
1,36136	-0,0019884		1,36136	-0,00201		1,36136	-0,00202
1,42619	-0,0021244		1,42619	-0,002149		1,42619	-0,00216
1,49101	-0,0022662		1,49101	-0,002295		1,49101	-0,00231
1,55584	-0,0024195		1,55584	-0,002453		1,55584	-0,00246
1,62067	-0,0025964		1,62067	-0,002635		1,62067	-0,00265
1,68549	-0,0027985		1,68549	-0,002841		1,68549	-0,00285
1,75032	-0,0030714		1,75032	-0,003107		1,75032	-0,00313
1,81515	-0,0032831		1,81515	-0,003316		1,81515	-0,00335
1,87997	-0,0033775		1,87997	-0,003418		1,87997	-0,00345
1,9448	-0,0034546		1,9448	-0,003487		1,9448	-0,00352
2,00963	-0,0033778		2,00963	-0,003418		2,00963	-0,00345
2,07445	-0,0032837		2,07445	-0,003317		2,07445	-0,00335
2,13928	-0,0030722		2,13928	-0,003108		2,13928	-0,00313
2,20411	-0,0027998		2,20411	-0,002843		2,20411	-0,00286
2,26893	-0,002598		2,26893	-0,002637		2,26893	-0,00265
2,33376	-0,0024215		2,33376	-0,002455		2,33376	-0,00247
2,39859	-0,0022685		2,39859	-0,002297		2,39859	-0,00231
2,46341	-0,002127		2,46341	-0,002151		2,46341	-0,00216
2,52824	-0,0019914		2,52824	-0,002013		2,52824	-0,00202
2,59307	-0,0018683		2,59307	-0,001886		2,59307	-0,0019
2,65789	-0,0017451		2,65789	-0,001761		2,65789	-0,00177
2,72272	-0,0016347		2,72272	-0,001648		2,72272	-0,00166
2,78755	-0,0015234		2,78755	-0,001535		2,78755	-0,00154
2,85237	-0,0014212		2,85237	-0,001431		2,85237	-0,00144
2,9172	-0,001321		2,9172	-0,001329		2,9172	-0,00134
2,98203	-0,001224		2,98203	-0,001231		2,98203	-0,00124
3,04685	-0,0011326		3,04685	-0,001138		3,04685	-0,00114
3,11168	-0,0010397		3,11168	-0,001045		3,11168	-0,00105
3,17651	-0,000954		3,17651	-0,000958		3,17651	-0,00096
3,24133	-0,0008656		3,24133	-0,000869		3,24133	-0,00087
3,30616	-0,0007827		3,30616	-0,000785		3,30616	-0,00079
3,37099	-0,0006986		3,37099	-0,000701		3,37099	-0,0007
3,43581	-0,0006163		3,43581	-0,000618		3,43581	-0,00062
3,50064	-0,0005356		3,50064	-0,000537		3,50064	-0,00054
3,56547	-0,000452		3,56547	-0,000453		3,56547	-0,00046
3,63029	-0,0003714		3,63029	-0,000372		3,63029	-0,00037
3,69512	-0,0002848		3,69512	-0,000285		3,69512	-0,00029
3,75995	-0,0001984		3,75995	-0,000198		3,75995	-0,0002
3,82E+00	-0,0001003		3,82477	-0,000102		3,82477	-0,0001
3,89E+00	5,06E-06		3,8896	1,60E-06		3,8896	1,50E-06

Mesh 7

Distance [m]	U2 [m]
0	4,29E-06
0,0648267	-9,86E-05
0,129653	-0,0001952
0,19448	-0,0002818
0,259307	-0,0003686
0,324133	-0,0004502
0,38896	-0,0005343
0,453787	-0,0006162
0,518613	-0,0006994
0,58344	-0,0007845
0,648267	-0,0008687
0,713093	-0,0009582
0,77792	-0,0010458
0,842747	-0,00114
0,907573	-0,0012335
0,9724	-0,0013325
1,03723	-0,001435
1,10205	-0,00154
1,16688	-0,0016539
1,23171	-0,0017681
1,29653	-0,0018945
1,36136	-0,0020221
1,42619	-0,0021622
1,49101	-0,002309
1,55584	-0,0024679
1,62067	-0,0026496
1,68549	-0,0028586
1,75032	-0,0031373
1,81515	-0,0033545
1,87997	-0,0034519
1,9448	-0,0035296
2,00963	-0,0034522
2,07445	-0,0033551
2,13928	-0,0031382
2,20411	-0,0028599
2,26893	-0,0026512
2,33376	-0,0024699
2,39859	-0,0023113
2,46341	-0,0021649
2,52824	-0,0020251
2,59307	-0,0018978
2,65789	-0,0017718
2,72272	-0,0016578
2,78755	-0,0015442
2,85237	-0,0014394
2,9172	-0,0013372

Mesh 8

Distance [m]	U2 [m]
0	3,89E-06
0,0648267	-9,84E-05
0,129653	-0,000195
0,19448	-0,000282
0,259307	-0,000369
0,324133	-0,000452
0,38896	-0,000536
0,453787	-0,000618
0,518613	-0,000702
0,58344	-0,000788
0,648267	-0,000873
0,713093	-0,000963
0,77792	-0,001051
0,842747	-0,001146
0,907573	-0,00124
0,9724	-0,00134
1,03723	-0,001444
1,10205	-0,00155
1,16688	-0,001665
1,23171	-0,001781
1,29653	-0,001909
1,36136	-0,002038
1,42619	-0,00218
1,49101	-0,00233
1,55584	-0,002491
1,62067	-0,002676
1,68549	-0,002888
1,75032	-0,003169
1,81515	-0,00339
1,87997	-0,00349
1,9448	-0,003567
2,00963	-0,00349
2,07445	-0,003391
2,13928	-0,00317
2,20411	-0,002889
2,26893	-0,002677
2,33376	-0,002493
2,39859	-0,002332
2,46341	-0,002183
2,52824	-0,002041
2,59307	-0,001912
2,65789	-0,001785
2,72272	-0,001669
2,78755	-0,001554
2,85237	-0,001448
2,9172	-0,001345

Mesh 9

Distance [m	U2[m]
0	9,76E-06
0,0648267	-9,3E-05
0,129653	-0,00019
0,19448	-0,00028
0,259307	-0,00036
0,324133	-0,00044
0,38896	-0,00053
0,453787	-0,00061
0,518613	-0,00069
0,58344	-0,00078
0,648267	-0,00086
0,713093	-0,00095
0,77792	-0,00104
0,842747	-0,00113
0,907573	-0,00123
0,9724	-0,00133
1,03723	-0,00143
1,10205	-0,00153
1,16688	-0,00165
1,23171	-0,00176
1,29653	-0,00189
1,36136	-0,00201
1,42619	-0,00215
1,49101	-0,0023
1,55584	-0,00246
1,62067	-0,00264
1,68549	-0,00285
1,75032	-0,00312
1,81515	-0,00334
1,87997	-0,00344
1,9448	-0,00352
2,00963	-0,00344
2,07445	-0,00334
2,13928	-0,00313
2,20411	-0,00285
2,26893	-0,00264
2,33376	-0,00246
2,39859	-0,0023
2,46341	-0,00216
2,52824	-0,00202
2,59307	-0,00189
2,65789	-0,00176
2,72272	-0,00165
2,78755	-0,00154
2,85237	-0,00143
2,9172	-0,00133

2,98203	-0,0012384
3,04685	-0,0011451
3,11168	-0,0010511
3,17651	-0,0009636
3,24133	-0,0008743
3,30616	-0,0007902
3,37099	-0,0007051
3,43581	-0,0006219
3,50064	-0,0005401
3,56547	-0,0004558
3,63029	-0,000374
3,69512	-0,0002869
3,75995	-0,0001996
3,82477	-0,0001023
3,8896	1,27E-06

2,98203	-0,001245
3,04685	-0,001151
3,11168	-0,001057
3,17651	-0,000968
3,24133	-0,000879
3,30616	-0,000794
3,37099	-0,000708
3,43581	-0,000625
3,50064	-0,000542
3,56547	-0,000457
3,63029	-0,000375
3,69512	-0,000287
3,75995	-0,0002
3,82477	-0,000103
3,8896	4,11E-07

2,98203	-0,00123
3,04685	-0,00114
3,11168	-0,00105
3,17651	-0,00096
3,24133	-0,00087
3,30616	-0,00078
3,37099	-0,0007
3,43581	-0,00062
3,50064	-0,00053
3,56547	-0,00045
3,63029	-0,00037
3,69512	-0,00028
3,75995	-0,00019
3,82477	-9,7E-05
3,8896	6,70E-06

Result : Global Deflection Upper Plate

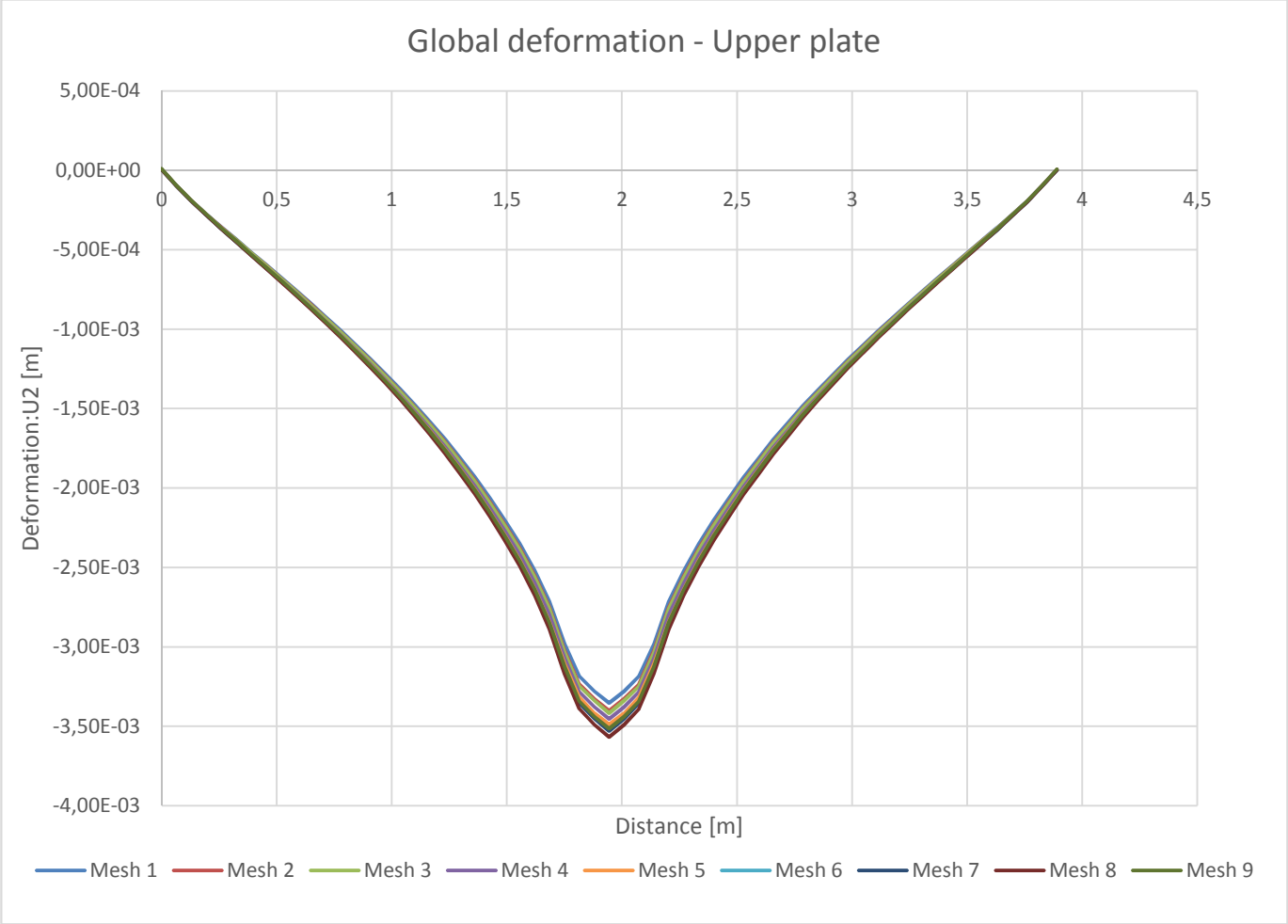

MIN values

Mesh 1	Mesh 2	Mesh 3	Mesh 4	Mesh 5	Mesh 6	Mesh 7	Mesh 8	Mesh 9
-3,35E-03	-3,40E-03	-3,4E-03	-3,45E-03	-3,49E-03	-3,5E-03	-3,53E-03	-3,6E-03	-3,5E-03

Differece in min value

Mesh 1-2	Mesh 2-3	Mesh 3-4	Mesh 4-5	Mesh 5-6	Mesh 6-7	Mesh 7-8
1,5%	0,4%	1,1%	0,9%	1,0%	0,2%	1,1%

Global Deflection - Bottom Plate

Additionally, a check of the global deflection of the lower plate were done. The values are taken in the center line of the slab at the bottom edge of the bottom plate, see figure below,

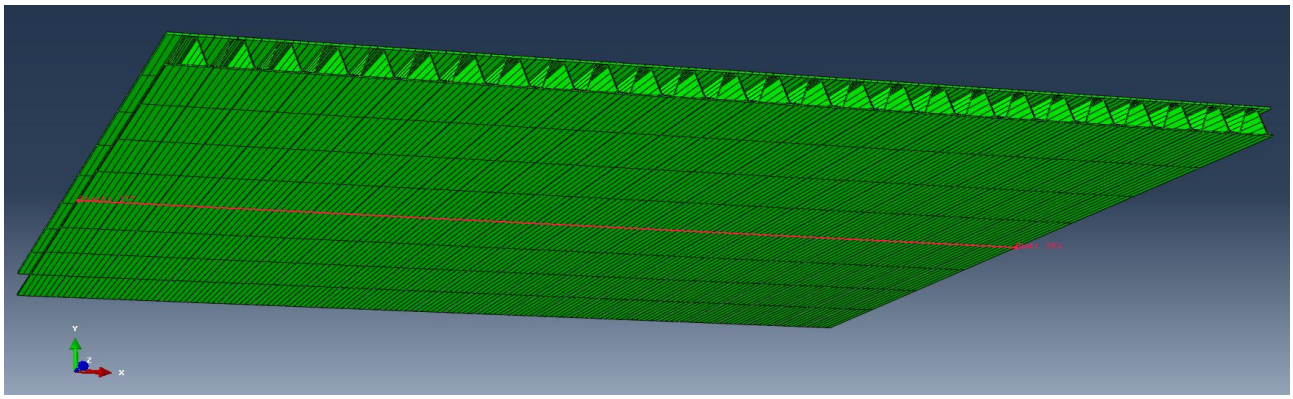

Mesh 1

Distance [m]	U2 [m]
0	-8,9E-34
0,0648268	-8,7E-05
0,129654	-0,0001754
0,19448	-0,00028
0,259307	-0,000338
0,324134	-0,0004384
0,388961	-0,0004999
0,453787	-0,0005885
0,518614	-0,0006702
0,583441	-0,000738
0,648268	-0,0008401
0,713094	-0,0009009
0,777921	-0,0010098
0,842748	-0,001079
0,907575	-0,0011811
0,972401	-0,001277
1,03723	-0,0013584
1,10205	-0,0014848
1,16688	-0,0015598
1,23171	-0,0017031
1,29654	-0,0017897
1,36136	-0,0019334
1,42619	-0,0020585
1,49102	-0,0021791
1,55584	-0,0023636
1,62067	-0,0024811
1,6855	-0,0027302
1,75032	-0,0028621
1,81515	-0,0030534

Mesh 2

Distance [m]	U2 [m]
0	-9E-34
0,0648268	-9E-05
0,129654	-0,000173
0,19448	-0,000279
0,259307	-0,00034
0,324134	-0,000442
0,388961	-0,000506
0,453787	-0,000593
0,518614	-0,000676
0,583441	-0,000743
0,648268	-0,000847
0,713094	-0,00091
0,777921	-0,001021
0,842748	-0,001092
0,907575	-0,001193
0,972401	-0,001289
1,03723	-0,001371
1,10205	-0,001499
1,16688	-0,001577
1,23171	-0,001725
1,29654	-0,001814
1,36136	-0,001958
1,42619	-0,002084
1,49102	-0,002205
1,55584	-0,002392
1,62067	-0,002516
1,6855	-0,002773
1,75032	-0,00291
1,81515	-0,003101

Mesh 3

Distance [m	U2 [m]
0	-9E-34
0,0648268	-9E-05
0,129654	-0,00017
0,19448	-0,00028
0,259307	-0,00034
0,324134	-0,00044
0,388961	-0,00051
0,453787	-0,00059
0,518614	-0,00068
0,583441	-0,00075
0,648268	-0,00085
0,713094	-0,00091
0,777921	-0,00102
0,842748	-0,0011
0,907575	-0,0012
0,972401	-0,00129
1,03723	-0,00138
1,10205	-0,00151
1,16688	-0,00158
1,23171	-0,00173
1,29654	-0,00182
1,36136	-0,00197
1,42619	-0,00209
1,49102	-0,00221
1,55584	-0,0024
1,62067	-0,00253
1,6855	-0,00278
1,75032	-0,00292
1,81515	-0,00311

1,87998	-0,0031859
1,9448	-0,0031515
2,00963	-0,0031862
2,07446	-0,0030539
2,13928	-0,002863
2,20411	-0,0027312
2,26894	-0,0024826
2,33376	-0,0023653
2,39859	-0,0021812
2,46342	-0,0020609
2,52824	-0,0019359
2,59307	-0,0017927
2,6579	-0,0017061
2,72272	-0,0015633
2,78755	-0,0014884
2,85238	-0,0013622
2,9172	-0,001281
2,98203	-0,0011851
3,04686	-0,0010834
3,11168	-0,001014
3,17651	-0,0009054
3,24134	-0,0008445
3,30616	-0,0007426
3,37099	-0,0006747
3,43582	-0,0005929
3,50064	-0,0005042
3,56547	-0,0004427
3,6303	-0,0003417
3,69513	-0,0002833
3,75995	-0,0001793
3,82478	-8,96E-05
3,88961	-8,87E-34

1,87998	-0,003232
1,9448	-0,003195
2,00963	-0,003232
2,07446	-0,003102
2,13928	-0,002911
2,20411	-0,002774
2,26894	-0,002517
2,33376	-0,002394
2,39859	-0,002207
2,46342	-0,002086
2,52824	-0,001961
2,59307	-0,001817
2,6579	-0,001728
2,72272	-0,001581
2,78755	-0,001503
2,85238	-0,001375
2,9172	-0,001293
2,98203	-0,001197
3,04686	-0,001096
3,11168	-0,001025
3,17651	-0,000915
3,24134	-0,000852
3,30616	-0,000748
3,37099	-0,00068
3,43582	-0,000598
3,50064	-0,00051
3,56547	-0,000447
3,6303	-0,000344
3,69513	-0,000282
3,75995	-0,000177
3,82478	-9,04E-05
3,88961	-8,73E-34

1,87998	-0,00325
1,9448	-0,00321
2,00963	-0,00325
2,07446	-0,00311
2,13928	-0,00292
2,20411	-0,00278
2,26894	-0,00253
2,33376	-0,00241
2,39859	-0,00221
2,46342	-0,0021
2,52824	-0,00197
2,59307	-0,00183
2,6579	-0,00173
2,72272	-0,00159
2,78755	-0,00151
2,85238	-0,00138
2,9172	-0,0013
2,98203	-0,0012
3,04686	-0,0011
3,11168	-0,00103
3,17651	-0,00092
3,24134	-0,00086
3,30616	-0,00075
3,37099	-0,00068
3,43582	-0,0006
3,50064	-0,00051
3,56547	-0,00045
3,6303	-0,00034
3,69513	-0,00028
3,75995	-0,00018
3,82478	-8,99E-05
3,88961	-8,72E-34

Mesh 4

Distance [m]	U2 [m]
0	-8,86E-35
0,0648268	-9,85E-05
0,129654	-0,0001806
0,19448	-0,0002914
0,259307	-0,0003558
0,324134	-0,0004572
0,388961	-0,0005236
0,453787	-0,0006142
0,518614	-0,0006946
0,583441	-0,0007683
0,648268	-0,000869
0,713094	-0,0009354
0,777921	-0,001047
0,842748	-0,0011172

Mesh 5

Distance [m]	U2 [m]
0	-1,72E-34
0,0648268	-9,86E-05
0,129654	-0,000181
0,19448	-0,00029
0,259307	-0,000357
0,324134	-0,000457
0,388961	-0,000525
0,453787	-0,000615
0,518614	-0,000696
0,583441	-0,000772
0,648268	-0,000871
0,713094	-0,00094
0,777921	-0,001051
0,842748	-0,001124

Mesh 6

Distance [m	U2 [m]
0	-8,60E-35
0,0648268	-9,92E-05
0,129654	-0,00018
0,19448	-0,00029
0,259307	-0,00036
0,324134	-0,00046
0,388961	-0,00053
0,453787	-0,00062
0,518614	-0,0007
0,583441	-0,00078
0,648268	-0,00088
0,713094	-0,00095
0,777921	-0,00106
0,842748	-0,00113

0,907575	-0,0012269
0,972401	-0,0013145
1,03723	-0,0014085
1,10205	-0,001528
1,16688	-0,001613
1,23171	-0,0017582
1,29654	-0,0018475
1,36136	-0,0020033
1,42619	-0,0021167
1,49102	-0,0022613
1,55584	-0,0024279
1,62067	-0,0025695
1,6855	-0,0028164
1,75032	-0,002957
1,81515	-0,0031669
1,87998	-0,0032745
1,9448	-0,0032842
2,00963	-0,0032748
2,07446	-0,0031674
2,13928	-0,002958
2,20411	-0,0028175
2,26894	-0,0025711
2,33376	-0,0024298
2,39859	-0,0022636
2,46342	-0,0021193
2,52824	-0,0020061
2,59307	-0,0018508
2,6579	-0,0017616
2,72272	-0,0016169
2,78755	-0,001532
2,85238	-0,0014128
2,9172	-0,0013189
2,98203	-0,0012315
3,04686	-0,0011222
3,11168	-0,0010519
3,17651	-0,0009407
3,24134	-0,0008741
3,30616	-0,0007737
3,37099	-0,0006998
3,43582	-0,0006194
3,50064	-0,0005289
3,56547	-0,0004621
3,6303	-0,0003604
3,69513	-0,0002953
3,75995	-0,0001848
3,82478	-0,0001032
3,88961	-8,89E-35

0,907575	-0,001233
0,972401	-0,001323
1,03723	-0,001418
1,10205	-0,001538
1,16688	-0,001627
1,23171	-0,001772
1,29654	-0,001867
1,36136	-0,002023
1,42619	-0,002141
1,49102	-0,002289
1,55584	-0,00246
1,62067	-0,002609
1,6855	-0,002854
1,75032	-0,003
1,81515	-0,003207
1,87998	-0,003316
1,9448	-0,003328
2,00963	-0,003316
2,07446	-0,003207
2,13928	-0,003001
2,20411	-0,002855
2,26894	-0,00261
2,33376	-0,002462
2,39859	-0,002292
2,46342	-0,002144
2,52824	-0,002025
2,59307	-0,00187
2,6579	-0,001775
2,72272	-0,001631
2,78755	-0,001542
2,85238	-0,001423
2,9172	-0,001327
2,98203	-0,001238
3,04686	-0,001129
3,11168	-0,001056
3,17651	-0,000946
3,24134	-0,000877
3,30616	-0,000777
3,37099	-0,000702
3,43582	-0,000621
3,50064	-0,000531
3,56547	-0,000462
3,6303	-0,000362
3,69513	-0,000294
3,75995	-0,000187
3,82478	-0,000105
3,88961	-1,72E-34

0,907575	-0,00124
0,972401	-0,00133
1,03723	-0,00143
1,10205	-0,00155
1,16688	-0,00164
1,23171	-0,00178
1,29654	-0,00188
1,36136	-0,00203
1,42619	-0,00215
1,49102	-0,0023
1,55584	-0,00247
1,62067	-0,00262
1,6855	-0,00287
1,75032	-0,00302
1,81515	-0,00323
1,87998	-0,00334
1,9448	-0,00336
2,00963	-0,00334
2,07446	-0,00323
2,13928	-0,00302
2,20411	-0,00287
2,26894	-0,00262
2,33376	-0,00247
2,39859	-0,0023
2,46342	-0,00216
2,52824	-0,00204
2,59307	-0,00188
2,6579	-0,00178
2,72272	-0,00164
2,78755	-0,00155
2,85238	-0,00143
2,9172	-0,00133
2,98203	-0,00124
3,04686	-0,00113
3,11168	-0,00106
3,17651	-0,00095
3,24134	-0,00088
3,30616	-0,00078
3,37099	-0,00071
3,43582	-0,00062
3,50064	-0,00053
3,56547	-0,00046
3,6303	-0,00036
3,69513	-0,0003
3,75995	-0,00019
3,82478	-0,00011
3,88961	-8,62E-35

Mesh 7

Distance [m]	U2 [m]
0	-8,58E-35
0,0648268	-9,96E-05
0,129654	-0,0001826
0,19448	-0,0002916
0,259307	-0,0003588
0,324134	-0,0004595
0,388961	-0,0005283
0,453787	-0,000619
0,518614	-0,0007005
0,583441	-0,0007762
0,648268	-0,0008765
0,713094	-0,0009461
0,777921	-0,0010568
0,842748	-0,0011304
0,907575	-0,0012402
0,972401	-0,0013305
1,03723	-0,0014272
1,10205	-0,0015476
1,16688	-0,0016376
1,23171	-0,0017827
1,29654	-0,0018783
1,36136	-0,0020351
1,42619	-0,0021548
1,49102	-0,0023039
1,55584	-0,0024749
1,62067	-0,0026258
1,6855	-0,0028743
1,75032	-0,003024
1,81515	-0,0032358
1,87998	-0,0033471
1,9448	-0,0033603
2,00963	-0,0033474
2,07446	-0,0032363
2,13928	-0,003025
2,20411	-0,0028754
2,26894	-0,0026275
2,33376	-0,0024768
2,39859	-0,0023062
2,46342	-0,0021574
2,52824	-0,002038
2,59307	-0,0018816
2,6579	-0,0017861
2,72272	-0,0016415
2,78755	-0,0015517
2,85238	-0,0014316
2,9172	-0,0013351

Mesh 8

Distance [m]	U2 [m]
0	-8,47E-35
0,0648268	-0,0001
0,129654	-0,000184
0,19448	-0,000291
0,259307	-0,00036
0,324134	-0,00046
0,388961	-0,00053
0,453787	-0,000621
0,518614	-0,000703
0,583441	-0,00078
0,648268	-0,00088
0,713094	-0,000951
0,777921	-0,001061
0,842748	-0,001137
0,907575	-0,001247
0,972401	-0,001338
1,03723	-0,001437
1,10205	-0,001557
1,16688	-0,00165
1,23171	-0,001795
1,29654	-0,001894
1,36136	-0,00205
1,42619	-0,002173
1,49102	-0,002325
1,55584	-0,002498
1,62067	-0,002654
1,6855	-0,002902
1,75032	-0,003058
1,81515	-0,003269
1,87998	-0,003382
1,9448	-0,003397
2,00963	-0,003382
2,07446	-0,003269
2,13928	-0,003059
2,20411	-0,002903
2,26894	-0,002655
2,33376	-0,0025
2,39859	-0,002327
2,46342	-0,002176
2,52824	-0,002053
2,59307	-0,001897
2,6579	-0,001798
2,72272	-0,001654
2,78755	-0,001561
2,85238	-0,001441
2,9172	-0,001343

Mesh 9

Distance [m	U2 [m]
0	-8,7E-35
0,0648268	-9,9E-05
0,129654	-0,00018
0,19448	-0,00029
0,259307	-0,00035
0,324134	-0,00045
0,388961	-0,00052
0,453787	-0,00061
0,518614	-0,0007
0,583441	-0,00077
0,648268	-0,00087
0,713094	-0,00094
0,777921	-0,00105
0,842748	-0,00112
0,907575	-0,00123
0,972401	-0,00132
1,03723	-0,00142
1,10205	-0,00154
1,16688	-0,00163
1,23171	-0,00178
1,29654	-0,00187
1,36136	-0,00202
1,42619	-0,00215
1,49102	-0,0023
1,55584	-0,00247
1,62067	-0,00262
1,6855	-0,00286
1,75032	-0,00301
1,81515	-0,00322
1,87998	-0,00333
1,9448	-0,00335
2,00963	-0,00333
2,07446	-0,00322
2,13928	-0,00301
2,20411	-0,00286
2,26894	-0,00262
2,33376	-0,00247
2,39859	-0,0023
2,46342	-0,00215
2,52824	-0,00203
2,59307	-0,00187
2,6579	-0,00178
2,72272	-0,00164
2,78755	-0,00155
2,85238	-0,00143
2,9172	-0,00133

2,98203	-0,001245
3,04686	-0,0011355
3,11168	-0,0010618
3,17651	-0,0009516
3,24134	-0,0008819
3,30616	-0,0007819
3,37099	-0,0007062
3,43582	-0,0006247
3,50064	-0,000534
3,56547	-0,0004649
3,6303	-0,0003641
3,69513	-0,0002961
3,75995	-0,0001878
3,82478	-0,0001055
3,88961	-8,59E-35

2,98203	-0,001251
3,04686	-0,001142
3,11168	-0,001067
3,17651	-0,000957
3,24134	-0,000885
3,30616	-0,000786
3,37099	-0,000709
3,43582	-0,000627
3,50064	-0,000536
3,56547	-0,000466
3,6303	-0,000366
3,69513	-0,000296
3,75995	-0,000189
3,82478	-0,000107
3,88961	-8,47E-35

2,98203	-0,00124
3,04686	-0,00113
3,11168	-0,00106
3,17651	-0,00095
3,24134	-0,00088
3,30616	-0,00078
3,37099	-0,0007
3,43582	-0,00062
3,50064	-0,00053
3,56547	-0,00046
3,6303	-0,00036
3,69513	-0,00029
3,75995	-0,00018
3,82478	-0,0001
3,88961	-8,6E-35

Result : Global Deflection Bottom Plate

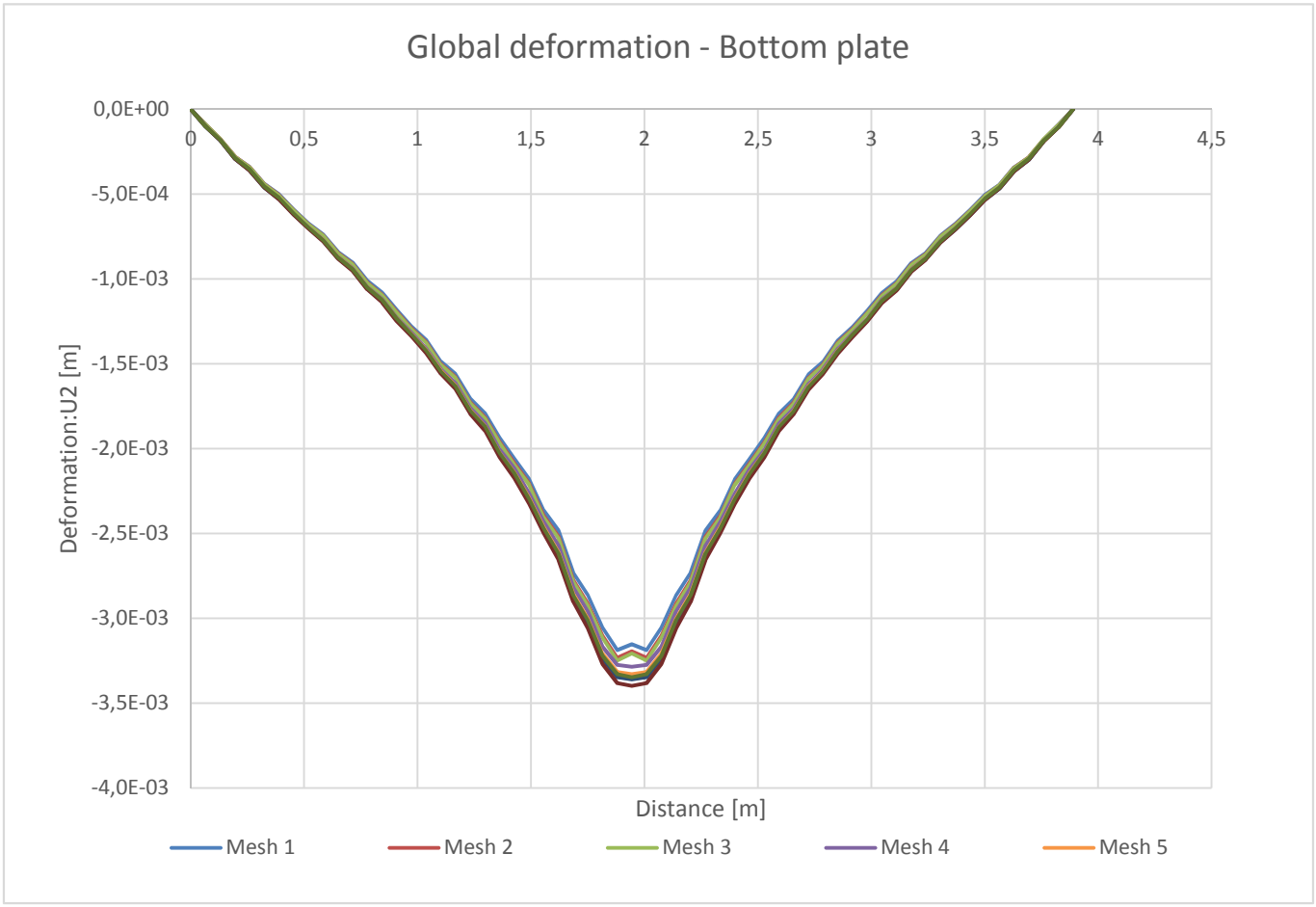

MID values

Mesh 1	Mesh 2	Mesh 3	Mesh 4	Mesh 5	Mesh 6	Mesh 7	Mesh 8	Mesh 9
-0,0031515	-0,0031946	-0,003206	-3,284E-03	-3,33E-03	-3,4E-03	-3,36E-03	-3,4E-03	-3,3E-03

Differece in min value

Mesh 1-2	Mesh 2-3	Mesh 3-4	Mesh 4-5	Mesh 5-6	Mesh 6-7	Mesh 7-8	Mesh 8-9
1,3%	0,4%	2,4%	1,3%	0,8%	0,2%	1,1%	1,5%

Local deflection - Upper Plate

To take account for the local impact of the patch load a convergence check of the local deflection of the upper plate were performed. The convergence check was done under the patch load, for exact position see figure below:

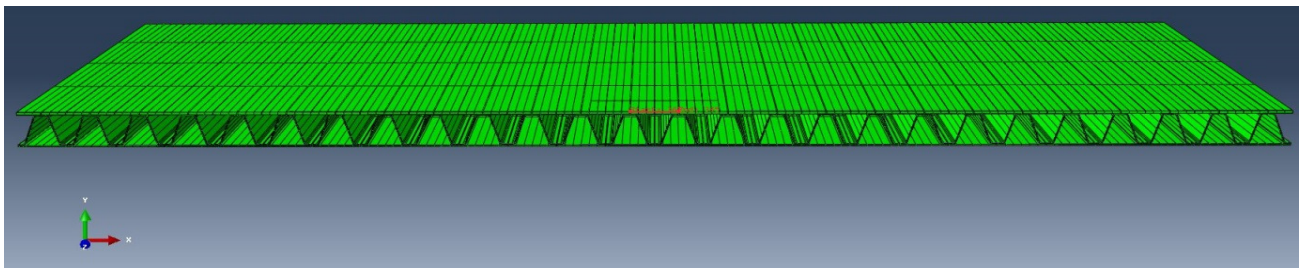

Mesh 1

Distance [m]	U2 [m]
0	-0,0032629
0,00244331	-0,0032679
0,00488663	-0,0032728
0,00732994	-0,0032775
0,00977337	-0,0032821
0,0122167	-0,0032866
0,01466	-0,0032909
0,0171033	-0,0032951
0,0195466	-0,0032992
0,0219901	-0,0033031
0,0244334	-0,0033069
0,0268767	-0,0033106
0,02932	-0,0033141
0,0317633	-0,0033175
0,0342066	-0,0033207
0,0366499	-0,0033238
0,0390934	-0,0033268
0,0415367	-0,0033296
0,04398	-0,0033323
0,0464233	-0,0033349
0,0488666	-0,0033373
0,0513101	-0,0033396
0,0537534	-0,0033418
0,0561967	-0,0033438
0,05864	-0,0033457
0,0610833	-0,0033474
0,0635266	-0,003349
0,0659699	-0,0033505
0,0684134	-0,0033518
0,0708567	-0,003353
0,0733	-0,0033541

Mesh 2

Distance [m]	U2 [m]
0	-0,003311
0,00244331	-0,003315
0,00488663	-0,00332
0,00732994	-0,003324
0,00977337	-0,003329
0,0122167	-0,003333
0,01466	-0,003337
0,0171033	-0,003341
0,0195466	-0,003346
0,0219901	-0,00335
0,0244334	-0,003354
0,0268767	-0,003358
0,02932	-0,003362
0,0317633	-0,003366
0,0342066	-0,00337
0,0366499	-0,003374
0,0390934	-0,003378
0,0415367	-0,003381
0,04398	-0,003384
0,0464233	-0,003387
0,0488666	-0,00339
0,0513101	-0,003392
0,0537534	-0,003395
0,0561967	-0,003397
0,05864	-0,003398
0,0610833	-0,0034
0,0635266	-0,003401
0,0659699	-0,003402
0,0684134	-0,003403
0,0708567	-0,003403
0,0733	-0,003404

Mesh 3

Distance [m	U2 [m]
0	-0,00332
0,0024433	-0,00333
0,0048866	-0,00333
0,0073299	-0,00334
0,0097734	-0,00334
0,0122167	-0,00335
0,01466	-0,00335
0,0171033	-0,00335
0,0195466	-0,00336
0,0219901	-0,00336
0,0244334	-0,00337
0,0268767	-0,00337
0,02932	-0,00338
0,0317633	-0,00338
0,0342066	-0,00338
0,0366499	-0,00339
0,0390934	-0,00339
0,0415367	-0,00339
0,04398	-0,0034
0,0464233	-0,0034
0,0488666	-0,0034
0,0513101	-0,00341
0,0537534	-0,00341
0,0561967	-0,00341
0,05864	-0,00341
0,0610833	-0,00341
0,0635266	-0,00342
0,0659699	-0,00342
0,0684134	-0,00342
0,0708567	-0,00342
0,0733	-0,00342

0,0757433	-0,0033531
0,0781866	-0,0033519
0,0806301	-0,0033505
0,0830734	-0,0033491
0,0855167	-0,0033475
0,08796	-0,0033457
0,0904033	-0,0033439
0,0928466	-0,0033419
0,0952899	-0,0033397
0,0977334	-0,0033374
0,100177	-0,003335
0,10262	-0,0033325
0,105063	-0,0033298
0,107507	-0,0033269
0,10995	-0,003324
0,112393	-0,0033209
0,114837	-0,0033176
0,11728	-0,0033143
0,119723	-0,0033108
0,122167	-0,0033071
0,12461	-0,0033034
0,127053	-0,0032994
0,129497	-0,0032954
0,13194	-0,0032912
0,134383	-0,0032869
0,136827	-0,0032824
0,13927	-0,0032778
0,141713	-0,0032731
0,144157	-0,0032682
0,1466	-0,0032632

0,0757433	-0,003403
0,0781866	-0,003403
0,0806301	-0,003402
0,0830734	-0,003401
0,0855167	-0,0034
0,08796	-0,003398
0,0904033	-0,003397
0,0928466	-0,003395
0,0952899	-0,003393
0,0977334	-0,00339
0,100177	-0,003387
0,10262	-0,003385
0,105063	-0,003381
0,107507	-0,003378
0,10995	-0,003374
0,112393	-0,00337
0,114837	-0,003366
0,11728	-0,003362
0,119723	-0,003358
0,122167	-0,003354
0,12461	-0,00335
0,127053	-0,003346
0,129497	-0,003342
0,13194	-0,003337
0,134383	-0,003333
0,136827	-0,003329
0,13927	-0,003324
0,141713	-0,00332
0,144157	-0,003316
0,1466	-0,003311

0,0757433	-0,00342
0,0781866	-0,00342
0,0806301	-0,00342
0,0830734	-0,00342
0,0855167	-0,00341
0,08796	-0,00341
0,0904033	-0,00341
0,0928466	-0,00341
0,0952899	-0,00341
0,0977334	-0,0034
0,100177	-0,0034
0,10262	-0,0034
0,105063	-0,00339
0,107507	-0,00339
0,10995	-0,00339
0,112393	-0,00338
0,114837	-0,00338
0,11728	-0,00338
0,119723	-0,00337
0,122167	-0,00337
0,12461	-0,00336
0,127053	-0,00336
0,129497	-0,00335
0,13194	-0,00335
0,134383	-0,00335
0,136827	-0,00334
0,13927	-0,00334
0,141713	-0,00333
0,144157	-0,00333
0,1466	-0,00332

Mesh 4

Distance [m]	U2 [m]
0	-0,0033627
0,00244331	-0,0033669
0,00488663	-0,0033712
0,00732994	-0,0033755
0,00977337	-0,0033798
0,0122167	-0,0033841
0,01466	-0,0033885
0,0171033	-0,0033928
0,0195466	-0,0033972
0,0219901	-0,0034016
0,0244334	-0,0034061
0,0268767	-0,0034104
0,02932	-0,0034145
0,0317633	-0,0034184
0,0342066	-0,0034222
0,0366499	-0,0034258

Mesh 5

Distance [m]	U2 [m]
0	-0,003402
0,00249338	-0,003405
0,00498664	-0,00341
0,00748003	-0,003414
0,00997329	-0,003418
0,0124667	-0,003422
0,0149599	-0,003426
0,0174533	-0,003431
0,0199467	-0,003435
0,02244	-0,003439
0,0249333	-0,003443
0,0274266	-0,003447
0,02992	-0,00345
0,0324134	-0,003454
0,0349066	-0,003458
0,0374	-0,003461

Mesh 6

Distance [m	U2 [m]
0	-0,00343
0,0024934	-0,00343
0,0049866	-0,00344
0,00748	-0,00344
0,0099733	-0,00345
0,0124667	-0,00345
0,0149599	-0,00346
0,0174533	-0,00346
0,0199467	-0,00346
0,02244	-0,00347
0,0249333	-0,00347
0,0274266	-0,00348
0,02992	-0,00348
0,0324134	-0,00349
0,0349066	-0,00349
0,0374	-0,00349

0,0390934	-0,0034293
0,0415367	-0,0034325
0,04398	-0,0034356
0,0464233	-0,0034386
0,0488666	-0,0034413
0,0513101	-0,0034438
0,0537534	-0,0034461
0,0561967	-0,003448
0,05864	-0,0034498
0,0610833	-0,0034512
0,0635266	-0,0034524
0,0659699	-0,0034534
0,0684134	-0,0034541
0,0708567	-0,0034545
0,0733	-0,0034546
0,0757433	-0,0034545
0,0781866	-0,0034541
0,0806301	-0,0034534
0,0830734	-0,0034525
0,0855167	-0,0034513
0,08796	-0,0034498
0,0904033	-0,0034481
0,0928466	-0,0034462
0,0952899	-0,0034439
0,0977334	-0,0034414
0,100177	-0,0034387
0,10262	-0,0034358
0,105063	-0,0034327
0,107507	-0,0034294
0,10995	-0,003426
0,112393	-0,0034224
0,114837	-0,0034186
0,11728	-0,0034147
0,119723	-0,0034106
0,122167	-0,0034063
0,12461	-0,0034019
0,127053	-0,0033975
0,129497	-0,0033931
0,13194	-0,0033887
0,134383	-0,0033844
0,136827	-0,0033801
0,13927	-0,0033758
0,141713	-0,0033715
0,144157	-0,0033673
0,1466	-0,003363

0,0398933	-0,003464
0,0423867	-0,003467
0,04488	-0,00347
0,0473733	-0,003473
0,0498667	-0,003475
0,0523599	-0,003477
0,0548533	-0,003479
0,0573466	-0,003481
0,05984	-0,003483
0,0623333	-0,003484
0,0648266	-0,003485
0,06732	-0,003486
0,0698133	-0,003487
0,0723066	-0,003487
0,0747999	-0,003487
0,0772933	-0,003487
0,0797867	-0,003487
0,0822799	-0,003486
0,0847733	-0,003485
0,0872666	-0,003484
0,0897599	-0,003483
0,0922533	-0,003481
0,0947466	-0,00348
0,09724	-0,003478
0,0997332	-0,003475
0,102227	-0,003473
0,10472	-0,00347
0,107213	-0,003467
0,109707	-0,003464
0,1122	-0,003461
0,114693	-0,003458
0,117187	-0,003454
0,11968	-0,003451
0,122173	-0,003447
0,124667	-0,003443
0,12716	-0,003439
0,129653	-0,003435
0,132146	-0,003431
0,13464	-0,003427
0,137133	-0,003422
0,139627	-0,003418
0,14212	-0,003414
0,144613	-0,00341
0,147107	-0,003406
0,1496	-0,003402

0,0398933	-0,0035
0,0423867	-0,0035
0,04488	-0,0035
0,0473733	-0,00351
0,0498667	-0,00351
0,0523599	-0,00351
0,0548533	-0,00351
0,0573466	-0,00352
0,05984	-0,00352
0,0623333	-0,00352
0,0648266	-0,00352
0,06732	-0,00352
0,0698133	-0,00352
0,0723066	-0,00352
0,0747999	-0,00352
0,0772933	-0,00352
0,0797867	-0,00352
0,0822799	-0,00352
0,0847733	-0,00352
0,0872666	-0,00352
0,0897599	-0,00352
0,0922533	-0,00352
0,0947466	-0,00352
0,09724	-0,00351
0,0997332	-0,00351
0,102227	-0,00351
0,10472	-0,0035
0,107213	-0,0035
0,109707	-0,0035
0,1122	-0,00349
0,114693	-0,00349
0,117187	-0,00349
0,11968	-0,00348
0,122173	-0,00348
0,124667	-0,00347
0,12716	-0,00347
0,129653	-0,00346
0,132146	-0,00346
0,13464	-0,00346
0,137133	-0,00345
0,139627	-0,00345
0,14212	-0,00344
0,144613	-0,00344
0,147107	-0,00343
0,1496	-0,00343

Mesh 7

Distance [m]	U2 [m]
0	-0,0034345
0,00249338	-0,0034386
0,00498664	-0,003443
0,00748003	-0,0034474
0,00997329	-0,0034519
0,0124667	-0,0034563
0,0149599	-0,0034608
0,0174533	-0,0034653
0,0199467	-0,0034698
0,02244	-0,0034744
0,0249333	-0,0034789
0,0274266	-0,0034834
0,02992	-0,0034876
0,0324134	-0,0034917
0,0349066	-0,0034956
0,0374	-0,0034994
0,0398933	-0,003503
0,0423867	-0,0035064
0,04488	-0,0035096
0,0473733	-0,0035127
0,0498667	-0,0035156
0,0523599	-0,0035182
0,0548533	-0,0035206
0,0573466	-0,0035226
0,05984	-0,0035244
0,0623333	-0,0035259
0,0648266	-0,0035272
0,06732	-0,0035282
0,0698133	-0,0035289
0,0723066	-0,0035294
0,0747999	-0,0035296
0,0772933	-0,0035294
0,0797867	-0,0035289
0,0822799	-0,0035282
0,0847733	-0,0035272
0,0872666	-0,003526
0,0897599	-0,0035245
0,0922533	-0,0035227
0,0947466	-0,0035207
0,09724	-0,0035183
0,0997332	-0,0035157
0,102227	-0,0035128
0,10472	-0,0035098
0,107213	-0,0035065
0,109707	-0,0035031
0,1122	-0,0034996

Mesh 8

Distance [m]	U2 [m]
0	-0,003472
0,00249338	-0,003476
0,00498664	-0,00348
0,00748003	-0,003485
0,00997329	-0,00349
0,0124667	-0,003494
0,0149601	-0,003499
0,0174533	-0,003503
0,0199467	-0,003508
0,02244	-0,003512
0,0249333	-0,003516
0,0274267	-0,003521
0,02992	-0,003525
0,0324134	-0,003529
0,0349066	-0,003533
0,0374	-0,003537
0,0398934	-0,003541
0,0423867	-0,003544
0,04488	-0,003548
0,0473733	-0,003551
0,0498667	-0,003553
0,0523601	-0,003556
0,0548533	-0,003558
0,0573467	-0,00356
0,05984	-0,003562
0,0623333	-0,003563
0,0648267	-0,003565
0,06732	-0,003566
0,0698134	-0,003566
0,0723066	-0,003567
0,0748	-0,003567
0,0772934	-0,003567
0,0797867	-0,003567
0,08228	-0,003566
0,0847733	-0,003565
0,0872667	-0,003564
0,0897601	-0,003562
0,0922533	-0,00356
0,0947467	-0,003558
0,09724	-0,003556
0,0997334	-0,003553
0,102227	-0,003551
0,10472	-0,003548
0,107213	-0,003544
0,109707	-0,003541
0,1122	-0,003537

Mesh 9

Distance [m	U2 [m]
0	-3,4E-03
0,0024934	-3,4E-03
0,0049866	-0,00343
0,00748	-0,00343
0,0099733	-0,00344
0,0124667	-0,00344
0,0149601	-0,00345
0,0174533	-0,00345
0,0199467	-0,00346
0,02244	-0,00346
0,0249333	-0,00346
0,0274267	-0,00347
0,02992	-0,00347
0,0324134	-0,00348
0,0349066	-0,00348
0,0374	-0,00349
0,0398934	-0,00349
0,0423867	-0,00349
0,04488	-0,0035
0,0473733	-0,0035
0,0498667	-0,0035
0,0523601	-0,0035
0,0548533	-0,00351
0,0573467	-0,00351
0,05984	-0,00351
0,0623333	-0,00351
0,0648267	-0,00351
0,06732	-0,00351
0,0698134	-0,00351
0,0723066	-0,00352
0,0748	-0,00352
0,0772934	-0,00352
0,0797867	-0,00351
0,08228	-0,00351
0,0847733	-0,00351
0,0872667	-0,00351
0,0897601	-0,00351
0,0922533	-0,00351
0,0947467	-0,00351
0,09724	-0,0035
0,0997334	-0,0035
0,102227	-0,0035
0,10472	-0,0035
0,107213	-0,00349
0,109707	-0,00349
0,1122	-0,00349

0,114693	-0,0034958
0,117187	-0,0034919
0,11968	-0,0034878
0,122173	-0,0034836
0,124667	-0,0034792
0,12716	-0,0034746
0,129653	-0,0034701
0,132146	-0,0034656
0,13464	-0,0034611
0,137133	-0,0034566
0,139627	-0,0034522
0,14212	-0,0034477
0,144613	-0,0034433
0,147107	-0,003439
0,1496	-0,0034348

0,114693	-0,003533
0,117187	-0,003529
0,11968	-0,003525
0,122173	-0,003521
0,124667	-0,003517
0,12716	-0,003512
0,129653	-0,003508
0,132147	-0,003504
0,13464	-0,003499
0,137133	-0,003495
0,139627	-0,00349
0,14212	-0,003485
0,144613	-0,003481
0,147107	-0,003476
0,1496	-0,003472

0,114693	-0,00348
0,117187	-0,00348
0,11968	-0,00347
0,122173	-0,00347
0,124667	-0,00347
0,12716	-0,00346
0,129653	-0,00346
0,132147	-0,00345
0,13464	-0,00345
0,137133	-0,00344
0,139627	-0,00344
0,14212	-0,00343
0,144613	-0,00343
0,147107	-3,4E-03
0,1496	-3,4E-03

Result : Local Deflection Upper Plate

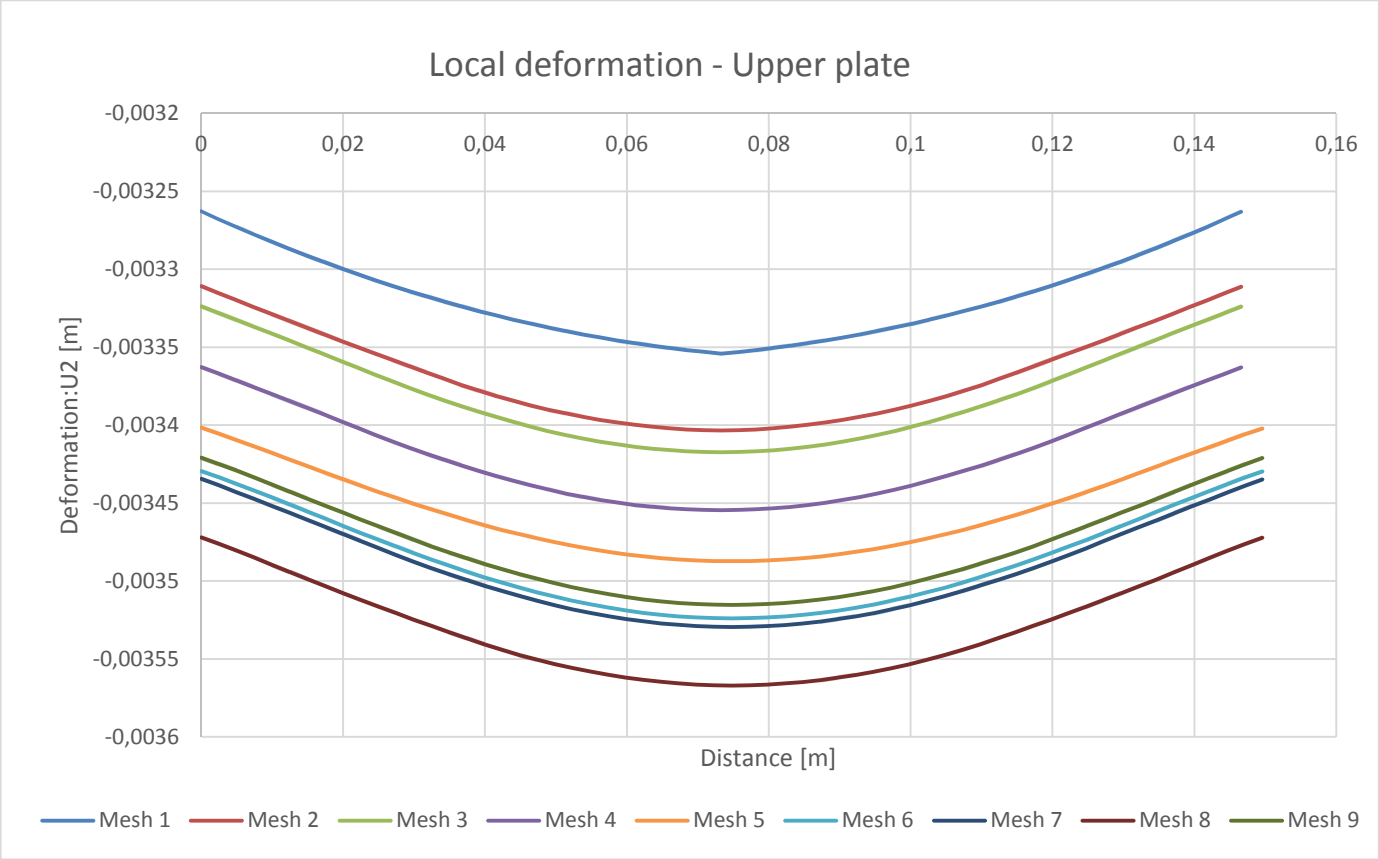

MIN values

Mesh 1	Mesh 2	Mesh 3	Mesh 4	Mesh 5	Mesh 6	Mesh 7	Mesh 8	Mesh 9
-3,35E-03	-3,40E-03	-3,4E-03	-3,45E-03	-3,49E-03	-3,5E-03	-3,53E-03	-3,6E-03	-3,5E-03

Differece in min value [%]

Mesh 1-2	Mesh 2-3	Mesh 3-4	Mesh 4-5	Mesh 5-6	Mesh 6-7	Mesh 7-8
1,5%	0,4%	1,1%	0,9%	1,0%	0,2%	1,1%

Local Deflection - Bottom Plate

The convergence check of the local deflection was also done at the bottom plate. The values were extracted at the lower plate under the patch load, see the figure below for the exact location:

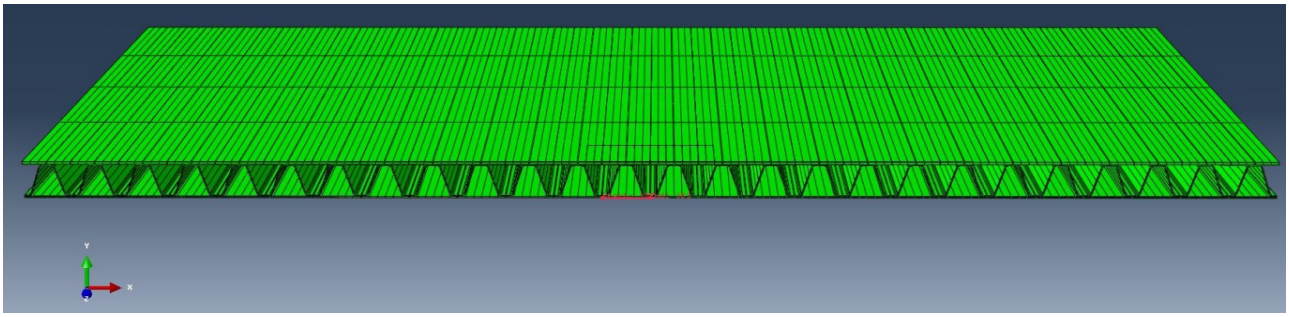

Mesh 1

Distance [m]	U2 [m]
0	-0,0029781
0,00244343	-0,0029889
0,00488687	-0,0029995
0,0073303	-0,0030099
0,00977373	-0,0030199
0,012217	-0,0030297
0,0146605	-0,0030392
0,0171039	-0,0030485
0,0195473	-0,0030574
0,0219908	-0,0030661
0,0244342	-0,0030746
0,0268776	-0,0030828
0,0293211	-0,0030907
0,0317645	-0,0030983
0,0342079	-0,0031056
0,0366514	-0,0031127
0,0390947	-0,0031196
0,0415381	-0,0031261
0,0439816	-0,0031324
0,046425	-0,0031384
0,0488684	-0,0031442
0,0513119	-0,0031496
0,0537553	-0,0031548
0,0561987	-0,0031598
0,0586421	-0,0031644
0,0610855	-0,0031688
0,0635289	-0,003173

Mesh 2

Distance [m]	U2 [m]
0	-0,003019
0,00244343	-0,003031
0,00488687	-0,003042
0,0073303	-0,003054
0,00977373	-0,003065
0,012217	-0,003076
0,0146605	-0,003086
0,0171039	-0,003096
0,0195473	-0,003106
0,0219908	-0,003115
0,0244342	-0,003124
0,0268776	-0,003133
0,0293211	-0,003141
0,0317645	-0,00315
0,0342079	-0,003157
0,0366514	-0,003165
0,0390947	-0,003171
0,0415381	-0,003176
0,0439816	-0,003182
0,046425	-0,003187
0,0488684	-0,003192
0,0513119	-0,003196
0,0537553	-0,003201
0,0561987	-0,003205
0,0586421	-0,003209
0,0610855	-0,003213
0,0635289	-0,003216

Mesh 3

Distance [m]	U2 [m]
0	-0,00303
0,0024434	-0,00304
0,0048869	-0,00305
0,0073303	-0,00307
0,0097737	-0,00308
0,012217	-0,00309
0,0146605	-0,0031
0,0171039	-0,00311
0,0195473	-0,00312
0,0219908	-0,00313
0,0244342	-0,00314
0,0268776	-0,00315
0,0293211	-0,00315
0,0317645	-0,00316
0,0342079	-0,00317
0,0366514	-0,00318
0,0390947	-0,00318
0,0415381	-0,00319
0,0439816	-0,0032
0,046425	-0,0032
0,0488684	-0,00321
0,0513119	-0,00321
0,0537553	-0,00322
0,0561987	-0,00322
0,0586421	-0,00322
0,0610855	-0,00323
0,0635289	-0,00323

0,0659723	-0,0031768
0,0684158	-0,0031804
0,0708592	-0,0031837
0,0733026	-0,0031868
0,0757461	-0,0031867
0,0781895	-0,0031865
0,0806329	-0,0031862
0,0830764	-0,0031859
0,0855198	-0,0031855
0,0879631	-0,0031851
0,0904065	-0,0031845
0,09285	-0,0031839
0,0952934	-0,0031832
0,0977368	-0,0031825
0,10018	-0,0031816
0,102624	-0,0031807
0,105067	-0,0031797
0,107511	-0,0031787
0,109954	-0,0031776
0,112397	-0,0031764
0,114841	-0,0031751
0,117284	-0,0031738
0,119728	-0,0031723
0,122171	-0,0031709
0,124614	-0,0031693
0,127058	-0,0031677
0,129501	-0,003166
0,131945	-0,0031642
0,134388	-0,0031623
0,136832	-0,0031604
0,139275	-0,0031584
0,141718	-0,0031563
0,144162	-0,0031542
0,146605	-0,003152

0,0659723	-0,00322
0,0684158	-0,003223
0,0708592	-0,003226
0,0733026	-0,003228
0,0757461	-0,003229
0,0781895	-0,00323
0,0806329	-0,003231
0,0830764	-0,003232
0,0855198	-0,003232
0,0879631	-0,003233
0,0904065	-0,003233
0,09285	-0,003234
0,0952934	-0,003234
0,0977368	-0,003234
0,10018	-0,003234
0,102624	-0,003233
0,105067	-0,003233
0,107511	-0,003232
0,109954	-0,003232
0,112397	-0,003229
0,114841	-0,003227
0,117284	-0,003225
0,119728	-0,003223
0,122171	-0,00322
0,124614	-0,003218
0,127058	-0,003216
0,129501	-0,003213
0,131945	-0,003211
0,134388	-0,003208
0,136832	-0,003206
0,139275	-0,003203
0,141718	-0,003201
0,144162	-0,003198
0,146605	-0,003196

0,0659723	-0,00324
0,0684158	-0,00324
0,0708592	-0,00324
0,0733026	-0,00324
0,0757461	-0,00324
0,0781895	-0,00325
0,0806329	-0,00325
0,0830764	-0,00325
0,0855198	-0,00325
0,0879631	-0,00325
0,0904065	-0,00325
0,09285	-0,00325
0,0952934	-0,00325
0,0977368	-0,00325
0,10018	-0,00325
0,102624	-0,00325
0,105067	-0,00325
0,107511	-0,00325
0,109954	-0,00324
0,112397	-0,00324
0,114841	-0,00324
0,117284	-0,00324
0,119728	-0,00324
0,122171	-0,00324
0,124614	-0,00323
0,127058	-0,00323
0,129501	-0,00323
0,131945	-0,00322
0,134388	-0,00322
0,136832	-0,00322
0,139275	-0,00322
0,141718	-0,00321
0,144162	-0,00321
0,146605	-0,00321

Mesh 4

Distance [m]	U2 [m]
0	-0,0031012
0,00244343	-0,003111
0,00488687	-0,0031205
0,0073303	-0,0031297
0,00977373	-0,0031385
0,012217	-0,0031469
0,0146605	-0,003155
0,0171039	-0,0031628
0,0195473	-0,0031702
0,0219908	-0,0031772
0,0244342	-0,0031839
0,0268776	-0,0031905

Mesh 5

Distance [m]	U2 [m]
0	-0,003136
0,00249338	-0,003146
0,00498664	-0,003156
0,00748003	-0,003166
0,00997329	-0,003175
0,0124667	-0,003183
0,0149601	-0,003191
0,0174533	-0,003199
0,0199467	-0,003207
0,02244	-0,003214
0,0249333	-0,003221
0,0274267	-0,003228

Mesh 6

Distance [m	U2 [m]
0	-0,00316
0,0024934	-0,00317
0,0049866	-0,00318
0,00748	-0,00319
0,0099733	-0,0032
0,0124667	-0,00321
0,0149601	-0,00322
0,0174533	-0,00322
0,0199467	-0,00323
0,02244	-0,00324
0,0249333	-0,00325
0,0274267	-0,00325

0,0293211	-0,0031968
0,0317645	-0,0032028
0,0342079	-0,0032086
0,0366514	-0,003214
0,0390947	-0,0032192
0,0415381	-0,0032241
0,0439816	-0,0032287
0,046425	-0,003233
0,0488684	-0,0032371
0,0513119	-0,003241
0,0537553	-0,0032448
0,0561987	-0,0032483
0,0586421	-0,0032516
0,0610855	-0,0032548
0,0635289	-0,0032577
0,0659723	-0,0032604
0,0684158	-0,0032629
0,0708592	-0,0032652
0,0733026	-0,0032672
0,0757461	-0,0032692
0,0781895	-0,0032711
0,0806329	-0,0032728
0,0830764	-0,0032744
0,0855198	-0,0032758
0,0879631	-0,0032771
0,0904065	-0,0032783
0,09285	-0,0032793
0,0952934	-0,0032802
0,0977368	-0,0032809
0,10018	-0,0032816
0,102624	-0,0032822
0,105067	-0,0032828
0,107511	-0,0032832
0,109954	-0,0032836
0,112397	-0,0032839
0,114841	-0,0032842
0,117284	-0,0032844
0,119728	-0,0032845
0,122171	-0,0032845
0,124614	-0,0032845
0,127058	-0,0032845
0,129501	-0,0032845
0,131945	-0,0032845
0,134388	-0,0032845
0,136832	-0,0032844
0,139275	-0,0032844
0,141718	-0,0032844
0,144162	-0,0032843
0,146605	-0,0032842

0,02992	-0,003235
0,0324134	-0,003241
0,0349066	-0,003246
0,0374	-0,003252
0,0398934	-0,003257
0,0423867	-0,003262
0,04488	-0,003267
0,0473733	-0,003272
0,0498667	-0,003276
0,0523601	-0,00328
0,0548533	-0,003284
0,0573467	-0,003288
0,05984	-0,003291
0,0623333	-0,003295
0,0648267	-0,003298
0,06732	-0,003301
0,0698134	-0,003303
0,0723066	-0,003306
0,0748	-0,003308
0,0772934	-0,00331
0,0797867	-0,003312
0,08228	-0,003314
0,0847733	-0,003316
0,0872667	-0,003318
0,0897601	-0,003319
0,0922533	-0,00332
0,0947467	-0,003321
0,09724	-0,003323
0,0997334	-0,003324
0,102227	-0,003324
0,10472	-0,003325
0,107213	-0,003326
0,109707	-0,003326
0,1122	-0,003327
0,114693	-0,003327
0,117187	-0,003328
0,11968	-0,003328
0,122173	-0,003328
0,124667	-0,003328
0,12716	-0,003329
0,129653	-0,003329
0,132147	-0,003329
0,13464	-0,003329
0,137133	-0,003329
0,139627	-0,003329
0,14212	-0,003328
0,144613	-0,003328
0,147107	-0,003328
0,1496	-0,003328

0,02992	-0,00326
0,0324134	-0,00327
0,0349066	-0,00327
0,0374	-0,00328
0,0398934	-0,00328
0,0423867	-0,00329
0,04488	-0,00329
0,0473733	-0,0033
0,0498667	-0,0033
0,0523601	-0,00331
0,0548533	-0,00331
0,0573467	-0,00331
0,05984	-0,00332
0,0623333	-0,00332
0,0648267	-0,00332
0,06732	-0,00333
0,0698134	-0,00333
0,0723066	-0,00333
0,0748	-0,00333
0,0772934	-0,00334
0,0797867	-0,00334
0,08228	-0,00334
0,0847733	-0,00334
0,0872667	-0,00334
0,0897601	-0,00335
0,0922533	-0,00335
0,0947467	-0,00335
0,09724	-0,00335
0,0997334	-0,00335
0,102227	-0,00335
0,10472	-0,00335
0,107213	-0,00335
0,109707	-0,00335
0,1122	-0,00335
0,114693	-0,00335
0,117187	-0,00335
0,11968	-0,00335
0,122173	-0,00335
0,124667	-0,00335
0,12716	-0,00336
0,129653	-0,00336
0,132147	-0,00336
0,13464	-0,00336
0,137133	-0,00336
0,139627	-0,00336
0,14212	-0,00336
0,144613	-0,00336
0,147107	-0,00336
0,1496	-0,00336

Mesh 7

Distance [m]	U2 [m]
0	-0,0031643
0,00249338	-0,0031745
0,00498664	-0,0031843
0,00748003	-0,0031937
0,00997329	-0,0032028
0,0124667	-0,0032115
0,0149601	-0,00322
0,0174533	-0,003228
0,0199467	-0,0032358
0,02244	-0,0032432
0,0249333	-0,0032503
0,0274267	-0,0032571
0,02992	-0,0032636
0,0324134	-0,0032699
0,0349066	-0,0032759
0,0374	-0,0032817
0,0398934	-0,0032871
0,0423867	-0,0032923
0,04488	-0,0032973
0,0473733	-0,0033019
0,0498667	-0,0033063
0,0523601	-0,0033105
0,0548533	-0,0033145
0,0573467	-0,0033183
0,05984	-0,0033219
0,0623333	-0,0033252
0,0648267	-0,0033284
0,06732	-0,0033314
0,0698134	-0,0033342
0,0723066	-0,0033367
0,0748	-0,0033391
0,0772934	-0,0033413
0,0797867	-0,0033434
0,08228	-0,0033453
0,0847733	-0,0033471
0,0872667	-0,0033487
0,0897601	-0,0033502
0,0922533	-0,0033516
0,0947467	-0,0033528
0,09724	-0,0033539
0,0997334	-0,0033549
0,102227	-0,0033557
0,10472	-0,0033565
0,107213	-0,0033572
0,109707	-0,0033578
0,1122	-0,0033584
0,114693	-0,0033588

Mesh 8

Distance [m]	U2 [m]
0	-0,003198
0,00249338	-0,003208
0,00498664	-0,003218
0,00748003	-0,003227
0,00997329	-0,003236
0,0124667	-0,003245
0,0149601	-0,003253
0,0174533	-0,003261
0,0199467	-0,003269
0,02244	-0,003276
0,0249333	-0,003283
0,0274267	-0,00329
0,02992	-0,003297
0,0324134	-0,003303
0,0349066	-0,003309
0,0374	-0,003315
0,0398934	-0,00332
0,0423867	-0,003325
0,04488	-0,00333
0,0473733	-0,003335
0,0498667	-0,003339
0,0523601	-0,003344
0,0548533	-0,003348
0,0573467	-0,003352
0,05984	-0,003355
0,0623333	-0,003359
0,0648267	-0,003362
0,06732	-0,003365
0,0698134	-0,003368
0,0723066	-0,003371
0,0748	-0,003373
0,0772934	-0,003376
0,0797867	-0,003378
0,08228	-0,00338
0,0847733	-0,003382
0,0872667	-0,003383
0,0897601	-0,003385
0,0922533	-0,003387
0,0947467	-0,003388
0,09724	-0,003389
0,0997334	-0,00339
0,102227	-0,003391
0,10472	-0,003392
0,107213	-0,003393
0,109707	-0,003394
0,1122	-0,003394
0,114693	-0,003395

Mesh 9

Distance [m	U2 [m]
0	-0,00315
0,0025356	-0,00316
0,0050712	-0,00317
0,0076067	-0,00318
0,0101423	-0,00319
0,012678	-0,0032
0,0152136	-0,00321
0,0177492	-0,00321
0,0202848	-0,00322
0,0228204	-0,00323
0,0253559	-0,00324
0,0278915	-0,00324
0,0304271	-0,00325
0,0329627	-0,00326
0,0354983	-0,00326
0,038034	-0,00327
0,0405695	-0,00327
0,0431051	-0,00328
0,0456407	-0,00328
0,0481763	-0,00329
0,0507119	-0,00329
0,0532475	-0,0033
0,055783	-0,0033
0,0583186	-0,0033
0,0608542	-0,00331
0,0633899	-0,00331
0,0659255	-0,00331
0,0684611	-0,00332
0,0709966	-0,00332
0,0735322	-0,00332
0,0760678	-0,00332
0,0786034	-0,00332
0,081139	-0,00333
0,0836746	-0,00333
0,0862101	-0,00333
0,0887458	-0,00333
0,0912814	-0,00333
0,093817	-0,00333
0,0963526	-0,00334
0,0988882	-0,00334
0,101424	-0,00334
0,103959	-0,00334
0,106495	-0,00334
0,10903	-0,00334
0,111566	-0,00334
0,114102	-0,00334
0,116637	-0,00334

0,117187	-0,0033592
0,11968	-0,0033595
0,122173	-0,0033598
0,124667	-0,0033599
0,12716	-0,00336
0,129653	-0,0033601
0,132147	-0,0033602
0,13464	-0,0033602
0,137133	-0,0033603
0,139627	-0,0033603
0,14212	-0,0033603
0,144613	-0,0033603
0,147107	-0,0033603
0,1496	-0,0033603

0,117187	-0,003395
0,11968	-0,003396
0,122173	-0,003396
0,124667	-0,003396
0,12716	-0,003397
0,129653	-0,003397
0,132147	-0,003397
0,13464	-0,003397
0,137133	-0,003397
0,139627	-0,003397
0,14212	-0,003397
0,144613	-0,003397
0,147107	-0,003397
0,1496	-0,003397

0,119173	-0,00334
0,121709	-0,00334
0,124244	-0,00335
0,12678	-0,00335
0,129315	-0,00335
0,131851	-0,00335
0,134386	-0,00335
0,136922	-0,00335
0,139458	-0,00335
0,141993	-0,00335
0,144529	-0,00335
0,147064	-0,00335
0,1496	-0,00335

Result : Local Deflection Bottom Plate

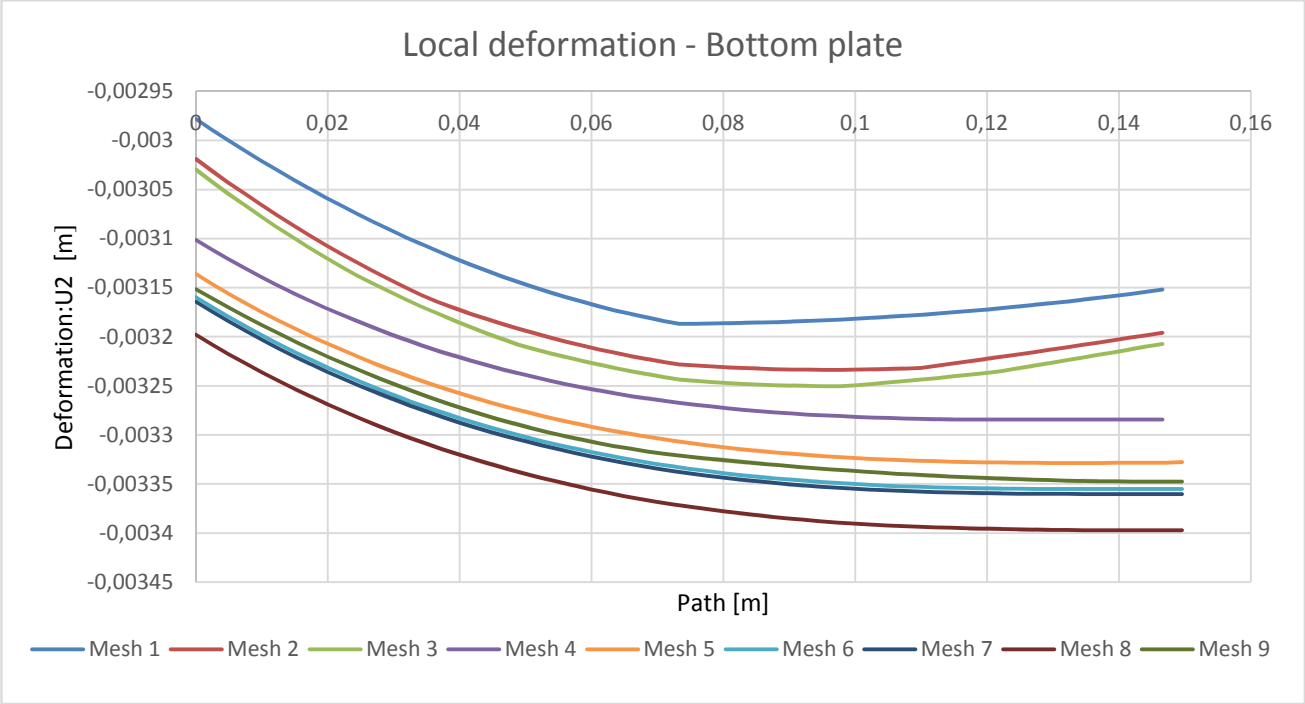

End Values

Mesh 1	Mesh 2	Mesh 3	Mesh 4	Mesh 5	Mesh 6	Mesh 7	Mesh 8	Mesh 9
-0,00315197	-0,0031958	-0,003207	-0,00328421	-0,003328	-0,003355	-0,00336	-0,0034	-0,00335

Differece in End value [%]

Mesh 1-2	Mesh 2-3	Mesh 3-4	Mesh 4-5	Mesh 5-6	Mesh 6-7	Mesh 7-8
1,4%	0,4%	2,3%	1,3%	0,8%	0,2%	1,1%

The convergence of the global and local deformation indicated that Mesh 1,2 and 3 was not created with sufficient mesh density. The meshes were therefore excluded for further studies.

Convergence of stresses

The stress behaviour was investigated to indentify at which position from the weld region linear stress realtion was obtained. At the postion of linear realtion there is no impact of the stress concentration from the weld region.
Initally, different positions in the upper and lower face panel were investigated with ambition of finding when the meshes indicated on convergence and when a linear relation was obtained in the

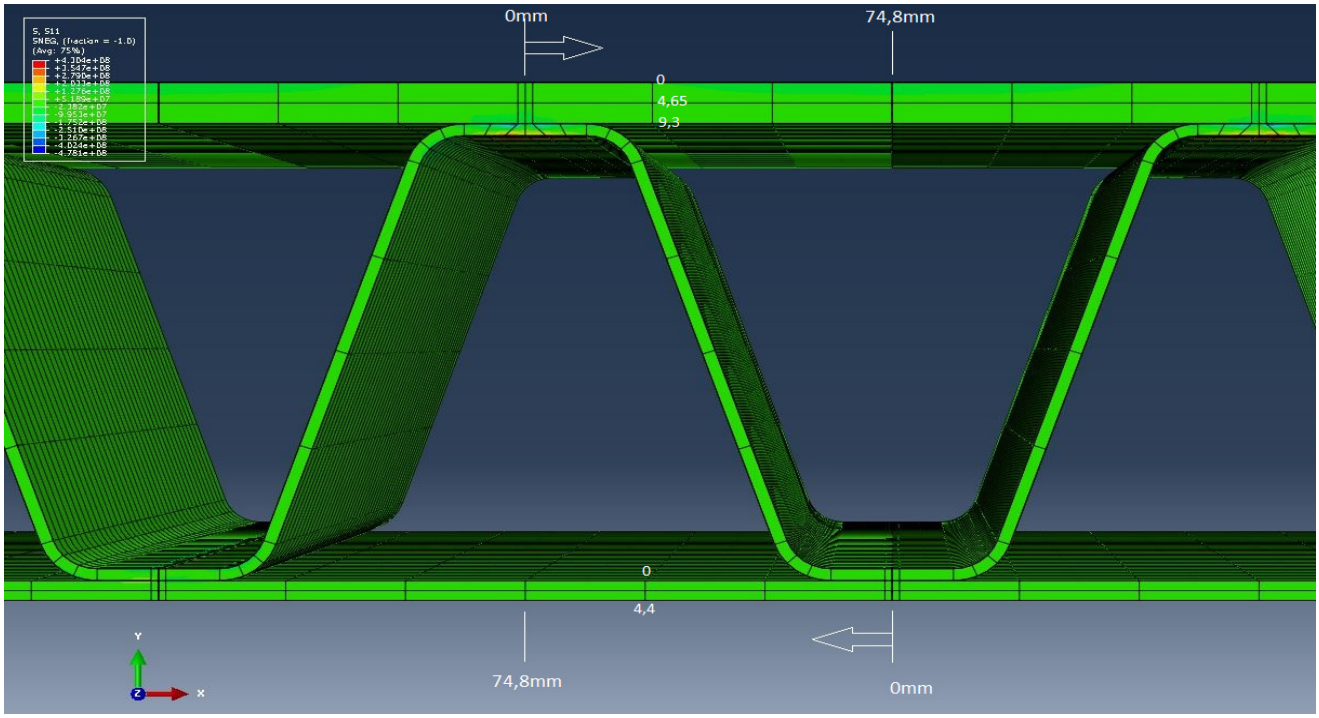

Mesh 4

Upper Plate

Distance weld	1,5mm	25,93mm	50,37mm	74,8mm
0	2,89E+07	-2,23E+07	-4,62E+07	-5,41E+07
4,65	-9,04E+06	-4,24E+06	-4,41E+06	-4,46E+06
9,3	-5,06E+07	1,39E+07	3,74E+07	4,52E+07

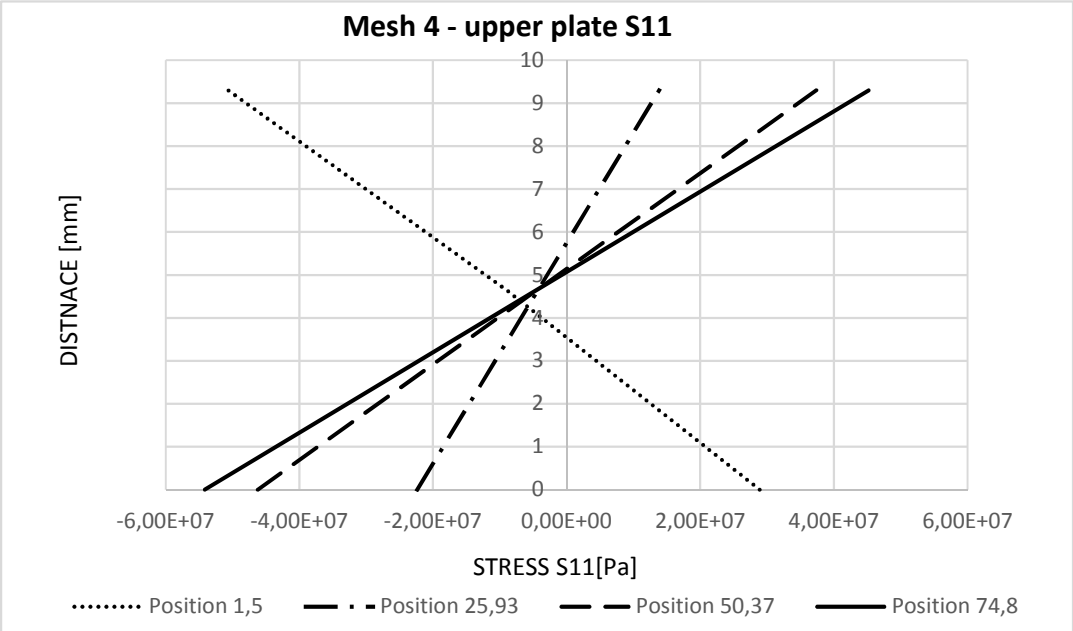

Bottom Plate

Distance weld	1,5mm	25,93mm	50,37mm	74,8mm
0	1,43E+07	8,50E+06	3,95E+06	-8,63E+05
2,2	1,14E+07	1,23E+07	1,28E+07	1,32E+07
4,4	1,02E+07	1,60E+07	2,17E+07	2,72E+07

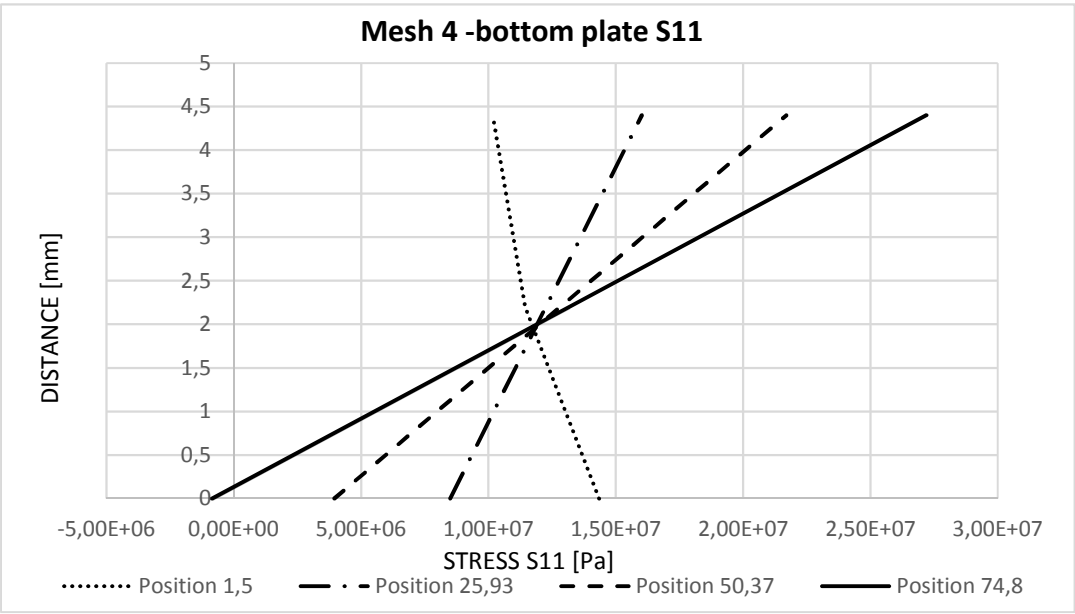

Mesh5

Upper Plate

Distance weld	1,5	19,83mm	38,15mm	56,48mm	74,8mm
0	1,17E+07	-1,63E+07	-3,11E+07	-4,07E+07	-4,4E+07
4,65	-7,38E+06	-3,38E+06	-1,59E+06	-6,95E+05	-3,9E+05
9,3	-3,00E+07	9,58E+06	2,80E+07	3,93E+07	4,30E+07

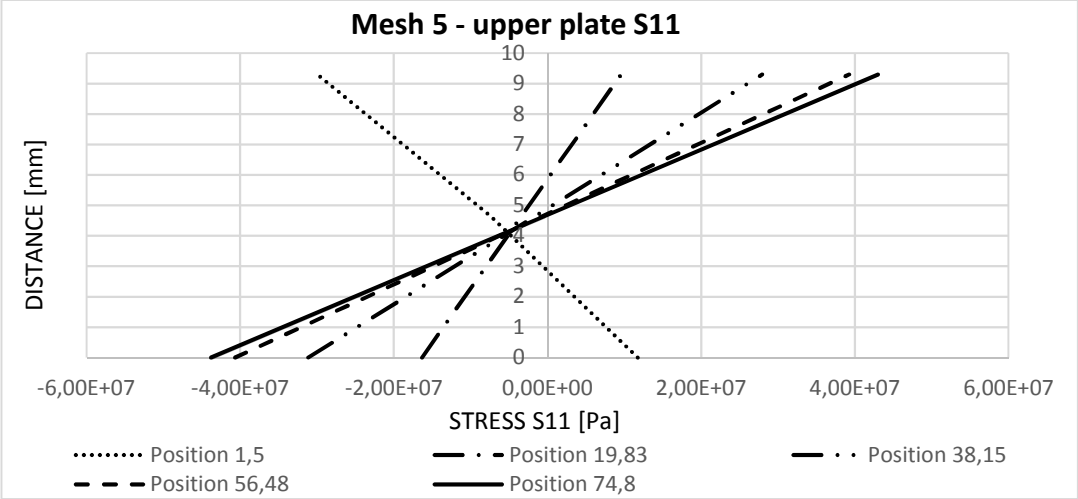

Bottom Plate

Distance weld	1,5mm	19,83mm	38,15mm	56,48mm	74,8mm
0,00E+00	1,23E+07	8,37E+06	5,38E+06	2,24E+06	-1,0E+06
2,20E+00	1,10E+07	1,16E+07	1,20E+07	1,24E+07	1,26E+07
4,40E+00	1,07E+07	1,48E+07	1,87E+07	2,26E+07	2,63E+07

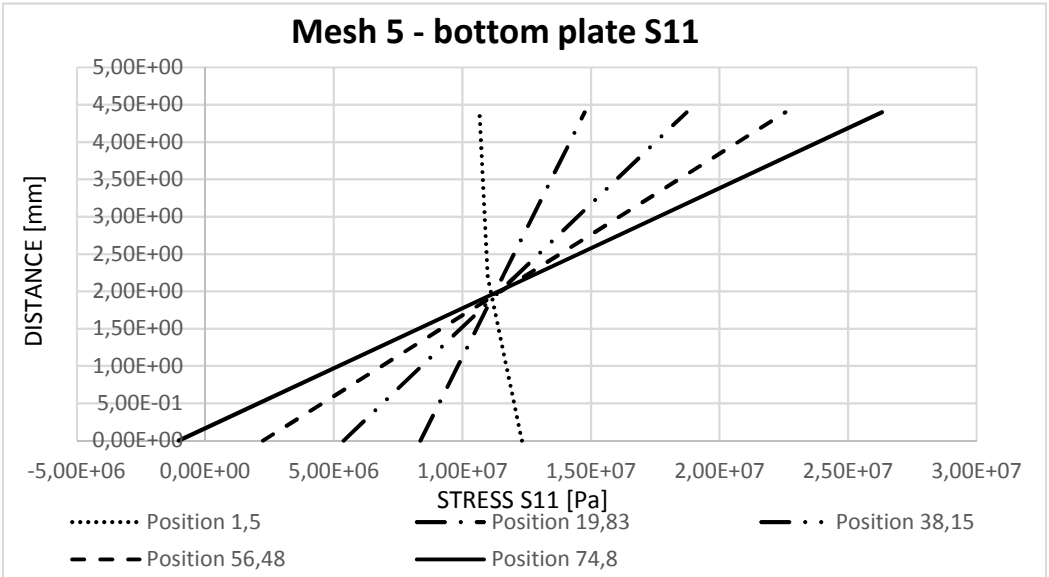

Mesh 6

Upper plate

Distance weld	1,5mm	19,83mm	38,15mm	56,48mm	74,8mm
0	2,26E+07	-1,31E+07	-3,56E+07	-4,90E+07	-5,3E+07
4,65	-5,66E+06	-3,88E+06	-4,02E+06	-4,12E+06	-4,1E+06
9,3	-3,69E+07	5,39E+06	2,75E+07	4,07E+07	4,5E+07

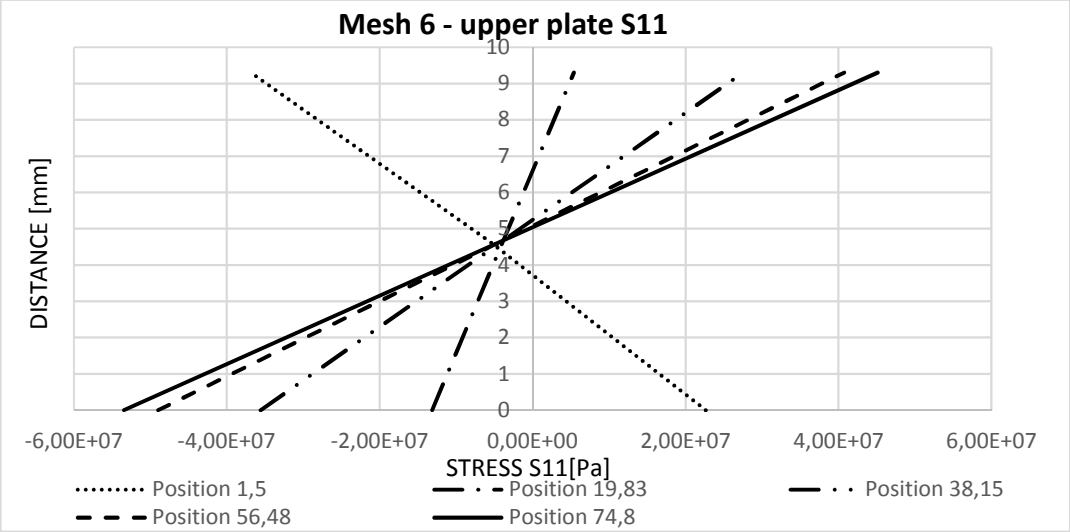

Bottom plate

Distance weld	1,5mm	19,83mm	38,15mm	56,48mm	74,8mm
0,00E+00	1,24E+07	8,37E+06	5,32E+06	2,13E+06	-1,2E+06
2,20E+00	1,10E+07	1,16E+07	1,21E+07	1,25E+07	1,27E+07
4,40E+00	1,07E+07	1,49E+07	1,89E+07	2,28E+07	2,66E+07

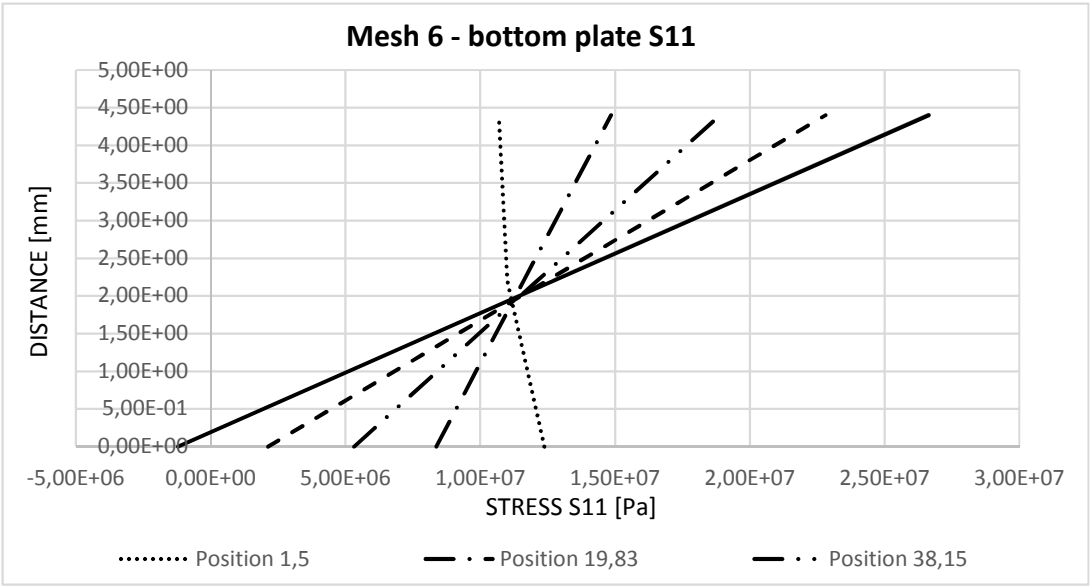

Mesh 7

Upper Plate

Distance weld	1,5mm	25,93mm	50,37mm	74,8mm
0	2,57E+07	-2,3E+07	-46475400	-5,42E+07
2,325	7,63E+06	-1,3E+07	-25082800	-2,91E+07
4,65	-7,83E+06	-2,9E+06	-3723970	-4,05E+06
6,975	-1,86E+07	5,18E+06	1,69E+07	2,08E+07
9,3	-3,58E+07	1,35E+07	3,76E+07	4,57E+07

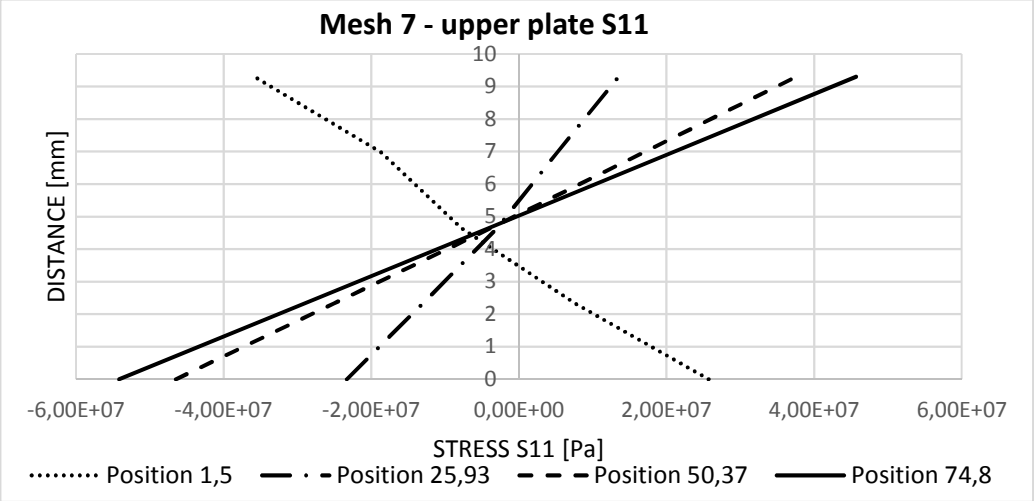

Bottom Plate

Distance weld	1,5mm	25,93mm	50,37mm	74,8mm
0	1,26E+07	7,34E+06	3,21E+06	-1,18E+06
1,1	1,07E+07	9,53E+06	7,75E+06	5,74E+06
2,2	1,18E+07	1,17E+07	1,23E+07	1,26E+07
3,3	1,11E+07	1,40E+07	1,69E+07	1,96E+07
4,4	9,50E+06	1,64E+07	2,16E+07	2,66E+07

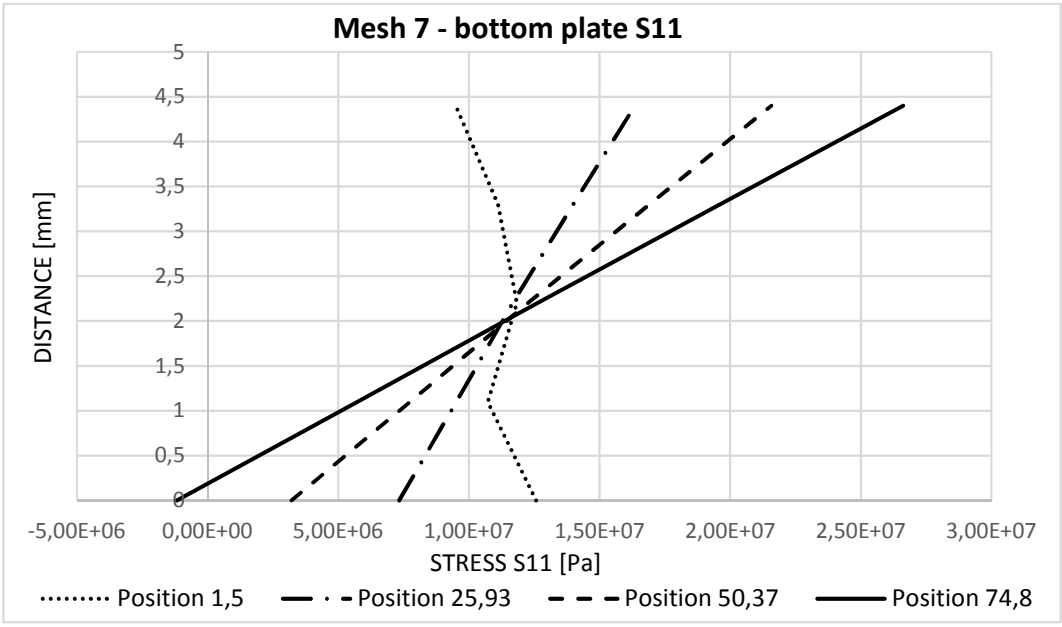

Mesh 8

Upper Plate

Distance weld	7mm	23,95mm	40,9mm	74,8mm
0	7,40E+06	-1,7E+07	-4,0E+07	-5,53E+07
2,325	1,90E+06		-2,2E+07	-2,96E+07
4,65	-3,61E+06	-4E+06	-3,9E+06	-4,00E+06
6,975	-9,12E+06		1,41E+07	2,16E+07
9,3	-1,46E+07	9,39E+06	3,21E+07	4,72E+07

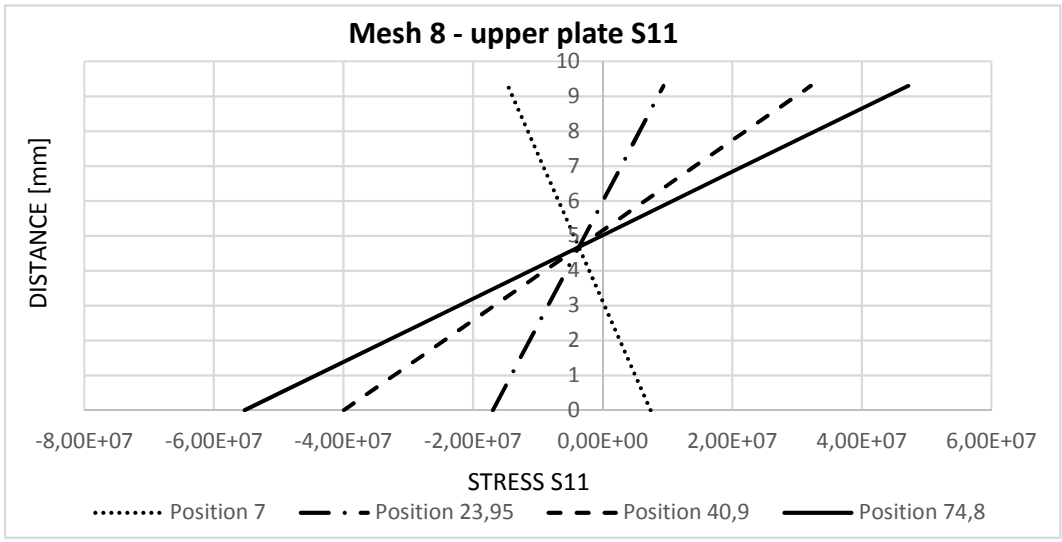

Bottom Plate

Distance weld	7mm	23,95mm	40,9mm	74,8mm
0	9,05E+06	6,79E+06	4,31E+06	-1,17E+06
1,1	1,01E+07		8,10E+06	5,61E+06
2,2	1,12E+07	1,14E+07	1,19E+07	1,24E+07
3,3	1,18E+07		1,57E+07	1,93E+07
4,4	1,23E+07	1,60E+07	1,96E+07	2,62E+07

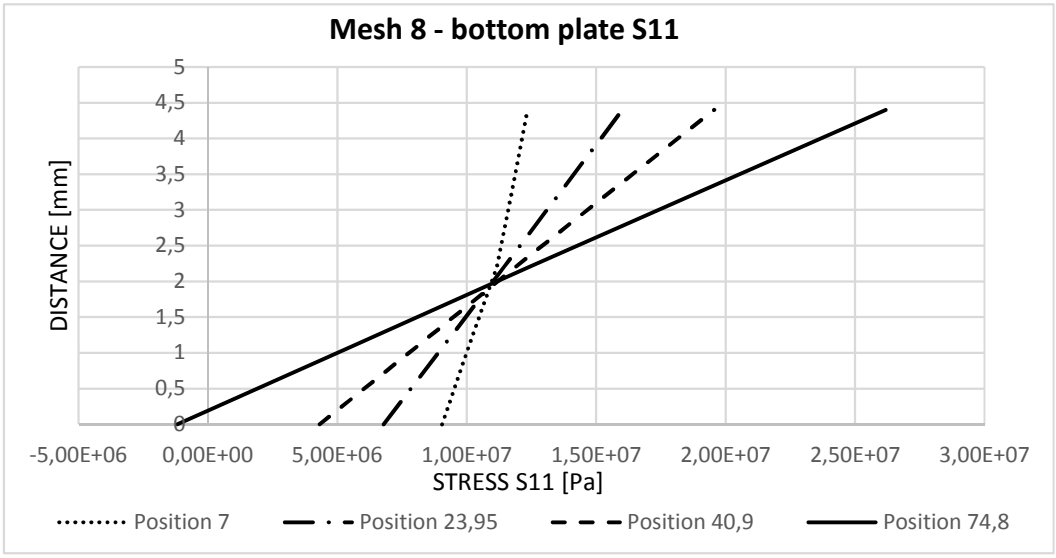

Mesh 9

Upper Plate

Distance weld	7mm	18,3mm	29,6mm	52,2mm	74,8mm
0	8,68E+06	-9,43E+06	-2,6E+07	-4,69E+07	-5,37E+07
1,55	4,28E+06		-1,9E+07	-3,25E+07	-3,72E+07
3,1	-106096	-5,64E+06	-1,1E+07	-1,83E+07	-2,06E+07
4,65	-3,92E+06		-4,0E+06	-4,11E+06	-4,16E+06
6,2	-7,51E+06	-2,10E+06	3,47E+06	1,01E+07	1,23E+07
7,75	-1,16E+07		1,10E+07	2,44E+07	2,88E+07
9,3	-1,60E+07	1,67E+06	1,85E+07	3,87E+07	4,53E+07

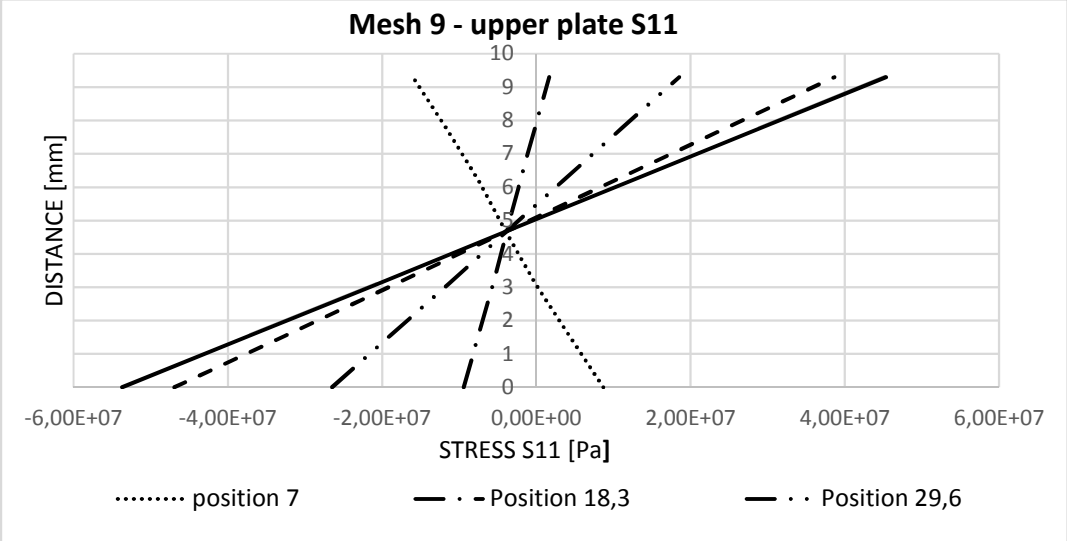

Bottom Plate

Distance weld	7mm	23,85mm	40,9mm	74,8mm
0	5,74E+06	5,86E+06	7,07E+06	-3,96E+05
1,1	8,47E+06		9,77E+06	6,41E+06
2,2	1,16E+07	1,15E+07	1,23E+07	1,32E+07
3,3	1,39E+07		1,50E+07	2,00E+07
4,4	1,61E+07	1,69E+07	1,78E+07	2,68E+07

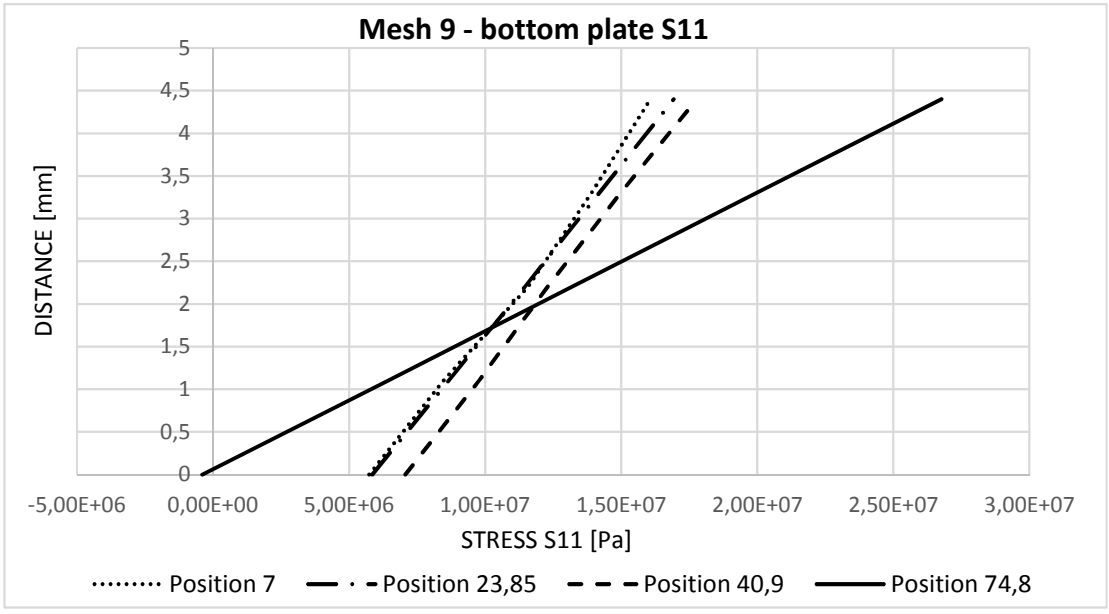

Result :

The meshes goes towards linearity at the distance 25,933mm away from the weld. Since it does not exist any nodes at that distance for Mesh 1, 2, 5, 6 and 8 a interpolation between the two closest nodes has been done.

Mesh 5

Upper Plate

	Delta stress	Position	Element lengt	X	S11
0	1,48E+07	0,0061083	0,018325	4,93E+06	-2,1E+07
4,65	1,79E+06	0,0061083	0,018325	5,96E+05	-2,8E+06
9,3	1,84E+07	0,0061083	0,018325	6,12E+06	1,57E+07

Bottom Plate

0	2,99E+06	0,0061083	0,018325	9,97E+05	7,37E+06
2,2	4,86E+05	0,0061083	0,018325	1,62E+05	1,17E+07
4,4	3,96E+06	0,0061083	0,018325	1,32E+06	1,61E+07

Mesh 6

Upper Plate

	Delta stress	Position	Elem. length	X	S11
0	2,24E+07	0,0061083	0,018325	7,48E+06	-2,1E+07
4,65	1,47E+05	0,0061083	0,018325	4,89E+04	-3,9E+06
9,3	2,21E+07	0,0061083	0,018325	7,38E+06	1,28E+07

Bottom Plate

0	3,05E+06	0,0061083	0,018325	1,02E+06	7,36E+06
2,2	6,08E+05	0,0061083	0,018325	2,03E+05	1,18E+07
4,4	4,04E+06	0,0061083	0,018325	1,35E+06	1,62E+07

Mesh 8

Upper Plate

	Delta stress	Position	Element L	X	S11
0	23004600	0,00198	0,01695	2687263	-2,0E+07
4,65	162880	0,00198	0,01695	19026,69	-3,8E+06
9,3	22748230	0,00198	0,01695	2657315	1,20E+07

Bottom Plate

0	2474020	0,00198	0,01695	289000,6	6,50E+06
2,2	443900	0,00198	0,01695	51853,81	1,15E+07
4,4	3547800	0,00198	0,01695	414433,3	1,64E+07

Mesh 9

Upper Plate

	Delta stress	Position	Element L	X	S11
0	17071440	0,00763	0,0113	11526999	-2,1E+07
3,1	5772200	0,00763	0,0113	3897512	-9,5E+06
6,2	5569770	0,00763	0,0113	3760827	1,66E+06
9,3	16856070	0,00763	0,0113	11381576	1,30E+07

Bottom Plate

0	1211650	0,00208	0,01705	147814,2	6,00E+06
2,2	826300	0,00208	0,01705	100803,8	1,16E+07
4,4	850900	0,00208	0,01705	103804,8	1,70E+07

In the diagram below is the verification of stresses at a position 25.93 mm from the weld region, both at the upper and bottom plate.

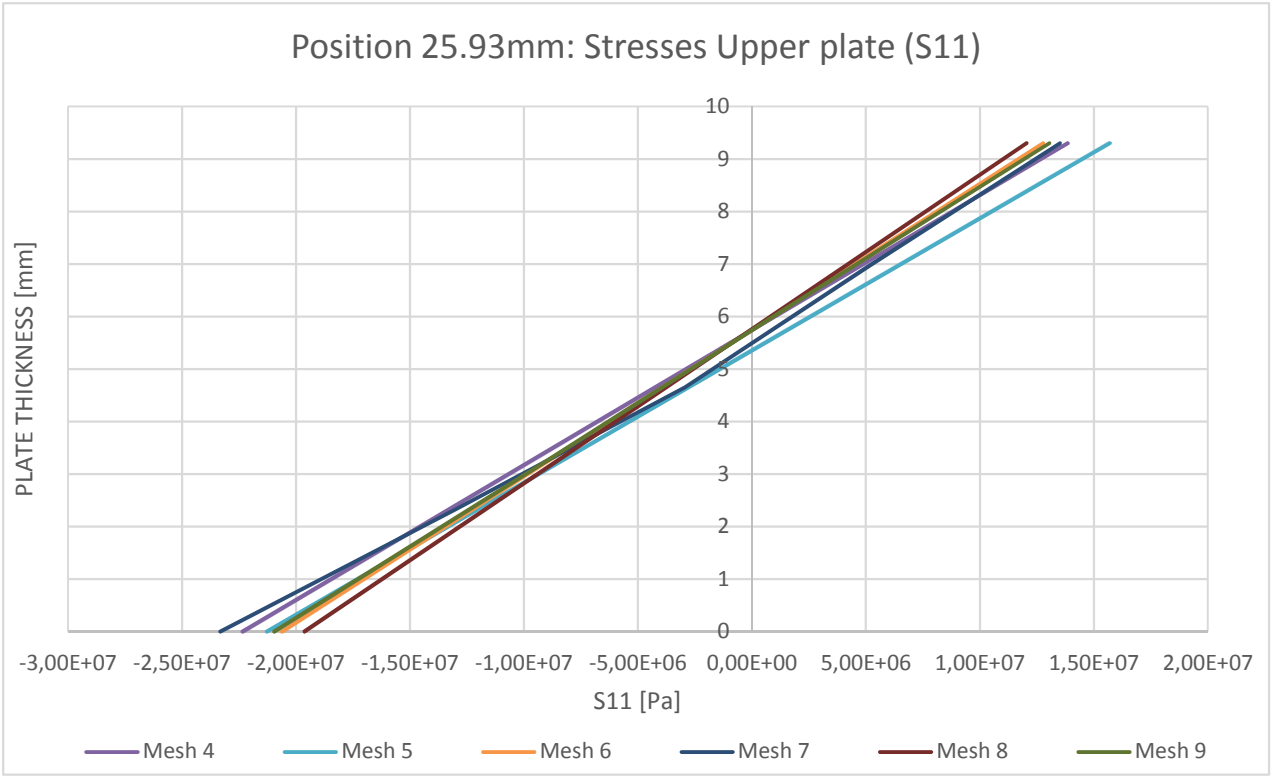

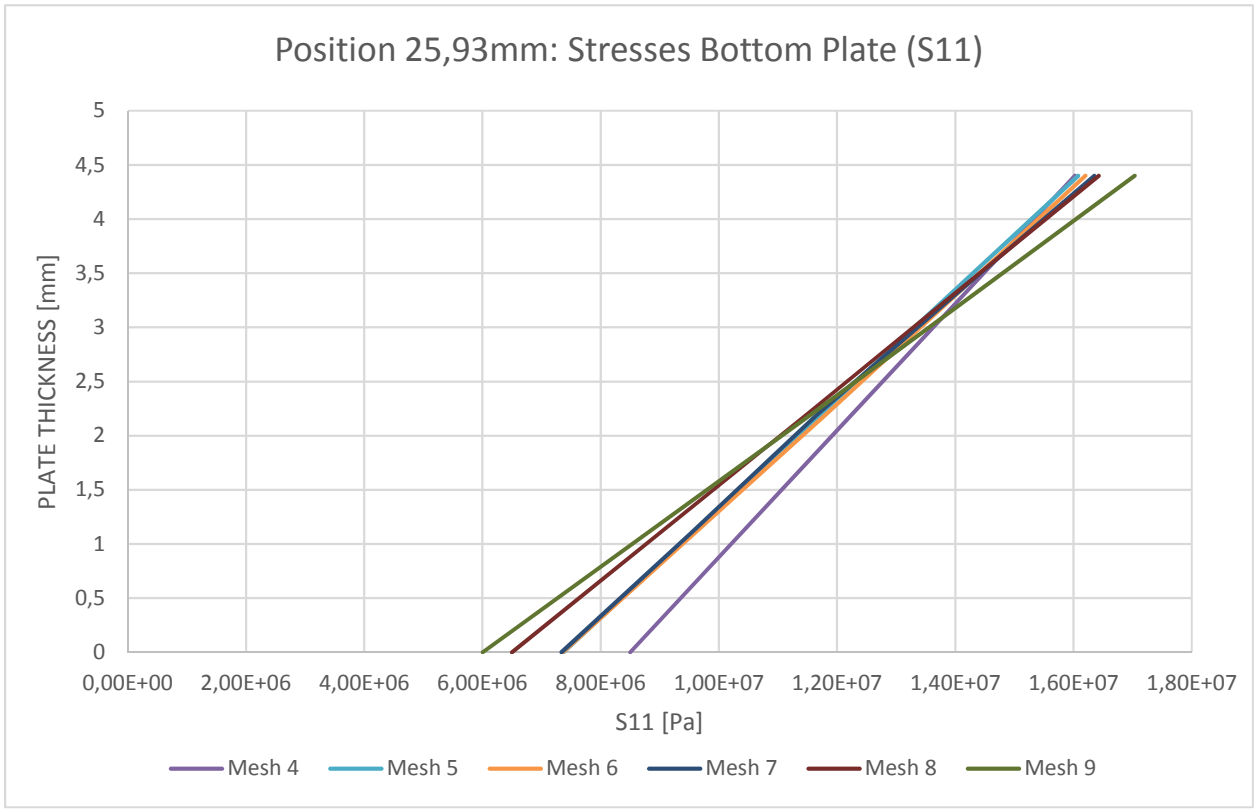

The verification of the stress showed that linear relation very not obtained at a distance 25.93 mm from the weld region. The ploted values showed and especielly at the bottom plate to large difference and therefore was the stress relation observed at a distance 74.8 mm from region instead, with hope that finding linear relation of the stresses.

In the diagram below is the verification of stresses at a position 74.8 mm from the weld region, both at the upper and bottom plate.

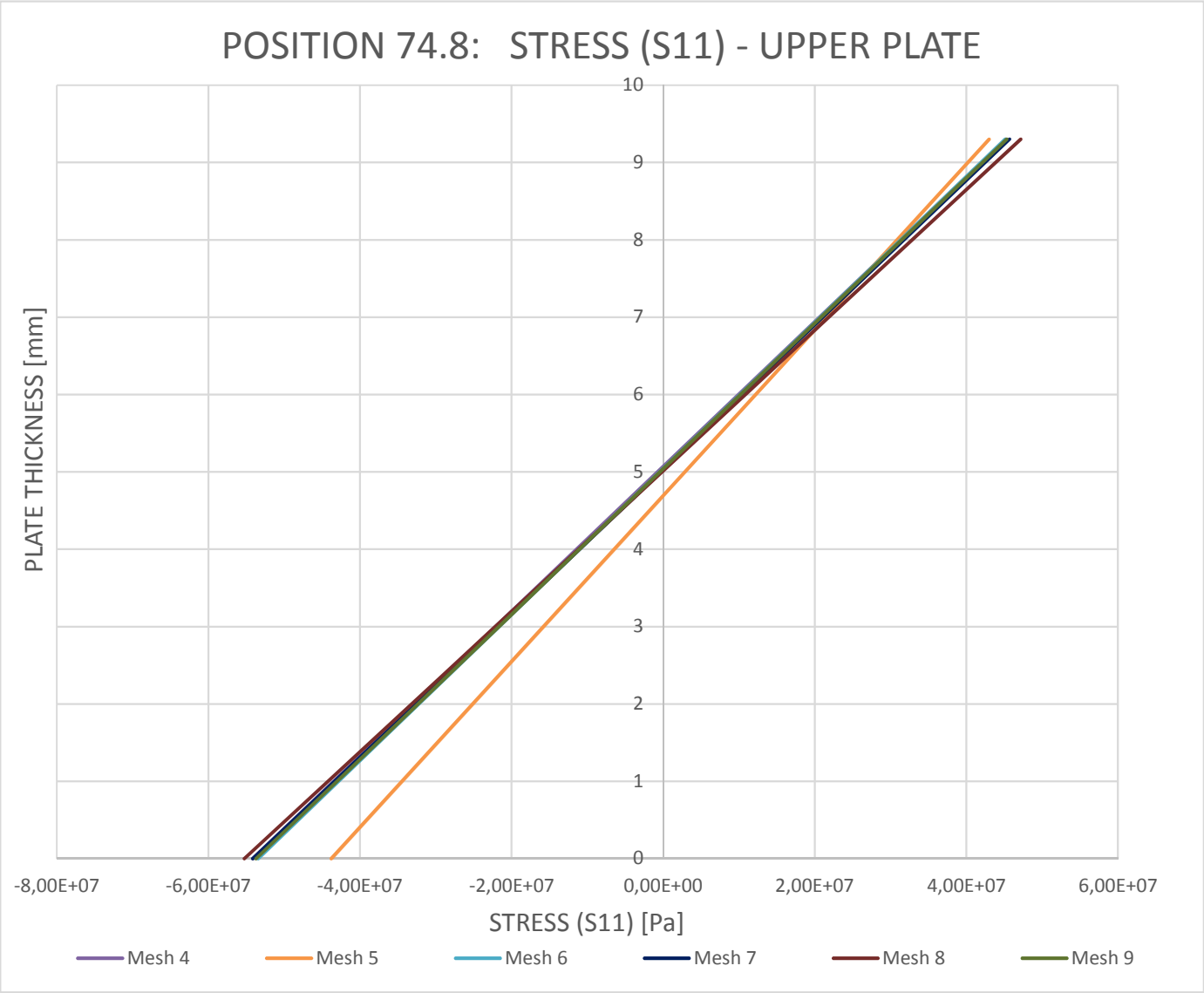

End Values

Position	Mesh 4	Mesh 5	Mesh 6	Mesh 7	Mesh 8	Mesh 9
9,3mm	4,52E+07	4,30E+07	4,51E+07	4,57E+07	4,7E+07	4,53E+07
0mm	-5,41E+07	-4,4E+07	-5,3E+07	-5,4E+07	-5,5E+07	-5,37E+07

Difference in end values [%]

Position	Mesh 4-5	Mesh 5-6	Mesh 6-7	Mesh 7-8	Mesh 8-9
9,3mm	4,9%	-5,0%	-1,2%	-3,3%	3,9%

Position	Mesh 4-5	Mesh 5-6	Mesh 6-7	Mesh 7-8	Mesh 8-9
0mm	19,1%	-22,0%	-1,3%	-2,0%	2,8%

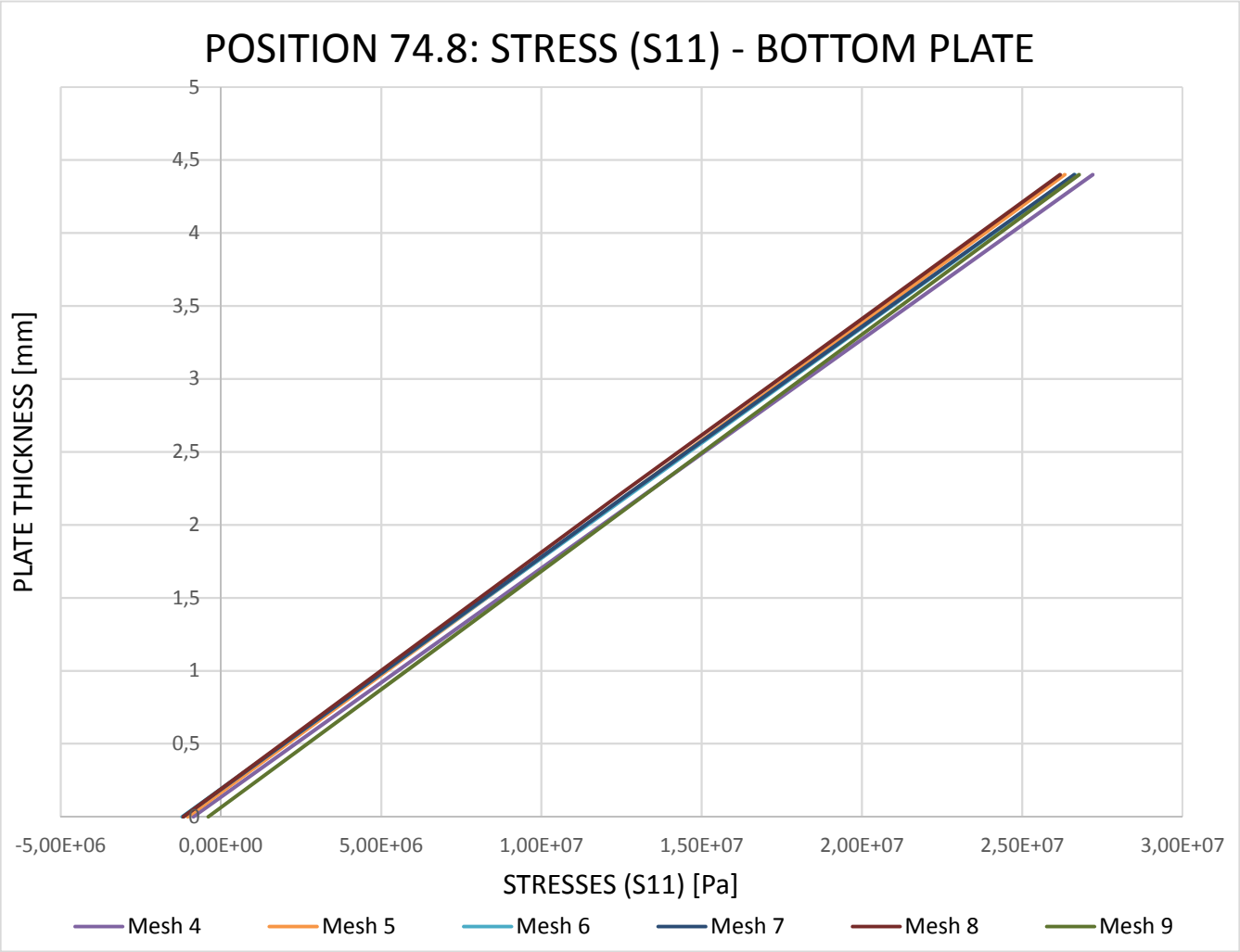

End Values

Position	Mesh 4	Mesh 5	Mesh 6	Mesh 7	Mesh 8	Mesh 9
4,4mm	2,72E+07	2,63E+07	2,66E+07	2,66E+07	2,6E+07	2,68E+07
0mm	-8,63E+05	-1,0E+06	-1,2E+06	-1,2E+06	-1,2E+06	-3,96E+05

Difference in end values [%]

Position	Mesh 4-5	Mesh 5-6	Mesh 6-7	Mesh 7-8	Mesh 8-9
4,4mm	3,2%	-1,2%	0,1%	1,6%	-2,3%

Position	Mesh 4-5	Mesh 5-6	Mesh 6-7	Mesh 7-8	Mesh 8-9
0mm	-20,2%	-17,0%	2,9%	0,3%	66,3%

The verification at a distance of 74.8 mm from the weld region showed convergence of the meshes and that a linear stress relation was found.
The postion is therefore suitable to be used for attachment of the submodels.

Stess convergence at boundaries for submodels

In the fatigue analysis of the deck submodels were used. The submodels were created with an area of 149,6x149,6 mm, seen from the above. To verify a correct response at the boundaries of the supposed submodel. A stress convergence were done at the boundaries ±74,8 mm from centre of the deck, see figure below

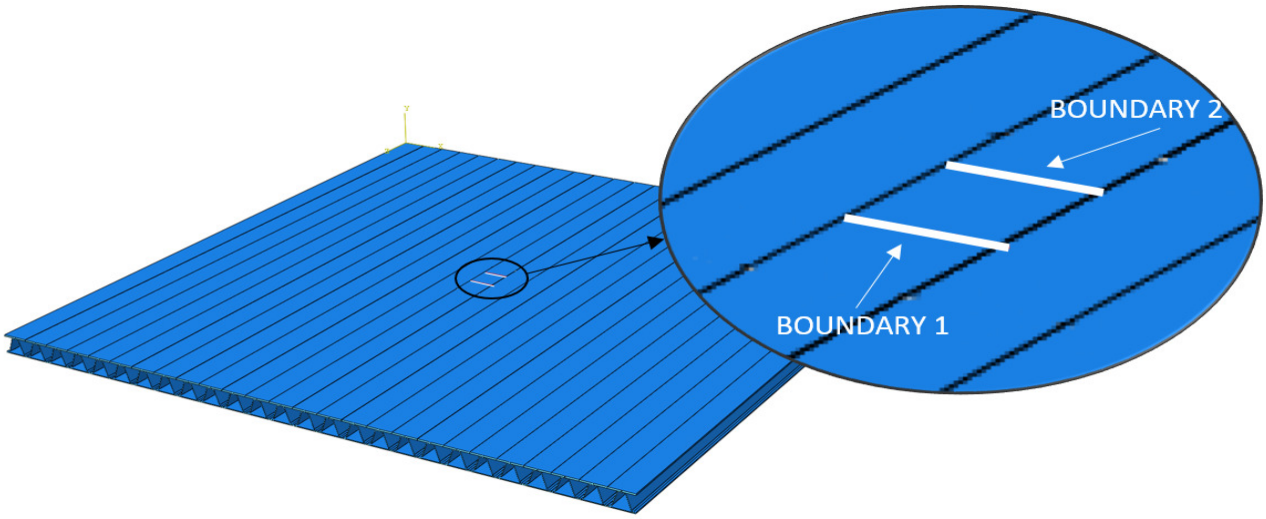

Mesh 4

Boundary 1

Distance	S33
0	-4,62E+07
0	-4,58E+07
0,0244334	-4,47E+07
0,0488666	-3,87E+07
0,0733	-2,54E+07
0,0763	-2,68E+07
0,100733	-4,14E+07
0,125167	-4,88E+07
0,1496	-5,09E+07
0,1496	-5,09E+07

Boundary 2

Distance	S33
0	-4,61E+07
0	-4,57E+07
0,0244334	-4,46E+07
0,0488666	-3,87E+07
0,0733	-2,53E+07
0,0763	-2,68E+07
0,100733	-4,14E+07
0,125167	-4,87E+07
0,1496	-5,09E+07
0,1496	-5,09E+07

Mesh 5

Boundary 1

Distance	S33
0	-4,14E+07
0	-4,14E+07
0,018325	-4,13E+07
0,0366501	-3,94E+07
0,054975	-3,65E+07
0,0733	-2,99E+07
0,0748	-2,99E+07
0,0763	-3,00E+07
0,094625	-3,84E+07
0,11295	-4,24E+07
0,131275	-4,50E+07
0,1496	-4,59E+07
0,1496	-4,59E+07

Boundary 2

Distance	S33
0	-4,13E+07
0	-4,13E+07
0,018325	-4,13E+07
0,0366501	-3,93E+07
0,054975	-3,64E+07
0,0733	-2,98E+07
0,0748	-2,98E+07
0,0763	-2,99E+07
0,094625	-3,83E+07
0,11295	-4,24E+07
0,131275	-4,49E+07
0,1496	-4,58E+07
0,1496	-4,58E+07

Mesh 6

Boundary 1

Distance	S33
0	-4,63E+07
0	-4,62E+07
0,018325	-4,58E+07
0,0366501	-4,25E+07
0,054975	-3,72E+07
0,0733	-2,84E+07
0,0748	-2,87E+07
0,0763	-2,88E+07
0,094625	-3,95E+07
0,11295	-4,60E+07
0,131275	-4,99E+07
0,1496	-5,12E+07
0,1496	-5,12E+07

Boundary 2

Distance	S33
0	-4,63E+07
0	-4,62E+07
0,018325	-4,57E+07
0,0366501	-4,25E+07
0,054975	-3,71E+07
0,0733	-2,83E+07
0,0748	-2,86E+07
0,0763	-2,87E+07
0,094625	-3,95E+07
0,11295	-4,60E+07
0,131275	-4,99E+07
0,1496	-5,12E+07
0,1496	-5,12E+07

Mesh7

Boundary 1

Distance	S33
0	-4,69E+07
0	-4,61E+07
0,0244334	-4,53E+07
0,0488666	-3,98E+07
0,0733	-2,78E+07
0,0748	-2,92E+07
0,0763	-2,85E+07
0,100733	-4,26E+07
0,125167	-4,93E+07
0,1496	-5,14E+07
0,1496	-5,14E+07

Boundary 2

Distance	S33
0	-4,68E+07
0	-4,60E+07
0,0244334	-4,53E+07
0,0488666	-3,97E+07
0,0733	-2,78E+07
0,0748	-2,92E+07
0,0763	-2,84E+07
0,100733	-4,25E+07
0,125167	-4,92E+07
0,1496	-5,14E+07
0,1496	-5,14E+07

Mesh 8

Boundary 1

Distance	S33
0	-4,70E+07
0	-4,71E+07
0,0148801	-4,58E+07
0,02976	-4,45E+07
0,0446401	-4,06E+07
0,05952	-3,51E+07
0,0744001	-2,81E+07
0,08928	-3,71E+07
0,10416	-4,32E+07
0,11904	-4,80E+07
0,13392	-5,00E+07
0,1488	-5,20E+07

Boundary 2

Distance	S33
0	-4,70E+07
0	-4,71E+07
0,0149601	-4,57E+07
0,02992	-4,45E+07
0,04488	-4,05E+07
0,05984	-3,49E+07
0,0748	-2,78E+07
0,0897601	-3,72E+07
0,10472	-4,33E+07
0,11968	-4,80E+07
0,13464	-5,00E+07
0,1496	-5,20E+07
0,1496	-5,20E+07

Mesh 9

Boundary 1

Distance	S33
0	-4,64E+07
0	-4,64E+07
0,0226033	-4,54E+07
0,0452067	-4,05E+07
0,0678099	-3,12E+07
0,0713056	-2,85E+07
0,0748017	-2,75E+07
0,0782974	-3,04E+07
0,0817931	-3,33E+07
0,104396	-4,34E+07
0,126998	-4,93E+07
0,1496	-5,13E+07
0,149601	-5,13E+07

Boundary 2

Distance	S33
0	-4,63E+07
0	-4,63E+07
0,0226033	-4,54E+07
0,0452067	-4,04E+07
0,0678099	-3,11E+07
0,0713056	-2,85E+07
0,0748015	-2,74E+07
0,0782972	-3,03E+07
0,081793	-3,32E+07
0,104395	-4,33E+07
0,126998	-4,93E+07
0,1496	-5,12E+07
0,149601	-5,12E+07

Results

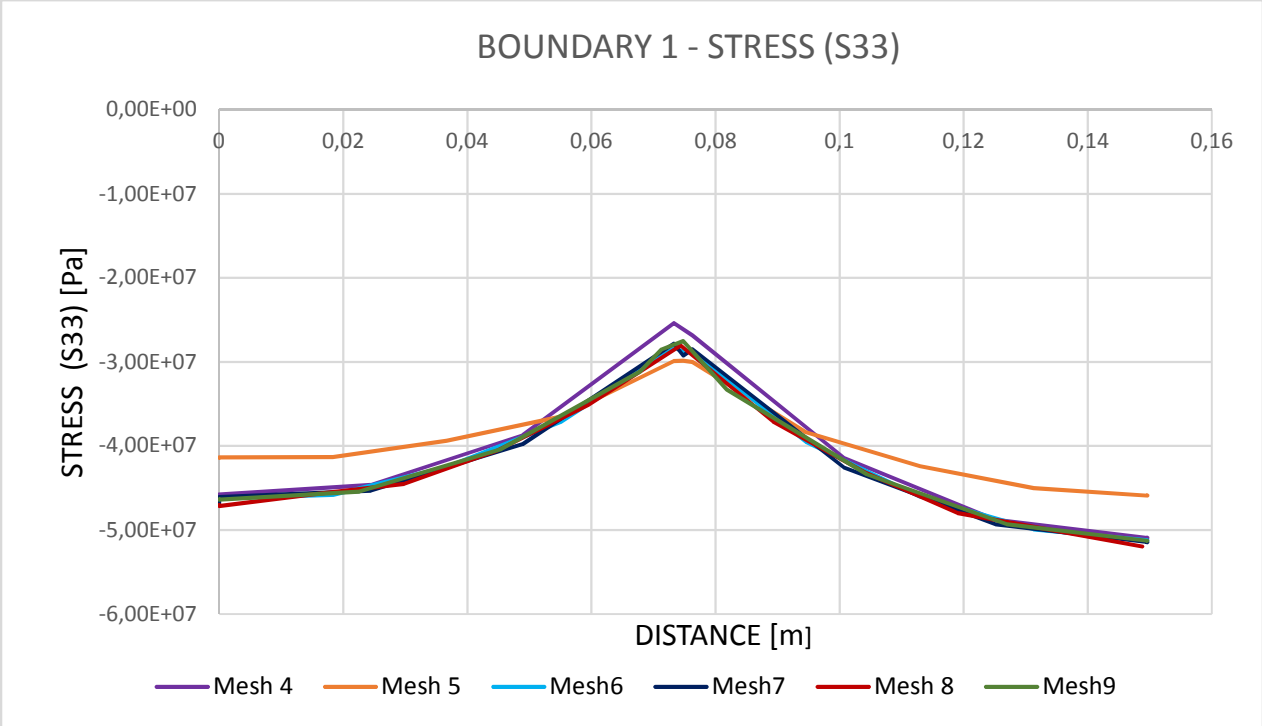

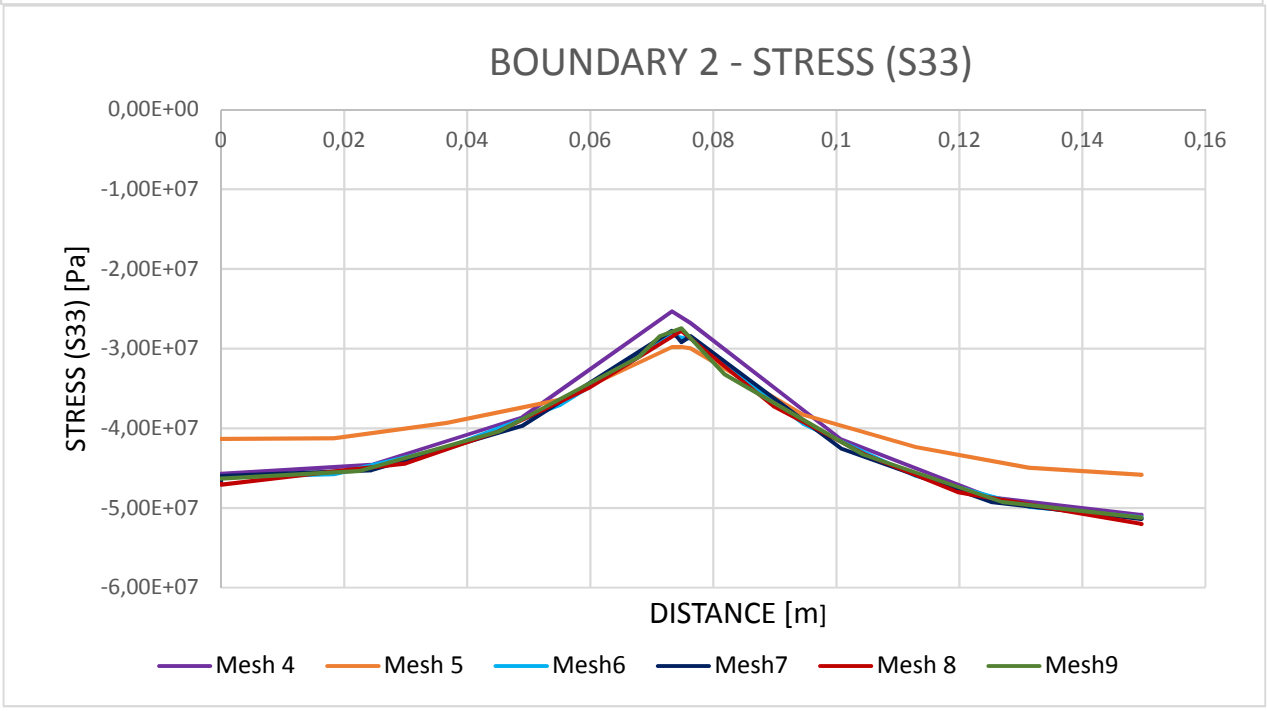

Max value boundary 1:

Mesh 4	Mesh 5	Mesh 6	Mesh 7	Mesh 8	Mesh 9
-2,54E+07	-2,99E+07	-2,84E+07	-2,78E+07	-2,81E+07	-2,75E+07

Difference in min values

Mesh 4 - 6: -11,7%

Mesh 6, 7, 8 and 9 showed good convergence. The difference between Mesh 4 and 6 was caluculated at maximum values to make clear that the Mesh 4 showed to large differnece.

Appendix D - Verification of submodels

Three submodels were created, named a) Submodel Cell b) Submodel Large c) Submodel Small, see figure below.

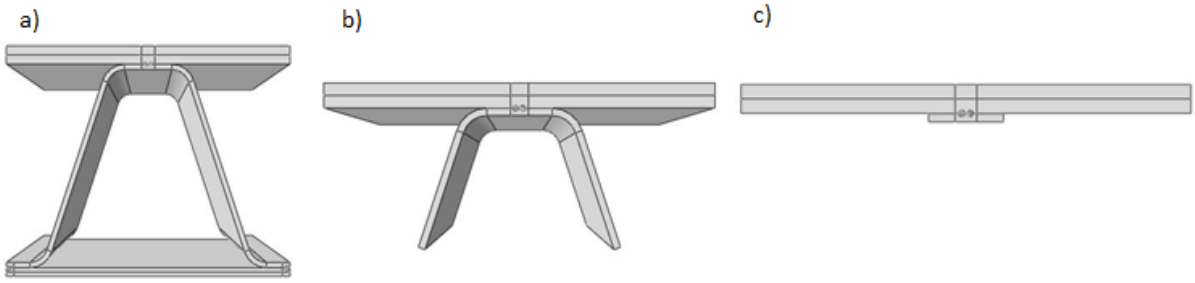

Figure D.1 Submodels a) Submodel Cell b) Submodel Large c) Submodel Small

By verification it was decided which of the models that was going to be used in the fatigue analysis. It was of interest to use a submodel with reduced geometry to decrease the run time. However, the models with decreased geometry had to show correct result and not jeopardize the accuracy of the result.

The load used for the verification of the submodels was applied at the center of the SSD. The load represented half an axel with a magnitude of 60kN. The area exposed for pressure is 400x400 mm, resulting in the total applied load 375 kPa. The verification involved comparison of deformation and Principal stress

DEFORMATIONS

The deformations, U2, were extracted from a path at the centerline of the submodel. See figure below.

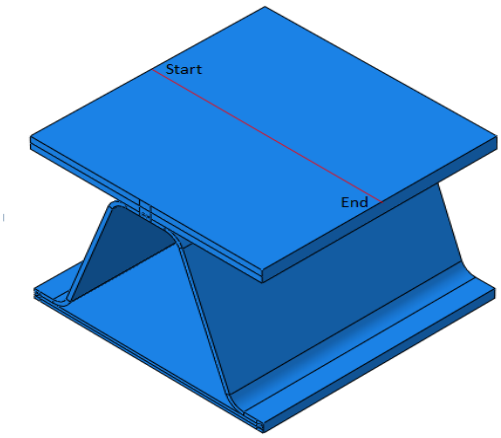

Figure D.2 Path were the deformations were extracted.

Submodel Cell

Distance	U2
0	-0,00331
0,00178099	-0,00331
0,00356197	-0,00332
0,00534296	-0,00332
0,00712395	-0,00332
0,00890493	-0,00333
0,0106859	-0,00333
0,0124669	-0,00334
0,0142478	-0,00334
0,0160288	-0,00334
0,0178097	-0,00335
0,0195907	-0,00335
0,0213717	-0,00335
0,0231527	-0,00336
0,0249337	-0,00336
0,0267147	-0,00336
0,0284957	-0,00337
0,0302767	-0,00337
0,0320576	-0,00337
0,0338386	-0,00337
0,0356196	-0,00338
0,0374006	-0,00338
0,0391816	-0,00338
0,0409626	-0,00338
0,0427436	-0,00338

Submodel Large

Distance	U2
0	-0,00330642
0,0017842	-0,00331131
0,0035685	-0,00331605
0,0053527	-0,00332061
0,0071371	-0,00332499
0,0089213	-0,00332919
0,0107056	-0,00333322
0,0124898	-0,00333709
0,0142741	-0,0033408
0,0160583	-0,00334436
0,0178427	-0,00334778
0,0196269	-0,00335106
0,0214112	-0,00335422
0,0231954	-0,00335726
0,0249797	-0,00336018
0,0267639	-0,003363
0,0285482	-0,00336571
0,0303324	-0,00336833
0,0321168	-0,00337087
0,0339011	-0,00337332
0,0356853	-0,0033757
0,0374696	-0,00337801
0,0392538	-0,00338027
0,0410382	-0,00338247
0,0428224	-0,00338463

Submodel Small

Distance	U2
0	-0,00330642
0,00178003	-0,00331133
0,00355995	-0,00331611
0,00533998	-0,00332072
0,00712001	-0,00332516
0,00889993	-0,00332944
0,01068	-0,00333357
0,01246	-0,00333755
0,0142399	-0,00334138
0,0160199	-0,00334509
0,0178	-0,00334866
0,01958	-0,0033521
0,0213599	-0,00335543
0,02314	-0,00335865
0,02492	-0,00336176
0,0266999	-0,00336477
0,0284799	-0,00336769
0,03026	-0,00337051
0,0320399	-0,00337326
0,0338199	-0,00337593
0,0355999	-0,00337853
0,03738	-0,00338107
0,0391599	-0,00338355
0,0409399	-0,00338597
0,04272	-0,00338835

0,0445246	-0,00339	0,0446067	-0,00338675	0,0444999	-0,00339069
0,0463054	-0,00339	0,0463909	-0,00338883	0,0462799	-0,003393
0,0480864	-0,00339	0,0481752	-0,0033909	0,0480599	-0,00339528
0,0498674	-0,00339	0,0499594	-0,00339295	0,0498399	-0,00339754
0,0516484	-0,00339	0,0517437	-0,00339499	0,0516199	-0,00339979
0,0534294	-0,0034	0,053528	-0,00339703	0,0533999	-0,00340203
0,0552104	-0,0034	0,0553123	-0,00339907	0,05518	-0,00340427
0,0569913	-0,0034	0,0570965	-0,00340114	0,0569599	-0,00340651
0,0587723	-0,0034	0,0588808	-0,00340322	0,0587399	-0,00340877
0,0605533	-0,0034	0,060665	-0,00340534	0,0605199	-0,00341105
0,0623343	-0,00341	0,0624493	-0,00340749	0,0622998	-0,00341335
0,0641153	-0,00341	0,0642335	-0,00340969	0,0640799	-0,00341568
0,0658963	-0,00341	0,0660179	-0,00341195	0,0658599	-0,00341805
0,0676773	-0,00341	0,0678021	-0,00341427	0,0676398	-0,00342047
0,0694582	-0,00342	0,0695864	-0,00341667	0,0694199	-0,00342294
0,0712392	-0,00342	0,0713706	-0,00341917	0,0711999	-0,00342548
0,0730196	-0,00342	0,0730853	-0,00342168	0,073	-0,00342815
0,0748	-0,00342	0,0748	-0,00342432	0,0748	-0,00343092
0,0765804	-0,00343	0,0765147	-0,00342709	0,0766001	-0,0034338
0,0783608	-0,00343	0,0782293	-0,00342996	0,0784001	-0,00343677
0,0801418	-0,00343	0,0800136	-0,00343305	0,08018	-0,00343978
0,0819228	-0,00344	0,0817978	-0,00343621	0,0819601	-0,00344283
0,0837038	-0,00344	0,0835822	-0,00343942	0,0837401	-0,00344592
0,0854847	-0,00344	0,0853664	-0,00344269	0,0855201	-0,00344905
0,0872657	-0,00345	0,0871507	-0,003446	0,0873001	-0,00345221
0,0890467	-0,00345	0,088935	-0,00344934	0,0890801	-0,00345538
0,0908277	-0,00345	0,0907192	-0,00345271	0,0908601	-0,00345857
0,0926086	-0,00346	0,0925035	-0,00345609	0,09264	-0,00346176
0,0943896	-0,00346	0,0942878	-0,00345949	0,0944201	-0,00346496
0,0961705	-0,00346	0,0960721	-0,00346289	0,0962001	-0,00346815
0,0979515	-0,00347	0,0978563	-0,00346628	0,09798	-0,00347132
0,0997325	-0,00347	0,0996406	-0,00346966	0,0997601	-0,00347448
0,101514	-0,00347	0,101425	-0,00347302	0,10154	-0,00347761
0,103294	-0,00348	0,103209	-0,00347635	0,10332	-0,00348071
0,105075	-0,00348	0,104993	-0,00347964	0,1051	-0,00348378
0,106856	-0,00348	0,106778	-0,00348289	0,10688	-0,0034868
0,108637	-0,00349	0,108562	-0,00348609	0,10866	-0,00348976
0,110418	-0,00349	0,110346	-0,00348923	0,11044	-0,00349268
0,112199	-0,00349	0,11213	-0,00349231	0,11222	-0,00349552
0,11398	-0,0035	0,113915	-0,00349532	0,114	-0,0034983
0,115761	-0,0035	0,115699	-0,00349825	0,11578	-0,00350101
0,117542	-0,0035	0,117483	-0,0035011	0,11756	-0,00350363
0,119323	-0,0035	0,119267	-0,00350385	0,11934	-0,00350616
0,121104	-0,00351	0,121052	-0,00350651	0,12112	-0,0035086
0,122885	-0,00351	0,122836	-0,00350906	0,1229	-0,00351095
0,124666	-0,00351	0,12462	-0,0035115	0,12468	-0,00351318
0,126447	-0,00351	0,126405	-0,00351382	0,12646	-0,00351531
0,128228	-0,00352	0,128189	-0,00351601	0,12824	-0,00351732
0,130009	-0,00352	0,129973	-0,00351808	0,13002	-0,00351921
0,13179	-0,00352	0,131757	-0,00352	0,1318	-0,00352096

0,133571	-0,00352
0,135352	-0,00352
0,137133	-0,00352
0,138914	-0,00353
0,140695	-0,00353
0,142476	-0,00353
0,144257	-0,00353
0,146038	-0,00353
0,147819	-0,00353
0,1496	-0,00353

0,133542	-0,00352178
0,135326	-0,00352341
0,13711	-0,00352488
0,138894	-0,00352619
0,140679	-0,00352732
0,142463	-0,00352827
0,144247	-0,00352903
0,146031	-0,0035296
0,147816	-0,00352998
0,1496	-0,00353022

0,13358	-0,00352259
0,13536	-0,00352407
0,13714	-0,00352541
0,13892	-0,00352659
0,1407	-0,00352762
0,14248	-0,00352848
0,14426	-0,00352916
0,14604	-0,00352968
0,14782	-0,00353002
0,1496	-0,00353022

RESULT - DEFORMATIONS

The deformations for the three submodels are plotted in the graph below.

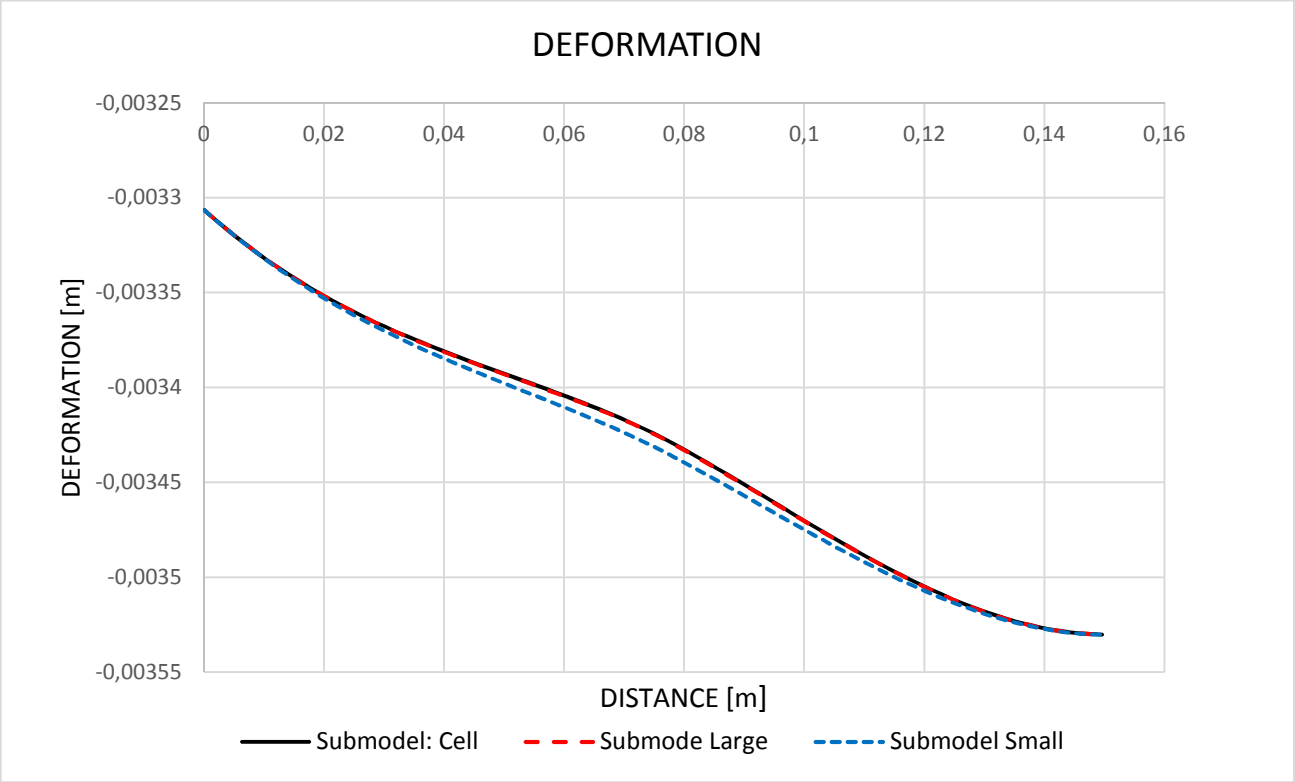

Value at a distance 0.075 m

Submodel Cell	Submodel Large	Submodel Small
-0,003424	-0,003424	-0,00343092

Difference

Submodel Cell and Large	Submodel Cell and Small
0,01%	0,2%

STRESSES

The mises stress and max principal stress (Abs) were compared at the U-shape of the weld, at both the right and the left side.

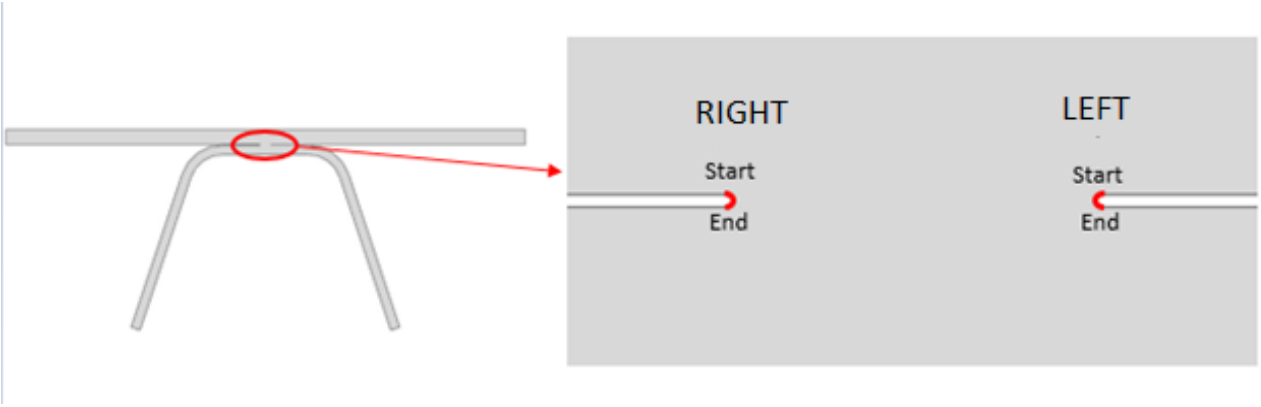

Figure D.3 The path were the stress components were extracted

Max Principle (Abs) =MPA

LEFT SIDE

Submodel Cell

Distance	Mises	MPA
0	1,06E+08	1,10E+08
0,00393689	1,19E+08	1,28E+08
0,00787378	1,19E+08	1,27E+08
0,0118107	1,06E+08	1,13E+08
0,0157476	8,50E+07	8,40E+07
0,0196845	5,00E+07	4,65E+07
0,0236213	3,09E+07	-3,13E+07
0,0275582	6,68E+07	-7,25E+07
0,0314951	1,31E+08	-1,54E+08
0,035432	2,12E+08	-2,46E+08
0,0393689	2,93E+08	-3,64E+08
0,0433058	4,03E+08	-4,73E+08
0,0472427	4,83E+08	-5,89E+08
0,0511796	5,99E+08	-7,16E+08
0,0551165	7,15E+08	-8,51E+08
0,0590534	8,26E+08	-9,83E+08
0,0629903	9,28E+08	-1,11E+09
0,0669271	1,02E+09	-1,22E+09
0,070864	1,08E+09	-1,30E+09
0,0748009	1,17E+09	-1,40E+09
0,0787378	1,23E+09	-1,44E+09
0,0826747	1,26E+09	-1,43E+09
0,0866116	1,31E+09	-1,48E+09
0,0905485	1,25E+09	-1,43E+09
0,0944854	1,17E+09	-1,31E+09

Submodel Large

Distance	Mises	MPA
0	1,03E+08	1,07E+08
0,00393689	1,21E+08	1,28E+08
0,00787378	1,19E+08	1,26E+08
0,0118107	1,07E+08	1,13E+08
0,0157476	8,45E+07	8,53E+07
0,0196845	5,23E+07	4,70E+07
0,0236213	2,60E+07	-3,07E+07
0,0275582	6,61E+07	-7,09E+07
0,0314951	1,26E+08	-1,56E+08
0,035432	2,10E+08	-2,45E+08
0,0393689	2,93E+08	-3,64E+08
0,0433058	3,97E+08	-4,71E+08
0,0472427	4,79E+08	-5,93E+08
0,0511796	5,95E+08	-7,19E+08
0,0551165	6,90E+08	-8,33E+08
0,0590534	8,10E+08	-9,74E+08
0,0629903	9,27E+08	-1,10E+09
0,0669271	1,03E+09	-1,22E+09
0,070864	1,09E+09	-1,29E+09
0,0748009	1,18E+09	-1,39E+09
0,0787378	1,24E+09	-1,45E+09
0,0826747	1,26E+09	-1,46E+09
0,0866116	1,26E+09	-1,45E+09
0,0905485	1,23E+09	-1,41E+09
0,0944854	1,16E+09	-1,32E+09

0,0984223	1,03E+09	-1,16E+09
0,102359	8,22E+08	-9,19E+08

0,0984223	1,03E+09	-1,17E+09
0,102359	8,18E+08	-8,87E+08

Submodel Small

Distance	Mises	MPA
0	1,32E+08	1,40E+08
0,00393689	1,55E+08	1,70E+08
0,00787378	1,61E+08	1,75E+08
0,0118107	1,52E+08	1,67E+08
0,0157476	1,33E+08	1,45E+08
0,0196845	1,02E+08	1,09E+08
0,0236213	6,60E+07	5,69E+07
0,0275582	3,01E+07	-2,36E+07
0,0314951	7,40E+07	-9,46E+07
0,035432	1,48E+08	-1,74E+08
0,0393689	2,33E+08	-2,90E+08
0,0433058	3,39E+08	-4,01E+08
0,0472427	4,24E+08	-5,22E+08
0,0511796	5,32E+08	-6,45E+08
0,0551165	6,42E+08	-7,72E+08
0,0590534	7,53E+08	-9,11E+08
0,0629903	8,56E+08	-1,03E+09
0,0669271	9,54E+08	-1,15E+09
0,070864	1,02E+09	-1,22E+09
0,0748009	1,11E+09	-1,33E+09
0,0787378	1,18E+09	-1,39E+09
0,0826747	1,21E+09	-1,41E+09
0,0866116	1,21E+09	-1,41E+09
0,0905485	1,18E+09	-1,36E+09
0,0944854	1,12E+09	-1,28E+09
0,0984223	1,00E+09	-1,13E+09
0,102359	7,95E+08	-8,72E+08

RIGHT SIDE

Submodel Cell

Distance	Mises	MPA
0	1,80E+08	1,86E+08
0,00393689	2,33E+08	2,54E+08
0,00787378	2,70E+08	2,94E+08
0,0118107	2,96E+08	3,30E+08
0,0157476	3,13E+08	3,50E+08
0,0196845	3,20E+08	3,59E+08
0,0236213	3,17E+08	3,56E+08
0,0275582	2,96E+08	3,38E+08
0,0314951	2,67E+08	2,97E+08
0,035432	2,18E+08	2,55E+08

Submodel Large

Distance	Mises	MPA
0	1,79E+08	1,84E+08
0,00393689	2,34E+08	2,55E+08
0,00787378	2,71E+08	2,96E+08
0,0118107	2,96E+08	3,30E+08
0,0157476	3,12E+08	3,48E+08
0,0196845	3,19E+08	3,60E+08
0,0236213	3,16E+08	3,56E+08
0,0275582	2,99E+08	3,39E+08
0,0314951	2,73E+08	3,02E+08
0,035432	2,18E+08	2,53E+08

0,0393689	1,61E+08	1,81E+08
0,0433058	1,03E+08	1,13E+08
0,0472427	4,21E+07	-34707
0,0511796	9,86E+07	-1,15E+08
0,0551165	1,89E+08	-2,47E+08
0,0590534	2,98E+08	-3,66E+08
0,0629903	3,91E+08	-4,83E+08
0,0669271	4,82E+08	-6,16E+08
0,070864	5,67E+08	-6,68E+08
0,0748009	7,04E+08	-7,87E+08
0,0787378	7,84E+08	-8,69E+08
0,0826747	8,37E+08	-9,56E+08
0,0866116	8,78E+08	-9,98E+08
0,0905485	8,74E+08	-1,00E+09
0,0944854	8,57E+08	-9,63E+08
0,0984223	7,61E+08	-8,76E+08
0,102359	6,18E+08	-6,79E+08

0,0393689	1,64E+08	1,78E+08
0,0433058	1,05E+08	1,13E+08
0,0472427	5,20E+07	-2,21E+06
0,0511796	1,09E+08	-1,13E+08
0,0551165	1,92E+08	-2,22E+08
0,0590534	2,85E+08	-3,40E+08
0,0629903	3,98E+08	-4,66E+08
0,0669271	5,03E+08	-5,97E+08
0,070864	5,89E+08	-6,98E+08
0,0748009	6,85E+08	-8,15E+08
0,0787378	7,58E+08	-8,82E+08
0,0826747	8,20E+08	-9,54E+08
0,0866116	8,65E+08	-1,00E+09
0,0905485	8,64E+08	-9,91E+08
0,0944854	8,45E+08	-9,53E+08
0,0984223	7,55E+08	-8,63E+08
0,102359	6,16E+08	-6,83E+08

Submodel Small

Distance	Mises	MPA
0	1,96E+08	2,05E+08
0,00393689	2,55E+08	2,80E+08
0,00787378	2,94E+08	3,21E+08
0,0118107	3,23E+08	3,59E+08
0,0157476	3,42E+08	3,79E+08
0,0196845	3,49E+08	3,92E+08
0,0236213	3,48E+08	3,85E+08
0,0275582	3,29E+08	3,60E+08
0,0314951	2,84E+08	3,18E+08
0,035432	2,47E+08	2,92E+08
0,0393689	1,98E+08	2,22E+08
0,0433058	1,22E+08	1,37E+08
0,0472427	6,18E+07	5,08E+07
0,0511796	6,99E+07	-7,44E+07
0,0551165	1,62E+08	-1,89E+08
0,0590534	2,64E+08	-3,14E+08
0,0629903	3,64E+08	-4,45E+08
0,0669271	4,75E+08	-5,68E+08
0,070864	5,57E+08	-6,59E+08
0,0748009	6,46E+08	-7,82E+08
0,0787378	7,28E+08	-8,29E+08
0,0826747	8,01E+08	-9,08E+08
0,0866116	8,50E+08	-9,62E+08
0,0905485	8,39E+08	-9,59E+08
0,0944854	8,17E+08	-9,17E+08
0,0984223	7,34E+08	-8,43E+08
0,102359	5,99E+08	-6,62E+08

RESULT - MAX PRINCIPAL STRESS (Abs)

The max principal stress (Abs) for the three submodels are plotted in the two graphs below.

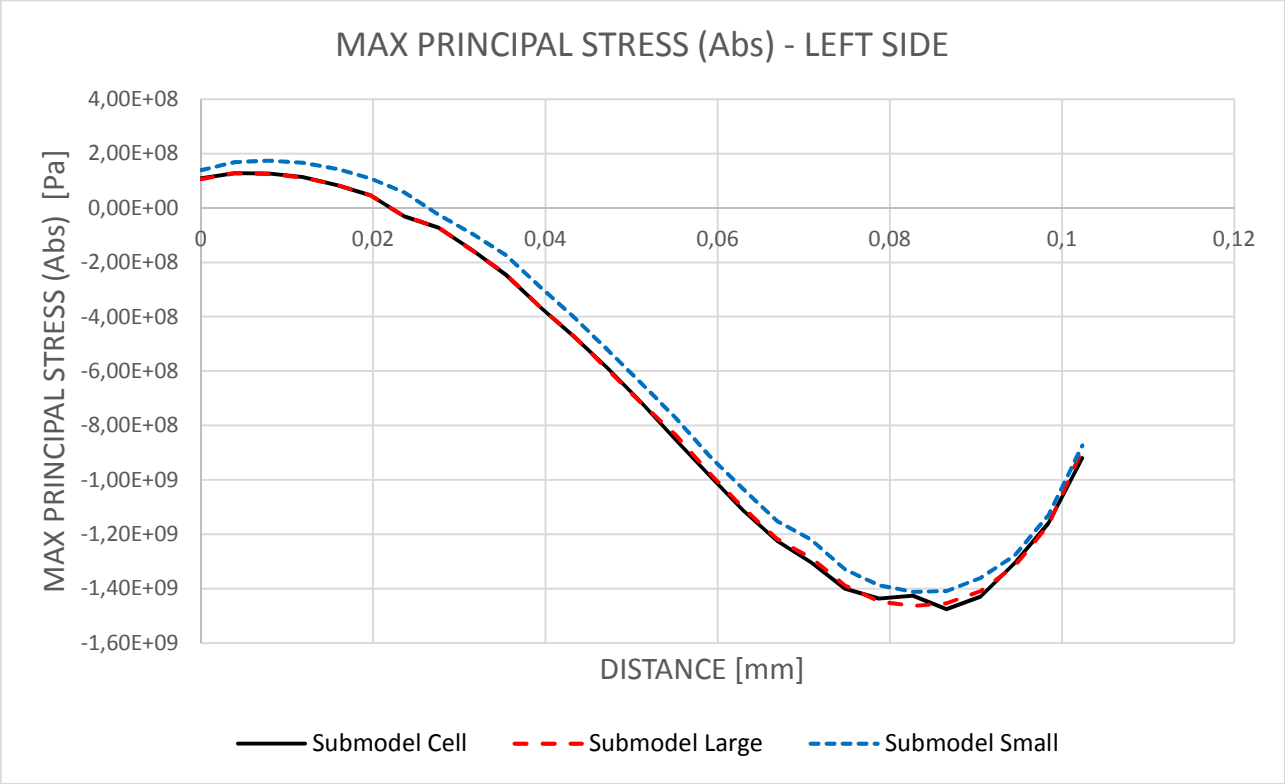

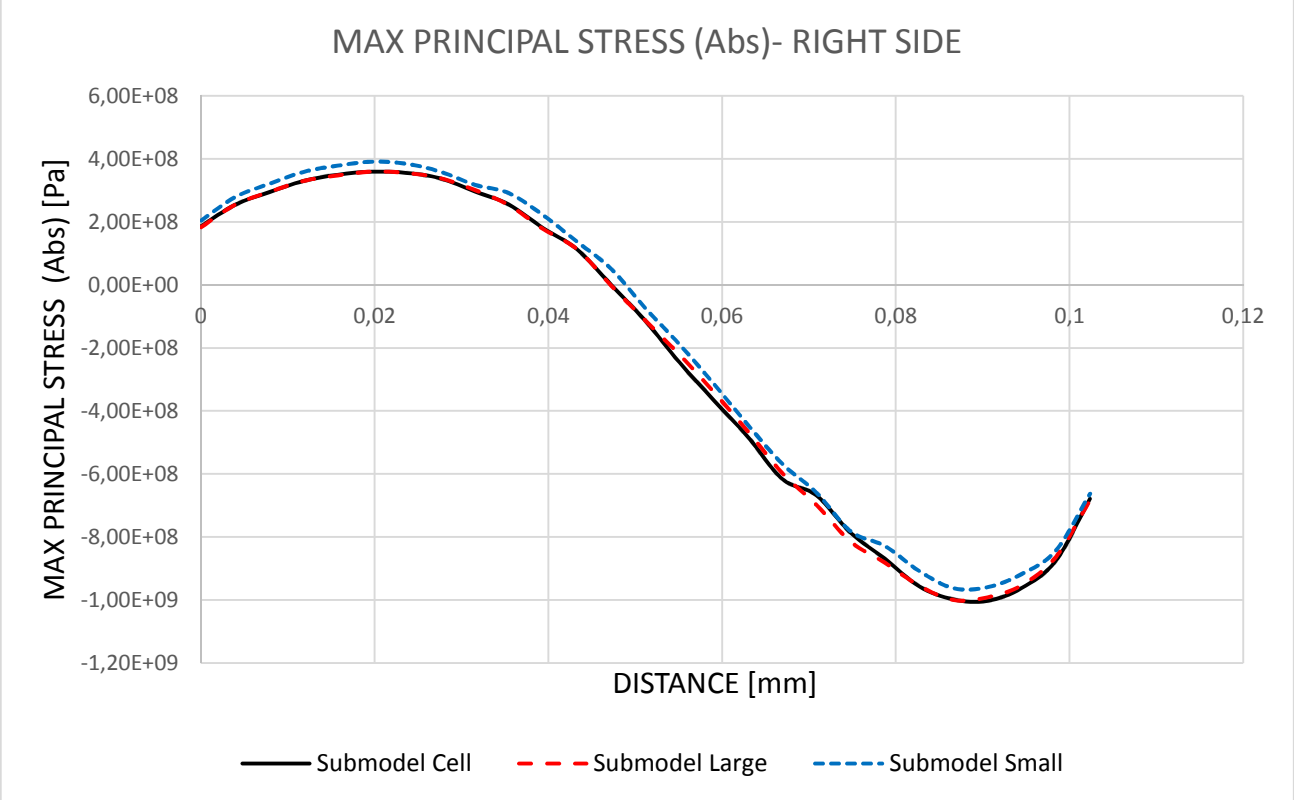

Difference

Submodel Cell and Large		Submodel Cell and Small	
LEFT	RIGHT	LEFT	RIGHT
2,8%	1,2%	27,5%	-10,1%
0,5%	0,4%	33,0%	-9,9%
0,4%	0,5%	37,9%	-9,2%
0,6%	0,2%	47,3%	-8,9%
1,6%	0,4%	72,2%	-8,4%
1,0%	0,2%	134,9%	-9,0%
1,7%	0,0%	281,8%	-8,2%
2,1%	0,2%	67,4%	-6,4%
1,4%	1,7%	38,6%	-7,3%
0,6%	0,7%	29,3%	-14,3%
0,1%	1,6%	20,3%	-22,8%
0,3%	0,5%	15,3%	-21,5%
0,7%	6267,0%	11,5%	146346,9%
0,3%	1,3%	10,0%	35,1%
2,1%	10,1%	9,4%	23,2%
1,0%	7,1%	7,3%	14,2%
0,9%	3,6%	7,1%	7,9%
0,6%	3,0%	5,9%	7,8%
1,3%	4,5%	6,4%	1,3%
0,8%	3,6%	5,0%	0,6%
0,8%	1,4%	3,4%	4,7%
2,6%	0,2%	1,1%	5,1%
1,5%	0,1%	4,5%	3,6%
1,4%	1,2%	4,8%	4,4%
0,7%	1,0%	2,3%	4,7%
0,5%	1,5%	2,7%	3,8%
3,5%	0,5%	5,1%	2,5%
1,2%	1,7%	33,0%	9,4%

The mean difference of 1.2%/1.7% between Submodel Cell and Large indicated on good coherence. However, Submodel Cell and Small showed a large discrepancy of 33%/9.4%.

RESULT - MISES STRESS

The mises stress for the three submodels in the two graphs below.

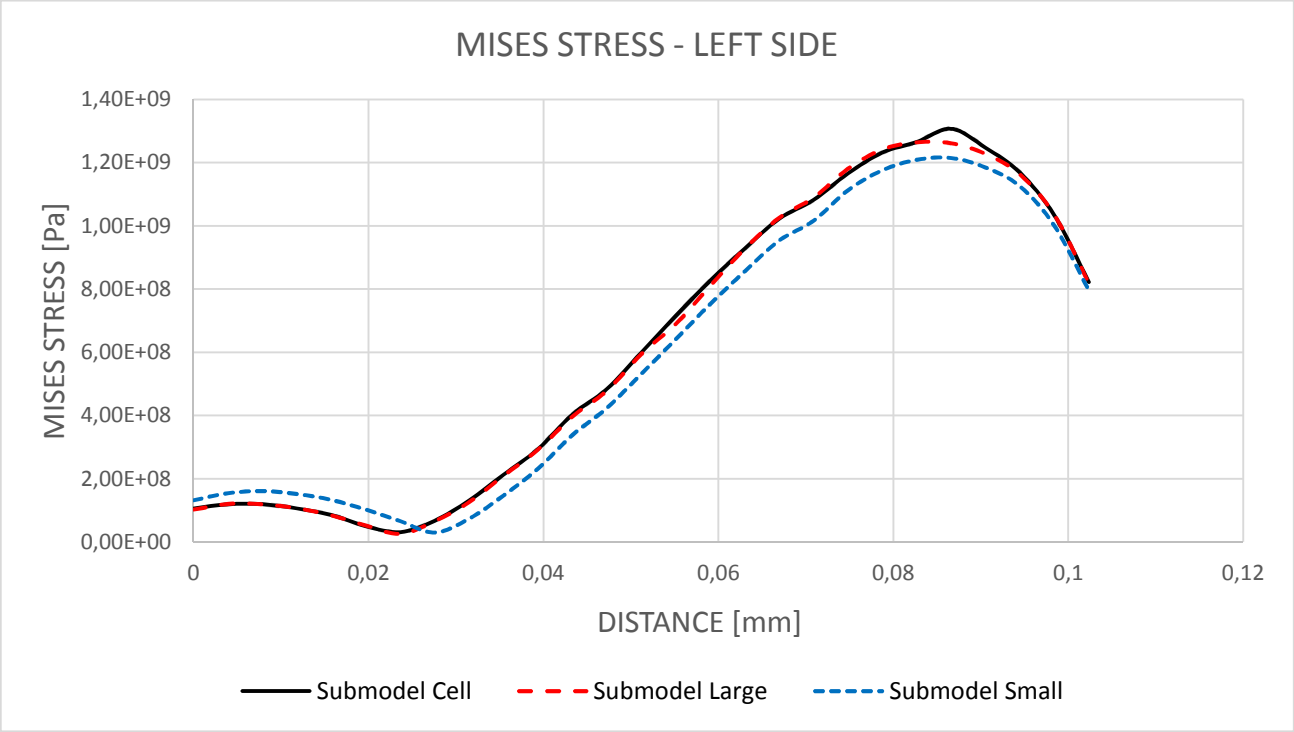

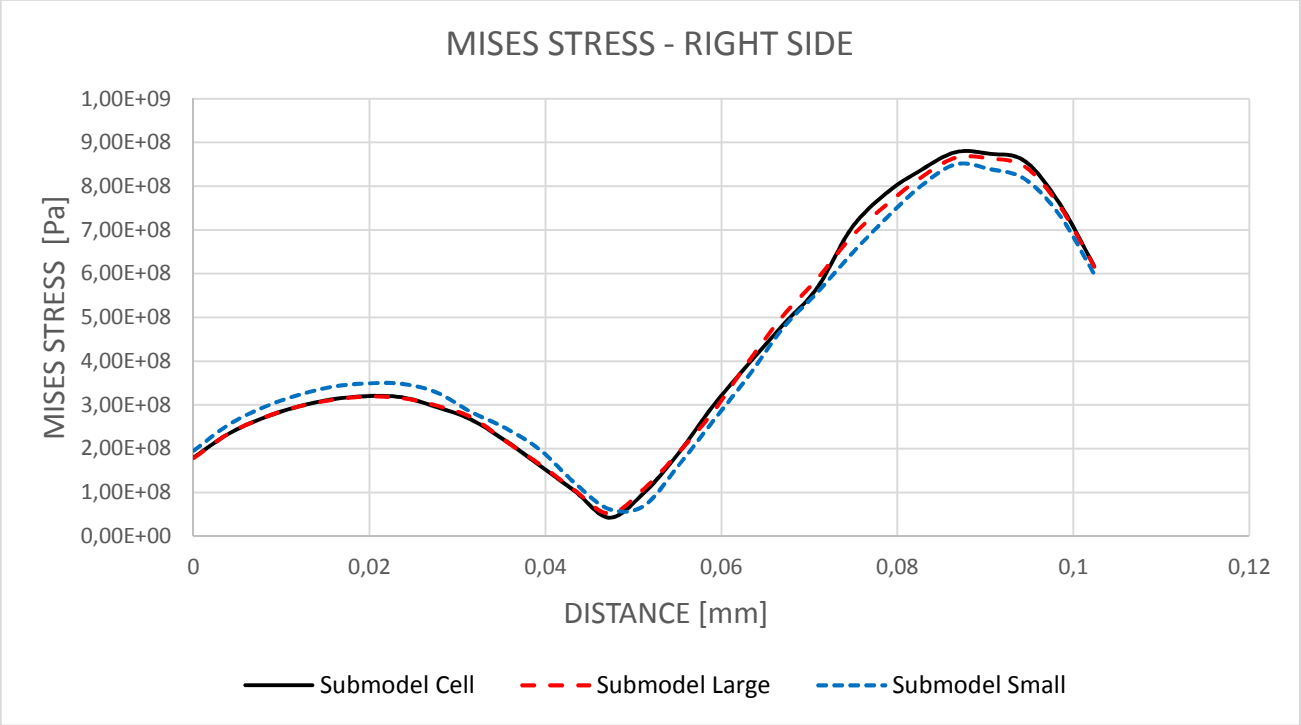

Appendix E - Fatigue analysis of SSD

The fatigue analysis involved investigation of welded details in a steel sandwich deck under a moving load. The fatigue analysis was conducted by implementing the effective notch stress method in conjunction with FE modelling.

A global model representing a 5984x4000 mm part of a bridge construction was created in ABAQUS. To the global model four submodels were attached according figure E.1. The submodels were created with U-shapes at the weld region according to IIW: recommendation, see figure 2. The left U-shape in the submodel was denoted A and the right one B. The notations, “Submodel 1A” means thus the left U-shape in Submodel 1.

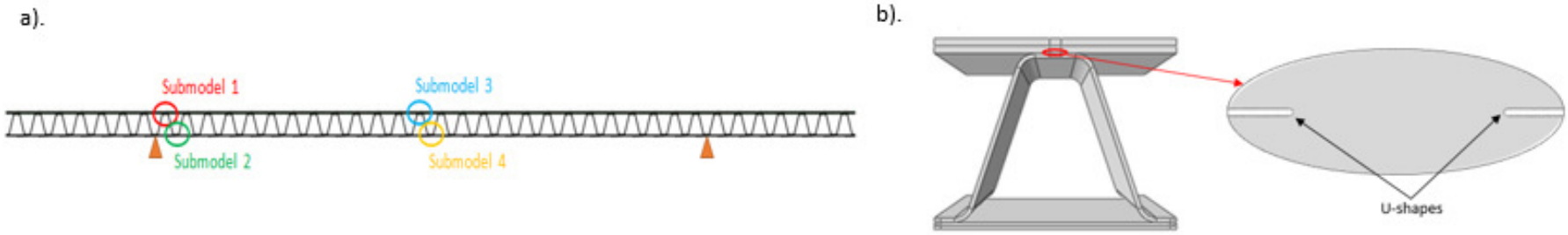

Figure E.1 a). Positions of submodels b). Submodel with U-shapes.

The applied load was a moving load transferred in the transverse direction of the deck. The load was applied through 42 load steps with different positions, see figure E.2. By investigate the stress concentrations at the U-shapes for all 42 load steps, critical hot spots with expected crack initiations positions were detected. The stress concentrations were extracted from paths placed at each U-shape, each path contained of 27 nodes. Consequently, for each load step and U-shape 27 values representing the stress concentration were extracted. To understand the variation of the stress concentration in each node, when the load was moving, influence lines were created. The influence lines were compared and for each submodel and U-shape maximum and minimum stress concentration was decided.

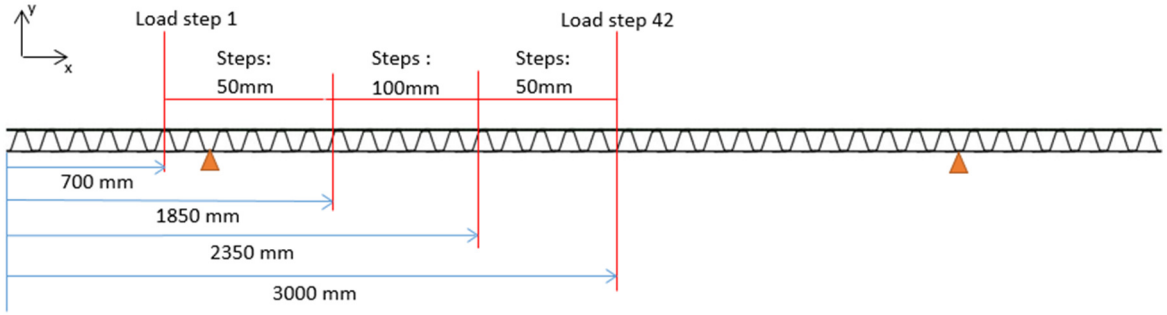

Figure E.2 Load steps.

In the following appendix are the extracted values from Abaqus presented and also the influence lines. The results are presented for each submodel at the time, both in Principal stress (Abs) and Mises stress.

SUBMODEL 1 A

MAX PRINCIPAL STRESS (Abs)

		Step 1	Step 2	Step 3	Step 4	Step 5	Step 6	Step 7	Step 8	Step 9	Step 10	Step 11
Node	Distance	0,7	0,75	0,8	0,85	0,9	0,95	1	1,05	1,1	1,15	1,2
1	0	-8,59E+07	-9,29E+07	-1,04E+08	-1,13E+08	-9,46E+07	-5,40E+07	-2,69E+07	-2,85E+07	-4,71E+07	-6,94E+07	-8,64E+07
2	0,00604	-1,14E+08	-1,23E+08	-1,38E+08	-1,54E+08	-1,36E+08	-8,83E+07	-5,52E+07	-6,04E+07	-9,05E+07	-1,25E+08	-1,52E+08
3	0,01208	-1,32E+08	-1,42E+08	-1,61E+08	-1,86E+08	-1,75E+08	-1,29E+08	-9,60E+07	-1,07E+08	-1,49E+08	-1,95E+08	-2,30E+08
4	0,01812	-1,47E+08	-1,58E+08	-1,81E+08	-2,16E+08	-2,17E+08	-1,77E+08	-1,48E+08	-1,67E+08	-2,22E+08	-2,83E+08	-3,28E+08
5	0,02416	-1,58E+08	-1,69E+08	-1,96E+08	-2,43E+08	-2,58E+08	-2,30E+08	-2,08E+08	-2,36E+08	-3,04E+08	-3,79E+08	-4,33E+08
6	0,0302	-1,66E+08	-1,76E+08	-2,09E+08	-2,68E+08	-3,01E+08	-2,87E+08	-2,75E+08	-3,14E+08	-3,97E+08	-4,86E+08	-5,49E+08
7	0,03624	-1,72E+08	-1,82E+08	-2,19E+08	-2,93E+08	-3,49E+08	-3,56E+08	-3,58E+08	-4,10E+08	-5,09E+08	-6,12E+08	-6,85E+08
8	0,04228	-1,76E+08	-1,85E+08	-2,27E+08	-3,16E+08	-3,95E+08	-4,23E+08	-4,41E+08	-5,06E+08	-6,19E+08	-7,36E+08	-8,17E+08
9	0,04832	-1,78E+08	-1,87E+08	-2,35E+08	-3,42E+08	-4,51E+08	-5,08E+08	-5,47E+08	-6,29E+08	-7,59E+08	-8,92E+08	-9,80E+08
10	0,05436	-1,77E+08	-1,86E+08	-2,39E+08	-3,64E+08	-5,02E+08	-5,86E+08	-6,47E+08	-7,46E+08	-8,90E+08	-1,03E+09	-1,13E+09
11	0,0604	-1,76E+08	-1,84E+08	-2,44E+08	-3,91E+08	-5,65E+08	-6,86E+08	-7,76E+08	-8,95E+08	-1,06E+09	-1,21E+09	-1,31E+09
12	0,06644	-1,72E+08	-1,79E+08	-2,44E+08	-4,10E+08	-6,15E+08	-7,67E+08	-8,83E+08	-1,02E+09	-1,19E+09	-1,36E+09	-1,46E+09
13	0,07248	-1,66E+08	-1,72E+08	-2,43E+08	-4,27E+08	-6,64E+08	-8,49E+08	-9,94E+08	-1,15E+09	-1,33E+09	-1,50E+09	-1,60E+09
14	0,07852	-1,63E+08	-1,69E+08	-2,46E+08	-4,52E+08	-7,24E+08	-9,44E+08	-1,12E+09	-1,29E+09	-1,49E+09	-1,67E+09	-1,77E+09
15	0,08456	-1,57E+08	-1,62E+08	-2,44E+08	-4,66E+08	-7,66E+08	-1,01E+09	-1,22E+09	-1,41E+09	-1,61E+09	-1,79E+09	-1,88E+09
16	0,0906	-1,52E+08	-1,57E+08	-2,46E+08	-4,89E+08	-8,25E+08	-1,11E+09	-1,34E+09	-1,56E+09	-1,77E+09	-1,96E+09	-2,04E+09
17	0,09664	-1,46E+08	-1,50E+08	-2,45E+08	-5,06E+08	-8,73E+08	-1,19E+09	-1,45E+09	-1,68E+09	-1,90E+09	-2,09E+09	-2,17E+09
18	0,10268	-1,38E+08	-1,41E+08	-2,40E+08	-5,15E+08	-9,06E+08	-1,25E+09	-1,54E+09	-1,78E+09	-2,01E+09	-2,19E+09	-2,26E+09
19	0,10872	-1,30E+08	-1,33E+08	-2,33E+08	-5,15E+08	-9,17E+08	-1,27E+09	-1,58E+09	-1,83E+09	-2,05E+09	-2,22E+09	-2,28E+09
20	0,11476	-1,22E+08	-1,26E+08	-2,30E+08	-5,22E+08	-9,46E+08	-1,33E+09	-1,65E+09	-1,92E+09	-2,14E+09	-2,30E+09	-2,36E+09
21	0,1208	-1,15E+08	-1,18E+08	-2,23E+08	-5,20E+08	-9,52E+08	-1,34E+09	-1,68E+09	-1,95E+09	-2,16E+09	-2,32E+09	-2,37E+09
22	0,12684	-1,05E+08	-1,08E+08	-2,11E+08	-5,04E+08	-9,32E+08	-1,32E+09	-1,66E+09	-1,93E+09	-2,14E+09	-2,28E+09	-2,31E+09
23	0,13288	-9,62E+07	-9,95E+07	-2,00E+08	-4,85E+08	-9,02E+08	-1,28E+09	-1,62E+09	-1,88E+09	-2,08E+09	-2,21E+09	-2,23E+09
24	0,13892	-8,60E+07	-8,92E+07	-1,84E+08	-4,55E+08	-8,54E+08	-1,22E+09	-1,55E+09	-1,80E+09	-1,98E+09	-2,09E+09	-2,11E+09
25	0,14496	-7,52E+07	-7,82E+07	-1,66E+08	-4,15E+08	-7,82E+08	-1,12E+09	-1,43E+09	-1,65E+09	-1,81E+09	-1,92E+09	-1,92E+09
26	0,151	-6,27E+07	-6,54E+07	-1,42E+08	-3,59E+08	-6,82E+08	-9,81E+08	-1,25E+09	-1,45E+09	-1,59E+09	-1,67E+09	-1,67E+09
27	0,15704	-4,45E+07	-4,66E+07	-1,04E+08	-2,67E+08	-5,08E+08	-7,33E+08	-9,37E+08	-1,09E+09	-1,19E+09	-1,25E+09	-1,24E+09

Step 12	Step 13	Step 14	Step 15	Step 16	Step 17	Step 18	Step 19	Step 20	Step 21	Step 22	Step 23	Step 24	Step 25
1,25	1,3	1,35	1,4	1,45	1,5	1,55	1,6	1,65	1,7	1,75	1,8	1,85	1,95
-1,01E+08	-1,38E+08	-1,97E+08	-2,40E+08	-2,51E+08	-2,41E+08	-2,23E+08	-2,06E+08	-1,92E+08	-1,81E+08	-1,70E+08	-1,61E+08	-1,53E+08	-1,38E+08
-1,71E+08	-2,19E+08	-2,94E+08	-3,52E+08	-3,67E+08	-3,52E+08	-3,27E+08	-3,02E+08	-2,82E+08	-2,65E+08	-2,50E+08	-2,37E+08	-2,25E+08	-2,02E+08
-2,52E+08	-3,03E+08	-3,86E+08	-4,51E+08	-4,68E+08	-4,49E+08	-4,18E+08	-3,86E+08	-3,61E+08	-3,39E+08	-3,20E+08	-3,03E+08	-2,87E+08	-2,59E+08
-3,52E+08	-4,04E+08	-4,91E+08	-5,64E+08	-5,82E+08	-5,59E+08	-5,20E+08	-4,82E+08	-4,50E+08	-4,23E+08	-4,00E+08	-3,78E+08	-3,58E+08	-3,23E+08
-4,59E+08	-5,07E+08	-5,93E+08	-6,67E+08	-6,86E+08	-6,59E+08	-6,13E+08	-5,69E+08	-5,32E+08	-5,00E+08	-4,72E+08	-4,47E+08	-4,23E+08	-3,82E+08
-5,75E+08	-6,17E+08	-6,99E+08	-7,74E+08	-7,93E+08	-7,60E+08	-7,09E+08	-6,58E+08	-6,15E+08	-5,79E+08	-5,46E+08	-5,17E+08	-4,90E+08	-4,42E+08
-7,08E+08	-7,40E+08	-8,13E+08	-8,85E+08	-9,01E+08	-8,63E+08	-8,05E+08	-7,48E+08	-7,00E+08	-6,59E+08	-6,22E+08	-5,88E+08	-5,58E+08	-5,03E+08
-8,37E+08	-8,57E+08	-9,20E+08	-9,86E+08	-9,99E+08	-9,57E+08	-8,93E+08	-8,30E+08	-7,77E+08	-7,31E+08	-6,91E+08	-6,53E+08	-6,19E+08	-5,58E+08
-9,94E+08	-9,96E+08	-1,04E+09	-1,10E+09	-1,10E+09	-1,06E+09	-9,86E+08	-9,17E+08	-8,59E+08	-8,08E+08	-7,63E+08	-7,22E+08	-6,85E+08	-6,17E+08
-1,14E+09	-1,12E+09	-1,14E+09	-1,19E+09	-1,19E+09	-1,13E+09	-1,06E+09	-9,87E+08	-9,25E+08	-8,71E+08	-8,22E+08	-7,78E+08	-7,37E+08	-6,65E+08
-1,31E+09	-1,26E+09	-1,26E+09	-1,29E+09	-1,28E+09	-1,22E+09	-1,14E+09	-1,06E+09	-9,94E+08	-9,36E+08	-8,84E+08	-8,37E+08	-7,93E+08	-7,15E+08
-1,44E+09	-1,37E+09	-1,35E+09	-1,35E+09	-1,33E+09	-1,27E+09	-1,18E+09	-1,11E+09	-1,04E+09	-9,76E+08	-9,22E+08	-8,72E+08	-8,27E+08	-7,45E+08
-1,57E+09	-1,47E+09	-1,42E+09	-1,40E+09	-1,37E+09	-1,29E+09	-1,21E+09	-1,13E+09	-1,06E+09	-9,99E+08	-9,44E+08	-8,93E+08	-8,46E+08	-7,63E+08
-1,72E+09	-1,60E+09	-1,51E+09	-1,47E+09	-1,42E+09	-1,35E+09	-1,26E+09	-1,18E+09	-1,10E+09	-1,04E+09	-9,83E+08	-9,30E+08	-8,82E+08	-7,95E+08
-1,82E+09	-1,67E+09	-1,56E+09	-1,49E+09	-1,43E+09	-1,35E+09	-1,26E+09	-1,18E+09	-1,11E+09	-1,04E+09	-9,86E+08	-9,34E+08	-8,85E+08	-7,97E+08
-1,96E+09	-1,78E+09	-1,64E+09	-1,54E+09	-1,46E+09	-1,37E+09	-1,28E+09	-1,20E+09	-1,13E+09	-1,06E+09	-1,01E+09	-9,52E+08	-9,02E+08	-8,13E+08
-2,07E+09	-1,86E+09	-1,68E+09	-1,56E+09	-1,46E+09	-1,37E+09	-1,28E+09	-1,20E+09	-1,13E+09	-1,06E+09	-1,00E+09	-9,50E+08	-9,01E+08	-8,12E+08
-2,14E+09	-1,90E+09	-1,69E+09	-1,54E+09	-1,43E+09	-1,33E+09	-1,24E+09	-1,17E+09	-1,10E+09	-1,04E+09	-9,79E+08	-9,26E+08	-8,78E+08	-7,91E+08
-2,15E+09	-1,89E+09	-1,67E+09	-1,50E+09	-1,37E+09	-1,27E+09	-1,19E+09	-1,12E+09	-1,05E+09	-9,95E+08	-9,40E+08	-8,90E+08	-8,43E+08	-7,60E+08
-2,21E+09	-1,92E+09	-1,67E+09	-1,47E+09	-1,33E+09	-1,23E+09	-1,15E+09	-1,08E+09	-1,02E+09	-9,63E+08	-9,10E+08	-8,62E+08	-8,17E+08	-7,36E+08
-2,21E+09	-1,91E+09	-1,64E+09	-1,42E+09	-1,27E+09	-1,17E+09	-1,10E+09	-1,03E+09	-9,72E+08	-9,17E+08	-8,67E+08	-8,21E+08	-7,78E+08	-7,01E+08
-2,15E+09	-1,84E+09	-1,56E+09	-1,33E+09	-1,17E+09	-1,08E+09	-1,01E+09	-9,49E+08	-8,95E+08	-8,45E+08	-7,99E+08	-7,56E+08	-7,17E+08	-6,46E+08
-2,06E+09	-1,75E+09	-1,47E+09	-1,24E+09	-1,08E+09	-9,86E+08	-9,22E+08	-8,70E+08	-8,21E+08	-7,76E+08	-7,33E+08	-6,94E+08	-6,58E+08	-5,93E+08
-1,94E+09	-1,64E+09	-1,36E+09	-1,13E+09	-9,71E+08	-8,81E+08	-8,24E+08	-7,78E+08	-7,35E+08	-6,95E+08	-6,57E+08	-6,22E+08	-5,90E+08	-5,31E+08
-1,76E+09	-1,48E+09	-1,22E+09	-9,95E+08	-8,47E+08	-7,65E+08	-7,16E+08	-6,77E+08	-6,40E+08	-6,05E+08	-5,72E+08	-5,41E+08	-5,13E+08	-4,63E+08
-1,53E+09	-1,27E+09	-1,04E+09	-8,39E+08	-7,07E+08	-6,35E+08	-5,94E+08	-5,62E+08	-5,32E+08	-5,03E+08	-4,76E+08	-4,50E+08	-4,27E+08	-3,85E+08
-1,13E+09	-9,36E+08	-7,59E+08	-6,01E+08	-4,99E+08	-4,46E+08	-4,17E+08	-3,95E+08	-3,74E+08	-3,53E+08	-3,34E+08	-3,17E+08	-3,00E+08	-2,71E+08

Step 26	Step 27	Step 28	Step 29	Step 30	Step 31	Step 32	Step 33	Step 34	Step 35	Step 36	Step 37	Step 38	Step 39
2,05	2,15	2,25	2,35	2,4	2,45	2,5	2,55	2,6	2,65	2,7	2,75	2,8	2,85
-1,25E+08	-1,13E+08	-1,03E+08	-9,35E+07	-8,93E+07	-8,52E+07	-8,14E+07	-7,77E+07	-7,42E+07	-7,09E+07	-6,77E+07	-6,46E+07	-6,17E+07	-5,90E+07
-1,83E+08	-1,66E+08	-1,51E+08	-1,37E+08	-1,31E+08	-1,25E+08	-1,19E+08	-1,14E+08	-1,09E+08	-1,04E+08	-9,92E+07	-9,47E+07	-9,04E+07	-8,63E+07
-2,34E+08	-2,12E+08	-1,93E+08	-1,75E+08	-1,67E+08	-1,60E+08	-1,53E+08	-1,46E+08	-1,39E+08	-1,33E+08	-1,27E+08	-1,21E+08	-1,16E+08	-1,10E+08
-2,92E+08	-2,65E+08	-2,41E+08	-2,19E+08	-2,09E+08	-1,99E+08	-1,90E+08	-1,81E+08	-1,73E+08	-1,65E+08	-1,58E+08	-1,51E+08	-1,44E+08	-1,37E+08
-3,45E+08	-3,13E+08	-2,84E+08	-2,58E+08	-2,47E+08	-2,35E+08	-2,25E+08	-2,14E+08	-2,05E+08	-1,95E+08	-1,86E+08	-1,78E+08	-1,70E+08	-1,62E+08
-3,99E+08	-3,62E+08	-3,29E+08	-2,99E+08	-2,85E+08	-2,72E+08	-2,60E+08	-2,48E+08	-2,37E+08	-2,26E+08	-2,16E+08	-2,06E+08	-1,96E+08	-1,87E+08
-4,54E+08	-4,12E+08	-3,74E+08	-3,40E+08	-3,25E+08	-3,10E+08	-2,95E+08	-2,82E+08	-2,69E+08	-2,57E+08	-2,45E+08	-2,34E+08	-2,23E+08	-2,13E+08
-5,05E+08	-4,58E+08	-4,15E+08	-3,78E+08	-3,60E+08	-3,44E+08	-3,28E+08	-3,13E+08	-2,99E+08	-2,85E+08	-2,72E+08	-2,60E+08	-2,48E+08	-2,36E+08
-5,58E+08	-5,06E+08	-4,59E+08	-4,18E+08	-3,98E+08	-3,80E+08	-3,63E+08	-3,46E+08	-3,30E+08	-3,15E+08	-3,01E+08	-2,87E+08	-2,74E+08	-2,61E+08
-6,01E+08	-5,45E+08	-4,95E+08	-4,50E+08	-4,29E+08	-4,09E+08	-3,90E+08	-3,73E+08	-3,56E+08	-3,39E+08	-3,24E+08	-3,09E+08	-2,95E+08	-2,81E+08
-6,46E+08	-5,86E+08	-5,32E+08	-4,84E+08	-4,61E+08	-4,40E+08	-4,20E+08	-4,01E+08	-3,82E+08	-3,65E+08	-3,48E+08	-3,32E+08	-3,17E+08	-3,02E+08
-6,74E+08	-6,11E+08	-5,55E+08	-5,04E+08	-4,81E+08	-4,59E+08	-4,38E+08	-4,18E+08	-3,99E+08	-3,80E+08	-3,63E+08	-3,46E+08	-3,30E+08	-3,15E+08
-6,90E+08	-6,25E+08	-5,68E+08	-5,16E+08	-4,92E+08	-4,70E+08	-4,48E+08	-4,28E+08	-4,08E+08	-3,89E+08	-3,71E+08	-3,54E+08	-3,38E+08	-3,23E+08
-7,19E+08	-6,52E+08	-5,92E+08	-5,38E+08	-5,13E+08	-4,89E+08	-4,67E+08	-4,45E+08	-4,25E+08	-4,06E+08	-3,87E+08	-3,69E+08	-3,52E+08	-3,36E+08
-7,21E+08	-6,54E+08	-5,94E+08	-5,40E+08	-5,15E+08	-4,91E+08	-4,68E+08	-4,47E+08	-4,27E+08	-4,07E+08	-3,88E+08	-3,71E+08	-3,54E+08	-3,37E+08
-7,35E+08	-6,66E+08	-6,05E+08	-5,50E+08	-5,25E+08	-5,01E+08	-4,77E+08	-4,56E+08	-4,35E+08	-4,15E+08	-3,96E+08	-3,78E+08	-3,60E+08	-3,44E+08
-7,34E+08	-6,66E+08	-6,04E+08	-5,49E+08	-5,24E+08	-5,00E+08	-4,77E+08	-4,55E+08	-4,34E+08	-4,14E+08	-3,95E+08	-3,77E+08	-3,60E+08	-3,43E+08
-7,16E+08	-6,49E+08	-5,89E+08	-5,36E+08	-5,11E+08	-4,87E+08	-4,65E+08	-4,44E+08	-4,23E+08	-4,04E+08	-3,85E+08	-3,68E+08	-3,51E+08	-3,35E+08
-6,88E+08	-6,23E+08	-5,66E+08	-5,15E+08	-4,91E+08	-4,68E+08	-4,47E+08	-4,26E+08	-4,07E+08	-3,88E+08	-3,70E+08	-3,53E+08	-3,37E+08	-3,21E+08
-6,66E+08	-6,04E+08	-5,48E+08	-4,98E+08	-4,75E+08	-4,54E+08	-4,33E+08	-4,13E+08	-3,94E+08	-3,76E+08	-3,59E+08	-3,42E+08	-3,26E+08	-3,11E+08
-6,34E+08	-5,75E+08	-5,22E+08	-4,75E+08	-4,53E+08	-4,32E+08	-4,12E+08	-3,93E+08	-3,75E+08	-3,58E+08	-3,42E+08	-3,26E+08	-3,11E+08	-2,97E+08
-5,84E+08	-5,30E+08	-4,81E+08	-4,37E+08	-4,17E+08	-3,98E+08	-3,80E+08	-3,62E+08	-3,46E+08	-3,30E+08	-3,15E+08	-3,00E+08	-2,86E+08	-2,73E+08
-5,37E+08	-4,86E+08	-4,42E+08	-4,02E+08	-3,83E+08	-3,66E+08	-3,49E+08	-3,33E+08	-3,17E+08	-3,03E+08	-2,89E+08	-2,76E+08	-2,63E+08	-2,51E+08
-4,81E+08	-4,36E+08	-3,96E+08	-3,60E+08	-3,43E+08	-3,27E+08	-3,12E+08	-2,98E+08	-2,84E+08	-2,71E+08	-2,59E+08	-2,47E+08	-2,36E+08	-2,25E+08
-4,18E+08	-3,79E+08	-3,45E+08	-3,13E+08	-2,99E+08	-2,85E+08	-2,72E+08	-2,60E+08	-2,48E+08	-2,36E+08	-2,25E+08	-2,15E+08	-2,05E+08	-1,96E+08
-3,48E+08	-3,16E+08	-2,87E+08	-2,61E+08	-2,49E+08	-2,37E+08	-2,26E+08	-2,16E+08	-2,06E+08	-1,97E+08	-1,88E+08	-1,79E+08	-1,71E+08	-1,63E+08
-2,45E+08	-2,22E+08	-2,02E+08	-1,83E+08	-1,75E+08	-1,67E+08	-1,59E+08	-1,52E+08	-1,45E+08	-1,38E+08	-1,32E+08	-1,26E+08	-1,20E+08	-1,15E+08

Step 40	Step 41	Step 42
2,9	2,95	3
-5,63E+07	-5,38E+07	-5,13E+07
-8,24E+07	-7,87E+07	-7,51E+07
-1,05E+08	-1,00E+08	-9,59E+07
-1,31E+08	-1,25E+08	-1,19E+08
-1,55E+08	-1,48E+08	-1,41E+08
-1,79E+08	-1,71E+08	-1,63E+08
-2,03E+08	-1,94E+08	-1,85E+08
-2,26E+08	-2,15E+08	-2,05E+08
-2,49E+08	-2,38E+08	-2,27E+08
-2,68E+08	-2,56E+08	-2,44E+08
-2,88E+08	-2,75E+08	-2,62E+08
-3,01E+08	-2,87E+08	-2,73E+08
-3,08E+08	-2,94E+08	-2,80E+08
-3,21E+08	-3,06E+08	-2,92E+08
-3,22E+08	-3,07E+08	-2,93E+08
-3,28E+08	-3,13E+08	-2,98E+08
-3,27E+08	-3,12E+08	-2,98E+08
-3,19E+08	-3,04E+08	-2,90E+08
-3,07E+08	-2,92E+08	-2,79E+08
-2,97E+08	-2,83E+08	-2,70E+08
-2,83E+08	-2,70E+08	-2,57E+08
-2,61E+08	-2,49E+08	-2,37E+08
-2,39E+08	-2,28E+08	-2,18E+08
-2,15E+08	-2,05E+08	-1,95E+08
-1,87E+08	-1,78E+08	-1,70E+08
-1,55E+08	-1,48E+08	-1,41E+08
-1,09E+08	-1,04E+08	-9,94E+07

MIN	MAX
-2,5102E+08	-2,6915E+07
-3,6726E+08	-5,5196E+07
-4,6830E+08	-9,5876E+07
-5,8236E+08	-1,1934E+08
-6,8640E+08	-1,4083E+08
-7,9290E+08	-1,6276E+08
-9,0078E+08	-1,7187E+08
-9,9930E+08	-1,7559E+08
-1,1038E+09	-1,7771E+08
-1,1885E+09	-1,7747E+08
-1,3116E+09	-1,7603E+08
-1,4576E+09	-1,7215E+08
-1,6004E+09	-1,6587E+08
-1,7671E+09	-1,6347E+08
-1,8832E+09	-1,5689E+08
-2,0438E+09	-1,5213E+08
-2,1703E+09	-1,4613E+08
-2,2580E+09	-1,3760E+08
-2,2845E+09	-1,2959E+08
-2,3563E+09	-1,2240E+08
-2,3663E+09	-1,1500E+08
-2,3124E+09	-1,0499E+08
-2,2313E+09	-9,6162E+07
-2,1078E+09	-8,6023E+07
-1,9230E+09	-7,5186E+07
-1,6725E+09	-6,2716E+07
-1,2459E+09	-4,4489E+07

Result - Principal stress (Abs)

The influence lines for Submodel 1A, for each node at the U-sape. Maximum principal stress 2366.3 MPa (compression) at node 21 in load step 1.2 m.

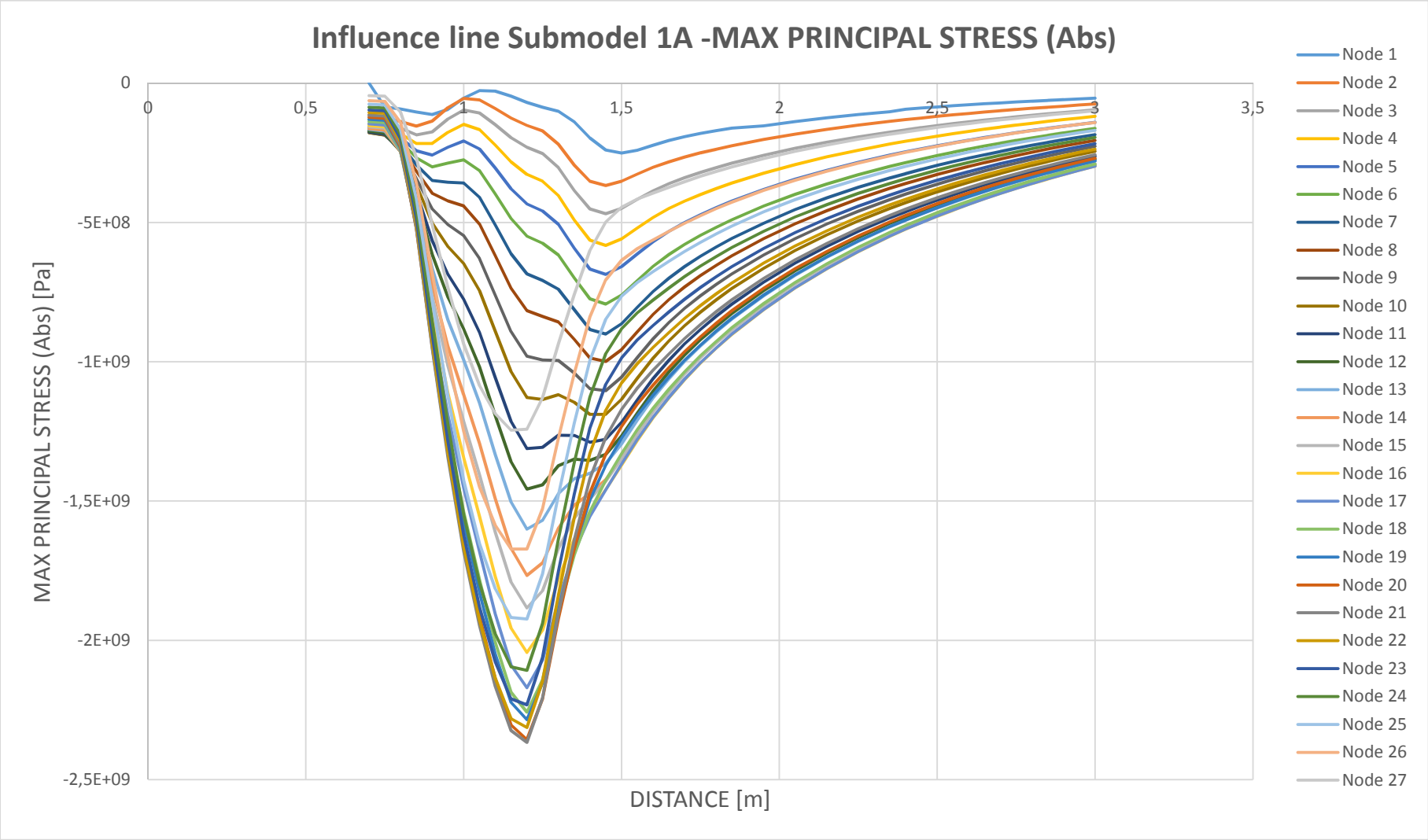

SUBMODEL 1A

MISES STRESS

		Step 1	Step2	Step3	Step 4	Step 5	Step 6	Step 7	Step 8	Step 9	Step 10	Step 11
Node	Distance	0,7	0,75	0,8	0,85	0,9	0,95	1	1,05	1,1	1,15	1,2
1	0	7,86E+07	8,49E+07	9,49E+07	1,05E+08	8,95E+07	5,41E+07	3,13E+07	3,39E+07	5,17E+07	7,28E+07	8,90E+07
2	0,00604	1,02E+08	1,10E+08	1,24E+08	1,39E+08	1,24E+08	8,22E+07	5,35E+07	5,89E+07	8,65E+07	1,18E+08	1,43E+08
3	0,01208	1,18E+08	1,27E+08	1,44E+08	1,67E+08	1,58E+08	1,18E+08	8,87E+07	9,92E+07	1,37E+08	1,79E+08	2,11E+08
4	0,01812	1,29E+08	1,39E+08	1,59E+08	1,91E+08	1,92E+08	1,57E+08	1,31E+08	1,48E+08	1,97E+08	2,51E+08	2,91E+08
5	0,02416	1,39E+08	1,49E+08	1,73E+08	2,14E+08	2,28E+08	2,03E+08	1,84E+08	2,09E+08	2,69E+08	3,35E+08	3,83E+08
6	0,0302	1,46E+08	1,55E+08	1,84E+08	2,36E+08	2,67E+08	2,55E+08	2,45E+08	2,80E+08	3,53E+08	4,32E+08	4,88E+08
7	0,03624	1,50E+08	1,59E+08	1,92E+08	2,56E+08	3,03E+08	3,08E+08	3,09E+08	3,53E+08	4,39E+08	5,29E+08	5,92E+08
8	0,04228	1,54E+08	1,63E+08	2,00E+08	2,78E+08	3,48E+08	3,73E+08	3,89E+08	4,47E+08	5,46E+08	6,49E+08	7,19E+08
9	0,04832	1,54E+08	1,63E+08	2,04E+08	2,96E+08	3,88E+08	4,35E+08	4,67E+08	5,37E+08	6,49E+08	7,63E+08	8,39E+08
10	0,05436	1,55E+08	1,62E+08	2,09E+08	3,18E+08	4,37E+08	5,10E+08	5,63E+08	6,49E+08	7,74E+08	9,00E+08	9,81E+08
11	0,0604	1,53E+08	1,59E+08	2,10E+08	3,35E+08	4,80E+08	5,79E+08	6,52E+08	7,52E+08	8,90E+08	1,02E+09	1,11E+09
12	0,06644	1,48E+08	1,54E+08	2,10E+08	3,51E+08	5,25E+08	6,53E+08	7,52E+08	8,68E+08	1,02E+09	1,16E+09	1,24E+09
13	0,07248	1,41E+08	1,46E+08	2,05E+08	3,58E+08	5,53E+08	7,04E+08	8,21E+08	9,49E+08	1,10E+09	1,25E+09	1,33E+09
14	0,07852	1,38E+08	1,43E+08	2,08E+08	3,80E+08	6,07E+08	7,89E+08	9,34E+08	1,08E+09	1,24E+09	1,39E+09	1,48E+09
15	0,08456	1,30E+08	1,34E+08	2,03E+08	3,87E+08	6,37E+08	8,43E+08	1,01E+09	1,17E+09	1,34E+09	1,49E+09	1,56E+09
16	0,0906	1,29E+08	1,33E+08	2,08E+08	4,12E+08	6,93E+08	9,32E+08	1,13E+09	1,30E+09	1,48E+09	1,64E+09	1,71E+09
17	0,09664	1,23E+08	1,27E+08	2,07E+08	4,28E+08	7,37E+08	1,00E+09	1,23E+09	1,42E+09	1,61E+09	1,76E+09	1,83E+09
18	0,10268	1,17E+08	1,21E+08	2,04E+08	4,37E+08	7,68E+08	1,06E+09	1,30E+09	1,51E+09	1,70E+09	1,85E+09	1,91E+09
19	0,10872	1,10E+08	1,13E+08	1,98E+08	4,37E+08	7,79E+08	1,08E+09	1,34E+09	1,55E+09	1,74E+09	1,89E+09	1,94E+09
20	0,11476	1,06E+08	1,09E+08	1,98E+08	4,49E+08	8,12E+08	1,14E+09	1,42E+09	1,64E+09	1,83E+09	1,98E+09	2,02E+09
21	0,1208	9,86E+07	1,02E+08	1,92E+08	4,48E+08	8,19E+08	1,15E+09	1,45E+09	1,68E+09	1,86E+09	2,00E+09	2,04E+09
22	0,12684	9,19E+07	9,48E+07	1,84E+08	4,39E+08	8,11E+08	1,15E+09	1,45E+09	1,68E+09	1,86E+09	1,98E+09	2,01E+09
23	0,13288	8,42E+07	8,70E+07	1,74E+08	4,23E+08	7,87E+08	1,12E+09	1,41E+09	1,64E+09	1,81E+09	1,93E+09	1,95E+09
24	0,13892	7,62E+07	7,90E+07	1,62E+08	4,00E+08	7,50E+08	1,07E+09	1,36E+09	1,57E+09	1,73E+09	1,84E+09	1,85E+09
25	0,14496	6,70E+07	6,96E+07	1,47E+08	3,69E+08	6,95E+08	9,95E+08	1,26E+09	1,47E+09	1,61E+09	1,70E+09	1,71E+09
26	0,151	5,66E+07	5,89E+07	1,27E+08	3,22E+08	6,09E+08	8,76E+08	1,12E+09	1,29E+09	1,42E+09	1,49E+09	1,50E+09
27	0,15704	4,23E+07	4,42E+07	9,75E+07	2,50E+08	4,75E+08	6,83E+08	8,72E+08	1,01E+09	1,11E+09	1,16E+09	1,16E+09

Step 12	Step 13	Step 14	Step 15	Step 16	Step 17	Step 18	Step 19	Step 20	Step 21	Step 22	Step 23	Step 24	Step 25
1,25	1,3	1,35	1,4	1,45	1,5	1,55	1,6	1,65	1,7	1,75	1,8	1,85	1,95
1,02E+08	1,35E+08	1,88E+08	2,27E+08	2,37E+08	2,28E+08	2,11E+08	1,95E+08	1,82E+08	1,71E+08	1,62E+08	1,53E+08	1,45E+08	1,31E+08
1,60E+08	2,02E+08	2,69E+08	3,21E+08	3,35E+08	3,21E+08	2,98E+08	2,76E+08	2,57E+08	2,42E+08	2,29E+08	2,16E+08	2,05E+08	1,85E+08
2,31E+08	2,76E+08	3,50E+08	4,08E+08	4,24E+08	4,07E+08	3,78E+08	3,50E+08	3,27E+08	3,07E+08	2,90E+08	2,75E+08	2,60E+08	2,35E+08
3,12E+08	3,58E+08	4,35E+08	4,98E+08	5,15E+08	4,94E+08	4,60E+08	4,26E+08	3,98E+08	3,74E+08	3,53E+08	3,35E+08	3,17E+08	2,86E+08
4,06E+08	4,48E+08	5,24E+08	5,90E+08	6,07E+08	5,83E+08	5,43E+08	5,03E+08	4,70E+08	4,42E+08	4,18E+08	3,95E+08	3,75E+08	3,38E+08
5,10E+08	5,47E+08	6,19E+08	6,85E+08	7,01E+08	6,72E+08	6,27E+08	5,82E+08	5,44E+08	5,12E+08	4,83E+08	4,58E+08	4,34E+08	3,91E+08
6,12E+08	6,41E+08	7,06E+08	7,69E+08	7,84E+08	7,51E+08	7,01E+08	6,51E+08	6,09E+08	5,73E+08	5,41E+08	5,12E+08	4,85E+08	4,37E+08
7,37E+08	7,53E+08	8,08E+08	8,66E+08	8,77E+08	8,39E+08	7,84E+08	7,29E+08	6,82E+08	6,42E+08	6,06E+08	5,74E+08	5,44E+08	4,90E+08
8,52E+08	8,55E+08	8,96E+08	9,46E+08	9,52E+08	9,11E+08	8,50E+08	7,92E+08	7,41E+08	6,98E+08	6,59E+08	6,23E+08	5,91E+08	5,33E+08
9,86E+08	9,71E+08	9,95E+08	1,03E+09	1,03E+09	9,85E+08	9,21E+08	8,58E+08	8,04E+08	7,57E+08	7,14E+08	6,76E+08	6,41E+08	5,77E+08
1,11E+09	1,07E+09	1,08E+09	1,10E+09	1,09E+09	1,04E+09	9,74E+08	9,08E+08	8,51E+08	8,01E+08	7,57E+08	7,16E+08	6,79E+08	6,12E+08
1,23E+09	1,17E+09	1,15E+09	1,15E+09	1,13E+09	1,08E+09	1,01E+09	9,41E+08	8,82E+08	8,31E+08	7,85E+08	7,43E+08	7,04E+08	6,35E+08
1,30E+09	1,23E+09	1,19E+09	1,17E+09	1,15E+09	1,09E+09	1,02E+09	9,49E+08	8,90E+08	8,38E+08	7,92E+08	7,49E+08	7,10E+08	6,40E+08
1,44E+09	1,33E+09	1,27E+09	1,23E+09	1,19E+09	1,13E+09	1,05E+09	9,84E+08	9,23E+08	8,70E+08	8,22E+08	7,78E+08	7,37E+08	6,64E+08
1,51E+09	1,39E+09	1,29E+09	1,24E+09	1,18E+09	1,12E+09	1,05E+09	9,78E+08	9,18E+08	8,65E+08	8,18E+08	7,74E+08	7,33E+08	6,61E+08
1,65E+09	1,49E+09	1,37E+09	1,29E+09	1,23E+09	1,15E+09	1,08E+09	1,01E+09	9,48E+08	8,94E+08	8,44E+08	7,99E+08	7,57E+08	6,83E+08
1,75E+09	1,57E+09	1,42E+09	1,31E+09	1,23E+09	1,15E+09	1,08E+09	1,01E+09	9,50E+08	8,96E+08	8,46E+08	8,01E+08	7,59E+08	6,84E+08
1,81E+09	1,61E+09	1,44E+09	1,30E+09	1,21E+09	1,13E+09	1,06E+09	9,90E+08	9,32E+08	8,79E+08	8,30E+08	7,86E+08	7,45E+08	6,71E+08
1,83E+09	1,61E+09	1,42E+09	1,27E+09	1,16E+09	1,08E+09	1,01E+09	9,49E+08	8,94E+08	8,43E+08	7,97E+08	7,54E+08	7,15E+08	6,44E+08
1,90E+09	1,65E+09	1,44E+09	1,27E+09	1,15E+09	1,06E+09	9,95E+08	9,36E+08	8,81E+08	8,32E+08	7,86E+08	7,44E+08	7,05E+08	6,36E+08
1,90E+09	1,64E+09	1,41E+09	1,22E+09	1,09E+09	1,00E+09	9,40E+08	8,84E+08	8,34E+08	7,87E+08	7,44E+08	7,04E+08	6,68E+08	6,02E+08
1,87E+09	1,60E+09	1,36E+09	1,16E+09	1,03E+09	9,41E+08	8,80E+08	8,29E+08	7,82E+08	7,39E+08	6,98E+08	6,61E+08	6,27E+08	5,65E+08
1,80E+09	1,53E+09	1,29E+09	1,08E+09	9,46E+08	8,63E+08	8,07E+08	7,62E+08	7,19E+08	6,79E+08	6,42E+08	6,08E+08	5,76E+08	5,19E+08
1,70E+09	1,44E+09	1,20E+09	9,95E+08	8,60E+08	7,81E+08	7,31E+08	6,90E+08	6,52E+08	6,16E+08	5,82E+08	5,51E+08	5,22E+08	4,71E+08
1,57E+09	1,31E+09	1,09E+09	8,87E+08	7,56E+08	6,83E+08	6,39E+08	6,04E+08	5,71E+08	5,40E+08	5,10E+08	4,83E+08	4,58E+08	4,13E+08
1,37E+09	1,14E+09	9,36E+08	7,56E+08	6,38E+08	5,75E+08	5,37E+08	5,08E+08	4,81E+08	4,55E+08	4,30E+08	4,07E+08	3,86E+08	3,48E+08
1,06E+09	8,78E+08	7,14E+08	5,69E+08	4,75E+08	4,25E+08	3,98E+08	3,77E+08	3,56E+08	3,37E+08	3,19E+08	3,02E+08	2,86E+08	2,58E+08

Step 26	Step 27	Step 28	Step 29	Step 30	Step 31	Step 32	Step 33	Step 34	Step 35	Step 36	Step 37	Step 38	Step 39
2,05	2,15	2,25	2,35	2,4	2,45	2,5	2,55	2,6	2,65	2,7	2,75	2,8	2,85
1,18E+08	1,07E+08	9,75E+07	8,88E+07	8,47E+07	8,09E+07	7,73E+07	7,38E+07	7,05E+07	6,73E+07	6,43E+07	6,14E+07	5,87E+07	5,61E+07
1,67E+08	1,52E+08	1,38E+08	1,25E+08	1,20E+08	1,14E+08	1,09E+08	1,04E+08	9,95E+07	9,50E+07	9,07E+07	8,66E+07	8,27E+07	7,90E+07
2,12E+08	1,92E+08	1,75E+08	1,59E+08	1,52E+08	1,45E+08	1,38E+08	1,32E+08	1,26E+08	1,20E+08	1,15E+08	1,10E+08	1,05E+08	1,00E+08
2,58E+08	2,34E+08	2,13E+08	1,94E+08	1,85E+08	1,76E+08	1,68E+08	1,61E+08	1,53E+08	1,46E+08	1,40E+08	1,34E+08	1,27E+08	1,22E+08
3,05E+08	2,77E+08	2,52E+08	2,29E+08	2,18E+08	2,08E+08	1,99E+08	1,90E+08	1,81E+08	1,73E+08	1,65E+08	1,58E+08	1,50E+08	1,44E+08
3,53E+08	3,20E+08	2,91E+08	2,65E+08	2,53E+08	2,41E+08	2,30E+08	2,20E+08	2,10E+08	2,00E+08	1,91E+08	1,82E+08	1,74E+08	1,66E+08
3,96E+08	3,59E+08	3,26E+08	2,96E+08	2,83E+08	2,70E+08	2,57E+08	2,46E+08	2,34E+08	2,24E+08	2,14E+08	2,04E+08	1,95E+08	1,86E+08
4,43E+08	4,02E+08	3,65E+08	3,32E+08	3,16E+08	3,02E+08	2,88E+08	2,75E+08	2,62E+08	2,50E+08	2,39E+08	2,28E+08	2,18E+08	2,08E+08
4,82E+08	4,37E+08	3,97E+08	3,61E+08	3,44E+08	3,28E+08	3,13E+08	2,99E+08	2,85E+08	2,72E+08	2,60E+08	2,48E+08	2,37E+08	2,26E+08
5,22E+08	4,73E+08	4,30E+08	3,91E+08	3,73E+08	3,56E+08	3,39E+08	3,24E+08	3,09E+08	2,95E+08	2,82E+08	2,69E+08	2,56E+08	2,45E+08
5,53E+08	5,01E+08	4,55E+08	4,14E+08	3,95E+08	3,77E+08	3,60E+08	3,43E+08	3,27E+08	3,12E+08	2,98E+08	2,85E+08	2,71E+08	2,59E+08
5,74E+08	5,20E+08	4,72E+08	4,30E+08	4,10E+08	3,91E+08	3,73E+08	3,56E+08	3,40E+08	3,24E+08	3,09E+08	2,95E+08	2,82E+08	2,69E+08
5,79E+08	5,25E+08	4,77E+08	4,33E+08	4,13E+08	3,94E+08	3,76E+08	3,59E+08	3,43E+08	3,27E+08	3,12E+08	2,98E+08	2,84E+08	2,71E+08
6,01E+08	5,45E+08	4,95E+08	4,50E+08	4,29E+08	4,09E+08	3,90E+08	3,73E+08	3,56E+08	3,39E+08	3,24E+08	3,09E+08	2,95E+08	2,81E+08
5,98E+08	5,42E+08	4,92E+08	4,47E+08	4,27E+08	4,07E+08	3,88E+08	3,71E+08	3,54E+08	3,38E+08	3,22E+08	3,07E+08	2,93E+08	2,80E+08
6,17E+08	5,60E+08	5,08E+08	4,62E+08	4,41E+08	4,20E+08	4,01E+08	3,83E+08	3,65E+08	3,48E+08	3,32E+08	3,17E+08	3,03E+08	2,89E+08
6,19E+08	5,61E+08	5,10E+08	4,63E+08	4,42E+08	4,22E+08	4,02E+08	3,84E+08	3,66E+08	3,49E+08	3,33E+08	3,18E+08	3,04E+08	2,90E+08
6,07E+08	5,51E+08	5,00E+08	4,55E+08	4,34E+08	4,14E+08	3,95E+08	3,77E+08	3,59E+08	3,43E+08	3,27E+08	3,12E+08	2,98E+08	2,84E+08
5,83E+08	5,28E+08	4,80E+08	4,36E+08	4,16E+08	3,97E+08	3,79E+08	3,61E+08	3,45E+08	3,29E+08	3,14E+08	3,00E+08	2,86E+08	2,73E+08
5,75E+08	5,21E+08	4,73E+08	4,30E+08	4,11E+08	3,92E+08	3,74E+08	3,57E+08	3,40E+08	3,25E+08	3,10E+08	2,96E+08	2,82E+08	2,69E+08
5,44E+08	4,94E+08	4,48E+08	4,07E+08	3,89E+08	3,71E+08	3,54E+08	3,38E+08	3,22E+08	3,07E+08	2,93E+08	2,80E+08	2,67E+08	2,55E+08
5,11E+08	4,63E+08	4,21E+08	3,82E+08	3,65E+08	3,48E+08	3,32E+08	3,17E+08	3,02E+08	2,88E+08	2,75E+08	2,63E+08	2,51E+08	2,39E+08
4,70E+08	4,26E+08	3,87E+08	3,52E+08	3,36E+08	3,20E+08	3,05E+08	2,91E+08	2,78E+08	2,65E+08	2,53E+08	2,42E+08	2,31E+08	2,20E+08
4,26E+08	3,86E+08	3,51E+08	3,19E+08	3,04E+08	2,90E+08	2,77E+08	2,64E+08	2,52E+08	2,41E+08	2,30E+08	2,19E+08	2,09E+08	1,99E+08
3,74E+08	3,39E+08	3,08E+08	2,80E+08	2,67E+08	2,55E+08	2,43E+08	2,32E+08	2,21E+08	2,11E+08	2,01E+08	1,92E+08	1,83E+08	1,75E+08
3,15E+08	2,85E+08	2,59E+08	2,36E+08	2,25E+08	2,15E+08	2,05E+08	1,95E+08	1,86E+08	1,78E+08	1,70E+08	1,62E+08	1,55E+08	1,47E+08
2,33E+08	2,12E+08	1,92E+08	1,75E+08	1,67E+08	1,59E+08	1,52E+08	1,45E+08	1,38E+08	1,32E+08	1,26E+08	1,20E+08	1,15E+08	1,09E+08

Step 40	Step 41	Step 42	MIN	MAX
2,9	2,95	3		
5,35E+07	5,11E+07	4,88E+07	3,1290E+07	2,3737E+08
7,54E+07	7,20E+07	6,88E+07	5,3517E+07	3,3473E+08
9,56E+07	9,12E+07	8,71E+07	8,7058E+07	4,2377E+08
1,16E+08	1,11E+08	1,06E+08	1,0579E+08	5,1474E+08
1,37E+08	1,31E+08	1,25E+08	1,2485E+08	6,0707E+08
1,58E+08	1,51E+08	1,44E+08	1,4422E+08	7,0116E+08
1,77E+08	1,69E+08	1,61E+08	1,5025E+08	7,8358E+08
1,98E+08	1,89E+08	1,80E+08	1,5391E+08	8,7687E+08
2,15E+08	2,05E+08	1,96E+08	1,5449E+08	9,5237E+08
2,33E+08	2,23E+08	2,12E+08	1,5473E+08	1,0327E+09
2,47E+08	2,36E+08	2,25E+08	1,5266E+08	1,1081E+09
2,56E+08	2,44E+08	2,33E+08	1,4782E+08	1,2404E+09
2,59E+08	2,47E+08	2,35E+08	1,4110E+08	1,3275E+09
2,68E+08	2,56E+08	2,44E+08	1,3825E+08	1,4752E+09
2,67E+08	2,55E+08	2,43E+08	1,3035E+08	1,5637E+09
2,75E+08	2,63E+08	2,51E+08	1,2895E+08	1,7132E+09
2,76E+08	2,63E+08	2,51E+08	1,2343E+08	1,8310E+09
2,71E+08	2,58E+08	2,46E+08	1,1741E+08	1,9129E+09
2,60E+08	2,48E+08	2,37E+08	1,0993E+08	1,9391E+09
2,57E+08	2,45E+08	2,33E+08	1,0635E+08	2,0212E+09
2,43E+08	2,32E+08	2,21E+08	9,8605E+07	2,0351E+09
2,28E+08	2,17E+08	2,07E+08	9,1860E+07	2,0112E+09
2,10E+08	2,00E+08	1,91E+08	8,4185E+07	1,9467E+09
1,90E+08	1,81E+08	1,73E+08	7,6178E+07	1,8512E+09
1,67E+08	1,59E+08	1,52E+08	6,7001E+07	1,7078E+09
1,41E+08	1,34E+08	1,28E+08	5,6557E+07	1,4957E+09
1,04E+08	9,96E+07	9,49E+07	4,2321E+07	1,1626E+09

Result - Mises stress

The influence lines for Submodel 1A, for each node at the U-sape. Maximum Mises stress 2035.1 MPa at node 21 in load step 1.2 m.

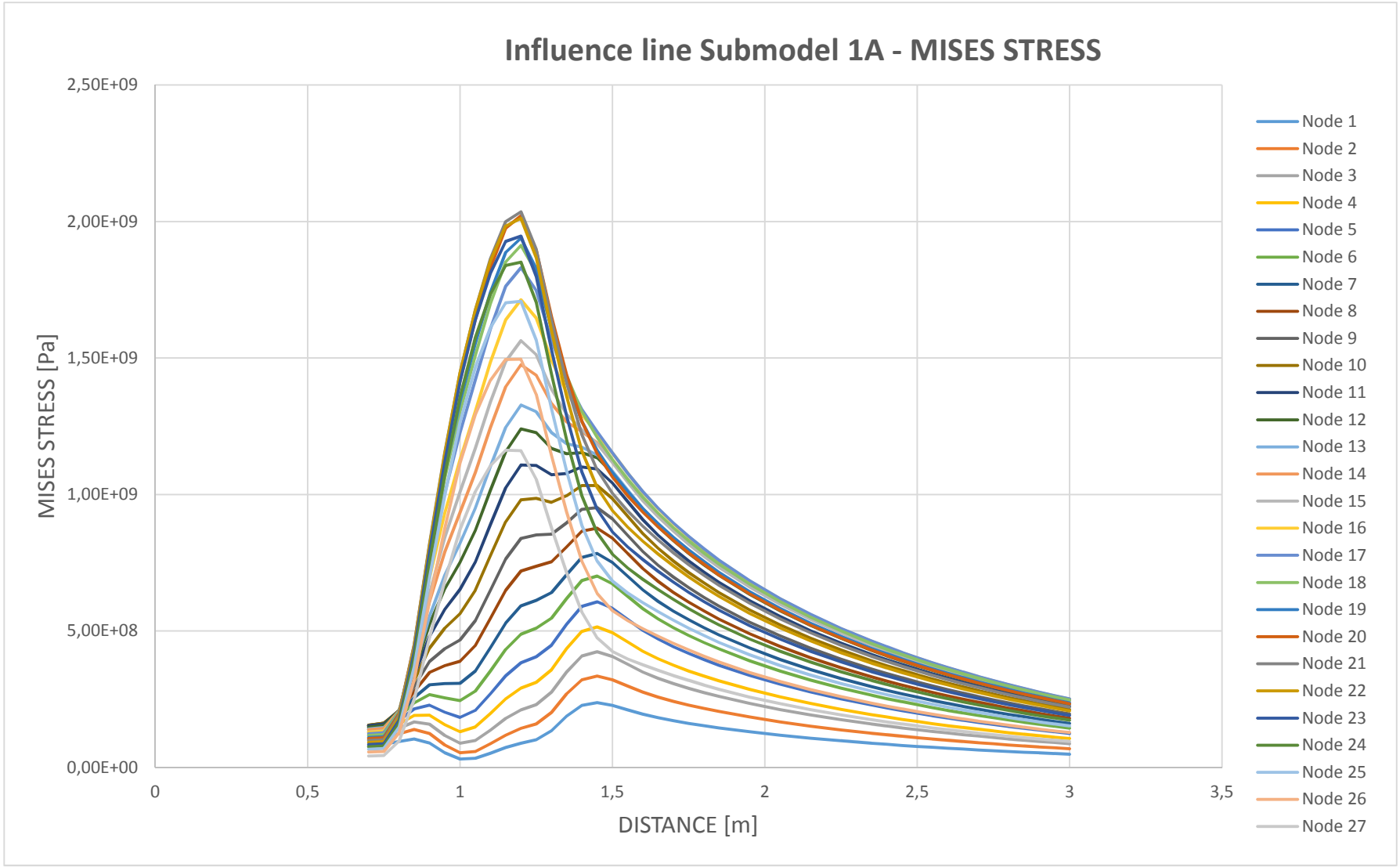

SUBMODEL 1 B

MAX PRINCIPAL STRESS (Abs)

		Step 1	Step 2	Step 3	Step 4	Step 5	Step 6	Step 7	Step 8	Step 9	Step 10	Step 11
Node	Distance	0,7	0,75	0,8	0,85	0,9	0,95	1	1,05	1,1	1,15	1,2
1	0	-3,37E+07	-3,85E+07	-3,28E+07	-6,49E+06	6,13E+07	1,37E+08	1,88E+08	2,15E+08	2,40E+08	2,64E+08	2,77E+08
2	0,00604	-3,53E+07	-4,12E+07	-3,10E+07	1,63E+07	1,07E+08	2,12E+08	2,83E+08	3,23E+08	3,64E+08	4,03E+08	4,25E+08
3	0,01208	-3,09E+07	-3,72E+07	-2,33E+07	3,54E+07	1,44E+08	2,65E+08	3,46E+08	3,96E+08	4,49E+08	5,01E+08	5,31E+08
4	0,01812	-2,12E+07	-2,74E+07	-9,73E+06	6,20E+07	1,87E+08	3,23E+08	4,13E+08	4,73E+08	5,41E+08	6,06E+08	6,46E+08
5	0,02416	-8,60E+06	-1,40E+07	9,64E+06	9,00E+07	2,27E+08	3,70E+08	4,65E+08	5,33E+08	6,14E+08	6,94E+08	7,44E+08
6	0,0302	8,82E+06	4,02E+06	2,94E+07	1,20E+08	2,68E+08	4,18E+08	5,16E+08	5,91E+08	6,86E+08	7,80E+08	8,40E+08
7	0,03624	2,65E+07	2,20E+07	5,22E+07	1,51E+08	3,06E+08	4,56E+08	5,53E+08	6,35E+08	7,42E+08	8,52E+08	9,23E+08
8	0,04228	4,48E+07	4,11E+07	7,45E+07	1,79E+08	3,37E+08	4,85E+08	5,78E+08	6,64E+08	7,83E+08	9,06E+08	9,89E+08
9	0,04832	6,62E+07	6,35E+07	9,96E+07	2,07E+08	3,64E+08	5,05E+08	5,89E+08	6,76E+08	8,07E+08	9,45E+08	1,04E+09
10	0,05436	8,40E+07	8,23E+07	1,20E+08	2,27E+08	3,79E+08	5,08E+08	5,80E+08	6,66E+08	8,05E+08	9,55E+08	1,06E+09
11	0,0604	1,01E+08	1,00E+08	1,37E+08	2,39E+08	3,77E+08	4,86E+08	5,40E+08	6,20E+08	7,64E+08	9,23E+08	1,04E+09
12	0,06644	1,18E+08	1,18E+08	1,55E+08	2,54E+08	3,82E+08	4,76E+08	5,13E+08	5,90E+08	7,41E+08	9,11E+08	1,04E+09
13	0,07248	1,34E+08	1,35E+08	1,69E+08	2,59E+08	3,66E+08	4,35E+08	4,48E+08	5,14E+08	6,68E+08	8,47E+08	9,89E+08
14	0,07852	1,45E+08	1,46E+08	1,78E+08	2,55E+08	3,39E+08	3,80E+08	3,69E+08	4,23E+08	5,76E+08	7,59E+08	9,11E+08
15	0,08456	1,50E+08	1,52E+08	1,78E+08	2,39E+08	2,98E+08	3,12E+08	2,75E+08	3,15E+08	4,62E+08	6,44E+08	8,02E+08
16	0,0906	1,60E+08	1,62E+08	1,84E+08	2,31E+08	2,64E+08	2,48E+08	1,84E+08	2,10E+08	3,54E+08	5,42E+08	7,11E+08
17	0,09664	1,65E+08	1,67E+08	1,83E+08	2,12E+08	2,16E+08	1,70E+08	8,01E+07	8,98E+07	2,25E+08	4,13E+08	5,89E+08
18	0,10268	1,64E+08	1,66E+08	1,75E+08	1,83E+08	1,54E+08	7,54E+07	-6,94E+07	-8,12E+07	7,46E+07	2,52E+08	4,31E+08
19	0,10872	1,59E+08	1,61E+08	1,64E+08	1,53E+08	9,74E+07	-2,60E+07	-1,67E+08	-1,96E+08	-8,32E+07	1,16E+08	2,93E+08
20	0,11476	1,55E+08	1,57E+08	1,52E+08	1,21E+08	3,62E+07	-1,08E+08	-2,86E+08	-3,33E+08	-2,25E+08	-5,99E+07	1,40E+08
21	0,1208	1,46E+08	1,47E+08	1,38E+08	9,15E+07	-2,03E+07	-1,74E+08	-3,68E+08	-4,28E+08	-3,32E+08	-1,69E+08	3,78E+07
22	0,12684	1,36E+08	1,37E+08	1,21E+08	5,84E+07	-7,32E+07	-2,51E+08	-4,64E+08	-5,38E+08	-4,55E+08	-3,01E+08	-1,26E+08
23	0,13288	1,25E+08	1,26E+08	1,05E+08	2,96E+07	-1,18E+08	-3,08E+08	-5,30E+08	-6,16E+08	-5,45E+08	-4,03E+08	-2,32E+08
24	0,13892	1,10E+08	1,10E+08	8,65E+07	4,11E+06	-1,51E+08	-3,45E+08	-5,67E+08	-6,58E+08	-6,01E+08	-4,74E+08	-3,17E+08
25	0,14496	9,41E+07	9,40E+07	6,85E+07	-1,74E+07	-1,72E+08	-3,60E+08	-5,74E+08	-6,66E+08	-6,22E+08	-5,12E+08	-3,70E+08
26	0,151	7,76E+07	7,73E+07	5,24E+07	-2,94E+07	-1,74E+08	-3,48E+08	-5,43E+08	-6,29E+08	-5,96E+08	-5,04E+08	-3,82E+08
27	0,15704	5,47E+07	5,43E+07	3,31E+07	-3,55E+07	-1,54E+08	-2,92E+08	-4,45E+08	-5,16E+08	-4,96E+08	-4,31E+08	-3,39E+08

Step 12	Step 13	Step 14	Step 15	Step 16	Step 17	Step 18	Step 19	Step 20	Step 21	Step 22	Step 23	Step 24	Step 25
1,25	1,3	1,35	1,4	1,45	1,5	1,55	1,6	1,65	1,7	1,75	1,8	1,85	1,95
2,65E+08	2,20E+08	1,63E+08	1,31E+08	1,23E+08	1,18E+08	1,13E+08	1,07E+08	1,01E+08	9,52E+07	8,99E+07	8,51E+07	8,06E+07	7,27E+07
4,11E+08	3,51E+08	2,75E+08	2,35E+08	2,25E+08	2,15E+08	2,05E+08	1,93E+08	1,82E+08	1,72E+08	1,62E+08	1,53E+08	1,45E+08	1,31E+08
5,16E+08	4,49E+08	3,68E+08	3,26E+08	3,15E+08	3,02E+08	2,86E+08	2,69E+08	2,53E+08	2,39E+08	2,25E+08	2,13E+08	2,02E+08	1,82E+08
6,32E+08	5,59E+08	4,74E+08	4,33E+08	4,23E+08	4,05E+08	3,83E+08	3,59E+08	3,38E+08	3,18E+08	3,01E+08	2,84E+08	2,70E+08	2,43E+08
7,32E+08	6,59E+08	5,77E+08	5,42E+08	5,33E+08	5,11E+08	4,81E+08	4,51E+08	4,24E+08	3,99E+08	3,77E+08	3,57E+08	3,38E+08	3,05E+08
8,31E+08	7,59E+08	6,82E+08	6,53E+08	6,47E+08	6,20E+08	5,83E+08	5,46E+08	5,13E+08	4,83E+08	4,56E+08	4,32E+08	4,09E+08	3,69E+08
9,20E+08	8,54E+08	7,87E+08	7,71E+08	7,68E+08	7,37E+08	6,93E+08	6,48E+08	6,08E+08	5,73E+08	5,41E+08	5,12E+08	4,85E+08	4,37E+08
9,92E+08	9,34E+08	8,80E+08	8,77E+08	8,79E+08	8,45E+08	7,93E+08	7,41E+08	6,95E+08	6,54E+08	6,18E+08	5,85E+08	5,54E+08	4,99E+08
1,06E+09	1,01E+09	9,77E+08	9,94E+08	1,00E+09	9,66E+08	9,06E+08	8,46E+08	7,93E+08	7,46E+08	7,05E+08	6,67E+08	6,32E+08	5,70E+08
1,09E+09	1,06E+09	1,04E+09	1,08E+09	1,10E+09	1,06E+09	9,92E+08	9,25E+08	8,67E+08	8,16E+08	7,70E+08	7,29E+08	6,91E+08	6,23E+08
1,08E+09	1,07E+09	1,08E+09	1,15E+09	1,18E+09	1,14E+09	1,06E+09	9,92E+08	9,29E+08	8,74E+08	8,25E+08	7,81E+08	7,40E+08	6,67E+08
1,09E+09	1,11E+09	1,14E+09	1,23E+09	1,27E+09	1,23E+09	1,15E+09	1,07E+09	1,00E+09	9,43E+08	8,90E+08	8,42E+08	7,98E+08	7,19E+08
1,06E+09	1,10E+09	1,17E+09	1,28E+09	1,34E+09	1,30E+09	1,22E+09	1,13E+09	1,06E+09	9,96E+08	9,40E+08	8,90E+08	8,43E+08	7,60E+08
1,00E+09	1,07E+09	1,17E+09	1,31E+09	1,38E+09	1,34E+09	1,26E+09	1,17E+09	1,09E+09	1,03E+09	9,70E+08	9,18E+08	8,70E+08	7,84E+08
9,06E+08	9,99E+08	1,13E+09	1,30E+09	1,38E+09	1,34E+09	1,26E+09	1,17E+09	1,09E+09	1,03E+09	9,70E+08	9,18E+08	8,70E+08	7,84E+08
8,36E+08	9,59E+08	1,12E+09	1,32E+09	1,42E+09	1,39E+09	1,30E+09	1,21E+09	1,13E+09	1,06E+09	1,00E+09	9,48E+08	8,99E+08	8,10E+08
7,34E+08	8,87E+08	1,08E+09	1,31E+09	1,43E+09	1,40E+09	1,31E+09	1,22E+09	1,14E+09	1,07E+09	1,01E+09	9,54E+08	9,04E+08	8,15E+08
5,94E+08	7,76E+08	1,00E+09	1,26E+09	1,39E+09	1,37E+09	1,29E+09	1,19E+09	1,11E+09	1,04E+09	9,85E+08	9,32E+08	8,84E+08	7,96E+08
4,68E+08	6,72E+08	9,16E+08	1,19E+09	1,34E+09	1,32E+09	1,24E+09	1,15E+09	1,07E+09	1,01E+09	9,49E+08	8,97E+08	8,51E+08	7,66E+08
3,29E+08	5,59E+08	8,30E+08	1,13E+09	1,29E+09	1,28E+09	1,20E+09	1,11E+09	1,03E+09	9,72E+08	9,17E+08	8,67E+08	8,22E+08	7,41E+08
2,15E+08	4,57E+08	7,37E+08	1,05E+09	1,21E+09	1,21E+09	1,13E+09	1,05E+09	9,74E+08	9,15E+08	8,63E+08	8,16E+08	7,74E+08	6,97E+08
8,23E+07	3,39E+08	6,34E+08	9,53E+08	1,12E+09	1,13E+09	1,06E+09	9,75E+08	9,08E+08	8,52E+08	8,03E+08	7,60E+08	7,20E+08	6,49E+08
-2,59E+07	2,41E+08	5,39E+08	8,61E+08	1,04E+09	1,04E+09	9,78E+08	9,01E+08	8,39E+08	7,87E+08	7,42E+08	7,02E+08	6,65E+08	5,99E+08
-1,16E+08	1,44E+08	4,34E+08	7,43E+08	9,13E+08	9,25E+08	8,67E+08	7,98E+08	7,42E+08	6,96E+08	6,56E+08	6,21E+08	5,88E+08	5,30E+08
-1,81E+08	6,49E+07	3,35E+08	6,24E+08	7,84E+08	7,99E+08	7,49E+08	6,89E+08	6,40E+08	6,00E+08	5,66E+08	5,35E+08	5,07E+08	4,57E+08
-2,14E+08	-1,06E+07	2,49E+08	5,06E+08	6,49E+08	6,64E+08	6,23E+08	5,72E+08	5,31E+08	4,98E+08	4,70E+08	4,44E+08	4,21E+08	3,79E+08
-2,09E+08	-3,87E+07	1,51E+08	3,49E+08	4,60E+08	4,75E+08	4,45E+08	4,08E+08	3,79E+08	3,55E+08	3,34E+08	3,16E+08	3,00E+08	2,70E+08

Step 26	Step 27	Step 28	Step 29	Step 30	Step 31	Step 32	Step 33	Step 34	Step 35	Step 36	Step 37	Step 38	Step 39
2,05	2,15	2,25	2,35	2,4	2,45	2,5	2,55	2,6	2,65	2,7	2,75	2,8	2,85
6,58E+07	5,96E+07	5,41E+07	4,91E+07	4,68E+07	4,46E+07	4,25E+07	4,05E+07	3,86E+07	3,68E+07	3,51E+07	3,34E+07	3,19E+07	3,03E+07
1,18E+08	1,07E+08	9,74E+07	8,84E+07	8,43E+07	8,04E+07	7,66E+07	7,31E+07	6,97E+07	6,64E+07	6,33E+07	6,03E+07	5,75E+07	5,48E+07
1,65E+08	1,49E+08	1,36E+08	1,23E+08	1,17E+08	1,12E+08	1,07E+08	1,02E+08	9,70E+07	9,25E+07	8,82E+07	8,41E+07	8,02E+07	7,64E+07
2,20E+08	1,99E+08	1,81E+08	1,64E+08	1,57E+08	1,49E+08	1,42E+08	1,36E+08	1,29E+08	1,23E+08	1,18E+08	1,12E+08	1,07E+08	1,02E+08
2,76E+08	2,50E+08	2,27E+08	2,06E+08	1,97E+08	1,87E+08	1,79E+08	1,70E+08	1,63E+08	1,55E+08	1,48E+08	1,41E+08	1,34E+08	1,28E+08
3,33E+08	3,02E+08	2,74E+08	2,49E+08	2,38E+08	2,27E+08	2,16E+08	2,06E+08	1,97E+08	1,88E+08	1,79E+08	1,71E+08	1,63E+08	1,55E+08
3,95E+08	3,58E+08	3,25E+08	2,95E+08	2,82E+08	2,69E+08	2,56E+08	2,44E+08	2,33E+08	2,22E+08	2,12E+08	2,02E+08	1,93E+08	1,84E+08
4,52E+08	4,09E+08	3,72E+08	3,38E+08	3,22E+08	3,07E+08	2,93E+08	2,79E+08	2,67E+08	2,54E+08	2,43E+08	2,31E+08	2,21E+08	2,11E+08
5,15E+08	4,67E+08	4,24E+08	3,85E+08	3,67E+08	3,50E+08	3,34E+08	3,19E+08	3,04E+08	2,90E+08	2,77E+08	2,64E+08	2,52E+08	2,40E+08
5,63E+08	5,10E+08	4,63E+08	4,21E+08	4,02E+08	3,83E+08	3,65E+08	3,49E+08	3,33E+08	3,17E+08	3,03E+08	2,89E+08	2,75E+08	2,63E+08
6,03E+08	5,47E+08	4,96E+08	4,51E+08	4,30E+08	4,10E+08	3,91E+08	3,73E+08	3,56E+08	3,40E+08	3,24E+08	3,09E+08	2,95E+08	2,81E+08
6,50E+08	5,89E+08	5,35E+08	4,86E+08	4,64E+08	4,42E+08	4,22E+08	4,03E+08	3,84E+08	3,66E+08	3,50E+08	3,34E+08	3,18E+08	3,04E+08
6,87E+08	6,23E+08	5,65E+08	5,14E+08	4,90E+08	4,67E+08	4,46E+08	4,25E+08	4,06E+08	3,87E+08	3,70E+08	3,53E+08	3,36E+08	3,21E+08
7,09E+08	6,43E+08	5,83E+08	5,30E+08	5,06E+08	4,82E+08	4,60E+08	4,39E+08	4,19E+08	4,00E+08	3,81E+08	3,64E+08	3,47E+08	3,31E+08
7,09E+08	6,42E+08	5,83E+08	5,30E+08	5,06E+08	4,82E+08	4,60E+08	4,39E+08	4,19E+08	4,00E+08	3,81E+08	3,64E+08	3,47E+08	3,31E+08
7,32E+08	6,64E+08	6,03E+08	5,48E+08	5,22E+08	4,98E+08	4,75E+08	4,53E+08	4,33E+08	4,13E+08	3,94E+08	3,76E+08	3,59E+08	3,42E+08
7,36E+08	6,67E+08	6,06E+08	5,51E+08	5,25E+08	5,01E+08	4,78E+08	4,56E+08	4,35E+08	4,15E+08	3,96E+08	3,78E+08	3,61E+08	3,44E+08
7,20E+08	6,52E+08	5,92E+08	5,38E+08	5,13E+08	4,90E+08	4,67E+08	4,46E+08	4,25E+08	4,06E+08	3,87E+08	3,69E+08	3,52E+08	3,36E+08
6,93E+08	6,28E+08	5,70E+08	5,18E+08	4,94E+08	4,71E+08	4,50E+08	4,29E+08	4,09E+08	3,91E+08	3,73E+08	3,56E+08	3,39E+08	3,24E+08
6,69E+08	6,07E+08	5,51E+08	5,01E+08	4,77E+08	4,55E+08	4,34E+08	4,14E+08	3,95E+08	3,77E+08	3,60E+08	3,43E+08	3,28E+08	3,13E+08
6,30E+08	5,71E+08	5,18E+08	4,71E+08	4,49E+08	4,29E+08	4,09E+08	3,90E+08	3,72E+08	3,55E+08	3,39E+08	3,23E+08	3,08E+08	2,94E+08
5,87E+08	5,32E+08	4,83E+08	4,39E+08	4,18E+08	3,99E+08	3,81E+08	3,63E+08	3,46E+08	3,31E+08	3,15E+08	3,01E+08	2,87E+08	2,74E+08
5,42E+08	4,91E+08	4,46E+08	4,05E+08	3,86E+08	3,68E+08	3,51E+08	3,35E+08	3,20E+08	3,05E+08	2,91E+08	2,78E+08	2,65E+08	2,53E+08
4,79E+08	4,34E+08	3,94E+08	3,58E+08	3,41E+08	3,26E+08	3,11E+08	2,96E+08	2,83E+08	2,70E+08	2,57E+08	2,46E+08	2,34E+08	2,24E+08
4,13E+08	3,74E+08	3,40E+08	3,09E+08	2,94E+08	2,81E+08	2,68E+08	2,55E+08	2,44E+08	2,33E+08	2,22E+08	2,12E+08	2,02E+08	1,93E+08
3,43E+08	3,10E+08	2,82E+08	2,56E+08	2,44E+08	2,33E+08	2,22E+08	2,12E+08	2,02E+08	1,93E+08	1,84E+08	1,76E+08	1,68E+08	1,60E+08
2,44E+08	2,21E+08	2,01E+08	1,82E+08	1,74E+08	1,66E+08	1,58E+08	1,51E+08	1,44E+08	1,37E+08	1,31E+08	1,25E+08	1,19E+08	1,14E+08

Step 40	Step 41	Step 42
2,9	2,95	3
2,89E+07	2,75E+07	2,62E+07
5,22E+07	4,97E+07	4,74E+07
7,28E+07	6,94E+07	6,61E+07
9,73E+07	9,27E+07	8,83E+07
1,22E+08	1,17E+08	1,11E+08
1,48E+08	1,41E+08	1,34E+08
1,76E+08	1,67E+08	1,60E+08
2,01E+08	1,91E+08	1,82E+08
2,29E+08	2,18E+08	2,08E+08
2,51E+08	2,39E+08	2,28E+08
2,68E+08	2,56E+08	2,44E+08
2,90E+08	2,76E+08	2,63E+08
3,06E+08	2,92E+08	2,78E+08
3,16E+08	3,01E+08	2,87E+08
3,16E+08	3,01E+08	2,87E+08
3,26E+08	3,11E+08	2,97E+08
3,28E+08	3,13E+08	2,98E+08
3,21E+08	3,06E+08	2,92E+08
3,09E+08	2,94E+08	2,81E+08
2,98E+08	2,84E+08	2,71E+08
2,81E+08	2,68E+08	2,55E+08
2,61E+08	2,49E+08	2,38E+08
2,41E+08	2,30E+08	2,19E+08
2,13E+08	2,03E+08	1,94E+08
1,84E+08	1,75E+08	1,67E+08
1,52E+08	1,45E+08	1,39E+08
1,09E+08	1,04E+08	9,88E+07

MIN	MAX
-3,8475E+07	2,7668E+08
-4,1208E+07	4,2529E+08
-3,7244E+07	5,3148E+08
-2,7416E+07	6,4645E+08
-1,4038E+07	7,4396E+08
4,0207E+06	8,3993E+08
2,1972E+07	9,2350E+08
4,1115E+07	9,9231E+08
6,3542E+07	1,0558E+09
8,2297E+07	1,0981E+09
1,0032E+08	1,1760E+09
1,1801E+08	1,2681E+09
1,3370E+08	1,3392E+09
1,4493E+08	1,3809E+09
1,4980E+08	1,3786E+09
1,5988E+08	1,4228E+09
8,0078E+07	1,4285E+09
-8,1243E+07	1,3934E+09
-1,9610E+08	1,3385E+09
-3,3307E+08	1,2902E+09
-4,2848E+08	1,2115E+09
-5,3818E+08	1,1281E+09
-6,1612E+08	1,0440E+09
-6,5792E+08	9,2482E+08
-6,6588E+08	7,9911E+08
-6,2911E+08	6,6445E+08
-5,1649E+08	4,7455E+08

Result - Principal stress (Abs)

The influence lines for Submodel 1B, for each node at the U-sape. Maximum principal stress 1428.5 MPa (tension) at node 17 in load step 1.45 m.

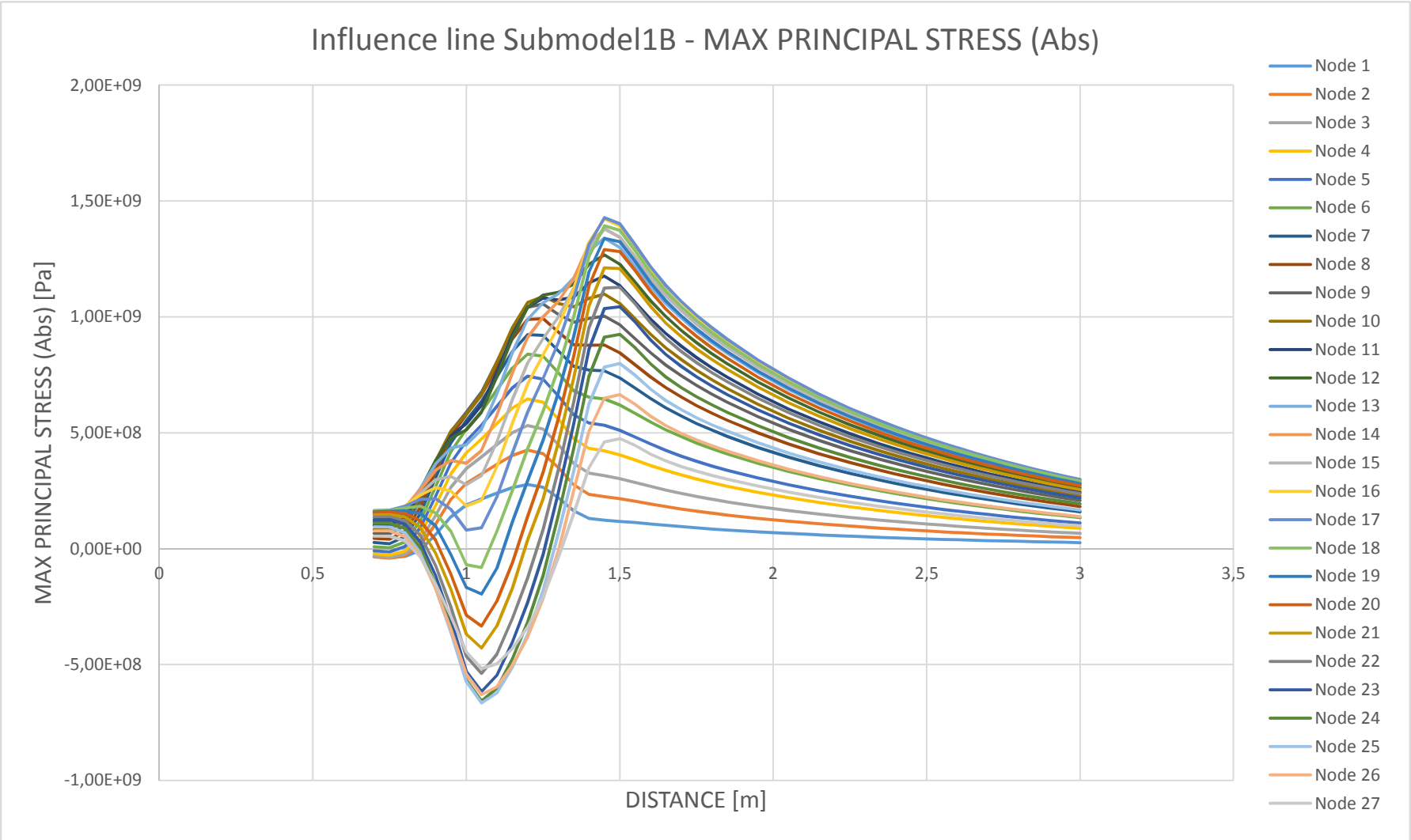

SUBMODEL 1B

MISES STRESS

		Step 1	Step 2	Step 3	Step 4	Step 5	Step 6	Step 7	Step 8	Step 9	Step 10	Step 11
Node	Distance	0,7	0,75	0,8	0,85	0,9	0,95	1	1,05	1,1	1,15	1,2
1	0	2,89E+07	3,32E+07	2,74E+07	5,45E+06	6,33E+07	1,35E+08	1,83E+08	2,09E+08	2,34E+08	2,58E+08	2,72E+08
2	0,00604	2,97E+07	3,49E+07	2,54E+07	1,75E+07	9,89E+07	1,94E+08	2,56E+08	2,93E+08	3,31E+08	3,66E+08	3,87E+08
3	0,01208	2,68E+07	3,23E+07	1,97E+07	3,30E+07	1,30E+08	2,39E+08	3,11E+08	3,56E+08	4,04E+08	4,51E+08	4,78E+08
4	0,01812	1,74E+07	2,27E+07	7,18E+06	5,66E+07	1,67E+08	2,87E+08	3,66E+08	4,19E+08	4,79E+08	5,38E+08	5,74E+08
5	0,02416	7,61E+06	1,21E+07	9,30E+06	7,92E+07	1,99E+08	3,25E+08	4,09E+08	4,68E+08	5,39E+08	6,09E+08	6,53E+08
6	0,0302	9,07E+06	5,66E+06	2,68E+07	1,05E+08	2,35E+08	3,66E+08	4,51E+08	5,18E+08	6,00E+08	6,83E+08	7,36E+08
7	0,03624	2,27E+07	1,89E+07	4,48E+07	1,30E+08	2,64E+08	3,96E+08	4,80E+08	5,51E+08	6,44E+08	7,39E+08	8,01E+08
8	0,04228	3,92E+07	3,61E+07	6,49E+07	1,55E+08	2,92E+08	4,21E+08	5,02E+08	5,76E+08	6,79E+08	7,86E+08	8,59E+08
9	0,04832	5,48E+07	5,25E+07	8,33E+07	1,76E+08	3,12E+08	4,35E+08	5,08E+08	5,84E+08	6,96E+08	8,13E+08	8,95E+08
10	0,05436	7,16E+07	7,02E+07	1,01E+08	1,92E+08	3,20E+08	4,30E+08	4,90E+08	5,62E+08	6,81E+08	8,09E+08	9,01E+08
11	0,0604	8,38E+07	8,31E+07	1,14E+08	2,00E+08	3,16E+08	4,11E+08	4,57E+08	5,25E+08	6,46E+08	7,79E+08	8,78E+08
12	0,06644	9,83E+07	9,82E+07	1,29E+08	2,11E+08	3,18E+08	3,97E+08	4,28E+08	4,92E+08	6,18E+08	7,61E+08	8,70E+08
13	0,07248	1,11E+08	1,12E+08	1,40E+08	2,15E+08	3,06E+08	3,65E+08	3,77E+08	4,33E+08	5,61E+08	7,10E+08	8,29E+08
14	0,07852	1,20E+08	1,22E+08	1,47E+08	2,10E+08	2,79E+08	3,13E+08	3,03E+08	3,47E+08	4,74E+08	6,27E+08	7,54E+08
15	0,08456	1,25E+08	1,26E+08	1,48E+08	1,98E+08	2,47E+08	2,59E+08	2,30E+08	2,63E+08	3,84E+08	5,35E+08	6,66E+08
16	0,0906	1,33E+08	1,35E+08	1,53E+08	1,92E+08	2,21E+08	2,09E+08	1,58E+08	1,80E+08	3,00E+08	4,56E+08	5,97E+08
17	0,09664	1,39E+08	1,41E+08	1,54E+08	1,77E+08	1,80E+08	1,41E+08	6,96E+07	7,81E+07	1,86E+08	3,43E+08	4,92E+08
18	0,10268	1,38E+08	1,40E+08	1,48E+08	1,54E+08	1,31E+08	6,91E+07	6,71E+07	7,81E+07	7,52E+07	2,18E+08	3,68E+08
19	0,10872	1,35E+08	1,36E+08	1,39E+08	1,30E+08	8,38E+07	3,50E+07	1,45E+08	1,70E+08	8,06E+07	1,06E+08	2,52E+08
20	0,11476	1,32E+08	1,34E+08	1,31E+08	1,05E+08	3,59E+07	8,91E+07	2,39E+08	2,78E+08	1,86E+08	5,20E+07	1,31E+08
21	0,1208	1,25E+08	1,26E+08	1,17E+08	7,62E+07	2,57E+07	1,56E+08	3,24E+08	3,77E+08	2,96E+08	1,59E+08	4,23E+07
22	0,12684	1,19E+08	1,20E+08	1,07E+08	5,33E+07	5,97E+07	2,13E+08	3,96E+08	4,60E+08	3,86E+08	2,52E+08	9,91E+07
23	0,13288	1,09E+08	1,10E+08	9,16E+07	2,57E+07	1,03E+08	2,68E+08	4,61E+08	5,36E+08	4,74E+08	3,50E+08	2,02E+08
24	0,13892	9,74E+07	9,77E+07	7,71E+07	5,57E+06	1,30E+08	2,99E+08	4,94E+08	5,73E+08	5,22E+08	4,10E+08	2,71E+08
25	0,14496	8,52E+07	8,52E+07	6,27E+07	1,34E+07	1,51E+08	3,18E+08	5,08E+08	5,89E+08	5,49E+08	4,50E+08	3,22E+08
26	0,151	6,98E+07	6,97E+07	4,81E+07	2,33E+07	1,50E+08	3,02E+08	4,73E+08	5,49E+08	5,18E+08	4,36E+08	3,27E+08
27	0,15704	5,17E+07	5,14E+07	3,26E+07	2,90E+07	1,35E+08	2,60E+08	3,99E+08	4,63E+08	4,43E+08	3,81E+08	2,97E+08

Step 12	Step 13	Step 14	Step 15	Step 16	Step 17	Step 18	Step 19	Step 20	Step 21	Step 22	Step 23	Step 24	Step 25
1,25	1,3	1,35	1,4	1,45	1,5	1,55	1,6	1,65	1,7	1,75	1,8	1,85	1,95
2,62E+08	2,21E+08	1,68E+08	1,39E+08	1,32E+08	1,26E+08	1,20E+08	1,14E+08	1,07E+08	1,01E+08	9,55E+07	9,04E+07	8,57E+07	7,72E+07
3,75E+08	3,21E+08	2,55E+08	2,19E+08	2,10E+08	2,01E+08	1,91E+08	1,80E+08	1,70E+08	1,60E+08	1,51E+08	1,43E+08	1,35E+08	1,22E+08
4,65E+08	4,05E+08	3,32E+08	2,95E+08	2,85E+08	2,73E+08	2,59E+08	2,43E+08	2,29E+08	2,16E+08	2,04E+08	1,93E+08	1,83E+08	1,65E+08
5,61E+08	4,98E+08	4,23E+08	3,88E+08	3,79E+08	3,63E+08	3,43E+08	3,22E+08	3,02E+08	2,85E+08	2,69E+08	2,54E+08	2,41E+08	2,17E+08
6,43E+08	5,79E+08	5,07E+08	4,76E+08	4,68E+08	4,49E+08	4,23E+08	3,96E+08	3,72E+08	3,51E+08	3,31E+08	3,13E+08	2,97E+08	2,68E+08
7,29E+08	6,67E+08	5,99E+08	5,75E+08	5,70E+08	5,46E+08	5,14E+08	4,81E+08	4,52E+08	4,25E+08	4,02E+08	3,80E+08	3,60E+08	3,25E+08
7,98E+08	7,40E+08	6,82E+08	6,67E+08	6,64E+08	6,37E+08	5,99E+08	5,60E+08	5,26E+08	4,95E+08	4,67E+08	4,42E+08	4,19E+08	3,78E+08
8,63E+08	8,13E+08	7,66E+08	7,64E+08	7,66E+08	7,36E+08	6,91E+08	6,46E+08	6,05E+08	5,70E+08	5,38E+08	5,09E+08	4,83E+08	4,35E+08
9,06E+08	8,66E+08	8,33E+08	8,45E+08	8,52E+08	8,20E+08	7,69E+08	7,18E+08	6,73E+08	6,34E+08	5,98E+08	5,66E+08	5,36E+08	4,83E+08
9,24E+08	9,00E+08	8,89E+08	9,21E+08	9,38E+08	9,04E+08	8,48E+08	7,91E+08	7,41E+08	6,97E+08	6,58E+08	6,23E+08	5,90E+08	5,32E+08
9,10E+08	9,02E+08	9,10E+08	9,60E+08	9,84E+08	9,50E+08	8,91E+08	8,30E+08	7,77E+08	7,31E+08	6,90E+08	6,53E+08	6,19E+08	5,58E+08
9,16E+08	9,26E+08	9,57E+08	1,03E+09	1,06E+09	1,03E+09	9,64E+08	8,98E+08	8,40E+08	7,91E+08	7,46E+08	7,06E+08	6,69E+08	6,03E+08
8,88E+08	9,20E+08	9,75E+08	1,07E+09	1,12E+09	1,08E+09	1,01E+09	9,44E+08	8,83E+08	8,30E+08	7,84E+08	7,42E+08	7,03E+08	6,33E+08
8,30E+08	8,87E+08	9,71E+08	1,09E+09	1,15E+09	1,12E+09	1,05E+09	9,76E+08	9,12E+08	8,58E+08	8,10E+08	7,66E+08	7,26E+08	6,54E+08
7,54E+08	8,31E+08	9,36E+08	1,08E+09	1,15E+09	1,12E+09	1,05E+09	9,74E+08	9,10E+08	8,56E+08	8,08E+08	7,64E+08	7,24E+08	6,53E+08
7,02E+08	8,05E+08	9,39E+08	1,11E+09	1,19E+09	1,17E+09	1,09E+09	1,01E+09	9,47E+08	8,90E+08	8,40E+08	7,95E+08	7,53E+08	6,79E+08
6,15E+08	7,45E+08	9,09E+08	1,11E+09	1,21E+09	1,18E+09	1,11E+09	1,03E+09	9,59E+08	9,01E+08	8,51E+08	8,05E+08	7,63E+08	6,87E+08
5,06E+08	6,60E+08	8,49E+08	1,07E+09	1,18E+09	1,16E+09	1,09E+09	1,01E+09	9,42E+08	8,86E+08	8,36E+08	7,90E+08	7,49E+08	6,75E+08
3,99E+08	5,71E+08	7,77E+08	1,01E+09	1,14E+09	1,12E+09	1,05E+09	9,73E+08	9,08E+08	8,53E+08	8,05E+08	7,61E+08	7,21E+08	6,50E+08
2,91E+08	4,86E+08	7,15E+08	9,71E+08	1,11E+09	1,10E+09	1,03E+09	9,51E+08	8,86E+08	8,33E+08	7,85E+08	7,43E+08	7,04E+08	6,34E+08
1,77E+08	3,85E+08	6,25E+08	8,91E+08	1,03E+09	1,03E+09	9,66E+08	8,92E+08	8,31E+08	7,80E+08	7,36E+08	6,96E+08	6,60E+08	5,94E+08
8,35E+07	3,05E+08	5,60E+08	8,37E+08	9,86E+08	9,88E+08	9,26E+08	8,54E+08	7,95E+08	7,46E+08	7,04E+08	6,66E+08	6,31E+08	5,69E+08
2,46E+07	2,11E+08	4,69E+08	7,49E+08	9,01E+08	9,08E+08	8,51E+08	7,84E+08	7,29E+08	6,84E+08	6,45E+08	6,11E+08	5,79E+08	5,21E+08
9,53E+07	1,34E+08	3,87E+08	6,59E+08	8,07E+08	8,18E+08	7,66E+08	7,05E+08	6,56E+08	6,15E+08	5,80E+08	5,48E+08	5,20E+08	4,68E+08
1,53E+08	6,67E+07	3,08E+08	5,66E+08	7,09E+08	7,22E+08	6,76E+08	6,22E+08	5,78E+08	5,42E+08	5,11E+08	4,83E+08	4,58E+08	4,13E+08
1,79E+08	1,79E+07	2,30E+08	4,57E+08	5,83E+08	5,96E+08	5,59E+08	5,14E+08	4,77E+08	4,47E+08	4,21E+08	3,99E+08	3,78E+08	3,40E+08
1,78E+08	2,40E+07	1,51E+08	3,33E+08	4,34E+08	4,46E+08	4,18E+08	3,84E+08	3,56E+08	3,34E+08	3,15E+08	2,98E+08	2,82E+08	2,54E+08

Step 26	Step 27	Step 28	Step 29	Step 30	Step 31	Step 32	Step 33	Step 34	Step 35	Step 36	Step 37	Step 38	Step 39
2,05	2,15	2,25	2,35	2,4	2,45	2,5	2,55	2,6	2,65	2,7	2,75	2,8	2,85
6,98E+07	6,33E+07	5,74E+07	5,21E+07	4,97E+07	4,73E+07	4,51E+07	4,30E+07	4,10E+07	3,91E+07	3,72E+07	3,55E+07	3,38E+07	3,22E+07
1,10E+08	9,99E+07	9,07E+07	8,23E+07	7,85E+07	7,48E+07	7,13E+07	6,80E+07	6,48E+07	6,18E+07	5,89E+07	5,61E+07	5,35E+07	5,10E+07
1,49E+08	1,35E+08	1,22E+08	1,11E+08	1,06E+08	1,01E+08	9,63E+07	9,18E+07	8,75E+07	8,35E+07	7,96E+07	7,59E+07	7,23E+07	6,89E+07
1,97E+08	1,78E+08	1,62E+08	1,47E+08	1,40E+08	1,33E+08	1,27E+08	1,21E+08	1,16E+08	1,10E+08	1,05E+08	1,00E+08	9,56E+07	9,12E+07
2,42E+08	2,19E+08	1,99E+08	1,81E+08	1,72E+08	1,64E+08	1,57E+08	1,49E+08	1,43E+08	1,36E+08	1,30E+08	1,24E+08	1,18E+08	1,12E+08
2,94E+08	2,66E+08	2,41E+08	2,19E+08	2,09E+08	1,99E+08	1,90E+08	1,81E+08	1,73E+08	1,65E+08	1,57E+08	1,50E+08	1,43E+08	1,37E+08
3,41E+08	3,09E+08	2,81E+08	2,55E+08	2,43E+08	2,32E+08	2,21E+08	2,11E+08	2,01E+08	1,92E+08	1,83E+08	1,75E+08	1,67E+08	1,59E+08
3,93E+08	3,56E+08	3,23E+08	2,94E+08	2,80E+08	2,67E+08	2,55E+08	2,43E+08	2,32E+08	2,21E+08	2,11E+08	2,01E+08	1,92E+08	1,83E+08
4,37E+08	3,96E+08	3,60E+08	3,27E+08	3,12E+08	2,97E+08	2,83E+08	2,70E+08	2,58E+08	2,46E+08	2,35E+08	2,24E+08	2,14E+08	2,04E+08
4,81E+08	4,36E+08	3,96E+08	3,60E+08	3,43E+08	3,27E+08	3,12E+08	2,98E+08	2,84E+08	2,71E+08	2,58E+08	2,46E+08	2,35E+08	2,24E+08
5,04E+08	4,57E+08	4,15E+08	3,77E+08	3,60E+08	3,43E+08	3,27E+08	3,12E+08	2,98E+08	2,84E+08	2,71E+08	2,59E+08	2,47E+08	2,35E+08
5,45E+08	4,94E+08	4,49E+08	4,08E+08	3,89E+08	3,71E+08	3,54E+08	3,37E+08	3,22E+08	3,07E+08	2,93E+08	2,80E+08	2,67E+08	2,54E+08
5,73E+08	5,19E+08	4,71E+08	4,28E+08	4,08E+08	3,90E+08	3,72E+08	3,55E+08	3,38E+08	3,23E+08	3,08E+08	2,94E+08	2,80E+08	2,67E+08
5,92E+08	5,36E+08	4,87E+08	4,42E+08	4,22E+08	4,02E+08	3,84E+08	3,66E+08	3,49E+08	3,33E+08	3,18E+08	3,03E+08	2,89E+08	2,76E+08
5,90E+08	5,35E+08	4,86E+08	4,41E+08	4,21E+08	4,02E+08	3,83E+08	3,65E+08	3,49E+08	3,33E+08	3,17E+08	3,03E+08	2,89E+08	2,76E+08
6,14E+08	5,56E+08	5,05E+08	4,59E+08	4,38E+08	4,17E+08	3,98E+08	3,80E+08	3,62E+08	3,46E+08	3,30E+08	3,15E+08	3,00E+08	2,86E+08
6,21E+08	5,63E+08	5,11E+08	4,65E+08	4,43E+08	4,23E+08	4,03E+08	3,85E+08	3,67E+08	3,50E+08	3,34E+08	3,19E+08	3,04E+08	2,90E+08
6,10E+08	5,53E+08	5,02E+08	4,56E+08	4,35E+08	4,15E+08	3,96E+08	3,78E+08	3,60E+08	3,44E+08	3,28E+08	3,13E+08	2,99E+08	2,85E+08
5,88E+08	5,32E+08	4,83E+08	4,39E+08	4,19E+08	4,00E+08	3,81E+08	3,64E+08	3,47E+08	3,31E+08	3,16E+08	3,01E+08	2,88E+08	2,74E+08
5,74E+08	5,20E+08	4,72E+08	4,29E+08	4,09E+08	3,90E+08	3,72E+08	3,55E+08	3,39E+08	3,23E+08	3,08E+08	2,94E+08	2,81E+08	2,68E+08
5,37E+08	4,87E+08	4,42E+08	4,02E+08	3,83E+08	3,65E+08	3,48E+08	3,32E+08	3,17E+08	3,03E+08	2,89E+08	2,75E+08	2,63E+08	2,51E+08
5,14E+08	4,66E+08	4,23E+08	3,84E+08	3,66E+08	3,49E+08	3,33E+08	3,18E+08	3,03E+08	2,89E+08	2,76E+08	2,63E+08	2,51E+08	2,40E+08
4,71E+08	4,27E+08	3,88E+08	3,52E+08	3,36E+08	3,20E+08	3,06E+08	2,92E+08	2,78E+08	2,65E+08	2,53E+08	2,42E+08	2,30E+08	2,20E+08
4,23E+08	3,83E+08	3,48E+08	3,16E+08	3,02E+08	2,88E+08	2,74E+08	2,62E+08	2,50E+08	2,38E+08	2,27E+08	2,17E+08	2,07E+08	1,97E+08
3,73E+08	3,38E+08	3,07E+08	2,79E+08	2,66E+08	2,53E+08	2,42E+08	2,31E+08	2,20E+08	2,10E+08	2,00E+08	1,91E+08	1,82E+08	1,74E+08
3,07E+08	2,79E+08	2,53E+08	2,30E+08	2,19E+08	2,09E+08	1,99E+08	1,90E+08	1,81E+08	1,73E+08	1,65E+08	1,57E+08	1,50E+08	1,43E+08
2,30E+08	2,08E+08	1,89E+08	1,72E+08	1,64E+08	1,56E+08	1,49E+08	1,42E+08	1,35E+08	1,29E+08	1,23E+08	1,18E+08	1,12E+08	1,07E+08

Step 40	Step 41	Step 42
2,9	2,95	3
3,07E+07	2,92E+07	2,78E+07
4,86E+07	4,63E+07	4,41E+07
6,57E+07	6,26E+07	5,96E+07
8,69E+07	8,28E+07	7,89E+07
1,07E+08	1,02E+08	9,73E+07
1,30E+08	1,24E+08	1,18E+08
1,52E+08	1,44E+08	1,38E+08
1,75E+08	1,67E+08	1,59E+08
1,94E+08	1,85E+08	1,77E+08
2,14E+08	2,04E+08	1,94E+08
2,24E+08	2,14E+08	2,04E+08
2,43E+08	2,31E+08	2,21E+08
2,55E+08	2,43E+08	2,32E+08
2,63E+08	2,51E+08	2,39E+08
2,63E+08	2,51E+08	2,39E+08
2,73E+08	2,61E+08	2,48E+08
2,77E+08	2,64E+08	2,52E+08
2,72E+08	2,59E+08	2,47E+08
2,62E+08	2,50E+08	2,38E+08
2,55E+08	2,43E+08	2,32E+08
2,39E+08	2,28E+08	2,17E+08
2,29E+08	2,18E+08	2,08E+08
2,10E+08	2,00E+08	1,91E+08
1,88E+08	1,80E+08	1,71E+08
1,66E+08	1,58E+08	1,51E+08
1,37E+08	1,30E+08	1,24E+08
1,02E+08	9,73E+07	9,28E+07

MIN	MAX
5,45E+06	2,72E+08
1,75E+07	3,87E+08
1,97E+07	4,78E+08
7,18E+06	5,74E+08
7,61E+06	6,53E+08
5,66E+06	7,36E+08
1,89E+07	8,01E+08
3,61E+07	8,63E+08
5,25E+07	9,06E+08
7,02E+07	9,38E+08
8,31E+07	9,84E+08
9,82E+07	1,06E+09
1,11E+08	1,12E+09
1,20E+08	1,15E+09
1,25E+08	1,15E+09
1,33E+08	1,19E+09
6,96E+07	1,21E+09
6,71E+07	1,18E+09
3,50E+07	1,14E+09
3,59E+07	1,11E+09
2,57E+07	1,03E+09
5,33E+07	9,88E+08
2,46E+07	9,08E+08
5,57E+06	8,18E+08
1,34E+07	7,22E+08
1,79E+07	5,96E+08
2,40E+07	4,63E+08

Result - Mises stress

The influence lines for Submodel 1B, for each node at the U-sape. Maximum Mises stress 1205.5 MPa at node 21 in load step 1.2 m.

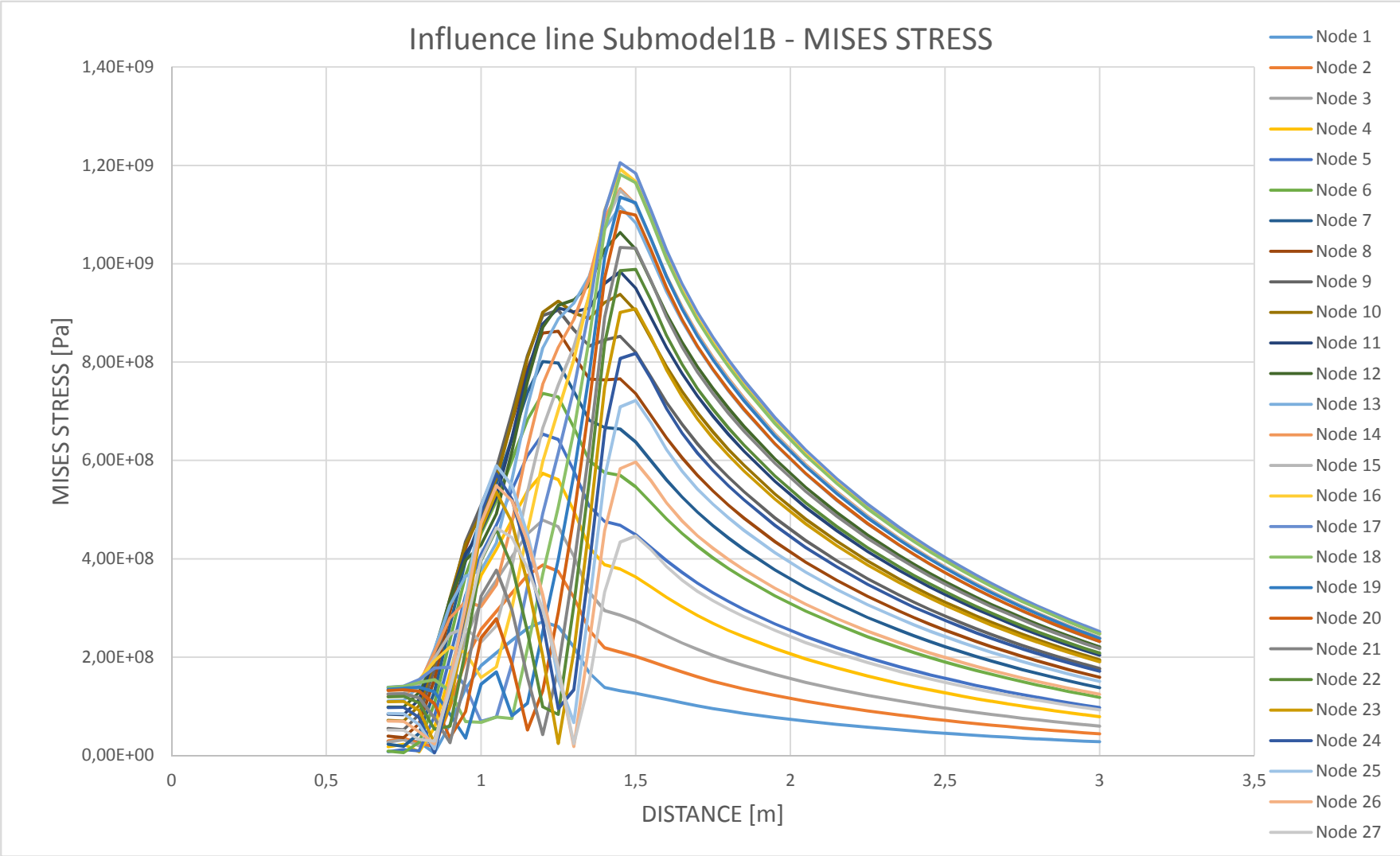

SUBMODEL 2 A

MAX PRINCIPAL STRESS (Abs)

		Step 1	Step 2	Step 3	Step 4	Step 5	Step 6	Step 7	Step 8	Step 9	Step 10	Step 11
Node	Distance	0,7	0,75	0,8	0,85	0,9	0,95	1	1,05	1,1	1,15	1,2
1	0	-3,33E+07	-4,47E+07	-5,74E+07	-7,04E+07	-8,13E+07	-8,56E+07	-6,70E+07	-1,44E+07	6,24E+07	1,45E+08	2,23E+08
2	0,00604	-4,29E+07	-5,80E+07	-7,50E+07	-9,28E+07	-1,08E+08	-1,14E+08	-9,02E+07	-2,03E+07	8,18E+07	1,92E+08	2,96E+08
3	0,01208	-5,03E+07	-6,85E+07	-8,94E+07	-1,12E+08	-1,31E+08	-1,40E+08	-1,11E+08	-2,62E+07	9,76E+07	2,31E+08	3,57E+08
4	0,01812	-5,56E+07	-7,63E+07	-1,00E+08	-1,26E+08	-1,50E+08	-1,61E+08	-1,28E+08	-3,17E+07	1,10E+08	2,61E+08	4,06E+08
5	0,02416	-5,98E+07	-8,28E+07	-1,10E+08	-1,40E+08	-1,67E+08	-1,81E+08	-1,46E+08	-3,79E+07	1,19E+08	2,89E+08	4,51E+08
6	0,0302	-6,30E+07	-8,78E+07	-1,17E+08	-1,50E+08	-1,82E+08	-1,98E+08	-1,60E+08	-4,37E+07	1,27E+08	3,10E+08	4,86E+08
7	0,03624	-6,47E+07	-9,06E+07	-1,22E+08	-1,57E+08	-1,92E+08	-2,11E+08	-1,72E+08	-4,98E+07	1,29E+08	3,21E+08	5,07E+08
8	0,04228	-6,77E+07	-9,53E+07	-1,29E+08	-1,68E+08	-2,06E+08	-2,27E+08	-1,87E+08	-5,67E+07	1,34E+08	3,39E+08	5,38E+08
9	0,04832	-6,94E+07	-9,79E+07	-1,33E+08	-1,74E+08	-2,16E+08	-2,40E+08	-1,99E+08	-6,40E+07	1,34E+08	3,47E+08	5,54E+08
10	0,05436	-7,10E+07	-1,00E+08	-1,36E+08	-1,80E+08	-2,24E+08	-2,50E+08	-2,09E+08	-7,12E+07	1,31E+08	3,50E+08	5,63E+08
11	0,0604	-7,23E+07	-1,02E+08	-1,38E+08	-1,83E+08	-2,29E+08	-2,58E+08	-2,18E+08	-7,89E+07	1,26E+08	3,47E+08	5,62E+08
12	0,06644	-7,36E+07	-1,03E+08	-1,39E+08	-1,85E+08	-2,33E+08	-2,63E+08	-2,24E+08	-8,60E+07	1,18E+08	3,39E+08	5,55E+08
13	0,07248	-7,44E+07	-1,03E+08	-1,39E+08	-1,85E+08	-2,33E+08	-2,64E+08	-2,27E+08	-9,20E+07	1,08E+08	3,25E+08	5,38E+08
14	0,07852	-7,70E+07	-1,05E+08	-1,42E+08	-1,88E+08	-2,37E+08	-2,70E+08	-2,35E+08	-1,01E+08	9,89E+07	3,15E+08	5,28E+08
15	0,08456	-7,71E+07	-1,04E+08	-1,39E+08	-1,84E+08	-2,32E+08	-2,65E+08	-2,33E+08	-1,05E+08	8,51E+07	2,91E+08	4,95E+08
16	0,0906	-7,94E+07	-1,05E+08	-1,39E+08	-1,83E+08	-2,32E+08	-2,66E+08	-2,35E+08	-1,12E+08	7,21E+07	2,72E+08	4,71E+08
17	0,09664	-8,26E+07	-1,08E+08	-1,41E+08	-1,84E+08	-2,33E+08	-2,67E+08	-2,39E+08	-1,21E+08	5,76E+07	2,52E+08	4,45E+08
18	0,10268	-8,25E+07	-1,05E+08	-1,35E+08	-1,76E+08	-2,21E+08	-2,55E+08	-2,31E+08	-1,23E+08	3,97E+07	2,17E+08	3,95E+08
19	0,10872	-8,17E+07	-1,02E+08	-1,30E+08	-1,67E+08	-2,10E+08	-2,41E+08	-2,21E+08	-1,24E+08	2,47E+07	1,87E+08	3,50E+08
20	0,11476	-8,34E+07	-1,02E+08	-1,28E+08	-1,63E+08	-2,03E+08	-2,34E+08	-2,17E+08	-1,28E+08	1,69E+07	1,60E+08	3,12E+08
21	0,1208	-8,29E+07	-9,97E+07	-1,23E+08	-1,55E+08	-1,92E+08	-2,22E+08	-2,08E+08	-1,28E+08	1,31E+07	1,32E+08	2,70E+08
22	0,12684	-8,05E+07	-9,50E+07	-1,15E+08	-1,44E+08	-1,77E+08	-2,04E+08	-1,93E+08	-1,25E+08	-1,71E+07	1,02E+08	2,23E+08
23	0,13288	-7,75E+07	-8,99E+07	-1,07E+08	-1,32E+08	-1,62E+08	-1,87E+08	-1,78E+08	-1,20E+08	-2,73E+07	7,62E+07	1,81E+08
24	0,13892	-7,36E+07	-8,40E+07	-9,89E+07	-1,20E+08	-1,46E+08	-1,68E+08	-1,63E+08	-1,14E+08	-3,53E+07	5,31E+07	1,43E+08
25	0,14496	-6,69E+07	-7,51E+07	-8,72E+07	-1,05E+08	-1,26E+08	-1,45E+08	-1,42E+08	-1,03E+08	-4,00E+07	3,15E+07	1,05E+08
26	0,151	-5,78E+07	-6,40E+07	-7,32E+07	-8,69E+07	-1,04E+08	-1,19E+08	-1,18E+08	-8,92E+07	-4,07E+07	2,03E+07	7,14E+07
27	0,15704	-4,53E+07	-4,96E+07	-5,62E+07	-6,61E+07	-7,85E+07	-9,00E+07	-8,97E+07	-6,96E+07	-3,52E+07	1,73E+07	4,53E+07

Step 12	Step 13	Step 14	Step 15	Step 16	Step 17	Step 18	Step 19	Step 20	Step 21	Step 22	Step 23	Step 24	Step 25
1,25	1,3	1,35	1,4	1,45	1,5	1,55	1,6	1,65	1,7	1,75	1,8	1,85	1,95
2,93E+08	3,56E+08	4,09E+08	4,38E+08	4,32E+08	4,02E+08	3,67E+08	3,37E+08	3,14E+08	2,96E+08	2,80E+08	2,66E+08	2,52E+08	2,28E+08
3,90E+08	4,74E+08	5,46E+08	5,85E+08	5,78E+08	5,38E+08	4,92E+08	4,51E+08	4,21E+08	3,97E+08	3,76E+08	3,56E+08	3,38E+08	3,06E+08
4,73E+08	5,77E+08	6,65E+08	7,14E+08	7,05E+08	6,58E+08	6,01E+08	5,53E+08	5,16E+08	4,86E+08	4,60E+08	4,36E+08	4,14E+08	3,74E+08
5,39E+08	6,60E+08	7,63E+08	8,19E+08	8,10E+08	7,56E+08	6,92E+08	6,37E+08	5,94E+08	5,60E+08	5,30E+08	5,02E+08	4,77E+08	4,31E+08
6,00E+08	7,37E+08	8,54E+08	9,18E+08	9,08E+08	8,49E+08	7,78E+08	7,17E+08	6,69E+08	6,30E+08	5,96E+08	5,66E+08	5,37E+08	4,85E+08
6,49E+08	7,99E+08	9,28E+08	9,99E+08	9,89E+08	9,25E+08	8,49E+08	7,82E+08	7,30E+08	6,88E+08	6,51E+08	6,18E+08	5,86E+08	5,30E+08
6,80E+08	8,41E+08	9,78E+08	1,05E+09	1,04E+09	9,78E+08	8,99E+08	8,29E+08	7,74E+08	7,30E+08	6,90E+08	6,55E+08	6,22E+08	5,62E+08
7,24E+08	8,98E+08	1,05E+09	1,13E+09	1,12E+09	1,05E+09	9,66E+08	8,91E+08	8,33E+08	7,85E+08	7,42E+08	7,04E+08	6,68E+08	6,04E+08
7,49E+08	9,32E+08	1,09E+09	1,18E+09	1,17E+09	1,10E+09	1,01E+09	9,32E+08	8,71E+08	8,21E+08	7,77E+08	7,37E+08	6,99E+08	6,32E+08
7,65E+08	9,54E+08	1,12E+09	1,21E+09	1,20E+09	1,13E+09	1,04E+09	9,62E+08	9,00E+08	8,48E+08	8,02E+08	7,61E+08	7,22E+08	6,53E+08
7,69E+08	9,63E+08	1,13E+09	1,23E+09	1,22E+09	1,15E+09	1,06E+09	9,79E+08	9,16E+08	8,63E+08	8,17E+08	7,74E+08	7,35E+08	6,64E+08
7,62E+08	9,59E+08	1,13E+09	1,23E+09	1,22E+09	1,15E+09	1,06E+09	9,83E+08	9,20E+08	8,67E+08	8,20E+08	7,78E+08	7,38E+08	6,67E+08
7,44E+08	9,39E+08	1,11E+09	1,21E+09	1,20E+09	1,13E+09	1,05E+09	9,70E+08	9,08E+08	8,56E+08	8,10E+08	7,68E+08	7,29E+08	6,59E+08
7,34E+08	9,31E+08	1,10E+09	1,20E+09	1,20E+09	1,13E+09	1,05E+09	9,71E+08	9,09E+08	8,57E+08	8,11E+08	7,69E+08	7,30E+08	6,60E+08
6,94E+08	8,85E+08	1,05E+09	1,15E+09	1,15E+09	1,08E+09	1,00E+09	9,31E+08	8,71E+08	8,21E+08	7,77E+08	7,37E+08	7,00E+08	6,32E+08
6,65E+08	8,53E+08	1,02E+09	1,11E+09	1,11E+09	1,05E+09	9,76E+08	9,06E+08	8,49E+08	8,00E+08	7,57E+08	7,18E+08	6,82E+08	6,16E+08
6,35E+08	8,19E+08	9,83E+08	1,08E+09	1,08E+09	1,02E+09	9,49E+08	8,81E+08	8,26E+08	7,78E+08	7,37E+08	6,99E+08	6,63E+08	6,00E+08
5,70E+08	7,41E+08	8,92E+08	9,82E+08	9,86E+08	9,34E+08	8,68E+08	8,07E+08	7,56E+08	7,13E+08	6,75E+08	6,40E+08	6,08E+08	5,49E+08
5,11E+08	6,68E+08	8,09E+08	8,93E+08	8,98E+08	8,52E+08	7,92E+08	7,36E+08	6,90E+08	6,51E+08	6,17E+08	5,85E+08	5,55E+08	5,02E+08
4,63E+08	6,10E+08	7,43E+08	8,24E+08	8,31E+08	7,89E+08	7,34E+08	6,83E+08	6,41E+08	6,05E+08	5,73E+08	5,43E+08	5,16E+08	4,66E+08
4,07E+08	5,42E+08	6,64E+08	7,40E+08	7,48E+08	7,11E+08	6,62E+08	6,16E+08	5,78E+08	5,46E+08	5,17E+08	4,90E+08	4,66E+08	4,21E+08
3,44E+08	4,63E+08	5,72E+08	6,40E+08	6,49E+08	6,18E+08	5,76E+08	5,37E+08	5,04E+08	4,76E+08	4,51E+08	4,28E+08	4,06E+08	3,67E+08
2,87E+08	3,92E+08	4,88E+08	5,49E+08	5,59E+08	5,33E+08	4,97E+08	4,64E+08	4,36E+08	4,11E+08	3,90E+08	3,70E+08	3,51E+08	3,17E+08
2,34E+08	3,24E+08	4,08E+08	4,62E+08	4,72E+08	4,51E+08	4,21E+08	3,93E+08	3,69E+08	3,49E+08	3,31E+08	3,14E+08	2,98E+08	2,69E+08
1,79E+08	2,53E+08	3,23E+08	3,68E+08	3,78E+08	3,62E+08	3,38E+08	3,16E+08	2,97E+08	2,81E+08	2,66E+08	2,53E+08	2,40E+08	2,17E+08
1,29E+08	1,87E+08	2,42E+08	2,79E+08	2,88E+08	2,76E+08	2,59E+08	2,42E+08	2,28E+08	2,15E+08	2,04E+08	1,94E+08	1,84E+08	1,66E+08
8,68E+07	1,29E+08	1,69E+08	1,96E+08	2,03E+08	1,96E+08	1,84E+08	1,72E+08	1,62E+08	1,53E+08	1,45E+08	1,38E+08	1,31E+08	1,18E+08

Step 26	Step 27	Step 28	Step 29	Step 30	Step 31	Step 32	Step 33	Step 34	Step 35	Step 36	Step 37	Step 38	Step 39
2,05	2,15	2,25	2,35	2,4	2,45	2,5	2,55	2,6	2,65	2,7	2,75	2,8	2,85
2,06E+08	1,87E+08	1,70E+08	1,55E+08	1,48E+08	1,41E+08	1,34E+08	1,28E+08	1,22E+08	1,17E+08	1,11E+08	1,06E+08	1,01E+08	9,66E+07
2,77E+08	2,51E+08	2,28E+08	2,08E+08	1,98E+08	1,89E+08	1,80E+08	1,72E+08	1,64E+08	1,56E+08	1,49E+08	1,42E+08	1,36E+08	1,30E+08
3,39E+08	3,08E+08	2,80E+08	2,54E+08	2,43E+08	2,31E+08	2,21E+08	2,11E+08	2,01E+08	1,92E+08	1,83E+08	1,74E+08	1,66E+08	1,59E+08
3,91E+08	3,54E+08	3,22E+08	2,93E+08	2,79E+08	2,67E+08	2,54E+08	2,43E+08	2,31E+08	2,21E+08	2,11E+08	2,01E+08	1,92E+08	1,83E+08
4,40E+08	3,99E+08	3,63E+08	3,30E+08	3,15E+08	3,00E+08	2,86E+08	2,73E+08	2,61E+08	2,49E+08	2,37E+08	2,26E+08	2,16E+08	2,06E+08
4,80E+08	4,36E+08	3,96E+08	3,60E+08	3,43E+08	3,28E+08	3,13E+08	2,98E+08	2,84E+08	2,71E+08	2,59E+08	2,47E+08	2,35E+08	2,25E+08
5,09E+08	4,62E+08	4,20E+08	3,82E+08	3,64E+08	3,47E+08	3,31E+08	3,16E+08	3,02E+08	2,88E+08	2,74E+08	2,62E+08	2,50E+08	2,38E+08
5,47E+08	4,97E+08	4,51E+08	4,10E+08	3,91E+08	3,73E+08	3,56E+08	3,40E+08	3,24E+08	3,09E+08	2,95E+08	2,81E+08	2,68E+08	2,56E+08
5,73E+08	5,20E+08	4,72E+08	4,29E+08	4,10E+08	3,91E+08	3,73E+08	3,56E+08	3,39E+08	3,24E+08	3,09E+08	2,94E+08	2,81E+08	2,68E+08
5,91E+08	5,37E+08	4,88E+08	4,43E+08	4,23E+08	4,03E+08	3,85E+08	3,67E+08	3,50E+08	3,34E+08	3,19E+08	3,04E+08	2,90E+08	2,76E+08
6,02E+08	5,46E+08	4,96E+08	4,51E+08	4,30E+08	4,11E+08	3,92E+08	3,74E+08	3,56E+08	3,40E+08	3,24E+08	3,09E+08	2,95E+08	2,81E+08
6,05E+08	5,49E+08	4,98E+08	4,53E+08	4,32E+08	4,12E+08	3,93E+08	3,75E+08	3,58E+08	3,41E+08	3,26E+08	3,11E+08	2,96E+08	2,82E+08
5,97E+08	5,42E+08	4,92E+08	4,47E+08	4,27E+08	4,07E+08	3,88E+08	3,70E+08	3,53E+08	3,37E+08	3,21E+08	3,06E+08	2,92E+08	2,79E+08
5,98E+08	5,42E+08	4,93E+08	4,48E+08	4,27E+08	4,07E+08	3,89E+08	3,71E+08	3,54E+08	3,37E+08	3,22E+08	3,07E+08	2,92E+08	2,79E+08
5,73E+08	5,20E+08	4,72E+08	4,29E+08	4,09E+08	3,90E+08	3,72E+08	3,55E+08	3,39E+08	3,23E+08	3,08E+08	2,94E+08	2,80E+08	2,67E+08
5,58E+08	5,06E+08	4,60E+08	4,18E+08	3,99E+08	3,80E+08	3,63E+08	3,46E+08	3,30E+08	3,15E+08	3,00E+08	2,86E+08	2,73E+08	2,60E+08
5,43E+08	4,93E+08	4,47E+08	4,07E+08	3,88E+08	3,70E+08	3,53E+08	3,36E+08	3,21E+08	3,06E+08	2,92E+08	2,78E+08	2,65E+08	2,53E+08
4,97E+08	4,51E+08	4,10E+08	3,72E+08	3,55E+08	3,39E+08	3,23E+08	3,08E+08	2,94E+08	2,80E+08	2,67E+08	2,55E+08	2,43E+08	2,31E+08
4,54E+08	4,12E+08	3,74E+08	3,40E+08	3,24E+08	3,09E+08	2,95E+08	2,81E+08	2,68E+08	2,56E+08	2,44E+08	2,32E+08	2,21E+08	2,11E+08
4,22E+08	3,83E+08	3,48E+08	3,16E+08	3,01E+08	2,87E+08	2,74E+08	2,61E+08	2,49E+08	2,37E+08	2,26E+08	2,16E+08	2,05E+08	1,96E+08
3,81E+08	3,46E+08	3,14E+08	2,85E+08	2,72E+08	2,59E+08	2,47E+08	2,35E+08	2,24E+08	2,14E+08	2,04E+08	1,94E+08	1,85E+08	1,76E+08
3,32E+08	3,01E+08	2,73E+08	2,48E+08	2,37E+08	2,26E+08	2,15E+08	2,05E+08	1,95E+08	1,86E+08	1,78E+08	1,69E+08	1,61E+08	1,54E+08
2,87E+08	2,60E+08	2,36E+08	2,15E+08	2,04E+08	1,95E+08	1,86E+08	1,77E+08	1,69E+08	1,61E+08	1,53E+08	1,46E+08	1,39E+08	1,33E+08
2,44E+08	2,21E+08	2,01E+08	1,82E+08	1,73E+08	1,65E+08	1,57E+08	1,50E+08	1,43E+08	1,36E+08	1,30E+08	1,24E+08	1,18E+08	1,12E+08
1,96E+08	1,78E+08	1,61E+08	1,46E+08	1,39E+08	1,33E+08	1,27E+08	1,21E+08	1,15E+08	1,09E+08	1,04E+08	9,94E+07	9,46E+07	9,01E+07
1,51E+08	1,36E+08	1,24E+08	1,12E+08	1,07E+08	1,02E+08	9,70E+07	9,24E+07	8,80E+07	8,38E+07	7,98E+07	7,60E+07	7,24E+07	6,90E+07
1,07E+08	9,70E+07	8,79E+07	7,97E+07	7,59E+07	7,23E+07	6,89E+07	6,56E+07	6,25E+07	5,95E+07	5,67E+07	5,40E+07	5,14E+07	4,89E+07

Step 40	Step 41	Step 42
2,9	2,95	3
9,21E+07	8,78E+07	8,37E+07
1,24E+08	1,18E+08	1,12E+08
1,51E+08	1,44E+08	1,37E+08
1,74E+08	1,66E+08	1,58E+08
1,96E+08	1,87E+08	1,78E+08
2,14E+08	2,04E+08	1,95E+08
2,27E+08	2,16E+08	2,06E+08
2,44E+08	2,33E+08	2,22E+08
2,55E+08	2,43E+08	2,32E+08
2,64E+08	2,51E+08	2,39E+08
2,68E+08	2,56E+08	2,44E+08
2,69E+08	2,57E+08	2,45E+08
2,66E+08	2,53E+08	2,41E+08
2,66E+08	2,53E+08	2,42E+08
2,55E+08	2,43E+08	2,31E+08
2,48E+08	2,36E+08	2,25E+08
2,41E+08	2,30E+08	2,19E+08
2,21E+08	2,10E+08	2,00E+08
2,01E+08	1,92E+08	1,83E+08
1,87E+08	1,78E+08	1,69E+08
1,68E+08	1,60E+08	1,53E+08
1,46E+08	1,39E+08	1,33E+08
1,26E+08	1,20E+08	1,15E+08
1,07E+08	1,02E+08	9,69E+07
8,58E+07	8,17E+07	7,78E+07
6,57E+07	6,25E+07	5,95E+07
4,66E+07	4,43E+07	4,22E+07

MIN	MAX
-8,5605E+07	4,3792E+08
-1,1449E+08	5,8512E+08
-1,3994E+08	7,1376E+08
-1,6089E+08	8,1903E+08
-1,8111E+08	9,1817E+08
-1,9789E+08	9,9858E+08
-2,1076E+08	1,0544E+09
-2,2738E+08	1,1295E+09
-2,3986E+08	1,1770E+09
-2,5003E+08	1,2103E+09
-2,5804E+08	1,2270E+09
-2,6315E+08	1,2272E+09
-2,6444E+08	1,2069E+09
-2,7039E+08	1,2032E+09
-2,6545E+08	1,1487E+09
-2,6574E+08	1,1144E+09
-2,6723E+08	1,0807E+09
-2,5455E+08	9,8648E+08
-2,4138E+08	8,9847E+08
-2,3447E+08	8,3115E+08
-2,2183E+08	7,4760E+08
-2,0394E+08	6,4909E+08
-1,8652E+08	5,5868E+08
-1,6814E+08	4,7176E+08
-1,4500E+08	3,7762E+08
-1,1934E+08	2,8767E+08
-9,0046E+07	2,0343E+08

Result - Principal stress (Abs)

The influence lines for Submodel 2A, for each node at the U-sape. Maximum principal stress 1227.2 MPa (tension) at node 12 in load step 1.4 m.

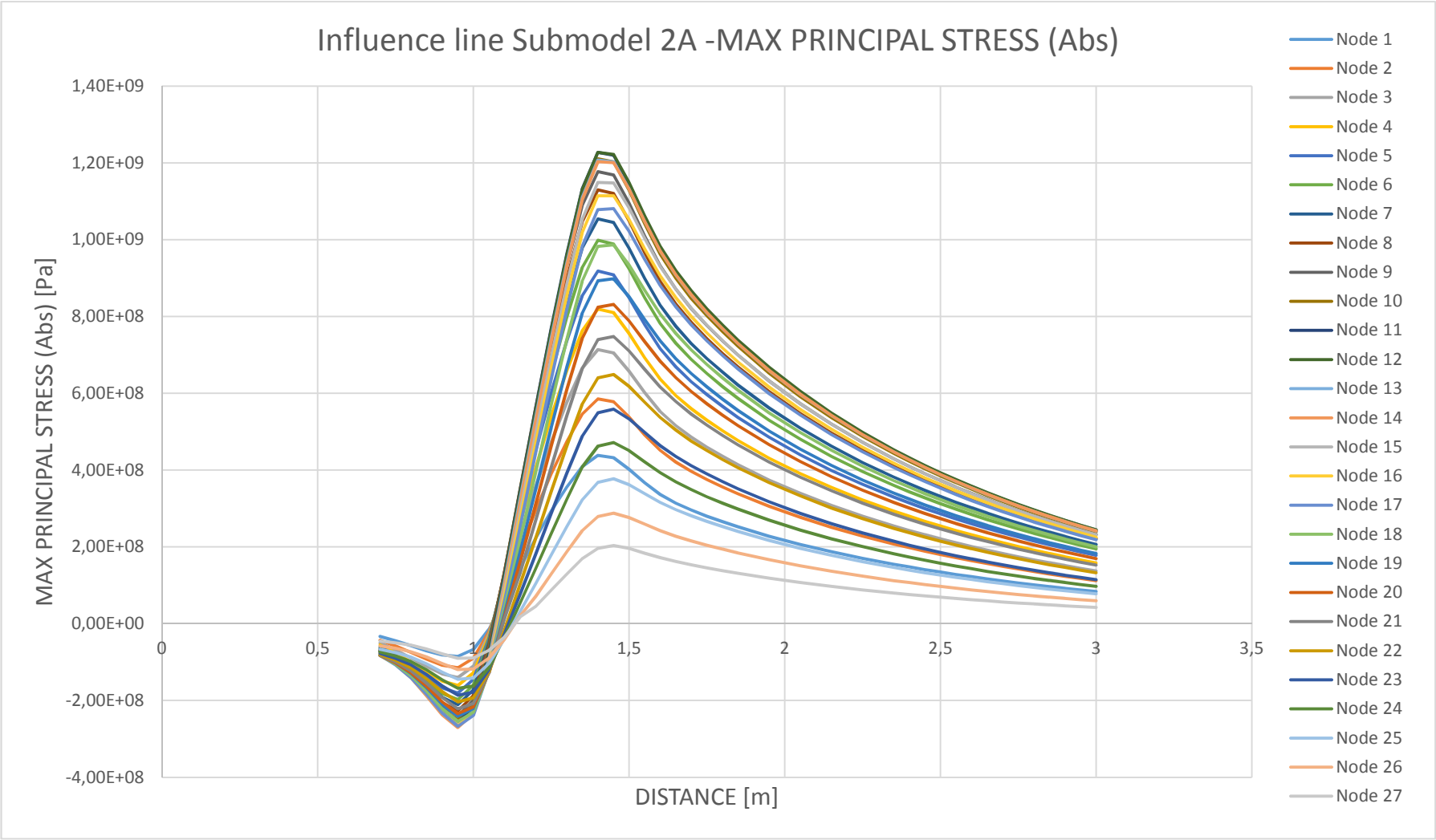

SUBMODEL 2A

MISES STRESS

		Step 1	Step 2	Step 3	Step 4	Step 5	Step 6	Step 7	Step 8	Step 9	Step 10	Step 11
Node	Distance	0,7	0,75	0,8	0,85	0,9	0,95	1	1,05	1,1	1,15	1,2
1	0	3,08E+07	4,14E+07	5,34E+07	6,57E+07	7,64E+07	8,11E+07	6,49E+07	1,96E+07	5,64E+07	1,32E+08	2,04E+08
2	0,00604	3,89E+07	5,26E+07	6,82E+07	8,46E+07	9,90E+07	1,06E+08	8,45E+07	2,41E+07	7,23E+07	1,71E+08	2,65E+08
3	0,01208	4,45E+07	6,05E+07	7,90E+07	9,88E+07	1,16E+08	1,25E+08	1,00E+08	2,82E+07	8,36E+07	2,00E+08	3,11E+08
4	0,01812	4,87E+07	6,68E+07	8,79E+07	1,11E+08	1,32E+08	1,43E+08	1,15E+08	3,28E+07	9,32E+07	2,25E+08	3,52E+08
5	0,02416	5,19E+07	7,18E+07	9,52E+07	1,21E+08	1,45E+08	1,58E+08	1,28E+08	3,73E+07	1,01E+08	2,46E+08	3,85E+08
6	0,0302	5,46E+07	7,59E+07	1,01E+08	1,30E+08	1,58E+08	1,72E+08	1,41E+08	4,25E+07	1,06E+08	2,63E+08	4,14E+08
7	0,03624	5,56E+07	7,78E+07	1,04E+08	1,35E+08	1,65E+08	1,81E+08	1,49E+08	4,68E+07	1,08E+08	2,71E+08	4,29E+08
8	0,04228	5,82E+07	8,18E+07	1,10E+08	1,44E+08	1,77E+08	1,96E+08	1,62E+08	5,28E+07	1,11E+08	2,85E+08	4,54E+08
9	0,04832	5,95E+07	8,39E+07	1,14E+08	1,49E+08	1,85E+08	2,06E+08	1,72E+08	5,86E+07	1,11E+08	2,92E+08	4,68E+08
10	0,05436	6,11E+07	8,59E+07	1,17E+08	1,54E+08	1,92E+08	2,15E+08	1,81E+08	6,48E+07	1,09E+08	2,94E+08	4,75E+08
11	0,0604	6,19E+07	8,69E+07	1,18E+08	1,56E+08	1,96E+08	2,21E+08	1,87E+08	7,04E+07	1,05E+08	2,92E+08	4,75E+08
12	0,06644	6,28E+07	8,75E+07	1,19E+08	1,57E+08	1,98E+08	2,24E+08	1,92E+08	7,65E+07	9,71E+07	2,82E+08	4,64E+08
13	0,07248	6,20E+07	8,57E+07	1,16E+08	1,54E+08	1,94E+08	2,21E+08	1,91E+08	8,00E+07	8,76E+07	2,66E+08	4,42E+08
14	0,07852	6,59E+07	8,97E+07	1,20E+08	1,60E+08	2,02E+08	2,30E+08	2,01E+08	8,91E+07	8,04E+07	2,61E+08	4,40E+08
15	0,08456	6,61E+07	8,87E+07	1,18E+08	1,56E+08	1,98E+08	2,26E+08	2,00E+08	9,41E+07	6,71E+07	2,39E+08	4,10E+08
16	0,0906	6,92E+07	9,16E+07	1,21E+08	1,59E+08	2,02E+08	2,31E+08	2,06E+08	1,01E+08	6,00E+07	2,31E+08	4,02E+08
17	0,09664	7,24E+07	9,42E+07	1,23E+08	1,61E+08	2,04E+08	2,35E+08	2,11E+08	1,09E+08	4,85E+07	2,16E+08	3,84E+08
18	0,10268	7,22E+07	9,19E+07	1,18E+08	1,54E+08	1,93E+08	2,23E+08	2,03E+08	1,11E+08	3,40E+07	1,86E+08	3,39E+08
19	0,10872	7,12E+07	8,90E+07	1,13E+08	1,46E+08	1,83E+08	2,11E+08	1,94E+08	1,11E+08	2,34E+07	1,60E+08	3,01E+08
20	0,11476	7,31E+07	8,97E+07	1,12E+08	1,43E+08	1,79E+08	2,07E+08	1,92E+08	1,15E+08	1,63E+07	1,40E+08	2,73E+08
21	0,1208	7,23E+07	8,70E+07	1,07E+08	1,35E+08	1,68E+08	1,94E+08	1,83E+08	1,15E+08	1,59E+07	1,12E+08	2,30E+08
22	0,12684	7,10E+07	8,39E+07	1,02E+08	1,27E+08	1,57E+08	1,81E+08	1,72E+08	1,13E+08	2,28E+07	8,94E+07	1,95E+08
23	0,13288	6,85E+07	7,95E+07	9,52E+07	1,17E+08	1,44E+08	1,66E+08	1,60E+08	1,09E+08	3,02E+07	6,71E+07	1,59E+08
24	0,13892	6,49E+07	7,42E+07	8,76E+07	1,07E+08	1,30E+08	1,50E+08	1,46E+08	1,04E+08	3,63E+07	4,84E+07	1,27E+08
25	0,14496	5,99E+07	6,73E+07	7,83E+07	9,42E+07	1,14E+08	1,31E+08	1,29E+08	9,55E+07	4,08E+07	3,10E+07	9,36E+07
26	0,151	5,24E+07	5,82E+07	6,68E+07	7,96E+07	9,56E+07	1,10E+08	1,09E+08	8,38E+07	4,12E+07	2,17E+07	6,77E+07
27	0,15704	4,12E+07	4,53E+07	5,16E+07	6,09E+07	7,27E+07	8,39E+07	8,42E+07	6,65E+07	3,69E+07	1,84E+07	4,53E+07

Step 12	Step 13	Step 14	Step 15	Step 16	Step 17	Step 18	Step 19	Step 20	Step 21	Step 22	Step 23	Step 24	Step 25
1,25	1,3	1,35	1,4	1,45	1,5	1,55	1,6	1,65	1,7	1,75	1,8	1,85	1,95
2,69E+08	3,28E+08	3,78E+08	4,05E+08	4,38E+08	3,73E+08	3,40E+08	3,13E+08	2,92E+08	2,75E+08	2,60E+08	2,47E+08	2,34E+08	2,12E+08
3,51E+08	4,28E+08	4,94E+08	5,30E+08	5,85E+08	4,88E+08	4,46E+08	4,10E+08	3,82E+08	3,60E+08	3,41E+08	3,24E+08	3,07E+08	2,78E+08
4,12E+08	5,04E+08	5,83E+08	6,26E+08	7,14E+08	5,78E+08	5,29E+08	4,86E+08	4,54E+08	4,28E+08	4,05E+08	3,84E+08	3,65E+08	3,30E+08
4,68E+08	5,74E+08	6,64E+08	7,14E+08	8,19E+08	6,60E+08	6,05E+08	5,57E+08	5,20E+08	4,90E+08	4,63E+08	4,40E+08	4,17E+08	3,77E+08
5,14E+08	6,32E+08	7,33E+08	7,89E+08	9,18E+08	7,30E+08	6,70E+08	6,17E+08	5,76E+08	5,43E+08	5,14E+08	4,87E+08	4,63E+08	4,18E+08
5,54E+08	6,84E+08	7,95E+08	8,57E+08	9,99E+08	7,95E+08	7,30E+08	6,73E+08	6,28E+08	5,92E+08	5,60E+08	5,32E+08	5,05E+08	4,56E+08
5,77E+08	7,14E+08	8,31E+08	8,97E+08	1,05E+09	8,33E+08	7,66E+08	7,06E+08	6,60E+08	6,22E+08	5,88E+08	5,58E+08	5,30E+08	4,79E+08
6,13E+08	7,61E+08	8,88E+08	9,59E+08	1,13E+09	8,92E+08	8,21E+08	7,58E+08	7,08E+08	6,68E+08	6,32E+08	5,99E+08	5,69E+08	5,14E+08
6,34E+08	7,89E+08	9,24E+08	9,99E+08	1,18E+09	9,31E+08	8,58E+08	7,92E+08	7,41E+08	6,98E+08	6,61E+08	6,26E+08	5,95E+08	5,38E+08
6,47E+08	8,08E+08	9,48E+08	1,03E+09	1,21E+09	9,59E+08	8,84E+08	8,18E+08	7,65E+08	7,21E+08	6,82E+08	6,47E+08	6,14E+08	5,55E+08
6,50E+08	8,16E+08	9,59E+08	1,04E+09	1,23E+09	9,73E+08	8,98E+08	8,31E+08	7,77E+08	7,33E+08	6,93E+08	6,58E+08	6,24E+08	5,64E+08
6,39E+08	8,05E+08	9,49E+08	1,03E+09	1,23E+09	9,67E+08	8,93E+08	8,27E+08	7,74E+08	7,30E+08	6,90E+08	6,55E+08	6,22E+08	5,62E+08
6,12E+08	7,74E+08	9,15E+08	9,96E+08	1,21E+09	9,36E+08	8,66E+08	8,02E+08	7,51E+08	7,08E+08	6,70E+08	6,35E+08	6,03E+08	5,45E+08
6,14E+08	7,80E+08	9,26E+08	1,01E+09	1,20E+09	9,51E+08	8,81E+08	8,17E+08	7,65E+08	7,21E+08	6,82E+08	6,47E+08	6,14E+08	5,55E+08
5,77E+08	7,38E+08	8,80E+08	9,62E+08	1,15E+09	9,08E+08	8,42E+08	7,81E+08	7,32E+08	6,90E+08	6,53E+08	6,19E+08	5,88E+08	5,31E+08
5,70E+08	7,32E+08	8,75E+08	9,58E+08	1,11E+09	9,06E+08	8,41E+08	7,81E+08	7,31E+08	6,90E+08	6,53E+08	6,19E+08	5,88E+08	5,31E+08
5,49E+08	7,10E+08	8,52E+08	9,37E+08	1,08E+09	8,88E+08	8,25E+08	7,67E+08	7,18E+08	6,77E+08	6,41E+08	6,08E+08	5,78E+08	5,22E+08
4,91E+08	6,40E+08	7,72E+08	8,51E+08	9,82E+08	8,10E+08	7,53E+08	7,00E+08	6,56E+08	6,19E+08	5,86E+08	5,56E+08	5,28E+08	4,77E+08
4,40E+08	5,77E+08	7,00E+08	7,73E+08	8,93E+08	7,38E+08	6,87E+08	6,39E+08	5,99E+08	5,65E+08	5,35E+08	5,08E+08	4,82E+08	4,36E+08
4,05E+08	5,35E+08	6,52E+08	7,23E+08	8,24E+08	6,93E+08	6,45E+08	6,01E+08	5,63E+08	5,32E+08	5,03E+08	4,78E+08	4,54E+08	4,10E+08
3,49E+08	4,66E+08	5,73E+08	6,39E+08	7,40E+08	6,14E+08	5,73E+08	5,34E+08	5,01E+08	4,73E+08	4,48E+08	4,25E+08	4,03E+08	3,65E+08
3,02E+08	4,08E+08	5,04E+08	5,65E+08	6,40E+08	5,46E+08	5,09E+08	4,74E+08	4,46E+08	4,21E+08	3,99E+08	3,78E+08	3,59E+08	3,25E+08
2,52E+08	3,45E+08	4,30E+08	4,85E+08	5,49E+08	4,71E+08	4,40E+08	4,10E+08	3,86E+08	3,64E+08	3,45E+08	3,28E+08	3,11E+08	2,81E+08
2,07E+08	2,87E+08	3,62E+08	4,10E+08	4,62E+08	4,01E+08	3,75E+08	3,50E+08	3,29E+08	3,11E+08	2,94E+08	2,79E+08	2,66E+08	2,40E+08
1,59E+08	2,26E+08	2,89E+08	3,30E+08	3,68E+08	3,25E+08	3,04E+08	2,84E+08	2,67E+08	2,53E+08	2,40E+08	2,28E+08	2,16E+08	1,95E+08
1,20E+08	1,73E+08	2,24E+08	2,58E+08	2,79E+08	2,55E+08	2,39E+08	2,24E+08	2,11E+08	1,99E+08	1,89E+08	1,80E+08	1,71E+08	1,54E+08
8,19E+07	1,20E+08	1,57E+08	1,82E+08	1,96E+08	1,82E+08	1,71E+08	1,60E+08	1,51E+08	1,43E+08	1,35E+08	1,28E+08	1,22E+08	1,10E+08

Step 26	Step 27	Step 28	Step 29	Step 30	Step 31	Step 32	Step 33	Step 34	Step 35	Step 36	Step 37	Step 38	Step 39
2,05	2,15	2,25	2,35	2,4	2,45	2,5	2,55	2,6	2,65	2,7	2,75	2,8	2,85
1,92E+08	1,74E+08	1,58E+08	1,44E+08	1,37E+08	1,31E+08	1,25E+08	1,19E+08	1,14E+08	1,08E+08	1,03E+08	9,87E+07	9,41E+07	8,98E+07
2,52E+08	2,28E+08	2,08E+08	1,89E+08	1,80E+08	1,72E+08	1,64E+08	1,56E+08	1,49E+08	1,42E+08	1,36E+08	1,29E+08	1,23E+08	1,18E+08
2,99E+08	2,71E+08	2,46E+08	2,24E+08	2,14E+08	2,04E+08	1,94E+08	1,85E+08	1,77E+08	1,69E+08	1,61E+08	1,53E+08	1,46E+08	1,40E+08
3,42E+08	3,10E+08	2,82E+08	2,56E+08	2,45E+08	2,33E+08	2,23E+08	2,12E+08	2,03E+08	1,93E+08	1,84E+08	1,76E+08	1,68E+08	1,60E+08
3,79E+08	3,44E+08	3,13E+08	2,84E+08	2,71E+08	2,59E+08	2,47E+08	2,35E+08	2,25E+08	2,14E+08	2,04E+08	1,95E+08	1,86E+08	1,77E+08
4,13E+08	3,75E+08	3,41E+08	3,10E+08	2,96E+08	2,82E+08	2,69E+08	2,57E+08	2,45E+08	2,34E+08	2,23E+08	2,12E+08	2,03E+08	1,93E+08
4,34E+08	3,94E+08	3,58E+08	3,25E+08	3,10E+08	2,96E+08	2,82E+08	2,69E+08	2,57E+08	2,45E+08	2,34E+08	2,23E+08	2,13E+08	2,03E+08
4,66E+08	4,23E+08	3,84E+08	3,49E+08	3,33E+08	3,18E+08	3,03E+08	2,89E+08	2,76E+08	2,63E+08	2,51E+08	2,39E+08	2,28E+08	2,18E+08
4,87E+08	4,42E+08	4,02E+08	3,65E+08	3,48E+08	3,32E+08	3,17E+08	3,02E+08	2,89E+08	2,75E+08	2,63E+08	2,50E+08	2,39E+08	2,28E+08
5,03E+08	4,56E+08	4,15E+08	3,77E+08	3,60E+08	3,43E+08	3,27E+08	3,12E+08	2,98E+08	2,84E+08	2,71E+08	2,58E+08	2,46E+08	2,35E+08
5,11E+08	4,64E+08	4,22E+08	3,83E+08	3,66E+08	3,49E+08	3,33E+08	3,17E+08	3,03E+08	2,89E+08	2,75E+08	2,63E+08	2,51E+08	2,39E+08
5,09E+08	4,62E+08	4,20E+08	3,82E+08	3,64E+08	3,47E+08	3,31E+08	3,16E+08	3,01E+08	2,87E+08	2,74E+08	2,61E+08	2,49E+08	2,38E+08
4,94E+08	4,48E+08	4,07E+08	3,70E+08	3,53E+08	3,37E+08	3,21E+08	3,06E+08	2,92E+08	2,79E+08	2,66E+08	2,53E+08	2,42E+08	2,30E+08
5,03E+08	4,56E+08	4,15E+08	3,77E+08	3,59E+08	3,43E+08	3,27E+08	3,12E+08	2,97E+08	2,84E+08	2,71E+08	2,58E+08	2,46E+08	2,35E+08
4,81E+08	4,37E+08	3,97E+08	3,61E+08	3,44E+08	3,28E+08	3,13E+08	2,98E+08	2,85E+08	2,71E+08	2,59E+08	2,47E+08	2,35E+08	2,24E+08
4,81E+08	4,37E+08	3,97E+08	3,60E+08	3,44E+08	3,28E+08	3,13E+08	2,98E+08	2,84E+08	2,71E+08	2,59E+08	2,47E+08	2,35E+08	2,24E+08
4,73E+08	4,29E+08	3,90E+08	3,54E+08	3,38E+08	3,22E+08	3,07E+08	2,93E+08	2,79E+08	2,66E+08	2,54E+08	2,42E+08	2,31E+08	2,20E+08
4,32E+08	3,92E+08	3,56E+08	3,23E+08	3,08E+08	2,94E+08	2,80E+08	2,67E+08	2,55E+08	2,43E+08	2,32E+08	2,21E+08	2,11E+08	2,01E+08
3,95E+08	3,58E+08	3,25E+08	2,95E+08	2,82E+08	2,68E+08	2,56E+08	2,44E+08	2,33E+08	2,22E+08	2,12E+08	2,02E+08	1,92E+08	1,83E+08
3,71E+08	3,37E+08	3,06E+08	2,78E+08	2,65E+08	2,52E+08	2,41E+08	2,29E+08	2,19E+08	2,09E+08	1,99E+08	1,90E+08	1,81E+08	1,72E+08
3,30E+08	2,99E+08	2,72E+08	2,47E+08	2,35E+08	2,24E+08	2,14E+08	2,04E+08	1,94E+08	1,85E+08	1,77E+08	1,68E+08	1,60E+08	1,53E+08
2,94E+08	2,67E+08	2,42E+08	2,20E+08	2,09E+08	2,00E+08	1,90E+08	1,81E+08	1,73E+08	1,65E+08	1,57E+08	1,50E+08	1,43E+08	1,36E+08
2,55E+08	2,31E+08	2,09E+08	1,90E+08	1,81E+08	1,73E+08	1,65E+08	1,57E+08	1,49E+08	1,42E+08	1,36E+08	1,29E+08	1,23E+08	1,17E+08
2,17E+08	1,97E+08	1,79E+08	1,62E+08	1,54E+08	1,47E+08	1,40E+08	1,34E+08	1,27E+08	1,21E+08	1,16E+08	1,10E+08	1,05E+08	1,00E+08
1,77E+08	1,60E+08	1,45E+08	1,32E+08	1,26E+08	1,20E+08	1,14E+08	1,09E+08	1,03E+08	9,86E+07	9,39E+07	8,95E+07	8,52E+07	8,11E+07
1,40E+08	1,26E+08	1,15E+08	1,04E+08	9,91E+07	9,44E+07	8,99E+07	8,56E+07	8,16E+07	7,77E+07	7,40E+07	7,05E+07	6,71E+07	6,39E+07
9,99E+07	9,05E+07	8,20E+07	7,44E+07	7,08E+07	6,74E+07	6,42E+07	6,12E+07	5,83E+07	5,55E+07	5,28E+07	5,03E+07	4,79E+07	4,56E+07

Step 40	Step 41	Step 42
2,9	2,95	3
8,56E+07	8,16E+07	7,77E+07
1,12E+08	1,07E+08	1,02E+08
1,33E+08	1,27E+08	1,21E+08
1,52E+08	1,45E+08	1,38E+08
1,69E+08	1,61E+08	1,54E+08
1,84E+08	1,76E+08	1,67E+08
1,93E+08	1,84E+08	1,76E+08
2,08E+08	1,98E+08	1,89E+08
2,17E+08	2,07E+08	1,97E+08
2,24E+08	2,14E+08	2,04E+08
2,28E+08	2,17E+08	2,07E+08
2,27E+08	2,16E+08	2,06E+08
2,20E+08	2,09E+08	2,00E+08
2,24E+08	2,13E+08	2,03E+08
2,14E+08	2,04E+08	1,94E+08
2,14E+08	2,04E+08	1,94E+08
2,10E+08	2,00E+08	1,90E+08
1,91E+08	1,82E+08	1,74E+08
1,75E+08	1,66E+08	1,59E+08
1,64E+08	1,56E+08	1,49E+08
1,46E+08	1,39E+08	1,32E+08
1,29E+08	1,23E+08	1,17E+08
1,12E+08	1,07E+08	1,01E+08
9,52E+07	9,07E+07	8,63E+07
7,73E+07	7,36E+07	7,00E+07
6,09E+07	5,79E+07	5,51E+07
4,34E+07	4,14E+07	3,94E+07

MIN	MAX
1,96E+07	4,38E+08
2,41E+07	5,85E+08
2,82E+07	7,14E+08
3,28E+07	8,19E+08
3,73E+07	9,18E+08
4,25E+07	9,99E+08
4,68E+07	1,05E+09
5,28E+07	1,13E+09
5,86E+07	1,18E+09
6,11E+07	1,21E+09
6,19E+07	1,23E+09
6,28E+07	1,23E+09
6,20E+07	1,21E+09
6,59E+07	1,20E+09
6,61E+07	1,15E+09
6,00E+07	1,11E+09
4,85E+07	1,08E+09
3,40E+07	9,82E+08
2,34E+07	8,93E+08
1,63E+07	8,24E+08
1,59E+07	7,40E+08
2,28E+07	6,40E+08
3,02E+07	5,49E+08
3,63E+07	4,62E+08
3,10E+07	3,68E+08
2,17E+07	2,79E+08
1,84E+07	1,96E+08

Result - Mises stress

The influence lines for Submodel 2A, for each node at the U-sape. Maximum Mises stress 1227.2 MPa at node 12 in load step 1.4 m.

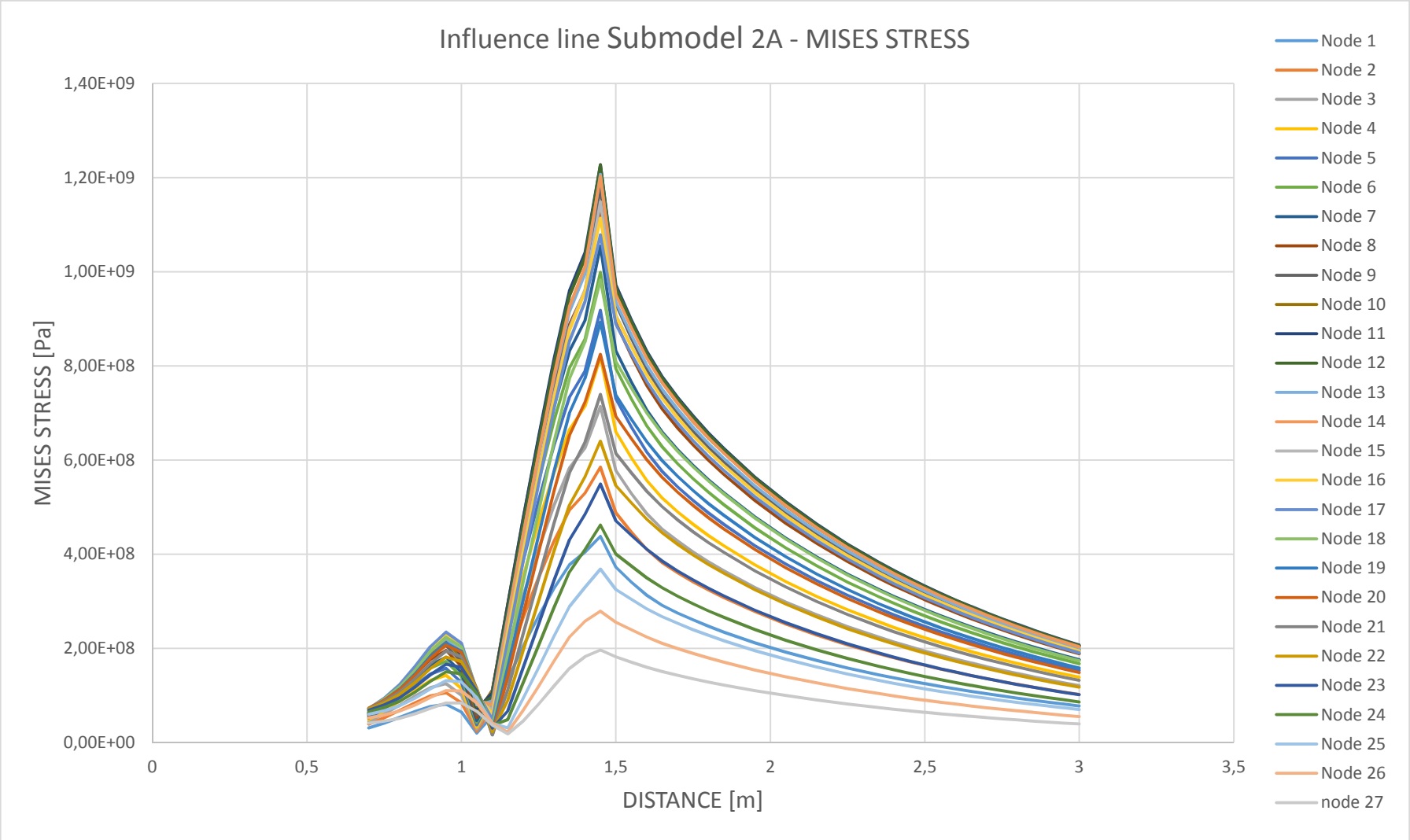

SUBMODEL 2 B

MAX PRINCIPAL STRESS (Abs)

		Step 1	Step 2	Step 3	Step 4	Step 5	Step 6	Step 7	Step 8	Step 9	Step 10	Step 11
Node	Distance	0,7	0,75	0,8	0,85	0,9	0,95	1	1,05	1,1	1,15	1,2
1	0	7,30E+06	1,47E+07	2,63E+07	4,49E+07	6,77E+07	8,44E+07	7,66E+07	3,67E+07	-2,20E+07	-8,63E+07	-1,55E+08
2	0,00604	1,15E+07	2,17E+07	3,75E+07	6,25E+07	9,30E+07	1,15E+08	1,04E+08	4,95E+07	-3,13E+07	-1,20E+08	-2,13E+08
3	0,01208	1,57E+07	2,82E+07	4,73E+07	7,73E+07	1,14E+08	1,40E+08	1,26E+08	5,91E+07	-3,99E+07	-1,48E+08	-2,62E+08
4	0,01812	2,04E+07	3,50E+07	5,71E+07	9,12E+07	1,32E+08	1,62E+08	1,45E+08	6,71E+07	-4,83E+07	-1,74E+08	-3,07E+08
5	0,02416	2,53E+07	4,19E+07	6,67E+07	1,05E+08	1,50E+08	1,83E+08	1,63E+08	7,40E+07	-5,73E+07	-2,01E+08	-3,50E+08
6	0,0302	2,98E+07	4,81E+07	7,51E+07	1,16E+08	1,64E+08	1,99E+08	1,77E+08	7,90E+07	-6,55E+07	-2,23E+08	-3,86E+08
7	0,03624	3,36E+07	5,33E+07	8,21E+07	1,25E+08	1,76E+08	2,11E+08	1,87E+08	8,17E+07	-7,37E+07	-2,43E+08	-4,18E+08
8	0,04228	3,79E+07	5,92E+07	9,00E+07	1,35E+08	1,89E+08	2,26E+08	1,99E+08	8,54E+07	-8,27E+07	-2,65E+08	-4,53E+08
9	0,04832	4,14E+07	6,42E+07	9,68E+07	1,44E+08	1,99E+08	2,38E+08	2,09E+08	8,69E+07	-9,25E+07	-2,87E+08	-4,86E+08
10	0,05436	4,31E+07	6,66E+07	9,99E+07	1,48E+08	2,03E+08	2,42E+08	2,11E+08	8,51E+07	-9,97E+07	-3,00E+08	-5,03E+08
11	0,0604	4,31E+07	6,70E+07	1,00E+08	1,48E+08	2,03E+08	2,40E+08	2,08E+08	8,08E+07	-1,06E+08	-3,08E+08	-5,13E+08
12	0,06644	4,39E+07	6,84E+07	1,03E+08	1,51E+08	2,06E+08	2,43E+08	2,09E+08	7,81E+07	-1,15E+08	-3,22E+08	-5,32E+08
13	0,07248	4,15E+07	6,58E+07	9,94E+07	1,46E+08	1,99E+08	2,35E+08	2,01E+08	7,10E+07	-1,19E+08	-3,24E+08	-5,30E+08
14	0,07852	3,98E+07	6,44E+07	9,80E+07	1,44E+08	1,97E+08	2,32E+08	1,96E+08	6,49E+07	-1,27E+08	-3,33E+08	-5,39E+08
15	0,08456	3,63E+07	6,07E+07	9,37E+07	1,39E+08	1,90E+08	2,23E+08	1,87E+08	5,67E+07	-1,33E+08	-3,36E+08	-5,39E+08
16	0,0906	3,05E+07	5,40E+07	8,54E+07	1,28E+08	1,75E+08	2,06E+08	1,71E+08	4,54E+07	-1,37E+08	-3,30E+08	-5,23E+08
17	0,09664	2,44E+07	4,69E+07	7,70E+07	1,17E+08	1,62E+08	1,90E+08	1,56E+08	3,43E+07	-1,40E+08	-3,26E+08	-5,09E+08
18	0,10268	1,72E+07	3,83E+07	6,63E+07	1,04E+08	1,44E+08	1,70E+08	1,37E+08	2,26E+07	-1,42E+08	-3,15E+08	-4,85E+08
19	0,10872	1,03E+07	2,94E+07	5,50E+07	8,88E+07	1,26E+08	1,48E+08	1,17E+08	1,51E+07	-1,39E+08	-2,97E+08	-4,53E+08
20	0,11476	4,01E+06	2,08E+07	4,44E+07	7,54E+07	1,09E+08	1,29E+08	9,84E+07	1,14E+07	-1,40E+08	-2,86E+08	-4,29E+08
21	0,1208	-6,01E+06	1,24E+07	3,35E+07	6,13E+07	9,09E+07	1,08E+08	7,98E+07	-1,07E+07	-1,37E+08	-2,69E+08	-3,98E+08
22	0,12684	-1,27E+07	4,06E+06	2,16E+07	4,54E+07	7,06E+07	8,48E+07	5,90E+07	-2,07E+07	-1,31E+08	-2,45E+08	-3,56E+08
23	0,13288	-1,85E+07	-5,88E+06	1,15E+07	3,18E+07	5,32E+07	6,48E+07	4,14E+07	-2,86E+07	-1,25E+08	-2,23E+08	-3,18E+08
24	0,13892	-2,27E+07	-1,17E+07	3,53E+06	1,96E+07	3,72E+07	4,62E+07	2,57E+07	-3,43E+07	-1,15E+08	-1,98E+08	-2,77E+08
25	0,14496	-2,55E+07	-1,66E+07	-5,85E+06	8,52E+06	2,20E+07	2,86E+07	1,15E+07	-3,75E+07	-1,03E+08	-1,68E+08	-2,30E+08
26	0,151	-2,57E+07	-1,86E+07	-1,01E+07	2,29E+06	1,12E+07	1,58E+07	8,22E+06	-3,73E+07	-8,83E+07	-1,39E+08	-1,87E+08
27	0,15704	-2,25E+07	-1,78E+07	-1,24E+07	-6,05E+06	-4,26E+05	6,46E+05	-7,11E+06	-3,21E+07	-6,48E+07	-9,69E+07	-1,27E+08

Step 12	Step 13	Step 14	Step 15	Step 16	Step 17	Step 18	Step 19	Step 20	Step 21	Step 22	Step 23	Step 24	Step 25
1,25	1,3	1,35	1,4	1,45	1,5	1,55	1,6	1,65	1,7	1,75	1,8	1,85	1,95
-2,29E+08	-3,04E+08	-3,70E+08	-4,10E+08	-4,15E+08	-4,01E+08	-3,81E+08	-3,59E+08	-3,38E+08	-3,19E+08	-3,01E+08	-2,86E+08	-2,71E+08	-2,45E+08
-3,13E+08	-4,15E+08	-5,05E+08	-5,58E+08	-5,65E+08	-5,44E+08	-5,16E+08	-4,87E+08	-4,58E+08	-4,32E+08	-4,08E+08	-3,87E+08	-3,68E+08	-3,32E+08
-3,83E+08	-5,06E+08	-6,14E+08	-6,78E+08	-6,86E+08	-6,60E+08	-6,25E+08	-5,88E+08	-5,54E+08	-5,22E+08	-4,93E+08	-4,68E+08	-4,44E+08	-4,02E+08
-4,46E+08	-5,87E+08	-7,10E+08	-7,83E+08	-7,91E+08	-7,60E+08	-7,19E+08	-6,76E+08	-6,36E+08	-5,99E+08	-5,67E+08	-5,37E+08	-5,10E+08	-4,61E+08
-5,07E+08	-6,64E+08	-8,02E+08	-8,83E+08	-8,91E+08	-8,55E+08	-8,07E+08	-7,58E+08	-7,13E+08	-6,72E+08	-6,35E+08	-6,02E+08	-5,72E+08	-5,17E+08
-5,56E+08	-7,26E+08	-8,76E+08	-9,63E+08	-9,71E+08	-9,30E+08	-8,76E+08	-8,22E+08	-7,73E+08	-7,29E+08	-6,89E+08	-6,53E+08	-6,20E+08	-5,61E+08
-5,98E+08	-7,78E+08	-9,36E+08	-1,03E+09	-1,04E+09	-9,89E+08	-9,31E+08	-8,72E+08	-8,20E+08	-7,73E+08	-7,31E+08	-6,93E+08	-6,58E+08	-5,95E+08
-6,46E+08	-8,37E+08	-1,01E+09	-1,10E+09	-1,11E+09	-1,06E+09	-9,95E+08	-9,32E+08	-8,75E+08	-8,25E+08	-7,80E+08	-7,40E+08	-7,03E+08	-6,35E+08
-6,89E+08	-8,90E+08	-1,07E+09	-1,17E+09	-1,17E+09	-1,12E+09	-1,05E+09	-9,81E+08	-9,21E+08	-8,68E+08	-8,21E+08	-7,79E+08	-7,39E+08	-6,68E+08
-7,10E+08	-9,14E+08	-1,09E+09	-1,20E+09	-1,20E+09	-1,14E+09	-1,07E+09	-9,99E+08	-9,38E+08	-8,84E+08	-8,36E+08	-7,92E+08	-7,53E+08	-6,80E+08
-7,20E+08	-9,24E+08	-1,10E+09	-1,20E+09	-1,21E+09	-1,15E+09	-1,07E+09	-1,00E+09	-9,39E+08	-8,85E+08	-8,37E+08	-7,93E+08	-7,53E+08	-6,81E+08
-7,42E+08	-9,48E+08	-1,13E+09	-1,23E+09	-1,23E+09	-1,17E+09	-1,09E+09	-1,02E+09	-9,56E+08	-9,01E+08	-8,52E+08	-8,08E+08	-7,67E+08	-6,93E+08
-7,36E+08	-9,37E+08	-1,11E+09	-1,21E+09	-1,21E+09	-1,15E+09	-1,07E+09	-9,98E+08	-9,36E+08	-8,82E+08	-8,34E+08	-7,91E+08	-7,51E+08	-6,79E+08
-7,44E+08	-9,44E+08	-1,12E+09	-1,22E+09	-1,21E+09	-1,15E+09	-1,07E+09	-9,96E+08	-9,33E+08	-8,80E+08	-8,32E+08	-7,89E+08	-7,49E+08	-6,77E+08
-7,39E+08	-9,34E+08	-1,10E+09	-1,20E+09	-1,19E+09	-1,13E+09	-1,05E+09	-9,77E+08	-9,15E+08	-8,62E+08	-8,15E+08	-7,73E+08	-7,34E+08	-6,63E+08
-7,13E+08	-8,97E+08	-1,06E+09	-1,14E+09	-1,14E+09	-1,07E+09	-9,97E+08	-9,27E+08	-8,68E+08	-8,18E+08	-7,74E+08	-7,33E+08	-6,96E+08	-6,29E+08
-6,90E+08	-8,64E+08	-1,01E+09	-1,10E+09	-1,09E+09	-1,02E+09	-9,51E+08	-8,83E+08	-8,27E+08	-7,79E+08	-7,36E+08	-6,98E+08	-6,63E+08	-5,99E+08
-6,53E+08	-8,13E+08	-9,51E+08	-1,03E+09	-1,02E+09	-9,55E+08	-8,85E+08	-8,21E+08	-7,68E+08	-7,24E+08	-6,84E+08	-6,48E+08	-6,16E+08	-5,56E+08
-6,04E+08	-7,50E+08	-8,74E+08	-9,40E+08	-9,29E+08	-8,72E+08	-8,07E+08	-7,49E+08	-7,00E+08	-6,59E+08	-6,23E+08	-5,91E+08	-5,61E+08	-5,07E+08
-5,68E+08	-7,00E+08	-8,14E+08	-8,72E+08	-8,60E+08	-8,05E+08	-7,44E+08	-6,90E+08	-6,45E+08	-6,07E+08	-5,74E+08	-5,44E+08	-5,16E+08	-4,67E+08
-5,22E+08	-6,40E+08	-7,41E+08	-7,92E+08	-7,78E+08	-7,27E+08	-6,71E+08	-6,22E+08	-5,81E+08	-5,47E+08	-5,17E+08	-4,90E+08	-4,65E+08	-4,20E+08
-4,63E+08	-5,64E+08	-6,49E+08	-6,91E+08	-6,77E+08	-6,31E+08	-5,82E+08	-5,38E+08	-5,03E+08	-4,73E+08	-4,47E+08	-4,23E+08	-4,02E+08	-3,63E+08
-4,10E+08	-4,96E+08	-5,68E+08	-6,02E+08	-5,88E+08	-5,46E+08	-5,03E+08	-4,65E+08	-4,34E+08	-4,08E+08	-3,85E+08	-3,65E+08	-3,46E+08	-3,13E+08
-3,53E+08	-4,24E+08	-4,83E+08	-5,09E+08	-4,95E+08	-4,59E+08	-4,22E+08	-3,90E+08	-3,63E+08	-3,41E+08	-3,22E+08	-3,05E+08	-2,90E+08	-2,62E+08
-2,90E+08	-3,45E+08	-3,90E+08	-4,10E+08	-3,97E+08	-3,66E+08	-3,36E+08	-3,10E+08	-2,89E+08	-2,71E+08	-2,56E+08	-2,42E+08	-2,30E+08	-2,08E+08
-2,32E+08	-2,74E+08	-3,08E+08	-3,22E+08	-3,10E+08	-2,85E+08	-2,61E+08	-2,40E+08	-2,24E+08	-2,10E+08	-1,98E+08	-1,88E+08	-1,78E+08	-1,61E+08
-1,55E+08	-1,81E+08	-2,01E+08	-2,08E+08	-1,99E+08	-1,82E+08	-1,66E+08	-1,53E+08	-1,42E+08	-1,33E+08	-1,25E+08	-1,19E+08	-1,13E+08	-1,02E+08

Step 26	Step 27	Step 28	Step 29	Step 30	Step 31	Step 32	Step 33	Step 34	Step 35	Step 36	Step 37	Step 38	Step 39
2,05	2,15	2,25	2,35	2,4	2,45	2,5	2,55	2,6	2,65	2,7	2,75	2,8	2,85
-2,22E+08	-2,02E+08	-1,83E+08	-1,66E+08	-1,59E+08	-1,51E+08	-1,44E+08	-1,38E+08	-1,31E+08	-1,25E+08	-1,19E+08	-1,14E+08	-1,09E+08	-1,03E+08
-3,01E+08	-2,73E+08	-2,48E+08	-2,26E+08	-2,15E+08	-2,05E+08	-1,96E+08	-1,87E+08	-1,78E+08	-1,70E+08	-1,62E+08	-1,54E+08	-1,47E+08	-1,40E+08
-3,64E+08	-3,30E+08	-3,00E+08	-2,72E+08	-2,60E+08	-2,48E+08	-2,36E+08	-2,25E+08	-2,15E+08	-2,05E+08	-1,95E+08	-1,86E+08	-1,78E+08	-1,69E+08
-4,18E+08	-3,79E+08	-3,44E+08	-3,13E+08	-2,98E+08	-2,85E+08	-2,71E+08	-2,59E+08	-2,47E+08	-2,35E+08	-2,24E+08	-2,14E+08	-2,04E+08	-1,95E+08
-4,68E+08	-4,25E+08	-3,86E+08	-3,51E+08	-3,34E+08	-3,19E+08	-3,04E+08	-2,90E+08	-2,77E+08	-2,64E+08	-2,52E+08	-2,40E+08	-2,29E+08	-2,18E+08
-5,08E+08	-4,61E+08	-4,18E+08	-3,80E+08	-3,63E+08	-3,46E+08	-3,30E+08	-3,15E+08	-3,00E+08	-2,86E+08	-2,73E+08	-2,60E+08	-2,48E+08	-2,36E+08
-5,39E+08	-4,89E+08	-4,44E+08	-4,04E+08	-3,85E+08	-3,67E+08	-3,50E+08	-3,34E+08	-3,18E+08	-3,04E+08	-2,90E+08	-2,76E+08	-2,63E+08	-2,51E+08
-5,75E+08	-5,22E+08	-4,74E+08	-4,31E+08	-4,11E+08	-3,92E+08	-3,74E+08	-3,56E+08	-3,40E+08	-3,24E+08	-3,09E+08	-2,95E+08	-2,81E+08	-2,68E+08
-6,05E+08	-5,49E+08	-4,99E+08	-4,53E+08	-4,32E+08	-4,12E+08	-3,93E+08	-3,75E+08	-3,58E+08	-3,41E+08	-3,25E+08	-3,10E+08	-2,96E+08	-2,82E+08
-6,16E+08	-5,59E+08	-5,08E+08	-4,62E+08	-4,40E+08	-4,20E+08	-4,00E+08	-3,82E+08	-3,64E+08	-3,47E+08	-3,31E+08	-3,16E+08	-3,01E+08	-2,87E+08
-6,17E+08	-5,60E+08	-5,08E+08	-4,62E+08	-4,41E+08	-4,20E+08	-4,01E+08	-3,82E+08	-3,65E+08	-3,48E+08	-3,32E+08	-3,16E+08	-3,02E+08	-2,88E+08
-6,28E+08	-5,70E+08	-5,18E+08	-4,71E+08	-4,49E+08	-4,28E+08	-4,08E+08	-3,89E+08	-3,71E+08	-3,54E+08	-3,38E+08	-3,22E+08	-3,07E+08	-2,93E+08
-6,15E+08	-5,58E+08	-5,07E+08	-4,61E+08	-4,39E+08	-4,19E+08	-4,00E+08	-3,81E+08	-3,64E+08	-3,47E+08	-3,31E+08	-3,15E+08	-3,01E+08	-2,87E+08
-6,13E+08	-5,56E+08	-5,05E+08	-4,60E+08	-4,38E+08	-4,18E+08	-3,99E+08	-3,80E+08	-3,63E+08	-3,46E+08	-3,30E+08	-3,15E+08	-3,00E+08	-2,86E+08
-6,01E+08	-5,45E+08	-4,95E+08	-4,50E+08	-4,30E+08	-4,10E+08	-3,91E+08	-3,73E+08	-3,56E+08	-3,39E+08	-3,24E+08	-3,09E+08	-2,94E+08	-2,81E+08
-5,70E+08	-5,17E+08	-4,70E+08	-4,28E+08	-4,08E+08	-3,89E+08	-3,71E+08	-3,54E+08	-3,38E+08	-3,22E+08	-3,07E+08	-2,93E+08	-2,79E+08	-2,67E+08
-5,43E+08	-4,92E+08	-4,48E+08	-4,07E+08	-3,88E+08	-3,70E+08	-3,53E+08	-3,37E+08	-3,22E+08	-3,07E+08	-2,93E+08	-2,79E+08	-2,66E+08	-2,54E+08
-5,04E+08	-4,58E+08	-4,16E+08	-3,78E+08	-3,61E+08	-3,44E+08	-3,28E+08	-3,13E+08	-2,99E+08	-2,85E+08	-2,72E+08	-2,60E+08	-2,48E+08	-2,36E+08
-4,59E+08	-4,17E+08	-3,79E+08	-3,45E+08	-3,29E+08	-3,14E+08	-2,99E+08	-2,86E+08	-2,73E+08	-2,60E+08	-2,48E+08	-2,37E+08	-2,26E+08	-2,15E+08
-4,23E+08	-3,84E+08	-3,49E+08	-3,17E+08	-3,03E+08	-2,89E+08	-2,76E+08	-2,63E+08	-2,51E+08	-2,40E+08	-2,29E+08	-2,18E+08	-2,08E+08	-1,99E+08
-3,81E+08	-3,46E+08	-3,14E+08	-2,86E+08	-2,73E+08	-2,60E+08	-2,49E+08	-2,37E+08	-2,26E+08	-2,16E+08	-2,06E+08	-1,97E+08	-1,88E+08	-1,79E+08
-3,29E+08	-2,99E+08	-2,72E+08	-2,48E+08	-2,36E+08	-2,25E+08	-2,15E+08	-2,05E+08	-1,96E+08	-1,87E+08	-1,79E+08	-1,71E+08	-1,63E+08	-1,55E+08
-2,84E+08	-2,58E+08	-2,35E+08	-2,14E+08	-2,04E+08	-1,95E+08	-1,86E+08	-1,77E+08	-1,69E+08	-1,62E+08	-1,54E+08	-1,47E+08	-1,41E+08	-1,34E+08
-2,37E+08	-2,16E+08	-1,96E+08	-1,79E+08	-1,71E+08	-1,63E+08	-1,56E+08	-1,49E+08	-1,42E+08	-1,36E+08	-1,29E+08	-1,24E+08	-1,18E+08	-1,13E+08
-1,88E+08	-1,71E+08	-1,56E+08	-1,42E+08	-1,36E+08	-1,30E+08	-1,24E+08	-1,18E+08	-1,13E+08	-1,08E+08	-1,03E+08	-9,84E+07	-9,40E+07	-8,97E+07
-1,46E+08	-1,33E+08	-1,21E+08	-1,10E+08	-1,05E+08	-1,01E+08	-9,61E+07	-9,18E+07	-8,77E+07	-8,38E+07	-8,01E+07	-7,65E+07	-7,31E+07	-6,98E+07
-9,24E+07	-8,41E+07	-7,66E+07	-6,99E+07	-6,68E+07	-6,39E+07	-6,11E+07	-5,84E+07	-5,58E+07	-5,33E+07	-5,10E+07	-4,87E+07	-4,66E+07	-4,45E+07

Step 40	Step 41	Step 42
2,9	2,95	3
-9,86E+07	-9,40E+07	-8,95E+07
-1,34E+08	-1,27E+08	-1,21E+08
-1,61E+08	-1,54E+08	-1,47E+08
-1,85E+08	-1,77E+08	-1,68E+08
-2,08E+08	-1,98E+08	-1,89E+08
-2,25E+08	-2,15E+08	-2,05E+08
-2,39E+08	-2,28E+08	-2,17E+08
-2,55E+08	-2,43E+08	-2,32E+08
-2,69E+08	-2,56E+08	-2,44E+08
-2,74E+08	-2,61E+08	-2,49E+08
-2,74E+08	-2,61E+08	-2,49E+08
-2,79E+08	-2,66E+08	-2,54E+08
-2,73E+08	-2,61E+08	-2,48E+08
-2,73E+08	-2,60E+08	-2,48E+08
-2,68E+08	-2,55E+08	-2,43E+08
-2,54E+08	-2,42E+08	-2,31E+08
-2,42E+08	-2,31E+08	-2,20E+08
-2,25E+08	-2,15E+08	-2,05E+08
-2,05E+08	-1,96E+08	-1,87E+08
-1,89E+08	-1,81E+08	-1,72E+08
-1,71E+08	-1,63E+08	-1,55E+08
-1,48E+08	-1,41E+08	-1,35E+08
-1,28E+08	-1,22E+08	-1,17E+08
-1,07E+08	-1,03E+08	-9,79E+07
-8,57E+07	-8,18E+07	-7,81E+07
-6,67E+07	-6,37E+07	-6,08E+07
-4,26E+07	-4,07E+07	-3,88E+07

MIN	MAX
-4,1533E+08	8,4387E+07
-5,6518E+08	1,1518E+08
-6,8591E+08	1,4001E+08
-7,9144E+08	1,6190E+08
-8,9144E+08	1,8251E+08
-9,7104E+08	1,9884E+08
-1,0351E+09	2,1145E+08
-1,1095E+09	2,2624E+08
-1,1732E+09	2,3798E+08
-1,1991E+09	2,4156E+08
-1,2058E+09	2,4031E+08
-1,2325E+09	2,4313E+08
-1,2120E+09	2,3523E+08
-1,2158E+09	2,3156E+08
-1,1983E+09	2,2290E+08
-1,1446E+09	2,0611E+08
-1,0962E+09	1,9026E+08
-1,0256E+09	1,6994E+08
-9,4032E+08	1,4814E+08
-8,7238E+08	1,2873E+08
-7,9171E+08	1,0819E+08
-6,9138E+08	8,4846E+07
-6,0197E+08	6,4801E+07
-5,0939E+08	4,6246E+07
-4,0975E+08	2,8570E+07
-3,2181E+08	1,5804E+07
-2,0811E+08	6,4602E+05

Result - Principal stress (Abs)

The influence lines for Submodel 2B, for each node at the U-sape. Maximum principal stress 1232.5 MPa (compression) at node 12 in load step 1.45 m.

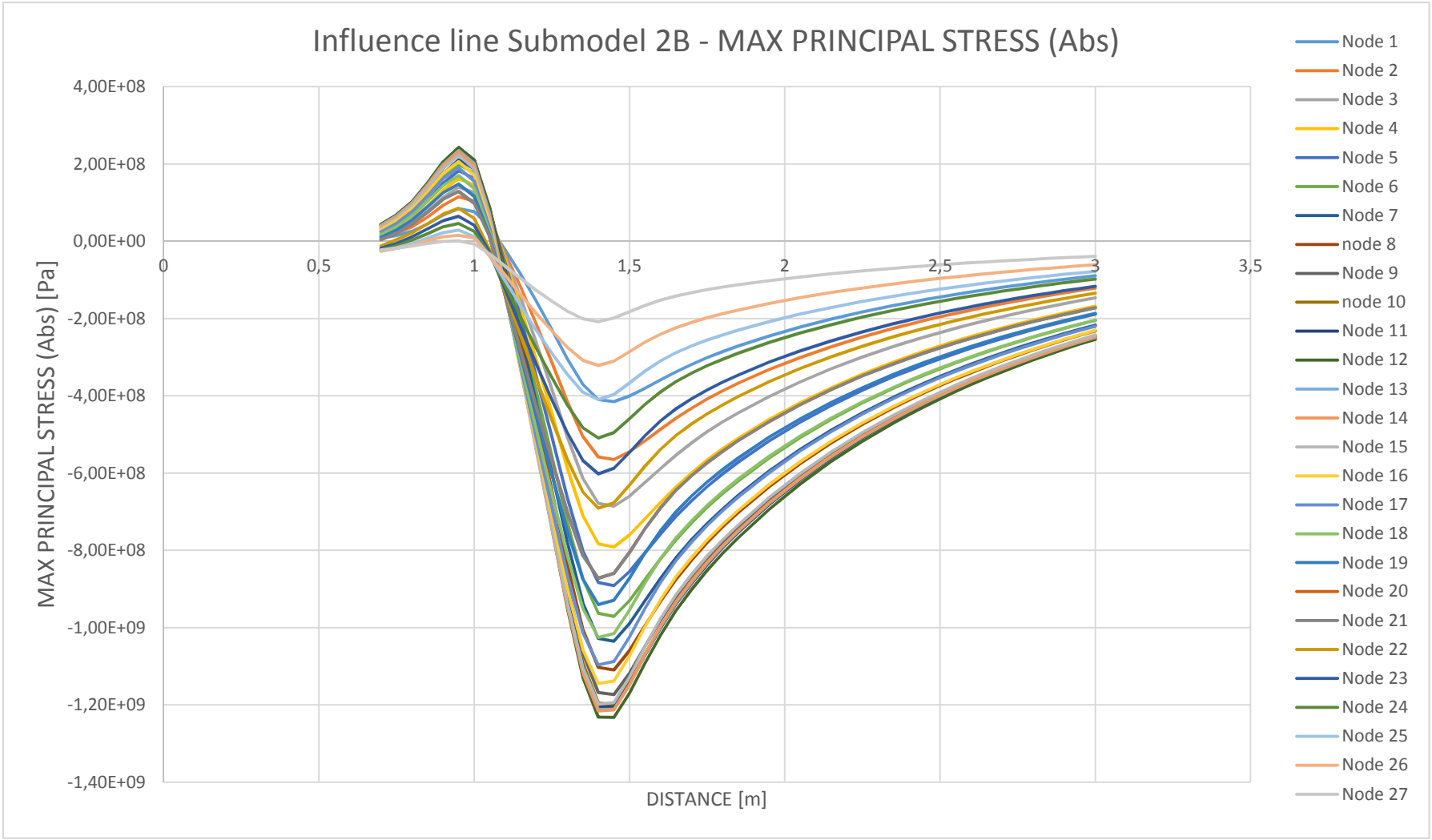

SUBMODEL 2B

MISES STRESS

		Step 1	Step 2	Step 3	Step 4	Step 5	Step 6	Step 7	Step 8	Step 9	Step 10	Step 11
Node	Distance	0,7	0,75	0,8	0,85	0,9	0,95	1	1,05	1,1	1,15	1,2
1	0	6,97E+06	1,38E+07	2,45E+07	4,15E+07	6,23E+07	7,73E+07	6,96E+07	3,34E+07	2,76E+07	8,56E+07	1,49E+08
2	0,00604	1,05E+07	1,97E+07	3,39E+07	5,63E+07	8,35E+07	1,03E+08	9,25E+07	4,35E+07	3,47E+07	1,13E+08	1,98E+08
3	0,01208	1,39E+07	2,50E+07	4,20E+07	6,84E+07	1,00E+08	1,23E+08	1,11E+08	5,11E+07	4,13E+07	1,37E+08	2,38E+08
4	0,01812	1,79E+07	3,07E+07	5,00E+07	7,98E+07	1,16E+08	1,41E+08	1,26E+08	5,72E+07	4,82E+07	1,58E+08	2,75E+08
5	0,02416	2,16E+07	3,60E+07	5,74E+07	9,01E+07	1,29E+08	1,57E+08	1,39E+08	6,25E+07	5,48E+07	1,78E+08	3,08E+08
6	0,0302	2,56E+07	4,15E+07	6,48E+07	1,00E+08	1,42E+08	1,71E+08	1,51E+08	6,63E+07	6,22E+07	1,98E+08	3,40E+08
7	0,03624	2,84E+07	4,51E+07	6,96E+07	1,06E+08	1,49E+08	1,79E+08	1,58E+08	6,80E+07	6,78E+07	2,12E+08	3,61E+08
8	0,04228	3,20E+07	5,01E+07	7,64E+07	1,15E+08	1,60E+08	1,92E+08	1,68E+08	7,08E+07	7,58E+07	2,32E+08	3,92E+08
9	0,04832	3,47E+07	5,39E+07	8,14E+07	1,21E+08	1,68E+08	2,00E+08	1,75E+08	7,16E+07	8,28E+07	2,47E+08	4,15E+08
10	0,05436	3,57E+07	5,55E+07	8,35E+07	1,24E+08	1,70E+08	2,02E+08	1,75E+08	6,91E+07	8,93E+07	2,58E+08	4,30E+08
11	0,0604	3,54E+07	5,52E+07	8,29E+07	1,22E+08	1,67E+08	1,98E+08	1,71E+08	6,52E+07	9,29E+07	2,61E+08	4,31E+08
12	0,06644	3,57E+07	5,62E+07	8,46E+07	1,25E+08	1,70E+08	2,01E+08	1,72E+08	6,23E+07	1,01E+08	2,74E+08	4,49E+08
13	0,07248	3,39E+07	5,41E+07	8,20E+07	1,21E+08	1,65E+08	1,94E+08	1,65E+08	5,62E+07	1,05E+08	2,76E+08	4,47E+08
14	0,07852	3,28E+07	5,36E+07	8,19E+07	1,21E+08	1,65E+08	1,94E+08	1,63E+08	5,23E+07	1,12E+08	2,86E+08	4,61E+08
15	0,08456	3,00E+07	5,07E+07	7,87E+07	1,17E+08	1,60E+08	1,87E+08	1,56E+08	4,54E+07	1,19E+08	2,91E+08	4,64E+08
16	0,0906	2,56E+07	4,57E+07	7,27E+07	1,09E+08	1,50E+08	1,75E+08	1,45E+08	3,74E+07	1,22E+08	2,89E+08	4,55E+08
17	0,09664	2,06E+07	3,98E+07	6,54E+07	9,98E+07	1,38E+08	1,61E+08	1,31E+08	2,86E+07	1,24E+08	2,83E+08	4,41E+08
18	0,10268	1,42E+07	3,22E+07	5,62E+07	8,81E+07	1,23E+08	1,44E+08	1,15E+08	1,93E+07	1,26E+08	2,75E+08	4,22E+08
19	0,10872	8,55E+06	2,45E+07	4,62E+07	7,49E+07	1,06E+08	1,25E+08	9,71E+07	1,27E+07	1,24E+08	2,59E+08	3,92E+08
20	0,11476	4,38E+06	1,81E+07	3,85E+07	6,53E+07	9,41E+07	1,11E+08	8,43E+07	1,20E+07	1,26E+08	2,53E+08	3,78E+08
21	0,1208	6,70E+06	9,84E+06	2,78E+07	5,15E+07	7,67E+07	9,10E+07	6,60E+07	1,69E+07	1,24E+08	2,37E+08	3,48E+08
22	0,12684	1,14E+07	4,17E+06	1,91E+07	3,99E+07	6,20E+07	7,41E+07	5,12E+07	2,35E+07	1,19E+08	2,21E+08	3,19E+08
23	0,13288	1,64E+07	5,74E+06	1,01E+07	2,78E+07	4,63E+07	5,62E+07	3,56E+07	2,97E+07	1,14E+08	2,01E+08	2,85E+08
24	0,13892	1,99E+07	1,04E+07	3,73E+06	1,76E+07	3,30E+07	4,08E+07	2,31E+07	3,43E+07	1,06E+08	1,80E+08	2,50E+08
25	0,14496	2,29E+07	1,48E+07	5,33E+06	8,41E+06	2,05E+07	2,65E+07	1,27E+07	3,75E+07	9,69E+07	1,57E+08	2,15E+08
26	0,151	2,24E+07	1,61E+07	8,56E+06	3,20E+06	1,12E+07	1,55E+07	8,83E+06	3,68E+07	8,29E+07	1,29E+08	1,73E+08
27	0,15704	2,01E+07	1,57E+07	1,05E+07	5,13E+06	5,47E+06	8,40E+06	1,09E+07	3,30E+07	6,50E+07	9,68E+07	1,27E+08

Step 12	Step 13	Step 14	Step 15	Step 16	Step 17	Step 18	Step 19	Step 20	Step 21	Step 22	Step 23	Step 24	Step 25
1,25	1,3	1,35	1,4	1,45	1,5	1,55	1,6	1,65	1,7	1,75	1,8	1,85	1,95
2,17E+08	2,87E+08	3,48E+08	3,84E+08	3,88E+08	3,73E+08	3,54E+08	3,34E+08	3,14E+08	2,96E+08	2,80E+08	2,65E+08	2,52E+08	2,28E+08
2,88E+08	3,80E+08	4,61E+08	5,08E+08	5,13E+08	4,94E+08	4,68E+08	4,41E+08	4,15E+08	3,91E+08	3,70E+08	3,50E+08	3,33E+08	3,01E+08
3,46E+08	4,55E+08	5,51E+08	6,07E+08	6,13E+08	5,89E+08	5,58E+08	5,25E+08	4,94E+08	4,65E+08	4,40E+08	4,17E+08	3,96E+08	3,58E+08
3,97E+08	5,21E+08	6,29E+08	6,92E+08	6,99E+08	6,70E+08	6,33E+08	5,95E+08	5,60E+08	5,28E+08	4,99E+08	4,73E+08	4,49E+08	4,06E+08
4,44E+08	5,80E+08	6,99E+08	7,69E+08	7,75E+08	7,43E+08	7,01E+08	6,58E+08	6,19E+08	5,83E+08	5,52E+08	5,23E+08	4,96E+08	4,49E+08
4,88E+08	6,35E+08	7,64E+08	8,39E+08	8,45E+08	8,09E+08	7,62E+08	7,14E+08	6,71E+08	6,33E+08	5,98E+08	5,67E+08	5,39E+08	4,87E+08
5,15E+08	6,69E+08	8,03E+08	8,81E+08	8,87E+08	8,47E+08	7,97E+08	7,47E+08	7,02E+08	6,61E+08	6,25E+08	5,93E+08	5,63E+08	5,09E+08
5,57E+08	7,21E+08	8,64E+08	9,47E+08	9,52E+08	9,08E+08	8,53E+08	7,98E+08	7,50E+08	7,07E+08	6,68E+08	6,33E+08	6,02E+08	5,44E+08
5,87E+08	7,57E+08	9,06E+08	9,92E+08	9,95E+08	9,48E+08	8,89E+08	8,32E+08	7,81E+08	7,36E+08	6,96E+08	6,60E+08	6,26E+08	5,66E+08
6,04E+08	7,76E+08	9,26E+08	1,01E+09	1,01E+09	9,65E+08	9,03E+08	8,44E+08	7,92E+08	7,46E+08	7,06E+08	6,69E+08	6,35E+08	5,74E+08
6,03E+08	7,72E+08	9,19E+08	1,00E+09	1,00E+09	9,54E+08	8,92E+08	8,33E+08	7,81E+08	7,36E+08	6,96E+08	6,60E+08	6,27E+08	5,66E+08
6,25E+08	7,97E+08	9,47E+08	1,03E+09	1,03E+09	9,78E+08	9,14E+08	8,52E+08	7,99E+08	7,53E+08	7,12E+08	6,75E+08	6,41E+08	5,79E+08
6,19E+08	7,86E+08	9,31E+08	1,01E+09	1,01E+09	9,58E+08	8,93E+08	8,32E+08	7,80E+08	7,35E+08	6,95E+08	6,59E+08	6,26E+08	5,66E+08
6,34E+08	8,03E+08	9,49E+08	1,03E+09	1,03E+09	9,72E+08	9,06E+08	8,43E+08	7,90E+08	7,45E+08	7,04E+08	6,67E+08	6,34E+08	5,73E+08
6,35E+08	8,00E+08	9,43E+08	1,02E+09	1,02E+09	9,61E+08	8,94E+08	8,32E+08	7,79E+08	7,34E+08	6,94E+08	6,58E+08	6,24E+08	5,64E+08
6,18E+08	7,76E+08	9,13E+08	9,88E+08	9,82E+08	9,26E+08	8,60E+08	7,99E+08	7,48E+08	7,05E+08	6,66E+08	6,32E+08	6,00E+08	5,42E+08
5,95E+08	7,44E+08	8,72E+08	9,42E+08	9,34E+08	8,79E+08	8,15E+08	7,57E+08	7,09E+08	6,67E+08	6,31E+08	5,98E+08	5,68E+08	5,13E+08
5,66E+08	7,03E+08	8,22E+08	8,85E+08	8,75E+08	8,22E+08	7,62E+08	7,07E+08	6,61E+08	6,23E+08	5,89E+08	5,58E+08	5,30E+08	4,79E+08
5,22E+08	6,45E+08	7,51E+08	8,07E+08	7,96E+08	7,47E+08	6,91E+08	6,41E+08	5,99E+08	5,64E+08	5,33E+08	5,05E+08	4,79E+08	4,33E+08
4,99E+08	6,14E+08	7,12E+08	7,63E+08	7,52E+08	7,04E+08	6,50E+08	6,02E+08	5,63E+08	5,30E+08	5,01E+08	4,74E+08	4,50E+08	4,07E+08
4,56E+08	5,57E+08	6,43E+08	6,86E+08	6,74E+08	6,29E+08	5,80E+08	5,37E+08	5,02E+08	4,72E+08	4,46E+08	4,22E+08	4,01E+08	3,62E+08
4,13E+08	5,02E+08	5,77E+08	6,14E+08	6,01E+08	5,60E+08	5,16E+08	4,77E+08	4,45E+08	4,19E+08	3,96E+08	3,75E+08	3,56E+08	3,22E+08
3,65E+08	4,41E+08	5,04E+08	5,33E+08	5,20E+08	4,83E+08	4,45E+08	4,11E+08	3,83E+08	3,60E+08	3,40E+08	3,22E+08	3,06E+08	2,76E+08
3,18E+08	3,81E+08	4,33E+08	4,56E+08	4,43E+08	4,11E+08	3,77E+08	3,48E+08	3,24E+08	3,05E+08	2,87E+08	2,72E+08	2,58E+08	2,34E+08
2,69E+08	3,20E+08	3,61E+08	3,78E+08	3,66E+08	3,38E+08	3,10E+08	2,85E+08	2,66E+08	2,49E+08	2,35E+08	2,23E+08	2,11E+08	1,91E+08
2,14E+08	2,53E+08	2,83E+08	2,95E+08	2,84E+08	2,61E+08	2,39E+08	2,20E+08	2,05E+08	1,92E+08	1,81E+08	1,71E+08	1,63E+08	1,47E+08
1,55E+08	1,80E+08	2,00E+08	2,07E+08	1,98E+08	1,82E+08	1,66E+08	1,52E+08	1,41E+08	1,33E+08	1,25E+08	1,18E+08	1,12E+08	1,01E+08

Step 26	Step 27	Step 28	Step 29	Step 30	Step 31	Step 32	Step 33	Step 34	Step 35	Step 36	Step 37	Step 38	Step 39
2,05	2,15	2,25	2,35	2,4	2,45	2,5	2,55	2,6	2,65	2,7	2,75	2,8	2,85
2,06E+08	1,87E+08	1,70E+08	1,54E+08	1,47E+08	1,40E+08	1,34E+08	1,28E+08	1,22E+08	1,16E+08	1,11E+08	1,06E+08	1,01E+08	9,61E+07
2,72E+08	2,47E+08	2,24E+08	2,04E+08	1,95E+08	1,85E+08	1,77E+08	1,69E+08	1,61E+08	1,53E+08	1,46E+08	1,40E+08	1,33E+08	1,27E+08
3,24E+08	2,94E+08	2,67E+08	2,43E+08	2,32E+08	2,21E+08	2,11E+08	2,01E+08	1,92E+08	1,83E+08	1,74E+08	1,66E+08	1,58E+08	1,51E+08
3,68E+08	3,34E+08	3,03E+08	2,75E+08	2,63E+08	2,50E+08	2,39E+08	2,28E+08	2,17E+08	2,07E+08	1,98E+08	1,88E+08	1,80E+08	1,71E+08
4,06E+08	3,69E+08	3,35E+08	3,04E+08	2,90E+08	2,77E+08	2,64E+08	2,52E+08	2,40E+08	2,29E+08	2,18E+08	2,08E+08	1,99E+08	1,89E+08
4,41E+08	4,00E+08	3,63E+08	3,30E+08	3,15E+08	3,00E+08	2,86E+08	2,73E+08	2,61E+08	2,49E+08	2,37E+08	2,26E+08	2,15E+08	2,05E+08
4,61E+08	4,18E+08	3,80E+08	3,45E+08	3,29E+08	3,14E+08	2,99E+08	2,85E+08	2,72E+08	2,60E+08	2,48E+08	2,36E+08	2,25E+08	2,15E+08
4,92E+08	4,47E+08	4,06E+08	3,69E+08	3,52E+08	3,35E+08	3,20E+08	3,05E+08	2,91E+08	2,78E+08	2,65E+08	2,52E+08	2,41E+08	2,29E+08
5,13E+08	4,65E+08	4,23E+08	3,84E+08	3,66E+08	3,49E+08	3,33E+08	3,18E+08	3,03E+08	2,89E+08	2,76E+08	2,63E+08	2,51E+08	2,39E+08
5,20E+08	4,72E+08	4,29E+08	3,90E+08	3,72E+08	3,54E+08	3,38E+08	3,22E+08	3,07E+08	2,93E+08	2,80E+08	2,67E+08	2,54E+08	2,42E+08
5,13E+08	4,66E+08	4,23E+08	3,84E+08	3,67E+08	3,50E+08	3,33E+08	3,18E+08	3,03E+08	2,89E+08	2,76E+08	2,63E+08	2,51E+08	2,39E+08
5,25E+08	4,76E+08	4,32E+08	3,93E+08	3,75E+08	3,58E+08	3,41E+08	3,25E+08	3,10E+08	2,96E+08	2,82E+08	2,69E+08	2,57E+08	2,45E+08
5,12E+08	4,65E+08	4,22E+08	3,84E+08	3,66E+08	3,49E+08	3,33E+08	3,18E+08	3,03E+08	2,89E+08	2,76E+08	2,63E+08	2,51E+08	2,39E+08
5,19E+08	4,71E+08	4,28E+08	3,89E+08	3,71E+08	3,54E+08	3,37E+08	3,22E+08	3,07E+08	2,93E+08	2,79E+08	2,66E+08	2,54E+08	2,42E+08
5,11E+08	4,64E+08	4,21E+08	3,83E+08	3,66E+08	3,49E+08	3,33E+08	3,17E+08	3,03E+08	2,89E+08	2,75E+08	2,63E+08	2,50E+08	2,39E+08
4,91E+08	4,46E+08	4,05E+08	3,68E+08	3,51E+08	3,35E+08	3,20E+08	3,05E+08	2,91E+08	2,77E+08	2,65E+08	2,52E+08	2,41E+08	2,30E+08
4,65E+08	4,22E+08	3,83E+08	3,49E+08	3,33E+08	3,17E+08	3,03E+08	2,89E+08	2,76E+08	2,63E+08	2,51E+08	2,39E+08	2,28E+08	2,18E+08
4,34E+08	3,94E+08	3,58E+08	3,25E+08	3,10E+08	2,96E+08	2,83E+08	2,70E+08	2,57E+08	2,45E+08	2,34E+08	2,23E+08	2,13E+08	2,03E+08
3,93E+08	3,56E+08	3,24E+08	2,95E+08	2,81E+08	2,68E+08	2,56E+08	2,44E+08	2,33E+08	2,22E+08	2,12E+08	2,02E+08	1,93E+08	1,84E+08
3,69E+08	3,35E+08	3,04E+08	2,77E+08	2,64E+08	2,52E+08	2,41E+08	2,30E+08	2,19E+08	2,09E+08	2,00E+08	1,90E+08	1,82E+08	1,73E+08
3,28E+08	2,98E+08	2,71E+08	2,47E+08	2,35E+08	2,25E+08	2,14E+08	2,05E+08	1,95E+08	1,86E+08	1,78E+08	1,70E+08	1,62E+08	1,55E+08
2,91E+08	2,65E+08	2,41E+08	2,19E+08	2,09E+08	2,00E+08	1,90E+08	1,82E+08	1,74E+08	1,66E+08	1,58E+08	1,51E+08	1,44E+08	1,38E+08
2,50E+08	2,27E+08	2,07E+08	1,88E+08	1,80E+08	1,72E+08	1,64E+08	1,57E+08	1,49E+08	1,43E+08	1,36E+08	1,30E+08	1,24E+08	1,18E+08
2,12E+08	1,92E+08	1,75E+08	1,59E+08	1,52E+08	1,45E+08	1,39E+08	1,33E+08	1,27E+08	1,21E+08	1,15E+08	1,10E+08	1,05E+08	1,00E+08
1,73E+08	1,57E+08	1,43E+08	1,31E+08	1,25E+08	1,19E+08	1,14E+08	1,09E+08	1,04E+08	9,92E+07	9,48E+07	9,05E+07	8,64E+07	8,26E+07
1,33E+08	1,21E+08	1,10E+08	1,01E+08	9,61E+07	9,18E+07	8,77E+07	8,38E+07	8,01E+07	7,65E+07	7,31E+07	6,99E+07	6,67E+07	6,38E+07
9,19E+07	8,36E+07	7,62E+07	6,95E+07	6,64E+07	6,35E+07	6,07E+07	5,80E+07	5,54E+07	5,30E+07	5,07E+07	4,85E+07	4,63E+07	4,43E+07

Step 40	Step 41	Step 42
2,9	2,95	3
9,16E+07	8,73E+07	8,32E+07
1,21E+08	1,15E+08	1,10E+08
1,44E+08	1,37E+08	1,31E+08
1,63E+08	1,56E+08	1,48E+08
1,81E+08	1,72E+08	1,64E+08
1,96E+08	1,87E+08	1,78E+08
2,05E+08	1,95E+08	1,86E+08
2,19E+08	2,08E+08	1,99E+08
2,28E+08	2,17E+08	2,07E+08
2,31E+08	2,20E+08	2,10E+08
2,28E+08	2,17E+08	2,07E+08
2,33E+08	2,22E+08	2,12E+08
2,28E+08	2,17E+08	2,07E+08
2,31E+08	2,20E+08	2,10E+08
2,28E+08	2,17E+08	2,07E+08
2,19E+08	2,09E+08	1,99E+08
2,08E+08	1,98E+08	1,89E+08
1,94E+08	1,85E+08	1,76E+08
1,76E+08	1,68E+08	1,60E+08
1,65E+08	1,58E+08	1,50E+08
1,48E+08	1,41E+08	1,34E+08
1,31E+08	1,25E+08	1,19E+08
1,13E+08	1,08E+08	1,03E+08
9,59E+07	9,15E+07	8,74E+07
7,88E+07	7,53E+07	7,18E+07
6,09E+07	5,82E+07	5,56E+07
4,23E+07	4,04E+07	3,86E+07

MIN	MAX
6,97E+06	3,88E+08
1,05E+07	5,13E+08
1,39E+07	6,13E+08
1,79E+07	6,99E+08
2,16E+07	7,75E+08
2,56E+07	8,45E+08
2,84E+07	8,87E+08
3,20E+07	9,52E+08
3,47E+07	9,95E+08
3,57E+07	1,01E+09
3,54E+07	1,00E+09
3,57E+07	1,03E+09
3,39E+07	1,01E+09
3,28E+07	1,03E+09
3,00E+07	1,02E+09
2,56E+07	9,88E+08
2,06E+07	9,42E+08
1,42E+07	8,85E+08
8,55E+06	8,07E+08
4,38E+06	7,63E+08
6,70E+06	6,86E+08
4,17E+06	6,14E+08
5,74E+06	5,33E+08
3,73E+06	4,56E+08
5,33E+06	3,78E+08
3,20E+06	2,95E+08
5,13E+06	2,07E+08

Result - Mises stress

The influence lines for Submodel 2B, for each node at the U-sape. Maximum Mises stress 1031.8 MPa at node 12 in load step 1.4 m.

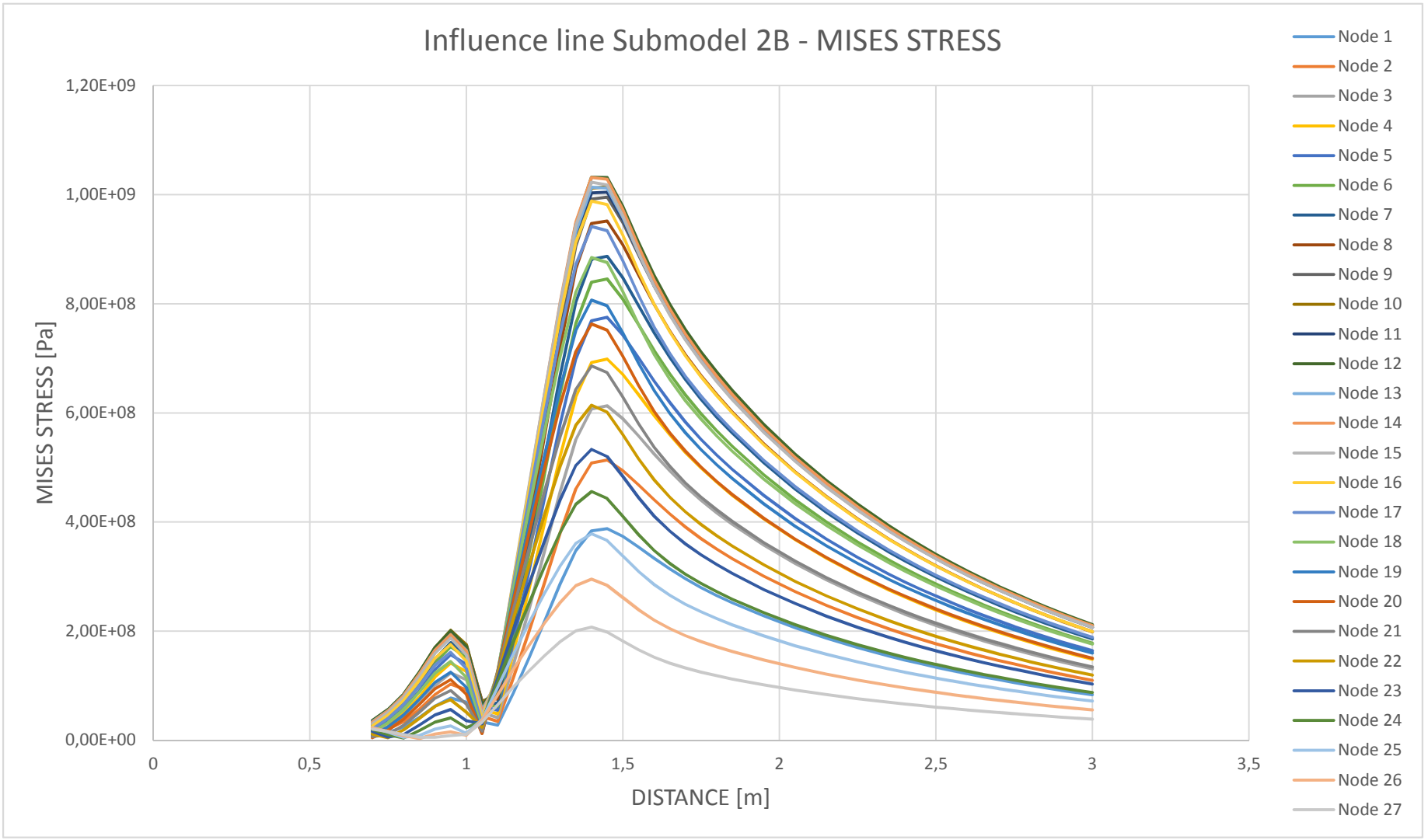

SUBMODEL 3 A

MAX PRINCIPAL STRESS (Abs)

		Step 1	Step 2	Step 3	Step 4	Step 5	Step 6	Step 7	Step 8	Step 9	Step 10
Node	Distance	0,7	0,75	0,8	0,85	0,9	0,95	1	1,05	1,1	1,15
1	0	-3,82E+06	-3,30E+06	-2,77E+06	-2,21E+06	-1,60E+06	-9,08E+05	-1,29E+05	8,62E+05	1,95E+06	3,17E+06
2	0,00604	-6,06E+06	-5,22E+06	-4,38E+06	-3,50E+06	-2,53E+06	-1,41E+06	-1,53E+05	1,41E+06	3,15E+06	5,12E+06
3	0,01208	-8,24E+06	-7,10E+06	-5,95E+06	-4,74E+06	-3,42E+06	-1,89E+06	-1,58E+05	1,97E+06	4,35E+06	7,05E+06
4	0,01812	-1,09E+07	-9,39E+06	-7,86E+06	-6,26E+06	-4,50E+06	-2,48E+06	-1,55E+05	2,66E+06	5,85E+06	9,44E+06
5	0,02416	-1,34E+07	-1,16E+07	-9,69E+06	-7,72E+06	-5,54E+06	-3,03E+06	-1,44E+05	3,34E+06	7,29E+06	1,17E+07
6	0,0302	-1,62E+07	-1,39E+07	-1,16E+07	-9,27E+06	-6,64E+06	-3,61E+06	-1,29E+05	4,07E+06	8,84E+06	1,42E+07
7	0,03624	-1,90E+07	-1,63E+07	-1,37E+07	-1,09E+07	-7,79E+06	-4,22E+06	-1,08E+05	4,84E+06	1,05E+07	1,68E+07
8	0,04228	-2,16E+07	-1,86E+07	-1,56E+07	-1,24E+07	-8,86E+06	-4,78E+06	-8,93E+04	5,56E+06	1,20E+07	1,92E+07
9	0,04832	-2,45E+07	-2,11E+07	-1,76E+07	-1,40E+07	-1,00E+07	-5,39E+06	1,04E+05	6,34E+06	1,36E+07	2,18E+07
10	0,05436	-2,69E+07	-2,31E+07	-1,93E+07	-1,54E+07	-1,10E+07	-5,89E+06	1,26E+05	7,00E+06	1,50E+07	2,40E+07
11	0,0604	-2,94E+07	-2,53E+07	-2,11E+07	-1,68E+07	-1,20E+07	-6,43E+06	1,47E+05	7,70E+06	1,65E+07	2,64E+07
12	0,06644	-3,10E+07	-2,67E+07	-2,23E+07	-1,77E+07	-1,26E+07	-6,77E+06	1,68E+05	8,17E+06	1,75E+07	2,79E+07
13	0,07248	-3,21E+07	-2,76E+07	-2,31E+07	-1,83E+07	-1,31E+07	-6,99E+06	1,83E+05	8,48E+06	1,81E+07	2,89E+07
14	0,07852	-3,38E+07	-2,90E+07	-2,43E+07	-1,93E+07	-1,37E+07	-7,33E+06	2,06E+05	8,95E+06	1,91E+07	3,05E+07
15	0,08456	-3,41E+07	-2,93E+07	-2,45E+07	-1,95E+07	-1,39E+07	-7,40E+06	2,15E+05	9,06E+06	1,93E+07	3,08E+07
16	0,0906	-3,50E+07	-3,01E+07	-2,51E+07	-2,00E+07	-1,42E+07	-7,58E+06	2,35E+05	9,32E+06	1,98E+07	3,17E+07
17	0,09664	-3,51E+07	-3,02E+07	-2,52E+07	-2,00E+07	-1,43E+07	-7,60E+06	2,42E+05	9,37E+06	1,99E+07	3,18E+07
18	0,10268	-3,43E+07	-2,95E+07	-2,47E+07	-1,96E+07	-1,40E+07	-7,42E+06	2,49E+05	9,19E+06	1,95E+07	3,12E+07
19	0,10872	-3,30E+07	-2,84E+07	-2,37E+07	-1,88E+07	-1,34E+07	-7,14E+06	2,43E+05	8,85E+06	1,88E+07	3,00E+07
20	0,11476	-3,20E+07	-2,75E+07	-2,30E+07	-1,83E+07	-1,30E+07	-6,92E+06	2,46E+05	8,61E+06	1,83E+07	2,92E+07
21	0,1208	-3,05E+07	-2,62E+07	-2,19E+07	-1,74E+07	-1,24E+07	-6,59E+06	2,37E+05	8,21E+06	1,74E+07	2,78E+07
22	0,12684	-2,81E+07	-2,41E+07	-2,02E+07	-1,60E+07	-1,14E+07	-6,06E+06	2,26E+05	7,57E+06	1,61E+07	2,56E+07
23	0,13288	-2,58E+07	-2,21E+07	-1,85E+07	-1,47E+07	-1,05E+07	-5,56E+06	2,09E+05	6,95E+06	1,47E+07	2,35E+07
24	0,13892	-2,31E+07	-1,98E+07	-1,66E+07	-1,32E+07	-9,37E+06	-4,97E+06	1,92E+05	6,22E+06	1,32E+07	2,11E+07
25	0,14496	-2,00E+07	-1,72E+07	-1,44E+07	-1,14E+07	-8,13E+06	-4,31E+06	1,67E+05	5,41E+06	1,15E+07	1,83E+07
26	0,151	-1,66E+07	-1,43E+07	-1,19E+07	-9,49E+06	-6,75E+06	-3,58E+06	1,42E+05	4,49E+06	9,52E+06	1,52E+07
27	0,15704	-1,16E+07	-1,00E+07	-8,37E+06	-6,65E+06	-4,73E+06	-2,51E+06	1,01E+05	3,15E+06	6,68E+06	1,07E+07

Step 11	Step 12	Step 13	Step 14	Step 15	Step 16	Step 17	Step 18	Step 19	Step 20	Step 21	Step 22	Step 23	Step 24
1,2	1,25	1,3	1,35	1,4	1,45	1,5	1,55	1,6	1,65	1,7	1,75	1,8	1,85
4,53E+06	6,00E+06	7,56E+06	9,18E+06	1,08E+07	1,25E+07	1,43E+07	1,60E+07	1,78E+07	1,96E+07	2,15E+07	2,35E+07	2,55E+07	2,76E+07
7,28E+06	9,64E+06	1,21E+07	1,47E+07	1,74E+07	2,01E+07	2,28E+07	2,56E+07	2,85E+07	3,14E+07	3,44E+07	3,76E+07	4,08E+07	4,41E+07
1,00E+07	1,32E+07	1,67E+07	2,02E+07	2,38E+07	2,75E+07	3,13E+07	3,51E+07	3,90E+07	4,30E+07	4,72E+07	5,14E+07	5,58E+07	6,04E+07
1,34E+07	1,77E+07	2,23E+07	2,70E+07	3,18E+07	3,67E+07	4,17E+07	4,68E+07	5,20E+07	5,73E+07	6,28E+07	6,85E+07	7,44E+07	8,05E+07
1,67E+07	2,20E+07	2,76E+07	3,35E+07	3,95E+07	4,55E+07	5,17E+07	5,80E+07	6,44E+07	7,11E+07	7,79E+07	8,49E+07	9,21E+07	9,97E+07
2,02E+07	2,66E+07	3,34E+07	4,05E+07	4,77E+07	5,50E+07	6,25E+07	7,01E+07	7,78E+07	8,58E+07	9,40E+07	1,02E+08	1,11E+08	1,20E+08
2,38E+07	3,14E+07	3,94E+07	4,77E+07	5,62E+07	6,49E+07	7,36E+07	8,26E+07	9,17E+07	1,01E+08	1,11E+08	1,21E+08	1,31E+08	1,42E+08
2,72E+07	3,59E+07	4,51E+07	5,46E+07	6,42E+07	7,41E+07	8,41E+07	9,43E+07	1,05E+08	1,15E+08	1,27E+08	1,38E+08	1,50E+08	1,62E+08
3,09E+07	4,08E+07	5,12E+07	6,19E+07	7,29E+07	8,41E+07	9,54E+07	1,07E+08	1,19E+08	1,31E+08	1,44E+08	1,56E+08	1,70E+08	1,84E+08
3,40E+07	4,48E+07	5,63E+07	6,81E+07	8,02E+07	9,25E+07	1,05E+08	1,18E+08	1,31E+08	1,44E+08	1,58E+08	1,72E+08	1,87E+08	2,02E+08
3,73E+07	4,92E+07	6,17E+07	7,46E+07	8,79E+07	1,01E+08	1,15E+08	1,29E+08	1,43E+08	1,58E+08	1,73E+08	1,88E+08	2,05E+08	2,21E+08
3,95E+07	5,20E+07	6,53E+07	7,90E+07	9,30E+07	1,07E+08	1,22E+08	1,36E+08	1,51E+08	1,67E+08	1,83E+08	1,99E+08	2,16E+08	2,34E+08
4,09E+07	5,39E+07	6,76E+07	8,18E+07	9,63E+07	1,11E+08	1,26E+08	1,41E+08	1,57E+08	1,73E+08	1,89E+08	2,06E+08	2,24E+08	2,42E+08
4,31E+07	5,68E+07	7,12E+07	8,61E+07	1,01E+08	1,17E+08	1,33E+08	1,49E+08	1,65E+08	1,82E+08	1,99E+08	2,17E+08	2,36E+08	2,55E+08
4,36E+07	5,74E+07	7,20E+07	8,71E+07	1,02E+08	1,18E+08	1,34E+08	1,50E+08	1,67E+08	1,84E+08	2,01E+08	2,20E+08	2,38E+08	2,58E+08
4,48E+07	5,90E+07	7,40E+07	8,95E+07	1,05E+08	1,21E+08	1,38E+08	1,54E+08	1,71E+08	1,89E+08	2,07E+08	2,26E+08	2,45E+08	2,65E+08
4,50E+07	5,93E+07	7,43E+07	8,98E+07	1,06E+08	1,22E+08	1,38E+08	1,55E+08	1,72E+08	1,90E+08	2,08E+08	2,26E+08	2,46E+08	2,66E+08
4,41E+07	5,80E+07	7,28E+07	8,80E+07	1,04E+08	1,19E+08	1,35E+08	1,52E+08	1,69E+08	1,86E+08	2,03E+08	2,22E+08	2,41E+08	2,60E+08
4,24E+07	5,59E+07	7,00E+07	8,47E+07	9,97E+07	1,15E+08	1,30E+08	1,46E+08	1,62E+08	1,79E+08	1,96E+08	2,13E+08	2,32E+08	2,51E+08
4,12E+07	5,43E+07	6,80E+07	8,23E+07	9,68E+07	1,12E+08	1,27E+08	1,42E+08	1,58E+08	1,74E+08	1,90E+08	2,07E+08	2,25E+08	2,43E+08
3,93E+07	5,17E+07	6,48E+07	7,84E+07	9,22E+07	1,06E+08	1,21E+08	1,35E+08	1,50E+08	1,65E+08	1,81E+08	1,98E+08	2,14E+08	2,32E+08
3,62E+07	4,77E+07	5,98E+07	7,23E+07	8,50E+07	9,80E+07	1,11E+08	1,25E+08	1,38E+08	1,53E+08	1,67E+08	1,82E+08	1,98E+08	2,14E+08
3,32E+07	4,37E+07	5,48E+07	6,63E+07	7,80E+07	8,99E+07	1,02E+08	1,14E+08	1,27E+08	1,40E+08	1,53E+08	1,67E+08	1,81E+08	1,96E+08
2,98E+07	3,92E+07	4,91E+07	5,94E+07	6,98E+07	8,05E+07	9,13E+07	1,02E+08	1,14E+08	1,25E+08	1,37E+08	1,50E+08	1,62E+08	1,76E+08
2,58E+07	3,40E+07	4,26E+07	5,15E+07	6,07E+07	6,99E+07	7,93E+07	8,89E+07	9,87E+07	1,09E+08	1,19E+08	1,30E+08	1,41E+08	1,53E+08
2,15E+07	2,83E+07	3,54E+07	4,28E+07	5,04E+07	5,81E+07	6,59E+07	7,39E+07	8,20E+07	9,04E+07	9,90E+07	1,08E+08	1,17E+08	1,27E+08
1,51E+07	1,98E+07	2,48E+07	3,00E+07	3,53E+07	4,07E+07	4,62E+07	5,18E+07	5,75E+07	6,34E+07	6,94E+07	7,57E+07	8,21E+07	8,89E+07

Step 25	Step 26	Step 27	Step 28	Step 29	Step 30	Step 31	Step 32	Step 33	Step 34	Step 35	Step 36	Step 37
1,95	2,05	2,15	2,25	2,35	2,4	2,45	2,5	2,55	2,6	2,65	2,7	2,75
3,20E+07	3,68E+07	4,22E+07	4,83E+07	5,56E+07	5,96E+07	6,35E+07	6,71E+07	6,95E+07	7,03E+07	7,50E+07	1,08E+08	1,58E+08
5,12E+07	5,90E+07	6,76E+07	7,74E+07	8,90E+07	9,55E+07	1,02E+08	1,09E+08	1,14E+08	1,15E+08	1,18E+08	1,58E+08	2,18E+08
7,01E+07	8,08E+07	9,26E+07	1,06E+08	1,22E+08	1,31E+08	1,41E+08	1,50E+08	1,58E+08	1,60E+08	1,60E+08	1,97E+08	2,60E+08
9,34E+07	1,08E+08	1,23E+08	1,41E+08	1,63E+08	1,75E+08	1,88E+08	2,02E+08	2,13E+08	2,15E+08	2,10E+08	2,42E+08	3,02E+08
1,16E+08	1,33E+08	1,53E+08	1,75E+08	2,02E+08	2,17E+08	2,34E+08	2,52E+08	2,67E+08	2,69E+08	2,57E+08	2,79E+08	3,32E+08
1,40E+08	1,61E+08	1,85E+08	2,12E+08	2,43E+08	2,62E+08	2,83E+08	3,06E+08	3,24E+08	3,26E+08	3,06E+08	3,15E+08	3,57E+08
1,65E+08	1,90E+08	2,18E+08	2,49E+08	2,87E+08	3,09E+08	3,34E+08	3,62E+08	3,85E+08	3,86E+08	3,54E+08	3,46E+08	3,73E+08
1,88E+08	2,17E+08	2,49E+08	2,85E+08	3,28E+08	3,53E+08	3,83E+08	4,15E+08	4,42E+08	4,41E+08	3,99E+08	3,72E+08	3,81E+08
2,13E+08	2,46E+08	2,82E+08	3,23E+08	3,72E+08	4,01E+08	4,35E+08	4,73E+08	5,04E+08	5,01E+08	4,43E+08	3,91E+08	3,76E+08
2,34E+08	2,70E+08	3,10E+08	3,55E+08	4,09E+08	4,41E+08	4,79E+08	5,22E+08	5,56E+08	5,51E+08	4,78E+08	4,00E+08	3,61E+08
2,57E+08	2,96E+08	3,40E+08	3,89E+08	4,48E+08	4,84E+08	5,26E+08	5,74E+08	6,12E+08	6,02E+08	5,10E+08	3,99E+08	3,27E+08
2,72E+08	3,13E+08	3,59E+08	4,12E+08	4,74E+08	5,12E+08	5,57E+08	6,09E+08	6,49E+08	6,35E+08	5,26E+08	3,86E+08	2,86E+08
2,81E+08	3,24E+08	3,72E+08	4,26E+08	4,91E+08	5,30E+08	5,78E+08	6,33E+08	6,74E+08	6,56E+08	5,27E+08	3,56E+08	2,25E+08
2,96E+08	3,41E+08	3,92E+08	4,49E+08	5,17E+08	5,59E+08	6,09E+08	6,68E+08	7,12E+08	6,88E+08	5,39E+08	3,35E+08	1,72E+08
2,99E+08	3,45E+08	3,96E+08	4,54E+08	5,23E+08	5,65E+08	6,17E+08	6,78E+08	7,22E+08	6,92E+08	5,25E+08	2,93E+08	1,05E+08
3,08E+08	3,54E+08	4,07E+08	4,66E+08	5,37E+08	5,81E+08	6,35E+08	6,98E+08	7,43E+08	7,07E+08	5,18E+08	2,50E+08	3,44E+07
3,09E+08	3,56E+08	4,08E+08	4,68E+08	5,40E+08	5,84E+08	6,39E+08	7,04E+08	7,49E+08	7,05E+08	4,96E+08	1,97E+08	-6,95E+07
3,02E+08	3,49E+08	4,00E+08	4,58E+08	5,29E+08	5,72E+08	6,27E+08	6,92E+08	7,35E+08	6,85E+08	4,59E+08	1,34E+08	-1,58E+08
2,91E+08	3,35E+08	3,85E+08	4,41E+08	5,09E+08	5,51E+08	6,05E+08	6,68E+08	7,09E+08	6,54E+08	4,19E+08	8,01E+07	-2,28E+08
2,83E+08	3,26E+08	3,74E+08	4,29E+08	4,95E+08	5,36E+08	5,89E+08	6,52E+08	6,91E+08	6,30E+08	3,80E+08	1,81E+07	-3,14E+08
2,69E+08	3,10E+08	3,56E+08	4,08E+08	4,71E+08	5,11E+08	5,62E+08	6,23E+08	6,60E+08	5,95E+08	3,37E+08	-4,16E+07	-3,81E+08
2,48E+08	2,86E+08	3,28E+08	3,76E+08	4,35E+08	4,72E+08	5,20E+08	5,77E+08	6,10E+08	5,42E+08	2,84E+08	-9,38E+07	-4,38E+08
2,28E+08	2,63E+08	3,01E+08	3,45E+08	3,99E+08	4,33E+08	4,78E+08	5,32E+08	5,61E+08	4,92E+08	2,37E+08	-1,35E+08	-4,75E+08
2,04E+08	2,35E+08	2,70E+08	3,09E+08	3,57E+08	3,88E+08	4,29E+08	4,78E+08	5,04E+08	4,36E+08	1,90E+08	-1,68E+08	-4,97E+08
1,77E+08	2,04E+08	2,34E+08	2,69E+08	3,11E+08	3,38E+08	3,74E+08	4,17E+08	4,39E+08	3,74E+08	1,46E+08	-1,87E+08	-4,93E+08
1,47E+08	1,70E+08	1,95E+08	2,23E+08	2,58E+08	2,81E+08	3,11E+08	3,48E+08	3,66E+08	3,07E+08	1,06E+08	-1,87E+08	-4,58E+08
1,03E+08	1,19E+08	1,37E+08	1,57E+08	1,81E+08	1,97E+08	2,19E+08	2,45E+08	2,57E+08	2,12E+08	6,01E+07	-1,62E+08	-3,67E+08

Step 38	Step 39	Step 40	Step 41	Step 42
2,8	2,85	2,9	2,95	3
1,89E+08	1,85E+08	1,61E+08	1,31E+08	1,02E+08
2,56E+08	2,49E+08	2,11E+08	1,65E+08	1,22E+08
2,99E+08	2,85E+08	2,35E+08	1,74E+08	1,18E+08
3,40E+08	3,18E+08	2,52E+08	1,73E+08	1,03E+08
3,65E+08	3,33E+08	2,52E+08	1,57E+08	7,42E+07
3,82E+08	3,40E+08	2,43E+08	1,30E+08	3,45E+07
3,86E+08	3,31E+08	2,17E+08	8,65E+07	-3,59E+07
3,81E+08	3,13E+08	1,83E+08	3,65E+07	-8,64E+07
3,58E+08	2,73E+08	1,24E+08	-4,62E+07	-1,73E+08
3,23E+08	2,23E+08	6,00E+07	-1,23E+08	-2,62E+08
2,64E+08	1,44E+08	-5,03E+07	-2,35E+08	-3,81E+08
1,99E+08	6,71E+07	-1,39E+08	-3,40E+08	-4,88E+08
1,14E+08	-6,85E+07	-2,56E+08	-4,63E+08	-6,09E+08
4,44E+07	-1,54E+08	-3,69E+08	-5,86E+08	-7,34E+08
-8,37E+07	-2,64E+08	-4,87E+08	-7,04E+08	-8,47E+08
-1,85E+08	-3,91E+08	-6,25E+08	-8,47E+08	-9,86E+08
-2,96E+08	-5,20E+08	-7,61E+08	-9,83E+08	-1,11E+09
-4,12E+08	-6,49E+08	-8,90E+08	-1,11E+09	-1,23E+09
-4,99E+08	-7,42E+08	-9,80E+08	-1,19E+09	-1,29E+09
-6,08E+08	-8,62E+08	-1,10E+09	-1,30E+09	-1,39E+09
-6,89E+08	-9,48E+08	-1,18E+09	-1,37E+09	-1,45E+09
-7,50E+08	-1,01E+09	-1,22E+09	-1,40E+09	-1,46E+09
-7,87E+08	-1,04E+09	-1,24E+09	-1,40E+09	-1,45E+09
-7,99E+08	-1,04E+09	-1,22E+09	-1,36E+09	-1,40E+09
-7,76E+08	-9,94E+08	-1,16E+09	-1,28E+09	-1,31E+09
-7,09E+08	-8,99E+08	-1,04E+09	-1,14E+09	-1,16E+09
-5,58E+08	-7,01E+08	-8,04E+08	-8,74E+08	-8,82E+08

MIN	MAX
-3,8210E+06	1,8852E+08
-6,0562E+06	2,5632E+08
-8,2352E+06	2,9917E+08
-1,0898E+07	3,3996E+08
-1,3445E+07	3,6481E+08
-1,6168E+07	3,8228E+08
-3,5895E+07	3,8619E+08
-8,6416E+07	4,4184E+08
-1,7277E+08	5,0384E+08
-2,6160E+08	5,5587E+08
-3,8087E+08	6,1183E+08
-4,8838E+08	6,4896E+08
-6,0924E+08	6,7446E+08
-7,3391E+08	7,1193E+08
-8,4699E+08	7,2156E+08
-9,8573E+08	7,4337E+08
-1,1136E+09	7,4858E+08
-1,2250E+09	7,3511E+08
-1,2924E+09	7,0926E+08
-1,3914E+09	6,9093E+08
-1,4479E+09	6,6015E+08
-1,4617E+09	6,1011E+08
-1,4505E+09	5,6128E+08
-1,4041E+09	5,0384E+08
-1,3110E+09	4,3887E+08
-1,1601E+09	3,6553E+08
-8,8153E+08	2,5721E+08

Result - Principal stress (Abs)

The influence lines for Submodel 3A, for each node at the U-sape. Maximum principal stress 1461.7 MPa (compression) at node 22 in load step 3 m.

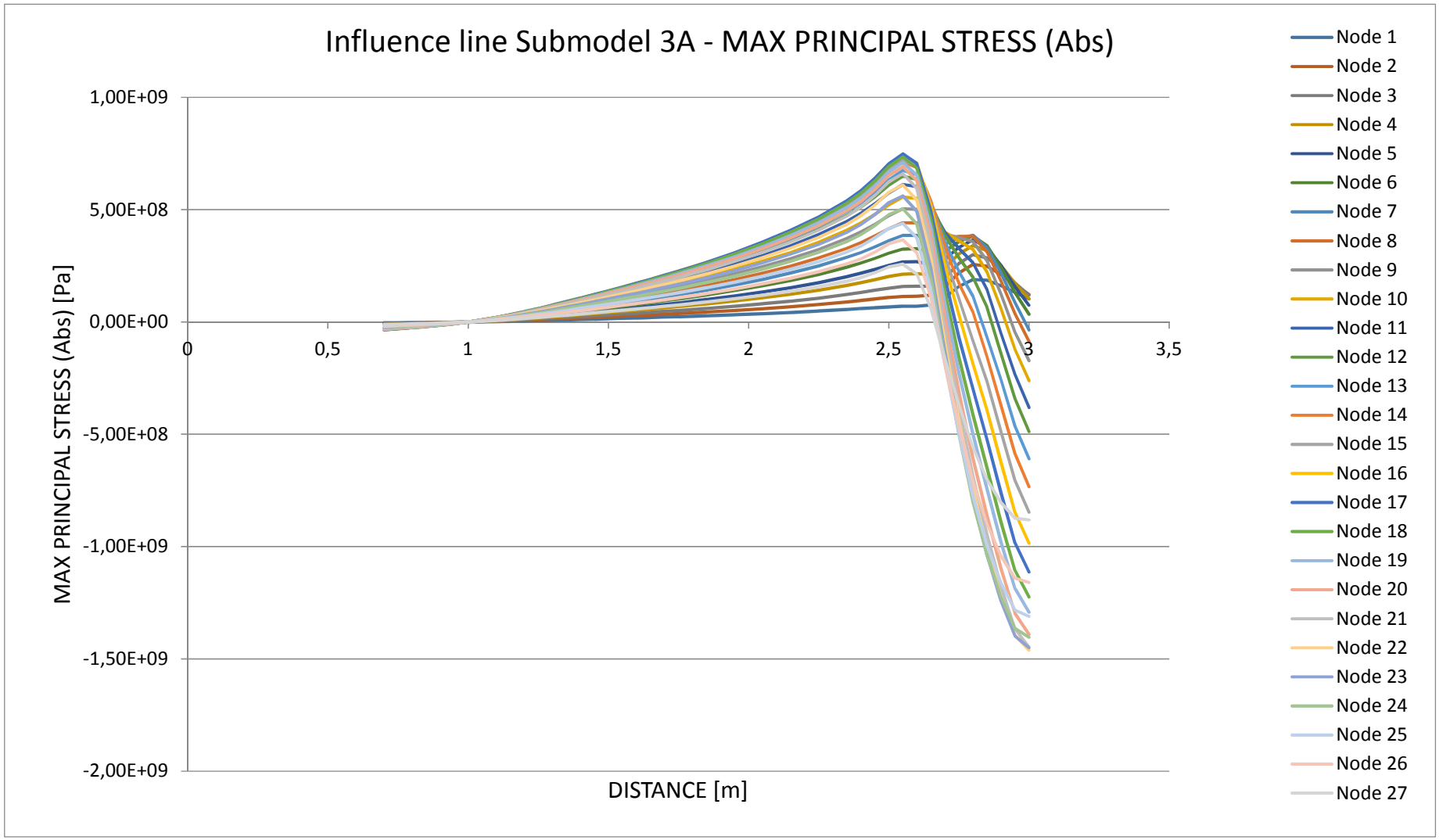

SUBMODEL 3 A

MISES STRESS

		Step 1	Step 2	Step 3	Step 4	Step 5	Step 6	Step 7	Step 8	Step 9	Step 10
Node	Distance	0,7	0,75	0,8	0,85	0,9	0,95	1	1,05	1,1	1,15
1	0	3,92E+06	3,38E+06	2,84E+06	2,27E+06	1,64E+06	9,28E+05	1,43E+05	9,02E+05	2,02E+06	3,29E+06
2	0,00604	5,79E+06	4,99E+06	4,19E+06	3,34E+06	2,42E+06	1,35E+06	1,67E+05	1,36E+06	3,03E+06	4,92E+06
3	0,01208	7,69E+06	6,63E+06	5,55E+06	4,43E+06	3,19E+06	1,77E+06	1,73E+05	1,84E+06	4,08E+06	6,60E+06
4	0,01812	9,85E+06	8,49E+06	7,11E+06	5,67E+06	4,07E+06	2,24E+06	1,75E+05	2,41E+06	5,29E+06	8,55E+06
5	0,02416	1,21E+07	1,04E+07	8,72E+06	6,95E+06	4,99E+06	2,73E+06	1,69E+05	3,01E+06	6,56E+06	1,06E+07
6	0,0302	1,45E+07	1,25E+07	1,05E+07	8,32E+06	5,97E+06	3,25E+06	1,65E+05	3,66E+06	7,94E+06	1,28E+07
7	0,03624	1,67E+07	1,44E+07	1,20E+07	9,56E+06	6,85E+06	3,71E+06	1,55E+05	4,24E+06	9,18E+06	1,48E+07
8	0,04228	1,92E+07	1,65E+07	1,38E+07	1,10E+07	7,85E+06	4,24E+06	1,52E+05	4,92E+06	1,06E+07	1,70E+07
9	0,04832	2,13E+07	1,83E+07	1,53E+07	1,22E+07	8,70E+06	4,69E+06	1,46E+05	5,50E+06	1,18E+07	1,90E+07
10	0,05436	2,35E+07	2,02E+07	1,69E+07	1,34E+07	9,60E+06	5,16E+06	1,51E+05	6,12E+06	1,31E+07	2,10E+07
11	0,0604	2,53E+07	2,17E+07	1,82E+07	1,44E+07	1,03E+07	5,53E+06	1,52E+05	6,61E+06	1,42E+07	2,27E+07
12	0,06644	2,66E+07	2,28E+07	1,91E+07	1,52E+07	1,08E+07	5,80E+06	1,64E+05	6,98E+06	1,49E+07	2,39E+07
13	0,07248	2,71E+07	2,33E+07	1,95E+07	1,55E+07	1,10E+07	5,90E+06	1,67E+05	7,14E+06	1,52E+07	2,44E+07
14	0,07852	2,83E+07	2,44E+07	2,04E+07	1,62E+07	1,15E+07	6,17E+06	1,82E+05	7,51E+06	1,60E+07	2,56E+07
15	0,08456	2,84E+07	2,44E+07	2,04E+07	1,62E+07	1,16E+07	6,18E+06	1,86E+05	7,55E+06	1,61E+07	2,57E+07
16	0,0906	2,95E+07	2,54E+07	2,12E+07	1,69E+07	1,20E+07	6,40E+06	2,01E+05	7,86E+06	1,67E+07	2,67E+07
17	0,09664	2,98E+07	2,56E+07	2,14E+07	1,70E+07	1,21E+07	6,45E+06	2,07E+05	7,94E+06	1,69E+07	2,70E+07
18	0,10268	2,93E+07	2,52E+07	2,10E+07	1,67E+07	1,19E+07	6,34E+06	2,12E+05	7,83E+06	1,67E+07	2,66E+07
19	0,10872	2,82E+07	2,42E+07	2,02E+07	1,61E+07	1,15E+07	6,09E+06	2,07E+05	7,54E+06	1,60E+07	2,56E+07
20	0,11476	2,78E+07	2,39E+07	2,00E+07	1,59E+07	1,13E+07	6,01E+06	2,11E+05	7,47E+06	1,59E+07	2,53E+07
21	0,1208	2,64E+07	2,27E+07	1,89E+07	1,51E+07	1,07E+07	5,70E+06	2,03E+05	7,09E+06	1,50E+07	2,40E+07
22	0,12684	2,47E+07	2,13E+07	1,78E+07	1,41E+07	1,01E+07	5,34E+06	1,96E+05	6,66E+06	1,41E+07	2,26E+07
23	0,13288	2,27E+07	1,95E+07	1,63E+07	1,30E+07	9,24E+06	4,91E+06	1,81E+05	6,12E+06	1,30E+07	2,07E+07
24	0,13892	2,06E+07	1,77E+07	1,48E+07	1,18E+07	8,38E+06	4,45E+06	1,67E+05	5,56E+06	1,18E+07	1,88E+07
25	0,14496	1,80E+07	1,55E+07	1,30E+07	1,03E+07	7,34E+06	3,90E+06	1,47E+05	4,87E+06	1,03E+07	1,65E+07
26	0,151	1,52E+07	1,31E+07	1,09E+07	8,69E+06	6,18E+06	3,28E+06	1,26E+05	4,11E+06	8,71E+06	1,39E+07
27	0,15704	1,13E+07	9,69E+06	8,10E+06	6,44E+06	4,59E+06	2,43E+06	9,39E+04	3,04E+06	6,46E+06	1,03E+07

Step 11	Step 12	Step 13	Step 14	Step 15	Step 16	Step 17	Step 18	Step 19	Step 20	Step 21	Step 22	Step 23	Step 24
1,2	1,25	1,3	1,35	1,4	1,45	1,5	1,55	1,6	1,65	1,7	1,75	1,8	1,85
4,70E+06	6,22E+06	7,84E+06	9,52E+06	1,12E+07	1,30E+07	1,48E+07	1,66E+07	1,84E+07	2,03E+07	2,23E+07	2,43E+07	2,64E+07	2,85E+07
7,00E+06	9,27E+06	1,17E+07	1,42E+07	1,67E+07	1,93E+07	2,19E+07	2,46E+07	2,74E+07	3,02E+07	3,31E+07	3,61E+07	3,92E+07	4,24E+07
9,38E+06	1,24E+07	1,56E+07	1,89E+07	2,23E+07	2,58E+07	2,93E+07	3,29E+07	3,66E+07	4,03E+07	4,42E+07	4,82E+07	5,23E+07	5,66E+07
1,21E+07	1,60E+07	2,02E+07	2,44E+07	2,88E+07	3,33E+07	3,78E+07	4,24E+07	4,71E+07	5,19E+07	5,69E+07	6,21E+07	6,74E+07	7,29E+07
1,50E+07	1,98E+07	2,49E+07	3,01E+07	3,55E+07	4,10E+07	4,66E+07	5,22E+07	5,80E+07	6,40E+07	7,01E+07	7,64E+07	8,30E+07	8,98E+07
1,81E+07	2,39E+07	3,00E+07	3,63E+07	4,28E+07	4,94E+07	5,61E+07	6,29E+07	6,99E+07	7,71E+07	8,45E+07	9,21E+07	9,99E+07	1,08E+08
2,09E+07	2,76E+07	3,46E+07	4,19E+07	4,94E+07	5,70E+07	6,47E+07	7,26E+07	8,06E+07	8,89E+07	9,74E+07	1,06E+08	1,15E+08	1,25E+08
2,41E+07	3,18E+07	4,00E+07	4,84E+07	5,70E+07	6,57E+07	7,46E+07	8,37E+07	9,29E+07	1,02E+08	1,12E+08	1,22E+08	1,33E+08	1,44E+08
2,69E+07	3,54E+07	4,45E+07	5,38E+07	6,34E+07	7,31E+07	8,30E+07	9,30E+07	1,03E+08	1,14E+08	1,25E+08	1,36E+08	1,48E+08	1,60E+08
2,98E+07	3,92E+07	4,92E+07	5,96E+07	7,02E+07	8,09E+07	9,18E+07	1,03E+08	1,14E+08	1,26E+08	1,38E+08	1,50E+08	1,63E+08	1,77E+08
3,21E+07	4,23E+07	5,30E+07	6,42E+07	7,56E+07	8,71E+07	9,89E+07	1,11E+08	1,23E+08	1,36E+08	1,49E+08	1,62E+08	1,76E+08	1,90E+08
3,38E+07	4,45E+07	5,59E+07	6,76E+07	7,96E+07	9,18E+07	1,04E+08	1,17E+08	1,30E+08	1,43E+08	1,57E+08	1,71E+08	1,85E+08	2,00E+08
3,45E+07	4,54E+07	5,70E+07	6,90E+07	8,12E+07	9,36E+07	1,06E+08	1,19E+08	1,32E+08	1,46E+08	1,60E+08	1,74E+08	1,89E+08	2,04E+08
3,62E+07	4,77E+07	5,98E+07	7,24E+07	8,52E+07	9,82E+07	1,11E+08	1,25E+08	1,39E+08	1,53E+08	1,67E+08	1,82E+08	1,98E+08	2,14E+08
3,64E+07	4,79E+07	6,01E+07	7,26E+07	8,55E+07	9,86E+07	1,12E+08	1,25E+08	1,39E+08	1,53E+08	1,68E+08	1,83E+08	1,99E+08	2,15E+08
3,78E+07	4,98E+07	6,24E+07	7,55E+07	8,89E+07	1,02E+08	1,16E+08	1,30E+08	1,45E+08	1,59E+08	1,75E+08	1,90E+08	2,07E+08	2,24E+08
3,82E+07	5,03E+07	6,30E+07	7,62E+07	8,97E+07	1,03E+08	1,17E+08	1,31E+08	1,46E+08	1,61E+08	1,76E+08	1,92E+08	2,09E+08	2,26E+08
3,76E+07	4,95E+07	6,21E+07	7,51E+07	8,84E+07	1,02E+08	1,16E+08	1,30E+08	1,44E+08	1,59E+08	1,74E+08	1,89E+08	2,05E+08	2,22E+08
3,62E+07	4,77E+07	5,98E+07	7,23E+07	8,50E+07	9,80E+07	1,11E+08	1,25E+08	1,38E+08	1,53E+08	1,67E+08	1,82E+08	1,98E+08	2,14E+08
3,58E+07	4,71E+07	5,91E+07	7,14E+07	8,41E+07	9,69E+07	1,10E+08	1,23E+08	1,37E+08	1,51E+08	1,65E+08	1,80E+08	1,95E+08	2,11E+08
3,40E+07	4,47E+07	5,60E+07	6,78E+07	7,97E+07	9,19E+07	1,04E+08	1,17E+08	1,30E+08	1,43E+08	1,57E+08	1,71E+08	1,85E+08	2,01E+08
3,19E+07	4,20E+07	5,26E+07	6,36E+07	7,49E+07	8,63E+07	9,79E+07	1,10E+08	1,22E+08	1,34E+08	1,47E+08	1,60E+08	1,74E+08	1,88E+08
2,93E+07	3,86E+07	4,84E+07	5,85E+07	6,88E+07	7,93E+07	9,00E+07	1,01E+08	1,12E+08	1,23E+08	1,35E+08	1,47E+08	1,60E+08	1,73E+08
2,66E+07	3,50E+07	4,39E+07	5,31E+07	6,24E+07	7,20E+07	8,16E+07	9,15E+07	1,02E+08	1,12E+08	1,23E+08	1,34E+08	1,45E+08	1,57E+08
2,33E+07	3,07E+07	3,84E+07	4,65E+07	5,47E+07	6,31E+07	7,15E+07	8,02E+07	8,90E+07	9,81E+07	1,07E+08	1,17E+08	1,27E+08	1,38E+08
1,96E+07	2,59E+07	3,24E+07	3,92E+07	4,61E+07	5,32E+07	6,03E+07	6,76E+07	7,51E+07	8,28E+07	9,06E+07	9,88E+07	1,07E+08	1,16E+08
1,46E+07	1,92E+07	2,40E+07	2,91E+07	3,42E+07	3,94E+07	4,47E+07	5,01E+07	5,57E+07	6,14E+07	6,72E+07	7,33E+07	7,95E+07	8,60E+07

Step 25	Step 26	Step 27	Step 28	Step 29	Step 30	Step 31	Step 32	Step 33	Step 34	Step 35	Step 36	Step 37
1,95	2,05	2,15	2,25	2,35	2,4	2,45	2,5	2,55	2,6	2,65	2,7	2,75
3,31E+07	3,81E+07	4,37E+07	5,00E+07	5,74E+07	6,16E+07	6,59E+07	6,99E+07	7,29E+07	7,41E+07	7,81E+07	1,08E+08	1,53E+08
4,92E+07	5,66E+07	6,49E+07	7,43E+07	8,54E+07	9,17E+07	9,83E+07	1,05E+08	1,10E+08	1,11E+08	1,14E+08	1,49E+08	2,03E+08
6,56E+07	7,56E+07	8,67E+07	9,93E+07	1,14E+08	1,23E+08	1,32E+08	1,41E+08	1,48E+08	1,50E+08	1,50E+08	1,84E+08	2,40E+08
8,46E+07	9,75E+07	1,12E+08	1,28E+08	1,47E+08	1,58E+08	1,70E+08	1,83E+08	1,93E+08	1,95E+08	1,91E+08	2,19E+08	2,73E+08
1,04E+08	1,20E+08	1,38E+08	1,58E+08	1,81E+08	1,95E+08	2,11E+08	2,27E+08	2,40E+08	2,42E+08	2,32E+08	2,52E+08	3,00E+08
1,26E+08	1,45E+08	1,66E+08	1,90E+08	2,19E+08	2,35E+08	2,54E+08	2,75E+08	2,92E+08	2,93E+08	2,75E+08	2,83E+08	3,21E+08
1,45E+08	1,67E+08	1,91E+08	2,19E+08	2,52E+08	2,72E+08	2,94E+08	3,18E+08	3,38E+08	3,39E+08	3,13E+08	3,07E+08	3,33E+08
1,67E+08	1,92E+08	2,20E+08	2,53E+08	2,91E+08	3,13E+08	3,39E+08	3,68E+08	3,92E+08	3,92E+08	3,54E+08	3,30E+08	3,39E+08
1,85E+08	2,14E+08	2,45E+08	2,81E+08	3,23E+08	3,48E+08	3,78E+08	4,11E+08	4,38E+08	4,36E+08	3,87E+08	3,44E+08	3,34E+08
2,05E+08	2,36E+08	2,71E+08	3,11E+08	3,58E+08	3,86E+08	4,19E+08	4,56E+08	4,86E+08	4,82E+08	4,19E+08	3,52E+08	3,19E+08
2,21E+08	2,55E+08	2,92E+08	3,35E+08	3,85E+08	4,16E+08	4,52E+08	4,93E+08	5,26E+08	5,18E+08	4,42E+08	3,51E+08	2,95E+08
2,33E+08	2,68E+08	3,08E+08	3,52E+08	4,06E+08	4,38E+08	4,77E+08	5,21E+08	5,56E+08	5,44E+08	4,51E+08	3,33E+08	2,50E+08
2,37E+08	2,73E+08	3,14E+08	3,59E+08	4,14E+08	4,47E+08	4,87E+08	5,33E+08	5,68E+08	5,53E+08	4,48E+08	3,09E+08	2,06E+08
2,49E+08	2,87E+08	3,29E+08	3,77E+08	4,34E+08	4,69E+08	5,12E+08	5,61E+08	5,98E+08	5,78E+08	4,54E+08	2,85E+08	1,54E+08
2,50E+08	2,88E+08	3,30E+08	3,79E+08	4,36E+08	4,71E+08	5,15E+08	5,65E+08	6,02E+08	5,77E+08	4,39E+08	2,48E+08	9,82E+07
2,60E+08	2,99E+08	3,43E+08	3,93E+08	4,53E+08	4,90E+08	5,36E+08	5,89E+08	6,27E+08	5,97E+08	4,39E+08	2,17E+08	5,03E+07
2,62E+08	3,02E+08	3,46E+08	3,97E+08	4,58E+08	4,95E+08	5,42E+08	5,97E+08	6,35E+08	5,98E+08	4,22E+08	1,72E+08	6,37E+07
2,58E+08	2,97E+08	3,41E+08	3,91E+08	4,51E+08	4,88E+08	5,35E+08	5,90E+08	6,27E+08	5,85E+08	3,94E+08	1,21E+08	1,31E+08
2,48E+08	2,86E+08	3,28E+08	3,76E+08	4,34E+08	4,70E+08	5,16E+08	5,70E+08	6,05E+08	5,59E+08	3,59E+08	7,56E+07	1,93E+08
2,46E+08	2,83E+08	3,25E+08	3,72E+08	4,29E+08	4,65E+08	5,11E+08	5,66E+08	6,00E+08	5,48E+08	3,34E+08	3,21E+07	2,58E+08
2,33E+08	2,68E+08	3,08E+08	3,53E+08	4,07E+08	4,42E+08	4,86E+08	5,39E+08	5,71E+08	5,14E+08	2,93E+08	3,95E+07	3,26E+08
2,19E+08	2,52E+08	2,89E+08	3,31E+08	3,83E+08	4,15E+08	4,57E+08	5,08E+08	5,37E+08	4,78E+08	2,54E+08	7,57E+07	3,72E+08
2,01E+08	2,32E+08	2,66E+08	3,05E+08	3,52E+08	3,82E+08	4,22E+08	4,69E+08	4,95E+08	4,35E+08	2,14E+08	1,13E+08	4,08E+08
1,82E+08	2,10E+08	2,41E+08	2,76E+08	3,19E+08	3,47E+08	3,83E+08	4,27E+08	4,50E+08	3,91E+08	1,77E+08	1,38E+08	4,25E+08
1,60E+08	1,84E+08	2,11E+08	2,42E+08	2,80E+08	3,05E+08	3,37E+08	3,76E+08	3,96E+08	3,39E+08	1,37E+08	1,60E+08	4,30E+08
1,35E+08	1,55E+08	1,78E+08	2,04E+08	2,36E+08	2,57E+08	2,85E+08	3,18E+08	3,34E+08	2,83E+08	1,05E+08	1,58E+08	3,99E+08
9,99E+07	1,15E+08	1,32E+08	1,52E+08	1,75E+08	1,91E+08	2,12E+08	2,37E+08	2,49E+08	2,07E+08	6,75E+07	1,41E+08	3,31E+08

Step 38	Step 39	Step 40	Step 41	Step 42
2,8	2,85	2,9	2,95	3
1,80E+08	1,77E+08	1,54E+08	1,25E+08	9,88E+07
2,37E+08	2,30E+08	1,96E+08	1,53E+08	1,15E+08
2,75E+08	2,62E+08	2,17E+08	1,62E+08	1,13E+08
3,06E+08	2,86E+08	2,28E+08	1,59E+08	9,87E+07
3,29E+08	3,01E+08	2,30E+08	1,46E+08	7,51E+07
3,42E+08	3,05E+08	2,19E+08	1,21E+08	4,34E+07
3,45E+08	2,98E+08	2,00E+08	8,80E+07	2,84E+07
3,39E+08	2,79E+08	1,65E+08	4,50E+07	7,86E+07
3,20E+08	2,48E+08	1,21E+08	3,59E+07	1,40E+08
2,86E+08	2,00E+08	6,39E+07	1,07E+08	2,25E+08
2,44E+08	1,45E+08	3,54E+07	1,83E+08	3,08E+08
1,78E+08	7,26E+07	1,19E+08	2,86E+08	4,12E+08
1,21E+08	6,16E+07	1,99E+08	3,69E+08	4,92E+08
6,18E+07	1,31E+08	3,05E+08	4,84E+08	6,08E+08
8,37E+07	2,23E+08	4,05E+08	5,84E+08	7,01E+08
1,53E+08	3,23E+08	5,19E+08	7,05E+08	8,21E+08
2,49E+08	4,37E+08	6,39E+08	8,26E+08	9,36E+08
3,44E+08	5,45E+08	7,49E+08	9,32E+08	1,03E+09
4,22E+08	6,29E+08	8,29E+08	1,00E+09	1,09E+09
5,09E+08	7,27E+08	9,30E+08	1,10E+09	1,18E+09
5,91E+08	8,13E+08	1,01E+09	1,17E+09	1,24E+09
6,42E+08	8,64E+08	1,05E+09	1,21E+09	1,26E+09
6,78E+08	8,95E+08	1,07E+09	1,21E+09	1,26E+09
6,89E+08	8,97E+08	1,06E+09	1,19E+09	1,22E+09
6,81E+08	8,74E+08	1,02E+09	1,13E+09	1,16E+09
6,22E+08	7,92E+08	9,20E+08	1,01E+09	1,03E+09
5,07E+08	6,40E+08	7,38E+08	8,04E+08	8,14E+08

MIN	MAX
1,43E+05	1,80E+08
1,67E+05	2,37E+08
1,73E+05	2,75E+08
1,75E+05	3,06E+08
1,69E+05	3,29E+08
1,65E+05	3,42E+08
1,55E+05	3,45E+08
1,52E+05	3,92E+08
1,46E+05	4,38E+08
1,51E+05	4,86E+08
1,52E+05	5,26E+08
1,64E+05	5,56E+08
1,67E+05	5,68E+08
1,82E+05	6,08E+08
1,86E+05	7,01E+08
2,01E+05	8,21E+08
2,07E+05	9,36E+08
2,12E+05	1,03E+09
2,07E+05	1,09E+09
2,11E+05	1,18E+09
2,03E+05	1,24E+09
1,96E+05	1,26E+09
1,81E+05	1,26E+09
1,67E+05	1,22E+09
1,47E+05	1,16E+09
1,26E+05	1,03E+09
9,39E+04	8,14E+08

Result - Mises stress

The influence lines for Submodel 3A, for each node at the U-sape. Maximum Mises stress 1263.5 MPa at node 22 in load step 3 m.

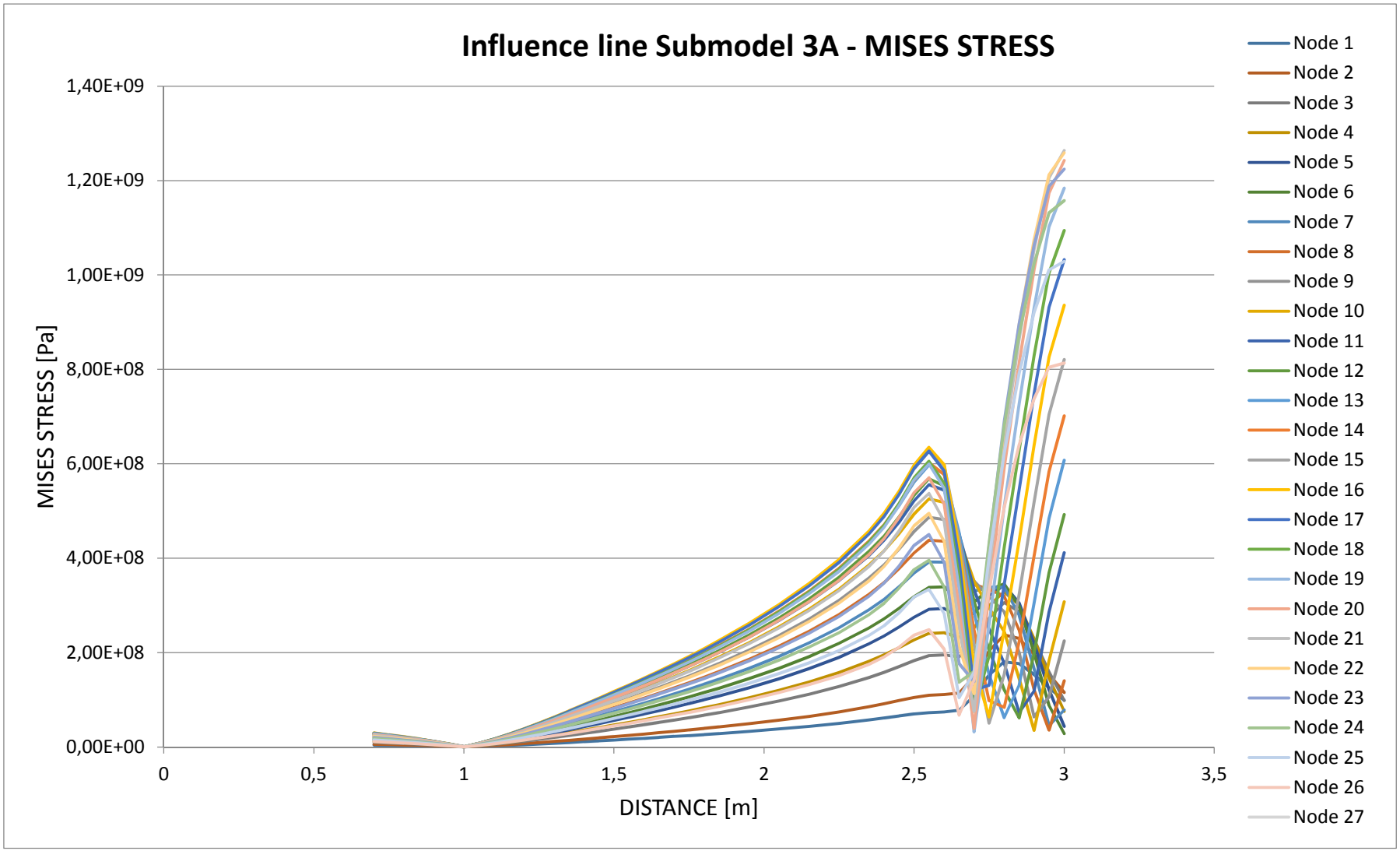

SUBMODEL 3B

MAX PRINCIPAL STRESS (Abs)

		Step 1	Step 2	Step 3	Step 4	Step 5	Step 6	Step 7	Step 8	Step 9	Step 10
Node	Distance	0,7	0,75	0,8	0,85	0,9	0,95	1	1,05	1,1	1,15
1	0	4,95E+06	4,25E+06	3,54E+06	2,81E+06	1,98E+06	1,01E+06	-1,31E+05	-1,47E+06	-3,02E+06	-4,76E+06
2	0,00604	7,94E+06	6,81E+06	5,68E+06	4,50E+06	3,18E+06	1,64E+06	-1,75E+05	-2,30E+06	-4,76E+06	-7,54E+06
3	0,01208	1,03E+07	8,87E+06	7,41E+06	5,87E+06	4,15E+06	2,15E+06	-1,98E+05	-2,95E+06	-6,14E+06	-9,74E+06
4	0,01812	1,30E+07	1,12E+07	9,31E+06	7,39E+06	5,23E+06	2,73E+06	-2,15E+05	-3,66E+06	-7,65E+06	-1,21E+07
5	0,02416	1,56E+07	1,34E+07	1,12E+07	8,87E+06	6,29E+06	3,29E+06	-2,24E+05	-4,34E+06	-9,10E+06	-1,45E+07
6	0,0302	1,82E+07	1,56E+07	1,30E+07	1,04E+07	7,35E+06	3,86E+06	-2,30E+05	-5,02E+06	-1,06E+07	-1,68E+07
7	0,03624	2,09E+07	1,79E+07	1,50E+07	1,19E+07	8,46E+06	4,46E+06	-2,29E+05	-5,72E+06	-1,21E+07	-1,92E+07
8	0,04228	2,33E+07	2,00E+07	1,67E+07	1,33E+07	9,45E+06	5,00E+06	-2,27E+05	-6,34E+06	-1,34E+07	-2,14E+07
9	0,04832	2,60E+07	2,23E+07	1,87E+07	1,48E+07	1,06E+07	5,60E+06	-2,19E+05	-7,01E+06	-1,49E+07	-2,37E+07
10	0,05436	2,80E+07	2,40E+07	2,01E+07	1,60E+07	1,14E+07	6,04E+06	-2,12E+05	-7,51E+06	-1,59E+07	-2,55E+07
11	0,0604	2,95E+07	2,54E+07	2,12E+07	1,69E+07	1,20E+07	6,39E+06	-1,98E+05	-7,89E+06	-1,68E+07	-2,68E+07
12	0,06644	3,15E+07	2,71E+07	2,26E+07	1,80E+07	1,28E+07	6,83E+06	-1,91E+05	-8,38E+06	-1,78E+07	-2,85E+07
13	0,07248	3,29E+07	2,83E+07	2,37E+07	1,88E+07	1,34E+07	7,16E+06	-1,78E+05	-8,73E+06	-1,86E+07	-2,98E+07
14	0,07852	3,37E+07	2,90E+07	2,43E+07	1,93E+07	1,37E+07	7,35E+06	-1,67E+05	-8,91E+06	-1,90E+07	-3,04E+07
15	0,08456	3,36E+07	2,88E+07	2,41E+07	1,92E+07	1,37E+07	7,32E+06	-1,54E+05	-8,83E+06	-1,89E+07	-3,02E+07
16	0,0906	3,45E+07	2,96E+07	2,48E+07	1,97E+07	1,41E+07	7,53E+06	-1,47E+05	-9,06E+06	-1,94E+07	-3,10E+07
17	0,09664	3,45E+07	2,97E+07	2,48E+07	1,97E+07	1,41E+07	7,55E+06	-1,37E+05	-9,05E+06	-1,94E+07	-3,10E+07
18	0,10268	3,37E+07	2,90E+07	2,42E+07	1,92E+07	1,37E+07	7,37E+06	-1,28E+05	-8,81E+06	-1,89E+07	-3,02E+07
19	0,10872	3,24E+07	2,78E+07	2,33E+07	1,85E+07	1,32E+07	7,09E+06	-1,20E+05	-8,45E+06	-1,81E+07	-2,90E+07
20	0,11476	3,13E+07	2,69E+07	2,25E+07	1,79E+07	1,28E+07	6,85E+06	-1,14E+05	-8,15E+06	-1,75E+07	-2,80E+07
21	0,1208	2,94E+07	2,53E+07	2,12E+07	1,68E+07	1,20E+07	6,45E+06	-1,07E+05	-7,66E+06	-1,64E+07	-2,63E+07
22	0,12684	2,74E+07	2,36E+07	1,97E+07	1,57E+07	1,12E+07	6,01E+06	-1,01E+05	-7,13E+06	-1,53E+07	-2,45E+07
23	0,13288	2,54E+07	2,18E+07	1,82E+07	1,45E+07	1,04E+07	5,56E+06	-9,47E+04	-6,58E+06	-1,41E+07	-2,26E+07
24	0,13892	2,25E+07	1,93E+07	1,61E+07	1,28E+07	9,17E+06	4,93E+06	-8,86E+04	-5,83E+06	-1,25E+07	-2,01E+07
25	0,14496	1,94E+07	1,67E+07	1,40E+07	1,11E+07	7,92E+06	4,26E+06	-8,12E+04	-5,03E+06	-1,08E+07	-1,73E+07
26	0,151	1,61E+07	1,39E+07	1,16E+07	9,23E+06	6,59E+06	3,55E+06	-7,30E+04	-4,18E+06	-8,99E+06	-1,44E+07
27	0,15704	1,15E+07	9,92E+06	8,29E+06	6,59E+06	4,71E+06	2,54E+06	-3,25E+03	-2,99E+06	-6,41E+06	-1,03E+07

Step 11	Step 12	Step 13	Step 14	Step 15	Step 16	Step 17	Step 18	Step 19	Step 20	Step 21	Step 22	Step 23	Step 24
1,2	1,25	1,3	1,35	1,4	1,45	1,5	1,55	1,6	1,65	1,7	1,75	1,8	1,85
-6,70E+06	-8,78E+06	-1,10E+07	-1,32E+07	-1,55E+07	-1,79E+07	-2,02E+07	-2,27E+07	-2,51E+07	-2,77E+07	-3,03E+07	-3,30E+07	-3,58E+07	-3,87E+07
-1,06E+07	-1,39E+07	-1,74E+07	-2,10E+07	-2,47E+07	-2,84E+07	-3,22E+07	-3,61E+07	-4,00E+07	-4,41E+07	-4,82E+07	-5,25E+07	-5,70E+07	-6,17E+07
-1,37E+07	-1,80E+07	-2,25E+07	-2,72E+07	-3,20E+07	-3,68E+07	-4,17E+07	-4,67E+07	-5,18E+07	-5,71E+07	-6,25E+07	-6,81E+07	-7,39E+07	-8,00E+07
-1,71E+07	-2,25E+07	-2,82E+07	-3,40E+07	-4,00E+07	-4,60E+07	-5,22E+07	-5,85E+07	-6,49E+07	-7,15E+07	-7,83E+07	-8,53E+07	-9,25E+07	-1,00E+08
-2,04E+07	-2,68E+07	-3,36E+07	-4,06E+07	-4,77E+07	-5,50E+07	-6,23E+07	-6,98E+07	-7,75E+07	-8,54E+07	-9,35E+07	-1,02E+08	-1,11E+08	-1,20E+08
-2,37E+07	-3,12E+07	-3,91E+07	-4,72E+07	-5,55E+07	-6,39E+07	-7,25E+07	-8,12E+07	-9,02E+07	-9,94E+07	-1,09E+08	-1,19E+08	-1,29E+08	-1,39E+08
-2,71E+07	-3,57E+07	-4,47E+07	-5,40E+07	-6,35E+07	-7,32E+07	-8,30E+07	-9,31E+07	-1,03E+08	-1,14E+08	-1,25E+08	-1,36E+08	-1,47E+08	-1,59E+08
-3,02E+07	-3,97E+07	-4,97E+07	-6,01E+07	-7,07E+07	-8,15E+07	-9,25E+07	-1,04E+08	-1,15E+08	-1,27E+08	-1,39E+08	-1,51E+08	-1,64E+08	-1,78E+08
-3,35E+07	-4,41E+07	-5,53E+07	-6,68E+07	-7,86E+07	-9,06E+07	-1,03E+08	-1,15E+08	-1,28E+08	-1,41E+08	-1,54E+08	-1,68E+08	-1,83E+08	-1,98E+08
-3,60E+07	-4,74E+07	-5,94E+07	-7,18E+07	-8,45E+07	-9,74E+07	-1,10E+08	-1,24E+08	-1,37E+08	-1,51E+08	-1,66E+08	-1,81E+08	-1,96E+08	-2,12E+08
-3,79E+07	-4,99E+07	-6,25E+07	-7,56E+07	-8,90E+07	-1,03E+08	-1,16E+08	-1,30E+08	-1,45E+08	-1,60E+08	-1,75E+08	-1,91E+08	-2,07E+08	-2,24E+08
-4,03E+07	-5,31E+07	-6,66E+07	-8,05E+07	-9,48E+07	-1,09E+08	-1,24E+08	-1,39E+08	-1,54E+08	-1,70E+08	-1,86E+08	-2,03E+08	-2,20E+08	-2,38E+08
-4,21E+07	-5,54E+07	-6,95E+07	-8,41E+07	-9,90E+07	-1,14E+08	-1,29E+08	-1,45E+08	-1,61E+08	-1,78E+08	-1,95E+08	-2,12E+08	-2,30E+08	-2,49E+08
-4,30E+07	-5,67E+07	-7,11E+07	-8,60E+07	-1,01E+08	-1,17E+08	-1,32E+08	-1,48E+08	-1,65E+08	-1,82E+08	-1,99E+08	-2,17E+08	-2,35E+08	-2,55E+08
-4,27E+07	-5,63E+07	-7,06E+07	-8,54E+07	-1,01E+08	-1,16E+08	-1,32E+08	-1,47E+08	-1,64E+08	-1,80E+08	-1,98E+08	-2,15E+08	-2,34E+08	-2,53E+08
-4,39E+07	-5,78E+07	-7,25E+07	-8,77E+07	-1,03E+08	-1,19E+08	-1,35E+08	-1,51E+08	-1,68E+08	-1,85E+08	-2,03E+08	-2,21E+08	-2,40E+08	-2,60E+08
-4,39E+07	-5,78E+07	-7,25E+07	-8,77E+07	-1,03E+08	-1,19E+08	-1,35E+08	-1,52E+08	-1,68E+08	-1,85E+08	-2,03E+08	-2,21E+08	-2,40E+08	-2,60E+08
-4,27E+07	-5,63E+07	-7,06E+07	-8,55E+07	-1,01E+08	-1,16E+08	-1,32E+08	-1,48E+08	-1,64E+08	-1,81E+08	-1,98E+08	-2,16E+08	-2,34E+08	-2,53E+08
-4,10E+07	-5,41E+07	-6,78E+07	-8,21E+07	-9,67E+07	-1,11E+08	-1,26E+08	-1,42E+08	-1,57E+08	-1,74E+08	-1,90E+08	-2,07E+08	-2,25E+08	-2,43E+08
-3,96E+07	-5,22E+07	-6,55E+07	-7,92E+07	-9,33E+07	-1,08E+08	-1,22E+08	-1,37E+08	-1,52E+08	-1,68E+08	-1,84E+08	-2,00E+08	-2,17E+08	-2,35E+08
-3,73E+07	-4,91E+07	-6,16E+07	-7,45E+07	-8,77E+07	-1,01E+08	-1,15E+08	-1,29E+08	-1,43E+08	-1,58E+08	-1,73E+08	-1,88E+08	-2,04E+08	-2,21E+08
-3,47E+07	-4,57E+07	-5,74E+07	-6,94E+07	-8,17E+07	-9,43E+07	-1,07E+08	-1,20E+08	-1,33E+08	-1,47E+08	-1,61E+08	-1,75E+08	-1,90E+08	-2,06E+08
-3,21E+07	-4,22E+07	-5,30E+07	-6,41E+07	-7,55E+07	-8,71E+07	-9,88E+07	-1,11E+08	-1,23E+08	-1,36E+08	-1,49E+08	-1,62E+08	-1,76E+08	-1,90E+08
-2,84E+07	-3,74E+07	-4,69E+07	-5,68E+07	-6,69E+07	-7,71E+07	-8,75E+07	-9,81E+07	-1,09E+08	-1,20E+08	-1,32E+08	-1,43E+08	-1,56E+08	-1,68E+08
-2,45E+07	-3,23E+07	-4,05E+07	-4,90E+07	-5,78E+07	-6,66E+07	-7,56E+07	-8,47E+07	-9,41E+07	-1,04E+08	-1,14E+08	-1,24E+08	-1,34E+08	-1,45E+08
-2,04E+07	-2,69E+07	-3,37E+07	-4,08E+07	-4,80E+07	-5,54E+07	-6,29E+07	-7,05E+07	-7,83E+07	-8,63E+07	-9,45E+07	-1,03E+08	-1,12E+08	-1,21E+08
-1,46E+07	-1,92E+07	-2,41E+07	-2,91E+07	-3,43E+07	-3,95E+07	-4,49E+07	-5,03E+07	-5,59E+07	-6,16E+07	-6,75E+07	-7,35E+07	-7,98E+07	-8,63E+07

Step 25	Step 26	Step 27	Step 28	Step 29	Step 30	Step 31	Step 32	Step 33	Step 34	Step 35	Step 36	Step 37	Step 38
1,95	2,05	2,15	2,25	2,35	2,4	2,45	2,5	2,55	2,6	2,65	2,7	2,75	2,8
-4,50E+07	-5,18E+07	-5,95E+07	-6,82E+07	-7,86E+07	-8,51E+07	-9,37E+07	-1,05E+08	-1,14E+08	-1,13E+08	-8,56E+07	-2,90E+07	4,41E+07	8,85E+07
-7,16E+07	-8,25E+07	-9,47E+07	-1,09E+08	-1,25E+08	-1,35E+08	-1,49E+08	-1,65E+08	-1,80E+08	-1,78E+08	-1,38E+08	-5,63E+07	3,89E+07	9,94E+07
-9,28E+07	-1,07E+08	-1,23E+08	-1,41E+08	-1,62E+08	-1,76E+08	-1,92E+08	-2,13E+08	-2,31E+08	-2,29E+08	-1,82E+08	-8,61E+07	2,19E+07	9,09E+07
-1,16E+08	-1,34E+08	-1,54E+08	-1,76E+08	-2,03E+08	-2,20E+08	-2,40E+08	-2,66E+08	-2,88E+08	-2,85E+08	-2,30E+08	-1,23E+08	-2,51E+07	7,08E+07
-1,39E+08	-1,60E+08	-1,84E+08	-2,11E+08	-2,43E+08	-2,62E+08	-2,87E+08	-3,16E+08	-3,41E+08	-3,39E+08	-2,79E+08	-1,64E+08	-4,45E+07	3,55E+07
-1,62E+08	-1,86E+08	-2,14E+08	-2,45E+08	-2,82E+08	-3,05E+08	-3,33E+08	-3,67E+08	-3,95E+08	-3,94E+08	-3,28E+08	-2,09E+08	-8,65E+07	-2,74E+07
-1,85E+08	-2,13E+08	-2,45E+08	-2,81E+08	-3,23E+08	-3,49E+08	-3,81E+08	-4,19E+08	-4,51E+08	-4,50E+08	-3,82E+08	-2,62E+08	-1,42E+08	-6,66E+07
-2,06E+08	-2,38E+08	-2,73E+08	-3,13E+08	-3,60E+08	-3,89E+08	-4,23E+08	-4,64E+08	-5,00E+08	-5,01E+08	-4,33E+08	-3,14E+08	-2,01E+08	-1,32E+08
-2,29E+08	-2,64E+08	-3,04E+08	-3,48E+08	-4,00E+08	-4,32E+08	-4,70E+08	-5,15E+08	-5,54E+08	-5,57E+08	-4,91E+08	-3,80E+08	-2,80E+08	-2,21E+08
-2,47E+08	-2,84E+08	-3,26E+08	-3,74E+08	-4,30E+08	-4,64E+08	-5,04E+08	-5,51E+08	-5,93E+08	-5,99E+08	-5,38E+08	-4,38E+08	-3,53E+08	-3,06E+08
-2,60E+08	-2,99E+08	-3,44E+08	-3,94E+08	-4,53E+08	-4,89E+08	-5,30E+08	-5,79E+08	-6,22E+08	-6,33E+08	-5,82E+08	-5,00E+08	-4,37E+08	-4,10E+08
-2,77E+08	-3,19E+08	-3,66E+08	-4,20E+08	-4,83E+08	-5,20E+08	-5,64E+08	-6,15E+08	-6,61E+08	-6,76E+08	-6,33E+08	-5,65E+08	-5,21E+08	-5,12E+08
-2,89E+08	-3,33E+08	-3,82E+08	-4,38E+08	-5,04E+08	-5,43E+08	-5,88E+08	-6,40E+08	-6,88E+08	-7,09E+08	-6,80E+08	-6,36E+08	-6,20E+08	-6,35E+08
-2,96E+08	-3,41E+08	-3,91E+08	-4,48E+08	-5,15E+08	-5,55E+08	-6,00E+08	-6,52E+08	-7,01E+08	-7,28E+08	-7,15E+08	-6,97E+08	-7,10E+08	-7,50E+08
-2,94E+08	-3,39E+08	-3,88E+08	-4,45E+08	-5,12E+08	-5,51E+08	-5,95E+08	-6,45E+08	-6,94E+08	-7,27E+08	-7,31E+08	-7,40E+08	-7,81E+08	-8,47E+08
-3,02E+08	-3,48E+08	-3,99E+08	-4,57E+08	-5,25E+08	-5,65E+08	-6,10E+08	-6,60E+08	-7,11E+08	-7,51E+08	-7,72E+08	-8,09E+08	-8,81E+08	-9,75E+08
-3,02E+08	-3,48E+08	-3,99E+08	-4,58E+08	-5,26E+08	-5,65E+08	-6,09E+08	-6,58E+08	-7,09E+08	-7,56E+08	-7,98E+08	-8,64E+08	-9,67E+08	-1,09E+09
-2,94E+08	-3,39E+08	-3,89E+08	-4,46E+08	-5,12E+08	-5,50E+08	-5,92E+08	-6,38E+08	-6,89E+08	-7,42E+08	-8,05E+08	-9,03E+08	-1,04E+09	-1,19E+09
-2,83E+08	-3,26E+08	-3,74E+08	-4,28E+08	-4,92E+08	-5,28E+08	-5,67E+08	-6,10E+08	-6,60E+08	-7,18E+08	-7,99E+08	-9,21E+08	-1,08E+09	-1,26E+09
-2,73E+08	-3,14E+08	-3,61E+08	-4,13E+08	-4,74E+08	-5,09E+08	-5,46E+08	-5,86E+08	-6,34E+08	-6,99E+08	-7,99E+08	-9,50E+08	-1,14E+09	-1,34E+09
-2,57E+08	-2,96E+08	-3,39E+08	-3,89E+08	-4,46E+08	-4,78E+08	-5,12E+08	-5,49E+08	-5,95E+08	-6,63E+08	-7,75E+08	-9,43E+08	-1,15E+09	-1,36E+09
-2,39E+08	-2,75E+08	-3,16E+08	-3,62E+08	-4,15E+08	-4,45E+08	-4,76E+08	-5,09E+08	-5,52E+08	-6,23E+08	-7,49E+08	-9,36E+08	-1,16E+09	-1,39E+09
-2,21E+08	-2,54E+08	-2,92E+08	-3,35E+08	-3,84E+08	-4,11E+08	-4,38E+08	-4,68E+08	-5,09E+08	-5,81E+08	-7,16E+08	-9,16E+08	-1,15E+09	-1,38E+09
-1,96E+08	-2,25E+08	-2,59E+08	-2,96E+08	-3,40E+08	-3,63E+08	-3,87E+08	-4,13E+08	-4,49E+08	-5,20E+08	-6,56E+08	-8,56E+08	-1,08E+09	-1,32E+09
-1,69E+08	-1,95E+08	-2,23E+08	-2,56E+08	-2,93E+08	-3,13E+08	-3,33E+08	-3,55E+08	-3,87E+08	-4,53E+08	-5,86E+08	-7,81E+08	-1,00E+09	-1,22E+09
-1,40E+08	-1,62E+08	-1,86E+08	-2,13E+08	-2,44E+08	-2,60E+08	-2,77E+08	-2,93E+08	-3,21E+08	-3,80E+08	-5,02E+08	-6,80E+08	-8,78E+08	-1,08E+09
-1,00E+08	-1,16E+08	-1,33E+08	-1,52E+08	-1,74E+08	-1,86E+08	-1,97E+08	-2,08E+08	-2,28E+08	-2,75E+08	-3,72E+08	-5,14E+08	-6,70E+08	-8,30E+08

Step 39	Step 40	Step 41	Step 42
2,85	2,9	2,95	3
1,14E+08	1,41E+08	1,68E+08	1,85E+08
1,38E+08	1,83E+08	2,28E+08	2,58E+08
1,39E+08	1,98E+08	2,58E+08	3,00E+08
1,29E+08	2,04E+08	2,81E+08	3,36E+08
1,02E+08	1,92E+08	2,87E+08	3,56E+08
6,87E+07	1,73E+08	2,86E+08	3,70E+08
-1,23E+06	1,36E+08	2,67E+08	3,68E+08
-4,87E+07	8,98E+07	2,37E+08	3,53E+08
-1,33E+08	-6,85E+05	1,84E+08	3,19E+08
-2,19E+08	-6,30E+07	1,24E+08	2,73E+08
-3,28E+08	-1,65E+08	4,51E+07	1,99E+08
-4,32E+08	-2,59E+08	-6,02E+07	1,37E+08
-5,64E+08	-3,86E+08	-1,70E+08	4,49E+07
-6,90E+08	-5,11E+08	-2,88E+08	-8,56E+07
-8,00E+08	-6,27E+08	-4,03E+08	-1,92E+08
-9,41E+08	-7,66E+08	-5,34E+08	-3,07E+08
-1,07E+09	-9,01E+08	-6,67E+08	-4,30E+08
-1,19E+09	-1,03E+09	-8,01E+08	-5,60E+08
-1,27E+09	-1,12E+09	-9,01E+08	-6,60E+08
-1,37E+09	-1,23E+09	-1,02E+09	-7,76E+08
-1,41E+09	-1,28E+09	-1,08E+09	-8,43E+08
-1,45E+09	-1,34E+09	-1,14E+09	-9,16E+08
-1,46E+09	-1,36E+09	-1,18E+09	-9,62E+08
-1,40E+09	-1,32E+09	-1,16E+09	-9,57E+08
-1,30E+09	-1,24E+09	-1,10E+09	-9,21E+08
-1,16E+09	-1,11E+09	-9,91E+08	-8,36E+08
-8,93E+08	-8,60E+08	-7,77E+08	-6,62E+08

MIN	MAX
-1,1406E+08	1,8513E+08
-1,7969E+08	2,5828E+08
-2,3132E+08	3,0011E+08
-2,8753E+08	3,3643E+08
-3,4149E+08	3,5615E+08
-3,9534E+08	3,6981E+08
-4,5075E+08	3,6781E+08
-5,0090E+08	3,5320E+08
-5,5740E+08	3,1879E+08
-5,9941E+08	2,7263E+08
-6,3335E+08	1,9943E+08
-6,7612E+08	1,3658E+08
-7,0889E+08	4,4944E+07
-7,5040E+08	3,3744E+07
-8,4660E+08	3,3550E+07
-9,7473E+08	3,4482E+07
-1,0899E+09	3,4545E+07
-1,1909E+09	3,3676E+07
-1,2714E+09	3,2377E+07
-1,3708E+09	3,1261E+07
-1,4068E+09	2,9431E+07
-1,4457E+09	2,7422E+07
-1,4557E+09	2,5358E+07
-1,3966E+09	2,2463E+07
-1,3041E+09	1,9412E+07
-1,1560E+09	1,6145E+07
-8,9258E+08	1,1538E+07

Result - Principal stress (Abs)

The influence lines for Submodel 3B, for each node at the U-sape. Maximum principal stress 1455.7 MPa (compression) at node 23 in load step2.85 m.

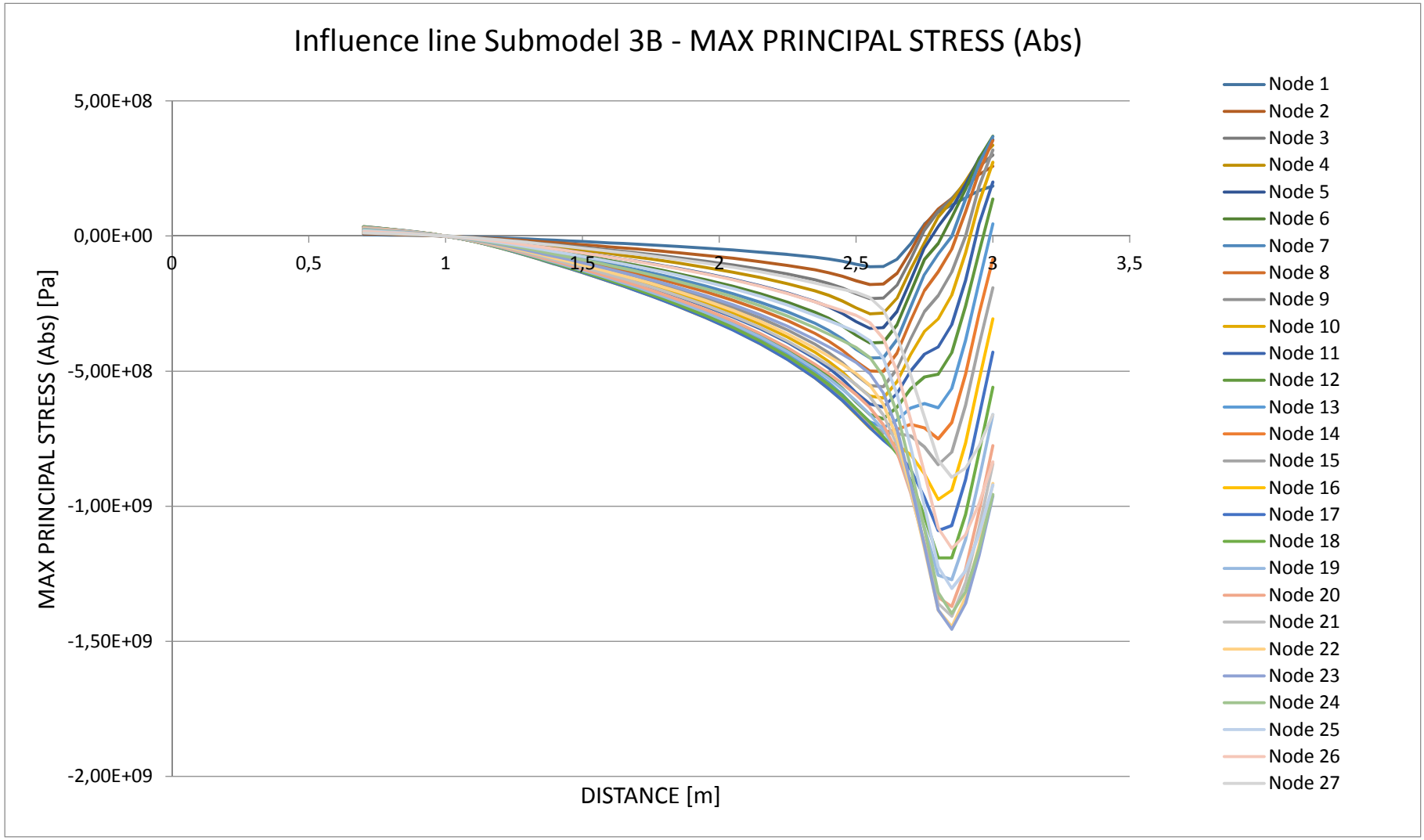

SUBMODEL 3B

MISES STRESS

		Step 1	Step 2	Step 3	Step 4	Step 5	Step 6	Step 7	Step 8	Step 9	Step 10
Node	Distance	0,7	0,75	0,8	0,85	0,9	0,95	1	1,05	1,1	1,15
1	0	4,91E+06	4,21E+06	3,52E+06	2,79E+06	1,96E+06	1,01E+06	1,26E+05	1,44E+06	2,97E+06	4,70E+06
2	0,00604	7,16E+06	6,14E+06	5,12E+06	4,06E+06	2,87E+06	1,48E+06	1,60E+05	2,07E+06	4,29E+06	6,79E+06
3	0,01208	9,16E+06	7,86E+06	6,56E+06	5,20E+06	3,68E+06	1,90E+06	1,81E+05	2,62E+06	5,44E+06	8,63E+06
4	0,01812	1,14E+07	9,80E+06	8,18E+06	6,49E+06	4,60E+06	2,39E+06	1,93E+05	3,22E+06	6,72E+06	1,07E+07
5	0,02416	1,35E+07	1,16E+07	9,69E+06	7,69E+06	5,45E+06	2,85E+06	2,00E+05	3,77E+06	7,90E+06	1,26E+07
6	0,0302	1,58E+07	1,36E+07	1,14E+07	9,02E+06	6,40E+06	3,36E+06	2,05E+05	4,38E+06	9,20E+06	1,46E+07
7	0,03624	1,79E+07	1,54E+07	1,29E+07	1,02E+07	7,25E+06	3,82E+06	2,05E+05	4,91E+06	1,03E+07	1,65E+07
8	0,04228	2,02E+07	1,73E+07	1,45E+07	1,15E+07	8,17E+06	4,32E+06	2,03E+05	5,48E+06	1,16E+07	1,85E+07
9	0,04832	2,20E+07	1,89E+07	1,58E+07	1,25E+07	8,91E+06	4,72E+06	1,97E+05	5,94E+06	1,26E+07	2,01E+07
10	0,05436	2,37E+07	2,04E+07	1,71E+07	1,35E+07	9,64E+06	5,12E+06	1,89E+05	6,38E+06	1,35E+07	2,16E+07
11	0,0604	2,46E+07	2,11E+07	1,77E+07	1,40E+07	9,99E+06	5,31E+06	1,77E+05	6,57E+06	1,40E+07	2,23E+07
12	0,06644	2,63E+07	2,26E+07	1,89E+07	1,50E+07	1,07E+07	5,70E+06	1,73E+05	7,00E+06	1,49E+07	2,38E+07
13	0,07248	2,73E+07	2,35E+07	1,96E+07	1,56E+07	1,11E+07	5,93E+06	1,63E+05	7,24E+06	1,54E+07	2,47E+07
14	0,07852	2,80E+07	2,41E+07	2,01E+07	1,60E+07	1,14E+07	6,10E+06	1,57E+05	7,40E+06	1,58E+07	2,53E+07
15	0,08456	2,78E+07	2,39E+07	2,00E+07	1,59E+07	1,13E+07	6,05E+06	1,49E+05	7,32E+06	1,56E+07	2,50E+07
16	0,0906	2,88E+07	2,47E+07	2,07E+07	1,64E+07	1,17E+07	6,28E+06	1,48E+05	7,56E+06	1,62E+07	2,59E+07
17	0,09664	2,90E+07	2,49E+07	2,08E+07	1,66E+07	1,18E+07	6,33E+06	1,43E+05	7,59E+06	1,63E+07	2,60E+07
18	0,10268	2,84E+07	2,44E+07	2,04E+07	1,62E+07	1,16E+07	6,21E+06	1,41E+05	7,43E+06	1,59E+07	2,55E+07
19	0,10872	2,73E+07	2,35E+07	1,96E+07	1,56E+07	1,11E+07	5,97E+06	1,38E+05	7,13E+06	1,53E+07	2,45E+07
20	0,11476	2,66E+07	2,29E+07	1,91E+07	1,52E+07	1,09E+07	5,83E+06	1,38E+05	6,95E+06	1,49E+07	2,38E+07
21	0,1208	2,49E+07	2,14E+07	1,79E+07	1,42E+07	1,02E+07	5,46E+06	1,36E+05	6,49E+06	1,39E+07	2,23E+07
22	0,12684	2,39E+07	2,05E+07	1,72E+07	1,36E+07	9,74E+06	5,23E+06	1,35E+05	6,21E+06	1,33E+07	2,13E+07
23	0,13288	2,19E+07	1,88E+07	1,57E+07	1,25E+07	8,94E+06	4,80E+06	1,33E+05	5,69E+06	1,22E+07	1,96E+07
24	0,13892	1,97E+07	1,69E+07	1,42E+07	1,13E+07	8,04E+06	4,32E+06	1,29E+05	5,12E+06	1,10E+07	1,76E+07
25	0,14496	1,74E+07	1,49E+07	1,25E+07	9,93E+06	7,09E+06	3,81E+06	1,24E+05	4,51E+06	9,68E+06	1,55E+07
26	0,151	1,43E+07	1,23E+07	1,03E+07	8,19E+06	5,85E+06	3,15E+06	1,16E+05	3,72E+06	7,98E+06	1,28E+07
27	0,15704	1,07E+07	9,22E+06	7,71E+06	6,13E+06	4,38E+06	2,35E+06	1,02E+05	2,78E+06	5,96E+06	9,55E+06

Step 11	Step 12	Step 13	Step 14	Step 15	Step 16	Step 17	Step 18	Step 19	Step 20	Step 21	Step 22	Step 23	Step 24
1,2	1,25	1,3	1,35	1,4	1,45	1,5	1,55	1,6	1,65	1,7	1,75	1,8	1,85
6,61E+06	8,67E+06	1,08E+07	1,31E+07	1,54E+07	1,77E+07	2,00E+07	2,24E+07	2,49E+07	2,74E+07	3,00E+07	3,26E+07	3,54E+07	3,83E+07
9,55E+06	1,25E+07	1,57E+07	1,89E+07	2,22E+07	2,56E+07	2,90E+07	3,25E+07	3,60E+07	3,97E+07	4,34E+07	4,73E+07	5,13E+07	5,55E+07
1,22E+07	1,60E+07	2,00E+07	2,41E+07	2,83E+07	3,26E+07	3,69E+07	4,14E+07	4,59E+07	5,06E+07	5,54E+07	6,03E+07	6,55E+07	7,08E+07
1,50E+07	1,98E+07	2,47E+07	2,99E+07	3,51E+07	4,04E+07	4,58E+07	5,13E+07	5,70E+07	6,28E+07	6,87E+07	7,49E+07	8,13E+07	8,79E+07
1,77E+07	2,33E+07	2,91E+07	3,52E+07	4,14E+07	4,77E+07	5,41E+07	6,06E+07	6,72E+07	7,40E+07	8,11E+07	8,84E+07	9,59E+07	1,04E+08
2,07E+07	2,72E+07	3,40E+07	4,11E+07	4,83E+07	5,57E+07	6,31E+07	7,07E+07	7,85E+07	8,65E+07	9,47E+07	1,03E+08	1,12E+08	1,21E+08
2,33E+07	3,06E+07	3,83E+07	4,63E+07	5,45E+07	6,28E+07	7,12E+07	7,98E+07	8,86E+07	9,76E+07	1,07E+08	1,16E+08	1,26E+08	1,37E+08
2,61E+07	3,43E+07	4,30E+07	5,20E+07	6,11E+07	7,04E+07	7,99E+07	8,95E+07	9,94E+07	1,10E+08	1,20E+08	1,31E+08	1,42E+08	1,53E+08
2,83E+07	3,73E+07	4,67E+07	5,65E+07	6,64E+07	7,66E+07	8,69E+07	9,73E+07	1,08E+08	1,19E+08	1,30E+08	1,42E+08	1,54E+08	1,67E+08
3,05E+07	4,02E+07	5,04E+07	6,09E+07	7,17E+07	8,26E+07	9,37E+07	1,05E+08	1,17E+08	1,29E+08	1,41E+08	1,53E+08	1,67E+08	1,80E+08
3,15E+07	4,15E+07	5,20E+07	6,29E+07	7,40E+07	8,53E+07	9,68E+07	1,09E+08	1,20E+08	1,33E+08	1,45E+08	1,59E+08	1,72E+08	1,86E+08
3,37E+07	4,43E+07	5,56E+07	6,72E+07	7,91E+07	9,12E+07	1,03E+08	1,16E+08	1,29E+08	1,42E+08	1,55E+08	1,69E+08	1,84E+08	1,99E+08
3,49E+07	4,59E+07	5,76E+07	6,97E+07	8,20E+07	9,46E+07	1,07E+08	1,20E+08	1,34E+08	1,47E+08	1,61E+08	1,76E+08	1,91E+08	2,06E+08
3,57E+07	4,71E+07	5,90E+07	7,14E+07	8,40E+07	9,69E+07	1,10E+08	1,23E+08	1,37E+08	1,51E+08	1,65E+08	1,80E+08	1,95E+08	2,11E+08
3,54E+07	4,66E+07	5,84E+07	7,07E+07	8,32E+07	9,59E+07	1,09E+08	1,22E+08	1,36E+08	1,49E+08	1,64E+08	1,78E+08	1,94E+08	2,09E+08
3,66E+07	4,82E+07	6,05E+07	7,31E+07	8,61E+07	9,93E+07	1,13E+08	1,26E+08	1,40E+08	1,55E+08	1,69E+08	1,85E+08	2,00E+08	2,17E+08
3,68E+07	4,85E+07	6,08E+07	7,36E+07	8,66E+07	9,99E+07	1,13E+08	1,27E+08	1,41E+08	1,56E+08	1,70E+08	1,86E+08	2,02E+08	2,18E+08
3,61E+07	4,75E+07	5,96E+07	7,21E+07	8,49E+07	9,79E+07	1,11E+08	1,24E+08	1,38E+08	1,52E+08	1,67E+08	1,82E+08	1,97E+08	2,14E+08
3,46E+07	4,56E+07	5,72E+07	6,92E+07	8,15E+07	9,39E+07	1,07E+08	1,20E+08	1,33E+08	1,46E+08	1,60E+08	1,75E+08	1,90E+08	2,05E+08
3,37E+07	4,45E+07	5,58E+07	6,75E+07	7,95E+07	9,16E+07	1,04E+08	1,17E+08	1,29E+08	1,43E+08	1,56E+08	1,70E+08	1,85E+08	2,00E+08
3,15E+07	4,16E+07	5,21E+07	6,31E+07	7,43E+07	8,57E+07	9,72E+07	1,09E+08	1,21E+08	1,33E+08	1,46E+08	1,59E+08	1,73E+08	1,87E+08
3,02E+07	3,98E+07	4,99E+07	6,04E+07	7,11E+07	8,20E+07	9,31E+07	1,04E+08	1,16E+08	1,28E+08	1,40E+08	1,53E+08	1,66E+08	1,79E+08
2,77E+07	3,65E+07	4,58E+07	5,54E+07	6,52E+07	7,52E+07	8,53E+07	9,56E+07	1,06E+08	1,17E+08	1,28E+08	1,40E+08	1,52E+08	1,64E+08
2,49E+07	3,28E+07	4,11E+07	4,98E+07	5,86E+07	6,76E+07	7,67E+07	8,60E+07	9,55E+07	1,05E+08	1,15E+08	1,26E+08	1,36E+08	1,48E+08
2,19E+07	2,89E+07	3,63E+07	4,39E+07	5,17E+07	5,96E+07	6,77E+07	7,59E+07	8,42E+07	9,29E+07	1,02E+08	1,11E+08	1,20E+08	1,30E+08
1,81E+07	2,38E+07	2,99E+07	3,62E+07	4,26E+07	4,92E+07	5,58E+07	6,26E+07	6,95E+07	7,66E+07	8,39E+07	9,14E+07	9,92E+07	1,07E+08
1,35E+07	1,78E+07	2,24E+07	2,71E+07	3,19E+07	3,67E+07	4,17E+07	4,67E+07	5,19E+07	5,72E+07	6,27E+07	6,83E+07	7,42E+07	8,02E+07

Step 25	Step 26	Step 27	Step 28	Step 29	Step 30	Step 31	Step 32	Step 33	Step 34	Step 35	Step 36	Step 37	Step 38
1,95	2,05	2,15	2,25	2,35	2,4	2,45	2,5	2,55	2,6	2,65	2,7	2,75	2,8
4,45E+07	5,12E+07	5,88E+07	6,74E+07	7,77E+07	8,42E+07	9,25E+07	1,03E+08	1,12E+08	1,11E+08	8,58E+07	3,62E+07	4,76E+07	8,58E+07
6,44E+07	7,43E+07	8,53E+07	9,78E+07	1,13E+08	1,22E+08	1,34E+08	1,49E+08	1,62E+08	1,60E+08	1,24E+08	5,38E+07	4,41E+07	9,40E+07
8,22E+07	9,48E+07	1,09E+08	1,25E+08	1,44E+08	1,56E+08	1,71E+08	1,89E+08	2,05E+08	2,03E+08	1,60E+08	7,63E+07	3,36E+07	8,90E+07
1,02E+08	1,18E+08	1,35E+08	1,55E+08	1,78E+08	1,93E+08	2,11E+08	2,34E+08	2,52E+08	2,50E+08	2,02E+08	1,08E+08	2,64E+07	6,97E+07
1,20E+08	1,39E+08	1,59E+08	1,83E+08	2,10E+08	2,27E+08	2,49E+08	2,74E+08	2,96E+08	2,94E+08	2,41E+08	1,41E+08	4,09E+07	4,44E+07
1,41E+08	1,62E+08	1,86E+08	2,13E+08	2,46E+08	2,66E+08	2,90E+08	3,19E+08	3,44E+08	3,43E+08	2,86E+08	1,82E+08	7,74E+07	2,90E+07
1,59E+08	1,83E+08	2,10E+08	2,41E+08	2,77E+08	2,99E+08	3,27E+08	3,59E+08	3,87E+08	3,86E+08	3,27E+08	2,22E+08	1,19E+08	5,62E+07
1,78E+08	2,05E+08	2,36E+08	2,70E+08	3,11E+08	3,36E+08	3,66E+08	4,01E+08	4,32E+08	4,33E+08	3,74E+08	2,71E+08	1,74E+08	1,15E+08
1,94E+08	2,23E+08	2,56E+08	2,94E+08	3,38E+08	3,65E+08	3,97E+08	4,35E+08	4,68E+08	4,71E+08	4,13E+08	3,16E+08	2,27E+08	1,75E+08
2,09E+08	2,41E+08	2,77E+08	3,17E+08	3,65E+08	3,94E+08	4,28E+08	4,68E+08	5,03E+08	5,09E+08	4,58E+08	3,73E+08	3,02E+08	2,64E+08
2,16E+08	2,49E+08	2,86E+08	3,28E+08	3,77E+08	4,06E+08	4,41E+08	4,82E+08	5,18E+08	5,27E+08	4,83E+08	4,12E+08	3,58E+08	3,35E+08
2,31E+08	2,66E+08	3,05E+08	3,50E+08	4,03E+08	4,34E+08	4,71E+08	5,13E+08	5,51E+08	5,64E+08	5,29E+08	4,72E+08	4,36E+08	4,29E+08
2,40E+08	2,76E+08	3,17E+08	3,63E+08	4,18E+08	4,50E+08	4,87E+08	5,30E+08	5,70E+08	5,87E+08	5,63E+08	5,26E+08	5,11E+08	5,23E+08
2,45E+08	2,83E+08	3,25E+08	3,72E+08	4,28E+08	4,60E+08	4,98E+08	5,41E+08	5,82E+08	6,05E+08	5,95E+08	5,81E+08	5,93E+08	6,29E+08
2,43E+08	2,80E+08	3,22E+08	3,69E+08	4,24E+08	4,56E+08	4,92E+08	5,34E+08	5,75E+08	6,02E+08	6,06E+08	6,14E+08	6,49E+08	7,05E+08
2,52E+08	2,90E+08	3,33E+08	3,81E+08	4,38E+08	4,71E+08	5,09E+08	5,50E+08	5,93E+08	6,26E+08	6,45E+08	6,75E+08	7,34E+08	8,13E+08
2,53E+08	2,92E+08	3,35E+08	3,84E+08	4,41E+08	4,74E+08	5,11E+08	5,52E+08	5,95E+08	6,34E+08	6,71E+08	7,28E+08	8,16E+08	9,22E+08
2,48E+08	2,86E+08	3,28E+08	3,76E+08	4,32E+08	4,64E+08	4,99E+08	5,38E+08	5,81E+08	6,26E+08	6,79E+08	7,62E+08	8,76E+08	1,00E+09
2,38E+08	2,74E+08	3,15E+08	3,61E+08	4,14E+08	4,45E+08	4,78E+08	5,15E+08	5,56E+08	6,06E+08	6,73E+08	7,77E+08	9,12E+08	1,06E+09
2,32E+08	2,68E+08	3,07E+08	3,52E+08	4,04E+08	4,33E+08	4,65E+08	5,00E+08	5,40E+08	5,95E+08	6,79E+08	8,06E+08	9,64E+08	1,13E+09
2,17E+08	2,50E+08	2,87E+08	3,29E+08	3,78E+08	4,05E+08	4,34E+08	4,65E+08	5,04E+08	5,62E+08	6,59E+08	8,04E+08	9,79E+08	1,16E+09
2,08E+08	2,40E+08	2,75E+08	3,15E+08	3,61E+08	3,87E+08	4,14E+08	4,43E+08	4,81E+08	5,42E+08	6,50E+08	8,11E+08	1,00E+09	1,20E+09
1,91E+08	2,20E+08	2,52E+08	2,89E+08	3,31E+08	3,54E+08	3,78E+08	4,04E+08	4,39E+08	5,02E+08	6,19E+08	7,92E+08	9,92E+08	1,20E+09
1,71E+08	1,97E+08	2,27E+08	2,60E+08	2,98E+08	3,18E+08	3,39E+08	3,62E+08	3,94E+08	4,55E+08	5,74E+08	7,49E+08	9,48E+08	1,15E+09
1,51E+08	1,74E+08	2,00E+08	2,29E+08	2,62E+08	2,80E+08	2,99E+08	3,18E+08	3,46E+08	4,05E+08	5,24E+08	6,97E+08	8,91E+08	1,09E+09
1,25E+08	1,44E+08	1,65E+08	1,89E+08	2,16E+08	2,31E+08	2,46E+08	2,61E+08	2,85E+08	3,37E+08	4,44E+08	6,00E+08	7,73E+08	9,52E+08
9,31E+07	1,07E+08	1,23E+08	1,41E+08	1,62E+08	1,72E+08	1,83E+08	1,94E+08	2,12E+08	2,54E+08	3,42E+08	4,71E+08	6,12E+08	7,57E+08

Step 39	Step 40	Step 41	Step 42
2,85	2,9	2,95	3
1,10E+08	1,36E+08	1,63E+08	1,80E+08
1,28E+08	1,68E+08	2,09E+08	2,37E+08
1,32E+08	1,83E+08	2,37E+08	2,74E+08
1,19E+08	1,84E+08	2,52E+08	3,02E+08
9,84E+07	1,75E+08	2,58E+08	3,18E+08
6,82E+07	1,57E+08	2,54E+08	3,28E+08
3,40E+07	1,28E+08	2,40E+08	3,26E+08
4,81E+07	8,58E+07	2,11E+08	3,11E+08
1,01E+08	4,19E+07	1,74E+08	2,87E+08
1,91E+08	6,55E+07	1,10E+08	2,34E+08
2,66E+08	1,33E+08	6,23E+07	1,81E+08
3,63E+08	2,20E+08	6,61E+07	1,23E+08
4,64E+08	3,17E+08	1,40E+08	6,04E+07
5,80E+08	4,32E+08	2,48E+08	8,87E+07
6,67E+08	5,24E+08	3,39E+08	1,67E+08
7,85E+08	6,40E+08	4,46E+08	2,57E+08
9,07E+08	7,64E+08	5,67E+08	3,67E+08
1,00E+09	8,70E+08	6,75E+08	4,71E+08
1,07E+09	9,48E+08	7,60E+08	5,56E+08
1,16E+09	1,04E+09	8,59E+08	6,52E+08
1,21E+09	1,10E+09	9,26E+08	7,25E+08
1,25E+09	1,15E+09	9,86E+08	7,87E+08
1,26E+09	1,18E+09	1,02E+09	8,33E+08
1,22E+09	1,15E+09	1,01E+09	8,33E+08
1,16E+09	1,10E+09	9,79E+08	8,17E+08
1,02E+09	9,71E+08	8,68E+08	7,31E+08
8,13E+08	7,81E+08	7,04E+08	5,97E+08

MIN	MAX
1,26E+05	1,80E+08
1,60E+05	2,37E+08
1,81E+05	2,74E+08
1,93E+05	3,02E+08
2,00E+05	3,18E+08
2,05E+05	3,44E+08
2,05E+05	3,87E+08
2,03E+05	4,33E+08
1,97E+05	4,71E+08
1,89E+05	5,09E+08
1,77E+05	5,27E+08
1,73E+05	5,64E+08
1,63E+05	5,87E+08
1,57E+05	6,29E+08
1,49E+05	7,05E+08
1,48E+05	8,13E+08
1,43E+05	9,22E+08
1,41E+05	1,00E+09
1,38E+05	1,07E+09
1,38E+05	1,16E+09
1,36E+05	1,21E+09
1,35E+05	1,25E+09
1,33E+05	1,26E+09
1,29E+05	1,22E+09
1,24E+05	1,16E+09
1,16E+05	1,02E+09
1,02E+05	8,13E+08

Result - Mises stress

The influence lines for Submodel 3B, for each node at the U-sape. Maximum Mises stress 1261.6 MPa at node 23 in load step 2.85 m.

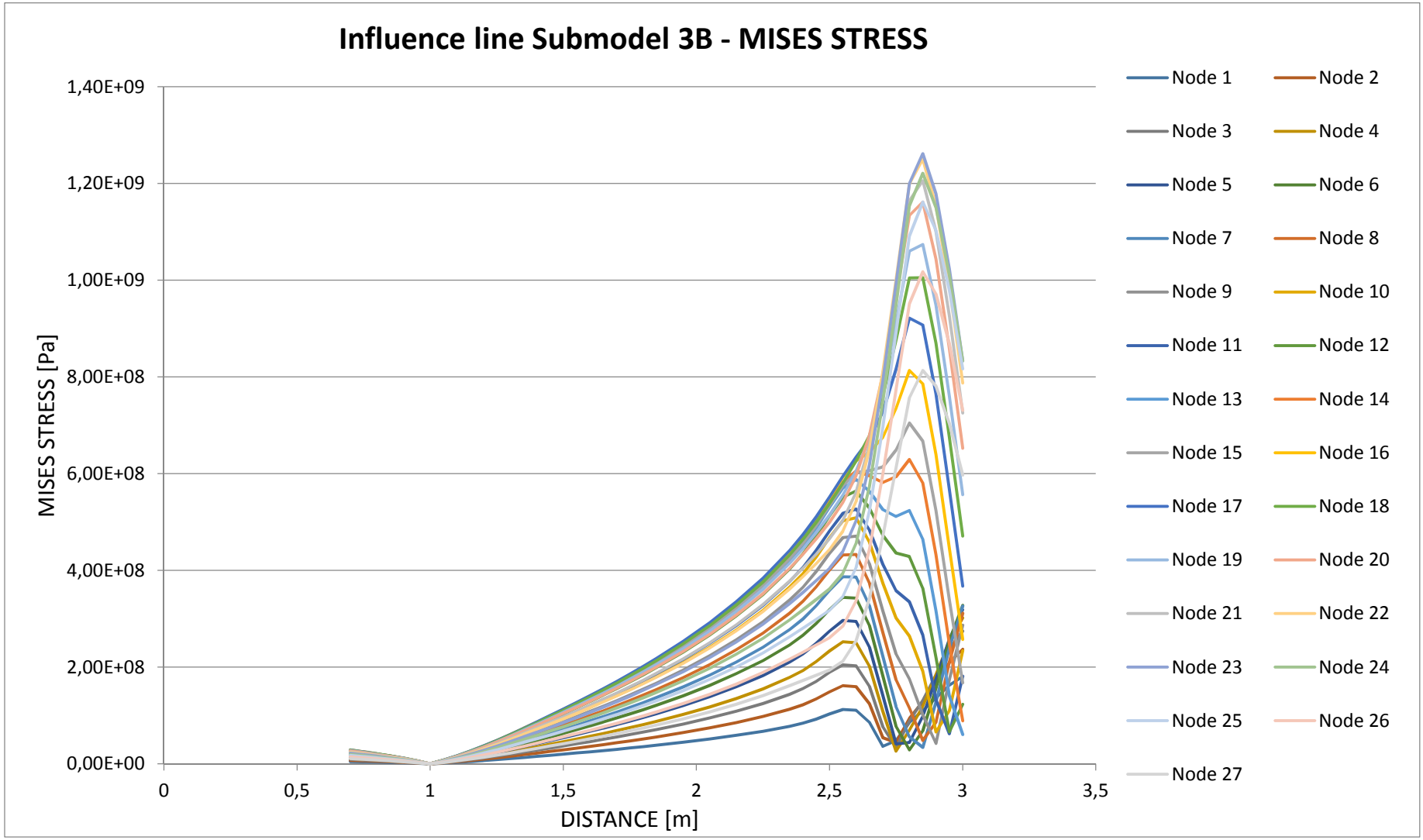

SUBMODEL 4A

MAX PRINCIPAL STRESS (Abs)

		Step 1	Step 2	Step 3	Step 4	Step 5	Step 6	Step 7	Step 8	Step 9	Step 10	Step 11
Node	Distance	0,7	0,75	0,8	0,85	0,9	0,95	1	1,05	1,1	1,15	1,2
1	0	1,34E+07	1,14E+07	9,45E+06	7,44E+06	5,31E+06	2,93E+06	2,53E+05	-2,87E+06	-6,38E+06	-1,03E+07	-1,46E+07
2	0,00604	1,79E+07	1,53E+07	1,26E+07	9,95E+06	7,09E+06	3,92E+06	3,09E+05	-3,84E+06	-8,54E+06	-1,38E+07	-1,95E+07
3	0,01208	2,18E+07	1,86E+07	1,54E+07	1,21E+07	8,65E+06	4,78E+06	3,74E+05	-4,68E+06	-1,04E+07	-1,68E+07	-2,38E+07
4	0,01812	2,50E+07	2,13E+07	1,77E+07	1,39E+07	9,92E+06	5,48E+06	4,23E+05	-5,38E+06	-1,20E+07	-1,93E+07	-2,74E+07
5	0,02416	2,80E+07	2,39E+07	1,98E+07	1,56E+07	1,11E+07	6,14E+06	4,72E+05	-6,04E+06	-1,34E+07	-2,16E+07	-3,07E+07
6	0,0302	3,04E+07	2,59E+07	2,15E+07	1,69E+07	1,21E+07	6,67E+06	5,06E+05	-6,57E+06	-1,46E+07	-2,35E+07	-3,34E+07
7	0,03624	3,20E+07	2,73E+07	2,26E+07	1,78E+07	1,27E+07	7,02E+06	5,28E+05	-6,93E+06	-1,54E+07	-2,48E+07	-3,52E+07
8	0,04228	3,42E+07	2,92E+07	2,42E+07	1,91E+07	1,36E+07	7,50E+06	5,55E+05	-7,43E+06	-1,65E+07	-2,66E+07	-3,77E+07
9	0,04832	3,55E+07	3,03E+07	2,51E+07	1,98E+07	1,41E+07	7,78E+06	5,70E+05	-7,74E+06	-1,72E+07	-2,77E+07	-3,92E+07
10	0,05436	3,63E+07	3,10E+07	2,57E+07	2,02E+07	1,44E+07	7,96E+06	5,69E+05	-7,95E+06	-1,76E+07	-2,84E+07	-4,02E+07
11	0,0604	3,65E+07	3,12E+07	2,58E+07	2,04E+07	1,45E+07	8,01E+06	5,63E+05	-8,04E+06	-1,78E+07	-2,87E+07	-4,06E+07
12	0,06644	3,62E+07	3,09E+07	2,56E+07	2,02E+07	1,44E+07	7,94E+06	5,42E+05	-8,03E+06	-1,77E+07	-2,86E+07	-4,05E+07
13	0,07248	3,52E+07	3,01E+07	2,49E+07	1,97E+07	1,41E+07	7,73E+06	5,20E+05	-7,87E+06	-1,74E+07	-2,80E+07	-3,96E+07
14	0,07852	3,47E+07	2,96E+07	2,46E+07	1,94E+07	1,38E+07	7,61E+06	4,93E+05	-7,82E+06	-1,72E+07	-2,77E+07	-3,93E+07
15	0,08456	3,26E+07	2,79E+07	2,31E+07	1,83E+07	1,30E+07	7,16E+06	4,58E+05	-7,42E+06	-1,63E+07	-2,63E+07	-3,73E+07
16	0,0906	3,10E+07	2,66E+07	2,21E+07	1,74E+07	1,24E+07	6,82E+06	4,20E+05	-7,16E+06	-1,57E+07	-2,53E+07	-3,58E+07
17	0,09664	2,94E+07	2,51E+07	2,09E+07	1,65E+07	1,18E+07	6,46E+06	3,88E+05	-6,88E+06	-1,51E+07	-2,42E+07	-3,43E+07
18	0,10268	2,60E+07	2,23E+07	1,85E+07	1,47E+07	1,05E+07	5,72E+06	3,41E+05	-6,21E+06	-1,35E+07	-2,18E+07	-3,08E+07
19	0,10872	2,29E+07	1,97E+07	1,64E+07	1,30E+07	9,28E+06	5,05E+06	3,09E+05	-5,59E+06	-1,21E+07	-1,95E+07	-2,76E+07
20	0,11476	2,03E+07	1,74E+07	1,46E+07	1,16E+07	8,26E+06	4,48E+06	2,74E+05	-5,09E+06	-1,10E+07	-1,77E+07	-2,50E+07
21	0,1208	1,74E+07	1,50E+07	1,25E+07	9,96E+06	7,12E+06	3,85E+06	2,50E+05	-4,50E+06	-9,69E+06	-1,55E+07	-2,20E+07
22	0,12684	1,42E+07	1,23E+07	1,03E+07	8,19E+06	5,86E+06	3,15E+06	2,22E+05	-3,83E+06	-8,19E+06	-1,31E+07	-1,86E+07
23	0,13288	1,14E+07	9,82E+06	8,26E+06	6,60E+06	4,73E+06	2,52E+06	2,03E+05	-3,22E+06	-6,82E+06	-1,09E+07	-1,55E+07
24	0,13892	8,76E+06	7,59E+06	6,41E+06	5,14E+06	3,69E+06	1,95E+06	-2,03E+05	-2,64E+06	-5,55E+06	-8,86E+06	-1,25E+07
25	0,14496	6,19E+06	5,40E+06	4,59E+06	3,70E+06	2,66E+06	1,39E+06	-2,23E+05	-2,04E+06	-4,23E+06	-6,74E+06	-9,54E+06
26	0,151	4,03E+06	3,54E+06	3,03E+06	2,46E+06	1,78E+06	9,21E+05	-2,22E+05	-1,50E+06	-3,05E+06	-4,84E+06	-6,85E+06
27	0,15704	2,44E+06	2,16E+06	1,87E+06	1,53E+06	1,11E+06	5,76E+05	-1,92E+05	-1,02E+06	-2,04E+06	-3,24E+06	-4,58E+06

Step 12	Step 13	Step 14	Step 15	Step 16	Step 17	Step 18	Step 19	Step 20	Step 21	Step 22	Step 23	Step 24	Step 25
1,25	1,3	1,35	1,4	1,45	1,5	1,55	1,6	1,65	1,7	1,75	1,8	1,85	1,95
-1,92E+07	-2,41E+07	-2,92E+07	-3,44E+07	-3,96E+07	-4,49E+07	-5,03E+07	-5,58E+07	-6,13E+07	-6,71E+07	-7,30E+07	-7,90E+07	-8,53E+07	-9,85E+07
-2,57E+07	-3,23E+07	-3,91E+07	-4,60E+07	-5,30E+07	-6,01E+07	-6,73E+07	-7,46E+07	-8,21E+07	-8,97E+07	-9,76E+07	-1,06E+08	-1,14E+08	-1,32E+08
-3,14E+07	-3,94E+07	-4,77E+07	-5,61E+07	-6,47E+07	-7,33E+07	-8,21E+07	-9,10E+07	-1,00E+08	-1,10E+08	-1,19E+08	-1,29E+08	-1,39E+08	-1,61E+08
-3,61E+07	-4,53E+07	-5,48E+07	-6,45E+07	-7,43E+07	-8,42E+07	-9,43E+07	-1,05E+08	-1,15E+08	-1,26E+08	-1,37E+08	-1,48E+08	-1,60E+08	-1,85E+08
-4,04E+07	-5,07E+07	-6,14E+07	-7,23E+07	-8,33E+07	-9,44E+07	-1,06E+08	-1,17E+08	-1,29E+08	-1,41E+08	-1,53E+08	-1,66E+08	-1,79E+08	-2,07E+08
-4,40E+07	-5,52E+07	-6,68E+07	-7,87E+07	-9,07E+07	-1,03E+08	-1,15E+08	-1,28E+08	-1,40E+08	-1,53E+08	-1,67E+08	-1,81E+08	-1,95E+08	-2,25E+08
-4,64E+07	-5,82E+07	-7,05E+07	-8,30E+07	-9,56E+07	-1,08E+08	-1,21E+08	-1,35E+08	-1,48E+08	-1,62E+08	-1,76E+08	-1,91E+08	-2,06E+08	-2,38E+08
-4,97E+07	-6,24E+07	-7,55E+07	-8,89E+07	-1,02E+08	-1,16E+08	-1,30E+08	-1,44E+08	-1,59E+08	-1,73E+08	-1,89E+08	-2,04E+08	-2,21E+08	-2,55E+08
-5,17E+07	-6,49E+07	-7,85E+07	-9,24E+07	-1,07E+08	-1,21E+08	-1,35E+08	-1,50E+08	-1,65E+08	-1,80E+08	-1,96E+08	-2,13E+08	-2,29E+08	-2,65E+08
-5,30E+07	-6,66E+07	-8,06E+07	-9,49E+07	-1,09E+08	-1,24E+08	-1,39E+08	-1,54E+08	-1,69E+08	-1,85E+08	-2,01E+08	-2,18E+08	-2,36E+08	-2,72E+08
-5,36E+07	-6,73E+07	-8,14E+07	-9,58E+07	-1,10E+08	-1,25E+08	-1,40E+08	-1,55E+08	-1,71E+08	-1,87E+08	-2,03E+08	-2,20E+08	-2,38E+08	-2,75E+08
-5,34E+07	-6,70E+07	-8,11E+07	-9,55E+07	-1,10E+08	-1,25E+08	-1,40E+08	-1,55E+08	-1,70E+08	-1,86E+08	-2,03E+08	-2,20E+08	-2,37E+08	-2,74E+08
-5,23E+07	-6,56E+07	-7,94E+07	-9,35E+07	-1,08E+08	-1,22E+08	-1,37E+08	-1,52E+08	-1,67E+08	-1,82E+08	-1,99E+08	-2,15E+08	-2,32E+08	-2,68E+08
-5,18E+07	-6,50E+07	-7,87E+07	-9,27E+07	-1,07E+08	-1,21E+08	-1,36E+08	-1,50E+08	-1,65E+08	-1,81E+08	-1,97E+08	-2,13E+08	-2,30E+08	-2,66E+08
-4,91E+07	-6,16E+07	-7,46E+07	-8,79E+07	-1,01E+08	-1,15E+08	-1,29E+08	-1,43E+08	-1,57E+08	-1,72E+08	-1,87E+08	-2,02E+08	-2,18E+08	-2,52E+08
-4,72E+07	-5,93E+07	-7,18E+07	-8,45E+07	-9,74E+07	-1,10E+08	-1,24E+08	-1,37E+08	-1,51E+08	-1,65E+08	-1,80E+08	-1,95E+08	-2,10E+08	-2,43E+08
-4,52E+07	-5,68E+07	-6,87E+07	-8,09E+07	-9,33E+07	-1,06E+08	-1,18E+08	-1,31E+08	-1,45E+08	-1,58E+08	-1,72E+08	-1,86E+08	-2,01E+08	-2,33E+08
-4,07E+07	-5,10E+07	-6,18E+07	-7,27E+07	-8,38E+07	-9,51E+07	-1,06E+08	-1,18E+08	-1,30E+08	-1,42E+08	-1,55E+08	-1,68E+08	-1,81E+08	-2,09E+08
-3,64E+07	-4,57E+07	-5,54E+07	-6,52E+07	-7,51E+07	-8,52E+07	-9,54E+07	-1,06E+08	-1,17E+08	-1,27E+08	-1,39E+08	-1,50E+08	-1,62E+08	-1,88E+08
-3,30E+07	-4,15E+07	-5,02E+07	-5,91E+07	-6,81E+07	-7,72E+07	-8,65E+07	-9,60E+07	-1,06E+08	-1,16E+08	-1,26E+08	-1,36E+08	-1,47E+08	-1,70E+08
-2,90E+07	-3,64E+07	-4,41E+07	-5,19E+07	-5,99E+07	-6,79E+07	-7,61E+07	-8,44E+07	-9,29E+07	-1,02E+08	-1,11E+08	-1,20E+08	-1,29E+08	-1,50E+08
-2,45E+07	-3,07E+07	-3,72E+07	-4,38E+07	-5,05E+07	-5,73E+07	-6,42E+07	-7,13E+07	-7,85E+07	-8,58E+07	-9,35E+07	-1,01E+08	-1,09E+08	-1,27E+08
-2,04E+07	-2,56E+07	-3,10E+07	-3,65E+07	-4,21E+07	-4,77E+07	-5,35E+07	-5,93E+07	-6,54E+07	-7,15E+07	-7,79E+07	-8,44E+07	-9,12E+07	-1,05E+08
-1,65E+07	-2,08E+07	-2,51E+07	-2,96E+07	-3,41E+07	-3,87E+07	-4,34E+07	-4,82E+07	-5,31E+07	-5,81E+07	-6,33E+07	-6,86E+07	-7,41E+07	-8,57E+07
-1,26E+07	-1,58E+07	-1,91E+07	-2,25E+07	-2,60E+07	-2,95E+07	-3,31E+07	-3,67E+07	-4,04E+07	-4,43E+07	-4,82E+07	-5,23E+07	-5,65E+07	-6,54E+07
-9,03E+06	-1,13E+07	-1,37E+07	-1,62E+07	-1,87E+07	-2,12E+07	-2,37E+07	-2,64E+07	-2,91E+07	-3,18E+07	-3,47E+07	-3,76E+07	-4,06E+07	-4,70E+07
-6,04E+06	-7,58E+06	-9,17E+06	-1,08E+07	-1,25E+07	-1,42E+07	-1,59E+07	-1,76E+07	-1,94E+07	-2,13E+07	-2,32E+07	-2,52E+07	-2,72E+07	-3,15E+07

Step 26	Step 27	Step 28	Step 29	Step 30	Step 31	Step 32	Step 33	Step 34	Step 35	Step 36	Step 37	Step 38	Step 39
2,05	2,15	2,25	2,35	2,4	2,45	2,5	2,55	2,6	2,65	2,7	2,75	2,8	2,85
-1,13E+08	-1,29E+08	-1,46E+08	-1,65E+08	-1,76E+08	-1,88E+08	-2,01E+08	-2,16E+08	-2,32E+08	-2,47E+08	-2,60E+08	-2,65E+08	-2,44E+08	-1,88E+08
-1,51E+08	-1,72E+08	-1,95E+08	-2,21E+08	-2,35E+08	-2,51E+08	-2,69E+08	-2,89E+08	-3,10E+08	-3,32E+08	-3,50E+08	-3,57E+08	-3,29E+08	-2,55E+08
-1,84E+08	-2,10E+08	-2,38E+08	-2,70E+08	-2,87E+08	-3,07E+08	-3,28E+08	-3,52E+08	-3,79E+08	-4,06E+08	-4,29E+08	-4,39E+08	-4,07E+08	-3,16E+08
-2,12E+08	-2,41E+08	-2,74E+08	-3,10E+08	-3,30E+08	-3,52E+08	-3,77E+08	-4,05E+08	-4,36E+08	-4,68E+08	-4,96E+08	-5,09E+08	-4,72E+08	-3,69E+08
-2,37E+08	-2,70E+08	-3,07E+08	-3,48E+08	-3,70E+08	-3,95E+08	-4,23E+08	-4,54E+08	-4,89E+08	-5,26E+08	-5,59E+08	-5,75E+08	-5,35E+08	-4,20E+08
-2,58E+08	-2,94E+08	-3,34E+08	-3,78E+08	-4,03E+08	-4,30E+08	-4,60E+08	-4,94E+08	-5,33E+08	-5,74E+08	-6,12E+08	-6,31E+08	-5,88E+08	-4,64E+08
-2,72E+08	-3,10E+08	-3,52E+08	-3,99E+08	-4,25E+08	-4,54E+08	-4,86E+08	-5,22E+08	-5,63E+08	-6,08E+08	-6,49E+08	-6,71E+08	-6,27E+08	-4,97E+08
-2,92E+08	-3,32E+08	-3,77E+08	-4,28E+08	-4,55E+08	-4,86E+08	-5,20E+08	-5,59E+08	-6,03E+08	-6,52E+08	-6,99E+08	-7,24E+08	-6,78E+08	-5,39E+08
-3,04E+08	-3,46E+08	-3,93E+08	-4,45E+08	-4,74E+08	-5,06E+08	-5,41E+08	-5,82E+08	-6,28E+08	-6,81E+08	-7,31E+08	-7,59E+08	-7,13E+08	-5,69E+08
-3,12E+08	-3,55E+08	-4,03E+08	-4,57E+08	-4,87E+08	-5,19E+08	-5,56E+08	-5,97E+08	-6,46E+08	-7,01E+08	-7,55E+08	-7,85E+08	-7,39E+08	-5,91E+08
-3,15E+08	-3,59E+08	-4,08E+08	-4,62E+08	-4,92E+08	-5,25E+08	-5,62E+08	-6,04E+08	-6,54E+08	-7,11E+08	-7,67E+08	-8,00E+08	-7,54E+08	-6,06E+08
-3,14E+08	-3,58E+08	-4,06E+08	-4,61E+08	-4,91E+08	-5,23E+08	-5,60E+08	-6,03E+08	-6,53E+08	-7,11E+08	-7,69E+08	-8,03E+08	-7,59E+08	-6,11E+08
-3,07E+08	-3,50E+08	-3,98E+08	-4,51E+08	-4,80E+08	-5,13E+08	-5,49E+08	-5,90E+08	-6,40E+08	-6,98E+08	-7,56E+08	-7,92E+08	-7,50E+08	-6,05E+08
-3,05E+08	-3,47E+08	-3,95E+08	-4,47E+08	-4,77E+08	-5,09E+08	-5,45E+08	-5,86E+08	-6,36E+08	-6,95E+08	-7,54E+08	-7,91E+08	-7,51E+08	-6,08E+08
-2,89E+08	-3,30E+08	-3,74E+08	-4,25E+08	-4,52E+08	-4,83E+08	-5,17E+08	-5,56E+08	-6,04E+08	-6,61E+08	-7,19E+08	-7,56E+08	-7,19E+08	-5,83E+08
-2,78E+08	-3,17E+08	-3,60E+08	-4,09E+08	-4,35E+08	-4,65E+08	-4,98E+08	-5,36E+08	-5,83E+08	-6,39E+08	-6,96E+08	-7,34E+08	-6,99E+08	-5,68E+08
-2,67E+08	-3,04E+08	-3,45E+08	-3,92E+08	-4,17E+08	-4,46E+08	-4,77E+08	-5,15E+08	-5,60E+08	-6,15E+08	-6,72E+08	-7,10E+08	-6,78E+08	-5,52E+08
-2,40E+08	-2,73E+08	-3,11E+08	-3,53E+08	-3,76E+08	-4,01E+08	-4,30E+08	-4,64E+08	-5,05E+08	-5,56E+08	-6,09E+08	-6,45E+08	-6,17E+08	-5,03E+08
-2,15E+08	-2,45E+08	-2,79E+08	-3,16E+08	-3,37E+08	-3,60E+08	-3,86E+08	-4,17E+08	-4,54E+08	-5,01E+08	-5,50E+08	-5,84E+08	-5,60E+08	-4,57E+08
-1,95E+08	-2,23E+08	-2,53E+08	-2,87E+08	-3,06E+08	-3,27E+08	-3,51E+08	-3,79E+08	-4,14E+08	-4,57E+08	-5,04E+08	-5,37E+08	-5,16E+08	-4,21E+08
-1,72E+08	-1,96E+08	-2,23E+08	-2,53E+08	-2,70E+08	-2,88E+08	-3,10E+08	-3,35E+08	-3,66E+08	-4,05E+08	-4,47E+08	-4,78E+08	-4,61E+08	-3,77E+08
-1,45E+08	-1,66E+08	-1,88E+08	-2,14E+08	-2,28E+08	-2,44E+08	-2,62E+08	-2,84E+08	-3,11E+08	-3,45E+08	-3,82E+08	-4,10E+08	-3,96E+08	-3,24E+08
-1,21E+08	-1,38E+08	-1,57E+08	-1,79E+08	-1,91E+08	-2,04E+08	-2,19E+08	-2,38E+08	-2,61E+08	-2,90E+08	-3,23E+08	-3,48E+08	-3,37E+08	-2,76E+08
-9,84E+07	-1,12E+08	-1,28E+08	-1,46E+08	-1,55E+08	-1,66E+08	-1,79E+08	-1,94E+08	-2,14E+08	-2,39E+08	-2,67E+08	-2,89E+08	-2,81E+08	-2,30E+08
-7,50E+07	-8,57E+07	-9,77E+07	-1,11E+08	-1,19E+08	-1,27E+08	-1,37E+08	-1,49E+08	-1,65E+08	-1,85E+08	-2,08E+08	-2,26E+08	-2,21E+08	-1,81E+08
-5,40E+07	-6,17E+07	-7,04E+07	-8,03E+07	-8,58E+07	-9,21E+07	-9,95E+07	-1,08E+08	-1,20E+08	-1,35E+08	-1,53E+08	-1,68E+08	-1,65E+08	-1,35E+08
-3,62E+07	-4,14E+07	-4,72E+07	-5,39E+07	-5,77E+07	-6,20E+07	-6,71E+07	-7,33E+07	-8,16E+07	-9,24E+07	-1,05E+08	-1,16E+08	-1,15E+08	-9,40E+07

Step 40	Step 41	Step 42
2,9	2,95	3
-1,08E+08	3,64E+07	6,17E+07
-1,49E+08	-3,51E+07	7,35E+07
-1,87E+08	-4,92E+07	8,35E+07
-2,22E+08	-6,38E+07	8,83E+07
-2,56E+08	-8,02E+07	9,06E+07
-2,86E+08	-9,54E+07	9,02E+07
-3,10E+08	-1,10E+08	8,69E+07
-3,40E+08	-1,26E+08	8,46E+07
-3,62E+08	-1,40E+08	8,00E+07
-3,80E+08	-1,52E+08	7,39E+07
-3,92E+08	-1,61E+08	6,86E+07
-3,99E+08	-1,68E+08	6,16E+07
-3,96E+08	-1,70E+08	6,12E+07
-4,00E+08	-1,75E+08	5,83E+07
-3,85E+08	-1,70E+08	5,75E+07
-3,77E+08	-1,68E+08	5,52E+07
-3,67E+08	-1,65E+08	5,45E+07
-3,35E+08	-1,51E+08	5,32E+07
-3,04E+08	-1,37E+08	5,27E+07
-2,80E+08	-1,26E+08	5,20E+07
-2,50E+08	-1,11E+08	5,20E+07
-2,15E+08	-9,40E+07	5,14E+07
-1,82E+08	-7,81E+07	5,11E+07
-1,51E+08	-6,31E+07	5,07E+07
-1,18E+08	-4,74E+07	5,00E+07
-8,74E+07	-3,35E+07	4,89E+07
-6,01E+07	3,62E+07	4,76E+07

MIN	MAX
-2,6477E+08	6,1678E+07
-3,5688E+08	7,3488E+07
-4,3924E+08	8,3504E+07
-5,0851E+08	8,8267E+07
-5,7528E+08	9,0582E+07
-6,3059E+08	9,0175E+07
-6,7093E+08	8,6856E+07
-7,2355E+08	8,4633E+07
-7,5894E+08	8,0003E+07
-7,8494E+08	7,3910E+07
-7,9963E+08	6,8634E+07
-8,0301E+08	6,1616E+07
-7,9178E+08	6,1238E+07
-7,9142E+08	5,8284E+07
-7,5628E+08	5,7506E+07
-7,3379E+08	5,5233E+07
-7,1001E+08	5,4515E+07
-6,4509E+08	5,3187E+07
-5,8426E+08	5,2730E+07
-5,3659E+08	5,1986E+07
-4,7826E+08	5,1975E+07
-4,1029E+08	5,1353E+07
-3,4815E+08	5,1118E+07
-2,8903E+08	5,0674E+07
-2,2636E+08	5,0005E+07
-1,6820E+08	4,8947E+07
-1,1615E+08	4,7638E+07

Result - Principal stress (Abs)

The influence lines for Submodel 4A, for each node at the U-sape. Maximum principal stress 803.01 MPa (compression) at node 12 in load step 2.75 m.

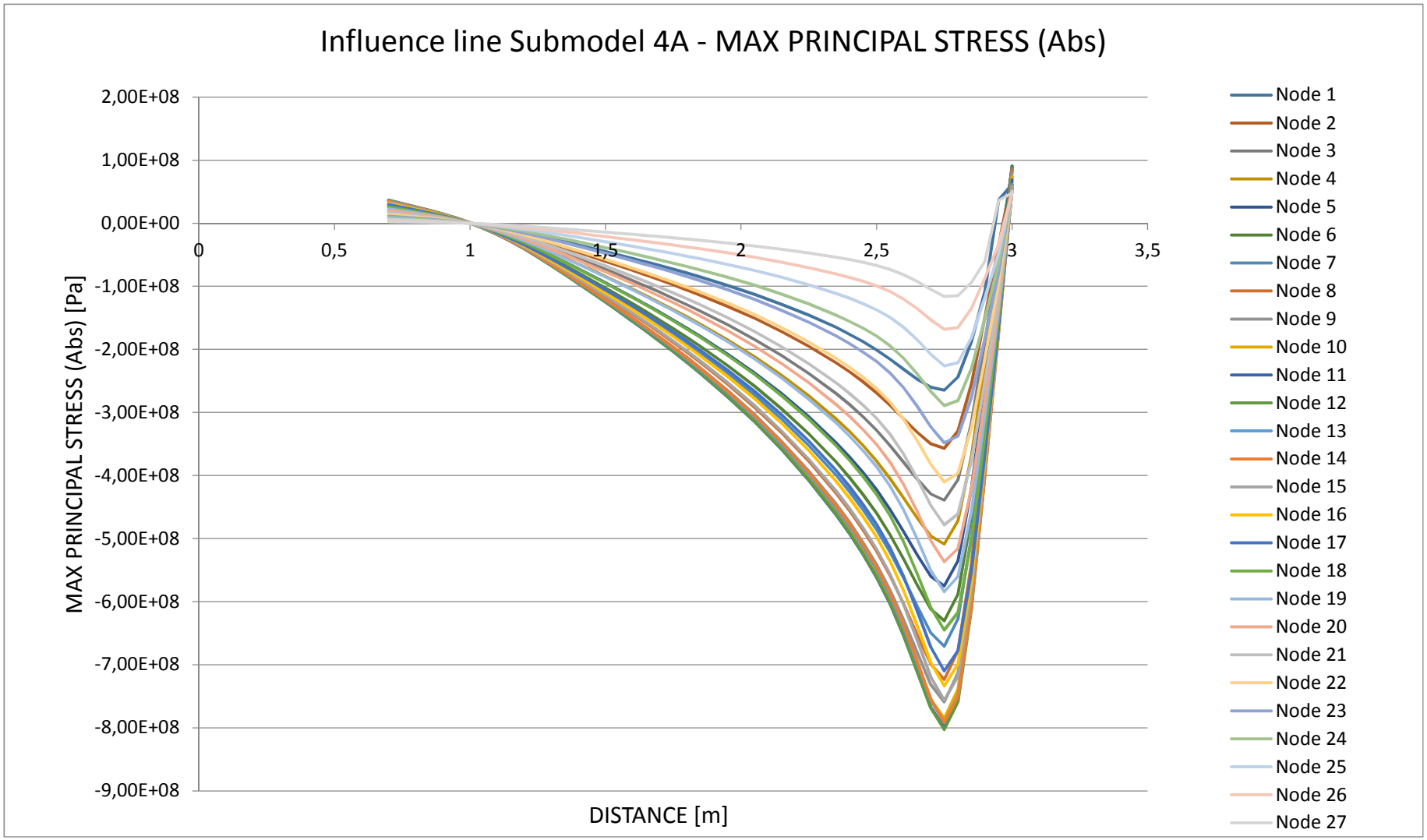

SUBMODEL 4A

MISES STRESS

		Step 1	Step 2	Step 3	Step 4	Step 5	Step 6	Step 7	Step 8	Step 9	Step 10	Step 11
Node	Distance	0,7	0,75	0,8	0,85	0,9	0,95	1	1,05	1,1	1,15	1,2
1	0	1,24E+07	1,06E+07	8,79E+06	6,93E+06	4,94E+06	2,72E+06	2,50E+05	2,76E+06	6,08E+06	9,79E+06	1,39E+07
2	0,00604	1,63E+07	1,39E+07	1,15E+07	9,05E+06	6,45E+06	3,55E+06	2,95E+05	3,58E+06	7,91E+06	1,27E+07	1,81E+07
3	0,01208	1,92E+07	1,64E+07	1,36E+07	1,07E+07	7,62E+06	4,20E+06	3,34E+05	4,22E+06	9,33E+06	1,50E+07	2,13E+07
4	0,01812	2,19E+07	1,87E+07	1,55E+07	1,22E+07	8,69E+06	4,78E+06	3,70E+05	4,81E+06	1,06E+07	1,71E+07	2,43E+07
5	0,02416	2,42E+07	2,06E+07	1,71E+07	1,35E+07	9,59E+06	5,28E+06	4,02E+05	5,30E+06	1,17E+07	1,89E+07	2,68E+07
6	0,0302	2,62E+07	2,23E+07	1,85E+07	1,46E+07	1,04E+07	5,72E+06	4,26E+05	5,75E+06	1,27E+07	2,05E+07	2,90E+07
7	0,03624	2,73E+07	2,33E+07	1,93E+07	1,52E+07	1,09E+07	5,98E+06	4,41E+05	6,01E+06	1,33E+07	2,14E+07	3,04E+07
8	0,04228	2,91E+07	2,48E+07	2,06E+07	1,62E+07	1,16E+07	6,37E+06	4,60E+05	6,43E+06	1,42E+07	2,29E+07	3,24E+07
9	0,04832	3,02E+07	2,58E+07	2,13E+07	1,68E+07	1,20E+07	6,61E+06	4,72E+05	6,68E+06	1,48E+07	2,38E+07	3,37E+07
10	0,05436	3,08E+07	2,63E+07	2,18E+07	1,72E+07	1,23E+07	6,75E+06	4,70E+05	6,86E+06	1,51E+07	2,44E+07	3,46E+07
11	0,0604	3,10E+07	2,65E+07	2,20E+07	1,73E+07	1,24E+07	6,80E+06	4,68E+05	6,93E+06	1,53E+07	2,46E+07	3,49E+07
12	0,06644	3,05E+07	2,60E+07	2,16E+07	1,70E+07	1,21E+07	6,67E+06	4,43E+05	6,86E+06	1,51E+07	2,43E+07	3,45E+07
13	0,07248	2,91E+07	2,49E+07	2,07E+07	1,63E+07	1,16E+07	6,39E+06	4,19E+05	6,61E+06	1,45E+07	2,34E+07	3,32E+07
14	0,07852	2,91E+07	2,49E+07	2,07E+07	1,63E+07	1,16E+07	6,38E+06	4,01E+05	6,68E+06	1,47E+07	2,36E+07	3,34E+07
15	0,08456	2,73E+07	2,33E+07	1,94E+07	1,53E+07	1,09E+07	5,98E+06	3,67E+05	6,33E+06	1,39E+07	2,23E+07	3,16E+07
16	0,0906	2,67E+07	2,29E+07	1,90E+07	1,50E+07	1,07E+07	5,86E+06	3,53E+05	6,27E+06	1,37E+07	2,20E+07	3,12E+07
17	0,09664	2,55E+07	2,19E+07	1,82E+07	1,44E+07	1,03E+07	5,61E+06	3,34E+05	6,08E+06	1,33E+07	2,13E+07	3,02E+07
18	0,10268	2,25E+07	1,93E+07	1,61E+07	1,27E+07	9,10E+06	4,95E+06	3,02E+05	5,49E+06	1,19E+07	1,91E+07	2,71E+07
19	0,10872	1,99E+07	1,71E+07	1,42E+07	1,13E+07	8,07E+06	4,38E+06	2,92E+05	4,95E+06	1,07E+07	1,72E+07	2,44E+07
20	0,11476	1,80E+07	1,54E+07	1,29E+07	1,02E+07	7,31E+06	3,95E+06	2,89E+05	4,59E+06	9,88E+06	1,58E+07	2,24E+07
21	0,1208	1,51E+07	1,30E+07	1,09E+07	8,64E+06	6,17E+06	3,32E+06	2,96E+05	4,00E+06	8,56E+06	1,37E+07	1,94E+07
22	0,12684	1,26E+07	1,09E+07	9,14E+06	7,29E+06	5,22E+06	2,79E+06	3,07E+05	3,50E+06	7,42E+06	1,19E+07	1,68E+07
23	0,13288	1,01E+07	8,77E+06	7,38E+06	5,90E+06	4,22E+06	2,25E+06	3,24E+05	2,96E+06	6,23E+06	9,95E+06	1,41E+07
24	0,13892	7,92E+06	6,87E+06	5,80E+06	4,66E+06	3,34E+06	1,76E+06	3,35E+05	2,47E+06	5,14E+06	8,20E+06	1,16E+07
25	0,14496	5,66E+06	4,94E+06	4,20E+06	3,39E+06	2,43E+06	1,27E+06	3,45E+05	1,96E+06	4,01E+06	6,37E+06	9,00E+06
26	0,151	3,92E+06	3,44E+06	2,94E+06	2,39E+06	1,72E+06	8,90E+05	3,37E+05	1,52E+06	3,05E+06	4,82E+06	6,82E+06
27	0,15704	2,45E+06	2,16E+06	1,87E+06	1,53E+06	1,10E+06	5,72E+05	3,12E+05	1,10E+06	2,15E+06	3,38E+06	4,77E+06

Step 12	Step 13	Step 14	Step 15	Step 16	Step 17	Step 18	Step 19	Step 20	Step 21	Step 22	Step 23	Step 24	Step 25
1,25	1,3	1,35	1,4	1,45	1,5	1,55	1,6	1,65	1,7	1,75	1,8	1,85	1,95
1,83E+07	2,29E+07	2,78E+07	3,27E+07	3,77E+07	4,27E+07	4,78E+07	5,30E+07	5,83E+07	6,38E+07	6,94E+07	7,52E+07	8,11E+07	9,37E+07
2,38E+07	2,99E+07	3,62E+07	4,26E+07	4,91E+07	5,56E+07	6,22E+07	6,90E+07	7,59E+07	8,30E+07	9,03E+07	9,78E+07	1,06E+08	1,22E+08
2,81E+07	3,52E+07	4,27E+07	5,02E+07	5,79E+07	6,56E+07	7,34E+07	8,14E+07	8,96E+07	9,80E+07	1,07E+08	1,15E+08	1,25E+08	1,44E+08
3,20E+07	4,01E+07	4,86E+07	5,72E+07	6,59E+07	7,47E+07	8,37E+07	9,28E+07	1,02E+08	1,12E+08	1,21E+08	1,32E+08	1,42E+08	1,64E+08
3,53E+07	4,43E+07	5,36E+07	6,31E+07	7,28E+07	8,25E+07	9,23E+07	1,02E+08	1,13E+08	1,23E+08	1,34E+08	1,45E+08	1,57E+08	1,81E+08
3,83E+07	4,81E+07	5,82E+07	6,85E+07	7,89E+07	8,95E+07	1,00E+08	1,11E+08	1,22E+08	1,34E+08	1,45E+08	1,57E+08	1,70E+08	1,96E+08
4,00E+07	5,02E+07	6,08E+07	7,16E+07	8,25E+07	9,35E+07	1,05E+08	1,16E+08	1,28E+08	1,40E+08	1,52E+08	1,65E+08	1,78E+08	2,05E+08
4,27E+07	5,36E+07	6,49E+07	7,64E+07	8,81E+07	9,98E+07	1,12E+08	1,24E+08	1,36E+08	1,49E+08	1,62E+08	1,76E+08	1,90E+08	2,19E+08
4,44E+07	5,57E+07	6,75E+07	7,94E+07	9,15E+07	1,04E+08	1,16E+08	1,29E+08	1,42E+08	1,55E+08	1,69E+08	1,83E+08	1,97E+08	2,28E+08
4,55E+07	5,72E+07	6,92E+07	8,15E+07	9,39E+07	1,06E+08	1,19E+08	1,32E+08	1,45E+08	1,59E+08	1,73E+08	1,87E+08	2,02E+08	2,34E+08
4,60E+07	5,77E+07	6,99E+07	8,23E+07	9,48E+07	1,08E+08	1,20E+08	1,33E+08	1,47E+08	1,61E+08	1,75E+08	1,89E+08	2,04E+08	2,36E+08
4,54E+07	5,70E+07	6,90E+07	8,13E+07	9,37E+07	1,06E+08	1,19E+08	1,32E+08	1,45E+08	1,59E+08	1,73E+08	1,87E+08	2,02E+08	2,33E+08
4,37E+07	5,49E+07	6,64E+07	7,82E+07	9,02E+07	1,02E+08	1,14E+08	1,27E+08	1,40E+08	1,53E+08	1,66E+08	1,80E+08	1,94E+08	2,25E+08
4,40E+07	5,53E+07	6,69E+07	7,88E+07	9,08E+07	1,03E+08	1,15E+08	1,28E+08	1,41E+08	1,54E+08	1,67E+08	1,81E+08	1,96E+08	2,26E+08
4,16E+07	5,22E+07	6,32E+07	7,45E+07	8,58E+07	9,73E+07	1,09E+08	1,21E+08	1,33E+08	1,45E+08	1,58E+08	1,71E+08	1,85E+08	2,14E+08
4,11E+07	5,17E+07	6,25E+07	7,36E+07	8,48E+07	9,62E+07	1,08E+08	1,19E+08	1,31E+08	1,44E+08	1,56E+08	1,70E+08	1,83E+08	2,12E+08
3,98E+07	5,00E+07	6,05E+07	7,12E+07	8,21E+07	9,31E+07	1,04E+08	1,16E+08	1,27E+08	1,39E+08	1,51E+08	1,64E+08	1,77E+08	2,05E+08
3,57E+07	4,49E+07	5,43E+07	6,39E+07	7,37E+07	8,35E+07	9,36E+07	1,04E+08	1,14E+08	1,25E+08	1,36E+08	1,47E+08	1,59E+08	1,84E+08
3,21E+07	4,03E+07	4,88E+07	5,74E+07	6,62E+07	7,51E+07	8,41E+07	9,33E+07	1,03E+08	1,12E+08	1,22E+08	1,32E+08	1,43E+08	1,65E+08
2,96E+07	3,71E+07	4,49E+07	5,29E+07	6,10E+07	6,92E+07	7,75E+07	8,60E+07	9,46E+07	1,04E+08	1,13E+08	1,22E+08	1,32E+08	1,52E+08
2,56E+07	3,21E+07	3,89E+07	4,58E+07	5,28E+07	5,99E+07	6,71E+07	7,44E+07	8,19E+07	8,96E+07	9,76E+07	1,06E+08	1,14E+08	1,32E+08
2,22E+07	2,78E+07	3,37E+07	3,97E+07	4,57E+07	5,19E+07	5,81E+07	6,45E+07	7,10E+07	7,77E+07	8,46E+07	9,17E+07	9,90E+07	1,15E+08
1,86E+07	2,33E+07	2,82E+07	3,32E+07	3,83E+07	4,35E+07	4,87E+07	5,41E+07	5,95E+07	6,52E+07	7,09E+07	7,69E+07	8,31E+07	9,61E+07
1,53E+07	1,92E+07	2,32E+07	2,74E+07	3,16E+07	3,58E+07	4,01E+07	4,46E+07	4,91E+07	5,37E+07	5,85E+07	6,34E+07	6,85E+07	7,92E+07
1,19E+07	1,49E+07	1,80E+07	2,13E+07	2,45E+07	2,78E+07	3,12E+07	3,46E+07	3,82E+07	4,18E+07	4,55E+07	4,93E+07	5,33E+07	6,17E+07
8,99E+06	1,13E+07	1,37E+07	1,61E+07	1,86E+07	2,11E+07	2,36E+07	2,63E+07	2,89E+07	3,17E+07	3,45E+07	3,74E+07	4,04E+07	4,68E+07
6,29E+06	7,89E+06	9,55E+06	1,13E+07	1,30E+07	1,47E+07	1,65E+07	1,84E+07	2,02E+07	2,22E+07	2,41E+07	2,62E+07	2,83E+07	3,28E+07

Step 26	Step 27	Step 28	Step 29	Step 30	Step 31	Step 32	Step 33	Step 34	Step 35	Step 36	Step 37	Step 38	Step 39
2,05	2,15	2,25	2,35	2,4	2,45	2,5	2,55	2,6	2,65	2,7	2,75	2,8	2,85
1,07E+08	1,22E+08	1,39E+08	1,57E+08	1,68E+08	1,79E+08	1,92E+08	2,06E+08	2,21E+08	2,37E+08	2,50E+08	2,55E+08	2,37E+08	1,87E+08
1,40E+08	1,59E+08	1,81E+08	2,05E+08	2,18E+08	2,33E+08	2,49E+08	2,68E+08	2,88E+08	3,08E+08	3,26E+08	3,34E+08	3,10E+08	2,44E+08
1,65E+08	1,88E+08	2,13E+08	2,42E+08	2,57E+08	2,75E+08	2,94E+08	3,16E+08	3,40E+08	3,65E+08	3,86E+08	3,96E+08	3,68E+08	2,90E+08
1,88E+08	2,14E+08	2,43E+08	2,75E+08	2,93E+08	3,13E+08	3,35E+08	3,60E+08	3,87E+08	4,16E+08	4,42E+08	4,54E+08	4,24E+08	3,35E+08
2,07E+08	2,36E+08	2,68E+08	3,04E+08	3,24E+08	3,45E+08	3,70E+08	3,97E+08	4,28E+08	4,61E+08	4,90E+08	5,05E+08	4,72E+08	3,74E+08
2,25E+08	2,56E+08	2,91E+08	3,30E+08	3,51E+08	3,75E+08	4,01E+08	4,31E+08	4,65E+08	5,01E+08	5,35E+08	5,52E+08	5,17E+08	4,11E+08
2,35E+08	2,68E+08	3,04E+08	3,45E+08	3,67E+08	3,92E+08	4,19E+08	4,51E+08	4,86E+08	5,25E+08	5,62E+08	5,81E+08	5,45E+08	4,35E+08
2,51E+08	2,86E+08	3,25E+08	3,68E+08	3,92E+08	4,18E+08	4,48E+08	4,81E+08	5,20E+08	5,62E+08	6,03E+08	6,25E+08	5,87E+08	4,70E+08
2,61E+08	2,97E+08	3,38E+08	3,83E+08	4,08E+08	4,35E+08	4,66E+08	5,01E+08	5,41E+08	5,87E+08	6,30E+08	6,55E+08	6,16E+08	4,95E+08
2,68E+08	3,05E+08	3,46E+08	3,93E+08	4,18E+08	4,46E+08	4,78E+08	5,14E+08	5,56E+08	6,03E+08	6,50E+08	6,76E+08	6,38E+08	5,14E+08
2,71E+08	3,08E+08	3,50E+08	3,97E+08	4,23E+08	4,51E+08	4,83E+08	5,19E+08	5,62E+08	6,11E+08	6,60E+08	6,88E+08	6,51E+08	5,25E+08
2,67E+08	3,04E+08	3,46E+08	3,92E+08	4,18E+08	4,46E+08	4,77E+08	5,13E+08	5,56E+08	6,06E+08	6,55E+08	6,85E+08	6,49E+08	5,26E+08
2,57E+08	2,93E+08	3,33E+08	3,78E+08	4,02E+08	4,29E+08	4,60E+08	4,95E+08	5,36E+08	5,85E+08	6,34E+08	6,65E+08	6,31E+08	5,12E+08
2,59E+08	2,95E+08	3,36E+08	3,81E+08	4,05E+08	4,33E+08	4,63E+08	4,99E+08	5,41E+08	5,92E+08	6,43E+08	6,75E+08	6,42E+08	5,22E+08
2,45E+08	2,79E+08	3,17E+08	3,60E+08	3,84E+08	4,10E+08	4,39E+08	4,72E+08	5,13E+08	5,62E+08	6,12E+08	6,44E+08	6,14E+08	5,01E+08
2,42E+08	2,76E+08	3,14E+08	3,56E+08	3,80E+08	4,05E+08	4,34E+08	4,68E+08	5,08E+08	5,57E+08	6,08E+08	6,41E+08	6,12E+08	5,00E+08
2,35E+08	2,68E+08	3,04E+08	3,45E+08	3,68E+08	3,93E+08	4,21E+08	4,53E+08	4,93E+08	5,42E+08	5,93E+08	6,27E+08	6,00E+08	4,91E+08
2,11E+08	2,40E+08	2,73E+08	3,10E+08	3,31E+08	3,53E+08	3,78E+08	4,08E+08	4,45E+08	4,89E+08	5,36E+08	5,69E+08	5,46E+08	4,48E+08
1,90E+08	2,16E+08	2,46E+08	2,79E+08	2,97E+08	3,18E+08	3,41E+08	3,68E+08	4,01E+08	4,42E+08	4,86E+08	5,16E+08	4,96E+08	4,08E+08
1,75E+08	1,99E+08	2,27E+08	2,57E+08	2,74E+08	2,93E+08	3,15E+08	3,40E+08	3,71E+08	4,10E+08	4,51E+08	4,81E+08	4,64E+08	3,82E+08
1,51E+08	1,73E+08	1,97E+08	2,23E+08	2,38E+08	2,55E+08	2,73E+08	2,96E+08	3,23E+08	3,58E+08	3,96E+08	4,23E+08	4,10E+08	3,38E+08
1,31E+08	1,50E+08	1,71E+08	1,94E+08	2,07E+08	2,21E+08	2,38E+08	2,57E+08	2,82E+08	3,13E+08	3,47E+08	3,72E+08	3,61E+08	2,99E+08
1,10E+08	1,26E+08	1,43E+08	1,63E+08	1,74E+08	1,86E+08	2,00E+08	2,17E+08	2,38E+08	2,65E+08	2,95E+08	3,18E+08	3,10E+08	2,57E+08
9,09E+07	1,04E+08	1,18E+08	1,35E+08	1,44E+08	1,54E+08	1,66E+08	1,80E+08	1,98E+08	2,21E+08	2,47E+08	2,68E+08	2,62E+08	2,18E+08
7,08E+07	8,09E+07	9,22E+07	1,05E+08	1,12E+08	1,20E+08	1,30E+08	1,41E+08	1,56E+08	1,75E+08	1,96E+08	2,14E+08	2,11E+08	1,76E+08
5,37E+07	6,14E+07	7,01E+07	7,99E+07	8,55E+07	9,18E+07	9,91E+07	1,08E+08	1,20E+08	1,35E+08	1,52E+08	1,67E+08	1,65E+08	1,40E+08
3,76E+07	4,31E+07	4,92E+07	5,62E+07	6,01E+07	6,47E+07	7,00E+07	7,64E+07	8,49E+07	9,58E+07	1,09E+08	1,20E+08	1,20E+08	1,03E+08

Step 40	Step 41	Step 42
2,9	2,95	3
1,17E+08	5,12E+07	6,10E+07
1,50E+08	5,86E+07	6,99E+07
1,79E+08	6,75E+07	7,56E+07
2,08E+08	7,80E+07	7,82E+07
2,34E+08	8,93E+07	7,98E+07
2,60E+08	1,01E+08	7,86E+07
2,78E+08	1,12E+08	7,63E+07
3,02E+08	1,24E+08	7,45E+07
3,21E+08	1,35E+08	7,12E+07
3,35E+08	1,45E+08	6,76E+07
3,45E+08	1,53E+08	6,38E+07
3,48E+08	1,57E+08	5,94E+07
3,41E+08	1,57E+08	5,49E+07
3,49E+08	1,62E+08	5,32E+07
3,37E+08	1,59E+08	4,95E+07
3,37E+08	1,60E+08	4,90E+07
3,32E+08	1,59E+08	4,78E+07
3,03E+08	1,47E+08	4,64E+07
2,77E+08	1,35E+08	4,56E+07
2,59E+08	1,27E+08	4,54E+07
2,30E+08	1,14E+08	4,47E+07
2,04E+08	1,02E+08	4,44E+07
1,76E+08	8,91E+07	4,42E+07
1,50E+08	7,77E+07	4,37E+07
1,22E+08	6,65E+07	4,34E+07
9,86E+07	5,76E+07	4,28E+07
7,63E+07	5,07E+07	4,21E+07

MIN	MAX
2,50E+05	2,55E+08
2,95E+05	3,34E+08
3,34E+05	3,96E+08
3,70E+05	4,54E+08
4,02E+05	5,05E+08
4,26E+05	5,52E+08
4,41E+05	5,81E+08
4,60E+05	6,25E+08
4,72E+05	6,55E+08
4,70E+05	6,76E+08
4,68E+05	6,88E+08
4,43E+05	6,85E+08
4,19E+05	6,65E+08
4,01E+05	6,75E+08
3,67E+05	6,44E+08
3,53E+05	6,41E+08
3,34E+05	6,27E+08
3,02E+05	5,69E+08
2,92E+05	5,16E+08
2,89E+05	4,81E+08
2,96E+05	4,23E+08
3,07E+05	3,72E+08
3,24E+05	3,18E+08
3,35E+05	2,68E+08
3,45E+05	2,14E+08
3,37E+05	1,67E+08
3,12E+05	1,20E+08

Result - Mises stress

The influence lines for Submodel 4A, for each node at the U-sape. Maximum Mises stress 688.22 MPa at node 12 in load step 2.75 m.

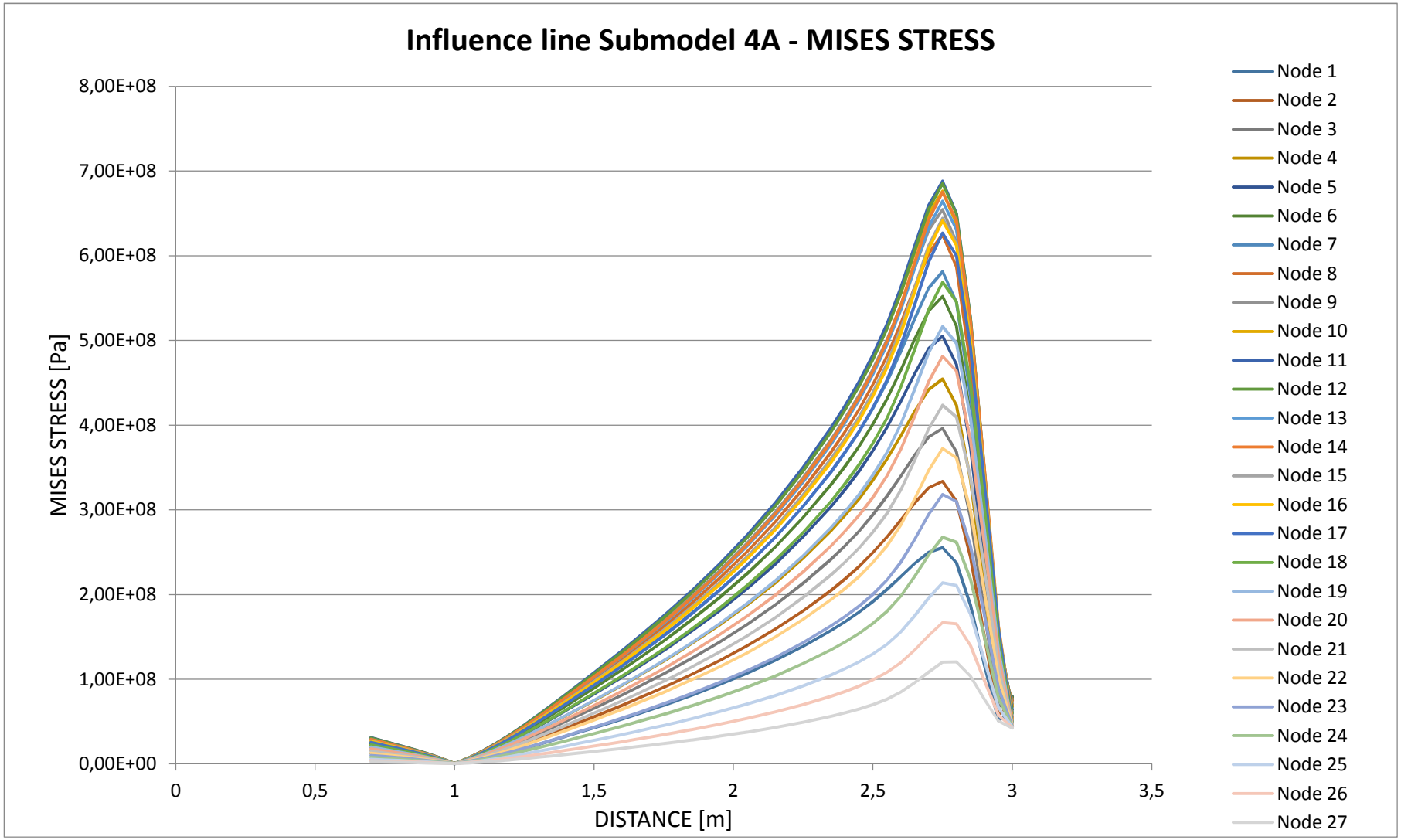

SUBMODEL 4B

MAX PRINCIPAL STRESS (Abs)

		Step 1	Step 2	Step 3	Step 4	Step 5	Step 6	Step 7	Step 8	Step 9	Step 10	Step 11
Node	Distance	0,7	0,75	0,8	0,85	0,9	0,95	1	1,05	1,1	1,15	1,2
1	0	-1,09E+07	-9,31E+06	-7,75E+06	-6,14E+06	-4,39E+06	-2,39E+06	1,63E+05	2,63E+06	5,72E+06	9,19E+06	1,30E+07
2	0,00604	-1,47E+07	-1,26E+07	-1,05E+07	-8,35E+06	-5,96E+06	-3,25E+06	1,57E+05	3,57E+06	7,77E+06	1,25E+07	1,77E+07
3	0,01208	-1,79E+07	-1,53E+07	-1,28E+07	-1,01E+07	-7,23E+06	-3,94E+06	1,51E+05	4,32E+06	9,41E+06	1,51E+07	2,14E+07
4	0,01812	-2,06E+07	-1,77E+07	-1,47E+07	-1,17E+07	-8,34E+06	-4,54E+06	1,47E+05	4,98E+06	1,08E+07	1,74E+07	2,47E+07
5	0,02416	-2,33E+07	-1,99E+07	-1,66E+07	-1,31E+07	-9,39E+06	-5,12E+06	-1,69E+05	5,59E+06	1,22E+07	1,96E+07	2,78E+07
6	0,0302	-2,53E+07	-2,17E+07	-1,81E+07	-1,43E+07	-1,02E+07	-5,58E+06	-1,89E+05	6,09E+06	1,33E+07	2,13E+07	3,02E+07
7	0,03624	-2,71E+07	-2,32E+07	-1,93E+07	-1,53E+07	-1,09E+07	-5,97E+06	-2,15E+05	6,48E+06	1,41E+07	2,27E+07	3,22E+07
8	0,04228	-2,91E+07	-2,50E+07	-2,08E+07	-1,65E+07	-1,18E+07	-6,41E+06	-2,39E+05	6,95E+06	1,52E+07	2,44E+07	3,45E+07
9	0,04832	-3,10E+07	-2,65E+07	-2,21E+07	-1,75E+07	-1,25E+07	-6,82E+06	-2,73E+05	7,35E+06	1,61E+07	2,58E+07	3,66E+07
10	0,05436	-3,19E+07	-2,73E+07	-2,27E+07	-1,80E+07	-1,28E+07	-7,01E+06	-2,96E+05	7,52E+06	1,64E+07	2,65E+07	3,75E+07
11	0,0604	-3,23E+07	-2,77E+07	-2,30E+07	-1,82E+07	-1,30E+07	-7,11E+06	-3,26E+05	7,58E+06	1,66E+07	2,67E+07	3,78E+07
12	0,06644	-3,33E+07	-2,85E+07	-2,37E+07	-1,88E+07	-1,34E+07	-7,33E+06	-3,56E+05	7,77E+06	1,70E+07	2,74E+07	3,88E+07
13	0,07248	-3,32E+07	-2,84E+07	-2,36E+07	-1,86E+07	-1,33E+07	-7,29E+06	-3,84E+05	7,65E+06	1,68E+07	2,70E+07	3,83E+07
14	0,07852	-3,36E+07	-2,88E+07	-2,39E+07	-1,89E+07	-1,35E+07	-7,39E+06	-4,16E+05	7,70E+06	1,69E+07	2,73E+07	3,86E+07
15	0,08456	-3,36E+07	-2,87E+07	-2,39E+07	-1,88E+07	-1,35E+07	-7,39E+06	-4,52E+05	7,62E+06	1,68E+07	2,70E+07	3,83E+07
16	0,0906	-3,27E+07	-2,79E+07	-2,32E+07	-1,83E+07	-1,31E+07	-7,19E+06	-4,78E+05	7,32E+06	1,61E+07	2,60E+07	3,69E+07
17	0,09664	-3,20E+07	-2,73E+07	-2,26E+07	-1,78E+07	-1,27E+07	-7,02E+06	-5,10E+05	7,05E+06	1,56E+07	2,51E+07	3,56E+07
18	0,10268	-3,06E+07	-2,61E+07	-2,16E+07	-1,70E+07	-1,22E+07	-6,72E+06	-5,31E+05	6,65E+06	1,47E+07	2,38E+07	3,37E+07
19	0,10872	-2,87E+07	-2,45E+07	-2,03E+07	-1,60E+07	-1,14E+07	-6,30E+06	-5,42E+05	6,14E+06	1,37E+07	2,20E+07	3,12E+07
20	0,11476	-2,74E+07	-2,33E+07	-1,93E+07	-1,52E+07	-1,08E+07	-6,01E+06	-5,59E+05	5,76E+06	1,29E+07	2,07E+07	2,94E+07
21	0,1208	-2,56E+07	-2,18E+07	-1,80E+07	-1,42E+07	-1,01E+07	-5,62E+06	-5,68E+05	5,28E+06	1,18E+07	1,91E+07	2,71E+07
22	0,12684	-2,32E+07	-1,97E+07	-1,63E+07	-1,28E+07	-9,13E+06	-5,09E+06	-5,59E+05	4,68E+06	1,05E+07	1,70E+07	2,41E+07
23	0,13288	-2,10E+07	-1,78E+07	-1,47E+07	-1,15E+07	-8,23E+06	-4,60E+06	-5,50E+05	4,13E+06	9,34E+06	1,51E+07	2,14E+07
24	0,13892	-1,85E+07	-1,57E+07	-1,29E+07	-1,01E+07	-7,23E+06	-4,05E+06	-5,22E+05	3,56E+06	8,08E+06	1,31E+07	1,85E+07
25	0,14496	-1,56E+07	-1,33E+07	-1,09E+07	-8,54E+06	-6,09E+06	-3,42E+06	-4,82E+05	2,92E+06	6,67E+06	1,08E+07	1,53E+07
26	0,151	-1,29E+07	-1,09E+07	-8,95E+06	-7,00E+06	-4,99E+06	-2,82E+06	-4,25E+05	2,35E+06	5,37E+06	8,71E+06	1,24E+07
27	0,15704	-8,92E+06	-7,54E+06	-6,19E+06	-4,83E+06	-3,44E+06	-1,95E+06	-3,27E+05	1,57E+06	3,61E+06	5,86E+06	8,31E+06

Step 12	Step 13	Step 14	Step 15	Step 16	Step 17	Step 18	Step 19	Step 20	Step 21	Step 22	Step 23	Step 24	Step 25
1,25	1,3	1,35	1,4	1,45	1,5	1,55	1,6	1,65	1,7	1,75	1,8	1,85	1,95
1,72E+07	2,15E+07	2,61E+07	3,07E+07	3,54E+07	4,01E+07	4,50E+07	4,99E+07	5,49E+07	6,00E+07	6,53E+07	7,08E+07	7,65E+07	8,84E+07
2,33E+07	2,93E+07	3,54E+07	4,17E+07	4,81E+07	5,45E+07	6,11E+07	6,77E+07	7,46E+07	8,16E+07	8,88E+07	9,62E+07	1,04E+08	1,20E+08
2,82E+07	3,55E+07	4,29E+07	5,05E+07	5,82E+07	6,60E+07	7,40E+07	8,21E+07	9,03E+07	9,88E+07	1,08E+08	1,17E+08	1,26E+08	1,45E+08
3,25E+07	4,08E+07	4,94E+07	5,82E+07	6,71E+07	7,61E+07	8,52E+07	9,45E+07	1,04E+08	1,14E+08	1,24E+08	1,34E+08	1,45E+08	1,68E+08
3,66E+07	4,59E+07	5,56E+07	6,55E+07	7,55E+07	8,56E+07	9,59E+07	1,06E+08	1,17E+08	1,28E+08	1,39E+08	1,51E+08	1,63E+08	1,88E+08
3,98E+07	5,00E+07	6,05E+07	7,13E+07	8,22E+07	9,32E+07	1,04E+08	1,16E+08	1,27E+08	1,39E+08	1,52E+08	1,64E+08	1,77E+08	2,05E+08
4,25E+07	5,33E+07	6,45E+07	7,60E+07	8,76E+07	9,93E+07	1,11E+08	1,23E+08	1,36E+08	1,49E+08	1,62E+08	1,75E+08	1,89E+08	2,19E+08
4,55E+07	5,72E+07	6,92E+07	8,15E+07	9,39E+07	1,07E+08	1,19E+08	1,32E+08	1,46E+08	1,59E+08	1,73E+08	1,88E+08	2,03E+08	2,34E+08
4,82E+07	6,05E+07	7,33E+07	8,63E+07	9,94E+07	1,13E+08	1,26E+08	1,40E+08	1,54E+08	1,69E+08	1,84E+08	1,99E+08	2,15E+08	2,48E+08
4,94E+07	6,20E+07	7,51E+07	8,84E+07	1,02E+08	1,16E+08	1,29E+08	1,44E+08	1,58E+08	1,73E+08	1,88E+08	2,04E+08	2,20E+08	2,54E+08
4,99E+07	6,26E+07	7,58E+07	8,92E+07	1,03E+08	1,17E+08	1,31E+08	1,45E+08	1,59E+08	1,74E+08	1,90E+08	2,06E+08	2,22E+08	2,56E+08
5,11E+07	6,42E+07	7,77E+07	9,15E+07	1,05E+08	1,20E+08	1,34E+08	1,49E+08	1,63E+08	1,79E+08	1,95E+08	2,11E+08	2,28E+08	2,63E+08
5,05E+07	6,34E+07	7,68E+07	9,04E+07	1,04E+08	1,18E+08	1,32E+08	1,47E+08	1,61E+08	1,77E+08	1,92E+08	2,08E+08	2,25E+08	2,60E+08
5,09E+07	6,39E+07	7,74E+07	9,11E+07	1,05E+08	1,19E+08	1,33E+08	1,48E+08	1,63E+08	1,78E+08	1,94E+08	2,10E+08	2,26E+08	2,62E+08
5,05E+07	6,33E+07	7,67E+07	9,03E+07	1,04E+08	1,18E+08	1,32E+08	1,46E+08	1,61E+08	1,76E+08	1,92E+08	2,08E+08	2,24E+08	2,59E+08
4,86E+07	6,10E+07	7,38E+07	8,69E+07	1,00E+08	1,14E+08	1,27E+08	1,41E+08	1,55E+08	1,70E+08	1,85E+08	2,00E+08	2,16E+08	2,50E+08
4,69E+07	5,89E+07	7,13E+07	8,40E+07	9,68E+07	1,10E+08	1,23E+08	1,36E+08	1,50E+08	1,64E+08	1,78E+08	1,93E+08	2,09E+08	2,41E+08
4,44E+07	5,58E+07	6,75E+07	7,95E+07	9,16E+07	1,04E+08	1,16E+08	1,29E+08	1,42E+08	1,55E+08	1,69E+08	1,83E+08	1,97E+08	2,28E+08
4,12E+07	5,17E+07	6,26E+07	7,37E+07	8,49E+07	9,62E+07	1,08E+08	1,19E+08	1,31E+08	1,44E+08	1,56E+08	1,69E+08	1,83E+08	2,11E+08
3,87E+07	4,86E+07	5,89E+07	6,93E+07	7,99E+07	9,05E+07	1,01E+08	1,12E+08	1,24E+08	1,35E+08	1,47E+08	1,59E+08	1,72E+08	1,99E+08
3,57E+07	4,48E+07	5,42E+07	6,38E+07	7,36E+07	8,34E+07	9,33E+07	1,03E+08	1,14E+08	1,24E+08	1,35E+08	1,47E+08	1,58E+08	1,83E+08
3,18E+07	3,99E+07	4,83E+07	5,68E+07	6,55E+07	7,42E+07	8,30E+07	9,20E+07	1,01E+08	1,11E+08	1,20E+08	1,30E+08	1,41E+08	1,63E+08
2,82E+07	3,54E+07	4,29E+07	5,05E+07	5,82E+07	6,59E+07	7,37E+07	8,17E+07	8,99E+07	9,83E+07	1,07E+08	1,16E+08	1,25E+08	1,44E+08
2,44E+07	3,07E+07	3,71E+07	4,37E+07	5,03E+07	5,70E+07	6,38E+07	7,07E+07	7,78E+07	8,50E+07	9,24E+07	1,00E+08	1,08E+08	1,25E+08
2,02E+07	2,53E+07	3,07E+07	3,61E+07	4,16E+07	4,71E+07	5,27E+07	5,84E+07	6,42E+07	7,02E+07	7,63E+07	8,26E+07	8,91E+07	1,03E+08
1,63E+07	2,04E+07	2,47E+07	2,91E+07	3,35E+07	3,80E+07	4,25E+07	4,71E+07	5,17E+07	5,65E+07	6,15E+07	6,66E+07	7,18E+07	8,29E+07
1,09E+07	1,37E+07	1,66E+07	1,96E+07	2,25E+07	2,55E+07	2,86E+07	3,16E+07	3,48E+07	3,80E+07	4,13E+07	4,47E+07	4,82E+07	5,57E+07

Step 26	Step 27	Step 28	Step 29	Step 30	Step 31	Step 32	Step 33	Step 34	Step 35	Step 36	Step 37	Step 38	Step 39
2,05	2,15	2,25	2,35	2,4	2,45	2,5	2,55	2,6	2,65	2,7	2,75	2,8	2,85
1,01E+08	1,16E+08	1,31E+08	1,49E+08	1,59E+08	1,70E+08	1,81E+08	1,96E+08	2,15E+08	2,41E+08	2,71E+08	2,91E+08	2,82E+08	2,40E+08
1,38E+08	1,57E+08	1,78E+08	2,03E+08	2,16E+08	2,30E+08	2,46E+08	2,66E+08	2,92E+08	3,27E+08	3,66E+08	3,93E+08	3,81E+08	3,23E+08
1,67E+08	1,90E+08	2,16E+08	2,45E+08	2,62E+08	2,79E+08	2,99E+08	3,22E+08	3,53E+08	3,95E+08	4,42E+08	4,74E+08	4,59E+08	3,88E+08
1,92E+08	2,19E+08	2,49E+08	2,83E+08	3,01E+08	3,21E+08	3,44E+08	3,71E+08	4,07E+08	4,54E+08	5,07E+08	5,42E+08	5,25E+08	4,42E+08
2,16E+08	2,46E+08	2,80E+08	3,18E+08	3,39E+08	3,62E+08	3,87E+08	4,17E+08	4,57E+08	5,10E+08	5,68E+08	6,07E+08	5,86E+08	4,92E+08
2,35E+08	2,68E+08	3,05E+08	3,46E+08	3,69E+08	3,93E+08	4,21E+08	4,54E+08	4,97E+08	5,54E+08	6,15E+08	6,57E+08	6,33E+08	5,29E+08
2,51E+08	2,86E+08	3,25E+08	3,69E+08	3,93E+08	4,19E+08	4,49E+08	4,84E+08	5,29E+08	5,89E+08	6,53E+08	6,96E+08	6,70E+08	5,58E+08
2,69E+08	3,06E+08	3,48E+08	3,95E+08	4,21E+08	4,49E+08	4,81E+08	5,19E+08	5,67E+08	6,30E+08	6,97E+08	7,42E+08	7,13E+08	5,92E+08
2,84E+08	3,24E+08	3,69E+08	4,18E+08	4,46E+08	4,76E+08	5,09E+08	5,49E+08	5,99E+08	6,65E+08	7,35E+08	7,81E+08	7,49E+08	6,20E+08
2,91E+08	3,32E+08	3,77E+08	4,28E+08	4,56E+08	4,87E+08	5,21E+08	5,62E+08	6,13E+08	6,79E+08	7,49E+08	7,95E+08	7,62E+08	6,28E+08
2,94E+08	3,35E+08	3,81E+08	4,32E+08	4,60E+08	4,91E+08	5,26E+08	5,66E+08	6,18E+08	6,83E+08	7,53E+08	7,98E+08	7,63E+08	6,28E+08
3,01E+08	3,44E+08	3,90E+08	4,43E+08	4,72E+08	5,04E+08	5,39E+08	5,80E+08	6,33E+08	6,99E+08	7,69E+08	8,13E+08	7,77E+08	6,37E+08
2,98E+08	3,39E+08	3,85E+08	4,37E+08	4,66E+08	4,97E+08	5,32E+08	5,73E+08	6,24E+08	6,88E+08	7,56E+08	7,99E+08	7,62E+08	6,24E+08
3,00E+08	3,42E+08	3,88E+08	4,40E+08	4,69E+08	5,01E+08	5,36E+08	5,76E+08	6,27E+08	6,91E+08	7,58E+08	8,00E+08	7,62E+08	6,22E+08
2,97E+08	3,39E+08	3,85E+08	4,36E+08	4,65E+08	4,96E+08	5,30E+08	5,71E+08	6,21E+08	6,83E+08	7,48E+08	7,88E+08	7,49E+08	6,10E+08
2,86E+08	3,26E+08	3,70E+08	4,20E+08	4,47E+08	4,77E+08	5,10E+08	5,48E+08	5,96E+08	6,55E+08	7,16E+08	7,53E+08	7,15E+08	5,81E+08
2,76E+08	3,15E+08	3,57E+08	4,05E+08	4,31E+08	4,60E+08	4,92E+08	5,29E+08	5,74E+08	6,30E+08	6,88E+08	7,22E+08	6,85E+08	5,55E+08
2,61E+08	2,97E+08	3,38E+08	3,83E+08	4,08E+08	4,34E+08	4,64E+08	4,99E+08	5,41E+08	5,93E+08	6,46E+08	6,78E+08	6,42E+08	5,20E+08
2,42E+08	2,76E+08	3,13E+08	3,54E+08	3,77E+08	4,02E+08	4,30E+08	4,62E+08	5,01E+08	5,48E+08	5,96E+08	6,25E+08	5,90E+08	4,77E+08
2,27E+08	2,59E+08	2,94E+08	3,33E+08	3,54E+08	3,78E+08	4,04E+08	4,33E+08	4,69E+08	5,13E+08	5,57E+08	5,83E+08	5,50E+08	4,44E+08
2,09E+08	2,38E+08	2,70E+08	3,06E+08	3,26E+08	3,47E+08	3,71E+08	3,98E+08	4,31E+08	4,70E+08	5,10E+08	5,32E+08	5,02E+08	4,05E+08
1,86E+08	2,12E+08	2,40E+08	2,72E+08	2,90E+08	3,08E+08	3,29E+08	3,53E+08	3,81E+08	4,16E+08	4,50E+08	4,69E+08	4,41E+08	3,56E+08
1,65E+08	1,88E+08	2,13E+08	2,41E+08	2,57E+08	2,73E+08	2,92E+08	3,12E+08	3,37E+08	3,67E+08	3,97E+08	4,13E+08	3,88E+08	3,12E+08
1,43E+08	1,62E+08	1,84E+08	2,08E+08	2,22E+08	2,36E+08	2,52E+08	2,69E+08	2,90E+08	3,16E+08	3,41E+08	3,54E+08	3,31E+08	2,67E+08
1,18E+08	1,34E+08	1,52E+08	1,72E+08	1,83E+08	1,94E+08	2,07E+08	2,21E+08	2,38E+08	2,59E+08	2,79E+08	2,89E+08	2,70E+08	2,17E+08
9,48E+07	1,08E+08	1,22E+08	1,38E+08	1,47E+08	1,56E+08	1,66E+08	1,78E+08	1,91E+08	2,07E+08	2,23E+08	2,30E+08	2,15E+08	1,73E+08
6,37E+07	7,24E+07	8,20E+07	9,27E+07	9,85E+07	1,05E+08	1,11E+08	1,19E+08	1,27E+08	1,38E+08	1,48E+08	1,52E+08	1,42E+08	1,14E+08

Step 40	Step 41	Step 42
2,9	2,95	3
1,78E+08	1,09E+08	5,27E+07
2,38E+08	1,43E+08	5,48E+07
2,84E+08	1,68E+08	5,58E+07
3,21E+08	1,86E+08	5,54E+07
3,54E+08	2,01E+08	5,44E+07
3,78E+08	2,10E+08	5,27E+07
3,95E+08	2,15E+08	5,06E+07
4,17E+08	2,23E+08	4,84E+07
4,33E+08	2,26E+08	4,59E+07
4,35E+08	2,24E+08	4,34E+07
4,32E+08	2,18E+08	4,12E+07
4,36E+08	2,16E+08	3,90E+07
4,25E+08	2,08E+08	3,80E+07
4,21E+08	2,03E+08	3,60E+07
4,11E+08	1,96E+08	3,54E+07
3,90E+08	1,84E+08	3,46E+07
3,72E+08	1,75E+08	3,47E+07
3,47E+08	1,63E+08	3,49E+07
3,19E+08	1,50E+08	3,60E+07
2,96E+08	1,39E+08	3,68E+07
2,70E+08	1,28E+08	3,81E+07
2,38E+08	1,14E+08	3,95E+07
2,10E+08	1,02E+08	4,10E+07
1,80E+08	8,87E+07	4,21E+07
1,47E+08	7,47E+07	4,34E+07
1,17E+08	6,10E+07	4,39E+07
7,82E+07	5,37E+07	4,44E+07

MIN	MAX
-1,0855E+07	2,9060E+08
-1,4744E+07	3,9278E+08
-1,7892E+07	4,7352E+08
-2,0628E+07	5,4236E+08
-2,3251E+07	6,0657E+08
-2,5350E+07	6,5658E+08
-2,7113E+07	6,9580E+08
-2,9132E+07	7,4202E+08
-3,0979E+07	7,8086E+08
-3,1862E+07	7,9514E+08
-3,2345E+07	7,9761E+08
-3,3336E+07	8,1346E+08
-3,3154E+07	7,9884E+08
-3,3639E+07	7,9976E+08
-3,3624E+07	7,8777E+08
-3,2709E+07	7,5295E+08
-3,1957E+07	7,2248E+08
-3,0598E+07	6,7811E+08
-2,8730E+07	6,2453E+08
-2,7407E+07	5,8255E+08
-2,5628E+07	5,3234E+08
-2,3213E+07	4,6924E+08
-2,1002E+07	4,1290E+08
-1,8513E+07	3,5358E+08
-1,5642E+07	2,8877E+08
-1,2865E+07	2,3015E+08
-8,9164E+06	1,5230E+08

Result - Principal stress (Abs)

The influence lines for Submodel 4B, for each node at the U-sape. Maximum principal stress 813.46 MPa (tension) at node 12 in load step 2.75 m.

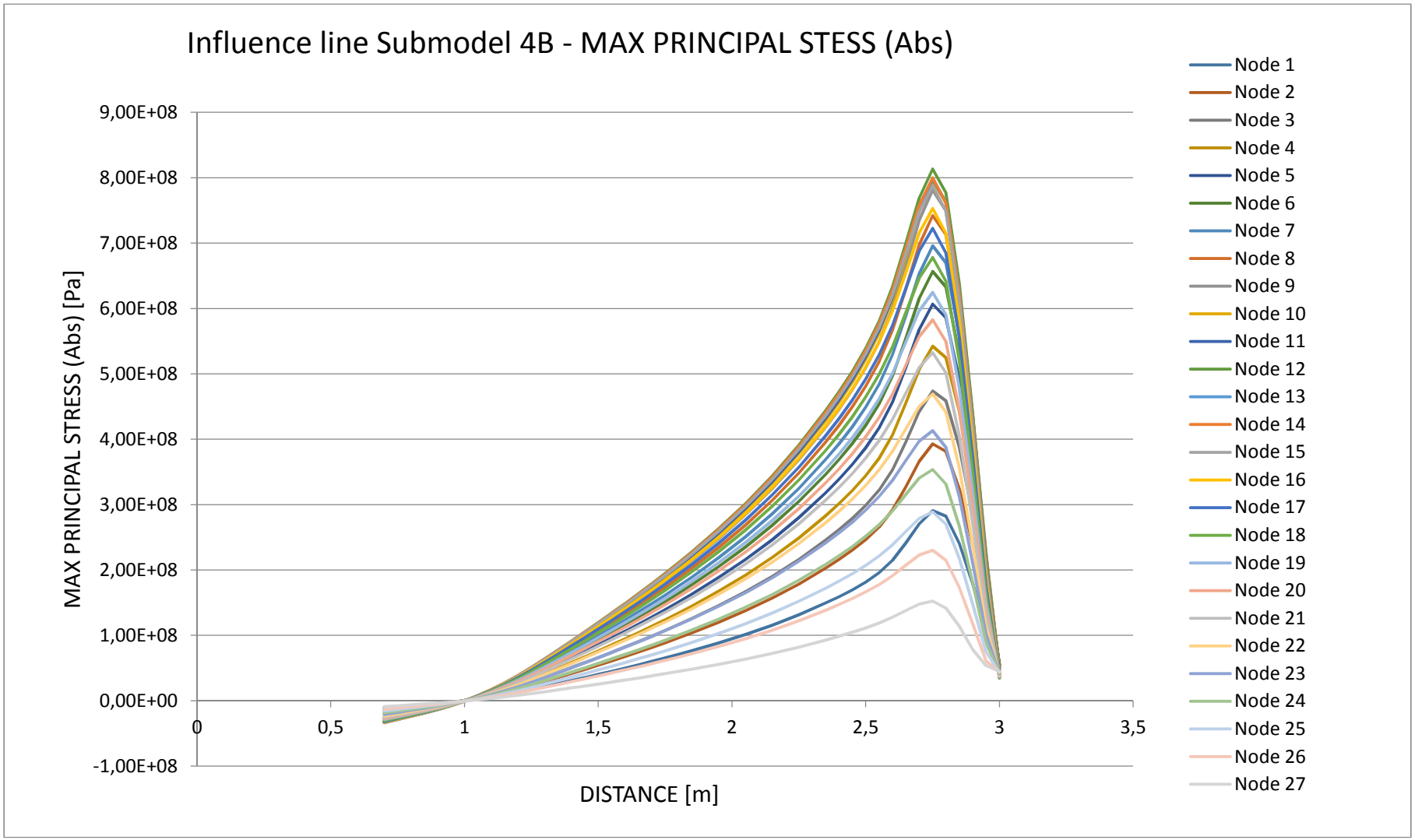

SUBMODEL 4B

MISES STRESS

		Step 1	Step 2	Step 3	Step 4	Step 5	Step 6	Step 7	Step 8	Step 9	Step 10	Step 11
Node	Distance	0,7	0,75	0,8	0,85	0,9	0,95	1	1,05	1,1	1,15	1,2
1	0	1,01E+07	8,65E+06	7,20E+06	5,70E+06	4,07E+06	2,23E+06	2,07E+05	2,38E+06	5,21E+06	8,38E+06	1,19E+07
2	0,00604	1,33E+07	1,14E+07	9,52E+06	7,54E+06	5,39E+06	2,95E+06	2,22E+05	3,16E+06	6,91E+06	1,11E+07	1,58E+07
3	0,01208	1,60E+07	1,37E+07	1,14E+07	9,01E+06	6,44E+06	3,52E+06	2,37E+05	3,78E+06	8,26E+06	1,33E+07	1,88E+07
4	0,01812	1,82E+07	1,56E+07	1,30E+07	1,03E+07	7,33E+06	4,01E+06	2,51E+05	4,31E+06	9,41E+06	1,51E+07	2,15E+07
5	0,02416	2,02E+07	1,73E+07	1,44E+07	1,14E+07	8,14E+06	4,45E+06	2,68E+05	4,78E+06	1,04E+07	1,68E+07	2,38E+07
6	0,0302	2,20E+07	1,89E+07	1,57E+07	1,24E+07	8,89E+06	4,86E+06	2,85E+05	5,21E+06	1,14E+07	1,83E+07	2,60E+07
7	0,03624	2,32E+07	1,99E+07	1,65E+07	1,31E+07	9,35E+06	5,11E+06	3,02E+05	5,46E+06	1,19E+07	1,92E+07	2,72E+07
8	0,04228	2,50E+07	2,14E+07	1,78E+07	1,41E+07	1,01E+07	5,51E+06	3,22E+05	5,87E+06	1,28E+07	2,07E+07	2,93E+07
9	0,04832	2,62E+07	2,25E+07	1,87E+07	1,48E+07	1,06E+07	5,78E+06	3,46E+05	6,14E+06	1,34E+07	2,16E+07	3,07E+07
10	0,05436	2,69E+07	2,31E+07	1,92E+07	1,52E+07	1,08E+07	5,94E+06	3,66E+05	6,27E+06	1,37E+07	2,21E+07	3,14E+07
11	0,0604	2,69E+07	2,30E+07	1,91E+07	1,51E+07	1,08E+07	5,93E+06	3,86E+05	6,21E+06	1,36E+07	2,20E+07	3,11E+07
12	0,06644	2,79E+07	2,39E+07	1,98E+07	1,57E+07	1,12E+07	6,15E+06	4,14E+05	6,41E+06	1,41E+07	2,27E+07	3,21E+07
13	0,07248	2,77E+07	2,37E+07	1,97E+07	1,56E+07	1,11E+07	6,11E+06	4,37E+05	6,30E+06	1,39E+07	2,23E+07	3,17E+07
14	0,07852	2,85E+07	2,44E+07	2,02E+07	1,60E+07	1,14E+07	6,28E+06	4,65E+05	6,44E+06	1,42E+07	2,29E+07	3,24E+07
15	0,08456	2,87E+07	2,45E+07	2,04E+07	1,61E+07	1,15E+07	6,32E+06	4,97E+05	6,41E+06	1,42E+07	2,28E+07	3,23E+07
16	0,0906	2,82E+07	2,41E+07	2,00E+07	1,58E+07	1,13E+07	6,21E+06	5,19E+05	6,22E+06	1,38E+07	2,22E+07	3,15E+07
17	0,09664	2,74E+07	2,34E+07	1,94E+07	1,53E+07	1,09E+07	6,03E+06	5,43E+05	5,96E+06	1,32E+07	2,13E+07	3,02E+07
18	0,10268	2,64E+07	2,25E+07	1,86E+07	1,47E+07	1,05E+07	5,80E+06	5,63E+05	5,64E+06	1,26E+07	2,03E+07	2,87E+07
19	0,10872	2,46E+07	2,10E+07	1,74E+07	1,37E+07	9,75E+06	5,42E+06	5,72E+05	5,17E+06	1,16E+07	1,87E+07	2,64E+07
20	0,11476	2,39E+07	2,03E+07	1,68E+07	1,32E+07	9,44E+06	5,25E+06	5,88E+05	4,94E+06	1,11E+07	1,79E+07	2,53E+07
21	0,1208	2,22E+07	1,89E+07	1,56E+07	1,23E+07	8,75E+06	4,88E+06	5,98E+05	4,49E+06	1,01E+07	1,63E+07	2,31E+07
22	0,12684	2,05E+07	1,74E+07	1,44E+07	1,13E+07	8,05E+06	4,51E+06	5,92E+05	4,06E+06	9,17E+06	1,48E+07	2,10E+07
23	0,13288	1,85E+07	1,57E+07	1,29E+07	1,02E+07	7,24E+06	4,07E+06	5,85E+05	3,57E+06	8,10E+06	1,31E+07	1,86E+07
24	0,13892	1,64E+07	1,39E+07	1,15E+07	8,99E+06	6,41E+06	3,61E+06	5,62E+05	3,10E+06	7,05E+06	1,14E+07	1,62E+07
25	0,14496	1,43E+07	1,21E+07	9,93E+06	7,78E+06	5,55E+06	3,14E+06	5,36E+05	2,62E+06	5,98E+06	9,70E+06	1,38E+07
26	0,151	1,16E+07	9,80E+06	8,05E+06	6,29E+06	4,49E+06	2,55E+06	4,84E+05	2,07E+06	4,75E+06	7,70E+06	1,09E+07
27	0,15704	8,54E+06	7,23E+06	5,92E+06	4,63E+06	3,30E+06	1,88E+06	4,12E+05	1,49E+06	3,42E+06	5,56E+06	7,88E+06

Step 12	Step 13	Step 14	Step 15	Step 16	Step 17	Step 18	Step 19	Step 20	Step 21	Step 22	Step 23	Step 24	Step 25
1,25	1,3	1,35	1,4	1,45	1,5	1,55	1,6	1,65	1,7	1,75	1,8	1,85	1,95
1,57E+07	1,96E+07	2,38E+07	2,80E+07	3,23E+07	3,66E+07	4,10E+07	4,55E+07	5,01E+07	5,48E+07	5,96E+07	6,46E+07	6,97E+07	8,06E+07
2,08E+07	2,61E+07	3,16E+07	3,71E+07	4,28E+07	4,86E+07	5,44E+07	6,03E+07	6,64E+07	7,26E+07	7,91E+07	8,57E+07	9,25E+07	1,07E+08
2,48E+07	3,12E+07	3,77E+07	4,44E+07	5,12E+07	5,80E+07	6,50E+07	7,21E+07	7,94E+07	8,68E+07	9,45E+07	1,02E+08	1,11E+08	1,28E+08
2,83E+07	3,55E+07	4,30E+07	5,06E+07	5,83E+07	6,61E+07	7,41E+07	8,22E+07	9,04E+07	9,89E+07	1,08E+08	1,17E+08	1,26E+08	1,46E+08
3,14E+07	3,94E+07	4,77E+07	5,61E+07	6,47E+07	7,34E+07	8,22E+07	9,12E+07	1,00E+08	1,10E+08	1,19E+08	1,29E+08	1,40E+08	1,62E+08
3,42E+07	4,30E+07	5,20E+07	6,13E+07	7,06E+07	8,01E+07	8,97E+07	9,95E+07	1,09E+08	1,20E+08	1,30E+08	1,41E+08	1,52E+08	1,76E+08
3,59E+07	4,51E+07	5,46E+07	6,43E+07	7,41E+07	8,40E+07	9,40E+07	1,04E+08	1,15E+08	1,26E+08	1,37E+08	1,48E+08	1,60E+08	1,85E+08
3,86E+07	4,85E+07	5,87E+07	6,91E+07	7,96E+07	9,03E+07	1,01E+08	1,12E+08	1,23E+08	1,35E+08	1,47E+08	1,59E+08	1,72E+08	1,99E+08
4,04E+07	5,08E+07	6,14E+07	7,23E+07	8,34E+07	9,45E+07	1,06E+08	1,17E+08	1,29E+08	1,41E+08	1,54E+08	1,67E+08	1,80E+08	2,08E+08
4,13E+07	5,19E+07	6,28E+07	7,40E+07	8,52E+07	9,66E+07	1,08E+08	1,20E+08	1,32E+08	1,45E+08	1,57E+08	1,70E+08	1,84E+08	2,13E+08
4,10E+07	5,15E+07	6,23E+07	7,34E+07	8,46E+07	9,59E+07	1,07E+08	1,19E+08	1,31E+08	1,43E+08	1,56E+08	1,69E+08	1,83E+08	2,11E+08
4,24E+07	5,32E+07	6,44E+07	7,58E+07	8,73E+07	9,90E+07	1,11E+08	1,23E+08	1,35E+08	1,48E+08	1,61E+08	1,75E+08	1,88E+08	2,18E+08
4,17E+07	5,24E+07	6,34E+07	7,47E+07	8,61E+07	9,76E+07	1,09E+08	1,21E+08	1,33E+08	1,46E+08	1,59E+08	1,72E+08	1,86E+08	2,15E+08
4,27E+07	5,36E+07	6,49E+07	7,64E+07	8,81E+07	9,98E+07	1,12E+08	1,24E+08	1,36E+08	1,49E+08	1,62E+08	1,76E+08	1,90E+08	2,19E+08
4,26E+07	5,35E+07	6,47E+07	7,62E+07	8,78E+07	9,96E+07	1,11E+08	1,24E+08	1,36E+08	1,49E+08	1,62E+08	1,75E+08	1,89E+08	2,19E+08
4,15E+07	5,21E+07	6,30E+07	7,42E+07	8,55E+07	9,69E+07	1,09E+08	1,20E+08	1,32E+08	1,45E+08	1,58E+08	1,71E+08	1,84E+08	2,13E+08
3,98E+07	5,00E+07	6,05E+07	7,13E+07	8,21E+07	9,31E+07	1,04E+08	1,16E+08	1,27E+08	1,39E+08	1,51E+08	1,64E+08	1,77E+08	2,04E+08
3,78E+07	4,75E+07	5,75E+07	6,77E+07	7,80E+07	8,84E+07	9,90E+07	1,10E+08	1,21E+08	1,32E+08	1,44E+08	1,56E+08	1,68E+08	1,94E+08
3,49E+07	4,38E+07	5,30E+07	6,23E+07	7,18E+07	8,14E+07	9,11E+07	1,01E+08	1,11E+08	1,22E+08	1,32E+08	1,43E+08	1,55E+08	1,79E+08
3,34E+07	4,19E+07	5,07E+07	5,97E+07	6,88E+07	7,80E+07	8,73E+07	9,68E+07	1,06E+08	1,16E+08	1,27E+08	1,37E+08	1,48E+08	1,71E+08
3,05E+07	3,83E+07	4,63E+07	5,45E+07	6,28E+07	7,12E+07	7,97E+07	8,83E+07	9,72E+07	1,06E+08	1,16E+08	1,25E+08	1,35E+08	1,56E+08
2,77E+07	3,48E+07	4,21E+07	4,96E+07	5,71E+07	6,47E+07	7,24E+07	8,03E+07	8,83E+07	9,65E+07	1,05E+08	1,14E+08	1,23E+08	1,42E+08
2,45E+07	3,08E+07	3,72E+07	4,38E+07	5,05E+07	5,72E+07	6,40E+07	7,09E+07	7,80E+07	8,53E+07	9,28E+07	1,00E+08	1,08E+08	1,25E+08
2,13E+07	2,68E+07	3,24E+07	3,82E+07	4,40E+07	4,98E+07	5,58E+07	6,18E+07	6,80E+07	7,43E+07	8,08E+07	8,75E+07	9,44E+07	1,09E+08
1,81E+07	2,28E+07	2,75E+07	3,24E+07	3,73E+07	4,23E+07	4,73E+07	5,24E+07	5,77E+07	6,30E+07	6,85E+07	7,42E+07	8,01E+07	9,24E+07
1,44E+07	1,81E+07	2,19E+07	2,57E+07	2,96E+07	3,36E+07	3,76E+07	4,16E+07	4,58E+07	5,00E+07	5,44E+07	5,89E+07	6,35E+07	7,33E+07
1,04E+07	1,30E+07	1,58E+07	1,86E+07	2,14E+07	2,42E+07	2,71E+07	3,00E+07	3,30E+07	3,60E+07	3,92E+07	4,24E+07	4,58E+07	5,28E+07

Step 26	Step 27	Step 28	Step 29	Step 30	Step 31	Step 32	Step 33	Step 34	Step 35	Step 36	Step 37	Step 38	Step 39
2,05	2,15	2,25	2,35	2,4	2,45	2,5	2,55	2,6	2,65	2,7	2,75	2,8	2,85
9,24E+07	1,05E+08	1,20E+08	1,36E+08	1,45E+08	1,55E+08	1,65E+08	1,78E+08	1,96E+08	2,20E+08	2,46E+08	2,64E+08	2,56E+08	2,17E+08
1,23E+08	1,40E+08	1,59E+08	1,80E+08	1,92E+08	2,05E+08	2,19E+08	2,36E+08	2,59E+08	2,91E+08	3,25E+08	3,49E+08	3,38E+08	2,85E+08
1,47E+08	1,67E+08	1,90E+08	2,16E+08	2,30E+08	2,45E+08	2,62E+08	2,83E+08	3,10E+08	3,47E+08	3,88E+08	4,15E+08	4,02E+08	3,38E+08
1,67E+08	1,90E+08	2,16E+08	2,46E+08	2,62E+08	2,79E+08	2,99E+08	3,22E+08	3,53E+08	3,94E+08	4,40E+08	4,70E+08	4,54E+08	3,81E+08
1,85E+08	2,11E+08	2,40E+08	2,72E+08	2,90E+08	3,10E+08	3,31E+08	3,57E+08	3,91E+08	4,37E+08	4,86E+08	5,19E+08	5,01E+08	4,19E+08
2,02E+08	2,30E+08	2,62E+08	2,97E+08	3,17E+08	3,38E+08	3,61E+08	3,90E+08	4,26E+08	4,75E+08	5,28E+08	5,63E+08	5,42E+08	4,51E+08
2,12E+08	2,42E+08	2,75E+08	3,12E+08	3,32E+08	3,54E+08	3,79E+08	4,09E+08	4,47E+08	4,97E+08	5,52E+08	5,87E+08	5,65E+08	4,69E+08
2,28E+08	2,60E+08	2,95E+08	3,35E+08	3,57E+08	3,81E+08	4,07E+08	4,39E+08	4,80E+08	5,33E+08	5,90E+08	6,28E+08	6,02E+08	4,99E+08
2,38E+08	2,72E+08	3,09E+08	3,51E+08	3,74E+08	3,99E+08	4,27E+08	4,60E+08	5,02E+08	5,57E+08	6,16E+08	6,54E+08	6,26E+08	5,17E+08
2,44E+08	2,78E+08	3,16E+08	3,58E+08	3,82E+08	4,07E+08	4,36E+08	4,69E+08	5,12E+08	5,67E+08	6,26E+08	6,64E+08	6,35E+08	5,22E+08
2,42E+08	2,76E+08	3,13E+08	3,55E+08	3,79E+08	4,04E+08	4,32E+08	4,66E+08	5,08E+08	5,62E+08	6,19E+08	6,55E+08	6,26E+08	5,13E+08
2,50E+08	2,84E+08	3,23E+08	3,67E+08	3,91E+08	4,17E+08	4,46E+08	4,80E+08	5,23E+08	5,78E+08	6,36E+08	6,72E+08	6,41E+08	5,24E+08
2,46E+08	2,80E+08	3,18E+08	3,61E+08	3,85E+08	4,10E+08	4,39E+08	4,73E+08	5,15E+08	5,68E+08	6,23E+08	6,58E+08	6,26E+08	5,11E+08
2,52E+08	2,87E+08	3,26E+08	3,69E+08	3,93E+08	4,20E+08	4,49E+08	4,83E+08	5,26E+08	5,79E+08	6,35E+08	6,69E+08	6,36E+08	5,18E+08
2,51E+08	2,86E+08	3,25E+08	3,68E+08	3,92E+08	4,18E+08	4,47E+08	4,81E+08	5,23E+08	5,76E+08	6,30E+08	6,63E+08	6,29E+08	5,11E+08
2,44E+08	2,78E+08	3,16E+08	3,58E+08	3,81E+08	4,07E+08	4,35E+08	4,67E+08	5,08E+08	5,58E+08	6,10E+08	6,41E+08	6,08E+08	4,92E+08
2,34E+08	2,67E+08	3,03E+08	3,43E+08	3,66E+08	3,90E+08	4,17E+08	4,48E+08	4,87E+08	5,34E+08	5,82E+08	6,11E+08	5,79E+08	4,68E+08
2,22E+08	2,53E+08	2,88E+08	3,26E+08	3,47E+08	3,70E+08	3,95E+08	4,25E+08	4,61E+08	5,05E+08	5,50E+08	5,76E+08	5,44E+08	4,39E+08
2,05E+08	2,33E+08	2,65E+08	3,00E+08	3,19E+08	3,40E+08	3,63E+08	3,90E+08	4,23E+08	4,63E+08	5,03E+08	5,27E+08	4,97E+08	4,00E+08
1,96E+08	2,23E+08	2,53E+08	2,87E+08	3,05E+08	3,25E+08	3,47E+08	3,73E+08	4,04E+08	4,41E+08	4,79E+08	5,01E+08	4,72E+08	3,79E+08
1,79E+08	2,03E+08	2,31E+08	2,61E+08	2,78E+08	2,96E+08	3,16E+08	3,39E+08	3,67E+08	4,00E+08	4,34E+08	4,53E+08	4,26E+08	3,42E+08
1,62E+08	1,85E+08	2,10E+08	2,37E+08	2,52E+08	2,69E+08	2,87E+08	3,07E+08	3,32E+08	3,62E+08	3,92E+08	4,08E+08	3,83E+08	3,07E+08
1,43E+08	1,63E+08	1,85E+08	2,09E+08	2,23E+08	2,37E+08	2,53E+08	2,71E+08	2,92E+08	3,18E+08	3,44E+08	3,57E+08	3,35E+08	2,68E+08
1,25E+08	1,42E+08	1,61E+08	1,82E+08	1,94E+08	2,06E+08	2,20E+08	2,35E+08	2,53E+08	2,75E+08	2,97E+08	3,08E+08	2,88E+08	2,31E+08
1,06E+08	1,20E+08	1,36E+08	1,54E+08	1,64E+08	1,74E+08	1,86E+08	1,99E+08	2,14E+08	2,32E+08	2,50E+08	2,59E+08	2,42E+08	1,94E+08
8,39E+07	9,54E+07	1,08E+08	1,22E+08	1,30E+08	1,38E+08	1,47E+08	1,57E+08	1,69E+08	1,83E+08	1,97E+08	2,03E+08	1,89E+08	1,52E+08
6,04E+07	6,87E+07	7,78E+07	8,80E+07	9,35E+07	9,94E+07	1,06E+08	1,13E+08	1,21E+08	1,31E+08	1,41E+08	1,45E+08	1,36E+08	1,10E+08

Step 40	Step 41	Step 42
2,9	2,95	3
1,61E+08	1,00E+08	4,63E+07
2,09E+08	1,26E+08	4,87E+07
2,46E+08	1,45E+08	4,99E+07
2,75E+08	1,59E+08	4,86E+07
3,00E+08	1,70E+08	4,77E+07
3,20E+08	1,77E+08	4,49E+07
3,30E+08	1,79E+08	4,36E+07
3,49E+08	1,85E+08	4,21E+07
3,59E+08	1,86E+08	4,20E+07
3,60E+08	1,83E+08	4,23E+07
3,51E+08	1,76E+08	4,42E+07
3,56E+08	1,75E+08	4,57E+07
3,45E+08	1,67E+08	4,78E+07
3,48E+08	1,67E+08	4,96E+07
3,42E+08	1,62E+08	5,16E+07
3,28E+08	1,54E+08	5,21E+07
3,11E+08	1,45E+08	5,25E+07
2,92E+08	1,36E+08	5,15E+07
2,65E+08	1,25E+08	5,04E+07
2,52E+08	1,19E+08	4,89E+07
2,27E+08	1,09E+08	4,75E+07
2,05E+08	9,98E+07	4,55E+07
1,79E+08	8,99E+07	4,42E+07
1,55E+08	8,03E+07	4,29E+07
1,32E+08	7,17E+07	4,23E+07
1,05E+08	6,10E+07	4,18E+07
7,91E+07	5,23E+07	4,17E+07

MIN	MAX
2,07E+05	2,64E+08
2,22E+05	3,49E+08
2,37E+05	4,15E+08
2,51E+05	4,70E+08
2,68E+05	5,19E+08
2,85E+05	5,63E+08
3,02E+05	5,87E+08
3,22E+05	6,28E+08
3,46E+05	6,54E+08
3,66E+05	6,64E+08
3,86E+05	6,55E+08
4,14E+05	6,72E+08
4,37E+05	6,58E+08
4,65E+05	6,69E+08
4,97E+05	6,63E+08
5,19E+05	6,41E+08
5,43E+05	6,11E+08
5,63E+05	5,76E+08
5,72E+05	5,27E+08
5,88E+05	5,01E+08
5,98E+05	4,53E+08
5,92E+05	4,08E+08
5,85E+05	3,57E+08
5,62E+05	3,08E+08
5,36E+05	2,59E+08
4,84E+05	2,03E+08
4,12E+05	1,45E+08

Result - Mises stress

The influence lines for Submodel 4B, for each node at the U-sape. Maximum Mises stress 671.96 MPa at node 12 in load step 2.75 m.